Report prepared by:
Yanbo Liu*,
Andres Suarez*,
Francisco J. Presuel-Moreno

Final Report

Characterization of New and Old Concrete Structures Using Surface Resistivity Measurements

(Contract Number BD546, RPWO #08)

Submitted to

Florida Department of Transportation Research Center
605 Suwannee Street
Tallahassee, Florida 32399

Submitted by

Francisco Presuel-Moreno
Principal Investigator
Department of Ocean and Mechanical Engineering
Florida Atlantic University
SeaTech Campus
101 North Beach Road
Dania Beach, Florida 33004

August 1, 2010

*Graduate Research Assistants

Disclaimer

The opinions, findings, and conclusions expressed in this publication are those of the authors and not necessarily those of the State of Florida Department of Transportation.

SI* (MODERN METRIC) CONVERSION FACTORS

APPROXIMATE CONVERSIONS TO SI UNITS

Symbol	When You Know	Multiply By	To Find	Symbol
		LENGTH		
in	inches	25.4	millimeters	mm
ft	feet	0.305	meters	m
yd	yards	0.914	meters	m
mi	miles	1.61	kilometers	km
		AREA		
in^2	square inches	645.2	square millimeters	mm^2
ft^2	square feet	0.093	square meters	m^2
yd^2	square yard	0.836	square meters	m^2
ac	acres	0.405	hectares	ha
mi^2	square miles	2.59	square kilometers	km^2
		VOLUME		
fl oz	fluid ounces	29.57	milliliters	mL
gal	gallons	3.785	liters	L
ft^3	cubic feet	0.028	cubic meters	m^3
yd^3	cubic yards	0.765	cubic meters	m^3
		NOTE: volumes greater than 1000 L shall be shown in m^3		
		MASS		
oz	ounces	28.35	grams	g
lb	pounds	0.454	kilograms	kg
T	short tons (2000 lb)	0.907	megagrams (or "metric ton")	Mg (or "t")
		TEMPERATURE (exact degrees)		
^oF	Fahrenheit	5 (F-32)/9 or (F-32)/1.8	Celsius	^oC
		ILLUMINATION		
fc	foot-candles	10.76	lux	lx
fl	foot-Lamberts	3.426	$candela/m^2$	cd/m^2
		FORCE and PRESSURE or STRESS		
lbf	poundforce	4.45	newtons	N
lbf/in^2	poundforce per square inch	6.89	kilopascals	kPa

APPROXIMATE CONVERSIONS FROM SI UNITS

Symbol	When You Know	Multiply By	To Find	Symbol
		LENGTH		
mm	millimeters	0.039	inches	in
m	meters	3.28	feet	ft
m	meters	1.09	yards	yd
km	kilometers	0.621	miles	mi
		AREA		
mm^2	square millimeters	0.0016	square inches	in^2
m^2	square meters	10.764	square feet	ft^2
m^2	square meters	1.195	square yards	yd^2
ha	hectares	2.47	acres	ac
km^2	square kilometers	0.386	square miles	mi^2
		VOLUME		
mL	milliliters	0.034	fluid ounces	fl oz
L	liters	0.264	gallons	gal
m^3	cubic meters	35.314	cubic feet	ft^3
m^3	cubic meters	1.307	cubic yards	yd^3
		MASS		
g	grams	0.035	ounces	oz
kg	kilograms	2.202	pounds	lb
Mg (or "t")	megagrams (or "metric ton")	1.103	short tons (2000 lb)	T
		TEMPERATURE (exact degrees)		
^oC	Celsius	1.8C+32	Fahrenheit	^oF
		ILLUMINATION		
lx	lux	0.0929	foot-candles	fc
cd/m^2	$candela/m^2$	0.2919	foot-Lamberts	fl
		FORCE and PRESSURE or STRESS		
N	newtons	0.225	poundforce	lbf
kPa	kilopascals	0.145	poundforce per square inch	lbf/in^2

*SI is the symbol for the International System of Units. Appropriate rounding should be made to comply with Section 4 of ASTM E380.
(Revised March 2003)

Technical Report Documentation Page

1. Report No.	2. Government Accession No.	3. Recipient's Catalog No.
4. Title and Subtitle Characterization of New and Old Concrete Structures Using Surface Resistivity Measurements		5. Report Date August, 2010
		6. Performing Organization Code FAU-OE-CMM-08-3
7. Author(s) Francisco Presuel-Moreno, Andres Suares, Yanbo Liu		8. Performing Organization Report No.
9. Performing Organization Name and Address Florida Atlantic University – Sea Tech Campus 101 North Beach Road, Dania Beach, FL 33004		10. Work Unit No. (TRAIS)
		11. Contract or Grant No. BD546, RPWO #08
12. Sponsoring Agency Name and Address Florida Department of Transportation – Research Center 605 Suwannee Street Tallahassee, Florida 32399		13. Type of Report and Period Covered Final Report May 31, 2007 – August 1, 2010
		14. Sponsoring Agency Code

15. Supplementary Notes

16. Abstract

This report describes the findings of concrete resistivity characterization using the surface resistivity test method. This characterization was conducted on Florida's new and old coastal bridge structures. The testing took place on partially-immersed substructures on more than 60 bridges. The surface resistivity measurements were performed in areas above the mean tide line (marine growth). The Surface resistivity (SR) profiles at several locations as a function of elevation were performed using a commercial Wenner probe. This Wenner probe is the same instrument used in Florida Department of Transportation's FM5-578 test method. A resistivity gradient from low to high proceeding from the submerged to atmospheric zone is usually observed. This gradient results from the elevation dependence of moisture saturation and pore solution composition. A conditioning procedure was designed and implemented as part of the field testing to increase the moisture content of the concrete being examined (tidal and splash zone). The characteristic surface resistivity after one or two days of monitoring is called herein the SR_{field}. This value was usually the minimum resistivity value observed at the second or higher examined elevation.

During the field trips nominal 2 inch concrete cores were obtained in the vicinity of where the surface resistivity profiles were made. These cores were used either to perform wet surface resistivity measurements in the laboratory or to obtain chloride profiles. The chloride profiles were then used to estimate the apparent chloride diffusivity (D_{Cl}). The wet surface resistivity was achieved after a few weeks of exposure in a high humidity chamber, and is named herein the SR_{wet}.

A correlation between SR_{field} and SR_{wet} was performed and it was found that SR_{field} was about 3 times that of SR_{wet}; i.e., no full saturation was obtained with the conditioning method. A correlation was computed between D_{Cl} (average per component) vs. SR_{wet}. However, due to the field nature of the data there is some scatter, the R^2 varied between 0.62 and 0.69 depending on whether all bridges visited were included or if only a subset was used in the fitting.

A second component of this project consisted of experiments on laboratory samples aimed at understanding how the resistivity varies over time depending upon the concrete mix and environmental exposure, as well as in the presence - and absence - of reinforcing steel. Numerical modeling was performed to obtain K (cell constants). The K values were used to normalize the SR measurements performed on laboratory samples. Additionally, numerical modeling was performed to investigate additional scenarios (different concrete cover thicknesses, multiple rebar presence, dimensions of the concrete block interrogated, presence of multiple concrete layers). Very useful insight was obtained from this research effort.

17. Key Word	18. Distribution Statement
Reinforced concrete, bridge substructure, marine, sea water, surface resistivity, wet surface resistivity, chloride diffusion coefficient	No restrictions.

19. Security Classif. (of this report)	20. Security Classif. (of this page)	21. No. of Pages	22. Price
Unclassified	Unclassified	263	

Form DOT F 1700.7 (8-72) Reproduction of completed page authorized

The authors are indebted to the Florida Department of Transportation - State Materials Office for logistical support during the field portion of this study and, in particular Mr. Rodney Powers, Ivan Lasa, Mario Paredes, Ronald Simmons, Richard Nalli and Dennis Baldi. The assistance of several undergraduate students who work in the corrosion lab as part of this project is also acknowledged.

EXECUTIVE SUMMARY

The surface resistivity of saturated concrete in the laboratory has been found to be a good measure of the concrete permeability to chlorides. The objective of the present research was to develop, design and test a surface resistivity measurement protocol that can be implemented in the field. These tests are intended to provide a more realistic assessment of the bulk concrete resistivity as the examined concrete approaches saturation. The designed-surface resistivity field testing protocol provides a non-destructive approach that assists in identifying the bulk concrete resistivity which can then be correlated to chloride diffusion coefficient.

Surface resistivity profiles as a function of elevation were measured on new and old marine partially-immersed reinforced concrete substructures at and above mean water on more than 60 bridges at coastal locations in Florida. The Surface resistivity (SR) profiles at several locations as a function of elevation were performed using a commercial Wenner probe using two electrode spacings: a=3 cm and a= 5 cm. This Wenner probe is the same instrument used in Florida Department of Transportation's (FDOT) FM5-578 test method. A resistivity gradient from low to high proceeding from the submerged to atmospheric zone results from the elevation dependence of moisture saturation.

Preliminary results of this investigation suggested that a conditioning method needed to be applied on-site to approximate water saturation conditions at the elevations of interest. A conditioning procedure was designed and implemented as part of the field testing to increase the moisture content of the concrete being examined (tidal and splash zone). The characteristic surface resistivity after one or two days of monitoring is called herein SR_{field}. This value was usually the minimum resistivity value observed at the second or higher examined elevation.

During the field trips nominal 2 inch concrete cores were obtained in the vicinity of where the surface resistivity profiles were made. These cores were used either to perform wet surface resistivity measurements in the laboratory or to obtain chloride

profiles. The chloride profiles were then used to estimate the apparent chloride diffusivity (D_{Cl}). The wet surface resistivity was achieved after a few weeks of exposure in a high humidity chamber, and is named herein the SR_{wet}.

A correlation between SR_{field} and SR_{wet} was performed and it was found that SR_{field} was about 3 times than SR_{wet}; i.e., no full saturation was obtained with the conditioning method. It is important to mention that SR_{field} measured after conditioning was significantly lower value than the resistivity value measured before the conditioning, suggesting that in most instances the degree of saturation increased but did not reach full saturation. Previous laboratory work suggests that a good correlation exists on saturated concrete between concrete resistivity and chloride diffusivity. A correlation was computed between D_{Cl} (average per component) vs. SR_{wet}. A good fit was obtained. However, due to the field nature of the data there is some scatter, the R^2 varied between 0.62 and 0.69 depending on whether all bridges visited were included or if only a subset was used in the fitting.

A second component of this project consisted of experiments in laboratory samples aimed at understanding how the resistivity varies over time depending on concrete mix and environmental exposure, as well as in the presence and absence of reinforcing steel. Five different concrete mixtures were prepared: three sample groups were prepared with single composition. The other two concrete mixtures were used to investigate the multiple layer effect by having two different types of concrete mixtures present in the same specimen. Two different probe spacing was also used on laboratory measurements a=3 cm and a=5 cm. Numerical modeling was performed to calculate K (cell constants) to correct laboratory readings due to finite geometry of laboratory samples or rebar presence/absence. These K values were used to normalize the surface resistivity measurements performed on laboratory samples. It was found that K values could range from 0.8 to 4 depending on geometry and rebar presence.

For saturated conditions very similar values were obtained after normalization when comparing readings made with both spacings at any given day. It was found that mixture composition is important, for e.g., a saturated-concrete-mixture prepared with

20% FA replacement, a stable normalized resistivity value was reached after 400 days (~95% of final value).

Laboratory samples exposed to laboratory temperature and relative humidity registered a gradual reduction on the degree of saturation. This moisture reduction produces a monotonic increase on the measured resistivity value. After a few days under this exposure the normalized values measured with a=3 cm were higher than those obtained with a=5 cm. The measured resistivity value in this exposure environment reached up to four times the saturated measured resistivity value. The normalized resistivity value under laboratory humidity could have reached higher values if exposed in this environment for a longer time.

Additionally, numerical modeling was performed to investigate additional scenarios (different concrete covers, multiple rebar presence, dimensions of the concrete block interrogated, presence of multiple concrete layers). Very useful insight was obtained and reported in here from the laboratory and numerical modeling component.

Table of Contents

List of Figures

List of Tables

1. INTRODUCTION

It is well known that concrete is one of the most used materials in construction. However, the deterioration of reinforced concrete structures has been a constant concern for years, and corrosion of the reinforcing steel is the main cause of this deterioration. Once corrosion has initiated, cracks in concrete propagate due to tension stress forces produced by corrosion products. The corrosion products occupy a larger volume when compared to the volume of a non-corroding rebar. A critical area in a partially-immersed reinforced concrete structure exposed to severe weather conditions (i.e., direct exposure to sea water) is the splash zone, where the most severe corrosion conditions could develop. A resistivity gradient from low to high upon proceeding from the submerged to the atmospheric zone results from the elevation dependence of moisture saturation. Consequently, macro-cells are likely to be more significant at lower elevations. Also, reinforcement in the submerged zone is expected to be active; and because of low [O_2] here, the potential is relatively negative (oxygen concentration polarization). The opposite is the case in the atmospheric zone where reinforcement remains passive due to low [Cl^-] and high [O_2], and so potential is relatively positive here. Thus, the concrete resistivity affects significantly how corrosion would proceed once corrosion has initiated.

The determination of concrete electrolytic resistivity has become an established non-destructive test method. This method is often used to assist in the assessment of concrete durability (Millard, Harrison and Gowers 1990, Millard and Gowers 1992). Pore water is an electrolytic solution containing mostly K^+, Na^+, Ca^{++}, and OH^- ions (Woelfl and Lauer 1979, Elkey and Sellevold 1995, Hunkeler 1996). Additionally ions, such as chloride, can also be present due to permeation as a result of exposure to external sources (such as seawater and de-icing salt), increasing the concentration of ions in the pore water and, presumably, reducing the electrolytic resistance of the pore water. One approach to measure the concrete resistivity is by using a Wenner probe. The Wenner probe method has been used in laboratory experiments for quite some time. This report describes research conducted with the aim to transfer this test method

to field measurements performed in marine substructures in service, either as to verify performance-based concrete quality or to assess the chloride diffusivity of the visited bridge structures.

The Florida Department of Transportation (FDOT) - State Materials Office (SMO) has developed a surface resistivity (SR) test method (FM5-578 2005) to assess concrete chloride permeability using a Wenner probe. FM5-578 or a slightly modified test has been used in recent FDOT research projects (e.g., Chini, Muszynski and Hicks 2003, Kessler, Powers and Paredes . 2005, Hamilton, Boyd and Vivas 2007, Kessler et al. 2008, Ferraro, Boyd and Ishee 2010) as part of the assessment of this test. Currently, other DOTs are considering adapting a similar test method. The test is performed on cylindrical concrete cores in a fully saturated condition. The Wenner probe has been in use for concrete resistivity as early as the mid-1980s (Millard, Harrison and Edwards 1986, Ewins 1990), and today there are a few commercial products, although to our knowledge, only one allows to adjust the electrode spacing. The main application of the Wenner probe has been in testing laboratory samples, with some use in the field for cathodic protection systems. It is important to note that the Wenner method was developed for geology (Wenner 1915) and has been adapted to measure concrete resistivity. There is considerable interest to assess if field surface resistivity measurements can be performed in situ and then use these obtained values to estimate concrete permeability properties.

FDOT uses a Wenner surface resistivity probe in the field for assessing the concrete resistivity before the installation of a cathodic protection system so as to estimate needed current. These measurements are particularly important for partially-immersed bridge components. When SR measurements are performed as a function of elevation a resistivity profile can be constructed. Sagüés and Lau 2009a, 2009b and Presuel and Hartt 2009 are examples of recent FDOT projects that used SR measurements in the field at various elevations. Higher SR values are usually observed as the distance from the water line increases. However, the higher SR values are due to a lower degree of

water saturation. A conditioning protocol was designed and implemented on 60 bridges along the coast of Florida.

2. BACKGROUND

Concrete electrical resistivity has been employed in a large number of laboratory tests (e.g., Elkey and Sellevold 1995, Hunkeler 1996, Hope and Ip 1985, Gowers and Millard1991, Millard et al. 1990, Saleem et al. 1996, Sengul and Gjorv 2008, Sengul and Gjorv 2009) and to some degree in the field (Naish 1990, Moreton 1997, Pruckner and Gjorv 2001, Sagüés et al. 2001, Presuel et al. 2010, Sagüés and Lau 2009) as a method to 1) characterize and/or monitor concrete quality, 2) assess the likelihood of corrosion in conjunction with corrosion potential and/or corrosion rate measurements, 3) monitor the evolution of the degree of hydration, and 4) characterize transport properties (e.g., permeability) of a given concrete. Other properties have been characterized using SR (e.g., degree of moisture (indirectly) in combination with relative humidity (RH) and temperature (T) sensors, cracks detection).

2.1 Electrical Resistivity in Concrete

Concrete electrical resistivity measures the ability of concrete to resist the passage of electrical current, passed by the ions in the case of concrete thru the pore solution contained in the pore structure of the concrete.

Concrete conductivity is fundamentally related to the permeability of fluids and the diffusivity of ions through a porous material. As a result, the electrical resistivity can be used as an indirect measure of the ease in which chloride ions can penetrate concrete.

2.1.1 Methods to Measure Concrete Resistivity other than Wenner Method

Recent publications have reviewed the concept of concrete resistivity (e.g., Elkey and Sellevold 1995, Lay et al. 2003, Chini, Muszynski, and Hicks 2003, Whiting and Nagi 2003, Hamilton, Boyd and Vivas 2007). There are multiple ways to measure the

concrete resistivity or concrete conductivity both for laboratory and field conditions. In the laboratory, one method consists of using external plates (e.g., McCarter 1996, McCarter, Ezirim and Emerson 1992) with the same geometry as the cross section of the specimen. Another approach to measure resistivity is to have the electrodes embedded (two or four electrodes), or a combination of embedded electrodes and plates (2 external plates and 2 embedded electrodes for a 4 point approach similar to that used in a soil resistivity cell). The embedded electrodes vary in size and location. Some of the set-ups have been designed to monitor changes as a function of depth (e.g., McCarter and Vennesland 2004, Brameshuber et al. 2003, Schiesl and Breit 1995, Weydert and Gehlen 1999); other set-ups have been used to monitor the resistivity very close to the reinforcing steel (e.g., Villagran Zaccardi et al. 2009). The reader is referred to recent literature reviews (Elkey and Sellevold 1995, Lay et al. 2003, Whiting and Nagi 2003) and the bibliography section of this report for more details on the multiple laboratory approaches. The method selected for both field and laboratory measurements for this investigation is a commercial Wenner probe that allows for adjustment in the electrode spacing.

Two methods other than the Wenner method used in the field are: 1) embedded electrodes of various sizes (e.g., Schiesl and Breit 1995, Burchler, Elsener and Bohni 1996, Weydert and Gehlen 1999, Brameshuber et al. 2003, McCarter et al. 2005, Butefuhr et al. 2006) or 2) through a connection to the reinforcing steel and external plate at the surface of the concrete (e.g., Weydert and Gehlen1999, Lay et al. 2003).

2.1.2 Wenner Method

The reader is referred to the open literature for a more detailed background on the surface resistivity Wenner method. Only a brief description of the method is included here. The resistivity of concrete close to the surface can be measured non-destructively by placing four equally-spaced electrodes on the surface of the concrete. The Wenner probe used here is a spring-loaded, hand-held instrument that is pushed upon until it comes into contact with the concrete surface (Broomfield and Millard 2002, Broomfield,

Kevin and Hladky 2002). Wetted wooden plugs are placed at the end of the probes of the model used to increase conductivity.

As shown in Figure 1, the Wenner method consists of four equi-spaced electrodes and the tips are placed in contact with the concrete surface. Once in contact with the concrete, a trapezoidal potential is applied between the outer probes which generates a current (I) inversely proportional to the resistivity of the concrete. The potential difference (V) is measured across the inner probes. The apparent resistivity is calculated through Ohm's Law and the solution is given by Equation 1.

$$\rho = \frac{2\pi a V}{I} \qquad \text{(Equation 1)}$$

Where ρ is the apparent resistivity, a is the spacing between probes.

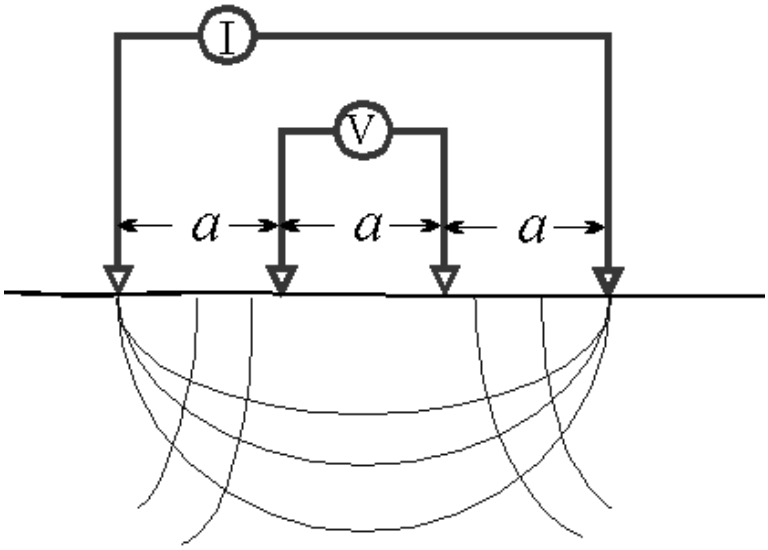

Figure B.1: Diagram of Wenner method used for measuring concrete resistivity.

Most instruments use alternating current (AC) with a frequency between 50 and 1000 Hz, usually sinusoidal or trapezoidal. DC is not recommended because it could polarize the electrodes and/or the under-laying reinforcement (Lay et al. 2003, Polder et al. 2000, Polder 2001). The spacing of the electrodes is critical for accurate measurements of concrete resistivity. The apparent resistivity obtained with a Wenner surface resistivity meter assumes that the concrete being measured is both semi-infinite and homogeneous. Concrete contains coarse aggregates (gravel) which normally have

a significantly higher resistivity than the cement paste; thus, the uniform bulk resistivity does not always hold. To minimize heterogeneity in the SR measurements, it has been suggested that the minimum electrode spacing should be 1.5 times the maximum aggregate size. Most laboratory concrete specimens that are measured have finite dimensions and cannot be considered as semi-infinite. Several researchers in the past have proposed correction factors (cell constants) (e.g., Morris, Moreno and Sagüés 1996) for different geometries. However, no publication was found that included cell constant values that accounted for the effects due the reinforcing steel.

2.2 Saturated Concrete Resistivity vs. D_{Cl}

It has been known for some time that the transport properties of concrete can be correlated to electrical resistivity (Garboczi 1990, Andrade 2005, Elkey and Sellevold 1995, Klinghoffer and Kofoed 1993, Klinghoffer and Rislund 1995). Moreover, under controlled conditions (i.e., saturated concrete in laboratory experiments), diffusivity and resistivity correlate well (e.g., Bamforth 1999, Bertolini and Polder 1997, Kessler, Powers and Paredes 2005, Kessler et al. 2008, Hamilton, Boyd and Vivas 2007, Polder 1997, Smith 2006, Castellote, Andrade and Alonso 2002). Other important parameters that could affect the measured resistivity have been discussed on references by Millard, Lay, Gowers, Elkey, Klinghoffer, Bertolini, Polder and others. A correlation between concrete resistivity measured with a Wenner probe and chloride permeability was reported recently (Kessler, Powers and Paredes 2005, Kessler et al. 2008) for saturated lab specimens. Recently, Andrade (Andrade 2005, Andrade and d'Andrea 2010) has suggested using the resistivity value of saturated concrete measured at 28 days to predict the service life of a structure. In actual exposure conditions the samples are not fully saturated all the time particularly at locations several feet above the water line. For this report, a correlation between SR_{wet} and D_{Cl} has been fitted to data obtained from tests performed on field cores.

2.3 Factors that Affect Surface Resistivity Measurements

It has been recognized for some time that field resistivity measurements are affected (Gowers and Millard 1991, 1999, Millard 1991) by environment (temperature and humidity), surface layers of different resistivity from the bulk, geometrical restrictions due to the shape and size of the bridge component being measured, electrode spacing, and the presence of the steel embedded in the concrete. Additionally, on partially-immersed structures, a resistivity gradient from low to high upon proceeding from the submerged to atmospheric zone results from the elevation dependence of moisture saturation.

High degrees of water saturation (wet concrete) and more and larger pores cause lower resistivity. The resistivity increases if concrete dries out and when it carbonates. (Pruckner and Gjorv 2001, 2004, 2010) describes how the degree of water saturation affects resistivity at two different temperatures. Pruckner suggests a relationship to normalize resistivity values based on temperature and relative humidity.

A partial list of factors that affect concrete electrical resistivity are

- Amount of cement paste (or amount of cement per unit volume)
- w/cm ratio (decreasing w/cm ratio increases the rate of change of resistance that can be observed due to moisture content variations)
- Curing conditions (temperature, high relative humidity or immersion, duration)
- Exposure temperature (3% decrease in resistivity for saturated concrete per °K increase, and 5% decrease in resistivity for not-saturated concrete for each degree °K increase) based on the influence of ion mobility, ion-ion, and ion-solid interaction
- Chlorides (e.g., wet concrete with chlorides (2% by wt of cement) has a resistivity ~50-60% lower than resistivity of a similar concrete with no chlorides); the contribution due to the chlorides is relatively modest. Nevertheless, due to the hygroscopic behavior of chlorides water is retained, which enhances the effect

- Moisture content (~3% resistivity decrease per 1% increase towards saturation). Usually, 70% or more degree of saturation is maintained for concrete cover beyond 2 cm
- Cement type and the presence and amount of pozzolans (e.g., FA, SF, UFA usually increase resistivity at relatively longer exposure times (Hamilton, Boyd and Vivas 2007)
- Aggregate type (chemical composition and porosity)
- Admixtures (inhibitors, water reducers, etc.)

2.3.1 Geometry Effect on Resistivity

The spacing of the electrodes is critical for accurate measurements of concrete resistivity. The Wenner method assumes that the concrete being measured is both semi-infinite and homogeneous. As concrete contains coarse and fine aggregates, which normally have a larger resistivity than cement paste, it is suggested that the minimum electrode spacing should be 1.5 times the maximum aggregate size. Placement of the electrode probes should be in a manner that avoids the edges of the concrete.

Most concrete laboratory specimens measured could not be considered as semi-infinite, thus, research has been done by (Broomfield and Millard 2002, Millard and Gowers 1992, Morris, Moreno and Sagüés 1996) regarding different specimen geometries. In this investigation additional geometric cell constants were calculated using numerical modeling for the geometries of interest. A few of the computed cases repeated some of the geometries and corresponding cell constants reported by others as a validation technique and also to provide an engineering curve for two commonly used concrete cylinders (10 cm diameter by 20 cm length cores and cores of 4.75 cm diameter (field-obtained cores using a 2 inch core drill bit) of various lengths.

2.3.2 Brief Review of Laboratory Specimens Similar to those Prepared for this Investigation

Two recent publications (Sengul and Gjorv 2008, Sengul and Gjorv 2009) investigated the concrete resistivity of FA cement (CEM II/A-V 42.5 R) 0.4 w/c concrete. The geometry investigated: cylinders 10 cm x 20 cm and 15 cm x 30 cm, concrete blocks 10 cm x 10 cm and 30 x 30 x 20 cm, concrete blocks with no rebars, specimens with a 1 cm diam rebar were 30 x 30 x 13.5 cm. For the latter geometry, the effect of rebar presence was also investigated. A commercial Wenner probe was used to measure the concrete resistivity at various spacings. Sengul also used the two-electrode method. The resistivity values measured by the Wenner method were divided by those measured by the two-electrode method to obtain relative resistivity values. The results presented by Sengul focus upon values obtained up to 29 days. These publications also report diffusivity values obtained at various ages that were compared to the measured resistivity at corresponding ages, a good correlation was found. With respect to the resistivity values trends appear to be similar to the findings described in chapters 2 and 3 of this report.

2.3.3 Pozzolanic Admixtures

For a constant moisture content the resistivity is increased by a lower w/c-ratio, longer curing periods, and particularly by additions of supplementary cementitious materials (SCM) as blast furnace slag, fly ash, silica fume, ultra fine fly ash, or metakaolin.

Modern concrete is a heterogeneous mixture made mostly of cement, coarse aggregate, sand and SCM’s. Pozzolans are commonly used as admixtures in modern concrete mixes to increase the long-term strength and to form compounds with cementitious properties which result in stronger, denser concrete. As a result, greater compressive, flexural, tensile strength, modulus of elasticity, reduced permeability and resistance to sulfate attack is developed in these concrete mixtures. Pozzolans are primarily vitreous siliceous materials which react with calcium hydroxide to form calcium silicates.

The most commonly-used pozzolans today are fly ash (FA), silica fume (SF), high-reactivity metakaolin (MET). Reaction of some of these pozzolans may be slower than the reactions that occur during cement hydration, and thus, the short-term strength of concrete made with pozzolans may not be as high as concrete made with purely cementitious materials, particularly when using fly ash. The slower-reacting pozzolans also take longer to achieve a denser structure. The evolution to a denser microstructure can be monitored via surface resistivity measurements. The experimental section results of this report indicate that it could take more than 400 days to reach a close-to-final resistivity value for a 20% FA 0.4 w/c concrete curing in a fog room. (Klinghoffer and Rislund 1995) suggests that close to two years are needed to achieve final resistivity on concrete with 9% FA. On the other hand, highly-reactive pozzolans, such as silica fume and high-reactivity metakaolin can produce "high early strength" concrete that increases the rate at which concrete gains strength. Concrete mixes with these admixtures also developed a denser microstructure with the associated higher resistivity values.

2.4 Resistivity and Reinforcing Steel Presence

The embedded reinforcing steel is highly conductive and could be expected to provide an easy path for the flow of current if located in the vicinity of the electrodes. Millard reports that, using an electrode spacing of 5 cm, reinforcement within 7.5 cm of the probes will affect measured values to a significant extent. This was likely for concrete with a thin concrete cover. Based on the results presented in the modeling and experimental sections of this report, the measured values is 10 percent smaller when using 5 cm spacing parallel and above the rebar for a concrete cover of 5 cm. Broomfield suggest an electrode spacing smaller than 2/3 the concrete cover thickness, so as to minimize any short circuit effects. This report presents findings on how the resistivity-measured value compare to the bulk resistivity by using several probe orientations and concrete covers (laboratory and numerical modeling).

The accuracy of resistivity measurements could be significantly affected if performed too closely to highly-conducting material such as reinforcing steel. A lower reading could

be recorded if the cover is small or if the spacing between Wenner probe electrodes is large. Therefore, surface resistivity measurements should be performed in a manner such that influences from the reinforcing steel are minimized or, if possible, avoided completely. It is recommended that readings be taken as far as possible from the rebars and/or in perpendicular orientation to the rebar orientation.

2.5 Resistivity Gradient

A surface layer is often present in the concrete closer to the outer surface with a resistivity value different from that of the bulk material. This layer could result from salt ingress, chemical changes such as carbonation or differential moisture content (due to low moisture during the dry season). It is likely that the concrete layer closer to the surface actually is composed of a resistivity gradient as a function of depth. This surface layer can be just a fraction of a millimeter deep, a few millimeters, or a few centimeters. At depths larger than 3 cm (McCarter, Starrs and Chrisp 2000, Saleem et al. 1996, Pruckner and Gjorv 2001) relative humidity has been found to be constant. Thus, the resistivity would be constant from that depth inwards except for situations when chlorides have reached more deeply. As indicated above, the degree of water saturation in a partially-immersed concrete pile is inversely proportional to the distance from the water level; i.e., as the distance from the water line is increased, the degree of water saturation decreases. Thus, surface resistivity measurements can vary as a function of depth and elevation simultaneously.

Techniques to achieve a more uniform saturation, such as water vacuum saturation or submerging in water for several days can be performed in the laboratory. For this project, an increase in the degree of water saturation in the field on the concrete structure was achieved by attaching a container filled with water against a relatively smooth region of the bridge component to be examined. This method will be explained in detail in the field section of this report. This report describes the results of a research project consisting of field visits to explore the implementation of surface resistivity profiles as a means to assess concrete permeability.

3. MODELING

3.1 Background

A commercial finite element method (FEM) software was used to model the laboratory size specimens as well as for selected cases assuming a concrete block of one cubic meter. Additionally, a geometry simulating a field rectangular pile was used in some instances. A three-dimensional approach was used to describe the concrete slabs with and without rebars. The rebars were implemented by introducing a very conductive cylinder with the same diameter as the rebar diameter used in the laboratory experiments.

Figure M.1 shows a diagram generated with the FEM software simulating a lab specimen with one rebar. This figure will assist in describing the model and boundary conditions. Potential in the domain will satisfy $\nabla^2\Phi = 0$ with the boundary conditions described below. In the sub-domain describing the concrete block (blk1) and rebar (cyc1), $\nabla^2\Phi = 0$, at the outer boundaries $\frac{\partial\Phi}{\partial\vec{n}} = 0$, at the boundary between blk1 and cyc1, $\Phi_1 = \Phi_2$, and $\frac{1}{\rho_1}\frac{\partial\Phi_1}{\partial\vec{n}} = \frac{1}{\rho_2}\frac{\partial\Phi_2}{\partial\vec{n}}$,

Finally, current sources are introduced at points 1 and 2. At point 1, a current source *I* with an arbitrary volume V_0, bounded by a surface S_0, and current density *J* (in units of $amps/m^2$) is described by $\int_{S_0} \vec{J}\cdot\vec{n}da = I$. Similarly, at point 2, $\int_{S_0} \vec{J}\cdot\vec{n}da = -I$ where $\vec{n}$ is the normal vector. ρ_1 is the resistivity of bulk concrete and ρ_2 is the resistivity of cyc1 (rebar) and was set to 5.99e7 s/m. For many cases the rebar was not present. The concrete block ρ_1 was assumed to have a constant value in most cases, but for selected cases the resistivity in the concrete block was allowed to vary by either assuming discrete layers of different resistivity or by assuming a transient in resistivity as a function of depth.

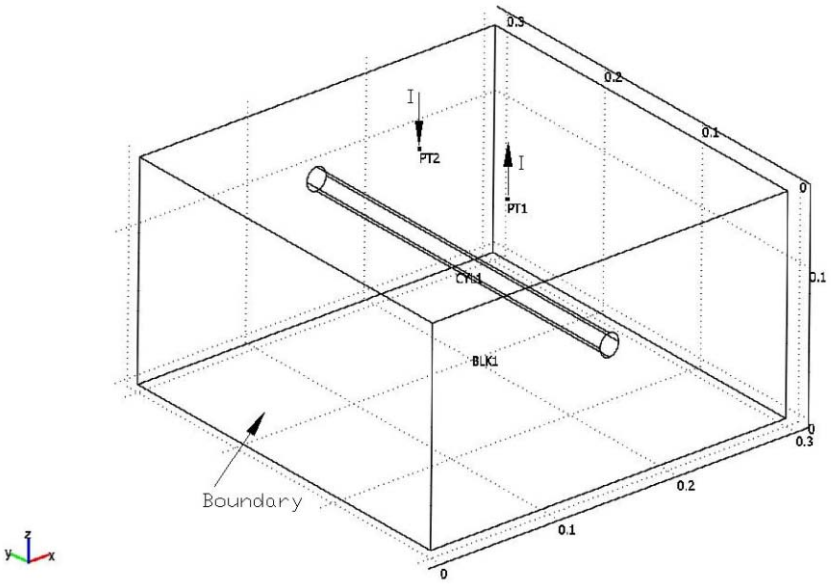

Figure M.1: Modeling geometry of one rebar specimen with dimension of 30 cm x 30 cm x 15 cm; shown electrode spacing a=3 cm.

Figure M.2 shows a specimen with the discretized mesh and the mesh density was increased at point 1 and at point 2 for more precise results. Figure M.3 shows a typical potential distribution between point 1 and point 2. ΔV was calculated by obtaining the potential difference between these two points. The resistivity was calculated using equation (M-1):

$$\rho = \frac{2\pi a \Delta V}{I} \qquad \text{Equation (M-1)}$$

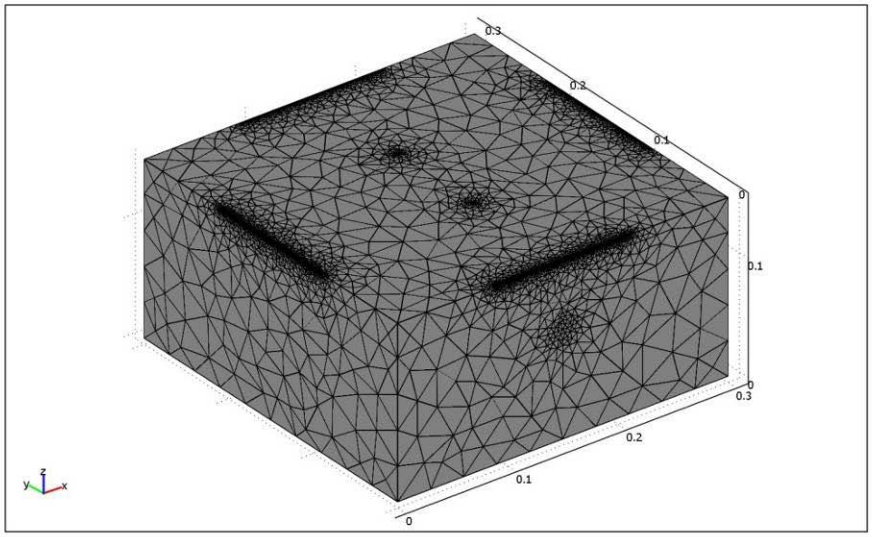

Figure M.2: Mesh style of modeling one rebar specimen with dimension of 30 cm x 30 cm x 15 cm, electrode spacing 3 cm; dimension of the graph in meters.

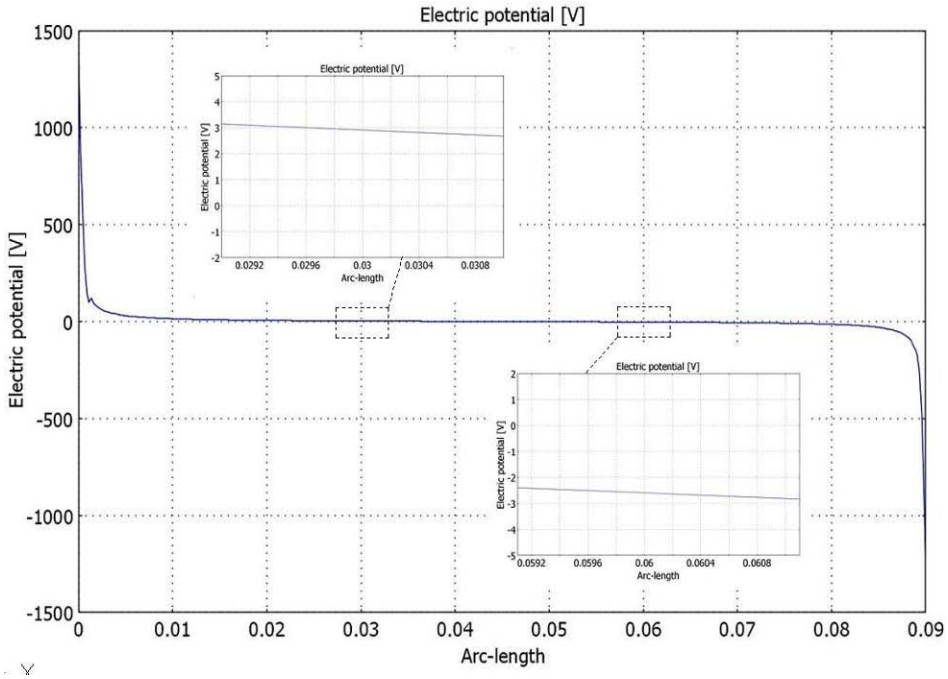

Figure M.3: Potential distributions between two external electrodes in blank specimen modeling, electrode spacing a=3 cm, dimension unit in the graph in meters.

The results obtained with the FEM software were validated by comparing selected cases to analytical solutions for cases with two layers and three layers. No analytical solution can be easily obtained for cases in which rebar are present, hence a numerical approach was used to obtain geometrical cell constants for the spacing and the locations of interest.

Geometries representing the laboratory specimens were modeled by assuming concrete single resistivity. Numerical modeling was conducted that reproduced the three types of prism-shaped laboratory specimens (no rebar, 1 rebar and 4 rebars). Computations replicated the location and spacing used during lab measurements. Geometrical correction factors were derived from these computations and are presented in this chapter.

3.2 Modeling Results

3.2.1 Cylindrical Geometry

Figure M.4 shows the computed cell constants due to restricted geometry that need to be accounted for when using a Wenner probe for concrete cylinders 10 cm (4 in) diameter by 20 cm (8 in) long. The value of the cell constant goes from K=1.2 when a=2 cm to K=3.5 when using a=6 cm, for FDOT resistivity test method FM5-578 that uses an a=3.8 cm (1.5 in) K=~1.8. The values shown in Figure M.4 could also be derived from (Morris, Moreno, and Sagüés 1996) but are provided in here for direct access to the corresponding K for this geometry.

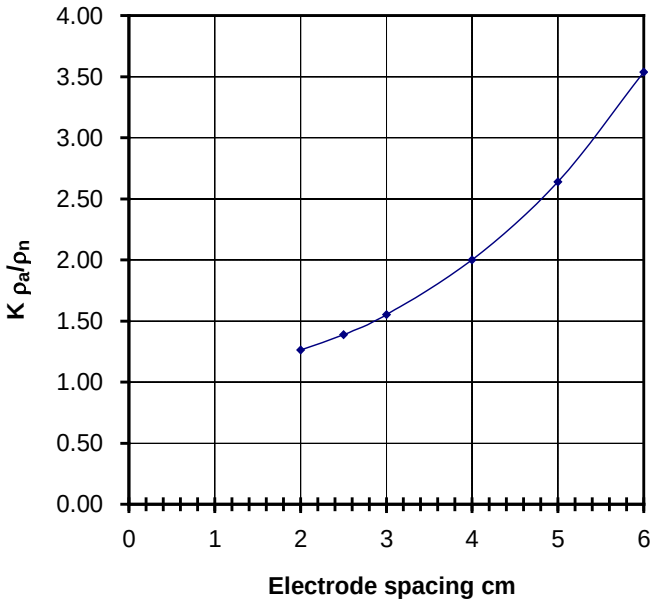

Figure M.4: Cell constant vs. spacing for a 4x8 cylinder.

Figure M.5 shows the computed cell constants due to restricted geometry that need to be considered when using a Wenner probe for field-obtained concrete cylinders using a 5 cm diameter core drill bit. The value of the cell constant is close to 3.95 when using a=3 cm and samples longer than 12 cm; the smallest length cylinder that can be measured using 3 cm spacing is 9 cm long, but a cell constant of 4.3 applies. Figure M.5 also includes the K values for a=2 cm and a=2.5 cm.

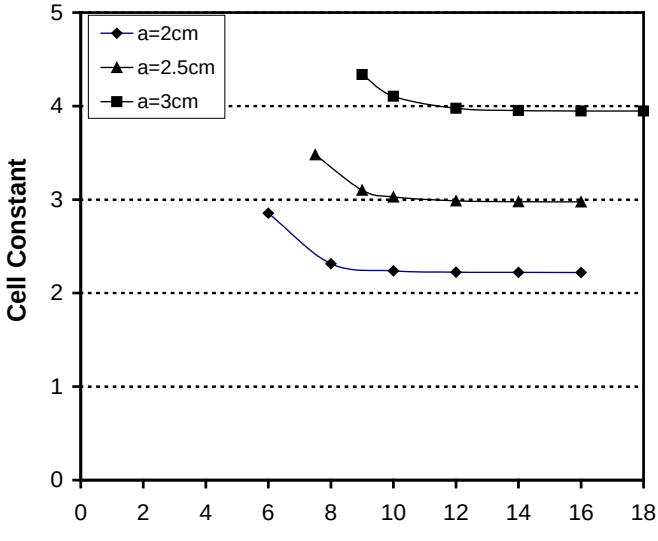

Figure M.5: Computed cell constant vs. core length for measurements centered with indicated spacing.

Some of the concrete cores from the field contained relatively large amounts of chlorides, in some cases at considerable depths. Modeling was performed to elucidate the contribution of these chlorides close to the structure surface, once the cores were obtained. An order of magnitude difference in resistivity was assumed between the bulk (the inner portion of the core, e.g., 50 KΩ-cm) and the high chloride region (concrete closer to the surface, e.g., 5 kΩ-cm). Although there is controversy as to how much chloride ions reduce the concrete resistivity, a 50% to 80% reduction has been suggested. The order of magnitude difference was used in here as a worst case scenario. Figure M.6 shows the ratio between apparent and bulk resistivity as a percentage of bulk resistivity for concrete cores with 4.5 cm diameter, a probe spacing a equal to 2 cm and L=10 cm or L=15 cm. The stepwise resistivity trend showed a somewhat larger reduction in the computed apparent resistivity for both core lengths. For the 15 cm long cores a value close to the bulk resistivity was obtained as long as the layer with the lower resistivity did not penetrate more than 3 cm. When this layer was 5 cm the apparent resistivity was about 90% and stayed there until the resistivity step was longer than 6.5 cm. The ratio eventually dropped to 72.5% when the layer with low resistivity was 7 cm long. Similar trends can be observed in the figure for L=10 cm. When the resistivity changed in a transient manner the resistivity ratio reduction was less than that observed with a step resistivity.

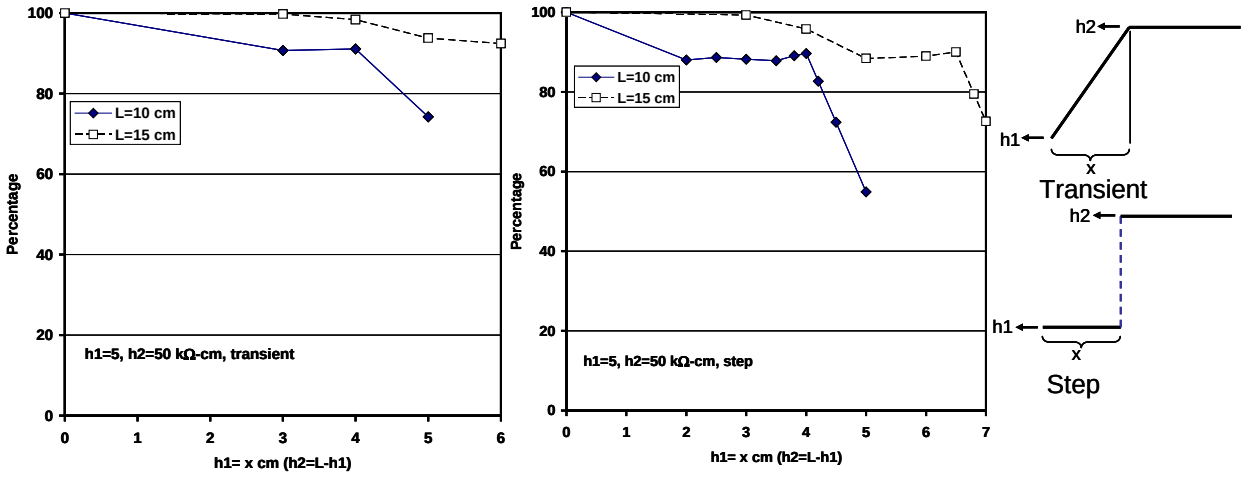

Figure M.6: Effect of two layer and transient resistivity profiles for 4.5 cm cores of L=10 or L=15 cm, and a=2 cm spacing.

3.2.2 Rectangular Prism Geometry

3.2.2.1 Specimen Size Effect for Specimens with No Rebars

Figure M.7 shows the effect of finite dimension on the apparent resistivity measurements of a blank 30 cm x 30 cm x 15 cm concrete specimen and assumes a uniform concrete resistivity thru the concrete block. Two parameters that effect the computed apparent resistivity are the specimen thickness and the location/orientation of the Wenner probe (Presuel, Liu and Paredes 2009). The locations computed correspond to sites where measurements were performed on laboratory specimens. Table M.1 shows K values at locations measured experimentally and electrode spacing a=3 cm and a=5 cm for specimens with no rebar. When a=3 cm, at locations L1 (d=0) and L2 (d=5), the ρ_a was about 4% higher than the assumed bulk resistivity and 9% higher at position L6 (d=10 cm). When a=5 cm, at position d=0 and d=5, the ρ_a was about 13-15% higher than the assumed bulk resistivity and 34% higher at position d=10 cm. These results suggest that 15 cm can not be considered a semi-infinite block.

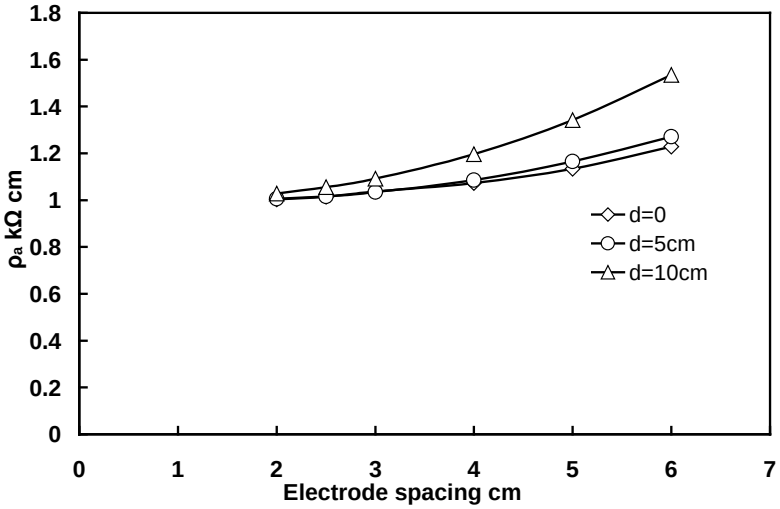

Figure M.7: Modeling of apparent resistivity of single layer concrete with no rebar; specimen dimension: 30 cm x 30 cm x 15 cm

Table M.1: Cell constant correction values K for blank specimens

	L1	L2	L3	L4	L5	L6
3 cm	1.04	1.04	1.04	1.04	1.04	1.09
5 cm	1.13	1.13	1.17	1.13	1.13	1.34

3.2.2.2 Rebar Location (concrete cover) and Specimen Size

Figure M.8 shows apparent resistivity values computed on concrete samples with one rebar. Two geometries (cubic meter compared to laboratory specimen geometry) were considered. Three different concrete covers were considered: 2.5 cm, 5 cm and 7.5 cm. The resistivity measurements were assumed to be made above the rebar at locations equivalent to location 1 in Figure E.4 (d=0). The largest effect is observed for the smaller concrete cover with a spacing a=6 cm (the largest computed spacing) which resulted in a computed apparent resistivity significantly smaller than the bulk resistivity. Additionally, there is almost no difference in the apparent resistivity values between the series for $1m^3$ and 30 cm x 30 cm x 15 cm concrete blocks. As the concrete cover increases, the apparent resistivity for the larger spacing tends to approach the bulk resistivity. There is a difference in computed resistivity values when comparing results from the two geometries and it is more evident at the larger electrode spacing, with the larger apparent resistivity computed in the $1m^3$ concrete block.

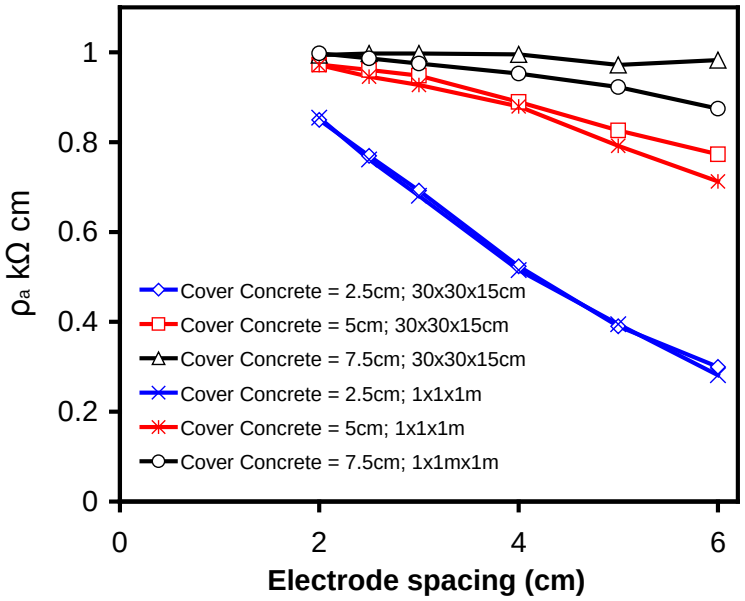

Figure M.8: Modeling of apparent resistivity of single layer concrete with single rebar with different cover concrete, specimen dimension: 1mx1mx1m vs. 30 cm x 30 cm x 15 cm

3.2.2.3 Effects of Measurement Location and Specimen Size:

Figure M.9 shows the apparent resistivity values corresponding to various electrodes spacing for concrete blocks with 1 rebar and a concrete cover of 5 cm. The plot on the left column corresponds to lab specimen geometry; the specimen on the right corresponds to a concrete block 1 m^3. Where the 1 m^3 concrete block approximates a semi-infinite dimension, the apparent resistivity values were never above the bulk resistivity. For the 1 m^3 specimen, the effect of the rebar is negligible at d=10 cm and in the perpendicular orientation. The ρ_a is 99% of the assumed bulk resistivity at a=3 cm and 97-99% when a=5 cm. The ρ_a is quite similar at d=5 cm and 45 degree, and 3% lower than the assumed bulk resistivity and 9% lower when a=5 cm. The largest effect due to the rebar presence is for location d=0, ρ_a is 7% lower than the actual resistivity when a=3 cm and 19% lower when a=5 cm.

However, the apparent resistivity at locations perpendicular (L2), 45 degrees (L4), and d=10 (L6), exceed the bulk resistivity for computations on the 30x30x15 cm block due to edge effects and the concrete not being thick enough. The largest difference corresponds to location d=10 (L6). For computation on the small concrete block, the effect of rebar is most significant at d=0, where ρ_a is 6% lower than the actual concrete bulk resistivity when a=3 cm, and 17% lower when a=5 cm. The ρ_a is almost the same as the actual resistivity at d=5 cm and 45 degrees. Dimension effect is still obvious at d=10, where ρ_a is 7% higher than the actual resistivity when a=3 cm and 26% higher when a=5 cm. When a measurement is done perpendicular to the rebar, ρ_a is 2% higher than the actual resistivity when a=3 cm and 11% lower when a=5 cm

Table M.2 shows K values at locations measured experimentally and electrode spacing a=3 cm and a=5 cm for specimens with one rebar.

Table M.2: Cell constant correction values K for one rebar specimens

	L1	L2	L3	L4	L5	L6
3 cm	0.94	1.02	0.99	0.99	0.99	1.07
5 cm	0.83	1.11	0.99	1	1	1.26

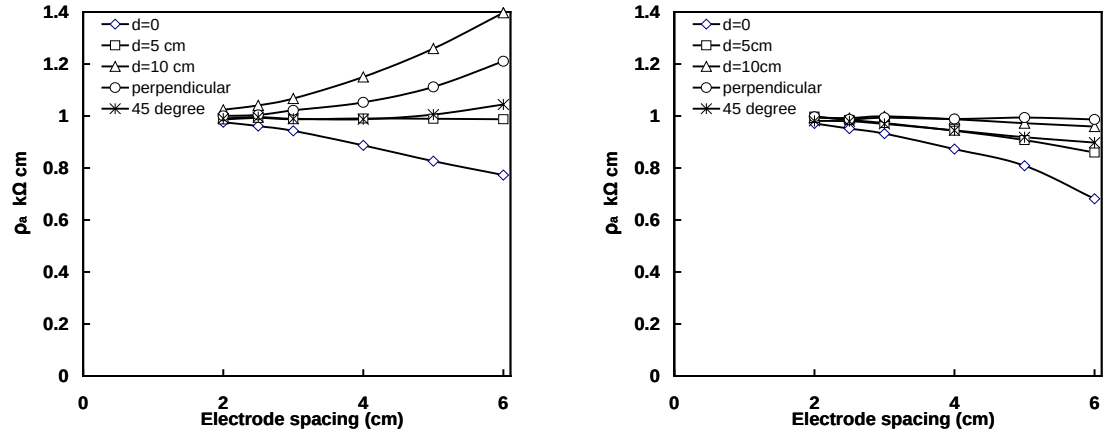

Figure M.9: Effect of geometry and location on apparent resistivity for concrete blocks with one rebar and 5 cm concrete cover. Left plot 30 cm x 30 cm x 15 cm and right 1 m^3.

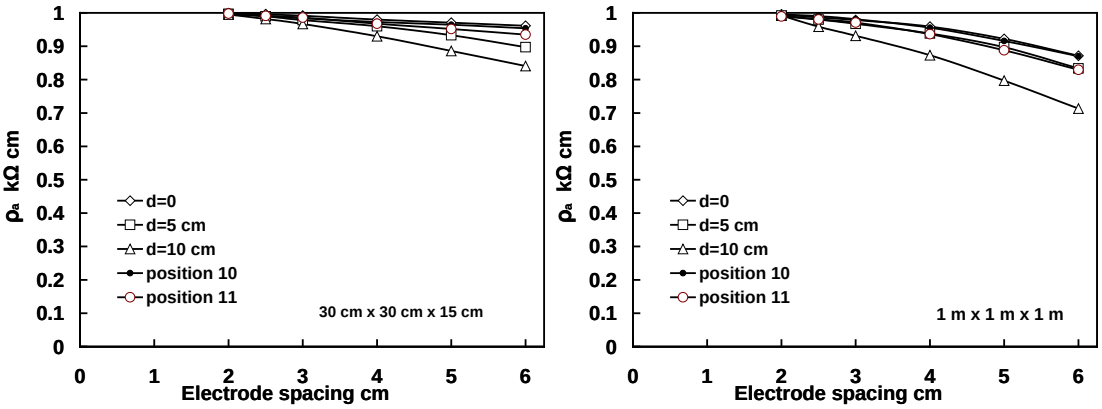

Figure M.10: Effect of geometry and location on apparent resistivity for concrete blocks with four rebars and 5 cm concrete cover. Left plot 30 cm x 30 cm x 15 cm and right 1 m^3.

Figure M.10 shows the apparent resistivity values computed for concrete blocks with four rebars. At all the locations shown, the apparent resistivity is always below the bulk resistivity due to the rebar mat. Smaller values are observed on the 1 m^3 concrete specimen. The finite size geometry and rebar presence are competing factors that counteract each other. For the specimen simulating the lab specimen the computed apparent resistivity with a=3 cm was 1-3% lower than the assumed bulk resistivity, and when a=5 cm, ρ_a varies from 3-11% lower than the bulk resistivity. Whereas, for the 1 m3 concrete block, the apparent resistivity computed with a=3 cm was 2-4% lower than the assumed bulk resistivity, and for a spacing of a=5 cm, ρ_a was 8-11% lower than the

bulk resistivity except when the computed measurement was at d=10 cm, which had a computed ρa ~20% lower.

Table M.3 shows K values at locations measured experimentally and electrode spacing a=3 cm and a=5 cm for specimens with four rebars.

Table M.3: Cell constant correction values K for four rebar specimens

	L1,L4	L2,L5	L3,L6	L7,L10	L11,L12
3 cm	0.99	0.98	0.96	0.98	0.97
5 cm	0.97	0.93	0.80	0.92	0.89

3.2.3 Apparent Resistivity for Multilayered Resistivity Concrete

Figure M.11 shows apparent resistivity values for cases with two and three layers. This figure compares results from an analytical approach and FEM computations for selected cases. Both types of computations assumed that there was no rebar present. For structures in which the concrete cover is large, it could be possible to use the analytic approach to assess the resistivity value at the rebar depth. Two- and three-layered concrete resistivity could be used as a first approximation to complex resistivity profiles.

Figure M.12 shows results for apparent resistivity computed for concrete specimens with two layers. The plots on the left column are apparent resistivity computed values for cases with a top resistivity layer ρ_1=1 kΩ-cm and a bottom layer ρ_2=10 kΩ-cm. On the column on the right, the layers order are inverted; i.e., ρ_1=10 kΩ-cm, and the bottom layer is ρ_2=1 kΩ-cm. The top row shows results for cases with no rebar, whereas the bottom row shows results for cases with one rebar. The measurements were assumed to be done at location L1. The thickness of the top layer (h1) was 0.2 cm, 0.5 cm, 1 cm and 2 cm. For cases with ρ_1=10 kΩ-cm, ρ_2=1 kΩ-cm, the thinner the top layer is and the smaller the spacing a is, the closer the computed apparent resistivity is to ρ_2. When h1=2 cm, the apparent resistivity gets closer to ρ_1. The rebar presence produces a

modest reduction on the computed apparent resistivity. The opposite trend is observed for cases with ρ_1=1 kΩ-cm and ρ_2=10 kΩ-cm.

FEM Results

Figure M.11: Apparent resistivity computed using an analytical approach and FEM computations for multilayered cases.

.

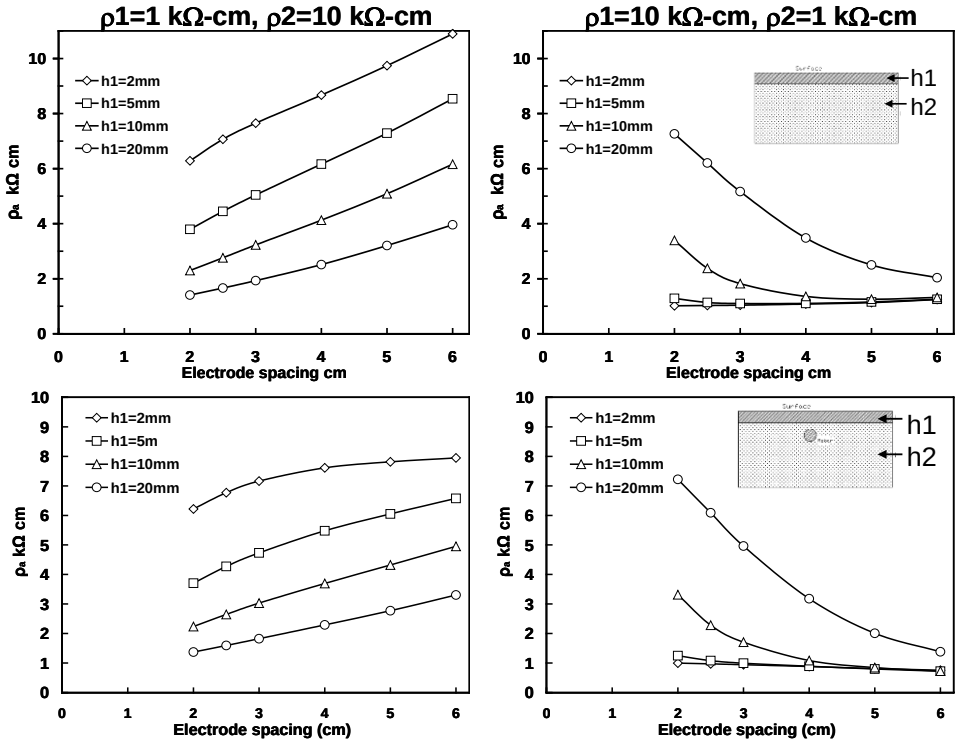

Figure M.12: Apparent resistivity computations of two resistivity layer concrete, h1 varies. Specimen 30 cm x 30 cm x15 cm. Top row cases with no rebar, bottom row with one rebar with 5 cm cover.

Figure M.13 shows computed apparent resistivity values for cases with two layers with h=1 cm, ρ1=1 kΩ-cm and ρ2=10 kΩ-cm, which were obtained at three different locations. The plot on the left assumes a concrete block with no rebar and the plot on the right assumes a concrete block with one rebar with a cover of 5 cm. The computed apparent resistivity is lower for the block with one rebar when comparing corresponding locations and spacings. The largest difference is observed at location d=0 with a=6, which is about 20 percent. When a=2 cm the difference is less than 5 percent.

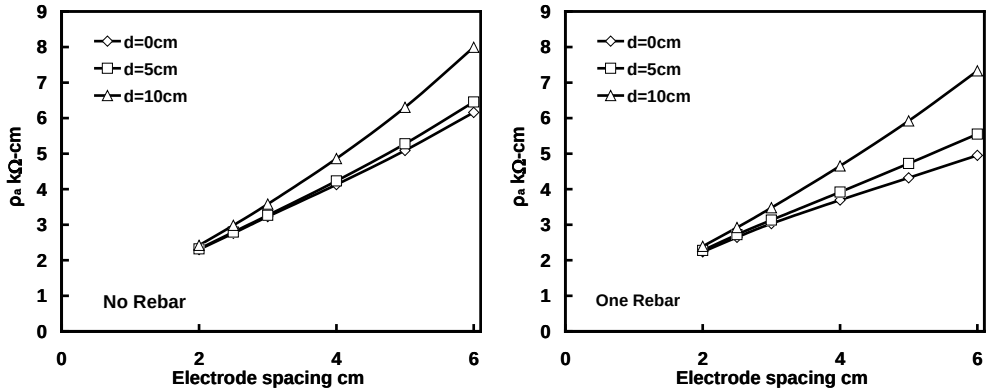

Figure M.13: Apparent resistivity computations of two layer concrete ρ1 =1 kΩ cm, ρ2 =10 kΩ cm; h1=1cm, with no rebar and with single rebar, rebar depth=5 cm; specimen 30 cm x 30 cm x 15 cm), comparison for three locations.

3.2.4 Geometry simulating field structure

The cross sectional dimensions and reinforcement spacing of the Key Royale Bridge was used to model measured apparent resistivity for conditions with uniform resistivity, and also for cases with two and three resistivity layers. Figure M.14 shows the simplified geometry for a uniform resistivity case; the orientation and location of the Wenner probe electrodes are also shown. An additional geometry was implemented attempting to describe the effects of two and three different resistivity layers when the moisture of the concrete closer to the surface is increased as might occur using the conditioning set-up described in the field section.

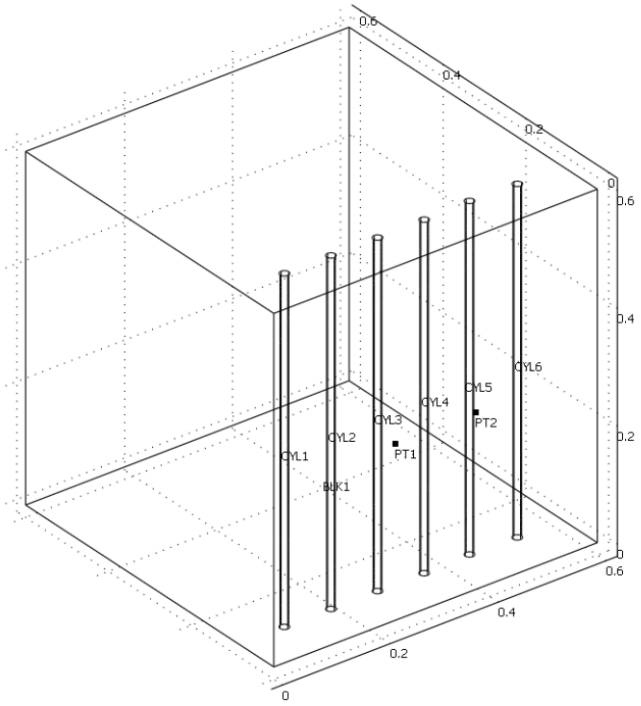

Figure M.14: Geometry used for modeling the SR, the concrete block emulates a portion of a Key Royale pile. CYL1 to CYL6 are very conductive cylinders that simulate the reinforcement, pt1 and pt2 are current source points simulating outer Wenner electrode probes.

A set of computations was performed where the bulk resistivity was uniform and included the conductive cylinders simulating the reinforcing steel. The apparent resistivity was 98.6% and 96.3% of the assumed bulk value for a=3 cm and a=5 cm, respectively. Hence, in principle, the effect of the reinforcing on the measured resistivity is less than 5 percent.

Figure M.15 shows the apparent resistivity calculated as the top layer becomes thicker (the top layer is the layer closest to the surface where the apparent resistivity is being measured). The top layer (h_1) was assumed to be ρ_1=100 kΩ.cm and the second layer (rest of the concrete) was assumed to be ρ_2=10 kΩ.cm. The computed apparent resistivity approximates ρ_2, the smaller h1 is for both a=3 cm and a=5 cm. The tendency towards ρ_1 is greater for a=3 cm.

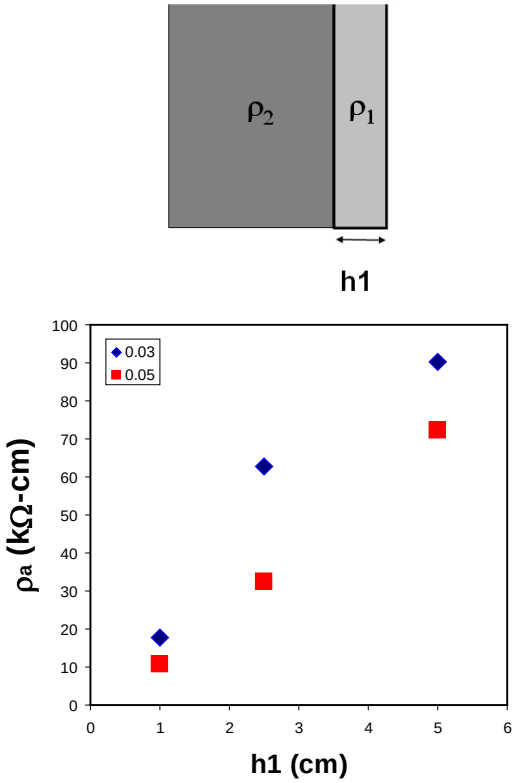

Figure M.15: Apparent resistivity calculated for a concrete with two resistivity layers. ρ1=100 kΩ-m and ρ2=10 kΩ-cm.

A second set of computations consisted of three resistivity layers, but with the two layers closest to the surface adding to 2.5 cm, the new layer was named h_1', was the top layer, and was assigned a resistivity value of 10 kΩ.cm, which is the same as ρ_2. This arrangement could represent a situation in which the concrete close to the surface is continuously wet; the longer it is exposed to this environment, the thicker **h_1**' becomes.

Figure M.16 shows results for selected combinations of h_1', h_1. The computed apparent resistivity values for cases with a=3 cm decay as h_1' is increased, whereas when a=5 cm, the apparent resistivity first goes up and eventually goes down when h_1'= 1 cm. These results partially explain some of the results from the field measurements when a=5 cm. It is likely that the resistivity profile in the field structure is significantly more complicated due to more complex resistivity profiles as a function of depth, and other parameters (e.g., concrete heterogeneity due to coarse aggregate, temperature, etc.) that are not being considered in the current model.

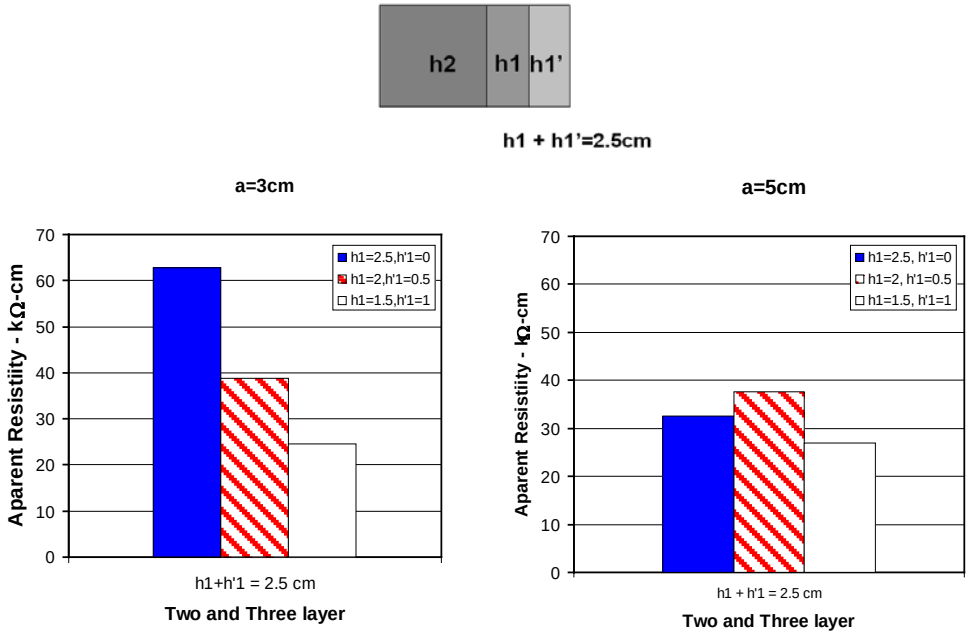

Figure M.16: Apparent resistivity calculated for a concrete with two or three resistivity layers: h1 with ρ1=100 kΩ-cm and h1' and h2 with ρ2=10 kΩ-cm. The top diagram shows the layers.

4. LABORATORY EXPERIMENTS

Concrete specimens with a w/cm ratio of 0.40 were prepared with 658 lb/yd^3 of cementitious material. In order to investigate the apparent resistivity under different conditions, four groups of specimens were prepared. Group 1 (1-A to 1-D) was prepared with ordinary Portland cement (OPC), Group 2 (1-E to 1-G) had 20% Fly Ash (FA) replacement. Group 3 simulated double layer conditions, with the top layer being 1 cm thick and concrete mix that contained either FA(top)/OPC(bottom) or OPC(Top)/FA(bottom), and Group 4 contained both FA and silica fume (SF). Table E.1 and Table E.2 show the quantity and properties of the samples prepared for each of the different groups.

Table E.1: Type and quantity of specimens

Specimen Design		W/C	Rebar	Admixture	Geometry	Number of Specimens
Group 1	1-A	0.4	-	-	RP	4
	1-B	0.4	1	-	RP	2
	1-C	0.4	1	-	RP	2
	1-D	0.4	4	-	RP	2
	1cy	0.4	-	-	Cylinder	12
Group 2	1-E	0.4	-	FA	RP	4
	1-F	0.4	1	FA	RP	2
	1-G	0.4	1	FA	RP	2
	1-H	0.4	4	FA	RP	2
	2cy	0.4	-	FA	Cylinder	12
	2-A	0.4	-	FA Bottom	RP	2
Group 3	2-B	0.4	1	FA Bottom	RP	2
	2-C	0.4	-	FA Top	RP	2
	2-D	0.4	1	FA Top	RP	2
	C, F, S	0.4	-	FA only	RP	7
	3-A	0.4	-	FA+SF	RP	4
Group 4	3-B	0.4	1	FA+SF	RP	4
	3cyl	0.4	-	FA+SF	Cylinder	7

NOTE: RP: Rectangular Prism

Table E.2: Plastic properties and compressive strength provided by SMO-FDOT.

Specimens cast	Cast Date	Initial Cl^- ($lbs./yd^3$)	Slump (in)	% air	Unit Weight ($lbs./ft^3$)	Mix Temp. (°F)	28 day SR (kΩ-cm)	28 Day Comp. (psi)	Notes
Group 1	3/3/2008	0.214	5	5.2	135.76	75	5.4	4610.0	#67 stone
Group 2	6/2/2008	0.253	3.5	1.7	139.44	77	6.5	5610.0	#67 stone
Group 3 OPC	8/19/2008	0.296	8	4.6	136.24	69	6	5790.0	#67 stone
Group 3 w/FA	8/19/2008	0.306	8	2.2	138.4	69	6	5870	#67 stone
Top G3	8/19/2008	0.465	NA		135.1	NA	5.2	6820	< ½
Top G3 w/FA	8/19/2008	0.49	NA		135.1	NA	4.8	6970	< ½
Group 4	10/6/2009	0.259	3.75	4.7	138.24	81	20.8	6520	#67 stone

Two types of geometries were prepared, cylinders 10 cm x 20 cm (4 in x 8 in), and prismatic concrete blocks. The concrete block specimens were 30 cm x 30 cm x 15 cm (12 in x 12 in x 6 in), and are named in here the rectangular prism (RP) geometry. The specimens with embedded reinforcement have Φ16mm (5/8 in) rebars. The concrete cover was 5 cm (2 in) for specimens with one rebar, and also for the top two rebars of specimens with 4 rebars. Table E.1 contains the detailed name of the groups. Additionally, at least 12 concrete cylinders 10 cm x 20 cm (4 in x 8 in) were also prepared per concrete mix for resistivity monitoring. Two specimens with one rebar for each group (1-C1, 1-C2, 1-F1, 1-F2, 3-B1 and 3B2) were exposed to a high moisture room all the time. In additiona, a number of cylinders remained in the fog room. The other samples were exposed to 60 days in the high moisture room followed by at least 60 days' exposure to laboratory environmental conditions.

4.1 Specimen Geometry

The geometries of the laboratory specimens are shown in Figures E.1, E.2, E.3 and E.4. The rectangular prism (RP) specimens were 30 cm x 30 cm x 15 cm (12 in x 12 in x 6 in). The specimens with embedded reinforcement have Φ16mm rebar. The concrete cover was 5 cm for specimens with one rebar; for the top, two rebars of specimens with four rebars.

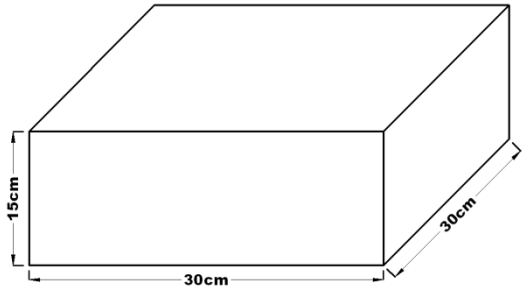

Figure E.1:Illustration of rectangular prism specimens without rebar. All dimensions in cm.

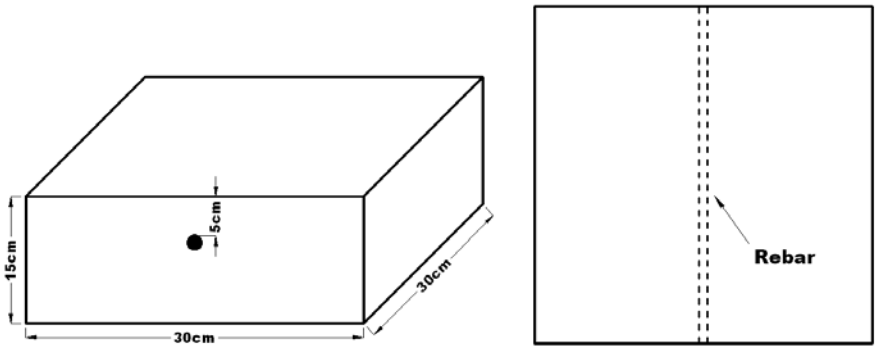

Figure E.2: Illustration of specimen with single rebar. All dimensions in cm. Rebar diameter Φ=1.6cm.

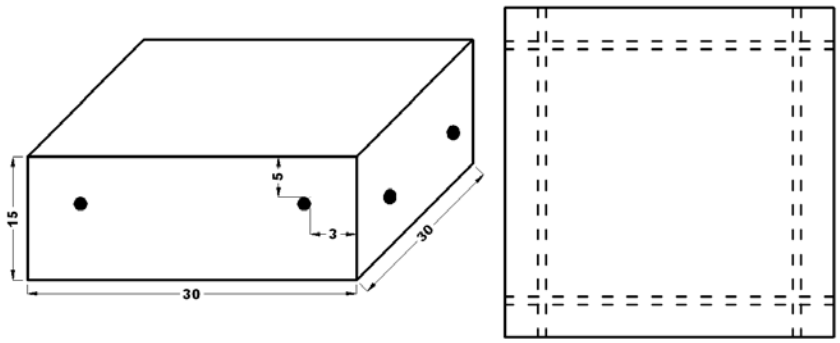

Figure E.3: Illustration of specimen with four rebars. All dimensions in cm. Rebar diameter Φ=1.6cm.

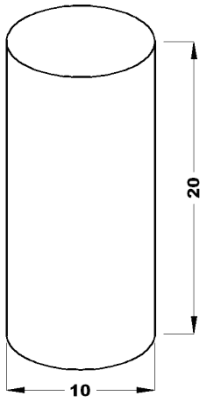

Figure E.4: Illustration of Cylinder specimens; all dimensions in cm.

4.2 Resistivity Measurements Schedule

The measurements were performed using a commercial surface resistivity meter with adjustable spacing. The four electrodes were equi-spaced, i.e., Wenner arrangement. The instrument reported values assume this arrangement and that the concrete examined is homogeneous and semi-infinite, which likely might not be the case for the selected geometries. The samples were de-molded after one day, shortly after the first set of measurements was performed. Resistivity measurements were made initially three times a week (the first two months). On most of the samples

measurements were then made twice a week or once a week; once the rate of the resistivity change slowed, the measurements were performed once every two weeks or at other frequencies. Figures E.5 and E.6 show the top view of the specimens and also indicate the locations where the measurements were made on the rectangular prism samples. The resistivity was measured using two spacings, a=3 cm and a=5 cm, on all specimens. The cylinders were measured with the probe centered along the longitudinal directions, rotating the sample every 90 degrees two times around for a total of eight readings each time. For the rectangular prism samples, templates were used to ensure reproducibility of the locations where measurements were made. Three readings were performed at each location in most instances. Figure E.7 shows pictures while the measurements were being performed.

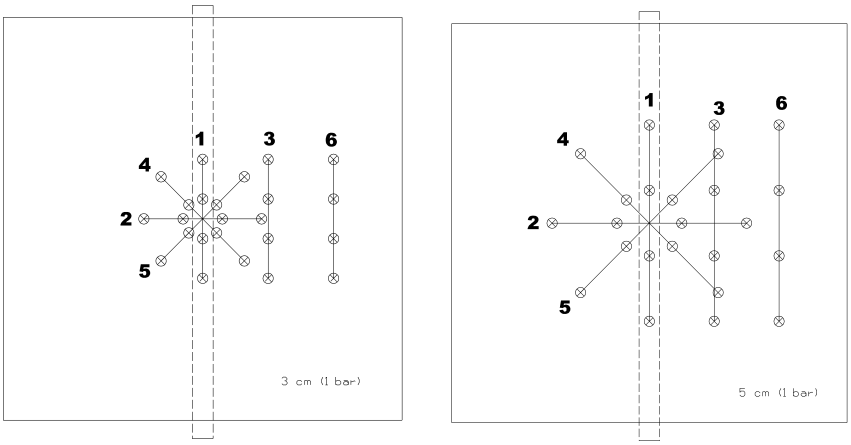

Figure E.5: Diagram showing the locations where SR measurements were conducted on blank and one rebar specimens.

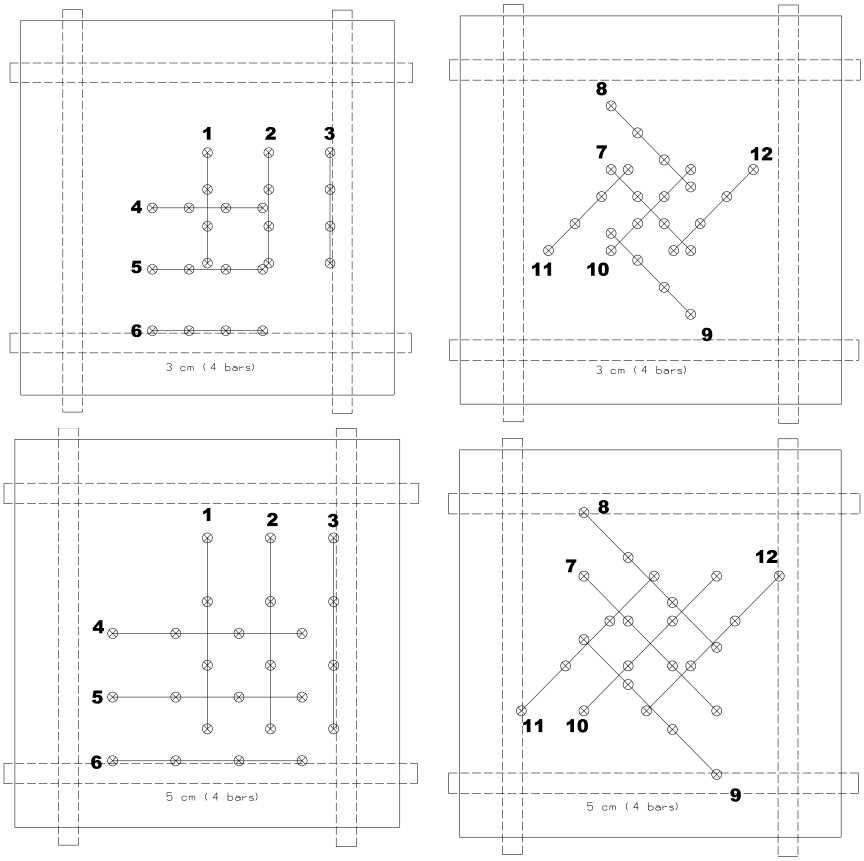

Figure E.6: Diagram showing the locations where the SR measurements were performed on specimens with four rebars.

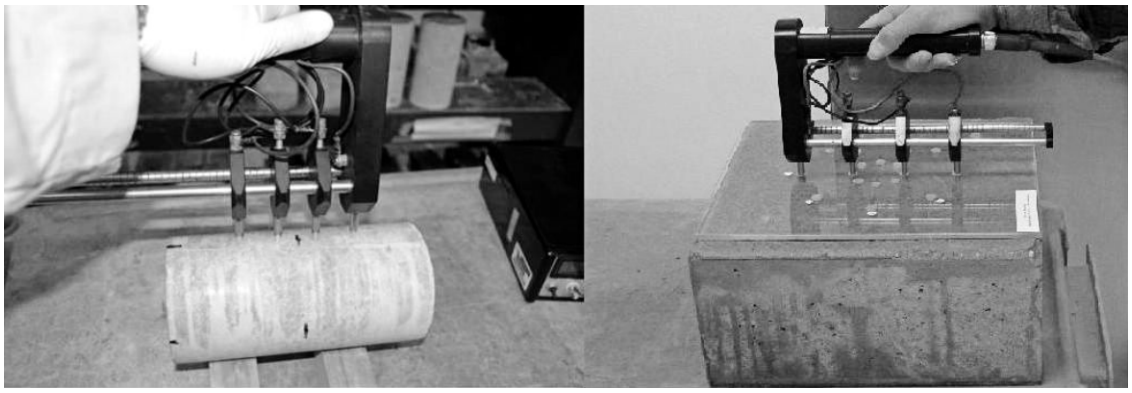

Figure E.7: Typical resistivity measurements on cylinders and RP specimens.

4.3 Exposure Environment

The initial planned exposure schedule is shown in Table E.3 for all samples; the actual schedule observed in results plots might be somewhat different. Various exposure environments were tested to examine the apparent resistivity under different environmental conditions. In some cases, modifications to the planned exposure environment were necessary. All specimens were exposed in a fog room for the first 60 days at SMO-FDOT. After this period of time selected samples remained in the fog room and continued to be monitored at SMO. All other samples were then transported to FAU-SeaTech. The majority of the samples were exposed to laboratory room temperature and humidity (About ~71 F and RH < 70%) for sixty days. After this second period of time a sub-set of samples was then exposed to cyclic ponding one week wet and one week dry; the solution used was sea water. The ponding produced large oscillations in the measured resistivity value. It was then decided to return the samples to laboratory conditions continuing the cyclic ponding, and at a later point in time the cyclic ponding was stopped. The samples were then exposed to a higher humidity (than that of the laboratory) by covering them in plastic wrap and periodically spraying water on the concrete samples (wet towels were placed on top of the samples between the plastic and the concrete).

The samples prepared with two layers (2A, 2B, 2C and 2D samples) were also exposed in the fog room for 60 days, and then were exposed to laboratory conditions. Exposure to the laboratory humidity and temperature on these double layered samples produced non-stable readings. (In particular, dry conditions were observed during the winter, and this may have contributed.) It was then decided to use a higher humidity than the laboratory humidity to achieve stable values. This was achieved by placing the samples in a mortar tub, with about five centimeters filled with water. The samples were elevated above the water line by using wood supports. The samples and part of the mortar tub were covered by a plastic wrap to maintain a higher humidity. This set up provided approximately ~80% RH. After more than 200 days in this environment, two of the tubs were inadvertently allowed to lose all the water and the resistivity increased,

this was realized after some time and the water refilled at a later date. Figures E.8, E.9, E.10 and E.11 show various exposure conditions.

Table E.3: Exposure plan for specimens tested in the experiment.

	Month													
	1	2	3	4	5	6	7	8	9	10	11	12	13	14
1A-1 1A-2	M		LR							HH-LR				
1A-3 1A-4	M		LR		CP				HH-LR					
1B1 1B2	M		LR		CP				HH-LR					
1C1 1C2	M													
1H1 1H2	M		LR		CP				HH-LR					
1cyl 1,2,3	M		LR								HH-LR			
1cyl 4,5,6	M		HH-LR											
1cyl (7 to12)	M													
1E1 1E2	M		LR											
1E3 1E4	M		LR		CP				HH-LR					
1C1 1C2	M													
1G1 1G2	M		LR		CP				HH-LR					
1H1 1H2	M		LR		CP				HH-LR					
2cyl 1,2,3	M		LR								HH-LR			
2cyl 4,5,6	M		HH-LR											
2cyl (7 to12)	M													
2A1, 2A2	M		IH-LR									HH-LR		
2B1, 2B2	M		IH-LR									HH-LR		
2C1, 2C2	M		IH-LR									Immersed		
2D1, 2D2	M		IH-LR									Immersed		
FA-TW (1 to 4)	Immersed in Tap water shortly after demolding													
FA-SS (1 to 4)	Immersed in 3.5 NaCl solution shortly after demolding													
3A (1 to 4)	M		LR											
3B1, 3B2	M													
3B3, 3B4	M		LR											
3 cyl 1,2,3	M													
3cyl 4,5,6	M		LR							HH-LR				
3 cyl 7,8,9	M		HH-LR											
3cyl 10,11,12	Immersed in Tap water shortly after demolding													
3cyl 13,14,15	Immersed in 3.5 NaCl solution shortly after demolding													

M: Fog room at SMO-FDOT
LR: Laboratory room temperature and humidity (laboratory environment)
CP Weekly Cyclic ponding with seawater
HH-LR High humidity in laboratory temperature
IH-LR Intermediate / higher humidity than laboratory humidity

Figure E.8: Samples store in the fog room at SMO-FDOT.

Figure E.9: Specimens under room temperature (68 F) and room humidity.

Figure E.10: Cylinder specimens under room temperature and high humidity environment.

Figure E.11: Specimens exposed outdoors with cyclic ponding.

4.4 Results

All values shown in this section have been normalized (Morris, Moreno and Sagüés 1996), i.e., corrected using the K values computed for a=3 cm and a=5 cm. The K values for the different geometries and locations are included in the modeling section.

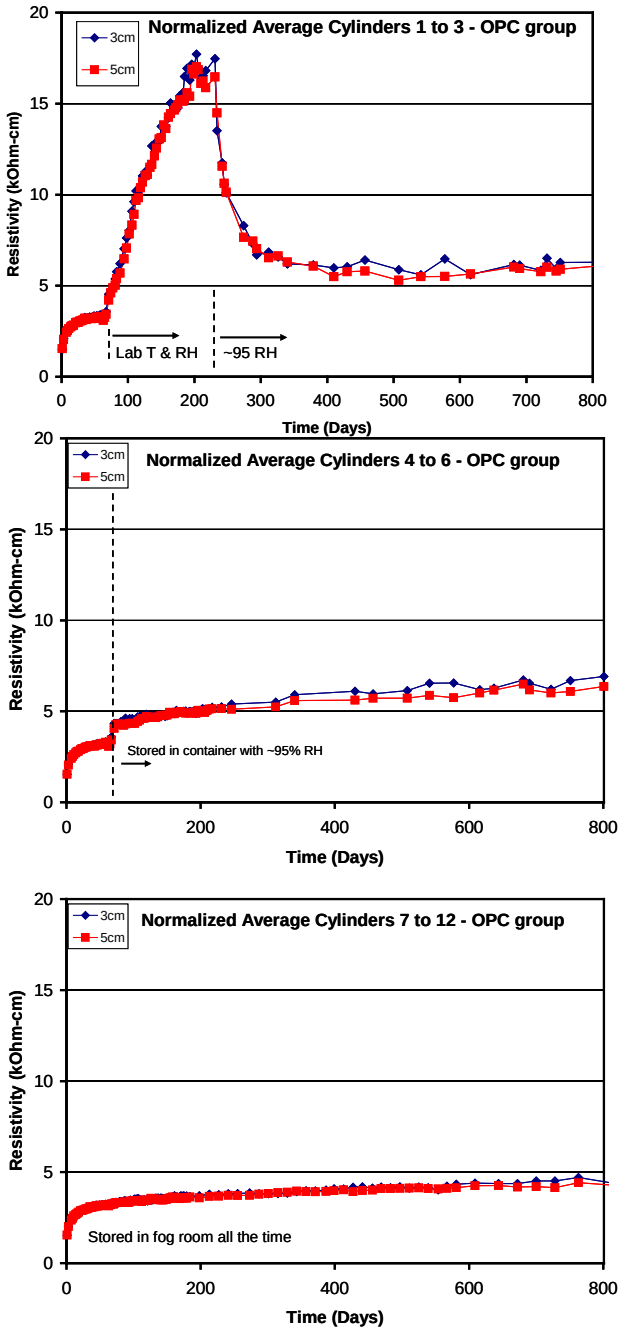

Figure E.12: Normalized SR vs. time on concrete specimens made of OPC subject to three exposure schedules

4.4.1 Resistivity on Cylindrical Samples

4.4.1.1 Environmental Exposure

Figure E.12 shows the normalized average SR values vs. time for OPC concrete cylinders. The top and middle plots correspond to an average of 3 samples each, and the bottom plot shows the average of six samples. All three plots show very similar trends for the first 60 days as all of them were exposed in the fog room. The plot on the top corresponds to resistivity values for samples exposed to laboratory temperature and RH after day 60, and it is identified by a linear increase in resistivity values with time. Upon the start of a third exposure in an environment close to 95% RH, the plot shows an exponential decay in resistivity value; the final SR is close to 6 kΩ-cm. The plot in the middle corresponds to samples exposed to ~90-95% RH after day 60. In this case, the final SR is close to 6.5 kΩ-cm, whereas the bottom plot corresponds to samples that remained all the time in the fog room and which, at the end of the test, reached a SR value of ~4.7 kΩ-cm. No significant difference was observed between measurements performed with a=3 cm and a=5 cm for this geometry. The lower final SR values for the cylinders exposed to laboratory RH for some time (top plot) is explained by the fact that these samples were subjected to full immersion on day 600. The difference in resistivity between samples exposed in high humidity (HH-LR 6.5 kΩ-cm) vs. those in the fog room (close to saturation 4. 7 kΩ-cm) is about 37%. The maximum value observed during laboratory exposure was ~17.5 kΩ-cm, almost four times the terminal value observed in the fog room.

Figure E.13 shows the normalized average SR values vs. time for concrete cylinders from group 2 (samples with FA) exposed to three different exposure schedules. All three plots show very similar resistivity trends and values for the first 60 days, as all of them were exposed in the fog room. The normalized resistivity values measured at day 60 is ~5 kΩ-cm, just slightly larger than the values measured at day 60 on samples of group 1 with only OPC. At day 60, the pozzolanic reaction continues, as suggested by the slope

describing the resistivity rate increase. All plots have 30 kΩ-cm as the maximum in the y-axis.

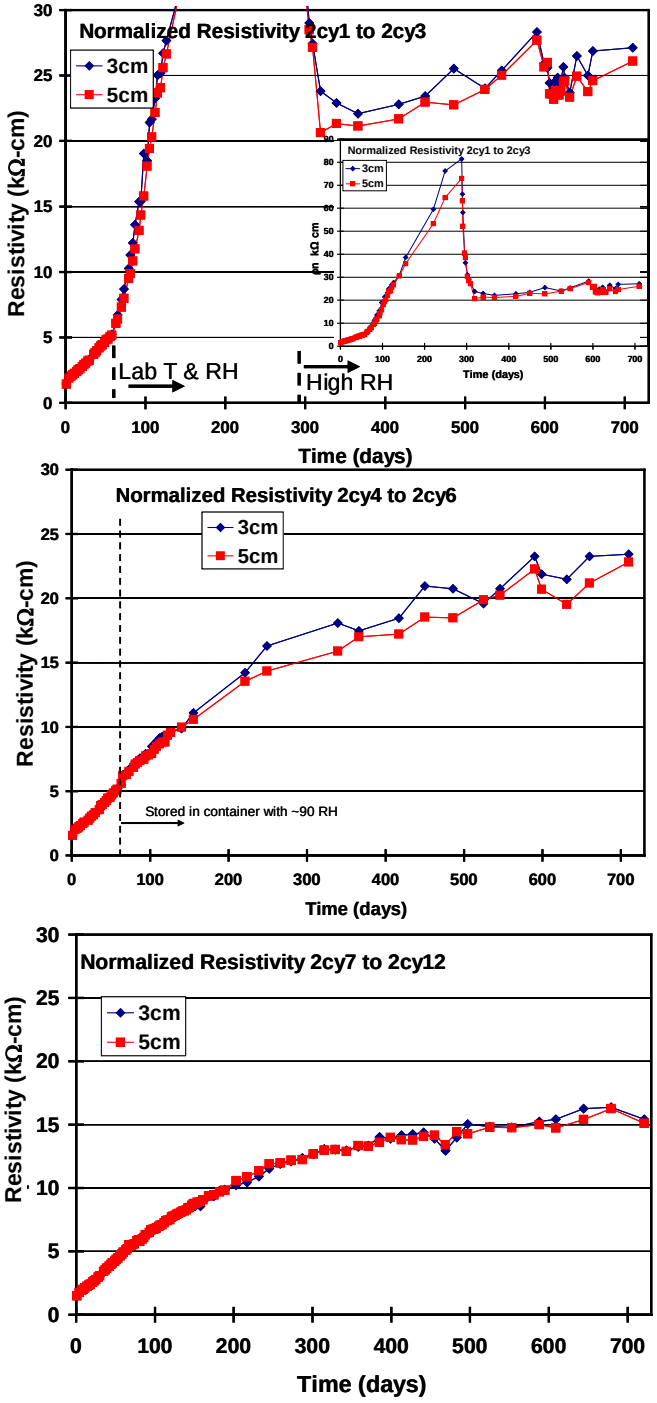

Figure E.13: Normalized SR vs. time on concrete specimens made of FA subject to three exposure schedules

The top plot corresponds to SR measured values on the cylinders that were exposed for ~200 days to laboratory temperature and RH, and later to a high humidity environment. For the top plot there is an inset plot that shows that the resistivity reached a maximum of 80 kΩ-cm (3 cm spacing) and 70 kΩ-cm (5 cm spacing) before changing to high humidity exposure. At day 700, the resistivity has reduced to ~27 kΩ-cm; the resistivity value is slightly higher when measured with 3 cm spacing. The second row shows a plot for resistivity vs. time, for cylinders where the second exposure was a high humidity ~90-95 RH, which is lower than the fog room (~100 RH). The trend of the resistivity values shows a continuous increase from the start, with a slightly different slope upon changing the humidity exposure condition. This trend was expected as the pozzolanic reaction for concrete with FA proceeds for an extended period of time, and appears to plateau around day 500, at day 700 the resistivity measured was about ~23 kΩ-cm. On these samples the resistivity measured using 3 cm spacing is slightly larger than when using 5 cm spacing. The third row shows results for specimens that remained in the high moisture environment throughout the duration of the test. On these samples the resistivity increased in a monotonic manner and the same slope for about 300 days. After that, the resistivity rate continues to increase but at a significantly slower rate. The maximum resistivity observed at day 700 was 15 kΩ-cm, and for this exposure condition, the same value was observed with both used spacings. The concrete in the fog room can be considered fully saturated, hence, the 15 kΩ-cm value reflects group 2 resistivity after 2 years. A 5% to 10% reduction in the RH allows the resistivity to increase to 23 kΩ-cm.

Figure E.14 shows the normalized average SR values vs. time for measurements on cylinders from group 4 (samples with FA+SF) exposed to three exposure schedules. Similar to what was indicated in E.12 and E.13, all samples in group 4 were exposed initially in the fog room. For this group, all samples remained in the fog room up until day 90. By day 60, the resistivity measured was ~15 kΩ-cm or three times that observed on samples of group 2; by day 90, the resistivity value measured reached ~28 kΩ-cm. The plot in the top row shows resistivity values after two additional exposure conditions; after ~60 days at laboratory temperature and humidity, the samples reached

a resistivity of 80 kΩ-cm (3 cm spacing) and 62 kΩ-cm (5 cm spacing), but the surface resistance (contact resistance) started to reach very high values and the measurements became somewhat erratic. It was then decided to transfer the cylinders to a slightly higher humidity.

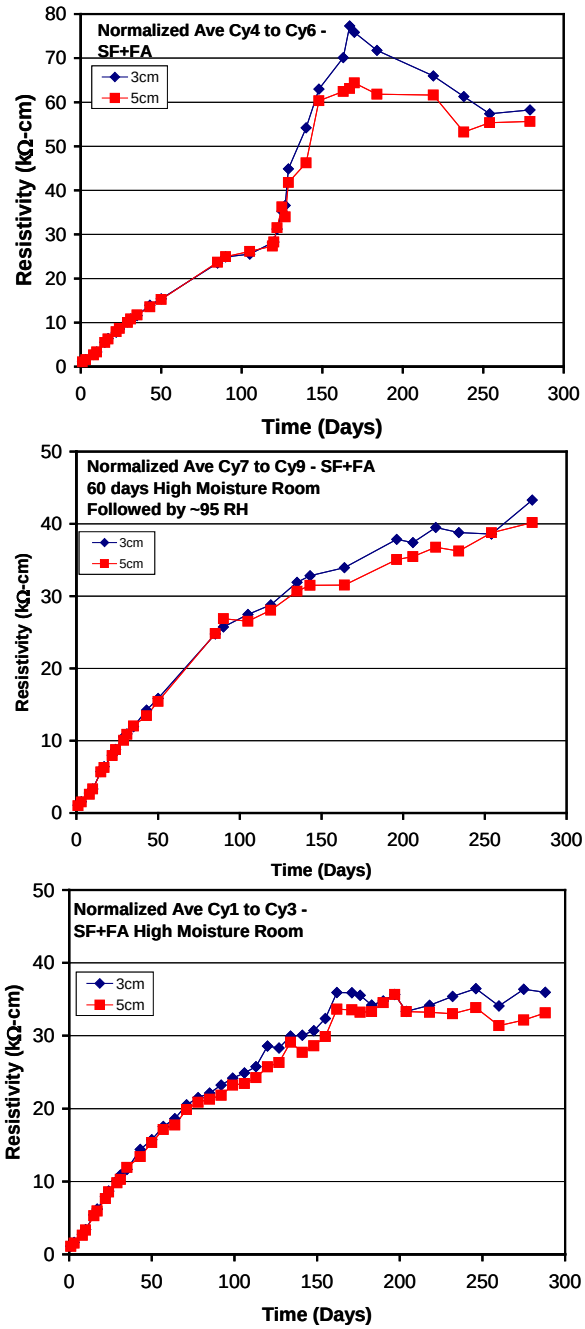

Figure E.14: Normalized SR vs. time on concrete specimens made of FA+SF subject to three exposure schedules

After 100 days in this environment, a resistivity value of ~ 55 kΩ-cm was measured, with both 3 cm and 5 cm spacing. The plot in the middle shows the resistivity values measured on samples that were transferred to ~90% RH; these samples reached an average resistivity of ~40 kΩ-cm at day 260. Finally, the plot in the last row which was exposed in the fog room all the time reached a resistivity of ~ 34 kΩ-cm at day 250. From the bottom two plots it can be observed that, at later times, the measurements made with 3 cm spacing were slightly larger than those measured with 5 cm spacing. This group was casted last, and not enough time has passed as to say what the final resistivity would be. However, the 34 kΩ-cm value at 250 days is more than twice the 15 kΩ-cm observed on samples of group 2 at day 700.

4.4.1.2 Chloride contribution

Figure E.15 shows the normalized average SR values vs. time for cylinder samples of group 2 and group 4 that were immersed in either tap water or 3.5 NaCl solutions. The resistivity values obtained in these exposures were compared to values obtained from samples stored in the fog room. The top row shows values for samples with FA. It is important to mention that these samples correspond to a different casting with very similar concrete mix, but with larger maximum aggregate size. Hence, the somewhat larger resistivity value observed at day 700 in the fog room was ~ 22 kΩ-cm (Figure E.15) vs. ~15 kΩ-cm (bottom plot Figure E.13).

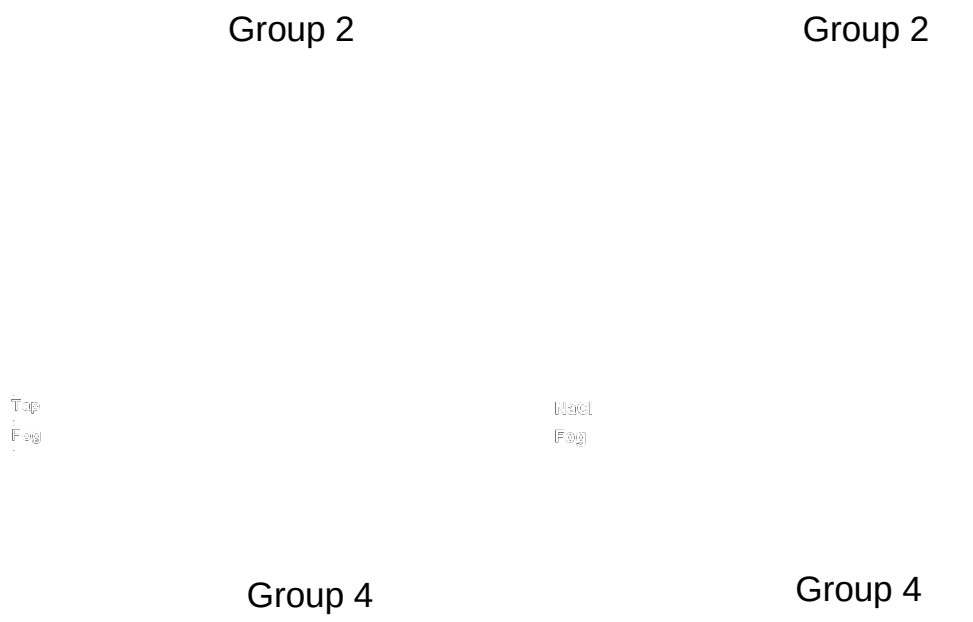

Figure E.15: Normalized SR vs. time on concrete specimens immersed in solution or exposed in the fog room

Note the different time scale for top row plots and bottom row plots. The average resistivity values measured on samples exposed to tap water were almost identical to those measured on samples exposed in the fog room for both systems (plots on the left column). Slightly larger values were measured when using 3 cm spacing on group 4 samples. Samples of group 2 exposed to 3.5 NaCl started to show lower resistivity after about 100 days; at day 700 the resistivity value measured is about 20% lower than those measured on samples exposed in the fog room. For samples of group 4 immersed in 3.% NaCl, there is hardly a reduction in resistivity. This could be explained in part because of a denser concrete and also because of the shorter exposure time. A longer exposure time will allow us to quantify what the effect is in the measured resistivity of exposing samples of group 4 in 3.5% NaCl solution.

4.4.2 Resistivity on Rectangular Prism Samples with no Rebars

4.4.2.1 Environmental Exposure

Figures E.16, E.17 and E.18 show normalized resistivity values for measurements on samples of group 1, group 2, and group 4, respectively. Each figure describes the resistivity evolution with time for two samples. The two plots in the top row correspond to resistivity values obtained using a=3 cm and the two in the second row to those obtained using a=5 cm. Similar to what is observed for the cylinders, the four plots in each figure show very similar trends for the first 60 days, as all of them were exposed in the fog room. Appendix 1 includes the plots for the resistivity evolution corresponding to the other two samples per mix prepared with no rebar.

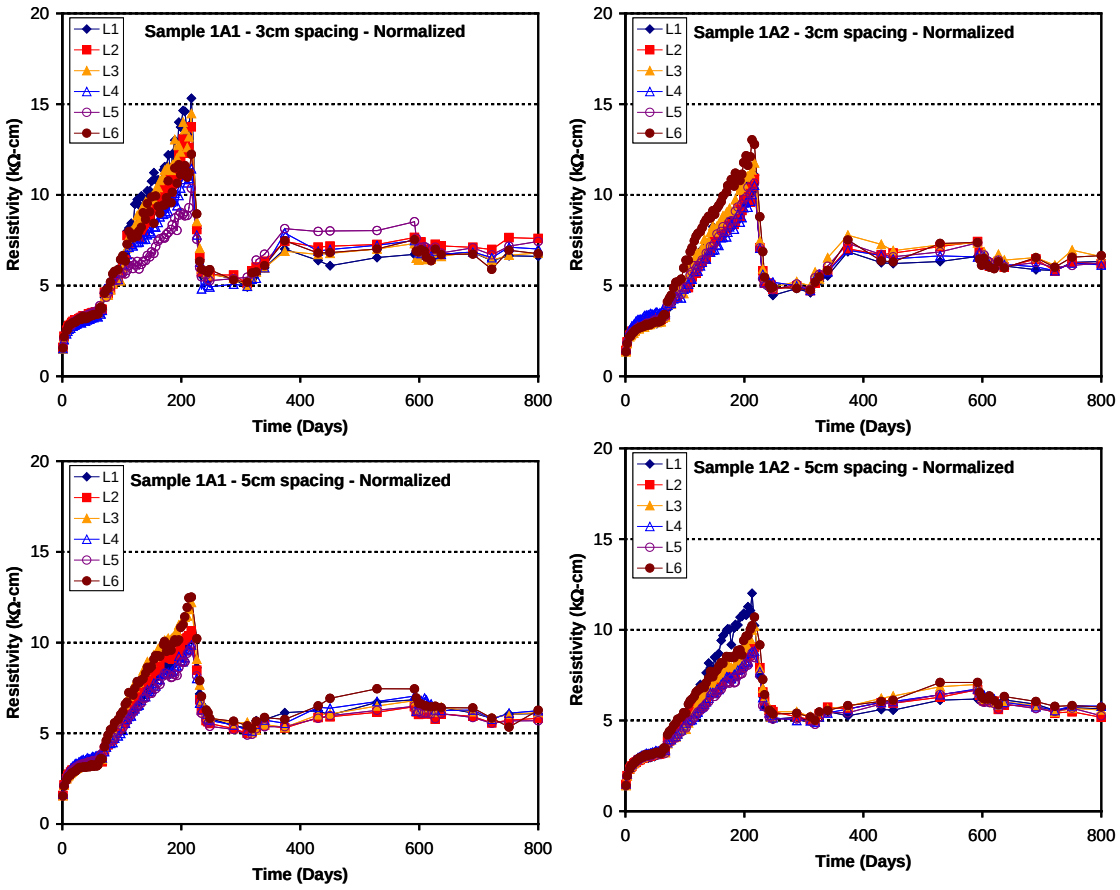

Figure E.16: Normalized SR vs. time on RP concrete specimens with no rebars made of OPC subject to three exposure schedules.

The environmental schedule after the first 60 days was somewhat different for each concrete group. Group 1 samples (Figure E.16) were exposed to laboratory temperature and RH for 150 days. Upon placing them in the laboratory environment, the spread between the normalized resistivity values measured on a given day increased as time passes. Figure E.16 shows that the largest resistivity value measured at day 210 was ~15 kΩ-cm on sample 1A1 with a=3 cm. This is due to the concrete closer to the surface drying with time and reaching deeper into the concrete creating a transient resistivity layer. Concrete heterogeneity is evident even when measurements have been normalized for geometry. Larger resistivity values were measured with a=3 cm spacing. The samples were then exposed to a higher humidity (constant spray initially could have brought the humidity close to 95% RH). This is identified in the plot by an exponential decay in resistivity values reaching a value of 5 kΩ-cm in all four plots at day 250. The relative humidity was somewhat reduced and the resistivity increased to resistivity values between 5.5 and 7 kΩ-cm with a larger separation in normalized resistivity values for the corresponding location when using 3 cm spacing (moisture of concrete close to surface decreases). Finally, when the samples were fully immersed around day 600, the resistivity decayed again to a value close to 6 kΩ-cm, which was very similar to that obtained on the cylinders.

Figure E.17 shows the resistivity evolution with time for specimens of group 2 that contain 20% Fly Ash. The second exposure was at laboratory temperature and humidity and lasted for 65 days. The rate in which the resistivity increased is faster (with a steeper slope) than during exposure in the fog room. A similar trend was observed for the cylinders of this group. The maximum normalized resistivity was 28 kΩ-cm on sample 1E1 and 3 cm spacing. For group 2, the resistivity increase during this period is probably due to continued curing of the inner concrete and drying of the concrete closer to the surface.

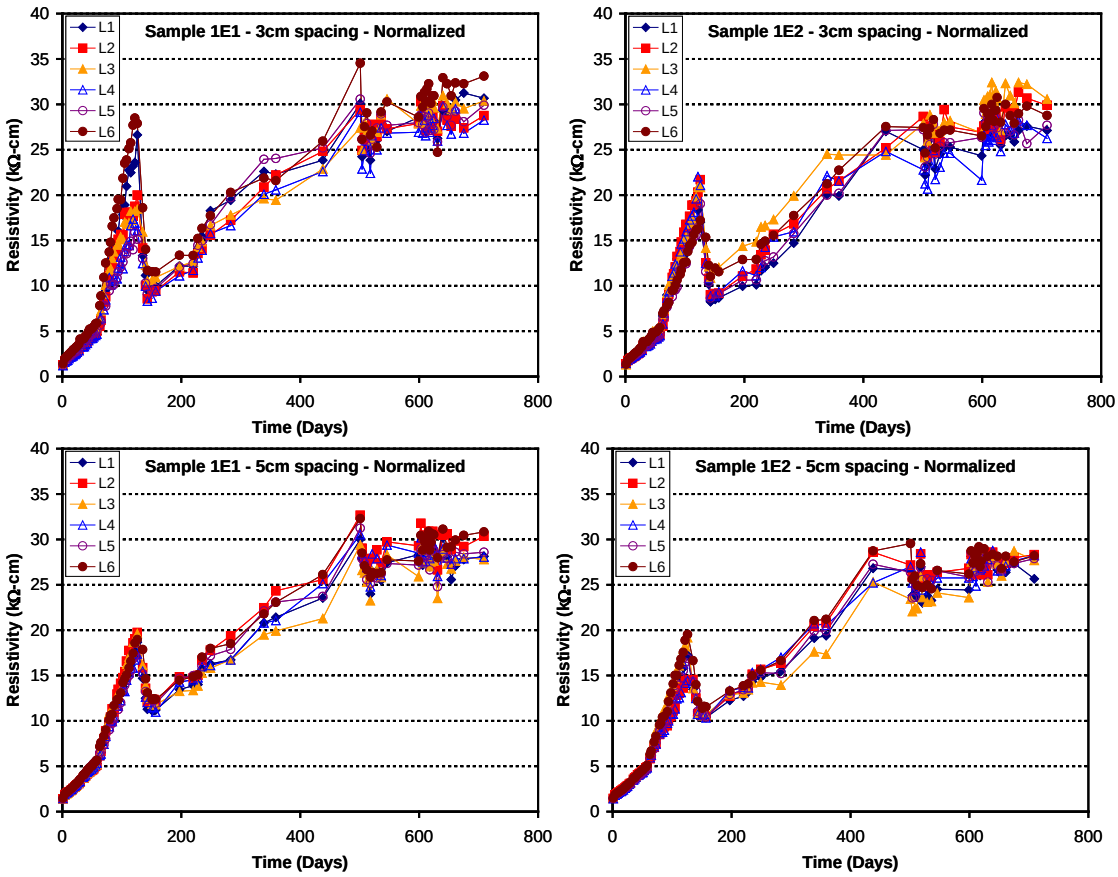

Figure E.17: Normalized SR vs. time on RP concrete specimens from group 2 with no rebars subject to three exposure schedules.

The samples were later exposed in a high humidity environment with the resistivity momentarily dropping to 10 kΩ-cm; the resistivity continued to increase as the pozzolanic reaction continued while in this environment. The resistivity values started to plateau after day 500. Resistivity values measured with a=3 cm spacing have a net range close to 5-6 kΩ-cm, whereas resistivity values measured with a=5 cm have a net range of about 3 kΩ-cm. The average resistivity at 700 days was 30 kΩ-cm, and 28 kΩ-cm for a=3 cm and a=5 cm, respectively.

Samples from group 4 shown in Figure E.18 have two distinctive resistivity increase rates as observed by the slopes during the first 150 days. The initial slope is the one developed during the exposure in the fog room.

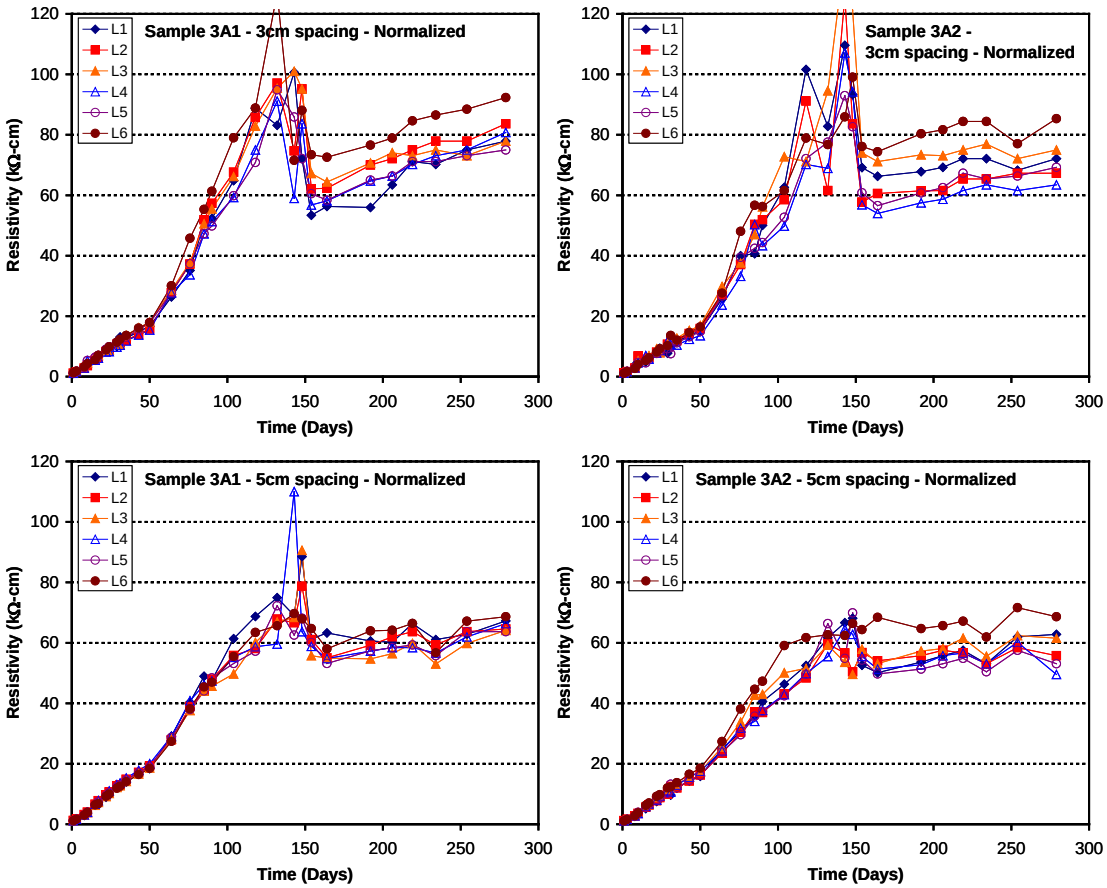

Figure E.18: Normalized SR vs. time on RP concrete specimens from group 4 with no rebars subject to three exposure schedules

The slope of the resistivity rate increase became steeper upon exposure to laboratory temperature and humidity. After day 120, the surface resistance between meter contact and the concrete surface reached such a high value that SR readings stopped being reproducible and reliable. Particularly for measurements performed with a=3 cm spacing and it is observed in the top row plots of Figure E.18 by sudden peaks and oscillation on the measured resistivity. It was decided to increase the humidity to augment the moisture content of the layer close to the surface. This was achieved similar to what has been described before, by placing two samples in a mortar tub with water at the bottom, the samples raised using 4”x4” wood pieces, and the entire set-up was then covered with a plastic wrap. As can be observed in Figure E.18, there is a temporary oscillation in the measured resistivity due to the high contact resistance. Upon increasing the humidity, the measurements were stable again. Recall that all

shown values are after normalization for geometry. It is evident that at early times the resistivity values collapse to the same value shown during the early stages of the lab exposure. The separation in the measured resistivity values is evident first with the 3 cm spacing from about day 65, and then appears also for measurements with 5 cm spacing from about day 90. After ~210 days, the resistivity values measured with 5 cm plateau to 50-55 kΩ-cm for 3A1 and 3A2, whereas the plateau for 3A3 and 3A4 (see Appendix 1) is between 60 and 70 kΩ-cm.

4.4.2.2 Two layer – OPC top, FA Bottom, No Rebar

Figure E.19 shows resistivity values as a function of time for samples with a top layer of OPC concrete and bottom layer made of concrete with FA. The low resistivity of the OPC layer acts as if chlorides have penetrated or a higher moisture is present close to the outer surface. The samples were subjected to an environmental schedule similar to those described in the previous section, except that the duration of the exposure to laboratory humidity and temperature was only 30 days and was not measured as frequently during this period of time. The samples were then exposed to a higher humidity environment of ~80% RH as described in the experimental detail. The RH was not controlled adequately from day 320 to 520. Because of this, the plateau observed on Figure E.17 is not seen at day 510. The moisture was increased again, and after a short time, the resistivity values reached a plateau. Figure E.19 has two plots for a=3 cm on the left. On the right, the plots were obtained with a=5 cm. Measurements made after day 600 with a=3 cm resulted in a lower normalized resistivity (average ~18 kΩ-cm); the value is almost 25 percent larger when measured with a=5 cm (average ~22 kΩ-cm). The 1 cm OPC concrete layer is responsible for this resistivity reduction. Although the top OPC layer was not poured until the bottom layer was almost set, a small fraction of the OPC might have moved within the top portion of the OPC+FA layer. These average values are smaller than those observed in Figure E.17, in which the final average resistivity value was 28-30 kΩ-cm. An interesting observation is that normalization works better on sample 2A2 which might indicate a more homogeneous specimen.

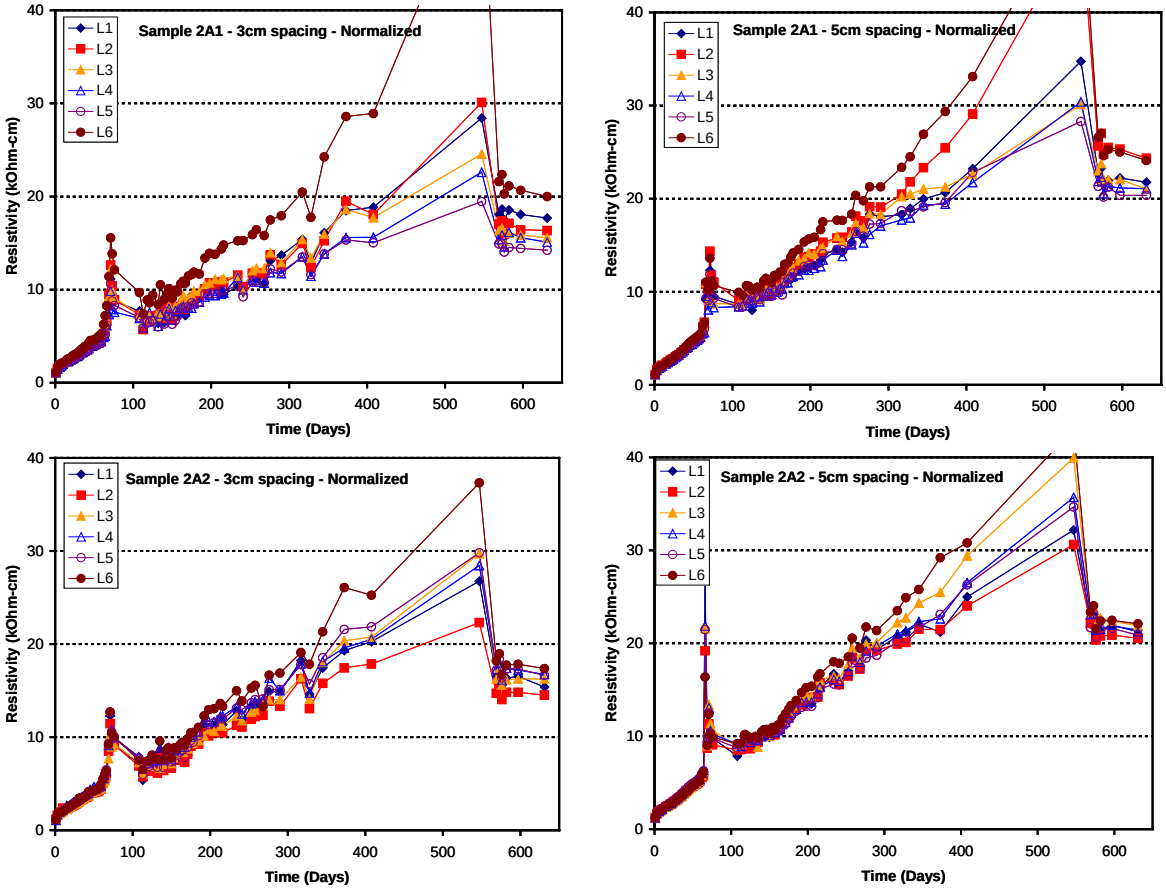

Figure E.19: Normalized SR vs. time on RP concrete specimens from group 3 with no rebars and two layers, with top layer being OPC subject to three exposure schedules.

4.4.2.3 Two layer – FA top, OPC Bottom, No Rebar

Figure E.20 shows that the top OPC+FA layer act as if concrete had carbonated or if the top layer had a lower moisture content. Measurements with a=3 cm resulted in a higher resistivity values; the value is close to 40 percent larger when measured with a=5 cm. This is more evident on the measurements performed at later times (>530 days). Measurements with a=5 cm allowed us to observe that the bottom layer is OPC. The water that helped keep the humidity high at the bottom of the tray was not lost as fast for samples 2C1 and 2C2 because when OPC is at the bottom layer, the resistivity values were not as affected. Still, an increase in resistivity was observed between days 400 and 520.

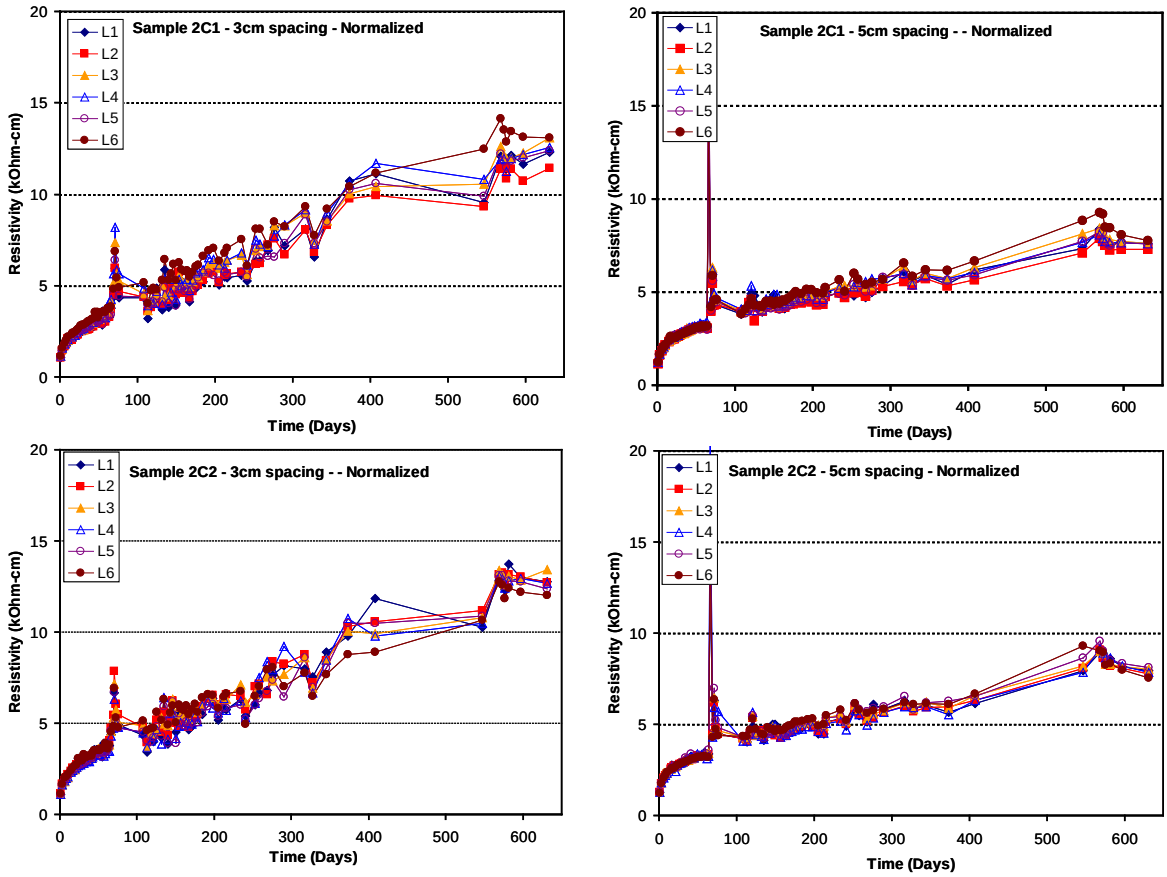

Figure E. 20: Normalized SR vs. time on RP concrete specimens from group 3 with no rebars and two layers, with top layer being OPC+FA subject to three exposure schedules

Upon increasing the moisture level the resistivity value stopped increasing. The two plots on the left correspond to measurements performed using a=3 cm; after day 120, a monotic increase is observed but it is a depressed slope when compared to the values shown in Figures E.17 and E.19. If you will recall in that case, the FA+OPC layer is only one cm thick and measurements made after day 620 with a=3 cm resulted in a normalized resistivity (average) ~12.5 kΩ-cm. This value is about 40 percent larger than the value measured with a=5 cm (average ~7.5 kΩ-cm). The 1 cm OPC+FA concrete layer is responsible for the larger resistivity measured when using a=3 cm.

4.4.3 Resistivity on Rectangular Prisms Samples with One Rebar

4.4.3.1 Environmental Exposure

Figure E.21 shows normalized resistivity values vs. time on samples 1C1 and 1C2 (RP OPC samples with one rebar kept in the moisture room all the time) at the six different locations and separated per spacing used. For these OPC samples the resistivity after normalization is very similar in all four cases. After an initial relatively fast rate of increase in resistivity during the first 50 days, the resistivity increase rate slows significantly. The additional curing provided by the longer exposure time in the fog room only provided a modest increase in resistivity. A value of ~5 kΩ-cm measured on these samples is typical of saturated OPC concrete, and is comparable to the values observed on the cylinder samples exposed under the same conditions. This is an indirect verification of the geometric cell constant applied.

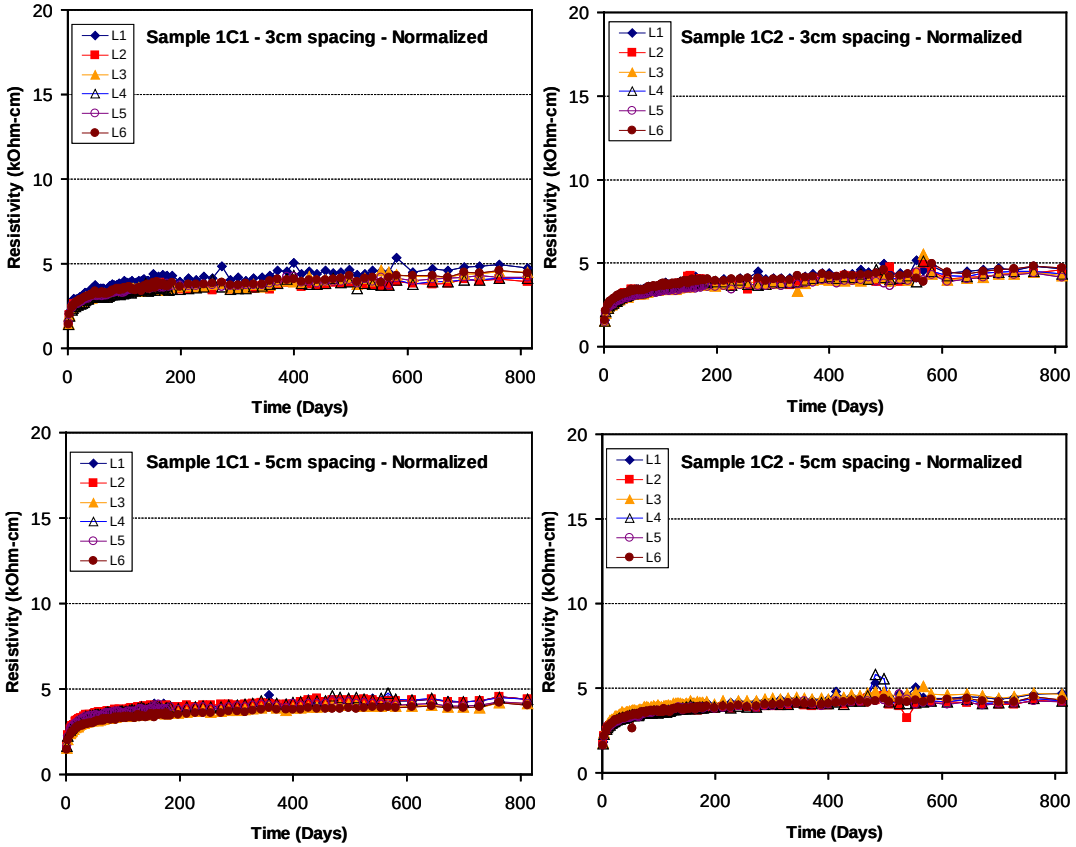

Figure E.21: Normalized SR vs. time on OPC RP concrete specimens with one rebar (1C1 and 1C2) exposed in the fog room all the time. Figures on the top and bottom rows correspond to readings performed using 3 cm and 5 cm spacing, respectively.

Figure E.22 shows normalized resistivity values vs. time on samples 1F1 and 1F2 (RP OPC+FA samples with one rebar kept in the moisture room all the time) at the six different locations. The resistivity trends obtained with a=3 cm spacing suggest that the measured resistivity plateaus after 400 days at an average resistivity value of 17.5 kΩ-cm for 1F1. The plateau is also observed when using a=5 cm but not until day 500, when the average resistivity value is ~18 kΩ-cm, but with a smaller spread between the values from the different locations is observed.

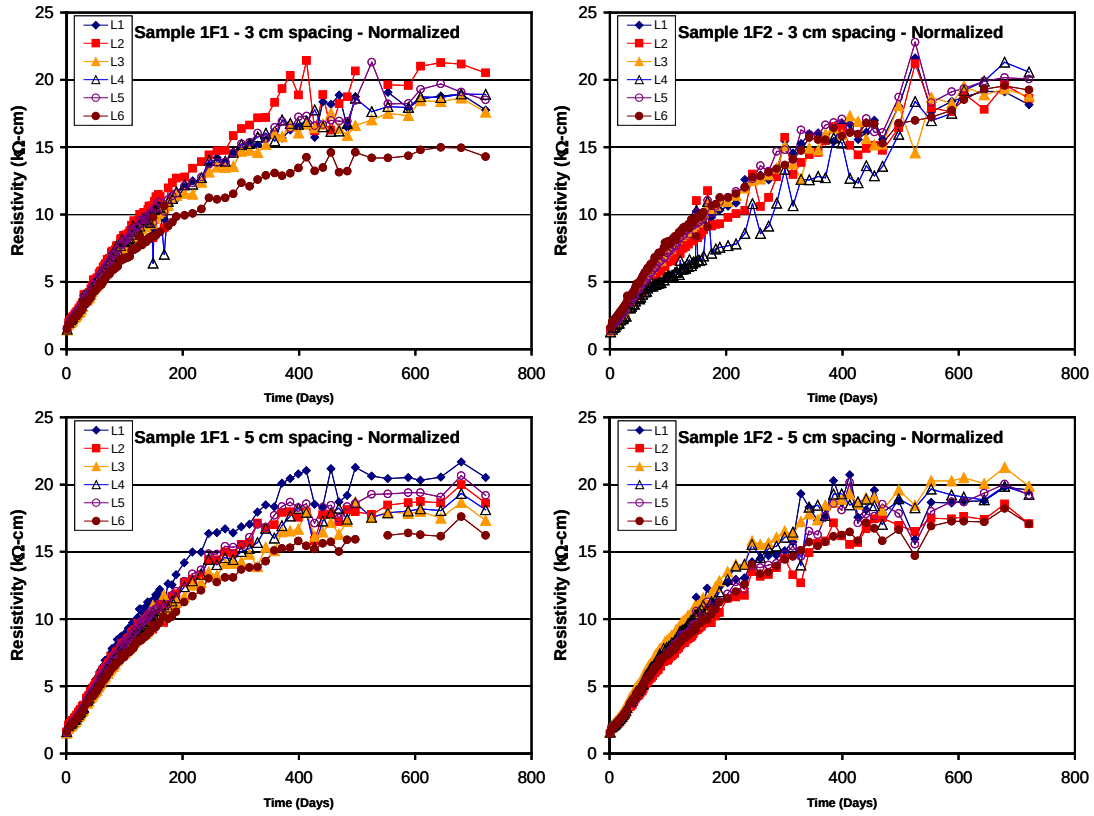

Figure E.22: Normalized SR vs. time on OPC+FA RP concrete specimens with one rebar (1F1 and 1F2) exposed in the fog room all the time. Figures on the top and bottom rows correspond to readings performed using 3 cm and 5 cm spacing, respectively.

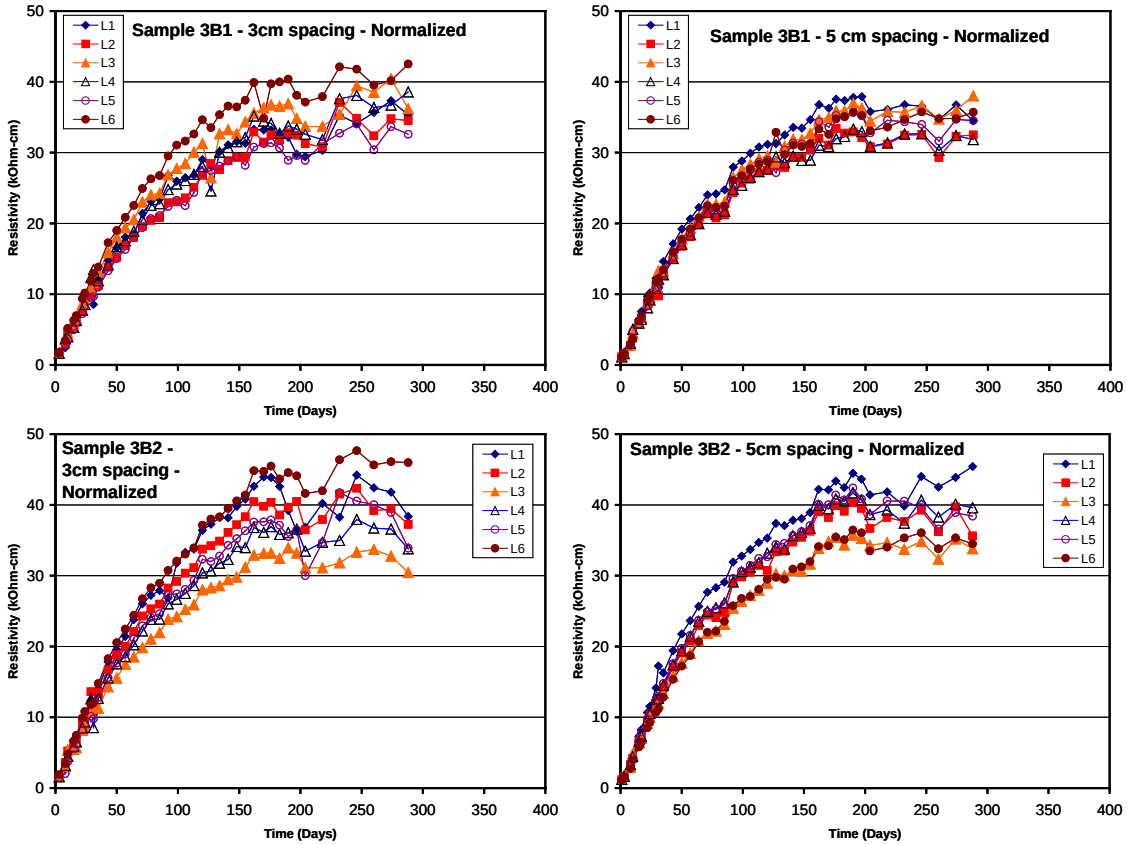

Figure E.23: Normalized SR vs. time on OPC+FA+SF RP concrete specimens with one rebar (3B1 and 3BF2) exposed in the fog room all the time. Figures on the top and bottom rows correspond to readings performed using 3 cm and 5 cm spacing, respectively.

Figure E.23 shows normalized resistivity values vs. time on samples 3B1 and 3B2 (RP OPC+FA+SF samples with one rebar kept in the moisture room all the time) at the six different locations. The spread between the maximum and the minimum resistivity values measured is larger for cases measured with 3 cm spacing. This would suggest that as concrete cures, the concrete closer to the surface develops a different resistivity than the inner concrete and cannot be corrected by the assumption of it being the same resistivity throughout all the sample. It also could mean that concrete heterogeneity is magnified in this type of concrete.

As time passed, the gap between the minimum and maximum increased and reached a somewhat stable difference by day 150. Sample 3B1 seemed to be slightly more homogeneous and also had lower resistivity. However, both samples have a

normalized SR larger than 30 kΩ-cm by day 150. Additionally, the values measured with 3 cm spacing are slightly larger than those obtained with a=5 cm spacing. These values are comparable to those obtained on the cylinders kept in the fog room.

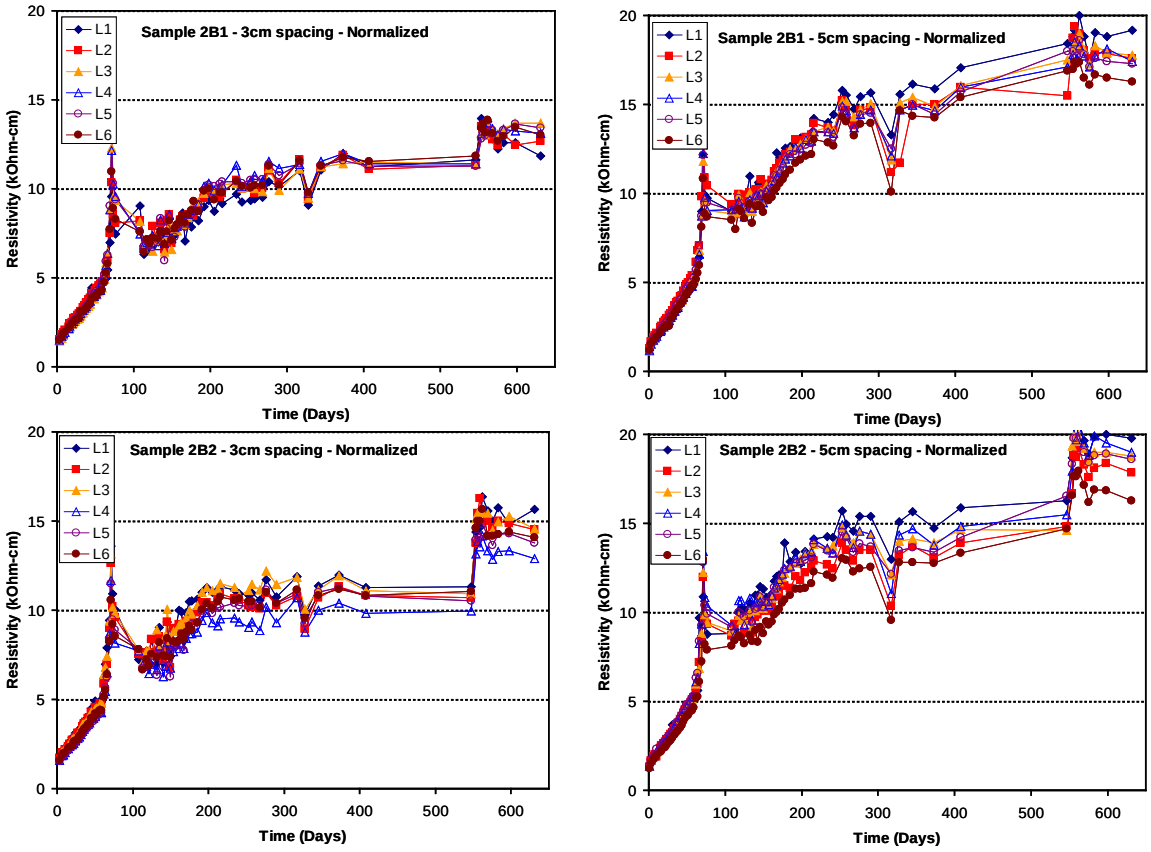

Figure E.24: Normalized SR vs. time on RP concrete specimens from group 3 with one rebar and two layers, with the top layer being OPC subject to three exposure schedules

4.4.3.2 Two layer – OPC top, FA Bottom, 1 Rebar

Figure E.24 shows the normalized resistivity values measured on two layer samples with one rebar that have OPC concrete as the top layer. The results shown here can be compared to those shown in E.19 for the companion samples with no rebars. The usual linear resistivity increase was observed for measurements performed during the time in the fog room. Upon exposure to ~80% RH, the resistivity rate increase was observed again, although with a milder slope, and a plateau was observed around 200 days (~12 kΩ-cm) on resistivity values measured with a=3 cm spacing, and at around 300 days for

a=5 cm spacing with an average resistivity value of 15 kΩ-cm. On day 520, the two samples were fully immersed, and larger resistivity values were then observed for both spacings. The average value measured using a=3 cm increased to ~14-15 kΩ-cm and the resistivity value measured with a=5 cm increased to a value of ~17.5 kΩ-cm. These are lower values than the final values observed on samples 2A1 and 2A2 (18 kΩ-cm with a=3 cm and 22 kΩ-cm with a=5 cm). These results confirm that higher moisture content was achieved on samples 2B1 and 2B2. During the intermediate exposure, the lower resistivity of the OPC layer dominates the apparent resistivity measured; however, note that the concrete is not fully saturated and might somewhat limit the amount of current reaching deeper into the concrete. The observed increase in resistivity upon immersion could be explained by current that reached deeper, which measured a larger volume of the bottom OPC+FA layer.

4.4.3.3 Two layer – OPC+FA top, OPC Bottom, 1 Rebar

Figure E.25 shows the normalized resistivity values measured on two layer samples with one rebar that have OPC+FA concrete as the top layer. The results shown here can be compared to those shown in E.20 for the companion samples with no rebars. The usual OPC resistivity increase was observed for measurements performed during the time in the fog room (see figures E.12 and E.16). Upon exposure to ~80% RH environment, a resistivity rate increase is observed again on measurements with a=3 cm. The slope is steeper than for OPC concrete, and is likely due to the fact that the concrete close to the surface was not being fully saturated and because of the composition of the top layer. By day 400, the average resistivity value is ~ 9 kΩ-cm. Measurements performed with a=5 cm during this exposure period did not show a significant resistivity increase; the average value by day 400 is about 5.5 kΩ-cm. On day 520, the two samples were fully immersed, and lower resistivity values were then observed for resistivity values obtained with a=3 cm, whereas those with a=5 cm spacing remained almost the same. The average value measured using a=3 cm on day 600 was about 7.5 kΩ-cm, and the resistivity value measured with a=5 cm was 5 kΩ-cm. These are lower values than the final values observed on samples 2C1 and 2C2 (12.5 kΩ-cm with a=3 cm and 7.5 kΩ-cm with a=5 cm). These results confirm that a

higher moisture content was achieved on samples 2D1 and 2D2. During the intermediate exposure, the top OPC+FA layer acts as if a drier concrete is present close to the surface; moreover, note that the concrete is not fully saturated and might somewhat limit the amount of current reaching deeper into the concrete. This is particularly easier to observe with a=3 cm. The observed reduction in resistivity upon immersion could be explained by a higher degree of moisture which allows to reach farther, measuring a larger volume of the bottom OPC layer.

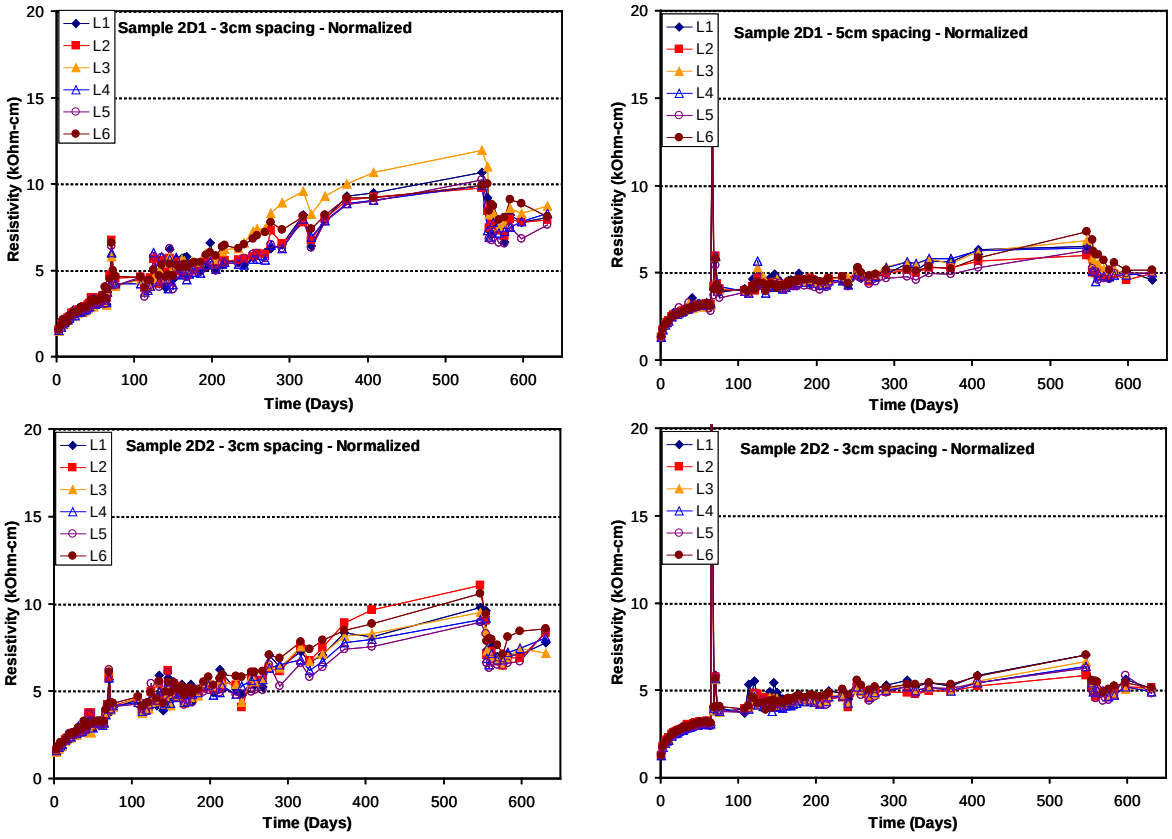

Figure E.25: Normalized SR vs. time on RP concrete specimens from group 3 with one rebar and two layers, with top layer being OPC+FA subject to three exposure schedules

NOTE: Plots for the other samples not described in this chapter can be found in Appendices 1, 2, and 3.

5. FIELD VISITS

5.1 Introduction

Several bridges along the west and east coasts of Florida were identified for field visits and evaluation based upon age and environment. Each field trip consisted of visiting two to five bridges, and one or two components partially immersed per bridge were selected for testing (footer, cylindrical column or square pile). During preliminary (initial) field evaluations, it was determined that a conditioning procedure was needed to increase the degree of saturation of the concrete close to the surface. Surface resistivity profiles were measured on at least three consecutive days: weather permitting, initial values, after ~24 hrs, and after ~48 hrs. The 24- and 48-hr measurements followed the conditioning set-up described below. Two other types of measurements were performed before obtaining the first surface resistivity profile: identification of the location of the rebar (reinforcing) mat and an estimate of the concrete moisture for the concrete closest to the surface. A magnetic wave rebar locator was used to identify the rebar mat and to estimate the concrete cover depth in most cases. The rebar mat outline was marked at the concrete surface. The locations that were selected as centers for the SR measurements were also marked. A commercial concrete moisture meter was used to record the apparent moisture content of the outermost 1.25 - 1.9 cm concrete layer before conducting each set of SR measurements. The moisture meter readings range from 20 (highly wet concrete) to 0 (dry concrete). The moisture measurements were made at the locations where SR measurements were to be made. In general, as the elevation from the marine growth increased, the obtained moisture value usually decreased during the first set of readings, and upon installing the conditioning set-up, the moisture level usually increased during the second- and third-day readings. SR measurements were made using a commercially-available Wenner probe with adjustable electrode spacing, identified here as a concrete resistivity meter. The spacing between electrode probes used corresponded to spacing a=3 cm and a=5 cm.

5.1.1 Water (Conditioning) Method

The designed conditioning method is based upon forcing water absorption onto the drier areas of the concrete. An edge-grip rubber seal was placed around the top of a 6-liter plastic container of 38.1 cm x 25.4 cm (15in x 10in) dimensions. A ~2.5 cm (1 in) diameter hole was drilled on the side that would be facing up. The containers were secured to the pile/column through two or three adjustable ratcheting tie downs with a wood piece milled to accommodate the back of the plastic container. This uniformly distributed the force applied. Once the container was in place, it was then filled with tap water and sealed with a cork rubber or tape to minimize losses of water due to evaporation. After approximately one day with the set-up in place, the SR measurements were performed. The SR measurements were done after removing the container and then using a towel to remove any excess water from the concrete surface. If an additional set of measurements was to be conducted the following day, the set-up was put back in place and the container refilled. This conditioning method has been used on more than 60 bridges.

In cases when the perimeter of the substructure was longer than the tie-downs (for example, some cast-in-place footers), a different approach was used to secure the container. Four holes were drilled per container to set 2 in x ½ in diameter stainless steel anchors. Two holes were drilled on both sides of the area where the container was to be placed, with a separation of at least 34 inches. Once the anchors were set up, galvanized screws with washers were placed, and tie downs winched to them. After the last set of SR measurements, the container and screws were removed, and a commercial polymeric cement mix was used to cover the anchors. This same polymeric cement mix was used to fill holes made from two-inch coring samples.

Figure F.1 shows a conditioning set-up used to increase the concrete moisture content. Figure F.1 shows a picture of the edge-grip rubber seal plastic container at the top row left column. Figure F.1 top row middle picture shows the container set-up full of water; the other four pictures in Figure F.1 show set-ups in place with tie downs around a pile, and with tie downs/ anchoring, respectively.

Figure F.1: Water saturation container set-up

5.1.2 Drilled Cores for D_{Cl} and Wet Resistivity

Once the surface resistivity measurements were performed two to four concrete cores were drilled on selected structures. The cores were obtained in the vicinity to the area where the SR measurements were performed. In some instances, a different face of the pile was cored due to easier access or a neighbor component. A nominal 5 cm (2 in) core bit was used that resulted in concrete cores ~4.5 cm in diameter. Approximately 315 cores have been obtained from ~80 different pile structures during 13 field trips including bridges in and close to: Apalachicola, Panama City, Daytona, Stewart Martin, Anna Marie Island, Tampa, Saint Petersburg, Florida Keys, Fort Lauderdale, Saint Augustine and Jacksonville.

The cores were usually obtained at two different elevations above the marine growth. The length of the cores varied depending on the concrete cover, concrete composition (e.g., type of aggregate), and other factors encountered in the field. The cores' lengths varied from 4.5 cm to 16 cm, depending upon the reinforcement depth of the component. At least two cores were obtained per location. In general, four concrete

cores were obtained as shown in Figure F.2. Figure F.2 also shows the set-up for conducting the coring of the piles, a cored space, and a picture of two concrete cores for chloride profiles and wet resistivity measurements. Once the two-inch samples were cored, the cores were stored in Ziploc bags. Usually, upon arriving to the laboratory, these cores were measured for length, resistivity, and weighed in a scale in an “as received” condition, to record the initial conditions. If one of the four cores was longer than 8.3 cm, it was then used to monitor wet resistivity. The rest of the cores were sliced and pulverized to obtain the chloride profiles via FDOT total chlorides method.

The cores selected for wet resistivity were placed in a high humidity chamber, weighed and the surface resistivity (with a=2 or a=2.5 cm) measured over time. SR measurements were taken every ninety degrees, twice around the sample. After the initial set of measurements was taken, the cores were then placed in high humidity chambers. Weight and SR measurements were conducted initially twice a week. The measurements were made once a week or more sporadically subsequent to four weeks. After several weeks in the high humidity chamber, the weight and the resistivity reached plateau values. Most of the measurements were performed with an electrode spacing of 2 cm (0.78in). Cell constant correction values were calculated and applied to determine the normalized wet concrete resistivity (see modeling chapter) to each measurement (SR_{wet}).

Figure F.2: Water saturation container set-up

5.1.3 Additional Field Measurements

Before conducting the surface resistivity (SR) measurements as a function of elevation, two additional measurements were performed: identification of the rebar

(reinforcing) mat location/depth and an estimate of the concrete moisture for the concrete closest to the surface. A rebar locator was used to identify the rebar mat. The rebar locator was also used to estimate the reinforcement bar size, and to determine the concrete cover depth when not available. The estimated location of the rebar mat was marked on the concrete surface and also the on locations that were used as the center for the SR measurements. This was done only the first day. Before conducting each set of SR measurements, a commercial concrete moisture meter was also used to record the apparent moisture content of the outer 1.25 to 1.9 cm concrete. The meter readings ranged from 0 (dry concrete) to 20 (highly wet concrete). The moisture measurements were made at the locations where SR measurements were to be made. As the elevation from the marine growth increased, the displayed moisture value usually decreased. This was particularly evident on day zero before the first set of SR measurements. SR measurements were made using a commercially-available Wenner probe with adjustable electrode spacing identified here as a concrete surface resistivity meter. The spacing used corresponded to a=3 cm and a=5 cm (a=1.18in, a=1.97in). Sets of measurements were performed with intervals of approximately 24 hours up to three to four days. Usually, four or five sets of measurements were conducted including day zero. Figure F.3 shows an example of the locations where the SRs were performed upon removing the conditioning set-up.

Initial field trips were made to relatively new structures. These structures were made with HPC concrete mixture and were recently characterized for RCP and chloride diffusivity. SR was measured on selected columns or other partially-immersed reinforced structures as a function of elevation. Resistivity measurements were made over the surface of concrete as it was, i.e., no surface conditioning was implemented. In one of the bridges, the selected structure was a retaining wall that had been recently repaired and still had the curing coating membrane. For this case, it was necessary to drill the coating at the electrode spacing. After the first two trips it was determined that a conditioning procedure was needed to increase the degree of saturation of the concrete close to the surface. Although the degree of saturation is very significant, it was determined that other factors besides the degree of saturation affect the apparent SR

measured (some of these other factors were described in the introduction). In addition, the degree of water saturation at the higher elevations is likely lower than close to the water line (marine growth).

Figure F.3: Bridge structure pile measurement set-up.

5.1.4 Temperature Correction

Field trips were made year-round; thus, the SR measurements were taken during different seasons of the year, and temperature varied considerably. There was a need to normalize SR values to a reference temperature. The selected temperature replicates laboratory conditions at 69.8°F (294°K, 21°C). No actual concrete surface temperature was measured; rather, the air temperature or water temperature were measured during the field trips. The air temperature was the temperature that was assumed for the correction. There are several approaches that have been reported to correct for temperature. Equation 1 developed by (Elkey and Sellevold 1995) was selected for the temperature correction.

$$\rho_{normalized} = \rho_{field} \exp\left(K.\left[\frac{1}{T^{\circ}_{Ks\tan dar}} - \frac{1}{T^{\circ}_{Kfield}} \right] \right) \qquad \textit{Equation (2)}$$

Where

K = 2889

$T^{\circ}_{Ks\tan dar}$ = 294.15 K°

5.1.5 Chloride Analysis

A set of field-obtained cores was assigned for chloride concentration profiles. This latter group of cores was cut transversely with a wet saw and seven slices were obtained per core whenever possible. Figure F.4 shows a diagram indicating the slices. In most cases, the slice thicknesses were: 0.4 cm for slice 1, 0.5 cm for slice 2, 0.6 cm for slice 3, 0.7 cm for slice 4, 0.7 cm for slice 5, 0.7 cm for slice 6, 0.7 cm for slice 7. The seventh slice cut was taken from the opposite edge of the core as shown in Figure F.4.

Concrete slices were pulverized, and the concrete powder was processed to get chloride concentration as per FDOT total chloride analysis. The choride concentration profiles per concrete core were then used to calculate the apparent chloride diffusion coefficient (D_{Cl}).

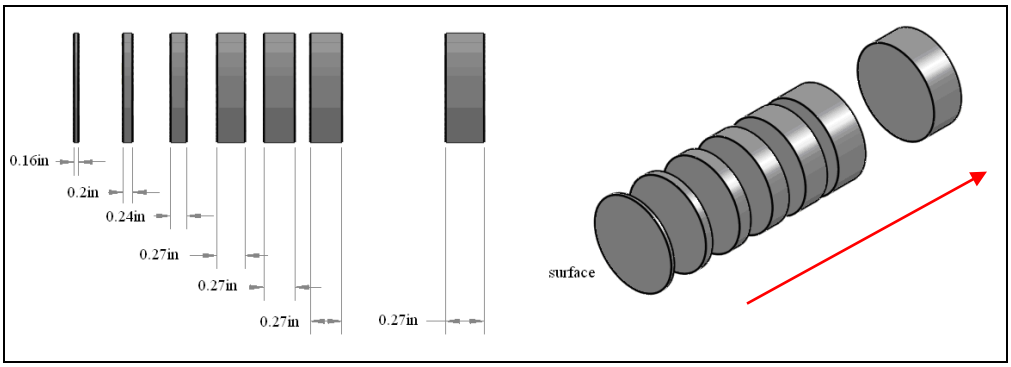

Figure F.4: Slicing of cores.

5.2 Field Results and Discussion

Table F.1 contains a list of all the bridges visited; the bridge number, age, and whether cores were obtained by showing the group ID. Tables F.2 and F.3 list the bridge components visited (i.e., footers, columns, piles); most of the components have been evaluated for SR profile measurements with the conditioning set-up. Tables F.4 to F.8 contains a list of all the cores, and the corresponding C_s, C_o, and D_{Cl} if used for chloride profiles, or the SR_{wet} if used for the SR measurements.

Table F.1: Bridges Visited

	Bridge	Bridge #	Abbreviation	County	Year Built	Core Group
1	Indian River 1	700181	IR1	Brevard	1985	1,7
2	Indian River 2	700174	IR2	Brevard	1978	3,5,6
3	SR-520 - Sykes Creek	700193	SC	Brevard	1995	2,4
4	Turkey Creek	700203	TC	Brevard	1999	8,9,10
5	US-1 Crane Cr. & City St	700006	CC	Brevard	1959/1990	11,12
6	Seabreeze Bridge -WB	790174	SBRZ	Volusia	1997	20, 21
7	International Speedway, US-92 WB	790187	SPEED	Volusia	2001	22, 23
8	Main St-Halifax River	794004	MainS	Volusia	1959	24
9	Seabreeze Bridge - EB	790175	OR	Volusia	1997	26
10	Apalachicola River - 490031	490031	APA	Franklin	1988	31
11	Saint George, test p.	490100*	SGB-T	Franklin	2003	32
12	Saint George, test p.	490100*	SGB-T	Franklin	2003	33
13	Old Saint George		OSG	Franklin		34
14	Apalachicola Bay	490032	APB	Franklin		30
15	Key Royale -UFA, FA,SF, Slag, Meta, OPC	136502*	KRB	Manatee	2007	40 to 45
16	Courtney C - Pile	150138		Pinellas	1974/1993	50, 51
17	Old Howard Franklin	150107	O-HFB	Pinellas	1959/1992	52
18	New Howard Franklin	150210	N-HFB	Pinellas	1991	53, 54
19	Old Ghandi-EB	100300		Hillsborough	1975	55
20	New Ghandi-WB	100585		Hillsborough	1996	56
21	Sunrise Blvd East Bound	860467	ITA	Broward	1987	60
22	Sunrise Blvd West Bound	860466	ITB	Broward	1989	61
23	Sunrise West West Bound	860061		Broward	1957/1981	62
24	Sunrise West Eastbound	860061		Broward	1957/1981	63
25	Las Olas	860018		Broward	1958	64, 65
26	Sheridan	860043		Broward	1962	66
27	Sunshine Sky Way 1 SB	150189	SSK-SB	Pinellas	1986	70
28	Sunshine Sky Way 1 NB	150189	SSK-NB	Pinellas		71
29	Dick Misener Bridge NB, I-275 NB	150214	DMB-NB	Pinellas	1992	72
30	Dick Misener Bridge SB, I-275 SB	150213	DMB-SB	Pinellas	1994	
31	I-275 NB Over Bunce Pass	150211	275-BP-NB	Pinellas	1991	
32	I-275 SB Over Bunce Pass	150038	275-BP-SB	Pinellas	1968/1990	73
33	SR 679 Over Bunces Pass	150243		Pinellas	2001	75
34	Structure E	150049		Pinellas	1961/1996	76
35	Structure C	150050		Pinellas	1962	77
36	SR732 Jensen Beach - Footer	890145 W/ 890146 E		Martin	2005	80, 81
37	SE Ocean Blvd. Footer. Bent 15	890158/60 River		Martin	2001	82
38	SE Ocean Blvd. Bent 10. Westbound	890150 Intercoastal		Martin	2007	83
39	SR714 Okeechobee. B10 foote	894037		Martin	1967	84
40	Roosebelt Brdge. B22.	890003		Martin	1964	85
41	US1. B13. Footer2. SB. WF/New Roosevelt	890151		Martin	1997	86
42	Hattaway- 460112	460113/460112		Bay	2003/2004	94
43	Hattaway 460012	460113/460112		Bay	2003/2004	95
44	Philips Outlet	460072		Bay	1989	96
45	William T Marler	570054		Okaloosa	1971	90,91
46	William T Marler	570082		Okaloosa	1979	92
47	120088-Matanzas	120088	MAT	Lee	1980	130
48	SR865- Over Hurricane Bay	120089	HUR	Lee	1980	131
49	SR865- Over Hurricane Bay with SF	120089	HUR	Lee	1991	132
50	Structure B - Sanibel Causeway	124115		Lee	2007	133
51	Structure A - Sanibel Causeway	124116		Lee	2007	134
52	Indian Key Channel	900095		Monroe	1981	120
53	Lignum Vitae Channel	900096		Monroe	1981	121
54	Seven Mile	900101	7MI	Monroe	1982	122c, 123
55	Missouri LittleE Duck Channel	900103		Monroe	1981	124
56	Bahia Honda NB	900045		Monroe	1972	125
57	Henry H. Buckman SR. - SB	720249		Duval	1970/1993	110, 111, 112
58	Henry H. Buckman SR. - NB	720343		Duval	1970/1993	115
59	Saint Elmo W. Acosta	720570		Duval	1991	116
60	Verle Allyn Pope Bridge - Matanzas IW	780090		St. Johns	1975	100, 105
61	Mickler O'Connel Bridge - Matanzas River - SR312 - EB	780089		St. Johns	1976	101
62	Mickler O'Connel Bridge - Matanzas River -SR312- WB	780100		St. Johns	1999??	102, 103

Table F.2: Bridge components visited

#	BRIDGE	BRIDGE #	BENT	PILE	FACE	Concrete Cover (in)	Cores
1	Indian River 1	700181	24		N	5	Y
2	Indian River 1	700181	20		N	5	Y
3	Indian River 2	700174	19		W	5	Y
4	Indian River 2	700174	24		N	5	Y
5	SR-520 - Sykes Creek	700193	3	11	N	2.9	Y
6	SR-520 - Sykes Creek	700193	4	11	N	2.9	Y
7	Turkey Creek	700203	5	15	W	3	Y
8	Turkey Creek	700203	3	15	W	3	Y
9	Turkey Creek	700203	5	14	E	3	Y
10	US-1 Crane Cr. & City St	700006	5	14	E	3.6	Y
11	Seabreeze Bridge -WB	790174	7		W		Y
12	Seabreeze Bridge -WB	790174	6		S		
13	International Speedway, US-92 WB	790187	8	1 (S)	N	3.85	Y
14	International Speedway, US-92 WB	790187	8	2 (N)	W	2.75	
15	Main St-Halifax River	794004	16	3	N		Y
16	Main St-Halifax River	794004	16	4	E		
17	Seabreeze Bridge - EB	790175	6		W		Y
18	Apalachicola River	490031	12	3	S	2.5	N
19	Apalachicola River - Column on top of footer	490031	15		S	3.85	Y
20	Saint George, test p.	490100*	36		W/SW	2.7	Y
21	Saint George, test p.	490100*	20		W/SW	3.5	Y
22	Saint George Bridge	490100	19	1	W	2.7	N
23	Saint George Bridge	490100	19	2	SW	2.65	N
24	Old Saint George Bridge - Fishing Pier		21	1	W	3.65	Y
25	Apalachicola Bay	490032	125	3	S	3.85	Y
26	Key Royale Bridge	136502	3	1	NF	3	N*
27	Key Royale Bridge	136502	3	2	SF	3	N
28	Key Royale Bridge	136502	3	3	NF	3	N
29	Key Royale Bridge	136502	3	4	NF	3	N
30	Key Royale Bridge	136502	3	5	NF	3	N
31	Key Royale Bridge	136502	2	1	NF	3	N
32	Key Royale Bridge	136502	2	2	SF	3	N
33	Key Royale Bridge	136502	2	3	NF	3	N
34	Key Royale Bridge	136502	2	4	NF	3	N
35	Key Royale Bridge	136502	2	5	NF	3	N
36	Courtney Cambell	150138	10	6	W	3.8	Y
37	Courtney Cambell	150138	23	Footer	W		Y
38	Old Howard Franklin	150107	141	8	S	3.45	Y
39	Old Howard Franklin	150107	141	5	S	3.3	N
40	New Howard Franklin	150210	26	1	E	5.5	Y
41	New Howard Franklin	150210	44	Footer	E	5.5	Y
42	Ghandy eastbound	100300	250	5	N	3.4	Y
43	Ghandy westbound New	100585	83	Footer	W	4.7	N**
44	Ghandy westbound New	100585	91	Footer	E	4.9	N
45	Sunrise Blvd -IWW- EB	860467	2	4	S		Y
46	Sunrise Blvd -IWW- WB	860466	2	3	S		Y
47	Sunrise west Blvd -EB	860061	2	14	E		Y
48	Sunrise west Blvd - WB	860061	2	10	E		Y
49	Las Olas Blvd	860018	6	2	N		Y
50	Las Olas Blvd	860018	2	5	E		Y
51	Sheridan	860043	5	1	W		Y

Table F.3:Bridge components visited (Continuation)

#	BRIDGE	BRIDGE #	BENT	PILE	FACE	Concrete Cover (in)	Cores
52	Sunshine Sky Way 1 SB	150189	173	Footer	N		Y
53	Sunshine Sky Way 1 NB	150189	171	Footer	N		Y
54	Dick Misener Bridge NB, I-275 NB	150214	22	4	N	3.2	N
55	Dick Misener Bridge SB, I-275 SB	150213	11	7	W	3.1	Y
56	I-275 NB Over Bunce Pass	150211	13	Footer 1	W		N
57	I-275 SB Over Bunce Pass	150038	17	Footer	S		Y
58	SR 679 Over Bunces Pass	150243	11	2 - Footer	E	6.2	N
59	SR 679 Over Bunces Pass	150243	11	2-Column	E	3.85	Y
60	Structure E	150049	6	3	N		Y
61	Structure C	150050				2.85	Y
62	SR 732 Jensen Beach Causeway	890145 W/ 890146 E	10	footer	N	4	Y
63	Jensen Beach Causeway Relief Bridge	890145 W/ 890146 E	9	2	W	3.15	Y
64	SE Ocean Blvd	890158/60 River	15	footer	E	3.8	Y
65	SE Ocean Blvd West bound	890150 Intercoastal	10	footer	E	4	Y
66	Palm City SR 714 Okeechobee ww 9.5m WB	894037	10	footer	N	6	Y
67	Roosebelt Bridge (opens)	890003	22			2.65	Y
68	US1 Southbound	890151	13	footer 2	W	4.2	Y
69	William Marter	570054	19	3	S	3	Y
70	William Marter	570082	20	3	W	3	Y
71	William Marter	570082	29	footer 1	E		Y
72	Hathaway 460112	460112	4	footer 2	W	3.5	Y
73	Hathaway 460112	460112	4	footer 1	E	3.5	Y
74	Phillips Inlet 460072	460072	18	2	E		Y
75	Phillips Inlet 460072	460072	16	2	E		N
76	Crescent Beach	780090	34	8	S		Y
77	Crescent Beach	780090	20	1	S	3.2	Y
78	State Road 312 -EB old	780089	25	footer	E	4	Y
79	State Road 312 -EB old	780100	27	footer	E	3.7	Y
80	State Road 312 - WB New	780100	16		W		Y
81	Vilano	780099	18	2	N		Y
82	Temporary Bridge		19	4	E		N
83	Buckman EB	720249	104	footer1	W	3	Y
84	Buckman EB	720249	123	3	W	2.5	Y
85	Buckman EB	720249	123	7	W	2.5	Y
86	Buckman WB	720343	123	3	S	3.1	Y
87	Buckman WB	720343	123	5	W	3.1	Y
88	Fuller Warn E to W	720343	21	footer1	N	3.5	Y
89	Acosta SB	720570	2	footer	S		Y
90	Isaiah D Hart -SB	720107	3	footer	S	2	Y
91	Indian Key Channel	900095	17	1			Y
92	Lignum Vitae Channel	900096	9	2			Y
93	7Mile	900101	14	2			Y
94	7Mile	900101	14	3 footer			Y
95	Missouri litle duck	900103	7	2			Y
96	Bahia Honda - NB	900045	71	5		2.65	Y
97	Bahia Honda - SB	900016	69	3			Y
98	Bogie	900106	35	4			Y
99	Matanzas Bay Bridge	120088	11	footer	North	3.85	Y
100	SR865- Over Hurricane Bay	120089	8	1		2.4	Y
101	SR865- Over Hurricane Bay	120089	8	4		3.5	Y
102	Structure B - Sanibel Causeway	124115	3	footer	East	4	Y
103	Structure A - Sanibel Causeway	124116	14	footer	East	3.5	Y

Table F.4: Core list including D_{app} and Wet Resistivity

#	CORE	BRIDGE	Bridge #	BENT	PILE	FACE	Length (in)	Length (cm)	Distance from MG (in)	Wet ρ kΩ-cm	Dapp cm^2/s	Cs kg/m^3	Co kg/m^3
1	1	Indian River 1	700181	24		N	5.00	12.9		5.1			
2	1b	Indian River 1	700181	24		N	4.00	10.3			3.7E-08	11.1	2.7
3	2	SR-520 - Sykes Creek	700193	3	11	S	3.75	9.7		8.8			
4	2b	SR-520 - Sykes Creek	700193	3	11	S	3.00	7.7			7.8E-09	13.6	0.1
5	3b	Indian River 2	700174	19		N	5.25	13.5			9.4E-09	20.5	0.9
6	3	Indian River 2	700174	19		N	5.75	14.8		3.8			
7	4b	SR-520 - Sykes Creek	700193	4	11	S	2.75	7.1			1.5E-08	10.9	0.1
8	4	SR-520 - Sykes Creek	700193	4	11	S	3.50	9.0		9.5			
9	5	Indian River 2	700174	24		N	4.25	11.0		4.8			
10	6	Indian River 2	700174	24		N	4.25	11.0		3.7			
11	7b	Indian River 1	700181	20		N	4.25	11.0			1.3E-07	9.5	4.7
12	7	Indian River 1	700181	20		N	5.00	12.9		4.0			
13	8	Turkey Creek	700203	5	15	W	4.25	11.0		29.2			
14	8b	Turkey Creek	700203	5	15	W	4.00	10.3			1.7E-09	6.9	0.1
15	9	Turkey Creek	700203	3	15	W	3.75	9.7		37.4			
16	9b	Turkey Creek	700203	3	15	W	3.50	9.0			3.2E-09	7.0	0.1
17	10b	Turkey Creek	700203	5	14	E	4.50	11.6			5.1E-10	0.7	0.1
18	10	Turkey Creek	700203	5	14	E	4.25	11.0		32.6			
19	11b	US-1 Crane Cr. & City St	700006	5	14	W	2.25	5.8			2.0E-09		0.0
20	11	US-1 Crane Cr. & City St	700006	5	14	W	5.25	13.5		5.5			
21	12	US-1 Crane Cr. & City St	700006	5	14	W	3.25	8.4		7.6			
22	12b	US-1 Crane Cr. & City St	700006	5	14	W	3.00	7.7			1.9E-09	4.2	0.0
23	20a	Seabreeze Bridge -WB	790174	7		W	5.38	13.9	14	58.8			
24	20b	Seabreeze Bridge -WB	790174	7		W	3.00	7.7	3		3.1E-09	17.4	0.3
25	20c	Seabreeze Bridge -WB	790174	7		W	3.00	7.7	-5		4.1E-09	9.8	0.2
26	21a	Seabreeze Bridge -WB	790174	6		S	1.75	4.5	14		3.8E-09	8.1	0.1
27	21b	Seabreeze Bridge -WB	790174	6		S	4.00	10.3	3	48.2			
28	21c	Seabreeze Bridge -WB	790174	6		S	3.00	7.7	-5		5.0E-09	13.9	0.3
29	22a	International Speedway, US-92 WB	790187	8	1	N	4.75	12.3	15	54.7			
30	22b	International Speedway, US-92 WB	790187	8	1	N	2.75	7.1	5		2.4E-09	9.4	0.2
31	22c	International Speedway, US-92 WB	790187	8	1	N	3.75	9.7	-4		2.9E-09	13.1	0.2
32	23a	International Speedway, US-92 WB	790187	8	2	W	5.00	12.9	14		3.6E-09	10.8	0.2
33	23b	International Speedway, US-92 WB	790187	8	2	W	3.50	9.0	4		1.9E-09	11.6	0.2
34	23c	International Speedway, US-92 WB	790187	8	2	W	5.00	12.9	-6	55.6			
35	24a	Main St-Halifax River	794004	16	3	N	3.00	7.7	13	2.5			
36	24b	Main St-Halifax River	794004	16	3	N	3.00	7.7	-1		7.3E-10	8.0	5.0
37	25a	Main St-Halifax River	794004	16	4	E	2.13	5.5	9.5		5.1E-08	2.7	3.3
38	25b	Main St-Halifax River	794004	16	4	E	2.50	6.5	-8		1.7E-07	4.9	7.0
39	26a	Seabreeze Bridge - EB	790175	6		W	3.50	9.0	11		3.9E-09	10.6	0.2
40	26b	Seabreeze Bridge - EB	790175	6		W	4.75	12.3	-1		2.5E-09	11.7	0.1
41	26c	Seabreeze Bridge - EB	790175	6		W	3.75	9.7	-8	50.8			
42	30a	Apalachicola Bay	490032	12	3	S	1.75	4.5	8		3.4E-09	7.6	N/A
43	30b	Apalachicola Bay	490032	12	3	S	2.00	5.2	6		6.9E-09	4.1	0.4
44	30c	Apalachicola Bay	490032	12	3	S	2.00	5.2	-7		9.6E-09	17.1	2.2
45	30d	Apalachicola Bay	490032	12	3	S	3.25	8.4	-7	11.4			
46	31a	Apalachicola Bay	490032	15		S	3.25	8.4	11		3.4E-09	9.1	0.3
47	31b	Apalachicola Bay	490032	15		S	2.50	6.5	11		3.5E-09	3.2	0.2
48	31c	Apalachicola Bay	490032	15		S	4.50	11.6	-7				
49	31d	Apalachicola Bay	490032	15		S	4.75	12.3	-7	31.7			
50	32a	Saint George, test p.	490003*	36		W	1.25	3.2	15		1.7E-09	18.7	0.3
51	32b	Saint George, test p.	490003*	36		W	2.25	5.8	15		2.9E-09	30.6	0.3
52	32c	Saint George, test p.	490003*	36		W	3.00	7.7	-1	61.3			
53	32d	Saint George, test p.	490003*	36		W	2.75	7.1	-1		3.0E-09	13.1	0.3
54	33a	Saint George, test p.	490003*	20		NW	3.00	7.7	17	49.2			
55	33b	Saint George, test p.	490003*	20		NW	2.75	7.1	17		1.5E-09	14.1	1.1
56	33c	Saint George, test p.	490003*	20		NW	2.50	6.5	7		1.2E-09	17.0	0.4
57	33d	Saint George, test p.	490003*	20		NW	2.50	6.5	7		1.4E-09	12.3	0.3
58	33e	Saint George, test p.	490003*	20		NW	3.00	7.7	-2		5.6E-09	15.8	0.3
59	33f	Saint George, test p.	490003*	20		NW	2.75	7.1	-2		3.6E-09	14.8	0.4
60	34a	Old Saint George		21	1	N	3.25	8.4	20	6.1			
61	34b	Old Saint George		21	1	N	3.00	7.7	20		6.1E-09	8.5	0.4
62	34c	Old Saint George		21	1	N	2.50	6.5	0		5.3E-09	15.5	5.5
63	34d	Old Saint George		21	1	N	2.50	6.5	0		8.2E-09	17.9	5.7
64	40a	Key Royale Bridge	136502	Fender	6		3.00	7.7	5 right	44.8			
65	40b	Key Royale Bridge	136502	Fender	6		2.75	7.1	5 left		2.2E-09	15.4	0.2

Table F.5: Core list including D_{app} and Wet Resistivity (Continuation)

#	CORE	BRIDGE	Bridge #	BENT	PILE	FACE	Length (in)	Length (cm)	Distance from MG (in)	Wet ρ kΩ-cm	Dapp cm^2/s	Cs kg/m^3	Co kg/m^3
66	40c	Key Royale Bridge	136502	Fender	6		2.75	7.1	-3 right		2.4E-09	11.3	0.2
67	40d	Key Royale Bridge	136502	Fender	6		2.75	7.1	-3 left		2.3E-09	8.7	0.2
68	41a	Key Royale Bridge	136502	Fender	7		3.00	7.7	4 right		2.1E-09	15.9	0.1
69	41b	Key Royale Bridge	136502	Fender	7		2.50	6.5	4 left		8.8E-10	18.1	0.1
70	41c	Key Royale Bridge	136502	Fender	7		3.00	7.7	-6 right	55.5			
71	41d	Key Royale Bridge	136502	Fender	7		3.00	7.7	-6 left		1.3E-09	13.8	0.1
72	42a	Key Royale Bridge	136502	Fender	8		2.75	7.1	5 right		1.4E-09		
73	42b	Key Royale Bridge	136502	Fender	8		3.00	7.7	5 left		3.1E-09	12.0	0.2
74	42c	Key Royale Bridge	136502	Fender	8		3.00	7.7	-7 right		3.6E-09	15.9	0.2
75	42d	Key Royale Bridge	136502	Fender	8		3.00	7.7	-7 left	51.1			
76	43a	Key Royale Bridge	136502	Fender	9		5.50	14.2	5 right	29.9			
77	43b	Key Royale Bridge	136502	Fender	9		2.75	7.1	5 left		2.5E-09	15.7	0.2
78	43c	Key Royale Bridge	136502	Fender	9		3.00	7.7	-5 right		2.9E-09	13.2	0.1
79	43d	Key Royale Bridge	136502	Fender	9		3.75	9.7	-5 left		3.4E-09	14.1	0.1
80	44a	Key Royale Bridge	136502	Fender	10		2.75	7.1	4 right		8.5E-10	14.6	0.1
81	44b	Key Royale Bridge	136502	Fender	10		6.00	15.5	4 left	50.1			
82	44c	Key Royale Bridge	136502	Fender	10		2.50	6.5	-5 right		1.6E-09	14.3	0.1
83	44d	Key Royale Bridge	136502	Fender	10		3.50	9.0	-5 left		9.5E-10	15.2	0.1
84	45a	Key Royale Bridge	136502	Fender	11		3.00	7.7	6 right		2.9E-09	13.4	0.0
85	45b	Key Royale Bridge	136502	Fender	11		3.00	7.7	6 left		3.9E-09	15.1	0.0
86	45c	Key Royale Bridge	136502	Fender	11		2.50	6.5	-5 right		8.0E-09	13.8	0.1
87	45d	Key Royale Bridge	136502	Fender	11		4.25	11.0	-5 left	5.9			
88	50a	Courtney Cambell	150138	10	6	W	4.25	11.0	13		ND	14.0	5.0
89	50b	Courtney Cambell	150138	10	6	W	4.25	11.0	13		ND	8.9	8.4
90	50c	Courtney Cambell	150138	10	6	W	5.25	13.5	-5	2.6			
91	50d	Courtney Cambell	150138	10	6	W	3.50	9.0	-5		1.2E-07	12.1	7.6
92	51a	Courtney Cambell	150138	23		W	3.25	8.4	16		1.3E-08	10.0	2.8
93	51b	Courtney Cambell	150138	23		W	3.50	9.0	16		4.9E-09	11.2	2.9
94	51c	Courtney Cambell	150138	23		W	3.50	9.0	-3		9.0E-09	11.6	4.0
95	51d	Courtney Cambell	150138	23		W	4.25	11.0	-3	4.0			
96	52a	Old Howard Franklin	150107	141	7		3.50	9.0	14		1.2E-08	7.0	1.6
97	52b	Old Howard Franklin	150107	141	7		4.50	11.6	14	7.5			
98	52d	Old Howard Franklin	150107	141	7		3.25	8.4	-5		4.9E-09	22.5	5.3
99	53a	New Howard Franklin	150210	44		E	3.00	7.7	11		1.8E-09	16.4	0.2
100	53b	New Howard Franklin	150210	44		E	5.00	12.9	11		1.3E-09	15.2	0.3
101	53c	New Howard Franklin	150210	44		E	4.25	11.0	-6		2.6E-09	16.2	0.2
102	53d	New Howard Franklin	150210	44		E	4.75	12.3	-6	31.5			
103	54a	New Howard Franklin	150210	44		E	4.75	12.3	21		2.8E-09	12.1	0.4
104	54b	New Howard Franklin	150210	44		E	5.00	12.9	21	29.4			
105	54c	New Howard Franklin	150210	44		E	4.25	11.0	0		9.1E-09	18.7	0.4
106	55a	Ghandy eastbound	100300	250	5	N	2.75	7.1	27		3.5E-08	19.1	6.5
107	55b	Ghandy eastbound	100300	250	5	N	3.00	7.7	27	3.1			
108	55c	Ghandy eastbound	100300	250	5	N	3.00	7.7	8		1.8E-08	31.0	7.9
109	56a	Ghandy westbound	100585	83	footer		4.75	12.3	16	40.3			
110	56b	Ghandy westbound	100585	84	footer		4.75	12.3	16		2.0E-09	27.6	0.3
111	56c	Ghandy westbound	100585	85	footer		4.75	12.3	0		2.2E-09	16.6	0.2
112	60a	Sunrise Blvd - EB	860467	2	4	S	4.50	11.6	12		2.4E-08	8.2	0.8
113	60b	Sunrise Blvd - EB	860467	2	4	S	3.00	7.7	12		ND	7.7	6.5
114	60c	Sunrise Blvd - EB	860467	2	4	S	3.75	9.7	-3		1.5E-08	10.3	2.8
115	60d	Sunrise Blvd - EB	860467	2	4	S	6.00	15.5	-3	3.0			
116	61a	Sunrise Blvd - WB	860466	2	3	S	3.50	9.0	14		1.6E-08	6.8	0.2
117	61b	Sunrise Blvd - WB	860466	2	3	S	3.50	9.0	14		2.4E-08	7.1	0.1
118	61c	Sunrise Blvd - WB	860466	2	3	S	3.75	9.7	-3		2.2E-08	16.0	3.2
119	61d	Sunrise Blvd - WB	860466	2	3	S	4.00	10.3	-3	3.5			
120	62a	Sunrise Blvd -WestBridge - EB	860061	2	14	E	2.75	7.1	10		1.5E-08	4.7	7.3
121	62b	Sunrise Blvd -WestBridge - EB	860061	2	14	E	5.25	13.5	10		6.5E-09	4.6	1.8
122	62c	Sunrise Blvd -WestBridge - EB	860061	2	14	E	7.00	18.1	-2	5.6			
123	62d	Sunrise Blvd -WestBridge - EB	860061	2	14	E	2.75	7.1	-2		2.4E-09	17.0	1.7
124	63a	Sunrise Blvd -WestBridge - WB	860061	2	10	E	3.00	7.7	16		7.3E-09	5.6	0.1
125	63b	Sunrise Blvd -WestBridge - WB	860061	2	10	E	3.00	7.7	16		8.3E-09	6.7	1.9
126	63c	Sunrise Blvd -WestBridge - WB	860061	2	10	E	4.00	10.3	0	3.9			
127	63d	Sunrise Blvd -WestBridge - WB	860061	2	10	E	3.00	7.7	0		6.8E-09	8.8	6.3
128	64a	Las Olas Blvd	860018	6	2	N	5.50	14.2	13		1.0E-08	3.3	1.7
129	64b	Las Olas Blvd	860018	6	2	N	5.00	12.9	13		1.1E-08	5.0	2.1
130	64c	Las Olas Blvd	860018	6	2	N	2.00	5.2	-4		5.8E-09	8.8	6.2

Table F.6: Core list including D_{app} and Wet Resistivity (Continuation)

#	CORE	BRIDGE	Bridge #	BENT	PILE	FACE	Length (in)	Length (cm)	Distance from MG (in)	Wet ρ kΩ-cm	Dapp cm^2/s	Cs kg/m^3	Co kg/m^3
131	64d	Las Olas Blvd	860018	6	2	N	4.25	11.0	-4	4.7			
132	65a	Las Olas Blvd	860018	2	5	E	2.00	5.2	10		2.9E-09	6.8	5.0
133	65b	Las Olas Blvd	860018	2	5	E	2.00	5.2	10		5.6E-09	6.4	6.9
134	65c	Las Olas Blvd	860018	2	5	E	2.25	5.8	-2		1.1E-08	13.0	8.2
135	65d	Las Olas Blvd	860018	2	5	E	2.00	5.2	-2		3.0E-08	11.8	8.0
136	66a	Sheridan	860043	5	1	W	3.00	7.7	14		1.1E-08	5.0	1.7
137	66b	Sheridan	860043	5	1	W	3.00	7.7	14		1.4E-08	6.7	2.0
138	66c	Sheridan	860043	5	1	W	2.75	7.1	0		2.5E-08	16.8	9.0
139	66d	Sheridan	860043	5	1	W	2.75	7.1	0	2.7			
140	70a	Sunshine Sky Way 1 SB	150189	173	footer	N	6.50	16.8	14 left	19.9			
141	70b	Sunshine Sky Way 1 SB	150189	173	footer	N	6.00	15.5	14 right		5.1E-09	33.1	0.2
142	70c	Sunshine Sky Way 1 SB	150189	173	footer	N	5.00	12.9	8 center		2.6E-09	33.1	0.3
143	71a	Sunshine Sky Way 1 NB	150189	171	footer	N	6.75	17.4	11 left		4.0E-09	33.0	0.2
144	71b	Sunshine Sky Way 1 NB	150189	171	footer	N	4.50	11.6	11 right	20.9			
145	71c	Sunshine Sky Way 1 NB	150189	171	footer	N	4.50	11.6	6 right		1.1E-08	16.0	0.2
146	72a	Dick Misener Bridge NB, I-275 NB	150214	11	7	W	2.75	7.1	12 left		1.6E-09	7.8	0.1
147	72b	Dick Misener Bridge NB, I-275 NB	150214	11	7	W	2.75	7.1	12 right		2.1E-09	12.3	0.2
148	72c	Dick Misener Bridge NB, I-275 NB	150214	11	7	W	3.00	7.7	6 left		2.2E-09	14.3	0.4
149	72d	Dick Misener Bridge NB, I-275 NB	150214	11	7	W	3.25	8.4	6 right	21.8			
150	73a	I-275 SB Over Bunces Pass	150038	17	footer		4.75	12.3	14.5 left		3.9E-09	27.3	0.6
151	73b	I-275 SB Over Bunces Pass	150038	17	footer		4.75	12.3	14.5 right	16.2			
152	73c	I-275 SB Over Bunces Pass	150038	17	footer		4.00	10.3	- 5 left		7.9E-09	30.1	0.1
153	73d	I-275 SB Over Bunces Pass	150038	17	footer		4.50	11.6	-5 right		1.9E-08	12.2	0.7
154	73e	I-275 SB Over Bunces Pass	150038	17"-crack	footer		4.25	11.0	7		1.3E-08	30.8	1.5
155	73f	I-275 SB Over Bunces Pass	150038	17"-Crack	footer		4.00	10.3	-5		8.3E-09	35.9	2.3
156	75a	SR 679 Over Bunces Pass	150243	11	2	E	4.75	12.3	44 left	11.3			
157	75b	SR 679 Over Bunces Pass	150243	11	2	E	2.50	6.5	44 right		6.7E-09	5.8	0.4
158	75c	SR 679 Over Bunces Pass	150243	11	2	E	5.50	14.2	24 left		1.2E-08	11.8	0.3
159	75d	SR 679 Over Bunces Pass	150243	11	2	E	2.25	5.8	24 right		2.8E-08	11.5	0.5
160	76a	Structure E -150049	150049	6	3	N	2.75	7.1	14		1.0E-08	13.4	2.5
161	76c	Structure E -150049	150049	6	3	N	3.00	7.7	8	9.4			
162	77a	Structure C - 150050	150050				6.00	15.5	14	2.8			
163	77c	Structure C - 150050	150050				5.50	14.2	7		1.6E-09	10.5	0.4
164	80a	SR 732 Jensen Beach Causeway	890145 W	10	footer	N	5.10	13.2	19		6.0E-09	20.9	0.4
165	80b	SR 732 Jensen Beach Causeway	890145 W	10	footer	N	5.40	13.9	19		1.3E-08	20.9	0.4
166	80c	SR 732 Jensen Beach Causeway	890145 W	10	footer	N			2	16.8			
167	80d	SR 732 Jensen Beach Causeway	890145 W	10	footer	N	4.40	11.4	2		8.4E-09	37.4	0.2
168	81a	Jensen Beach Causeway Relief Bridge	890146 E	9	2	W	3.20	8.3	20		9.0E-09	21.0	0.2
169	81b	Jensen Beach Causeway Relief Bridge	890146 E	9	2	W	3.30	8.5	20		6.7E-09	16.8	0.2
170	81c	Jensen Beach Causeway Relief Bridge	890146 E	9	2	W			0	20.1			
171	81d	Jensen Beach Causeway Relief Bridge	890146 E	9	2	W	3.00	7.7	0		9.1E-09	14.9	0.2
172	82a	SE Ocean Blvd	890158	15	footer	E	4.30	11.1	19		1.1E-09	21.3	0.3
173	82b	SE Ocean Blvd	890158	15	footer	E			19	37.7			
174	82c	SE Ocean Blvd	890158	15	footer	E	4.00	10.3	2		2.4E-09	21.5	0.2
175	82d	SE Ocean Blvd	890158	15	footer	E	4.30	11.1	2		2.4E-09	25.9	0.2
176	83a	SE Ocean Blvd West bound	890150	10	footer	E	4.20	10.8	21		1.2E-09	20.9	0.4
177	83b	SE Ocean Blvd West bound	890150	10	footer	E	4.00	10.3	21		2.8E-09	17.2	0.1
178	83c	SE Ocean Blvd West bound	890150	10	footer	E			3	16.3			
179	83d	SE Ocean Blvd West bound	890150	10	footer	E			3		3.2E-09	37.7	0.6
180	84a	Palm City SR 714 Okeechobee WWay m 9.5 WB	894037	10	footer	N	4.30	11.1	21		9.8E-10	7.5	0.0
181	84b	Palm City SR 714 Okeechobee WWay m 9.5 WB	894037	10	footer	N			21		7.8E-10	8.9	0.1
182	84c	Palm City SR 714 Okeechobee WWay m 9.5 WB	894037	10	footer	N			3	26.6			
183	84d	Palm City SR 714 Okeechobee WWay m 9.5 WB	894037	10	footer	N	4.10	10.6	3		ND	17.0	0.1
184	85a	Roosebelt Bridge (opens)	890003	22					18	6.1			
185	85b	Roosebelt Bridge (opens)	890003	22			2.60	6.7	18		3.4E-09	9.8	0.4
186	85c	Roosebelt Bridge (opens)	890003	22			1.90	4.9	3		4.6E-09	31.6	5.4
187	85d	Roosebelt Bridge (opens) 890003	890003	22			2.60	6.7	3		9.0E-09	11.3	7.1
188	86a	US1 Southbound	890151	13	footer	W			18	80.4			
189	86b	US1 Southbound	890151	13	footer	W	3.90	10.1	18		1.1E-09	14.4	0.3
190	86c	US1 Southbound	890151	13	footer	W	4.40	11.4	3		2.0E-09	14.4	0.2
191	86d	US1 Southbound	890151	13	footer	W	5.10	13.2	3		1.8E-09	15.3	0.2
192	90a	William Marter	570054	19	3	S	2.50	6.5	17		1.2E-08	12.2	2.8
193	90b	William Marter	570054	19	3	S	2.00	5.2	17		1.7E-08	12.1	
194	90c	William Marter	570054	19	3	S	2.50	6.5	4		1.3E-08	17.9	5.3
195	90d	William Marter	570054	19	3	S	2.00	5.2	4		2.5E-08	22.7	4.6

Table F.7: Core list including D_{app} and Wet Resistivity (Continuation)

#	CORE	BRIDGE	Bridge #	BENT	PILE	FACE	Length (in)	Length (cm)	Distance from MG (in)	Wet ρ kΩ-cm	Dapp cm^2/s	Cs kg/m^3	Co kg/m^3
196	91a	William Marter	570054	20	3	W	2.25	5.8	2		1.3E-08	8.1	1.4
197	91b	William Marter	570054	20	3	W	1.75	4.5	2		1.4E-08	8.8	3.8
198	91c	William Marter	570054	20	3	W	1.50	3.9	7		1.1E-08	12.1	
199	91d	William Marter	570054	20	3	W	1.75	4.5	7		3.7E-08	11.7	3.9
200	92a	William Marter	570054	29	footer1	E	1.25	3.2	15				
201	92b	William Marter	570054	30	footer1	E	1.75	4.5	15		8.1E-09	18.0	
202	92c	William Marter	570054	31	footer1	E	2.25	5.8	5		6.1E-09	18.6	4.0
203	92d	William Marter	570054	32	footer1	E	2.00	5.2	5				
204	94a	Hathaway 460112	460112	4	footer2	W	3.00	7.7	11		6.3E-09	13.8	0.3
205	94c	Hathaway 460112	460112	4	footer2	W	2.50	6.5	2		5.2E-09	22.2	0.1
206	95a	Hathaway 460112	460112	4	footer1	E	5.50	14.2	20	20.7			
207	95c	Hathaway 460112	460112	4	footer1	E	5.50	14.2	7		4.8E-09	19.2	0.2
208	96a	Phillips Inlet 460072	460072	18	2	E	3.75	9.7	18	12.3			
209	96b	Phillips Inlet 460072	460072	18	2	E	3.50	9.0	18		3.9E-09	5.4	0.2
210	96c	Phillips Inlet 460072	460072	18	2	E	3.50	9.0	0		3.5E-09	13.0	0.3
211	96d	Phillips Inlet 460072	460072	18	2	E	3.50	9.0	0		8.3E-09	12.8	0.4
212	100a	Crescent Beach	780090	34	8	S	3.75	9.7	18	4.1			
213	100b	Crescent Beach	780090	34	8	S	3.50	9.0	18		8.4E-09	3.2	1.5
214	100c	Crescent Beach	780090	34	8	S	3.50	9.0	-1		1.2E-08	9.8	2.3
215	100d	Crescent Beach	780090	34	8	S	3.50	9.0	-1		2.1E-08	8.1	1.9
216	101a	Mickler O'Connel B. - Matanzas River -SR312 EB	780089	25	footer	E	5.00	12.9	20		6.8E-09	9.3	0.9
217	101b	Mickler O'Connel B. - Matanzas River -SR312 EB	780089	25	footer	E	5.75	14.8	20		2.0E-08	5.3	0.6
218	101c	Mickler O'Connel B. - Matanzas River -SR312 EB	780089	25	footer	E	6.50	16.8	0	3.4			
219	101d	Mickler O'Connel B. - Matanzas River -SR312 EB	780089	25	footer	E	7.00	18.1	0		8.7E-09	23.3	5.3
220	102a	Mickler O'Connel B. - Matanzas River -SR312- WB	780100	27	footer	E	6.25	16.1	3		1.2E-08	11.5	0.9
221	102b	Mickler O'Connel B. - Matanzas River -SR312- WB	780100	27	footer	E	5.75	14.8	3		1.8E-08	24.1	5.5
222	102c	Mickler O'Connel B. - Matanzas River -SR312- WB	780100	27	footer	E	6.25	16.1	-10		1.2E-08	27.1	2.8
223	102d	Mickler O'Connel B. - Matanzas River -SR312- WB	780100	27	footer	E	6.25	16.1	-10	4.6			
224	103a	State Road 312 - WB New Bridge	780100	16		W	5.25	13.5	17		3.7E-09	14.8	0.1
225	103b	State Road 312 - WB New Bridge	780100	16		W	4.75	12.3	17		4.1E-09	17.2	0.2
226	103c	State Road 312 - WB New Bridge	780100	16		W	6.25	16.1	0	18.2			
227	103d	State Road 312 - WB New Bridge	780100	16		W	6.50	16.8	0		6.2E-09	31.0	0.2
228	104a	Vilano	780099	18	2	N	2.50	6.5	30		9.3E-10	8.5	0.2
229	104b	Vilano	780099	18	2	N	3.00	7.7	30		1.4E-09	10.4	0.2
230	104c	Vilano	780099	18	2	N	2.75	7.1	17		3.1E-09	11.4	0.1
231	105a	Crescent Beach	780090	20	1	S	5.25	13.5	17	2.2			
232	105b	Crescent Beach	780090	20	1	S	5.50	14.2	17		9.7E-09	8.3	1.6
233	105c	Crescent Beach	780090	20	1	S	5.25	13.5	4		1.4E-08	10.9	2.6
234	105d	Crescent Beach	780090	20	1	S	5.50	14.2	4		1.2E-08	10.6	1.8
235	110a	Henry H. Buckman SR. - SB	720249	104	footer1	W	4.75	12.3	19		4.8E-10	3.8	0.0
236	110b	Henry H. Buckman SR. - SB	720249	104	footer1	W	5.00	12.9	19	34.0			
237	110c	Henry H. Buckman SR. - SB	720249	104	footer1	W	3.75	9.7	3		5.6E-10	6.4	0.1
238	110d	Henry H. Buckman SR. - SB	720249	104	footer1	W	3.75	9.7	3		1.1E-09	6.7	0.1
239	111a	Henry H. Buckman SR. - SB	720249	123	3	W	3.50	9.0	19		2.9E-09	3.1	0.3
240	111b	Henry H. Buckman SR. - SB	720249	123	3	W	3.25	8.4	19		2.2E-09	2.3	0.2
241	111c	Henry H. Buckman SR. - SB	720249	123	3	W	3.75	9.7	3	13.9			
242	111d	Henry H. Buckman SR. - SB	720249	123	3	W	3.25	8.4	3		9.7E-10	11.9	0.3
243	112a	Henry H. Buckman SR. - SB	720249	123	7	W	4.25	11.0	18		9.1E-09	3.4	0.1
244	112b	Henry H. Buckman SR. - SB	720249	123	7	W	5.25	13.5	18	3.6			
245	112c	Henry H. Buckman SR. - SB	720249	123	7	W	2.50	6.5	2		1.3E-07	8.4	7.7
246	112d	Henry H. Buckman SR. - SB	720249	123	7	W	2.75	7.1	2		2.9E-08	12.6	6.6
247	113a	Henry H. Buckman SR. - NB	720343	123	3	S	2.25	5.8	18		3.4E-09	7.1	1.3
248	113b	Henry H. Buckman SR. - NB	720343	123	3	S	3.00	7.7	18		9.5E-09	6.4	1.1
249	113c	Henry H. Buckman SR. - NB	720343	123	3	S	4.25	11.0	3		1.4E-08	18.0	4.2
250	113d	Henry H. Buckman SR. - NB	720343	123	3	S	2.75	7.1	3		2.1E-08	20.6	7.8
251	114a	Henry H. Buckman SR. - NB	720343	123	5	W	3.25	8.4	20		4.4E-09	5.8	0.2
252	114b	Henry H. Buckman SR. - NB	720343	123	5	W	3.50	9.0	20		9.4E-10	4.7	0.1
253	114c	Henry H. Buckman SR. - NB	720343	123	5	W	3.50	9.0	3		1.1E-09	9.7	0.2
254	114d	Henry H. Buckman SR. - NB	720343	123	5	W	3.50	9.0	3		1.5E-09	7.6	0.1
255	115a	Fuller Warn - WB	720343	21	footer1	N	3.75	9.7	19		2.5E-09	6.7	0.3
256	115b	Fuller Warn - WB	720343	21	footer1	N	4.50	11.6	19		2.7E-09	6.6	0.2
257	115c	Fuller Warn - WB	720343	21	footer1	N	4.00	10.3	2		5.5E-09	16.1	0.2
258	115d	Fuller Warn - WB	720343	21	footer1	N	5.25	13.5	2	16.1			
259	116a	Acosta - SB	720570	2	footer	S	4.50	11.6	18		8.2E-10	1.8	0.2
260	116b	Acosta - SB	720570	2	footer	S	4.50	11.6	18		1.3E-09	1.6	0.3

Table F.8: Core list including D_{app} and Wet Resistivity (Continuation)

#	CORE	BRIDGE	Bridge #	BENT	PILE	FACE	Length (in)	Length (cm)	Distance from MG (in)	Wet ρ kΩ-cm	Dapp cm^2/s	Cs kg/m^3	Co kg/m^3
261	116c	Acosta - SB	720570	2	footer	S	4.75	12.3	3	49.7			
262	116d	Acosta - SB	720570	2	footer	S	4.50	11.6	3		1.8E-09	10.5	0.2
263	117a	Hart	720107	3	footer	S	4.25	11.0	20		3.9E-09	3.7	0.5
264	117b	Hart	720107	3	footer	S	4.00	10.3	20		1.8E-07	3.4	0.8
265	117c	Hart	720107	3	footer	S	4.25	11.0	3		ND	10.4	0.8
266	117d	Hart	720107	3	footer	S	4.75	12.3	3		6.6E-09	4.7	1.5
267	120a	Indian Key Channel	900095	17	1		4.00	10.3	26	2.8			
268	120b	Indian Key Channel	900095	17	1		4.00	10.3	26		3.8E-08	3.4	4.3
269	120c	Indian Key Channel	900095	17	1		3.50	9.0	6		1.2E-07	7.6	4.1
270	120d	Indian Key Channel	900095	17	1		2.00	5.2	6		6.2E-08	7.4	7.9
271	121a	Lignum Vitae Channel	900096	9	2		4.00	10.3	30		1.8E-07	4.0	3.7
272	121b	Lignum Vitae Channel	900096	9	2		4.00	10.3	30	2.4			
273	121c	Lignum Vitae Channel	900096	9	2		4.00	10.3	5		2.2E-08	12.3	5.5
274	121d	Lignum Vitae Channel	900096	9	2		4.00	10.3	5		1.6E-08	13.6	5.6
275	122a	7Mile - Column	900101	14	2		4.00	10.3	40		1.9E-08	11.9	10.0
276	122c	7Mile - Column	900101	14	2		4.00	10.3	10	1.4			
277	122d	7Mile - Column	900101	14	2		4.00	10.3	10		8.0E-07	16.4	9.4
278	123a	7Mile - Footer	900101	14	2		4.50	11.6	35	2.9			
279	123b	7Mile - Footer	900101	14	2		4.50	11.6	35		1.3E-07	2.9	2.6
280	123c	7Mile - Footer	900101	14	2		3.50	9.0	10		3.5E-08	6.7	4.9
281	123d	7Mile - Footer	900101	14	2		3.75	9.7	10		2.4E-08	6.9	4.1
282	124a	Missouri litle duck	900103	7	2		4.50	11.6	35		ND	8.6	10.7
283	124b	Missouri litle duck	900103	7	2		4.50	11.6	35	2.1			
284	124c	Missouri litle duck	900103	7	2		4.25	11.0	15		ND	10.9	9.7
285	124d	Missouri litle duck	900103	7	2		4.50	11.6	15		1.4E-07	11.5	11.1
286	125a	Bahia Honda - NB	900045	71	5		2.00	5.2	30		ND	8.7	4.4
287	125b	Bahia Honda - NB	900045	71	5		3.50	9.0	30	4.3			
288	125c	Bahia Honda - NB	900045	71	5		2.50	6.5	10		ND	11.0	3.8
289	125d	Bahia Honda - NB	900045	71	5		2.00	5.2	10		1.7E-08	9.9	4.5
290	126a	Bahia Honda - SB	900016	69	3		1.75	4.5	35		1.0E-08	9.5	7.2
291	126b	Bahia Honda - SB	900016	69	3		1.50	3.9	35		1.6E-08	8.9	5.5
292	126c	Bahia Honda - SB	900016	69	3		1.75	4.5	12		8.7E-09	12.5	6.3
293	126d	Bahia Honda - SB	900016	69	3		2.00	5.2	12		ND	11.8	6.3
294	127a	Bogie	900106	35	4		2.00	5.2	28		4.4E-08	10.4	11.4
295	127b	Bogie	900106	35	4		1.75	4.5	28		2.7E-08	9.9	12.6
296	127c	Bogie	900106	35	4		3.00	7.7	7		2.9E-08	11.1	6.9
297	127d	Bogie	900106	35	4		2.75	7.1	7		2.5E-08	10.0	6.9
298	130a	Matanzas Bay Bridge	120088	11	footer	N	4.50	11.6	19		1.9E-09	3.4	0.2
299	130b	Matanzas Bay Bridge	120088	11	footer	N	4.75	12.3	19		3.2E-09	2.8	0.3
300	130c	Matanzas Bay Bridge	120088	11	footer	N	4.75	12.3	0	10.0			
301	130d	Matanzas Bay Bridge	120088	11	footer	N	4.50	11.6	0		7.5E-09	20.8	0.8
302	131a	SR865- Over Hurricane Bay	120089	8	1		2.50	6.5	20		1.3E-09	15.7	0.3
303	131b	SR865- Over Hurricane Bay	120089	8	1		2.00	5.2	20		2.4E-09	16.5	0.3
304	131c	SR865- Over Hurricane Bay	120089	8	1		2.75	7.1	3		1.2E-09	21.1	0.2
305	131d	SR865- Over Hurricane Bay	120089	8	1		3.00	7.7	3	63.5			
306	132a	SR865- Over Hurricane Bay	120089	8	4		4.00	10.3	21	3.6			
307	132b	SR865- Over Hurricane Bay	120089	8	4		3.75	9.7	21		ND	3.9	1.3
308	132c	SR865- Over Hurricane Bay	120089	8	4		3.00	7.7	1		3.8E-08	11.5	5.4
309	132d	SR865- Over Hurricane Bay	120089	8	4		2.75	7.1	1		2.8E-08	12.4	5.9
310	133a	Structure B Sanibel Causeway	124115	2	footer	E	5.00	12.9	20	14.7			
311	133b	Structure B Sanibel Causeway	124115	2	footer	E	5.00	12.9	20		1.0E-08	31.0	0.7
312	133c	Structure B Sanibel Causeway	124115	2	footer	E	5.00	12.9	5		8.0E-09	37.8	0.9
313	133d	Structure B Sanibel Causeway	124115	2	footer	E	4.50	11.6	5		9.6E-09	36.7	0.9
314	134a	Structure A Sanibel Causeway	124116	13	footer	E	4.25	11.0	18	16.2			
315	134b	Structure A Sanibel Causeway	124116	13	footer	E	3.75	9.7	18		1.0E-08	19.8	1.0
316	134c	Structure A Sanibel Causeway	124116	13	footer	E	3.50	9.0	2		1.5E-08	21.2	1.1
317	134d	Structure A Sanibel Causeway	124116	13	footer	E	3.75	9.7	2		1.4E-08	19.4	0.7

As indicated in the introduction and background chapter, pre-wetting the concrete surface is not recommended if SR measurements are going to be performed shortly after wetting. Our approach is different in the sense that we did not spray water on the surface, but rather used a water container to attempt to increase the moisture of the concrete. According to McCarter, water could reach about 2 cm in nine hours of water exposure for OPC concrete if starting from a dry state. For high performance concrete, the amount of water transported might be lower, due to lower porosity. Additionally, the water going into the concrete might not be confined only to the area below the container. Depending on the season and weather conditions, the concrete at the interrogated location might not be significantly dry. From the measurements conducted in the different field trips it appears that when the concrete is dry and there are no wetting events other than the water in the container; the resistivity decreases as a function of time, for measurements performed with a=3 cm.

Results for eight piles out of ~100 piles/footers visited are presented in this section. The next sub-section will describe the results of the measurements on five piles that correspond to a recently built (~3 years old) research bridge made with five different high performance concrete mix designs. The results for the other selected piles will follow. Two of these other piles correspond to older bridges with more than 40 years in service. Each bridge group section will be divided into several subsections. The first subsection describes the results for SR measurements vs. time, taken in-situ, followed by a subsection of measurements performed in the lab on field-obtained 2 in diameter concrete cores: SR_{wet} vs. time and weight increment vs. time. These measurements show how weight and SR_{wet} values evolved when the cores were exposed to a high humidity environment. A third subsection describes the chloride diffusivity results.

All field surface resistivity measured values presented in this section are based on measurements performed while subjecting the piles to the water conditioning method. However, it is important to briefly describe how this research began by testing without conditioning, and why later the water conditioning method was implemented.

Initial field trips were made to relatively new structures, with typical mix designs available and/or that were recently characterized for chloride diffusivity. SR was measured on selected columns or other partially-immersed reinforced structures as a function of elevation. First, SR measurements on this project were made over the surface of concrete as it was found, without any surface preconditioning. The SR profiles showed a dramatic increase in the SR measured value as the elevation from the water line increased. After the first two trips, it was realized that a conditioning procedure was needed to increase the degree moisture content of the concrete close to the surface.

As described in the background section, the degree of water saturation at the higher elevations might be lower than close to the water line (marine growth). A conditioning method was developed to increase the moisture content of the concrete close to the surface by employing a water reservoir (1.6 gallons). The set-up of this water reservoir has been described in the experimental field section.

5.2.1 Bridge #136502 – Key Royale Bridge

5.2.1.1 Bridge #136502 -SR Measurements

The results are presented as surface resistivity profiles, i.e., SR measurements vs. elevation, at various days with two different spacings, and three orientations of the Wenner probe. Bridge #136502, named Key Royale Bridge, is located in Anna Marie Island, FL, and constructed in 2007, was selected to describe typical results. This is a research bridge designed with five different high performance concrete mixes where each bent of piles corresponds to concrete made with: ultra fly ash (UFA), fly ash (FA), silica fume (SF), blast furnace slag (BFS), and metakaolin (MET). Adjacent to both sides of the bridge there are fender walls. These walls are supported by reinforced concrete piles made with the same composition as the main piles. An additional concrete mix made only with Portland cement (OPC) was used on two of the fender piles as part of the fender wall. Incidentally, two piles of each high performance concrete mix were also part of the fender wall. It is from these piles that the cores were

obtained. Figure F.5 shows a diagram with the distribution of concrete types, piles and bents for this research bridge (only the immersed piles are shown in here); not shown are two bents, one per side. This bridge was visited four times during the duration of this project. Surface resistivity profiles for the four trips are including in Appendix 4. Two bents (or rows of piles) were measured during each visit. During the first trip to this structure, a different conditioning method was used (Presuel et al. 2009). Many of the profiles showed a reduction in the measured SR value as a function of time. In the following paragraphs, the resistivity profiles described correspond to measurements performed during October 2008 on bent 2.

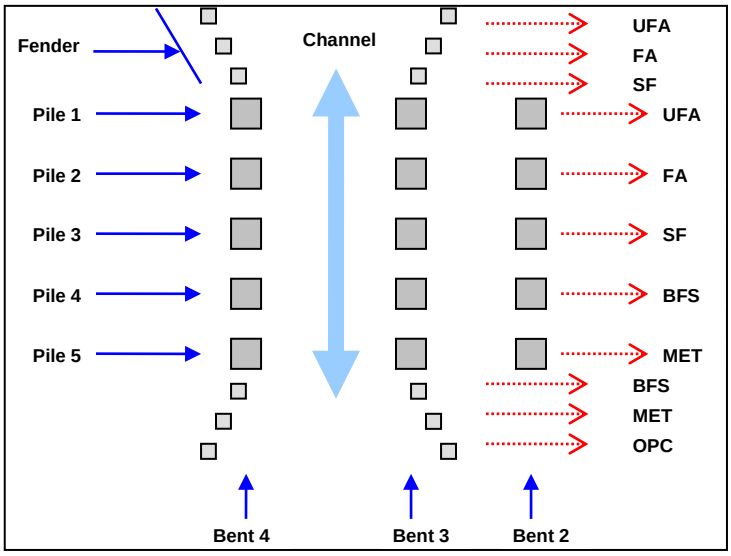

Figure F.5: Concrete mixture distribution diagram KRB.

SR measurements were taken at different orientations: 0° right plot, 45° left plot and 135° middle plot; conserving the same point as the center for each elevation. Two containers were used in these piles, the bottom one was positioned close to the marine growth, and the second above the first one. No leaks were observed; in most cases the water level was about 2 cm lower than the completely filled container, and it was speculated that most of this water was absorbed by the concrete. Figures F.6 to F.10 have two columns of plots. The column on the left shows results for spacing a=3 cm (1.18in), and the column on the right for spacing a=5 cm (2in).

The high resistivity values measured confirm the low permeability of the concrete. From the measured-resistivity values, it is clearly observed that the resistivity increases with elevation during the initial set of measurements. The lowest resistivity values were observed close to the water line (marine growth). Usually, field resistivity values measured after conditioning decreased significantly when compared to initial values, particularly when the concrete was initially dry.

Figure F.6 shows SR profiles for concrete with ultra fly ash (UFA). The highest SR values were measured during the first day without conditioning. After the water conditioning method was implemented, SR values reduced during the next days, and tended to stabilize, apparently reaching a high moisture content close to the surface after conditioning. Resistivity values recorded are in the range between 150 kΩ-cm when the condition of the surface was dry, and 110 kΩ-cm when wet.

#136502 KRB – Bent 2 Pile 1

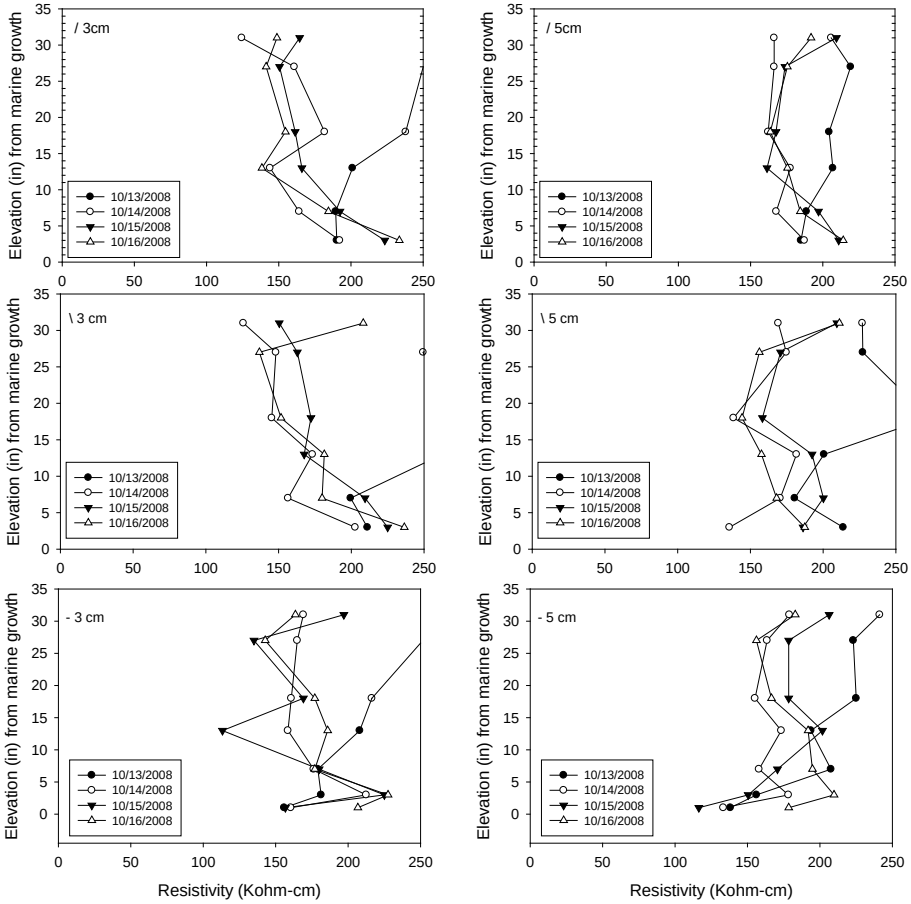

Figure F.6: Results of ρ vs. elevation for UFA. Bridge #136502.

SR profiles made on piles with fly ash (FA) are shown in Figure F.7. Resistivity on the first day was slightly higher than the following days. SR values for the second, third and fourth day remain relatively stable in the same average range of resistivity values between 170 kΩ-cm when dry and 140 kΩ-cm when wet, suggesting that moisture content of concrete close to the surface increased, confirming that when the moisture content is increased, the electrical resistivity of concrete decreases. There is not a significant difference in values when comparing the two spacings used.

#136502 KRB – Bent 2 Pile 2

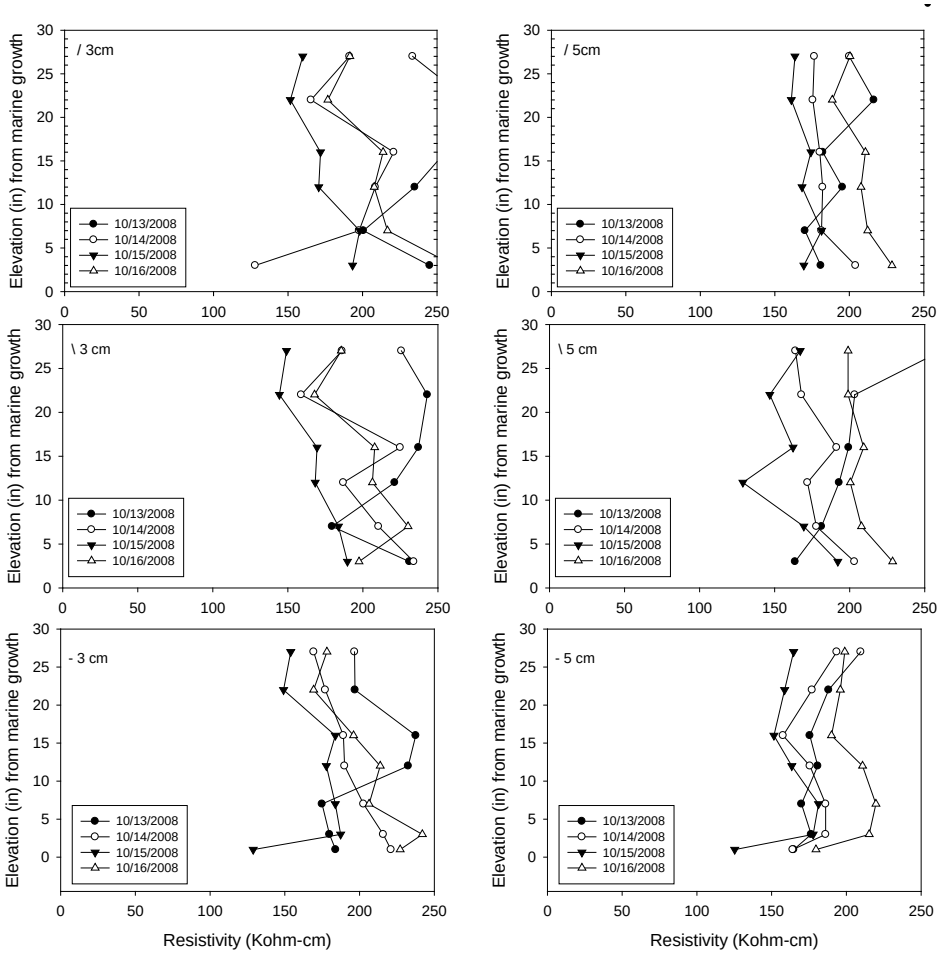

Figure F.7: Results of ρ vs. elevation for FA. Bridge #136502

.

In Figure F.8a, SR profile for concrete with SF, it can be seen that a strange case is presented when the initial set of values of SR is the lowest in comparison with the following days. However, for the second, third and fourth days, SR measurements were stable in the range between 100 kΩ-cm and 160 kΩ-cm, which suggest that a transient resistivity layer was created on the surface of the concrete. Figure F.8b shows the moisture profile under conditioning during 68 hours.

#136502 KRB – Bent 2 Pile 3

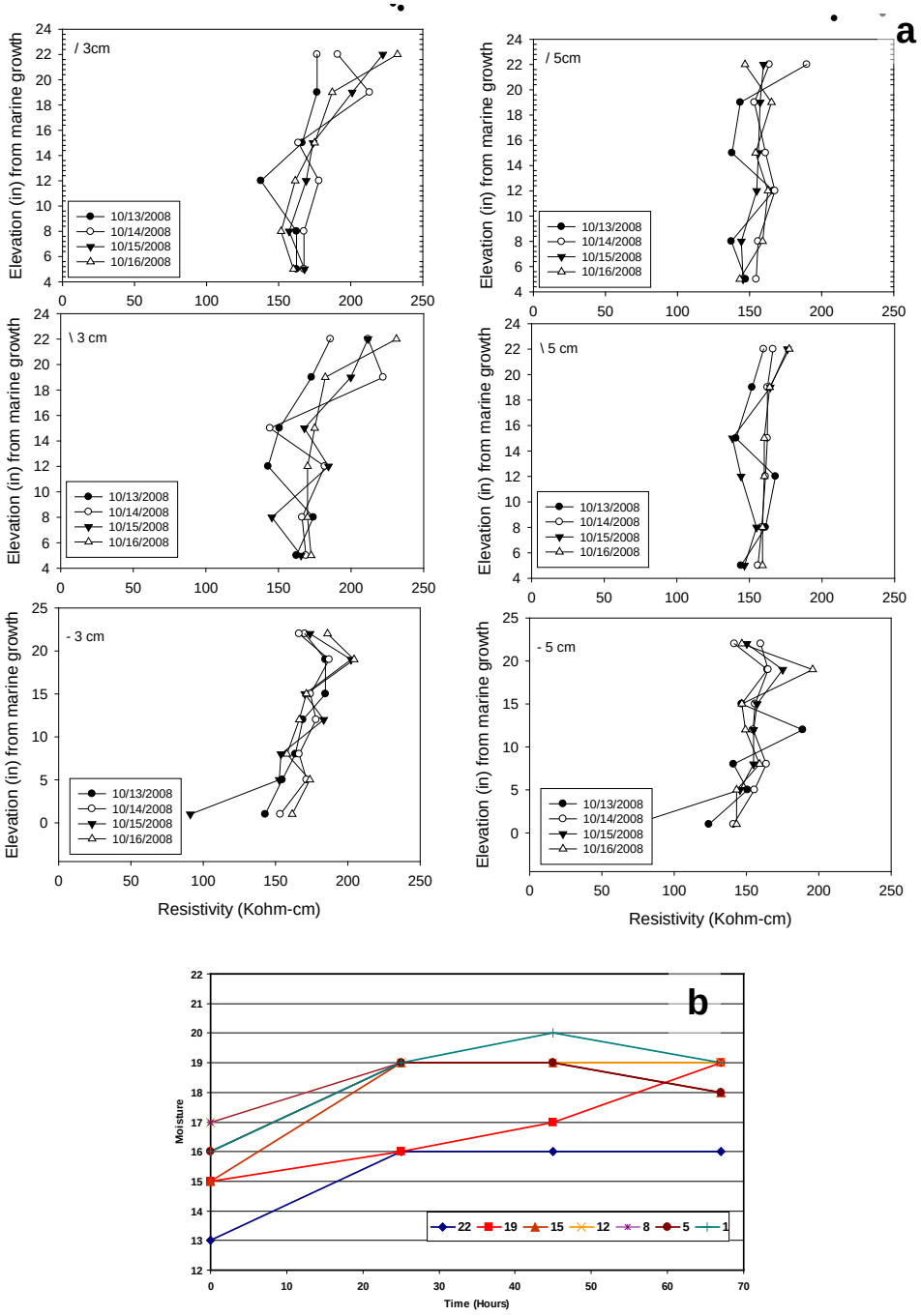

Figure F.8: Results of ρ vs. elevation and moisture vs. time for SF. Bridge #136502.

SR profile for concrete with blast furnace slag (BFS) is shown in Figure F.9a. The resistivity on the first day was lower than the rest of the days. From the second to the last set of measurements, SR values were stable with good reproducibility. However, the behavior of moisture after 68 hours shown in Figure F.8b indicates that moisture for

different elevations was not stable, and in some cases decreased, instead of increasing or reaching stable values. As moisture readings changed every day, it is possible that the container was not full all days of the conditioning period.

#136502 KRB – Bent 2 Pile 4

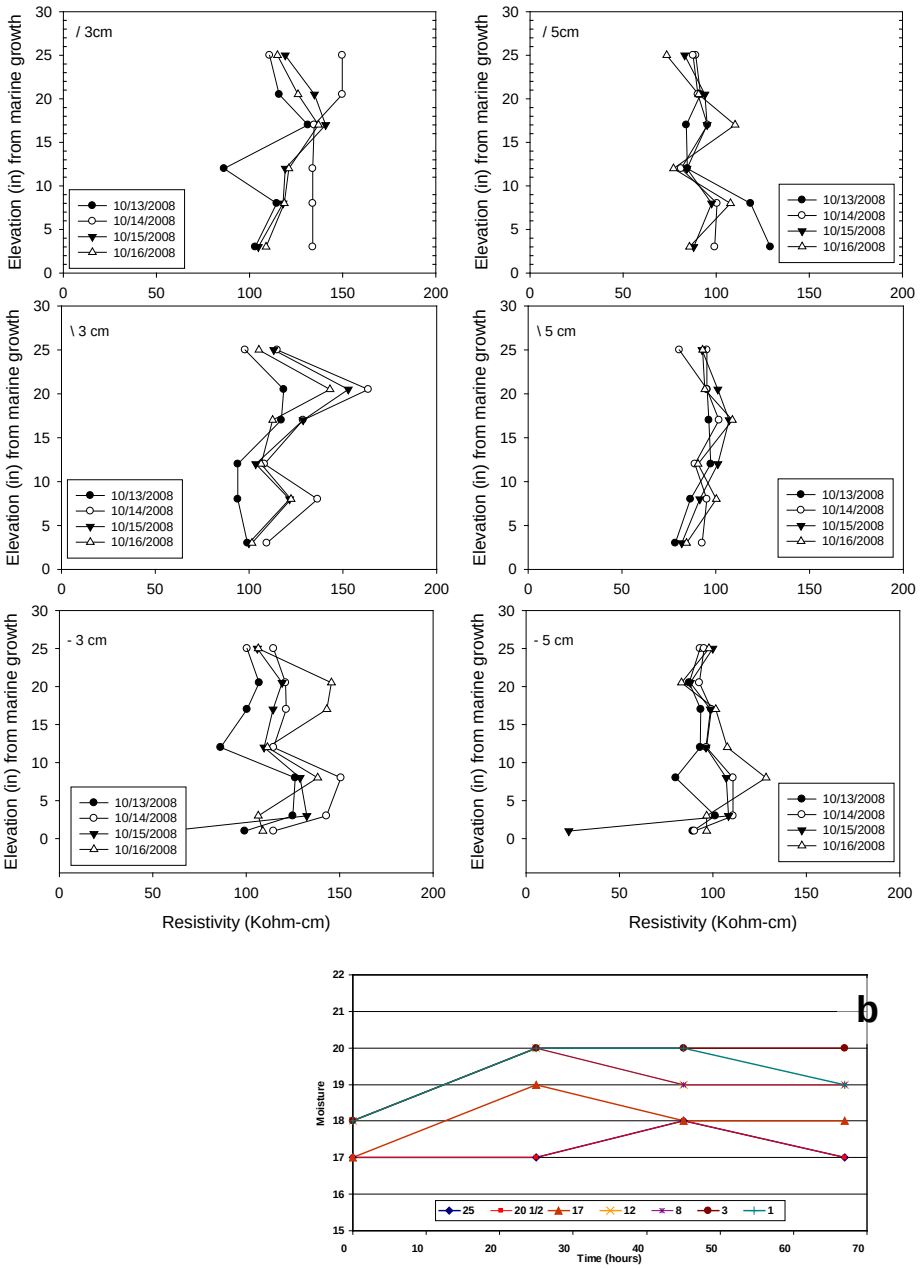

Figure F.9: Results of ρ vs. elevation and moisture vs. time for BFS. Bridge #136502.

Measurements of piles with BFS showed the lowest SR values when compared to the measured SR values on concrete piles with UFA, FA and SF. The measured SR

values for BFS with a=5 cm spacing were in an approximate range between 75 kΩ-cm to 100 kΩ-cm, while for the other concrete mixtures, the measured SR values were higher than 110 kΩ–cm.

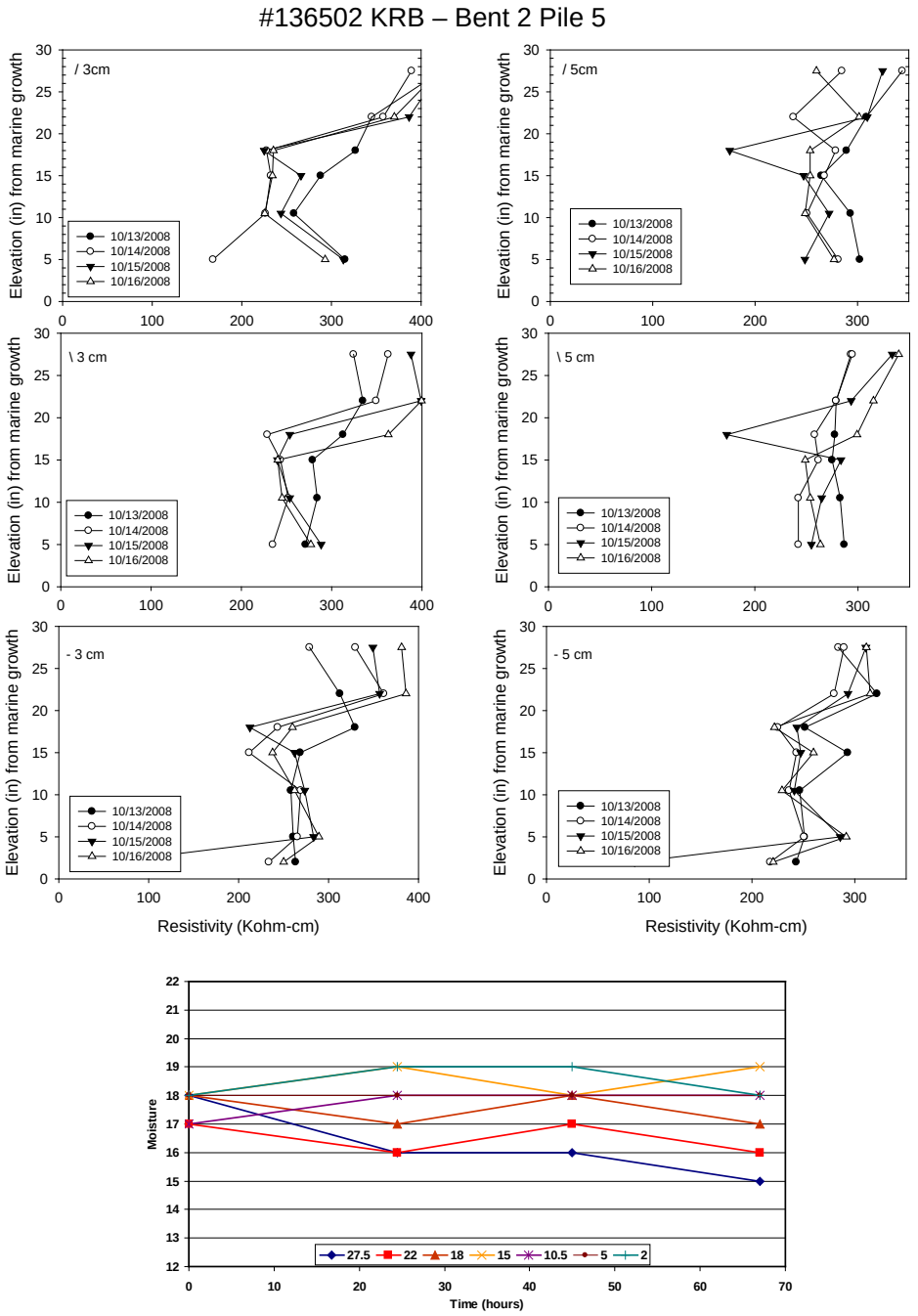

Figure F.10: Results of ρ vs. elevation and moisture vs. time for MET. Bridge #136502.

SR profiles and moisture content on concrete piles with MET are shown in Figures F.10a and b. The SR values measured on this pile presents the highest resistivity values when compared with the other four HPC concrete of this Bridge on bent 2.

The results presented show how SR measurements vary when the moisture of the concrete is altered, and how the measured resistivity changes as a function of elevation. Readings of moisture content, on surfaces made of different mix composition, indicate that for this ~3 year-old bridge, low permeability (related to high density and good pore control of concrete) does allow the water go into the concrete just close to the surface.

5.2.1.2 Bridge #136502 – SR_{wet} measurements on two-inch cores

At least one concrete core per pile was selected to be placed in a high humidity chamber. Two different measurements were taken on these two-inch cores: 1) resistivity measurements along the longitudinal direction of the concrete core SR_{wet} vs. time, and 2) weight percent change vs. time. The weight percent change referred to the initial weight was calculated and is the value reported. These measurements started about a week after being collected from the field which might have allowed the cores to get drier when compared to field conditions. It was expected that the measured SR_{wet} would show a high resistivity value for the initial day as the concrete was relatively dry, then SR values would drop as the moisture increased until it stabilized due to increased moisture content. Additionally, due to the high moisture condition, it was expected that resistivity would decrease, and the cores would gain weight. Figures F.11 to F.16 show results for cores obtained from fender piles with the different concrete mixes: UFA, FA, SF, BFS, MET and OPC.

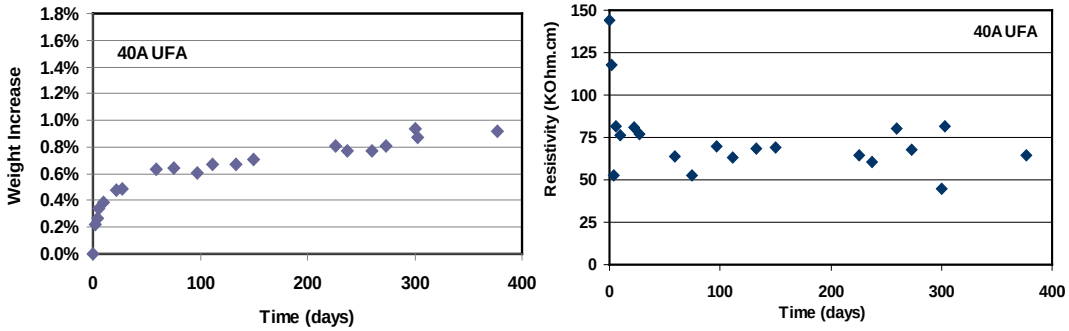

Figure F.11: Results of Weight increase (%) vs. time, and SR_{wet} vs. time, for concrete with UFA. Bridge #136502.

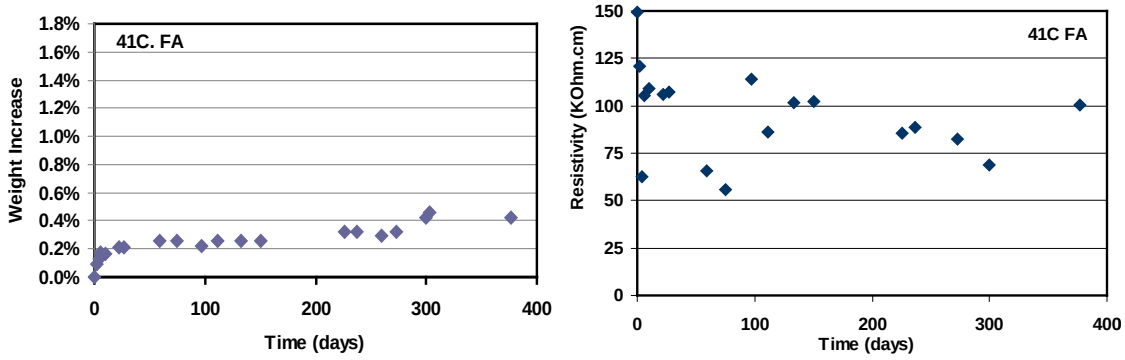

Figure F.12: Results of Weight increase (%) vs. time, and SR_{wet} vs. time, for concrete with FA. Bridge #136502.

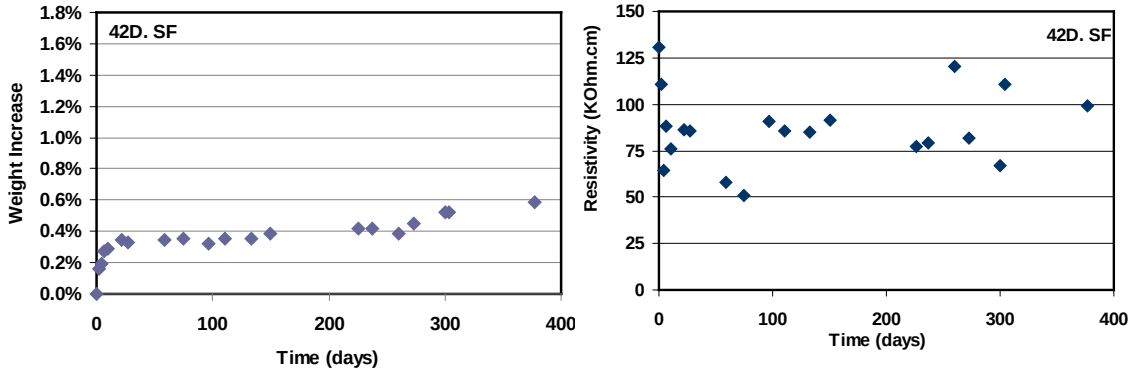

Figure F.13: Results of Weight increase (%) vs. time, and SR_{wet} vs. time, for concrete with SF. Bridge #136502.

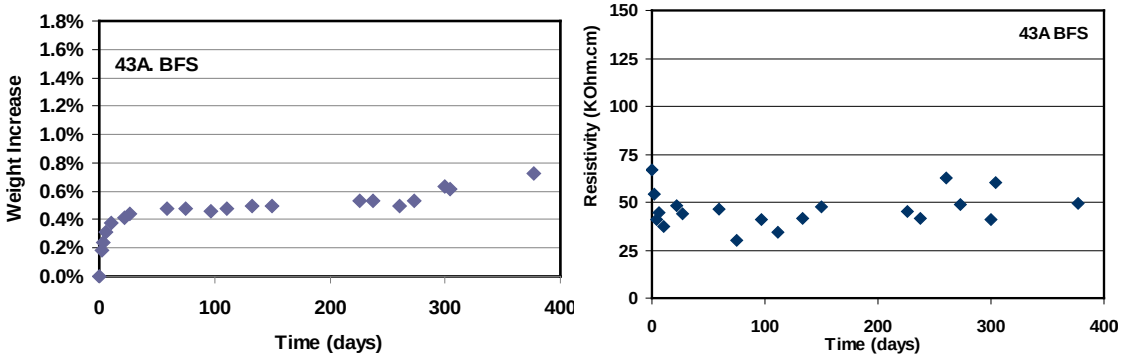

. Figure F.14: Results of Weight increase (%) vs. time, and SR_{wet} vs. time, for concrete with BFS. Bridge #136502.

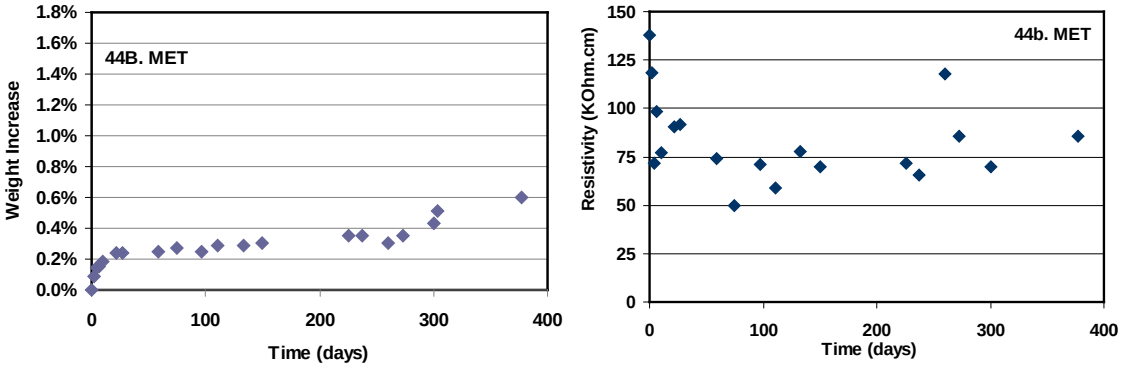

Figure F.15: Results of Weight increase (%) vs. time, and SR_{wet} vs. time, for concrete with MET. Bridge #136502.

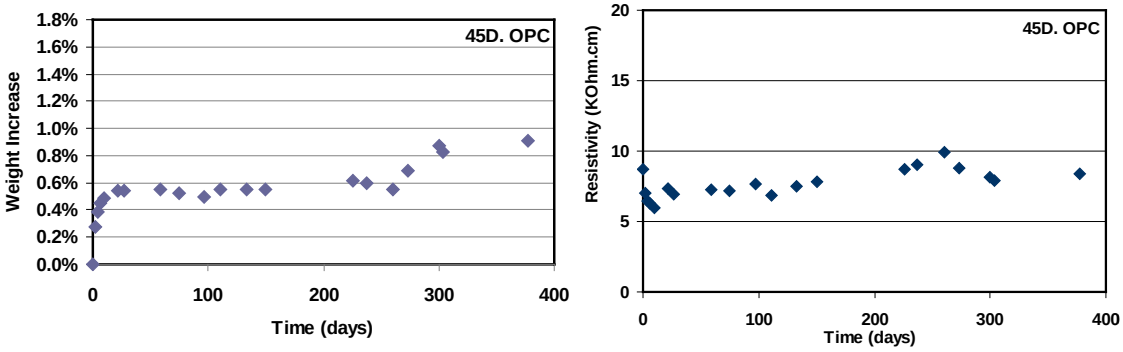

Figure F.16: Results of Weight increase (%) vs. time, and SR_{wet} vs. time, for concrete with OPC. Bridge #136502.

5.2.1.3 Bridge #136502 - SR_{wet} Discussion

The results of resistivity in concrete with UFA shown in Figure F.11 show SR_{wet} values vs. time. The initial SR value measured was 140 kΩ-cm and it monotonically

decayed until it reached a minimum SR_{wet} value of 70 kΩ-cm. The weight increased until reaching a weight percentage change of 0.9%. Thus, for moisture content increase there is a corresponding reduction in the SR_{wet} value measured. For all the mixtures in this section, the maximum weight increase reached is a relative weight increase that the depends on the initial degree of saturation.

Figure F.12 corresponds to cores with FA where the initial resistivity value was 150 kΩ-cm and had a final average value ~80 kΩ-cm. The total weight increase was ~0.4%. For the case of concrete with SF shown in Figure F.13, the initial resistivity was 130 kΩ-cm and the final average was ~75 kΩ-cm, with a total of 0.4% variation of the weight at day 250.In the case of concrete with BFS, shown in Figure F.14, initial resistivity values were lower when compared with UFA, FA, SF and MET. The initial SR measured value was 70 kΩ-cm, and was ~35 kΩ-cm for high moisture content conditions. Again, it can be seen that resistivity values decrease while the weight increment reached 0.6%.

The results for concrete with MET, in Figure F.15, present a light variation of resistivity values after day 60 but with a tendency to become stable. When dry, the core registered a resistivity value of 140 kΩ-cm and the average for saturated conditions was 70 kΩ-cm. The weight in the core increased 0.4% by day 250. Finally, concrete with OPC, shown in Figure F16, presented the lowest resistivity measurement values starting with just 9 kΩ-cm for initial condition and 7 kΩ-cm when wet, and also the second highest increment of weight in comparison with the other five mixes with 0.7%.

Figure F.17 combines resistivity values vs. percentage of weight increased for the six different concrete mixtures. Thus, it is clear that electrical resistivity decreases when the moisture of concrete is increased. Concrete with FA, SF and MET had similar results with respect to weight increase and resistivity, while concrete with UFA showed the highest increment of weight, reaching a 0.80% change. Also, concrete with BFS has moderate-resistivity values with an intermediate increment in weight percent (0.55%), and OPC got the lowest resistivity measurements combined with a relatively high

increase in weight. It is important to note that these are relative weight increases since the concrete cores were not oven dry, as it was important to keep the initial conditions.

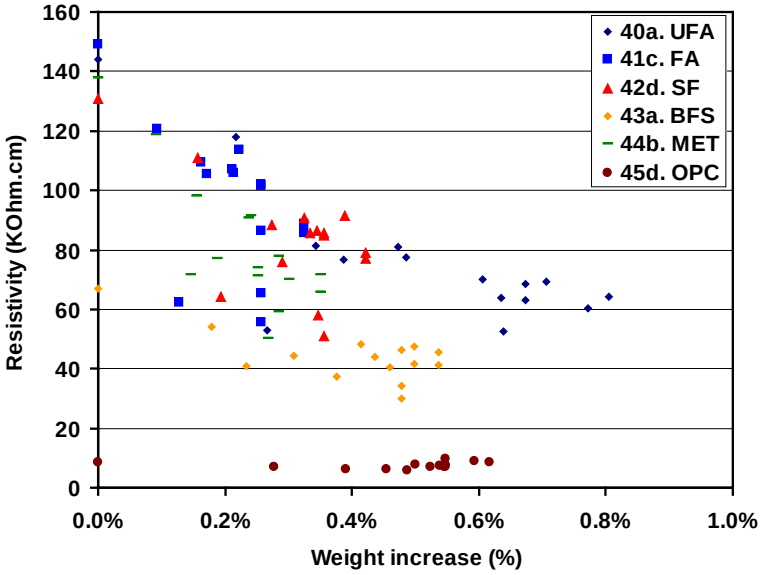

Figure F.17: SRwet vs. Weight increase for six different concrete mixes.

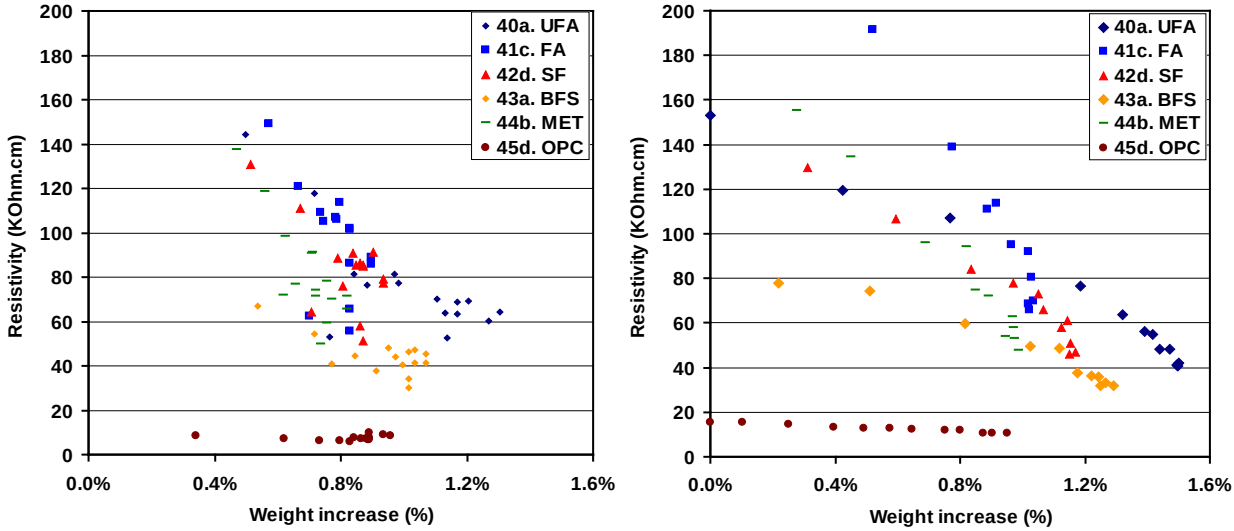

Figure F. 18: SRwet vs. Weight increase for six different concrete mixes. Left plot updated F16 and plot on the right after second weight increase cycle

A group of cores was selected to be dry and subjected to a second cycle in the high relative humidity exposure condition. Drying consisted of placing the concrete cores for two days in a 38 ºC room, then for 20 hours in an oven at 60 ºC so as to minimize any microstructure changes. Figure F.18 shows two plots. The plot on the left corresponds to an updated Figure F.17 but with the weight increase calculated relative to the drier

weight. The plot on the right corresponds to the weight increase and SR_{wet} measured during the second cycle in the high humidity chamber. A better ranking can be observed from this plot. UFA gained the most weight ~1.5% with a SR_{wet} value of 40 kΩ-cm; followed by BFS which gained ~1.3% which had the lower SR_{wet} (SR_{wet}=32 kΩ-cm) of the five HPC mixtures. Samples with SF and MET had similar SR_{wet} of ~47 kΩ-cm, with SF gaining 1.2% weight and MET gaining 1%. The sample with FA had a SR_{wet} of 66 kΩ-cm and a weight increase of 1%. The sample with only OPC gained 0.95% and a SR_{wet} of 10.6 kΩ-cm.

5.2.1.4 Bridge #136502 Chloride Concentration for Two-Inch Cores

In Table F.9, the chloride diffusivity fitted to the chloride profiles obtained on the two-inch cores is presented for the six concrete mixes. The diffusivity values shown are the average of three diffusivity values. The minimum chloride diffusivity was recorded for Metakaolin with 1.14E-09 cm^2/s followed by the FA with 1.42E-09 cm^2/s showing low permeability. Diffusivity values calculated for concrete with UFA, SF and BFS are in an intermediate range of diffusivity after 2 to 3 years since having been built. Concrete with BFS has the highest chloride diffusivity of the HPC mixes. Concrete with OPC showed the highest chloride diffusivity with 4.92E-09 cm^2/s confirming the higher permeability and lower resistivity values. Still, the diffusivity is relatively low due to the low water cement ratio (w/c) used in the mix.

Table F.9: Chloride Diffusion for OPC and HPC mixes.

Concrete	D cm^2/s
UFA	2.19E-09
FA	1.42E-09
SF	2.64E-09
BFS	2.84E-09
MET	1.14E-09
OPC	4.92E-09

5.2.2 Bridge # 700203 - Turkey Creek Bridge

5.2.2.1 Bridge # 700203 - Resistivity Profiles –- Turkey Creek Bridge

Figure F19 shows the resistivity profiles obtained for Bridge #700203, bent 5 pile 14. Resistivity profiles are shown in two columns. The three plots on the left correspond to measurements performed using a=3 cm and the three plots to the right correspond to measurements with a=5 cm. Each plot corresponds to a different orientation indicated by the direction of the line on front of the electrode spacing label (/ top plot, \ middle, -- bottom plot). The resistivity values shown have been normalized to 21 ºC, but no cell constant corrected (either for geometry or rebar presence). In all the plots of Figure F.18, there was a decline in the apparent resistivity values measured from day 0 to day 1, an additional decline from day 1 to day 2, and an additional decline from day 2 to day 3. This pattern was not found when comparing profiles from day 3 to profiles from day 4. Rain took place between days 3 and 4 that likely modified the moisture conditions of the concrete surrounding the set-up.

5.2.2.2 Bridge # 700203 - Turkey Creek Bridge- Moisture Profiles

Figure F.20 shows typical moisture profiles measured before taking the daily surface resistivity readings during the field trip to the Turkey Creek Bridge. The initial readings could have been significantly affected by the predominant weather previous to day zero. This is somewhat monitored by the moisture meter readings. The measured moisture values were between 12-13 on the initial day and increased to values between 16 and 17 after one day. After three days, the moisture values ranged between 17 and 20 suggesting that the highest moisture value was observed then.

#700203 Turkey Creek – Bent 5 Pile 14

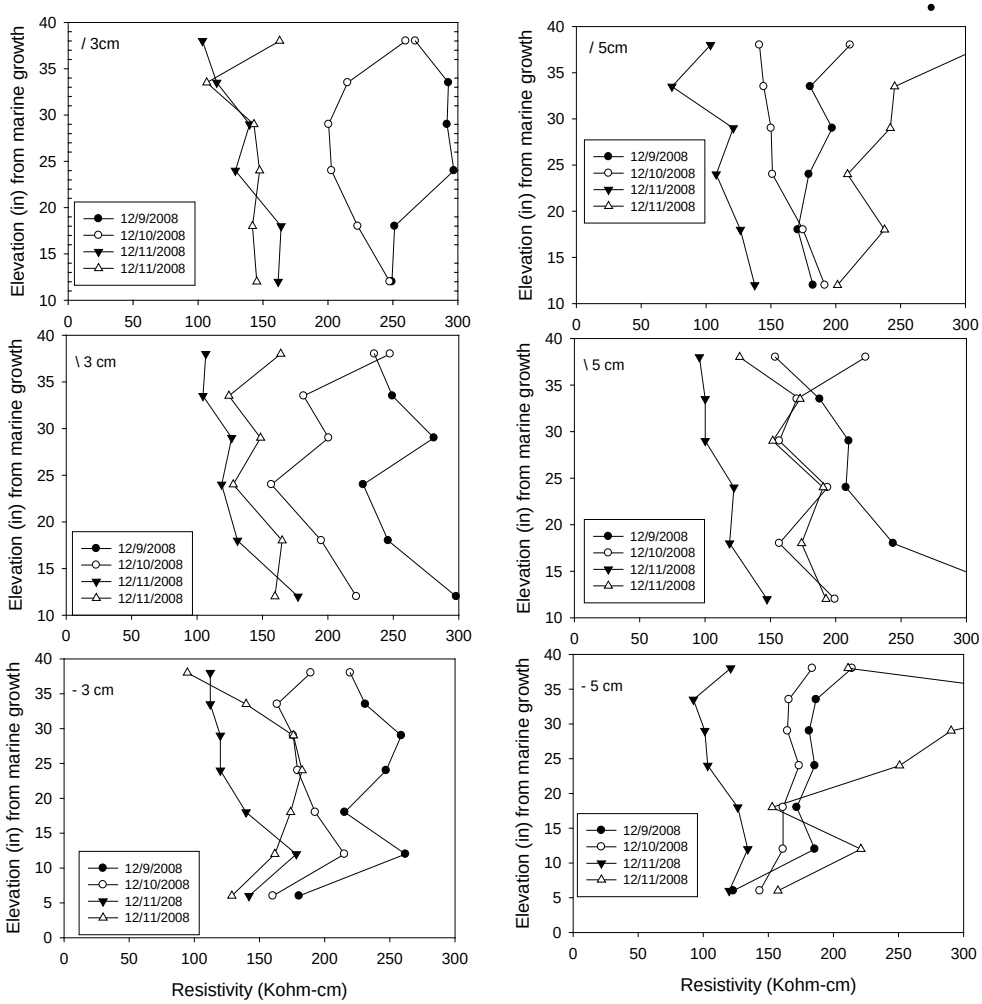

Figure F.19: Results of ρ vs. elevation for Bridge #700203.

Elevation (m)

Figure F.20: Moisture vs. time for Bridge #700203

5.2.2.3 Bridge # 700203 - Turkey Creek Bridge - SRwet on two-inch cores

Figure F.21 shows the SR_{wet} vs. time and weight gain on a core from Bridge #700203. These results are divided into two different sets of measurements. The first set was performed up to day 100 when the core was removed from the high humidity chamber. Up to day 100, a monotonic decay of the normalized resistivity values was observed, accompanied with an increase in weight. It was decided to place the core back in the high humidity environment on day 150. During the 50 days not in the chamber, the core was store in a Ziploc bag and in contact with laboratory temperature and humidity. The specimen dried some, but did not returned to the initial moisture content. The weight and SR measurements on day 150 reflected an increment of resistivity and a reduction of weight. After 50 additional days in a high humidity environment, relatively stable values of resistivity and weight were recorded.

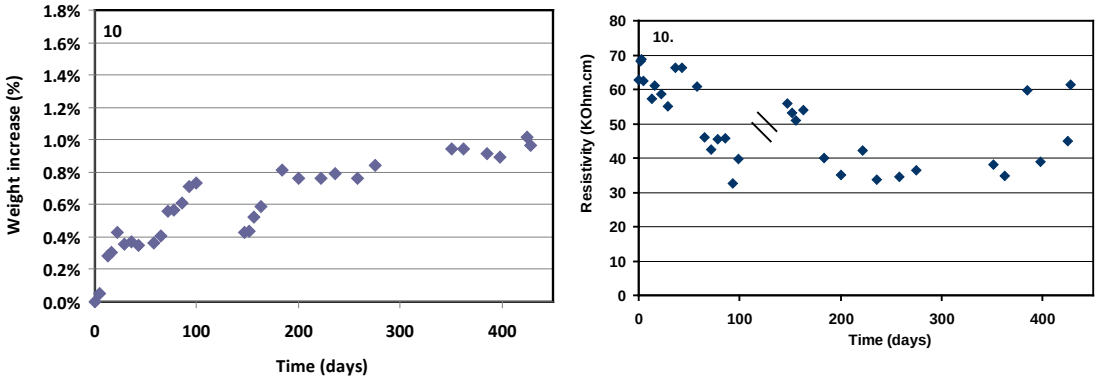

Figure F.21: SR_{wet} vs. Time and weight increase percentage vs. time for Bridge #700203.

From the field profiles shown in Figure F.19, high SR measurements and low moisture increase registered with the moisture meter suggest a concrete with low permeability. A relevant difference was observed between the SR measured values obtained with the two different spacings in dry conditions, while at later days in higher moisture content conditions, this difference is reduced significantly.

The concrete core exposed in a high humidity environment experienced, during the first 80 days, an evident reduction of resistivity and an increase in weight. Recall that the core was removed from the high humidity chamber. Thus, the reading on day 150 registered a high resistivity value and a loss of weight. It took 50 days to increase the moisture content to those observed on day 50; thereafter, relatively stable values were recorded. The chloride diffusivity from a core from this pile was $5x10^{-10}$ cm^2/s and the average apparent diffusivity for this Bridge was $1.8x10^{-9}$ cm^2/s.

5.2.3 Bridge # 700-006

5.2.3.1 Bridge # 700-006 - Resistivity Profiles

The Bridge called US-1 Crane Cr. & City St (known as C. Creek), is located in Melbourne, FL. It was built in 1959 with reconstruction of some piles in 1990. It is assumed that the original concrete was OPC due to the age of the bridge. The SR profiles for bent 5, pile 14 plotted in Figure F.22 show a progressive drop in the SR measurements during the four days under the conditioning. Again, SR profiles are plotted in two columns, where the left column shows results for spacing a=3 cm and the right column shows spacing of a=5 cm. Resistivity measurements are more stable using spacing 5 cm during the first three days with no significant alterations or sudden changes.

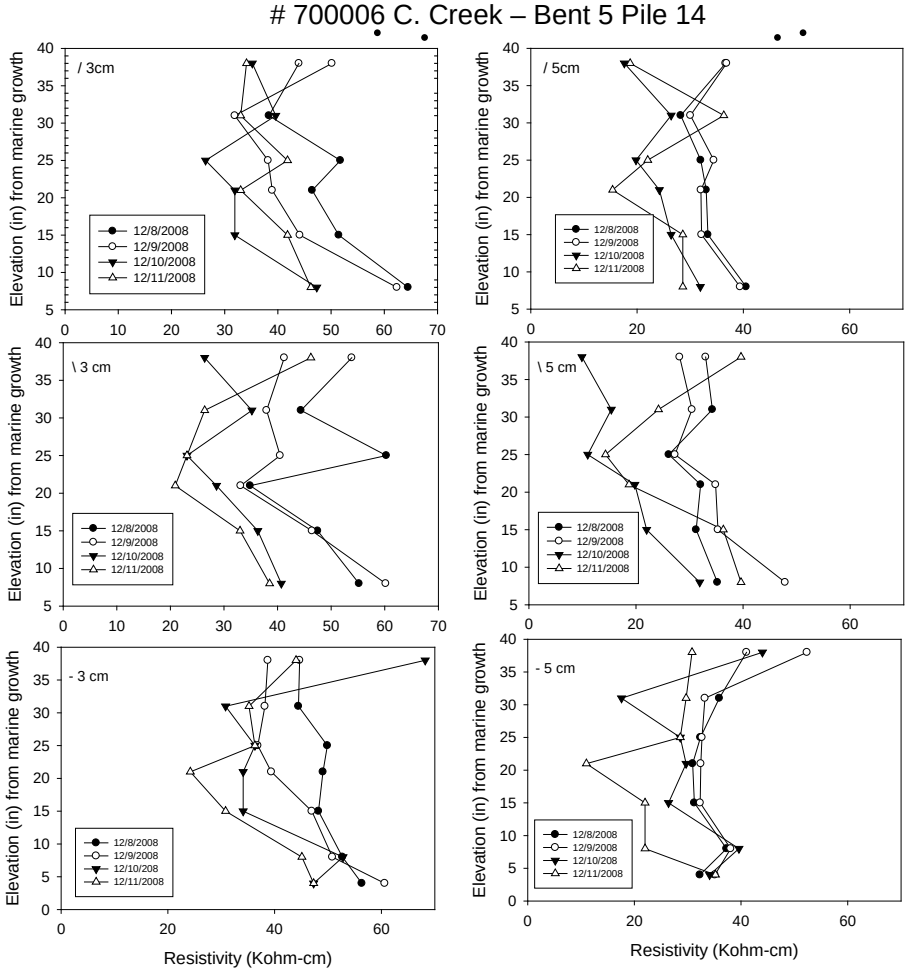

Figure F.22: Results of ρ vs. elevation for Bridge #700-006.

The surface moisture readings are shown in Figure F.23. The initial measurements of moisture at day one indicate relatively high values starting on 15 and 16 out of a maximum 20. From the second day of readings and the rest of the days, the moisture content reached the maximum values on the scale of the moisture meter showing that absorption close to the surface is high, and also confirming that OPC concrete gains moisture faster than other concrete mixtures. The moisture level remained high after two and three days.

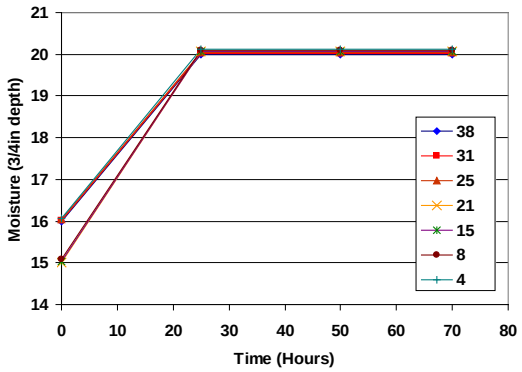

Figure F.23: Moisture vs. Time for Bridge #700-006.

5.2.3.2 Bridge # 700-006 SRwet on two-inch cores

From Figure F.24 it can be seen that a stable plateau for the normalized wet resistivity was achieved around 18 days and remained relatively stable for the remainder of the monitored time. Also, it indicates the change of weight becoming stable from day 20, with a weight change percent greater than 1.2%. The apparent diffusivity calculated from the chloride concentration profiles was 1.94 x10^{-9} cm^2/s.

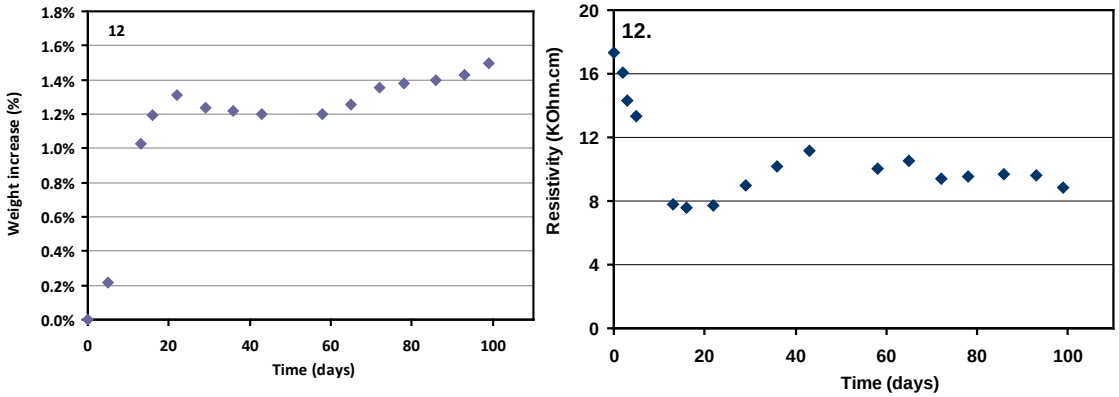

Figure F.24: SR_{wet} vs. Time and Weight increase % vs. Time for bridge #700-006.

Typical results for an 18-year old rebuilt OPC bridge were shown above (assuming that the examined piles were the ones of the re-built ones). In the first two days of measurements, SR_{field} values do not have a significant reduction when seeing the results for the horizontal orientation of the probe at low elevations and spacing 5 cm. For the third day, a reduction of SR_{field} values is more evident. On the last day of

measurements, an unstable behavior of SR values was found, where for 0 (horizontal) and 135 degree orientation of the Wenner probe with a=3 cm, resistivity shows the lowest values, while for 45 degrees, resistivity values increased more than the third day. This case is also found, for spacing 5 cm, when measured at 135 degrees, but not for 0 and 45 degrees. The moisture meter reached the maximum values from the second day. The same rain event that was described for Bridge #700203 also affected Brige #700006, as they were visit during the same field trip.

From the SR_{wet} on the cores, the weight was stabilized after 20 days in high humidity exposure, and SR_{wet} values reached a plateau. In general, this 18-year-old structure presents good condition showing relatively low resistivity values and a low chloride diffusivity.

5.2.4 Bridge # 720249

5.2.4.1 Bridge # 720249. SR_{field} visited during summer time.

Typical SR profiles for Bridge #720249 are shown in Figure F.25. This bridge, called Buckman Bridge, was constructed in 1970 with OPC. Results shown correspond to bent 123, pile 3 on the west face of column during summer time for four consecutive days. On Figure F.25, the left column corresponds for spacing a=3 cm (1.18in). It can be seen that SR measurements did not vary significantly compared to the first set of measurements with those on the fourth day. Measurements during the last day could not be taken for the first two elevations at 12.7 and 21.59 centimeters (5 and 8.5 inches) above the marine growth due to a high tide incident which covered these two measurement points. A special case is presented for the results for spacing a=5 cm (1.96in), where measurements during first day, without conditioning, are the lowest for SR when compared with SR measurements taken on other days. SR measurements taken on the second, third and fourth days have almost identical values. It is believed that no rain had fallen before the first set of measurements. Again, an assumption of a new layer due to water could be the reason for the opposite resistivity values.

#072109 - Buckman WB - Bent 123 Pile 7

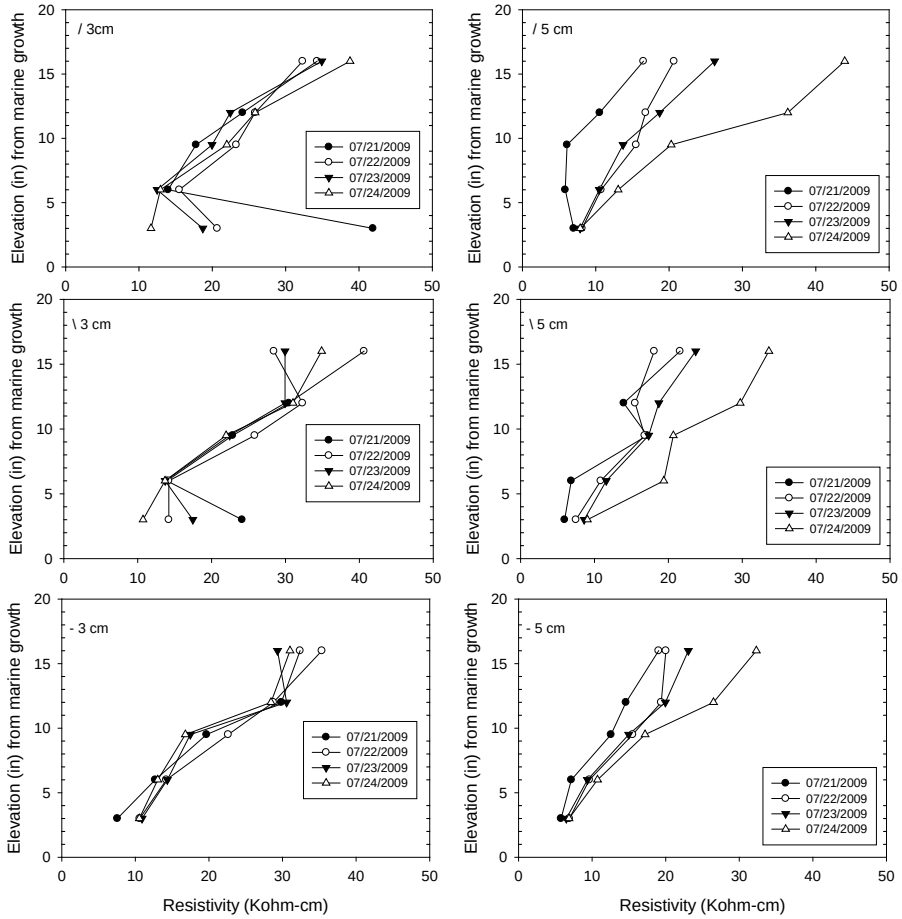

Figure F.25: Results of ρ vs. elevation for Bridge #720249.

The profile of moisture vs. time shown in Figure F.26 suggested an increase of moisture with time reaching the maximum value of 20 after one day.

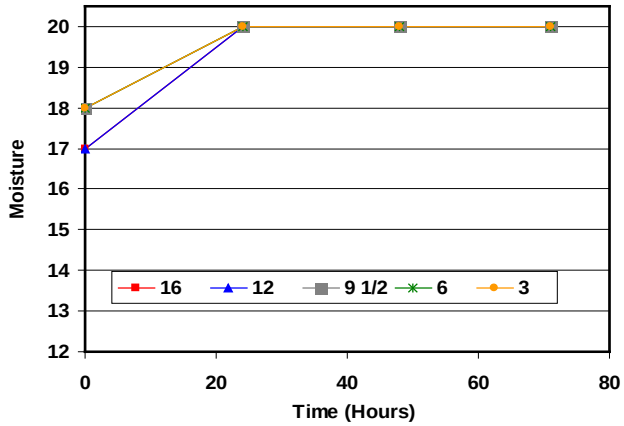

Figure F.26: Moisture vs. Time for Bridge #720249.

5.2.4.2 Bridge # 720249 SRwet on two-inch cores

Figure F.27 shows the results for the normalized resistivity vs. time, and weight percent increase vs. time for the selected core taken from Bridge #720249**.** Resistivity values reached a plateau after day 10 with SR_{wet} of 4 KΩ-cm, and also saw the stabilization of the percentage of weight increased. The calculated apparent diffusivity was 5.7E-08 cm^2/s. It is notable that the moisture increase corresponded to a weight change of ~3.2% by day 300. These three values suggest that this structure likely has a high permeability and consequently the concrete quality is low.

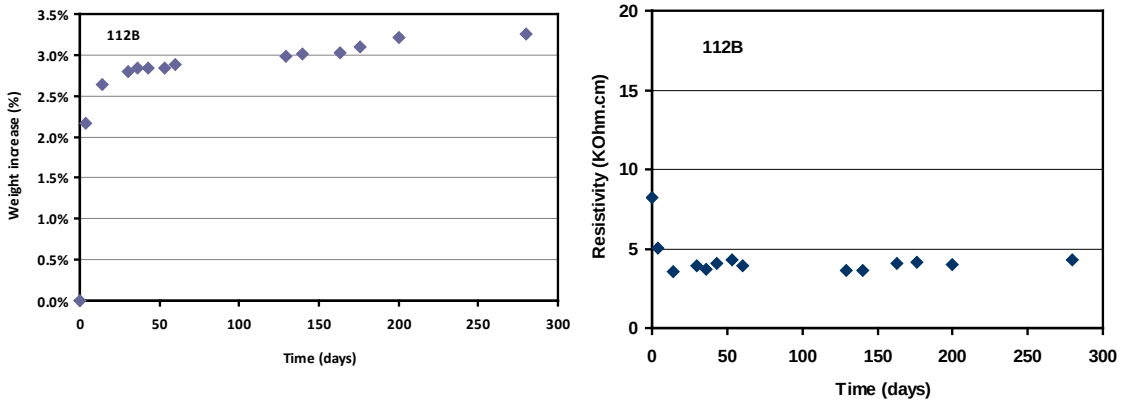

Figure F.27: SR_{wet} vs. time and, weight increase percentage vs. time for Bridge #720249.

A combination of relatively low SR values from the field, low SR_{wet} values from cores, plus the high increment of weight under high humidity exposure and high chloride diffusion indicate a highly permeable concrete.

5.2.5 General Comments - SR Profiles

The following paragraphs describe the general findings for SR_{field} profiles. The SR measurements conducted just above the marine growth (shown as elevation 0 inches) were quite reproducible, and were consistently smaller SR values in most instances with respect to each column/pile. The spread on the observed SR values at higher elevations was significant, particularly at day zero. For cases in which concrete was initially significantly dry, and after two or three days with the conditioning set up, the SR values observed at all elevations were lower than initially-measured SR and also were

very similar. This trend suggests a somewhat uniform moisture increase of the concrete closer to the surface at all elevations tested.

SR values as high as 800 kΩ-cm were recorded (the bridge component with this measured value is included in the SR profiles in Appendix 5). The profile corresponded to a structure visited during the winter time and which was protected from the environment. A combination of low moisture content, high performance concrete and low temperature affected the SR value obtained. Hence, the field results were affected by the temperature, humidity and other weather related conditions (e.g., rain).

Wether a concrete element was subjected to partial shade or not, orientation (predominant winds), could also affect measurements. The face of the element exposed to the sun longer would likely have a drier concrete. Note that from the SR field data, values of 20 to 40 kΩ-cm might indicate that the concrete is not HPC but rather OPC, particularly if concrete had moderate moisture content. Concrete with HPC usually had a value larger than 70 kΩ-cm when not saturated. During the different visits it was realized that when visiting older structures it was difficult to find a bridge component with a smooth surface. It is likely that the concrete surface had degraded due to wind, splash or other type of wear.

Rain during a field visit appears to skew the measured SR values toward higher values. It is possible that a wet thin layer all over the concrete creates an increase in the area examined. In some instances, the minimum SR profile values (i.e., minimums corresponding to each elevation) were measured during day 0, and it was speculated that rain or tide conditions were significantly different on day 0 than on the subsequent days. Thus, a careful record of the weather preceding and during the field evaluation is important when analyzing the measurements.

5.2.6 General Observations Regarding Moisture

In some cases, the maximum moisture was registered during day 0. On one occasion, SR profiles were recorded on the same footer at two close-by parallel locations, one with, and the other one without, the set-up. The SR measured decreased at the higher locations of the profiles with the set-up on subsequent days, whereas it remained large for those with no conditioning container. At the lower locations, the SR values were lower for the case with no set-up; it is not clear why this occurred. One possible explanation is that due to the set-up present, some of the water was transported toward the higher locations. The location with no set-up, although close to the location with set-up, might have experienced different environmental exposure resulting in more saturated conditions at the lower locations of the examined area, hence, the lower SR values measured.

Additional alternative conditioning methods should be investigated that allow for a faster and more uniform moisture increase of the area to be examined, but at the same time isolate it from the surrounding concrete that might adversely influence the measurements. From laboratory measurements, it was also learned that waiting a few minutes could prevent skin resistivity. In the lab, it was found that waiting 30 minutes was best, but this amount of time might be too long for field implementation. Another way to improve is to empty the container by using a pump rather than just removing the container, to prevent wetting the surrounding concrete. (This last comment might not be as important if all concrete is close to saturation).

This report, besides presenting findings on how D_{Cl} correlates to SR measurements, will describe some relevant factors that should be recorded in field visits. Whenever possible, measure the water temperature, air temperature and also the concrete surface temperature. If possible, obtain recent weather conditions preceding the visit. A concrete moisture meter could provide an idea of the moisture content of the concrete closer to the surface. Particularly note if it has rained, as this significantly affects the SR value measured. It might be interesting to record in what part of the tidal cycle the visit is taking place, and how far/close the water level is from the marine growth mark (or

MWL). If the moisture reading is less than 12, it might be ok to only perform measurements at 5 cm spacing; however, if the reading is higher then it would be important to measure resistivity using additional electrode spacings of a =2 cm, a =3 and possibly a=7.5 cm spacing. Using additional electrode spacings allow a better understanding of the SR values at different depths and thus a better estimate of the bulk resistivity underneath can be obtained. An additional practice is to use a rebar meter to try to minimize reading above the reinforcing steel, particularly if the cover found is 5 cm or less, as the SR value measured would be lower than the bulk resistivity.

5.2.7 General Observations concerning SRwet on 2 in cores

How affected the resistivity is due to the temperature depends upon the concrete composition and the degree of water saturation. Measurements on the samples obtained from the field suggest that the higher the bulk resistivity, the larger the possible oscillation on the value measured. These oscillations were more pronounced during the winter time, where the room temperature and humidity fluctuated more than the rest of the year. This could be due to a combination of several factors; temperature probably was the main factor. For the days in which the laboratory temperature and the laboratory RH were both low, then a thin drying-concrete layer at the surface of the sample would tend to dry faster on HPC samples (as there is a smaller amount of water in the less permeable concrete, and wicking might be accelerated by the smaller size of the pores)than concrete samples with only OPC.

Figure F.28 shows additional cores that were subjected to a second high humidity cycle that followed the drying of the concrete. Each plot in Figure F.28 shows how SR_{wet} relates to the increase in moisture content measured by weight percent increase (M%). The plot on the top row shows the cores with the largest terminal SR_{wet} and most of them have maximum M% smaller than 1%. The final SR_{wet} ranged between 50 kΩ-cm and 100 kΩ-cm. The middle plot shows SR_{wet} for cases that had an intermediate SR_{wet}. The final SR_{wet} ranged between 20 and 70 kΩ-cm for this group. The maximum M% ranged between 1% and 2.2%. Finally, the cores with the lower SR_{wet} had final values

that ranged between 5 and 12 kΩ-cm. In this group, three of the cores reached M% between 3% and 4%.

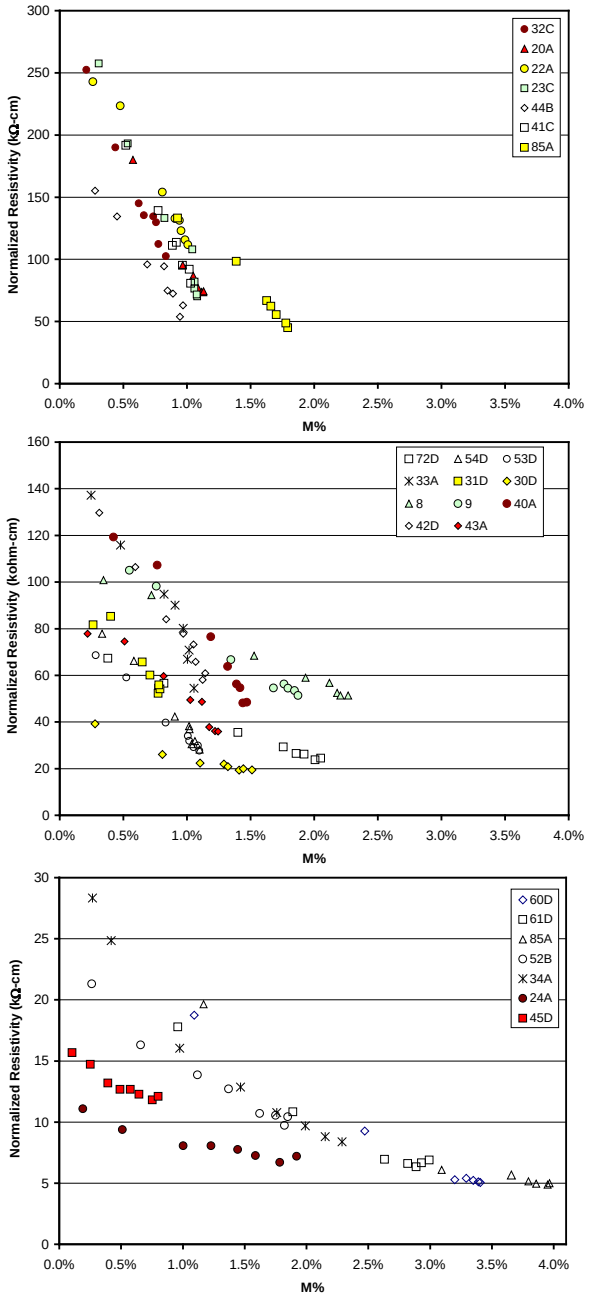

Figure F.28: SR_{wet} vs. Weight increase (M%) for selected cores after second weight increase cycle.

5.3 Summary of Results (D_{Cl}, SR_{field}, SR_{wet}, C_s, C_o)

5.3.1 Wet Resistivity vs. Minimum Field Resistivity

The minimum field resistivity values (SR_{field}) (one for a=3 cm and another for a=5 cm) were obtained from within the profile values measured after at least one day with the set-up on a given component, usually from the upper portion of the profiles. The corresponding normalized wet resistivity value measured on a concrete core from the same component was used to compare wet resistivity vs. field resistivity values.

Figure F.29 compares the normalized wet resistivity vs. the minimum measured field resistivity values for both a=3 cm and a=5 cm. The plot on the left shows both axes in linear scale, whereas the plot on the right shows the axis in a log-log scale. It is apparent that there is no one-to-one relationship between SR_{field} and SR_{wet} values. One-to-one relation is only found for a few of the concrete mixtures with low resistivity values; additionally, a good number of pair-values showed a less steep slope. The surface resistivity minimum value from the field measurements is usually higher than the wet resistivity. This is likely due to mass transport limitations encountered in the conditioning set-up. The concrete resistivity (from the surface into the concrete) as a function of the depth in the field is likely significantly different than SR_{wet} from the cores. It usually took ~10 days to reach the minimum/plateau on the wet resistivity measurements on concrete with SR_{wet}<10 kΩ-cm and >20 days for concrete cores with SR_{wet}>20 kΩ-cm. This suggests that a longer period of time is needed to reach saturation in the field, but probably this is not practical to implement. The water transported into the concrete in the field set-up is probably not constrained to the area covered by the container. Moreover, the SR_{field} values were not cell constant corrected (as the geometry and concrete cover varies from element to element). An updated set-up could be a two-chamber combination. The two chambers would be filled with water, with the inner chamber designed to withstand vacuum. This alternative set-up might expedite the water transport and could be part of a future research project.

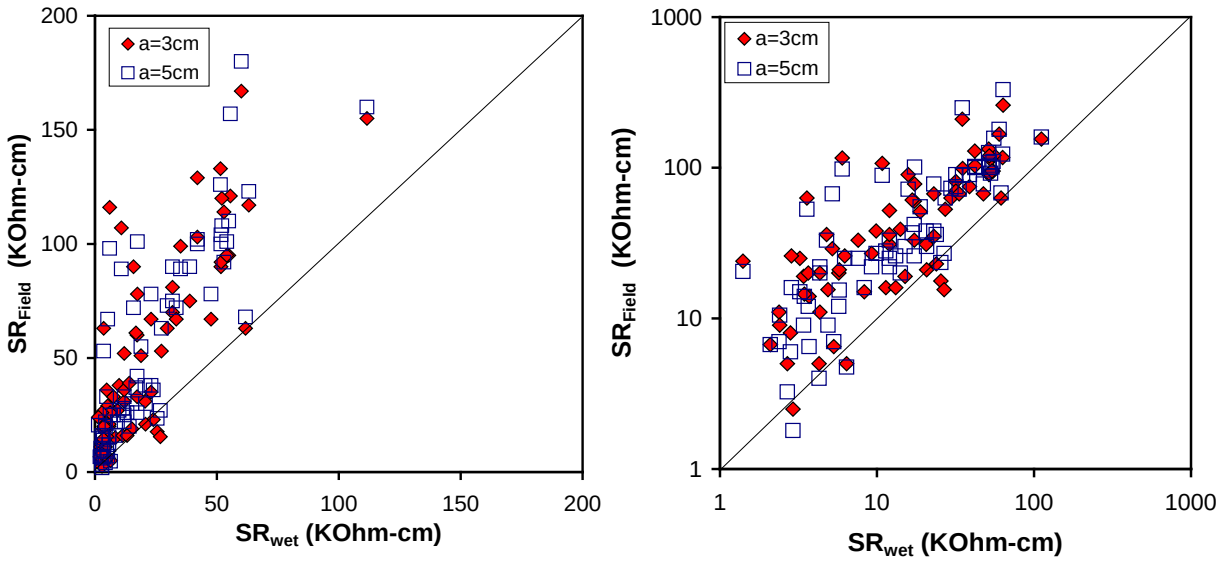

Figure F.29: Correlation between SR_{wet} and SR_{field} (a=3 cm diamonds, a=5 cm squares)

5.3.2 Wet Resistivity vs. Bridge Age

Figure F.30 shows the SR_{wet} values vs. the age of the bridge where the cores were obtained. Normalized wet resistivity values for structures older than 20 years are typically less than 10 KΩ-cm; for structures younger than 20 years, most of bridges registered resistivity values larger than 20 KΩ-cm consistent with the period when pozzolanic admixtures began to be used on FDOT marine substructures.

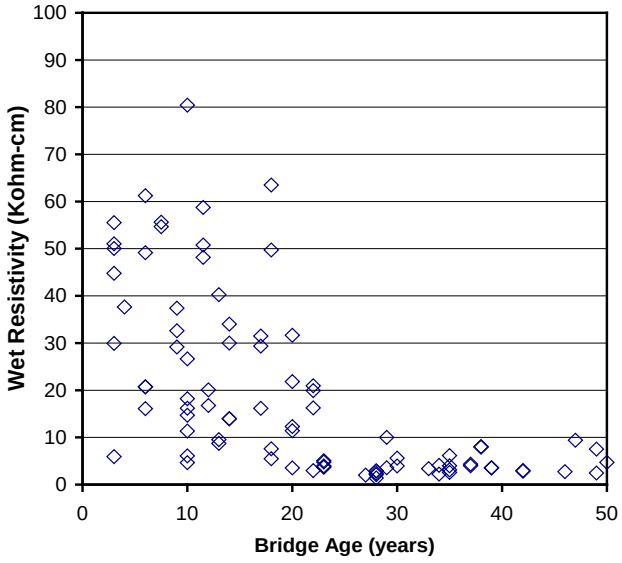

Figure F.30: SR_{wet} vs. age (years).

5.3.3 D_{Cl} vs. Bridge Age

Figure F.31 shows the apparent chloride diffusivity (D_{Cl}) values obtained from the field cores vs. bridge age. Although not as evident as for the resistivity values, the larger D_{Cl} values were observed on cores from bridges that are 20 years old or older. Values greater than 1E-7 cm2/s were only observed on cores from bridges older than 20 years. There are number of bridges that have D_{Cl} values similar to those observed from cores from newer structures. This is likely due to due to the aging effect on D_{Cl} reported by (Bamforth 1999) and others, i.e., as the bridge gets older, the diffusivity gets lower.

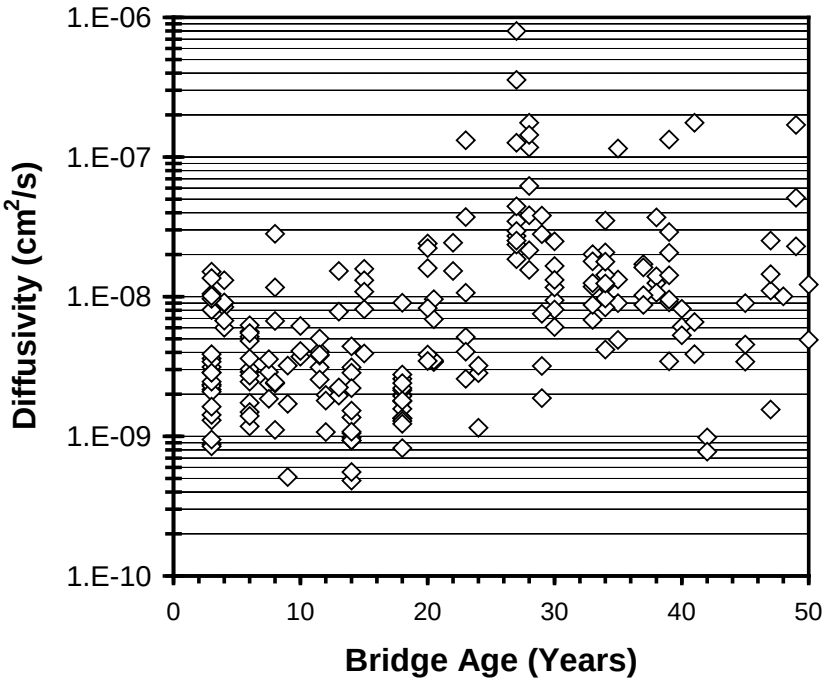

Figure F.31:Chloride Diffusivity vs. Age (years)

5.3.4 C_s vs. Elevation from MWL

Figure F.32 shows that the data of the C_s concentration vs. distance from mean water line (marine growth) is grouped in four series by bridge age. It can be observed that C_s values ranged from 1.5 kg/m^3 to almost 40 kg/m^3. The salinity and type of exposure at the structure location seems to influence more the observed C_s than the distance from

marine growth. On a few structures, one- to ten-year old bridges showed C_s concentration values close to the largest C_s values observed.

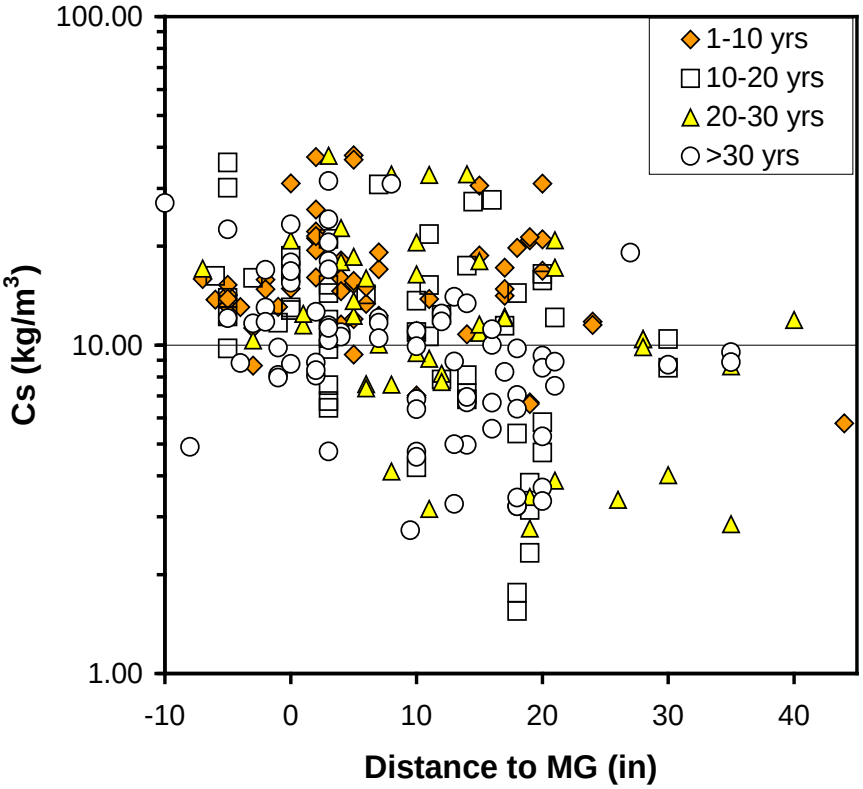

Figure F.32: C_s values vs. distance from the marine growth grouped by bridge age.

5.3.5 C_o vs. Elevation from MWL

Figure F.33 shows that the data of the C_o concentration vs. distance from mean water line (marine growth) is grouped in four series by bridge age. It is important to mention that the core lengths varied as can be seen in Tables F.4 to F.8). Some of the older structures had a small C_o value and usually corresponded to longer cores (e.g., 15 cm). The larger C_o values in older structures corresponded to shorter length cores. It is evident that the two series with the largest C_o are for structures 20-30 years and for structures >30 years. As expected, the C_o is smallest for structures less than 10 years old. No clear trend was observed for C_o as a function of elevation.

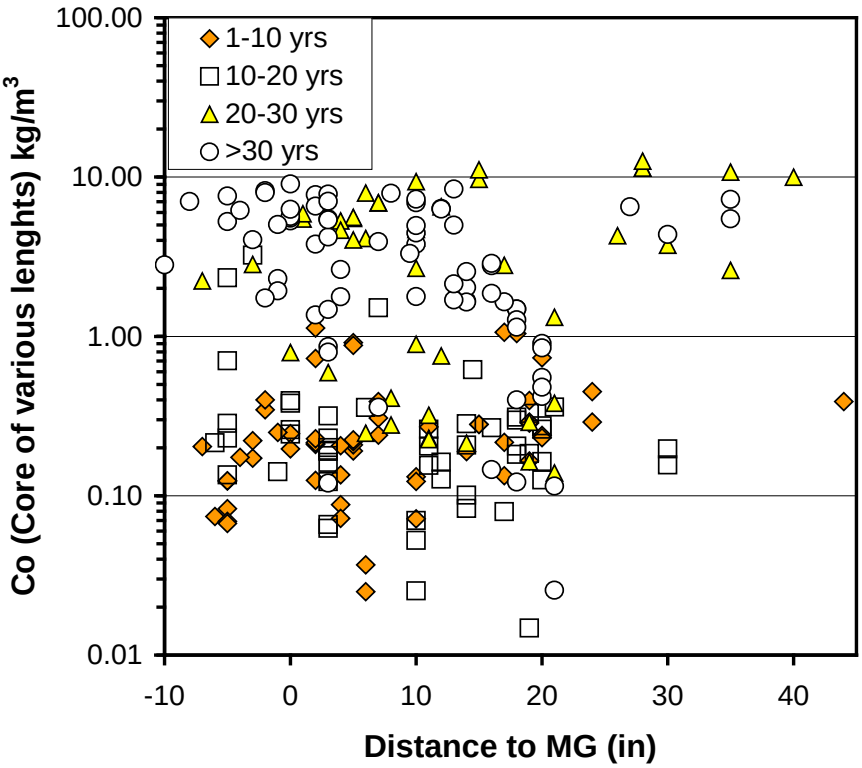

Figure F. 33: C_o values vs. distance from the marine growth grouped by bridge age.

D_{Cl} vs. Elevation from MWL

Figure F.34 shows that the data of the D_{Cl} values vs. distance from mean water line (marine growth) is grouped in four series by bridge age. No clear trend was observed as a function of elevation. The two series with the largest D_{Cl} corresponds to structures older than 20 years.

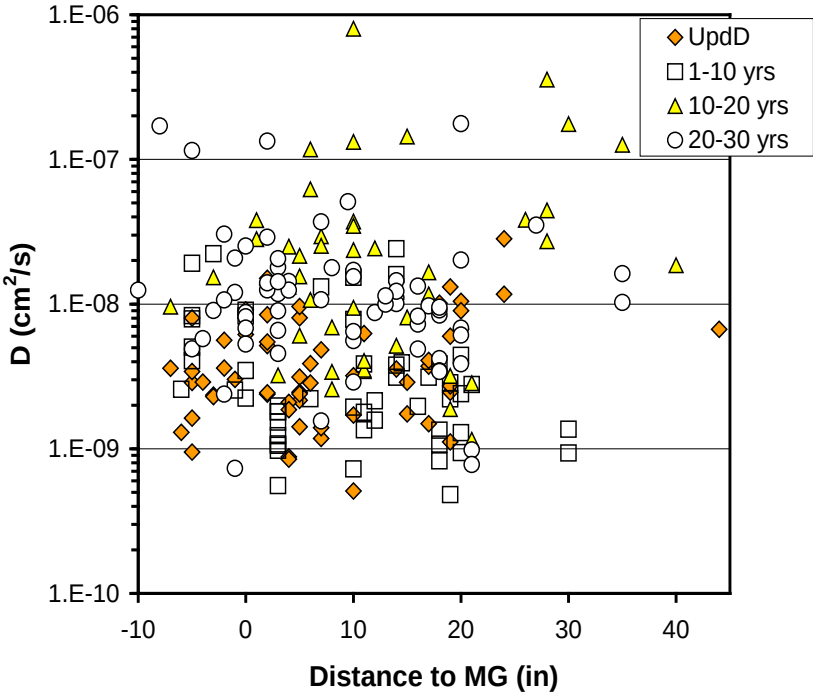

Figure F.34: D_{Cl} values vs. distance from the marine growth grouped by bridge age.

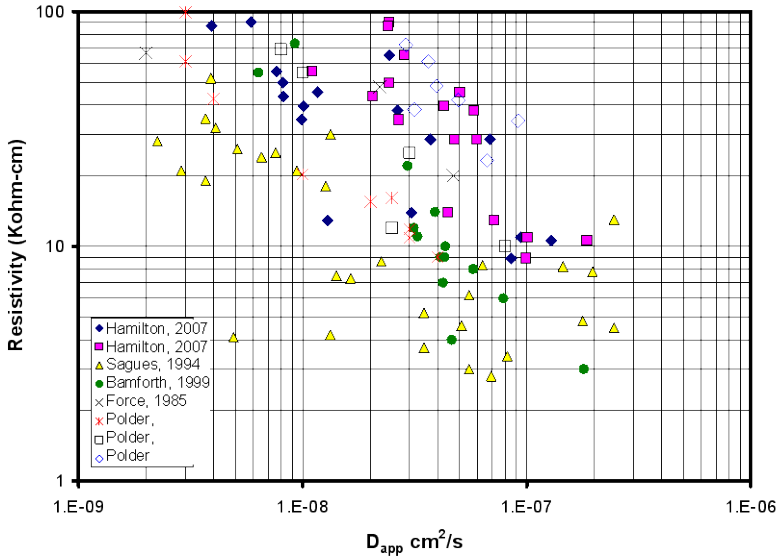

Figure F. 35: D_{Cl} values vs. Resistivity collected from the literature.

5.3.6 Literature D_{Cl} vs. SR

Figure F35 shows a literature compilation of resistivity (by various methods) vs. diffusivity from laboratory and field concrete cores with most of them water saturated

before measuring the resistivity. The trends observed in Figure F.35 and those in Figure F.36 seem to confirm that there is a correlation between D_{Cl} and resistivity. Unfortunately, for data shown in Figure F.35 the D_{Cl} vs. ρ series do not coincide along one single line, suggesting that the procedure by which D_{Cl} and ρ were obtained is important and need to be normalized.

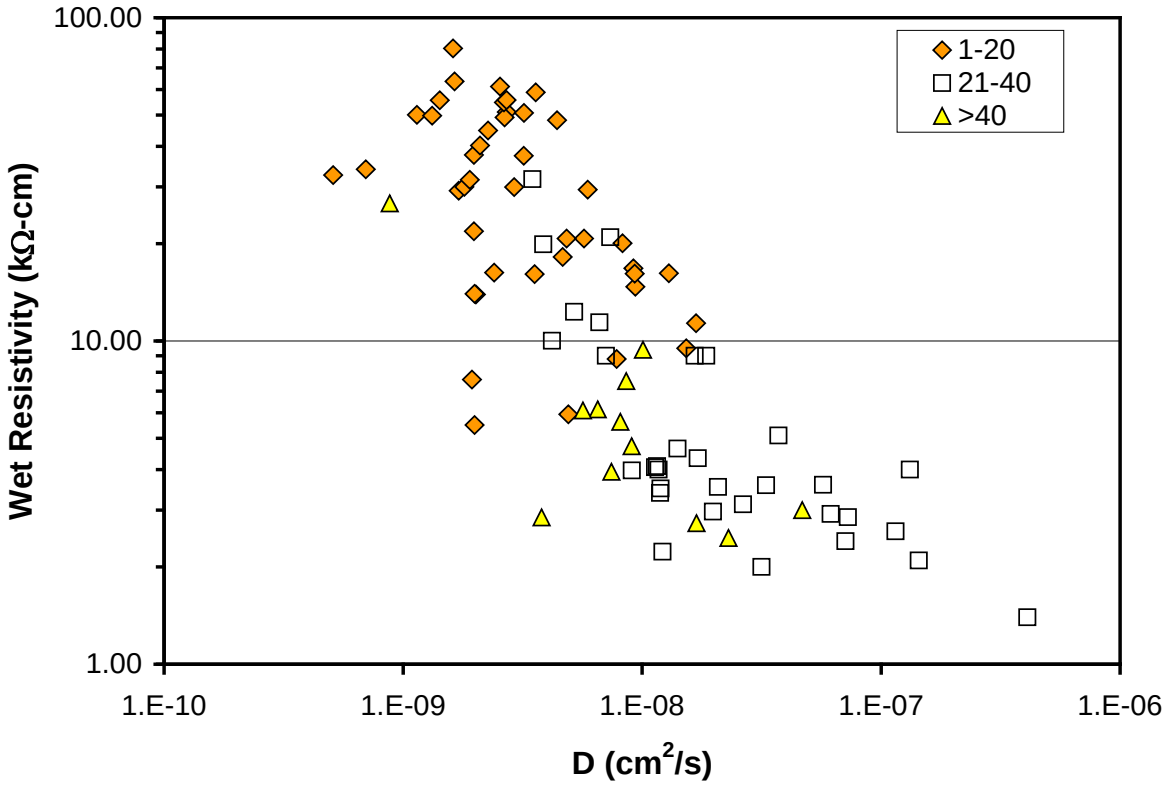

Figure F. 36: Chloride Diffusivity vs. Wet Resistivity grouped by structure age.

5.3.7 Wet Resistivity vs. D_{Cl}

Figure F.36 shows a compilation of wet resistivity vs. diffusivity measured from field concrete cores grouped in three series. Each D_{Cl} value shown is the average of two or three D_{Cl} values measured on any given pile/column. The normalized resistivity values shown were measured on cores from the corresponding pile/column after reaching a constant weight and resistivity value. There is an evident trend: the higher the wet resistivity, the lower the D_{Cl}, and the lower the normalized wet resistivity, the larger the

corresponding D_{Cl}. Unfortunately, not all values converge into a single straight line (in the log-log scale). This is likely due to the age range of the structures, different mix designs, and possibly different water-to-cement ratios (e.g., a recent pile with low w/c and only OPC had a low wet resistivity and also a relatively low D_{Cl}). The bridges 1-20 years old had the higher wet resistivity values and the lower D_{Cl}. Bridges 20 to 40 years old had some of the highest D_{Cl} and the lowest wet resistivity. There are a few data points from this series that fall within the range for structures 1 to 20 years. It is known that pozzolans have been in use for a little over 20 years, and that these structures are just a few years older. A normalized resistivity value higher than 9 kΩ-cm appears to indicate the presence of pozzolanic admixtures (i.e., FA, FA+SF, and others).

Both the wet resistivity and the D_{Cl} values shown in Figures F.36 were re-plotted by applying the log base 10 to each axis so that a linear fitting for a log–log scale can be computed. This is shown in Figure F.37. The x and y in the equations in Table F.10 are: x = the $\log_{10}(D_{Cl})$ and y = $\log_{10}$ (wet resistivity). Table F.10 shows the three different correlations performed. As indicated on the left column of the table, one included all the data available; a second grouping included values from bridges <40 years, and a third fitting considered values for bridges <30 years. The largest R^2 value (R^2=0.67) was found when only considering bridges younger than 30 years. The smallest R^2 value (R^2=0.63) was found when including all bridges. (The R^2 also goes down if only bridges <20 years were used in the fitting, but are not included in here). Figure F.46 shows the fitting line for when using only data for bridges <30 years.

Table F.10: Correlation equations for log10(D_{Cl}) vs. log10(wet resistivity)

Fitting	Equation	R^2
All Data	y = -0.6709x - 4.4192	0.628
< 40 years	y = -0.6725x - 4.3907	0.664
< 30 years	y = -0.6374x - 4.0522	0.672

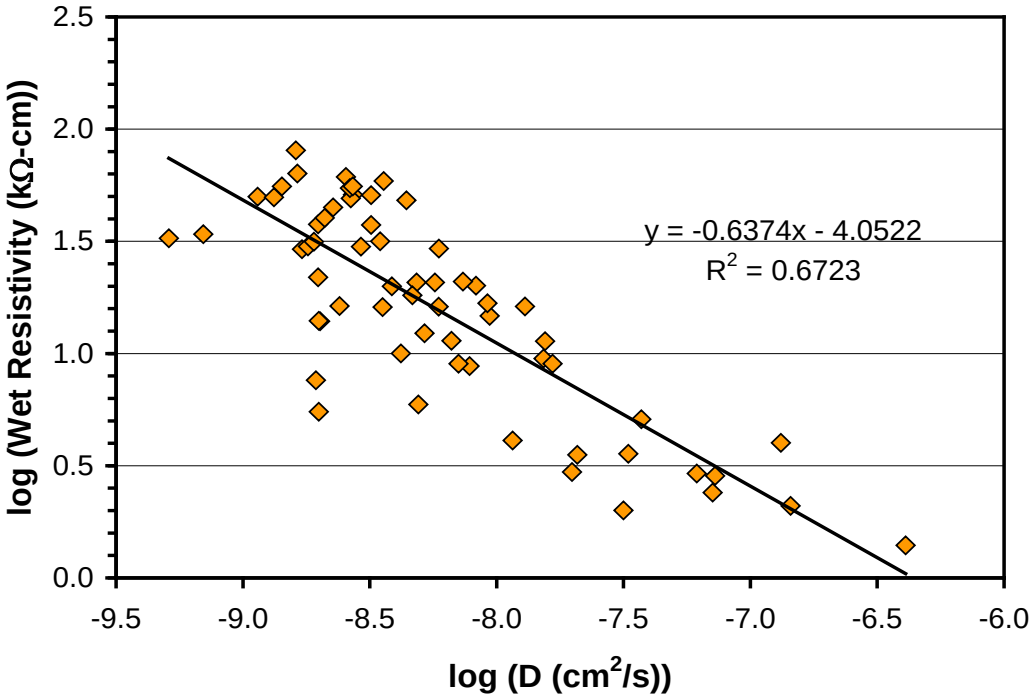

Figure F.37: log10(D) vs. log10(wet resistivity) and corresponding fitting.

6. CONCLUSIONS

Laboratory and Modeling

- FEM modeling allows for the calculation of cell constant parameter (K) values. K values normalize the measured values for finite geometry and rebar presence.

- Results from numerical computations to estimate a cell constant correction for the field values (assuming uniform SR) indicates that the presence of reinforcing steel with cover > 7.5 cm has a negligible effect on the resistivity measured with a=3 cm and a=5 cm.

- The normalized SR measured on the laboratory specimens provides a qualitative insight on how rebar presence, probe location and orientation affect the apparent resistivity measured when subjected to various environmental conditions.

- Concrete with Fly Ash replacement cured in a fog room needs more than 400 days to reach final resistivity value. Concrete mixture with Silica Fume and Fly Ash replacements require about 250 days to reach final resistivity value.

- Immersion in 3.5 NaCl solution reduced the SR value measured by 20% on FA concrete when compared to saturated SR measured value.

- Environmental conditions have a significant effect on the SR value measured. Exposure to laboratory temperature and relative humidity produces a monotonic increase in the measured SR value. The measured resistivity value in this environment reached up to four times the resistivity value measured in saturated conditions.

- Modeling results suggest that the conditioning methods could introduce a third resistivity layer. Depending on initial moisture conditions, concrete type, how fast the water is absorbed, an apparent increase in resistivity could be observed.

Field

- The conditioning method increases the moisture content of the concrete layer closer to the surface. Best results are obtained if concrete is dry and in the absence of other wetting events (rain). The resistivity values measured after conditioning was significantly lower than the resistivity values before conditioning.

- The wet resistivity measued on field obtained cores was lower than the minimum field resistivity values measured. On average, SR_{field} was about three times SR_{wet}.

- A good correlation was observed between SR_{wet} and D_{Cl} from field values (R^2=0.67). The structures age ranged from 50 years to 3 years old.

- The use of two electrode spacing a=3 and a=5 cm provides insight on the resistivity of the concrete layer closer to the surface and how the apparent resistivity evolves upon water absorption (conditioning).

- Normalized wet resistivity values for structures older than 20 years were typically less than 10 KΩ-cm.

- The SR_{wet} values measured on structures younger than 20 years were usually higher than 10 KΩ-cm (most > 20 KΩ-cm) consistent with the period when pozzolanic admixtures began to be used on FDOT marine substructures.

References

Andrade, C., (2005) “Model for Prediction of Reinforced Concrete Service Life Based on Electrical Resistivity,” IBRACON Materials Journal (Revista IBRACON de Materiais) Vol. 1, p. 61-65.

Andrade, C., and d’Andrea, R., (2010) “The Use Of Electrical Resistivity As A NDT For The Specification Of Concrete Durability,” in Concrete Under Severe Conditions, Eds. Castro-Borges, Moreno, et.al., Taylor & Francis Group, London, p. 195-200.

Bamforth, P. B., (1999) “The Derivation Of Input Data For Modelling Chloride Ingress From Eight-Year UK Coastal Exposure Trials,” Magazine of Concrete Research, Vol. 51, p.87-96.

Bertolini, L., and R.B. Polder, (1997) “Concrete resistivity and reinforcement corrosion rate as a function of temperature and humidity of the environment,” Final Report TNO report 97-BT-R0574.

Brameshuber, W.; Raupach ,M.; Schroder ,P.; and Dauberschmidt ,C., (2003) “Non-destructive determination of the Water-Content in Concrete Cover using the Multi-ring-electrode,” International Symposium (NDT-CE).

Broomfield, J., and Millard, S.,(2002) “Measuring Concrete Resistivity to assess Corrosion Rates,” A report from The Concrete Society/Institute of Corrosion liaison committee Current Practice Sheet no. 128, Concrete, p. 37-39.

Broomfield, J.P.; Kevin D.B.; and Hladky K., (2002) Cement & Concrete Composites, Vol. 24 p. 27.

Burchler, D., Elsener, B.; and Bohni, H., (1996) “Electrical Resistivity and Dielectric Properties of Hardened Cement Paste and Mortar,” in Corrosion of Reinforcement in Concrete Construction, Ed. C.L. Page, P.B. Bamforth, J.W. Figg, The Royal Society of Chemistry pp 283-293.

Butefuhr, M.; Fischer, C.; Gehlen, C.; Menzel, K.; and Nurberger, U., (2006) “On-Site investigation on concrete resistivity – a parameter of durability calculation of reinforced concrete structures,” Materials and Corrosion Vol. 57 p 932-939.

Castellote, M.; Andrade, C.; and Alonso, M.C., (2002) “Standardization, to a Reference of 25C, of electrical resistivity for Mortars and Concretes in Saturated or Isolated Conditions,” ACI Materials Journal, Vol. 99 p. 127.

Chini, A.R.; Muszynski, L.C.; and Hicks, J., (2003) “Determination of Acceptance Permeability Characteristics for Performance-Related Specifications for Portland Cement Concrete,” Final Report submitted to Florida Department of Transportation (Contract No. BC 354-41).

Elkey, W., and Sellevold, E.J., (1995) “Electrical Resistivity of Concrete,” Publication No. 80, Norwegian Road Research Laboratory, Oslo, Norway, 36pp.

Ewins, A.J., (1990) “Resistivity measurements on concrete,” British Journal of NDT, Vol. 32 p. 120-126.

Ferraro, C.C.; Boyd, A.J.; and Ishee, C.A., (2010) “Qualification of repair materials by mechanical and durability properties,” in Concrete under Severe Conditions, Eds. Castro-Borges, Moreno, et.al., 2010 Taylor & Francis Group, London, p. 91-98.

FM5-516 (2005). “Florida Method of Test For Determining Low-Levels of Chloride in Concrete and Raw Materials,” Florida Department of Transportation (FDOT).

FM5-578 (2004). “Florida Method of Test for Concrete Resistivity as an Electrical Indicator of its Permeability,” Florida Department of Transportation (FDOT).

Garboczi, E.J., (1990) “Permeability, Diffusivity, and Microstructural Parameters: A critical Review,” Cement and Concrete Research Vol. 20, pp 591-601.

Gowers, K.R., and Millard S.G. (1991) “The effect of steel reinforcement bars on the measurement of concrete resistivity,” British Journal of NDT Vol. 32 p. 551-556.

Gowers ,K.R., and Millard SG (1999) “Measurement of concrete resistivity for assessment of corrosion severity of steel using Wenner technique,” ACI Materials Journal Vol. 96 p. 536-541.

Hamilton, H.R.; Boyd, A.J.; and Vivas, E.A., (2007) “Permeability of Concrete – Comparison of Conductive and Diffusion Methods,” Final Report submitted to Florida Department of Transportation” (Contract No. BD536).

Hope, B.B.; Ip, A.K.; and Manning, D.G., (1985) “Corrosion and Electrical Impedance in Concrete”, Cement and Concrete Research Vol. 15 p. 525-534.

Hunkeler, F., (1996) “The resistivity of pore water solution – a decisive parameter of rebar corrosion and repair methods,” Construction and Building Materials, Vol. 10 p. 381.

Kessler, R.; Powers, R.; and Paredes, M., (2005) “Resistivity Measurements of Water Saturated Concrete as an Indicator of Permeability,” paper No 05261 in Corrosion/2005.

Kessler, R.J.; Powers, R.G.; Vivas, E.; Paredes, M.A.; and Virmani, P., (2008) “Surface Resistivity as an Indicator of Concrete Chloride Penetration Resistance,” 2008 Concrete Bridge Conference, May 4-7, 2008, St. Louis, MO (Proceedings published on CD).

Klinghoffer, O., and Kofoed, B., (1993) “Resistivity Measurements in Concrete, Techniques and Applications. Limitations using resistivity as a measure of diffusivity,” in Nordic Miniseminar, Chalmers University of Technology, Goteborg.

Klinghoffer, O., and Rislund, E., (1995) “Determination of Chloride Diffusivity in Matured Concrete based on Electrical Conductivity Measurements Hardening Material,” in International Symposium Non-Destructive Testing in Civil Engineering (NDT-CE) pp 539-550.

Lay, S.; Schießl, P.; Law, D.; Lahus, O.; and Gjørv, O., (2003) “Prototype of condition assessment protocol” Program: GROWTH RDT Project: Life Cycle management of Concrete Infrastructures for Improved Sustainability: LIFECON, Chapter 4.7.6 “Electrical Resistivity of Concrete” p, 85-100.

McCarter, W.J.; Ezirim, H.; Emerson, M., (1992) “Absorption of water and chloride into concrete,” Magazine of Concrete Research, Vol. 44 p 31-37.

McCarter, W., (1996) “Monitoring the Influence of Water and Ionic Ingress on Cover-Zone Concrete Subjected to Repeated Absortpion,” Cement Concrete and Aggregates, Vol. 18 p 55.

McCarter, W.J.; Starrs, G.; Chrisp, T.M., (2000) “Electrical conductivity, diffusion, and permeability of Portland cement-based mortars,” Cement and Concrete Research Vol. 30 p. 1395.

McCarter, W.J., Vennesland O., (2004) “Sensor systems for use in reinforced concrete structures,” Construction and Building Materials Vol. 18 p. 351-358.

McCarter, W.J.; Chrisp, T.M.; Starrs, G., Basheer P.A.M., Blewett J., (2005) “Field monitoring of electrical conductivity of cover-zone concrete,” Cement & Concrete Composites Vol. 27: 809-817.

Millard, S.G.; Harrison, J.A.; and Edwards A.J. (1986) “Measurement of the electrical resistivity of reinforced concrete structures for the assessment of corrosion risk,” British Journal of NDT, Vol. 31 p. 617-621.

Millard, S.G.; Ghassemi, M.H.; Bungey, J.; Jafar, M.I., (1990) “Assessing the Electrical Resistivity of Concrete Structures for Corrosion Durability Studies,” Corrosion of Reinforcement in Concrete (Eds.: Page, Treadaway, Bamforth), Elsevier, London, 1990, p. 303-313.

Millard, S.G.; Harrison, J.A.; Gowers, K.R., (1990) “Practical measurement of concrete resistivity,” British Journal of NDT, Vol. 32 p. 120-126.

Millard, S.G., (1991) “Reinforced concrete resistivity measurement techniques,” Proc Inst Civil Engineers, Part 2, Vol. 91 p. 71-78.

Millard, S.G., and Gowers, K.R., (1992) “Resistivity assessment of in-situ concrete: the influence of conductive and resistive surface layers,” Proc. Instn Civ. Engrs. Strucs & Blds, Vol. 94 p. 389-395.

Moreton, A.J., (1997) Transportation Research Record, Vol. 1610 paper No. 97-0561.

Morris, W.; Moreno E.I.; and Sagues, A.A., (1996) “Practical Evaluation of Resistivity of Concrete in Test Cylinders using a Wenner Array Probe,” Cement and Concrete Research, Vol. 26, p.1779-1787.

Naish, C.C., (1990) “Concrete inspection: interpretation of potential and resistivity measurements”, Proc. “Corrosion of reinforcement in concrete,” Eds. C.L. Page, K.W.J. Treadaway, P.B. Bamfoth, Elsevier, p. 314-332.

Polder, R.B., (1997) “Chloride diffusion and resistivity testing of five concrete mixes for marine environment,” Proc. RILEM. International Workshop on Chloride Penetration into Concrete, St-Remy-les-Chevreuses, October 15–18, 1995, Eds. L.-O. Nilsson, J.-P. Ollivier, RILEM.

Polder, R.; Andrade, C.; Elsener, B.; Vennesland, O.; Gulikers, J.; Weidert, R.; and Raupach, M., (2000) “Rilem TC 154-EMC: Electrochemical techniques for Measuring Metallic Corrosion,” Materials and Structures, Vol. 33 p. 603-611.

Polder, R.B., (2001) “Test methods for on-site measurement of resistivity of concrete - A RILEM TC-154 technical recommendation,” Construction and building materials Vol. 15 p. 125-131.

Presuel-Moreno, F.; Suarez, A.; Lasa, I.; and Paredes M., (2009) “Preliminary Results of Surface Resistivity Readings (Wenner Method) on Field Marine Substructures as a Mean to Assess Concrete Permeability,” paper 09218 in CORROION/2009, Atlanta, GA (2009) (Proceedings published on CD).

Presuel, F.; Liu, Y.; and Paredes, M., (2009) “Understanding the Effect of Rebar Presence and/or Multilayered Concrete Resistivity on the Apparent Surface Resistivity Measured via the Four-Point Wenner Method,” paper paper 09217 in CORROION/2009, Atlanta, GA (2009) (Proceedings published on CD)..

Presuel-Moreno, F.J., and Hartt, W., (2009) “Protection of Reinforced Concrete Bridge Substructures Using Submerged Bulk Anodes,” Final Report submitted to Florida Department of Transportation (Contract No. BD546-03).

Presuel-Moreno, F.J.; Suarez, A.; Lasa, I., and Paredes, M., (2010), “Surface resistivity profiles on marine substructures to assess concrete permeability,” in Concrete under Severe Conditions, Eds. Castro-Borges, Moreno, et.al., 2010 Taylor & Francis Group, London, p.227-235

Pruckner, F., and Gjørv O.E., Cement and Concrete Research Vol. 34 p. 1209 (2004)

Pruckner, F., and Gjørv, O.E., (2001) “ Electrical Resistivity for Evaluation of Concrete Corrosivity,” in Concrete under Severe Conditions, Eds. Banthia, K. Sakai, and O.E. Gjorv, The University of British Columbia, Vancouver, Canada, p. 2070-2078.

Pruckner, F., and Gjorv, O.E., (2010), “ RH measurements for assessing moisture conditions in concrete structures,” in Concrete under Severe Conditions 2010, Eds. Castro-Borges, Moreno, et.al., 2010 Taylor & Francis Group, London, p. 1141-1146.

Sagüés, A.A.; Kranc, S.C.; Yao, L.; Presuel-Moreno, F.; and Rey, D., (2001) Torres-Acosta A. “Corrosion Forecasting for 75-Year Durability Design of Reinforced Concrete,” Final Report submitted to Florida Department of Transportation (Contract No. 0510805).

Sagüés, A.A., and Lau, K., (2009) “Corrosion evaluation of Bridges with Epoxy-Coated Rebar,” Final Report submitted to Florida Department of Transportation (Contract No. BD544-23).

Sagüés, A.A., and Lau, K., (2009) “Corrosion of steel in locally deficient concrete,” Final Report submitted to Florida Department of Transportation (Contract No. BD544-31).

Sagüés, A.A.; Lau, K.; and Yao, L., (2005) “Corrosion Performance of Concrete Cylinder Piles,” Final Report submitted to Florida Department of Transportation (Contract No. BC353-10).

Saleem, M.; Shemeem, M.; Hussain, S.E.; and Maslehuddin, M., (1996) “Effect of Moisture, Chloride and Sulfate Contamination on the Electrical Resistivity of Portland Cement Concrete,” Construction and Building Materials, Vol. 10 n 3, pp 209-214.

Schiesl, P., and W. Breit (1995) “Monitoring of the Depth-Dependent Moisture Content of Concrete Using Multi-ring-Electrodes,” E&FN Spon, London, Proceeding of the International conference on Concrete under Severe Conditions, Ed. K. Sakai; et al, Sapporo, Japan Vol. II p 964-973.

Sengul, O., and Gjørv, O.E., (2008) “Electrical Resistivity Measuremetns for Quality Control during Concrete Construction,” ACI Materials Journal, Vol. 105 p. 541-547.

Sengul, O., and Gjørv, O.E., (2009) “Effect of Embedded Steel on Electrical Resistivity Measuremetns on Concrete Structures,” ACI Materials Journal, Vol. 106 pp 11-18.

Smith, D., (2006) “The Development of a Rapid Test for Determining the Transport Properties of Concrete,” University of New Brunswick, Master’s Thesis.

Villagran Zaccardi, Y.A.; Fullea Garcia, J.; Huelamo, P.; and Di Maio, A.A., (2009) “Influence of temperatura and humidity on Pórtland cement mortar resistivity monitored with inner sensors,” Materials and Corrosion, Vol. 60 p. 294-299.

Wenner, F., (1915) “A method of measuring earth resistivity,” Bulletin of the Bureau of Standards, Vol. 12 p. 469-4778.

Weydert, R., and Gehlen, C., (1999) “Electrolytic Resistivity of cover Concrete: Relevance, Measurement and Interpretation,” Durability of Building Materials and Components 8 (Vol 1). Ed by M.A. Lacasse and D.J. Vanier. NRC Research Press, pp 409-419.

Whiting, D.A., and Nagi, M. A., (2003) “Electrical Resistivity of Concrete,” R&D No. 2457, Portland Cement Association, Skokie, IL, 57 pp.

Woelfl. G.A., and Lauer, K., (1979) “The electrical resistivity of concrete with emphasis on the use of electrical resistance for measuring moisture content,” Journal of Cement, Concrete and Aggregates, Vol. 1 p. 64-67.

Appendix 1– Resistivity vs. time on rectangular blank specimens, subjected to various exposure conditions.

From day 120 to day 425 samples 1A3 and 1A4 (top face only) were subjected to cyclic ponding with seawater

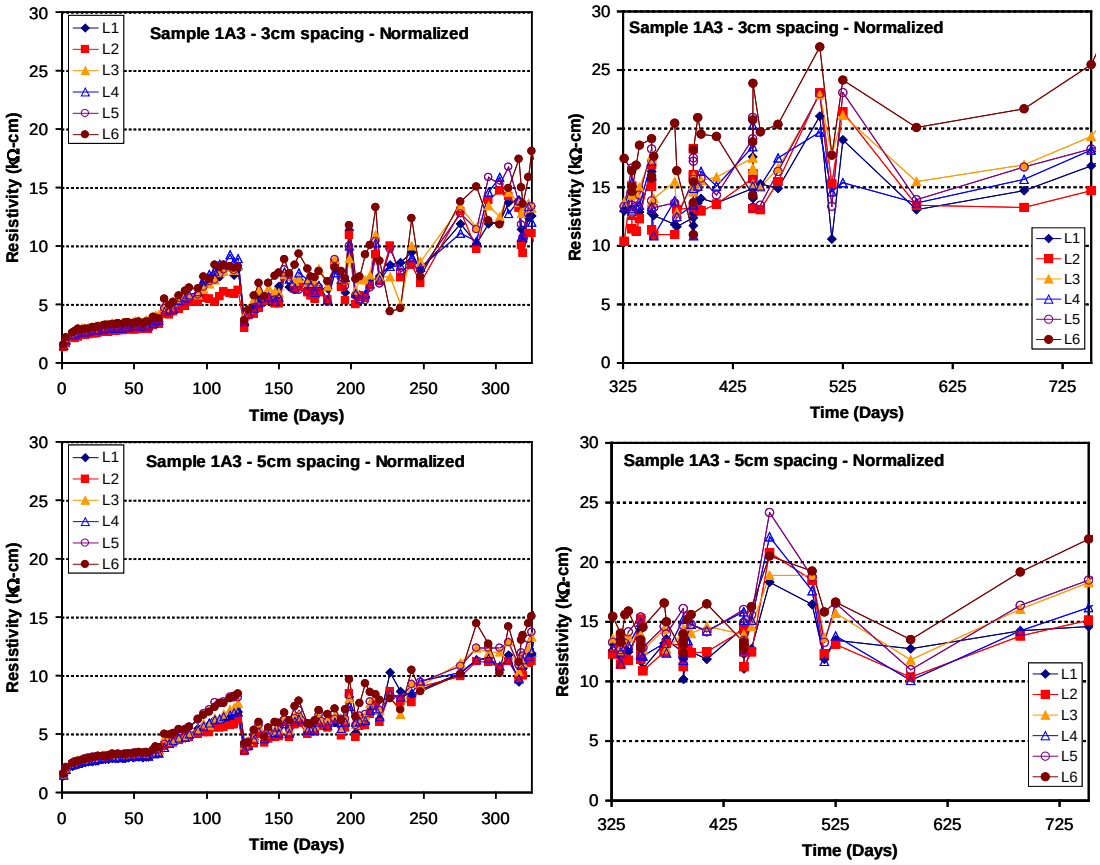

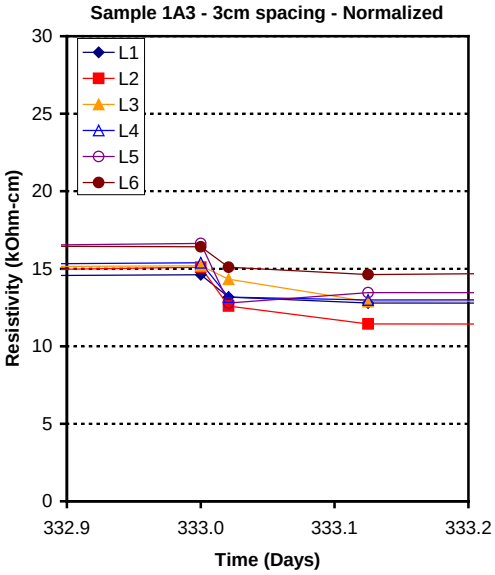
Sample 1A3 - 3cm spacing - Normalized
Resistivity (kOhm-cm)
Time (Days)
L1
L2
L3
L4
L5
L6
30
25
20
15
10
5
0
332.9
333.0
333.1
333.2

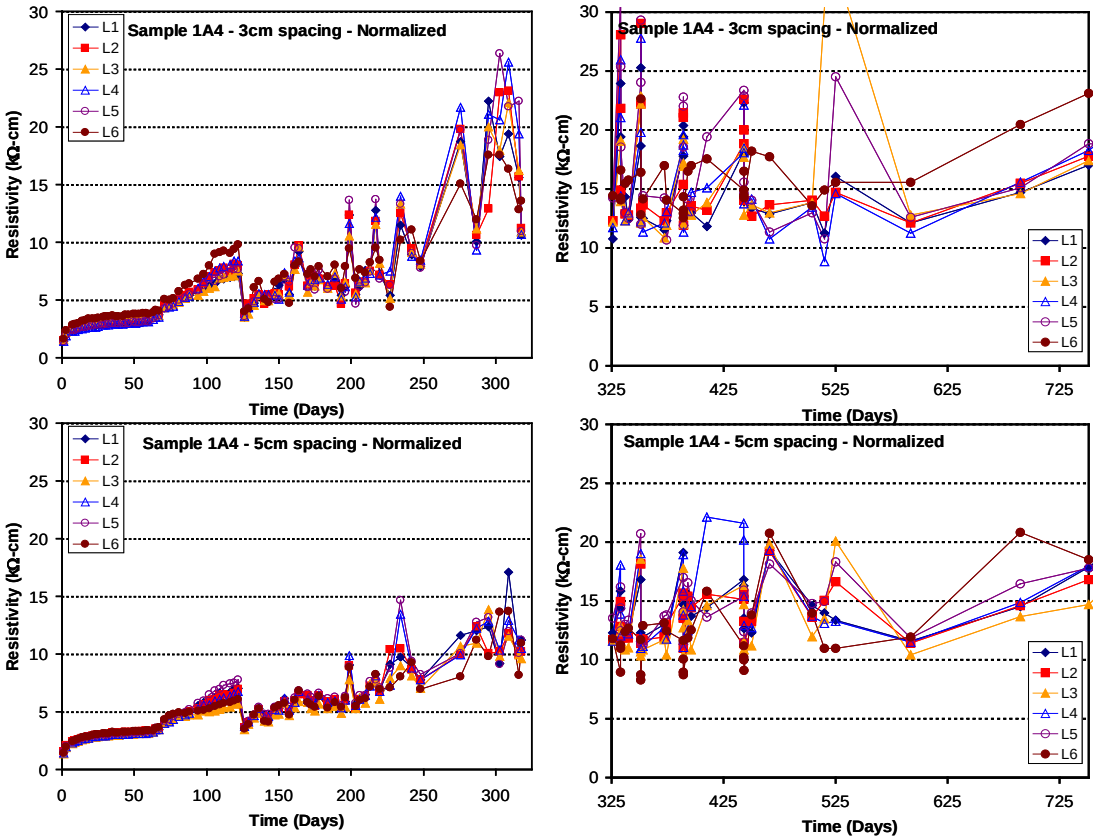

An interesting behavior was observed for samples that were ponded with seawater. There was considerable oscillation on the measured resistivity values, somewhat similar to what sometimes was observed in the field. After day 425 samples 1A3 and 1A4 were kept in laboratory temperature but at higher humidity than laboratory humidity.

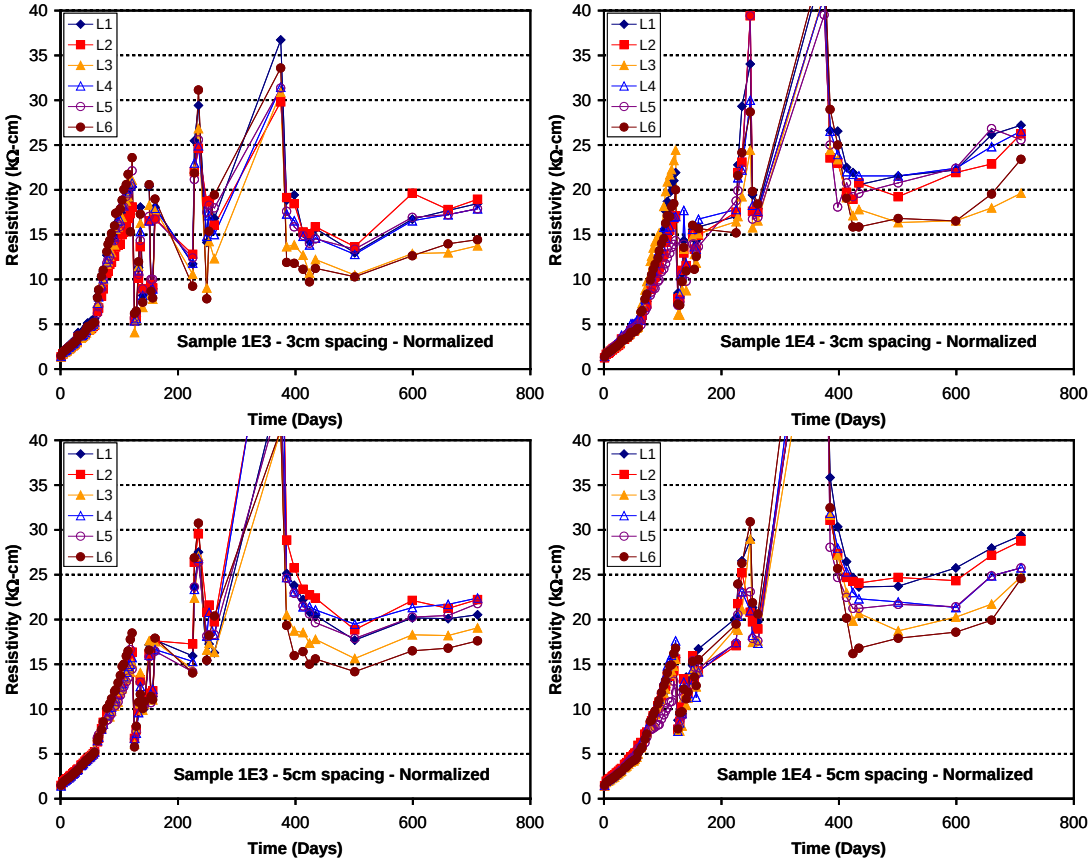

OPC+FA Samples

Day 120 to day 250 samples were subjected to cyclic ponding with seawater

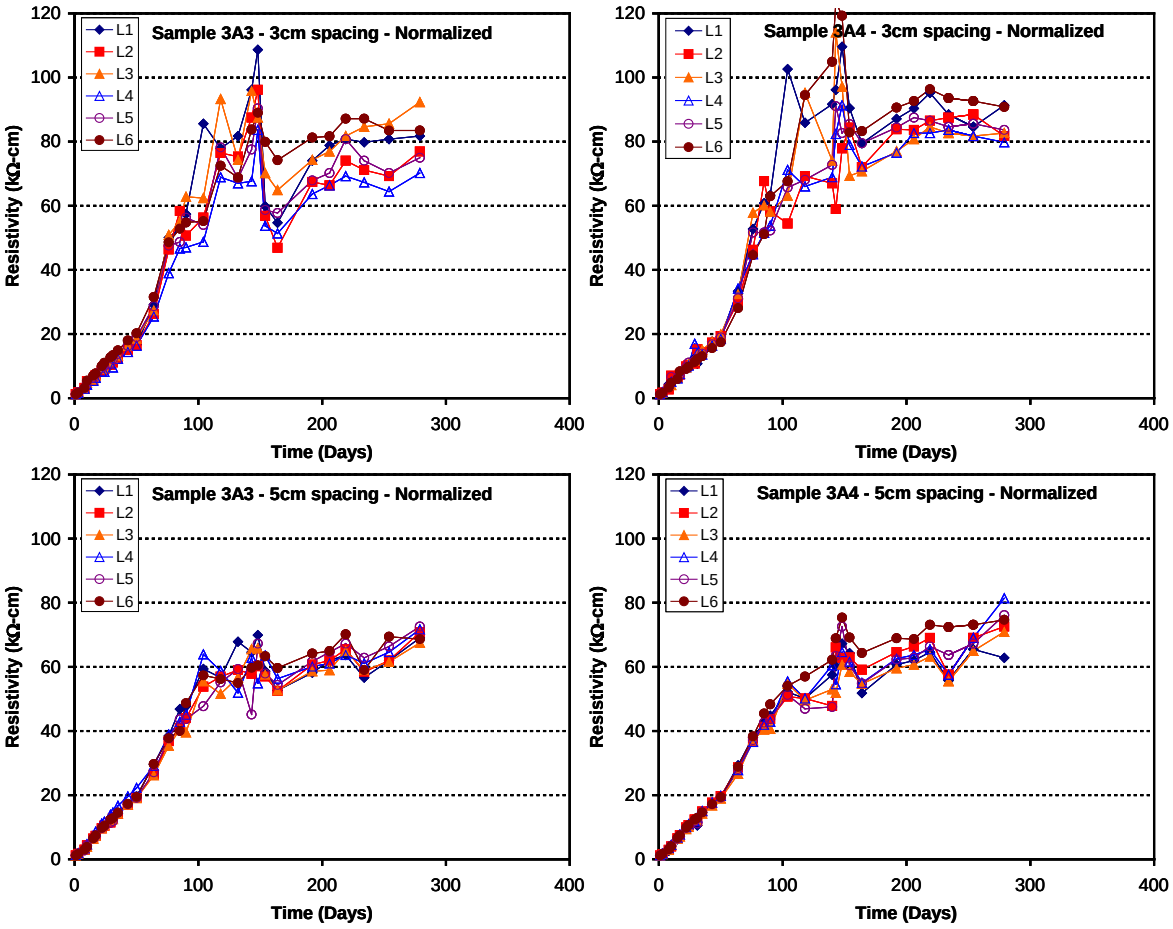

FA+SF Samples

Appendix 2– Resistivity vs. time on rectangular specimens with one rebar, subjected to various exposure conditions.

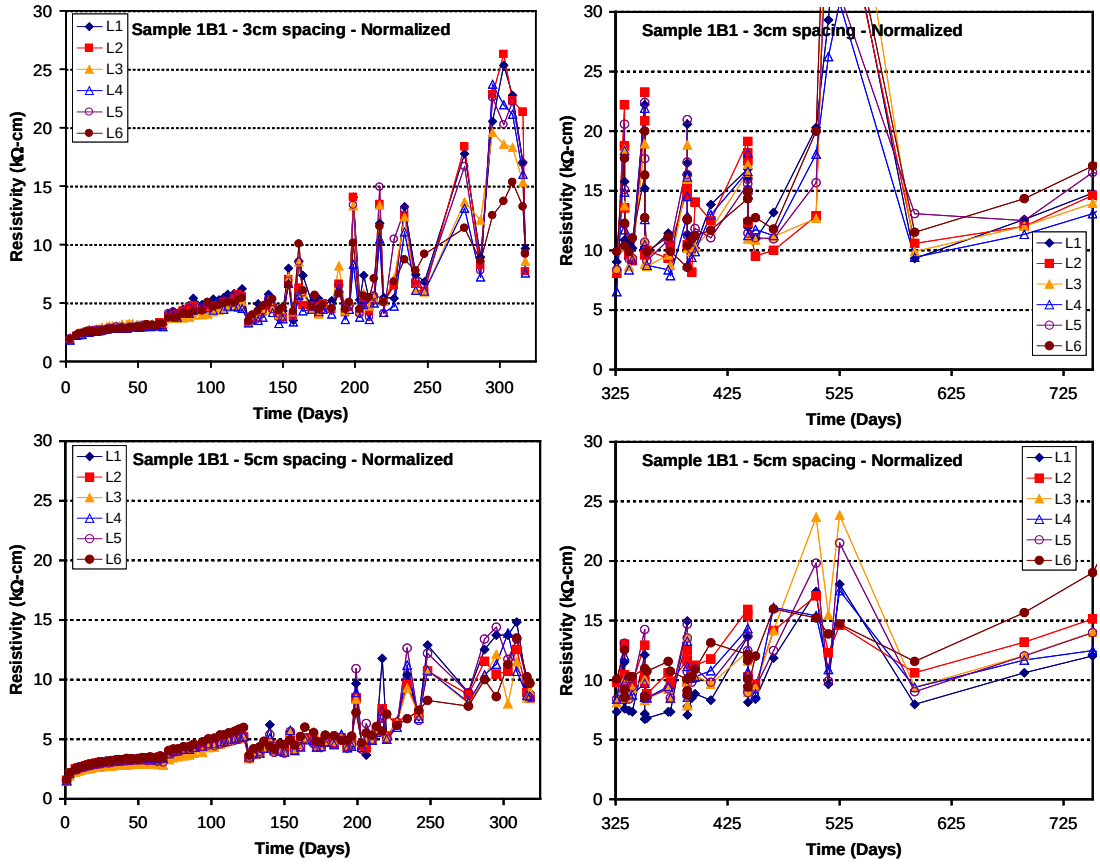

OPC Sample 1B1

Day 120 to 425 samples were subjected to cyclic ponding with seawater

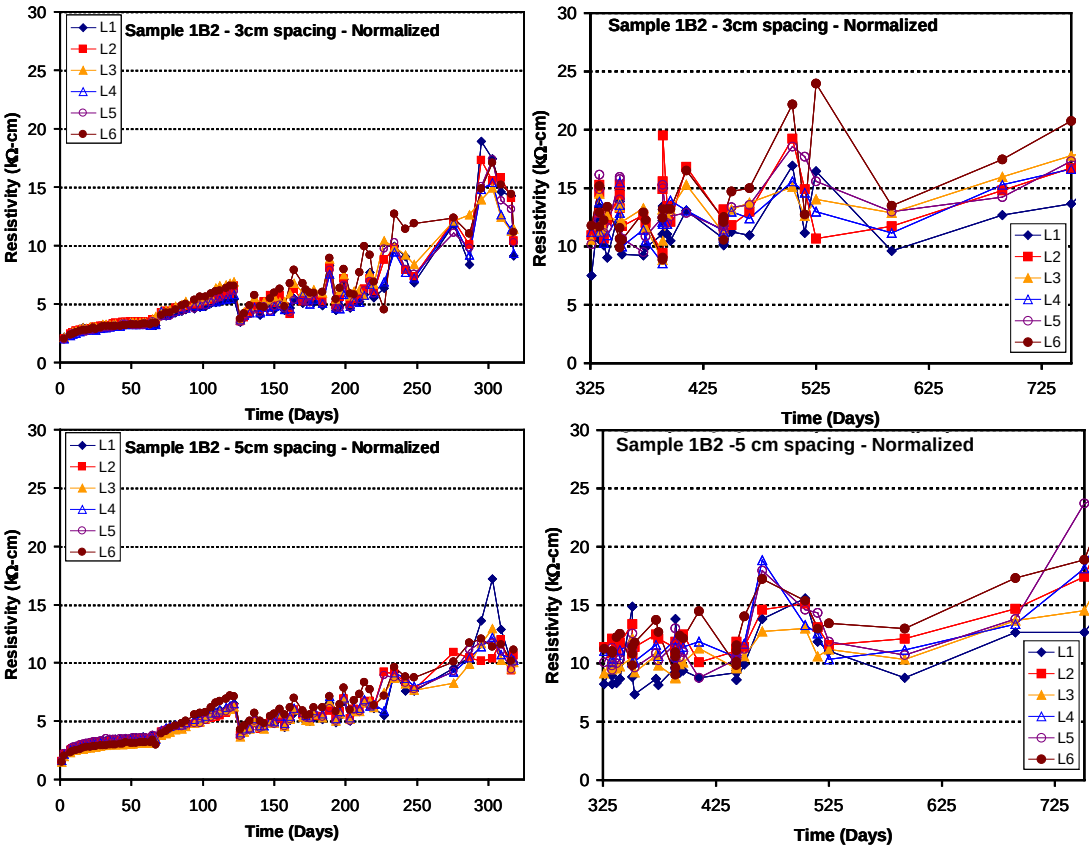

OPC Sample 1B2

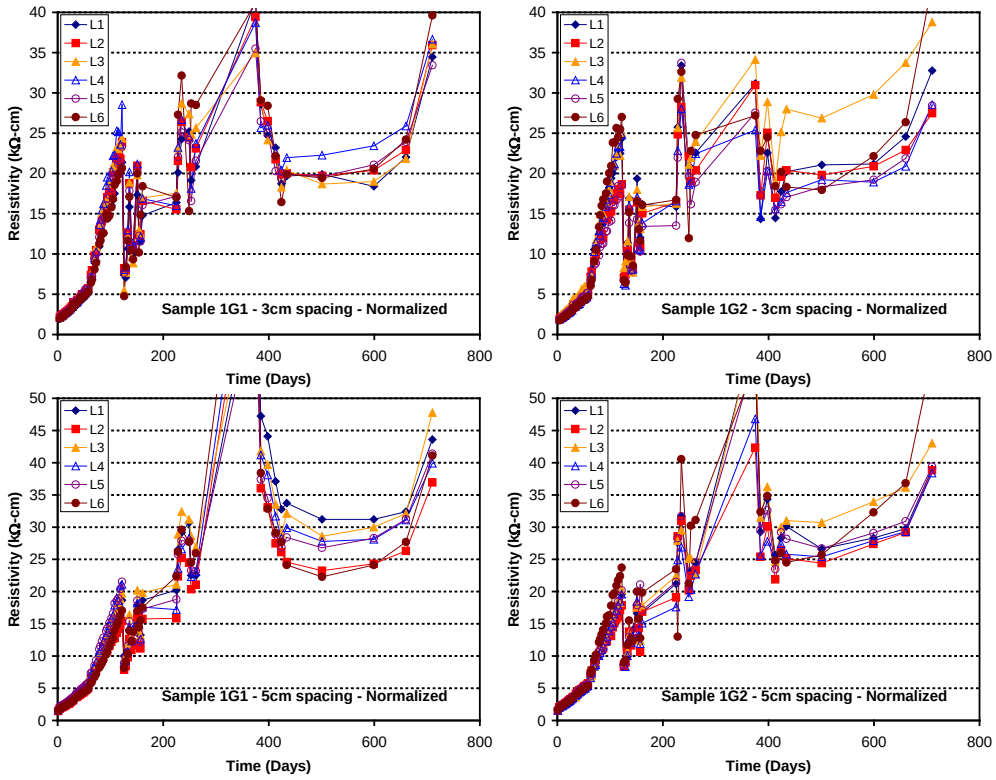

OPC+FA Samples 1G1 and 1G2

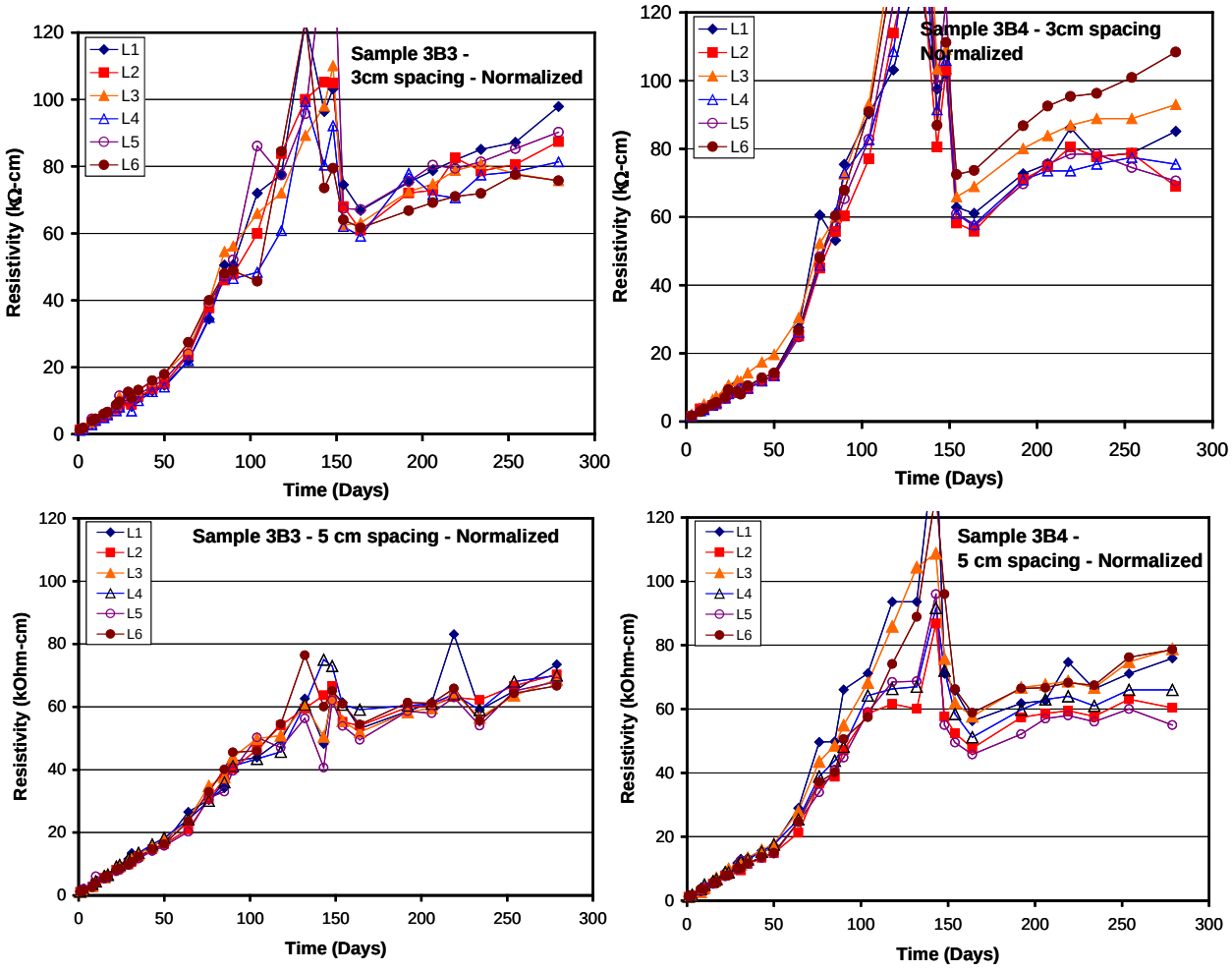

OPC+FA+SF Samples 3B3 and 3B4

Appendix 3. Resistivity vs. time on rectangular specimens with four rebars, subjected to various exposure conditions

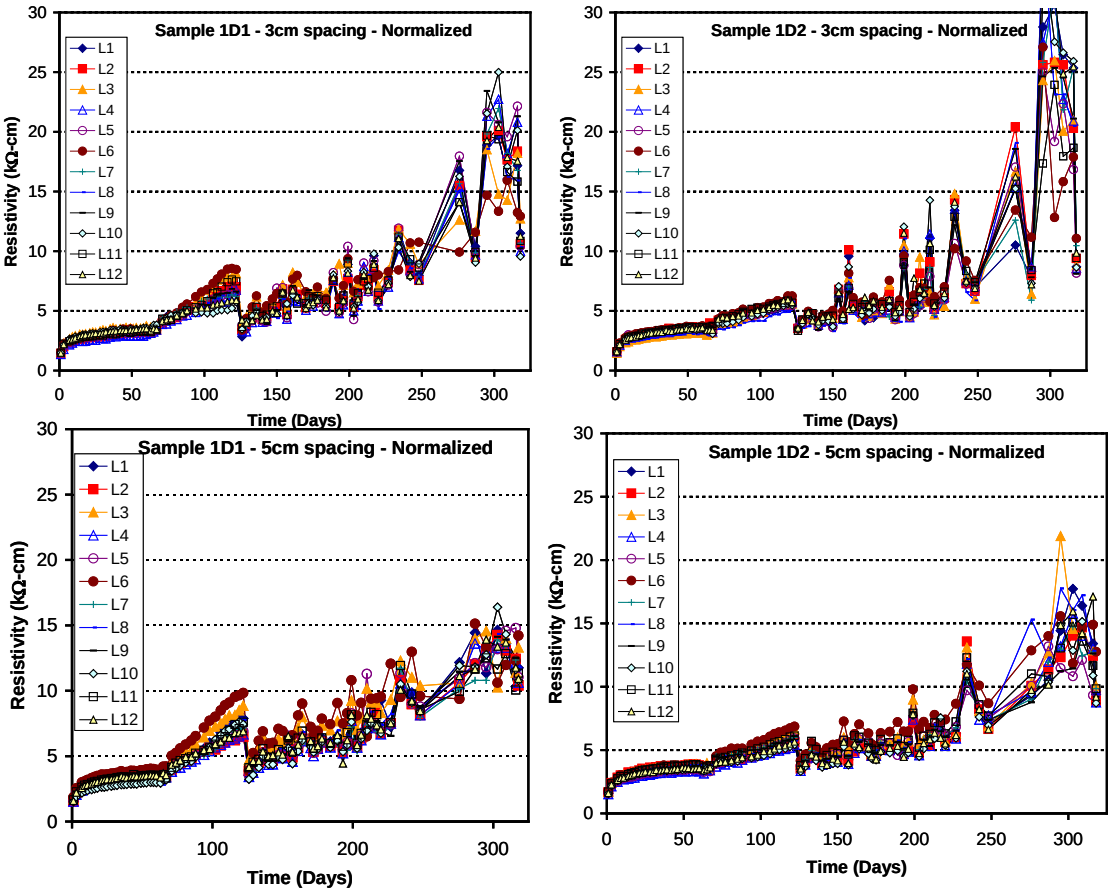

OPC Samples 1D1 and 1D2, samples with four rebars

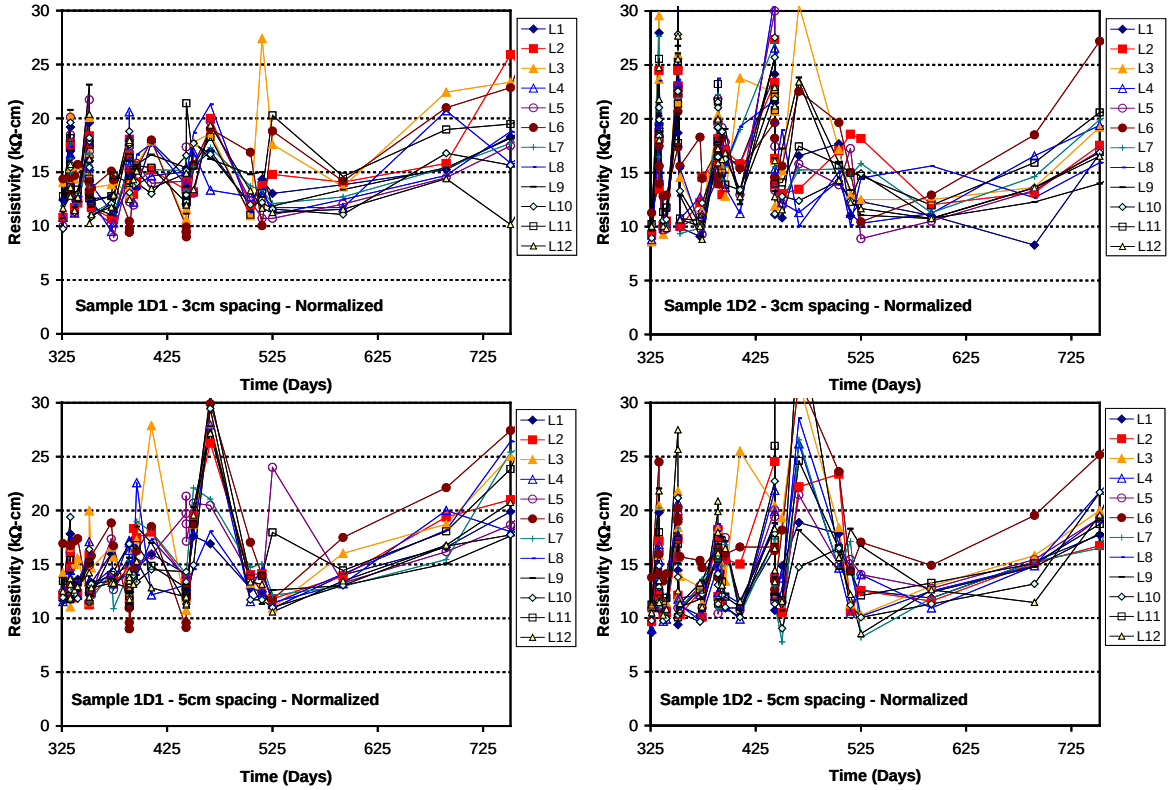

OPC Samples 1D1 and 1D2, samples with four rebars after day 325

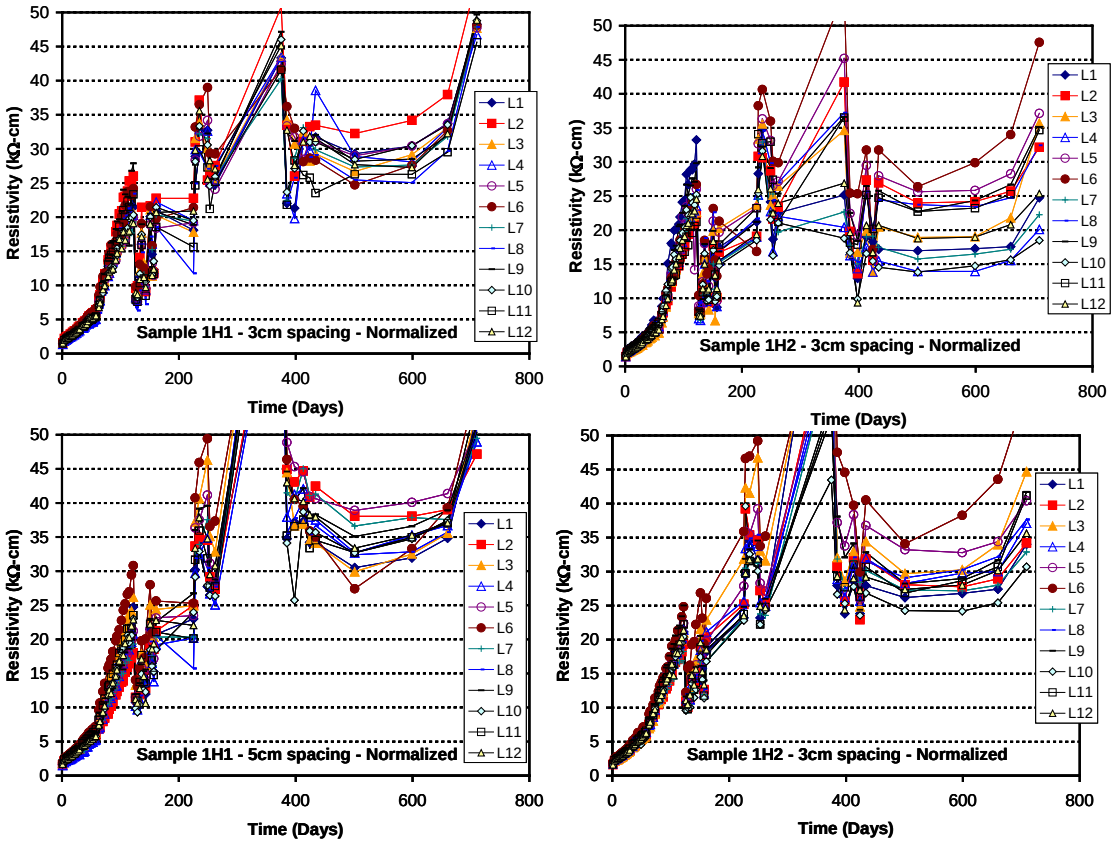

OPC+FA Samples 1H1 and 1H2, samples with four rebars

Appendix 4. Chloride profiles from field cores

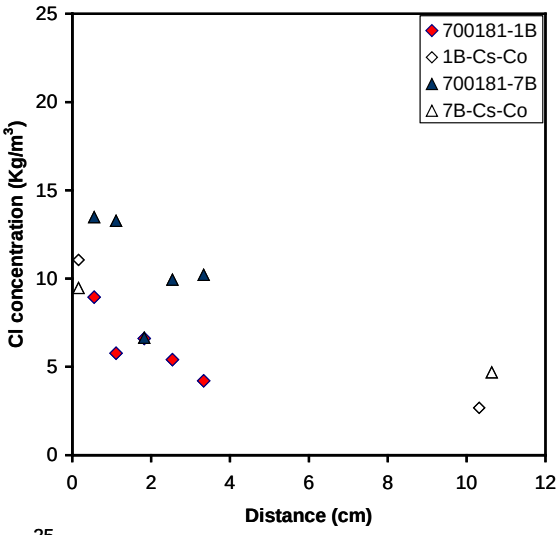

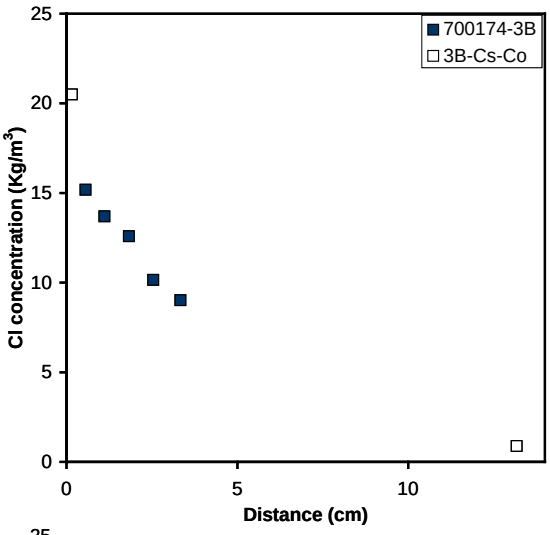

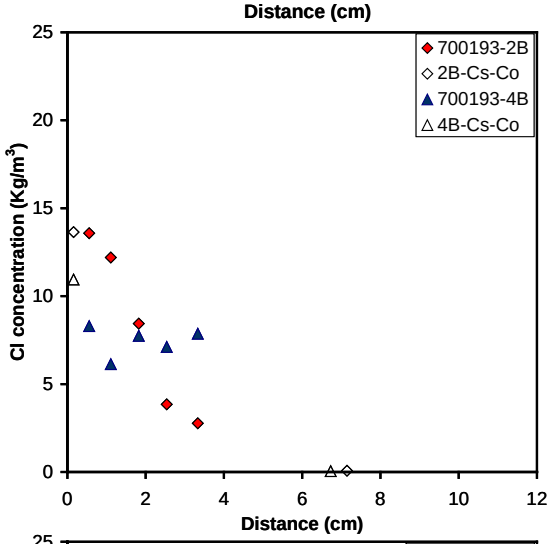

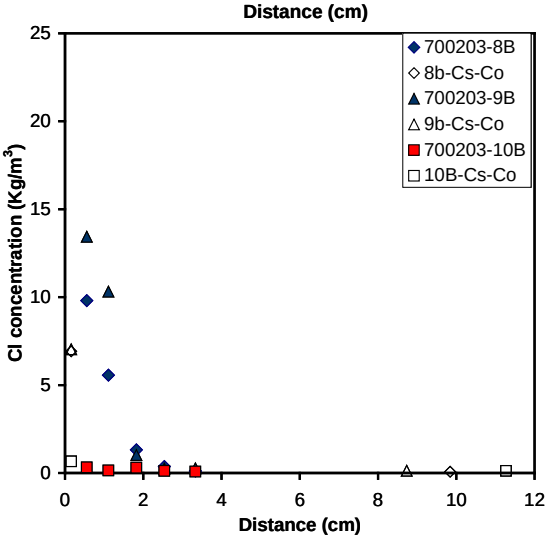

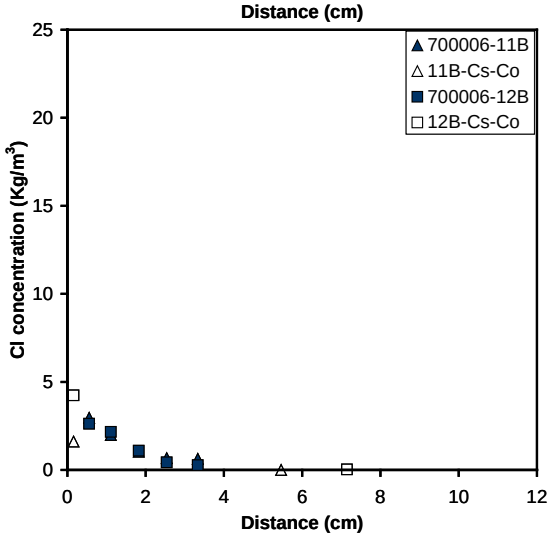

NOTE: Label next to color symbol is the Bridge# followed by core-ID number.

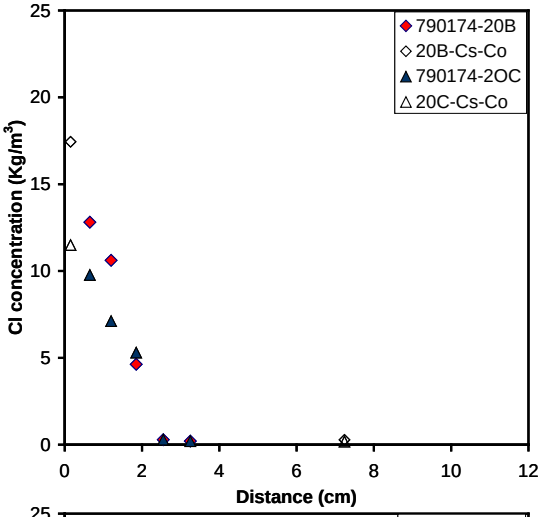
790174-20B
20B-Cs-Co
790174-2OC
20C-Cs-Co
Cl concentration (Kg/m3)
Distance (cm)

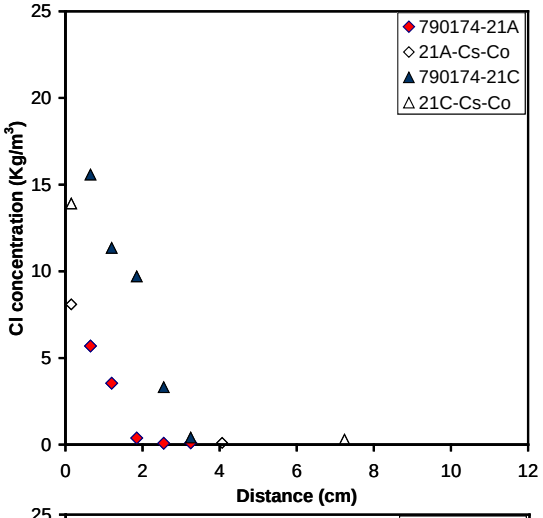
790174-21A
21A-Cs-Co
790174-21C
21C-Cs-Co
Cl concentration (Kg/m3)
Distance (cm)

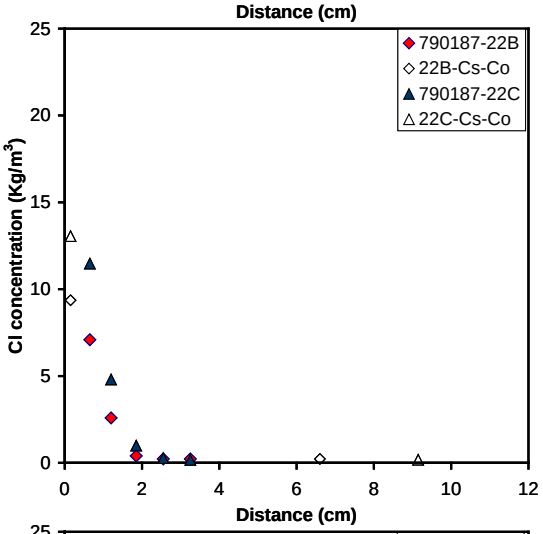
790187-22B
22B-Cs-Co
790187-22C
22C-Cs-Co
Cl concentration (Kg/m3)
Distance (cm)

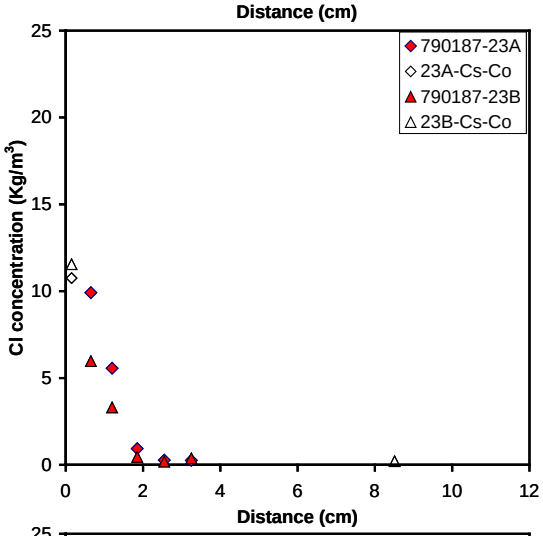
790187-23A
23A-Cs-Co
790187-23B
23B-Cs-Co
Cl concentration (Kg/m3)
Distance (cm)

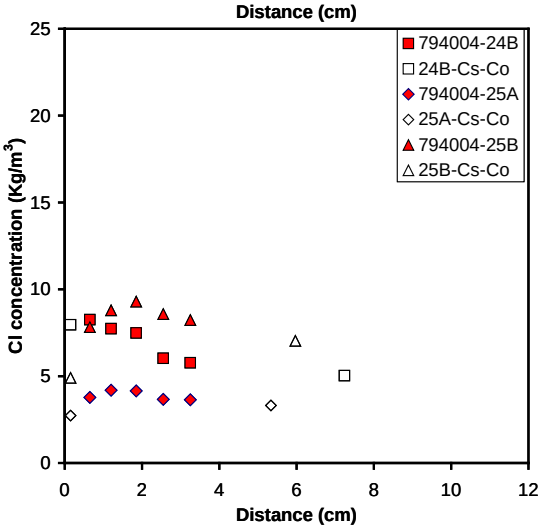
794004-24B
24B-Cs-Co
794004-25A
25A-Cs-Co
794004-25B
25B-Cs-Co
Cl concentration (Kg/m3)
Distance (cm)

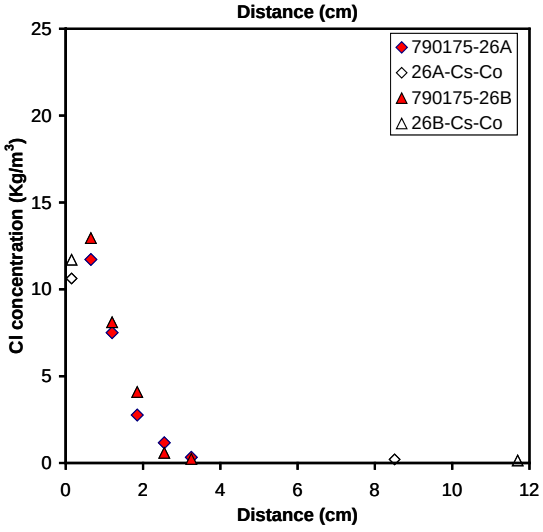
790175-26A
26A-Cs-Co
790175-26B
26B-Cs-Co
Cl concentration (Kg/m3)
Distance (cm)

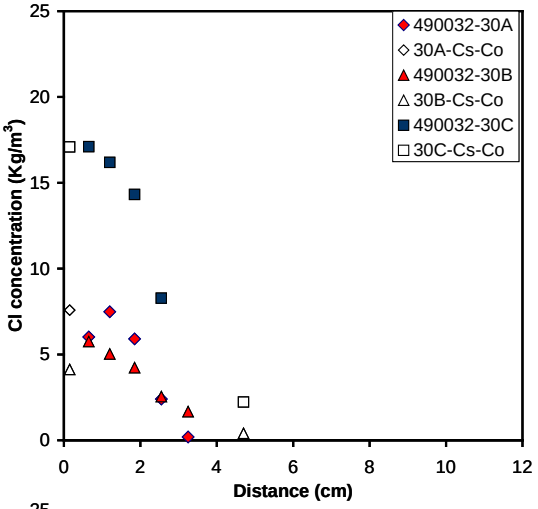
490032-30A
30A-Cs-Co
490032-30B
30B-Cs-Co
490032-30C
30C-Cs-Co
Cl concentration (Kg/m3)
Distance (cm)

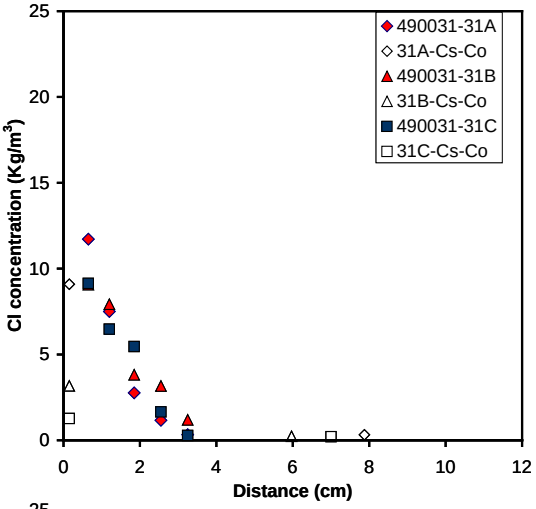
490031-31A
31A-Cs-Co
490031-31B
31B-Cs-Co
490031-31C
31C-Cs-Co
Cl concentration (Kg/m3)
Distance (cm)

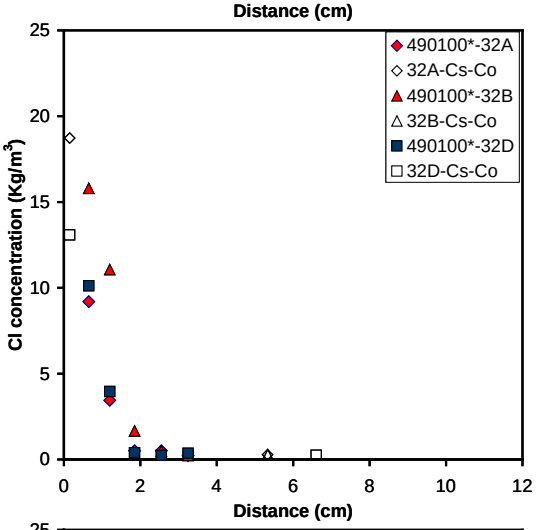
490100*-32A
32A-Cs-Co
490100*-32B
32B-Cs-Co
490100*-32D
32D-Cs-Co
Cl concentration (Kg/m3)
Distance (cm)

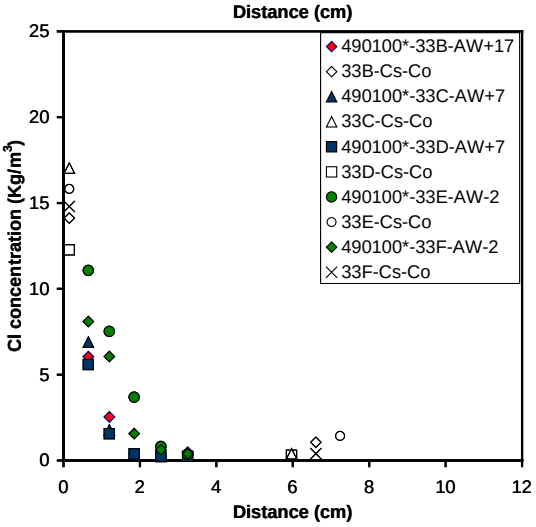
490100*-33B-AW+17
33B-Cs-Co
490100*-33C-AW+7
33C-Cs-Co
490100*-33D-AW+7
33D-Cs-Co
490100*-33E-AW-2
33E-Cs-Co
490100*-33F-AW-2
33F-Cs-Co
Cl concentration (Kg/m3)
Distance (cm)

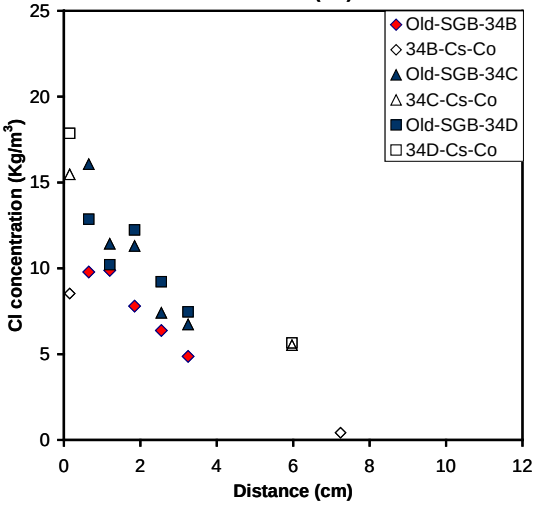
Old-SGB-34B
34B-Cs-Co
Old-SGB-34C
34C-Cs-Co
Old-SGB-34D
34D-Cs-Co
Cl concentration (Kg/m3)
Distance (cm)

UFA+FA

FA

SF+FA

Slag+FA

MK+FA

OPC

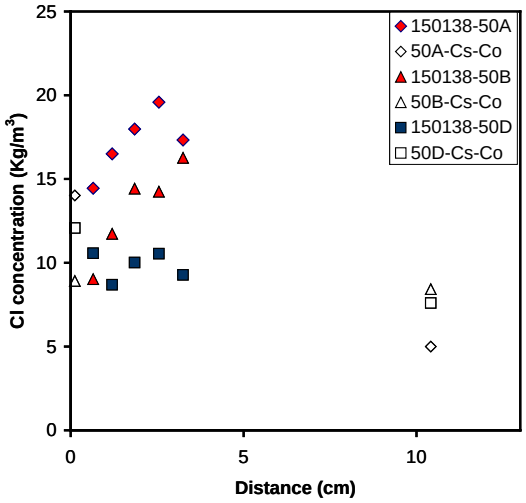
150138-50A
50A-Cs-Co
150138-50B
50B-Cs-Co
150138-50D
50D-Cs-Co
Cl concentration (Kg/m3)
Distance (cm)

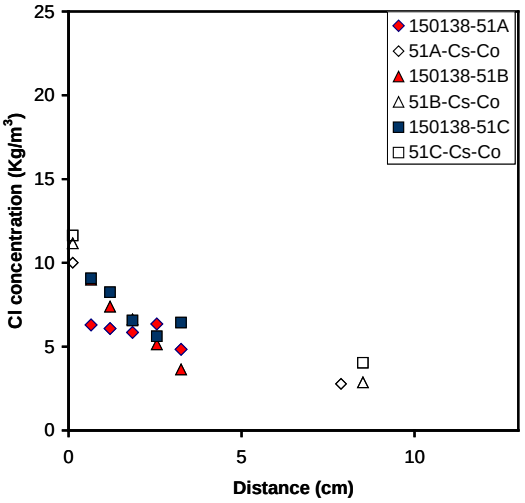
150138-51A
51A-Cs-Co
150138-51B
51B-Cs-Co
150138-51C
51C-Cs-Co
Cl concentration (Kg/m3)
Distance (cm)

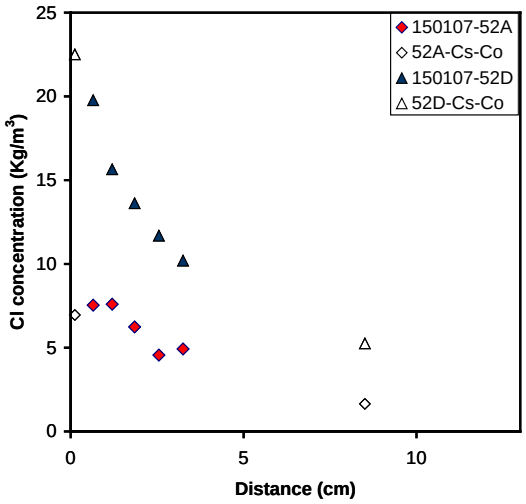
150107-52A
52A-Cs-Co
150107-52D
52D-Cs-Co
Cl concentration (Kg/m3)
Distance (cm)

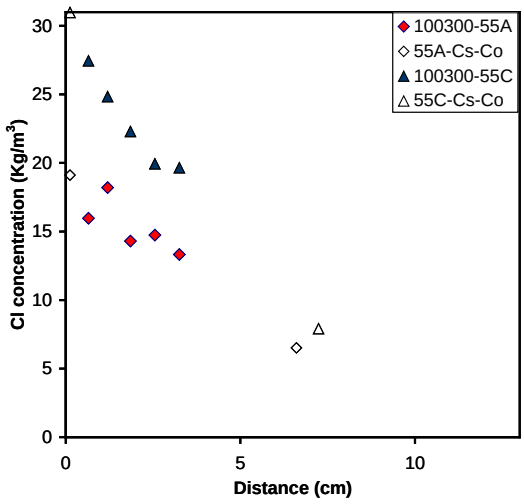
100300-55A
55A-Cs-Co
100300-55C
55C-Cs-Co
Cl concentration (Kg/m3)
Distance (cm)

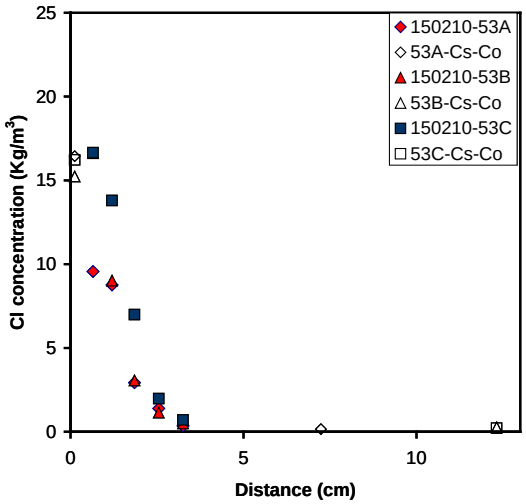
150210-53A
53A-Cs-Co
150210-53B
53B-Cs-Co
150210-53C
53C-Cs-Co
Cl concentration (Kg/m3)
Distance (cm)

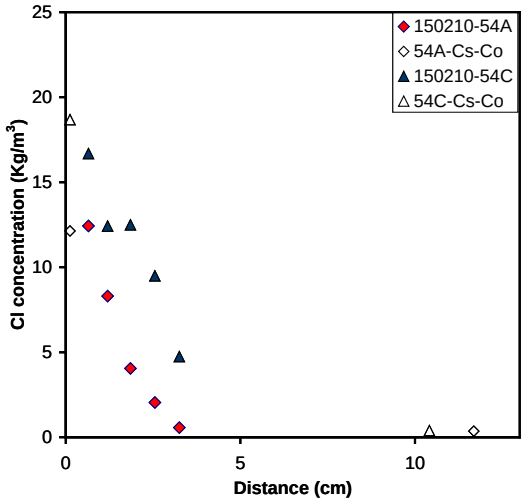
150210-54A
54A-Cs-Co
150210-54C
54C-Cs-Co
Cl concentration (Kg/m3)
Distance (cm)

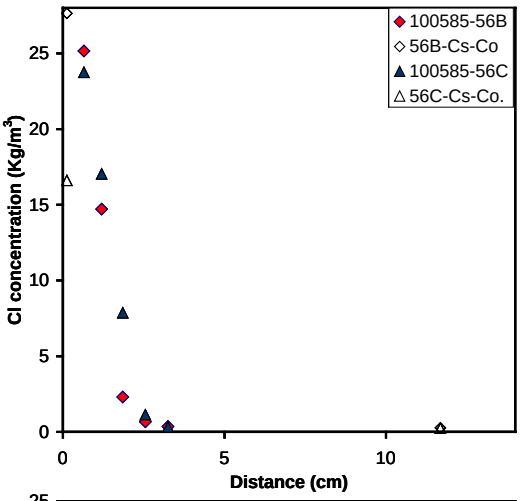
100585-56B
56B-Cs-Co
100585-56C
56C-Cs-Co.
Cl concentration (Kg/m3)
Distance (cm)

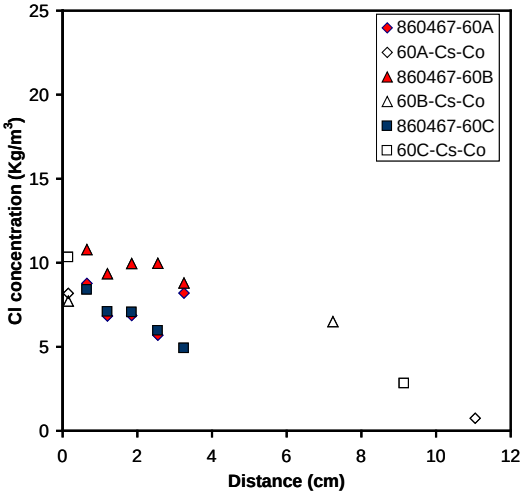
860467-60A
60A-Cs-Co
860467-60B
60B-Cs-Co
860467-60C
60C-Cs-Co
Cl concentration (Kg/m3)
Distance (cm)

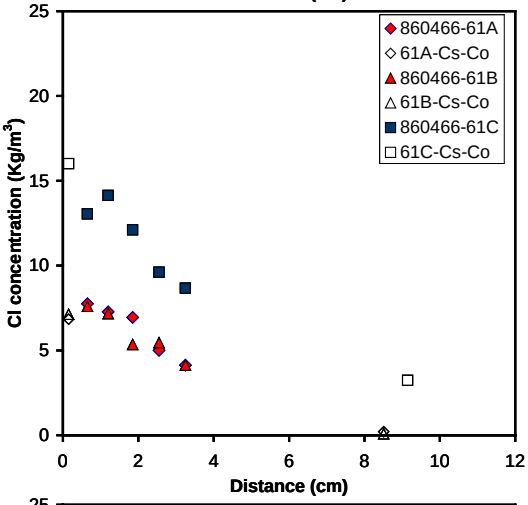
860466-61A
61A-Cs-Co
860466-61B
61B-Cs-Co
860466-61C
61C-Cs-Co
Cl concentration (Kg/m3)
Distance (cm)

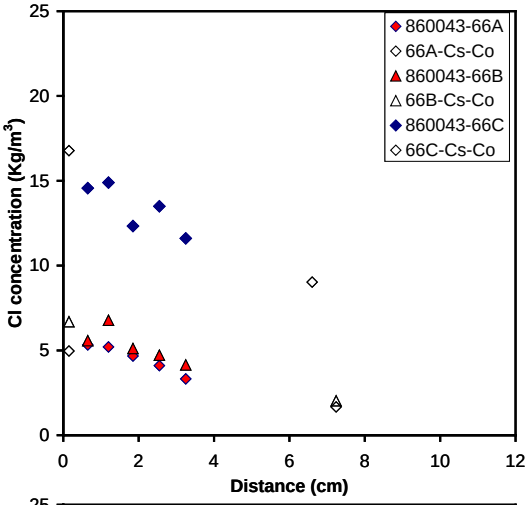
860043-66A
66A-Cs-Co
860043-66B
66B-Cs-Co
860043-66C
66C-Cs-Co
Cl concentration (Kg/m3)
Distance (cm)

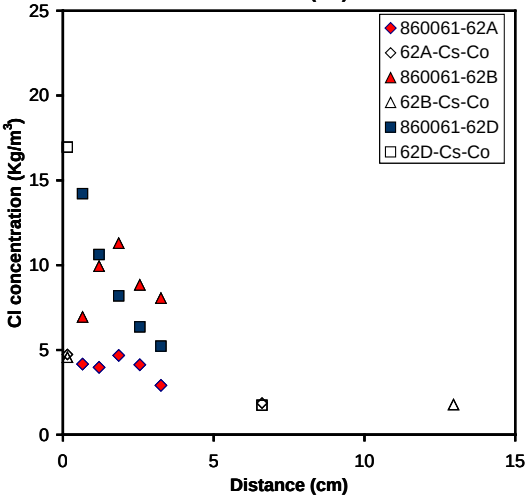
860061-62A
62A-Cs-Co
860061-62B
62B-Cs-Co
860061-62D
62D-Cs-Co
Cl concentration (Kg/m3)
Distance (cm)

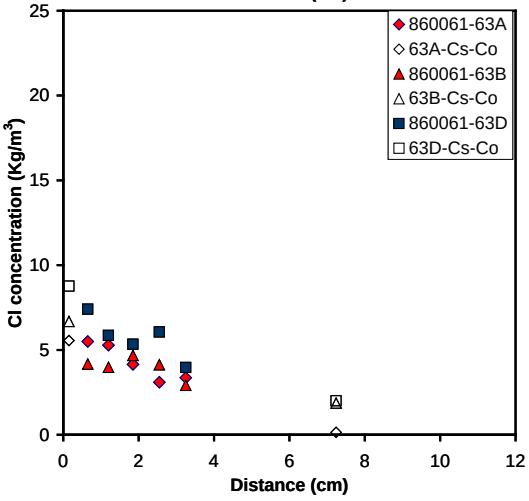
860061-63A
63A-Cs-Co
860061-63B
63B-Cs-Co
860061-63D
63D-Cs-Co
Cl concentration (Kg/m3)
Distance (cm)

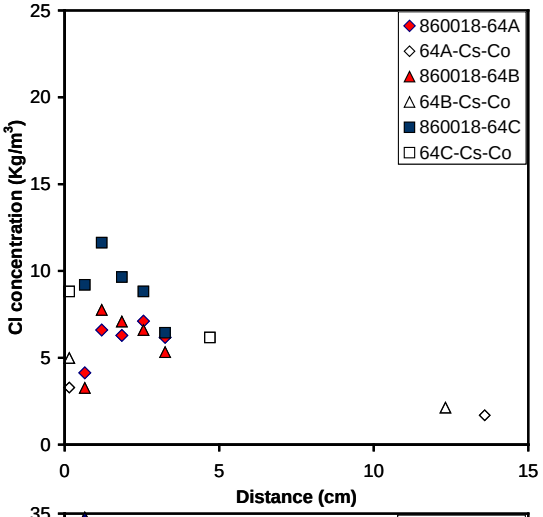
860018-64A
64A-Cs-Co
860018-64B
64B-Cs-Co
860018-64C
64C-Cs-Co
Cl concentration (Kg/m3)
Distance (cm)

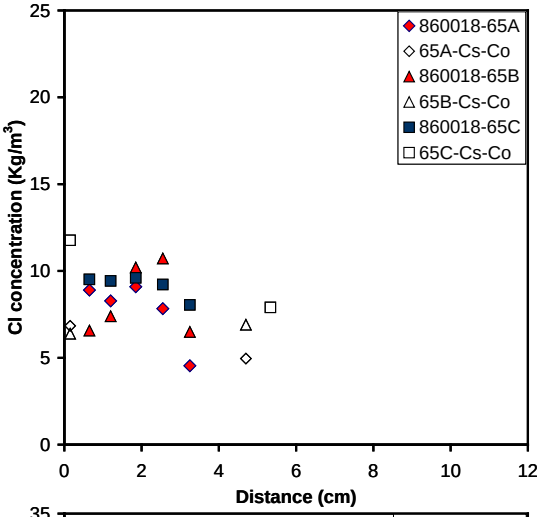
860018-65A
65A-Cs-Co
860018-65B
65B-Cs-Co
860018-65C
65C-Cs-Co
Cl concentration (Kg/m3)
Distance (cm)

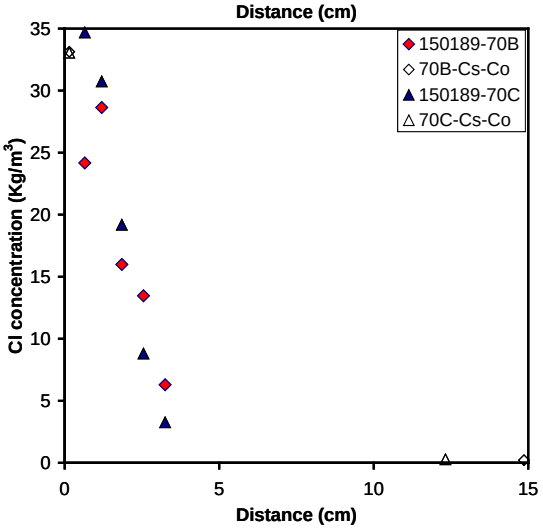
150189-70B
70B-Cs-Co
150189-70C
70C-Cs-Co
Cl concentration (Kg/m3)
Distance (cm)

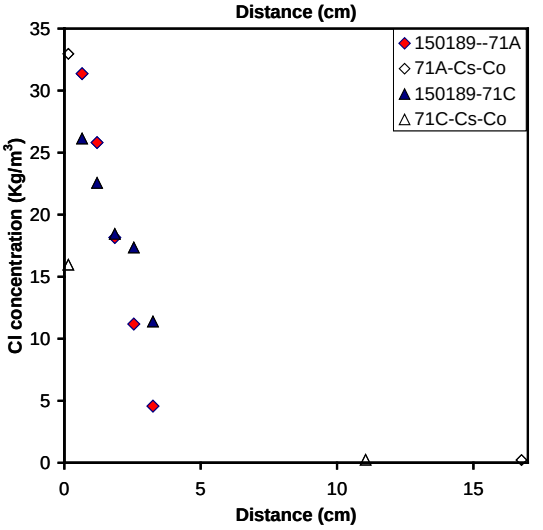
150189--71A
71A-Cs-Co
150189-71C
71C-Cs-Co
Cl concentration (Kg/m3)
Distance (cm)

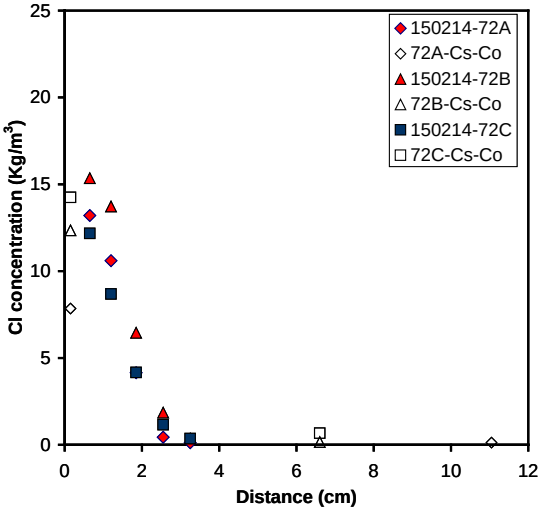
150214-72A
72A-Cs-Co
150214-72B
72B-Cs-Co
150214-72C
72C-Cs-Co
Cl concentration (Kg/m3)
Distance (cm)

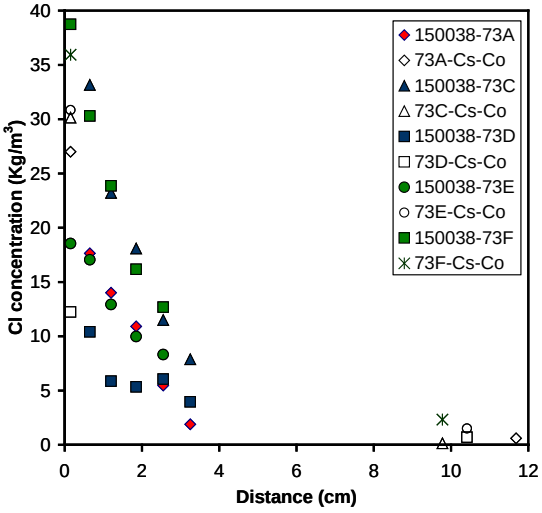
150038-73A
73A-Cs-Co
150038-73C
73C-Cs-Co
150038-73D
73D-Cs-Co
150038-73E
73E-Cs-Co
150038-73F
73F-Cs-Co
Cl concentration (Kg/m3)
Distance (cm)

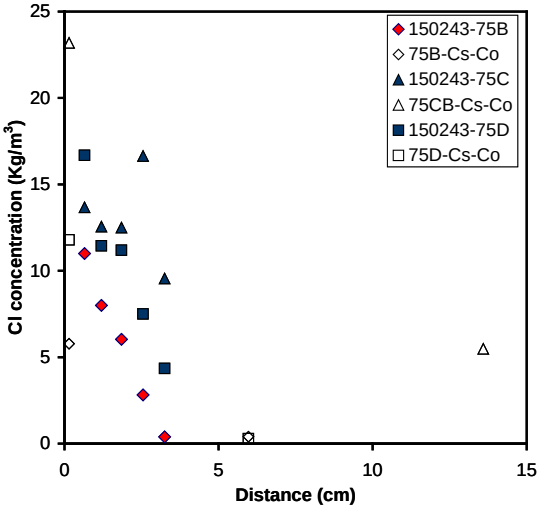
150243-75B
75B-Cs-Co
150243-75C
75CB-Cs-Co
150243-75D
75D-Cs-Co
Cl concentration (Kg/m3)
Distance (cm)
0
5
10
15
20
25

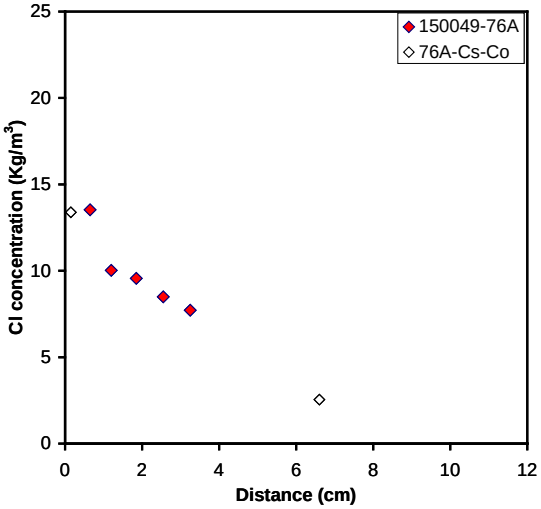
150049-76A
76A-Cs-Co
Cl concentration (Kg/m3)
Distance (cm)
0
2
4
6
8
10
12
0
5
10
15
20
25

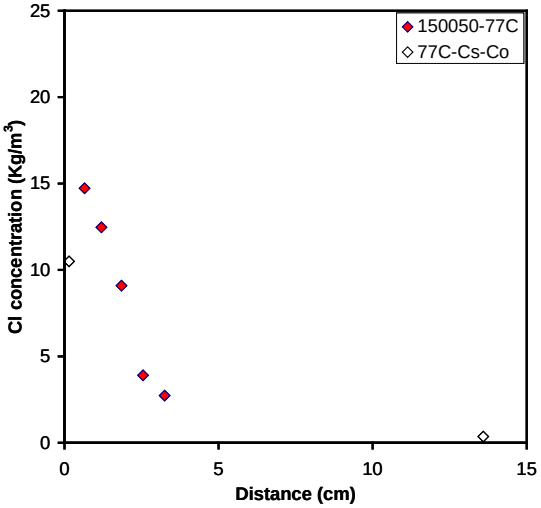
150050-77C
77C-Cs-Co
Cl concentration (Kg/m3)
Distance (cm)
0
5
10
15
20
25

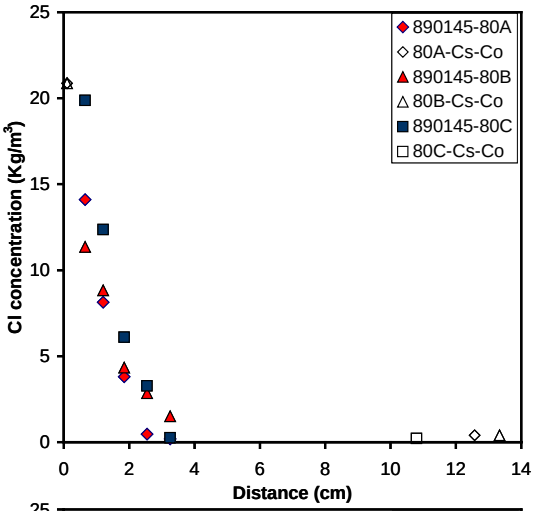
890145-80A
80A-Cs-Co
890145-80B
80B-Cs-Co
890145-80C
80C-Cs-Co
Cl concentration (Kg/m3)
Distance (cm)

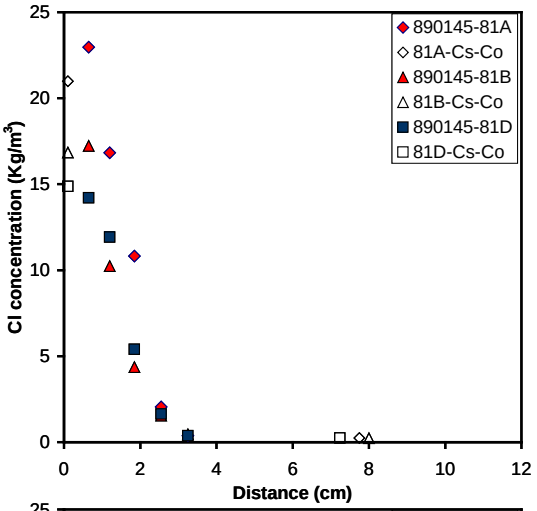
890145-81A
81A-Cs-Co
890145-81B
81B-Cs-Co
890145-81D
81D-Cs-Co
Cl concentration (Kg/m3)
Distance (cm)

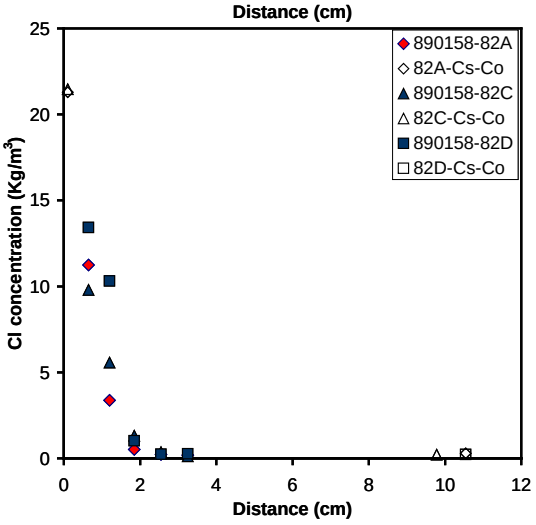
890158-82A
82A-Cs-Co
890158-82C
82C-Cs-Co
890158-82D
82D-Cs-Co
Cl concentration (Kg/m3)
Distance (cm)

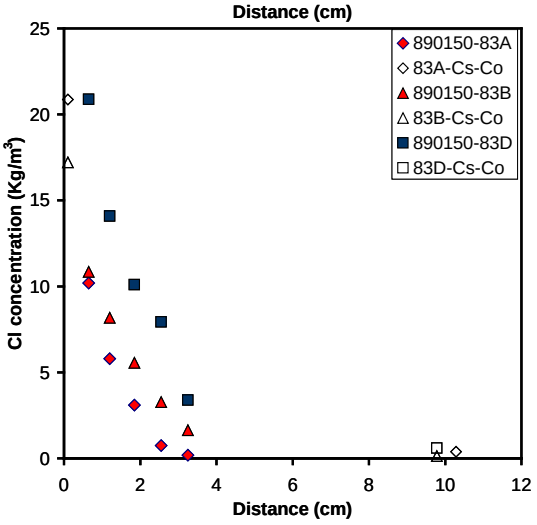
890150-83A
83A-Cs-Co
890150-83B
83B-Cs-Co
890150-83D
83D-Cs-Co
Cl concentration (Kg/m3)
Distance (cm)

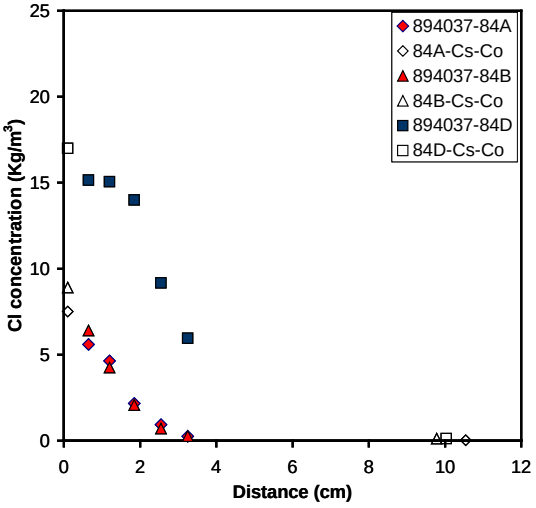
894037-84A
84A-Cs-Co
894037-84B
84B-Cs-Co
894037-84D
84D-Cs-Co
Cl concentration (Kg/m3)
Distance (cm)

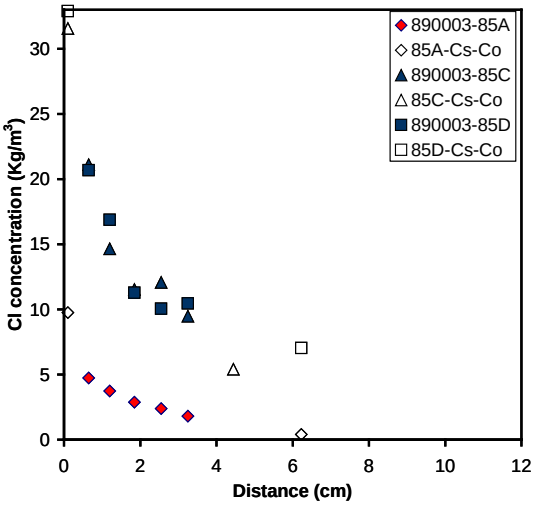
890003-85A
85A-Cs-Co
890003-85C
85C-Cs-Co
890003-85D
85D-Cs-Co
Cl concentration (Kg/m3)
Distance (cm)

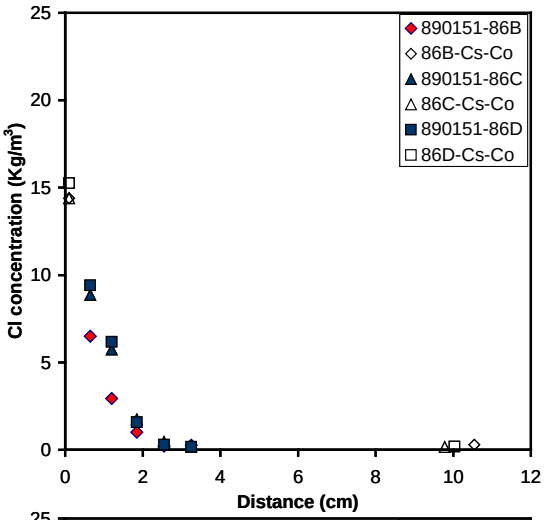
890151-86B
86B-Cs-Co
890151-86C
86C-Cs-Co
890151-86D
86D-Cs-Co
Cl concentration (Kg/m3)
Distance (cm)

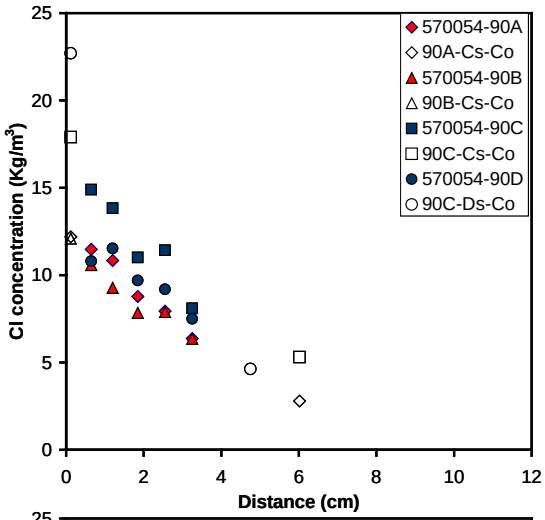
570054-90A
90A-Cs-Co
570054-90B
90B-Cs-Co
570054-90C
90C-Cs-Co
570054-90D
90C-Ds-Co
Cl concentration (Kg/m3)
Distance (cm)

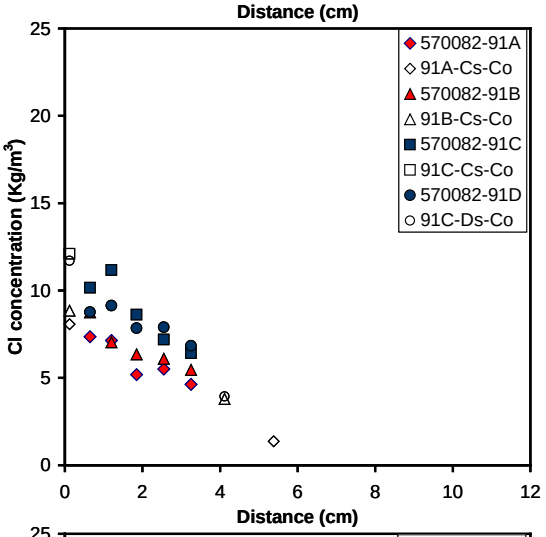
570082-91A
91A-Cs-Co
570082-91B
91B-Cs-Co
570082-91C
91C-Cs-Co
570082-91D
91C-Ds-Co
Cl concentration (Kg/m3)
Distance (cm)

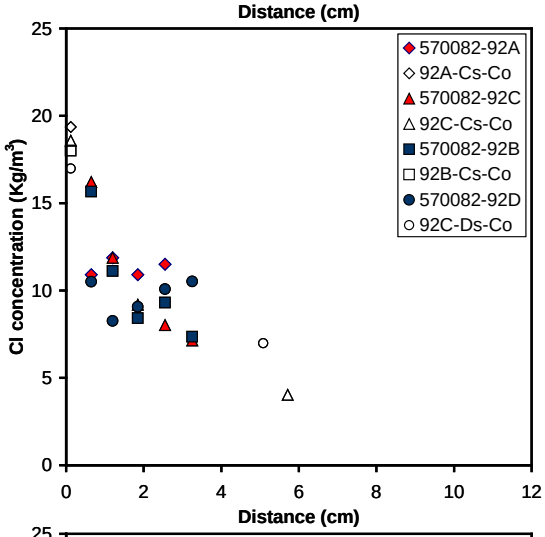
570082-92A
92A-Cs-Co
570082-92C
92C-Cs-Co
570082-92B
92B-Cs-Co
570082-92D
92C-Ds-Co
Cl concentration (Kg/m3)
Distance (cm)

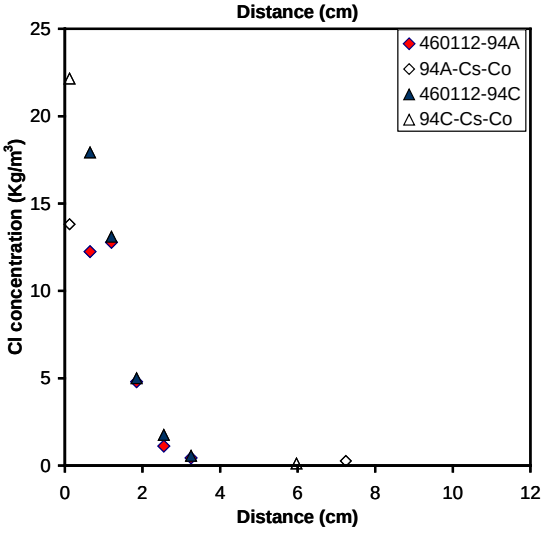
460112-94A
94A-Cs-Co
460112-94C
94C-Cs-Co
Cl concentration (Kg/m3)
Distance (cm)

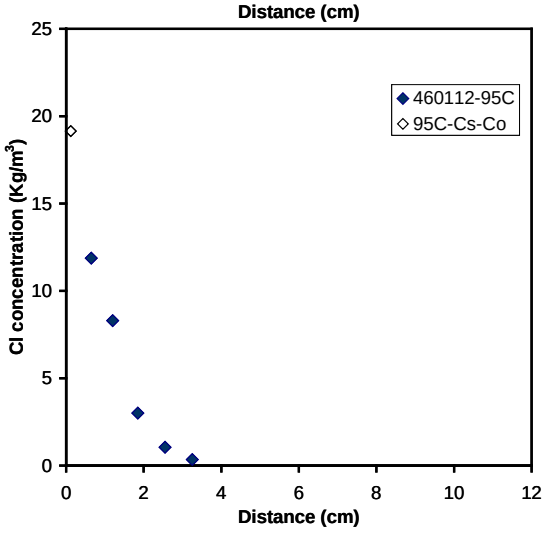
460112-95C
95C-Cs-Co
Cl concentration (Kg/m3)
Distance (cm)

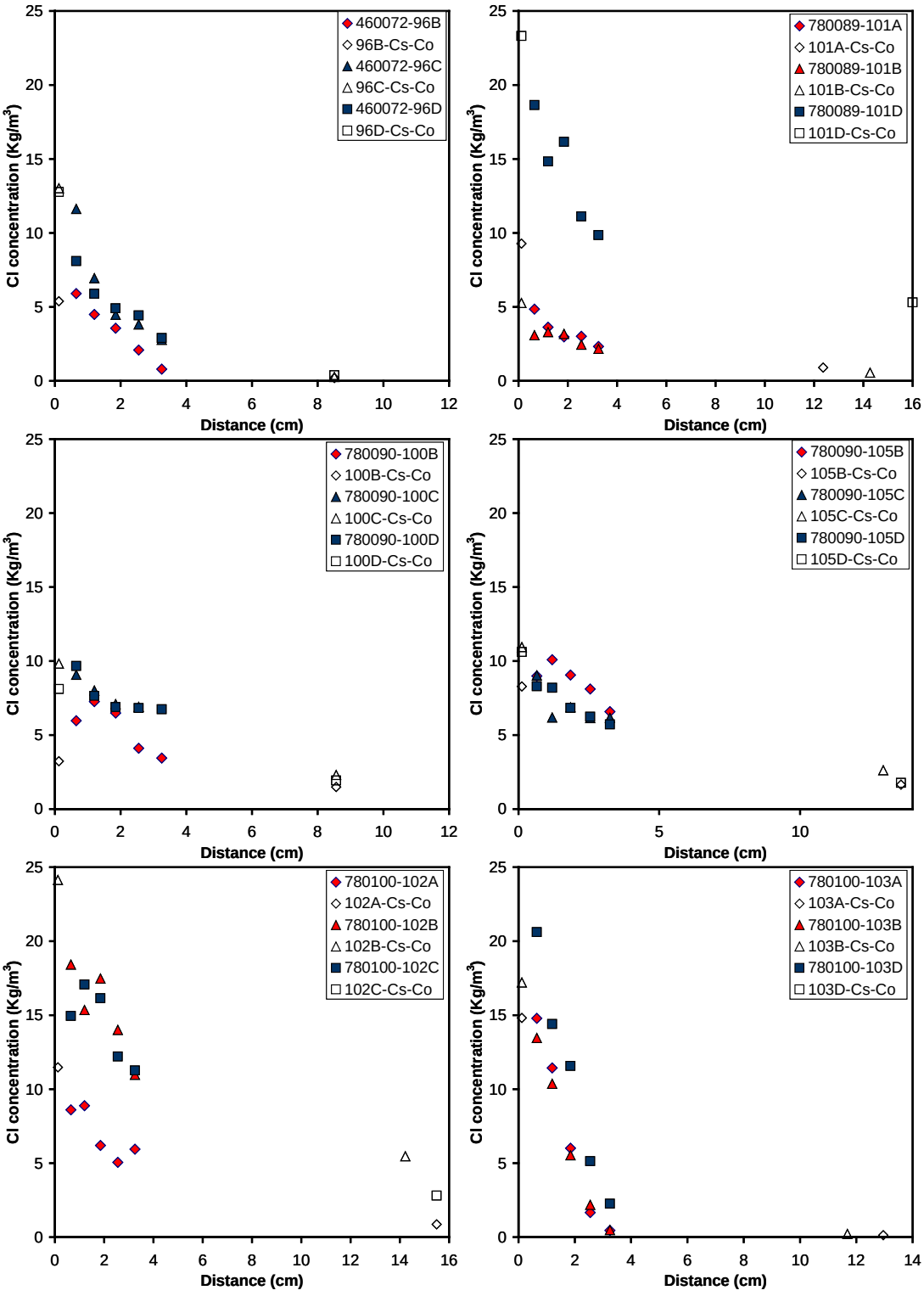
460072-96B
96B-Cs-Co
460072-96C
96C-Cs-Co
460072-96D
96D-Cs-Co
780089-101A
101A-Cs-Co
780089-101B
101B-Cs-Co
780089-101D
101D-Cs-Co
780090-100B
100B-Cs-Co
780090-100C
100C-Cs-Co
780090-100D
100D-Cs-Co
780090-105B
105B-Cs-Co
780090-105C
105C-Cs-Co
780090-105D
105D-Cs-Co
780100-102A
102A-Cs-Co
780100-102B
102B-Cs-Co
780100-102C
102C-Cs-Co
780100-103A
103A-Cs-Co
780100-103B
103B-Cs-Co
780100-103D
103D-Cs-Co
Cl concentration (Kg/m3)
Distance (cm)

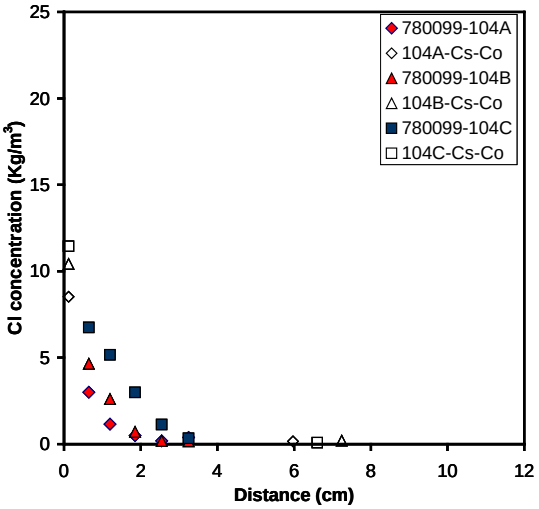
780099-104A
104A-Cs-Co
780099-104B
104B-Cs-Co
780099-104C
104C-Cs-Co
Cl concentration (Kg/m3)
Distance (cm)

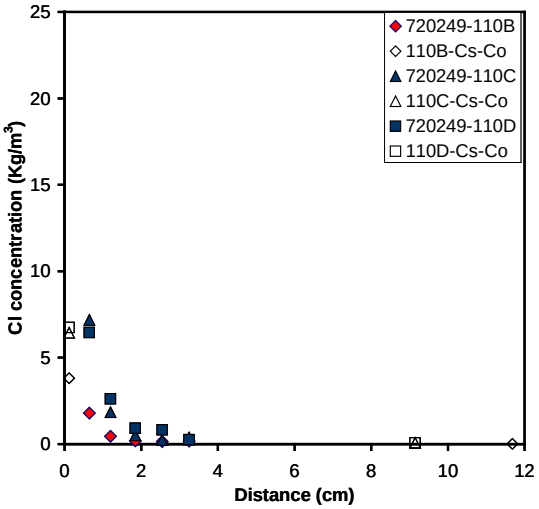
720249-110B
110B-Cs-Co
720249-110C
110C-Cs-Co
720249-110D
110D-Cs-Co
Cl concentration (Kg/m3)
Distance (cm)

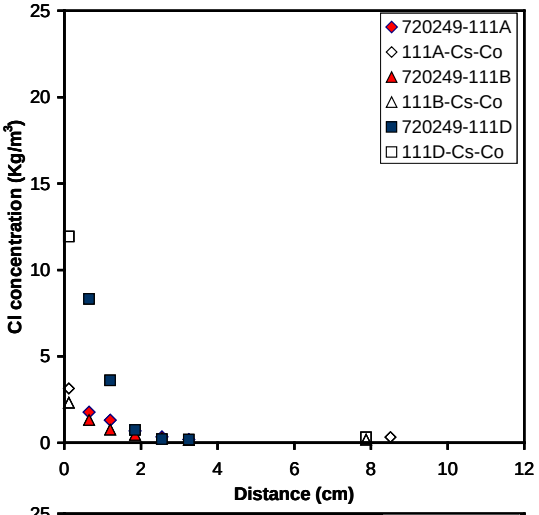
720249-111A
111A-Cs-Co
720249-111B
111B-Cs-Co
720249-111D
111D-Cs-Co
Cl concentration (Kg/m3)
Distance (cm)

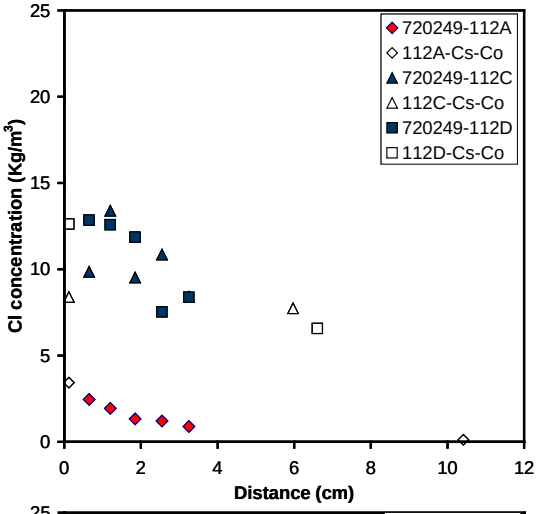
720249-112A
112A-Cs-Co
720249-112C
112C-Cs-Co
720249-112D
112D-Cs-Co
Cl concentration (Kg/m3)
Distance (cm)

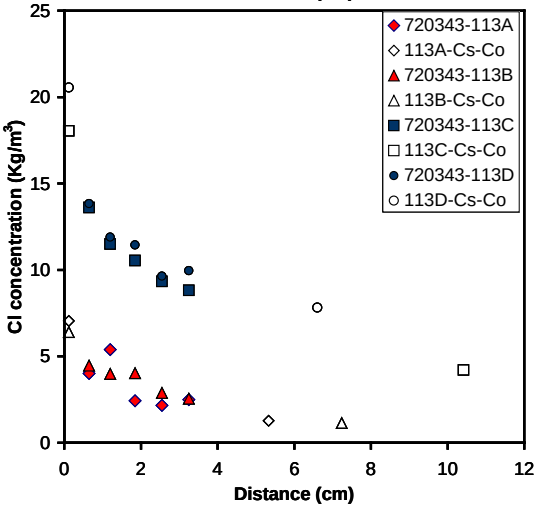
720343-113A
113A-Cs-Co
720343-113B
113B-Cs-Co
720343-113C
113C-Cs-Co
720343-113D
113D-Cs-Co
Cl concentration (Kg/m3)
Distance (cm)

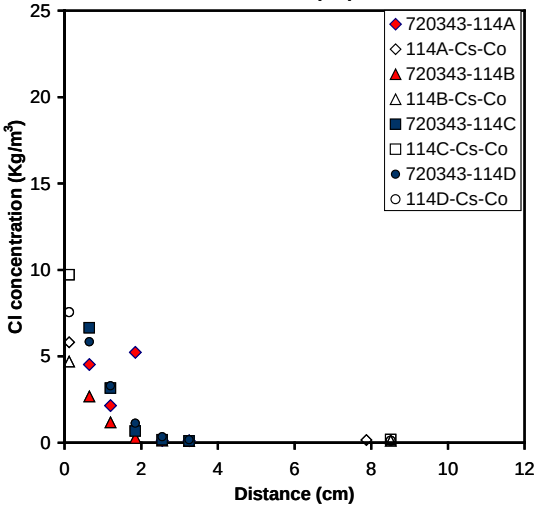
720343-114A
114A-Cs-Co
720343-114B
114B-Cs-Co
720343-114C
114C-Cs-Co
720343-114D
114D-Cs-Co
Cl concentration (Kg/m3)
Distance (cm)

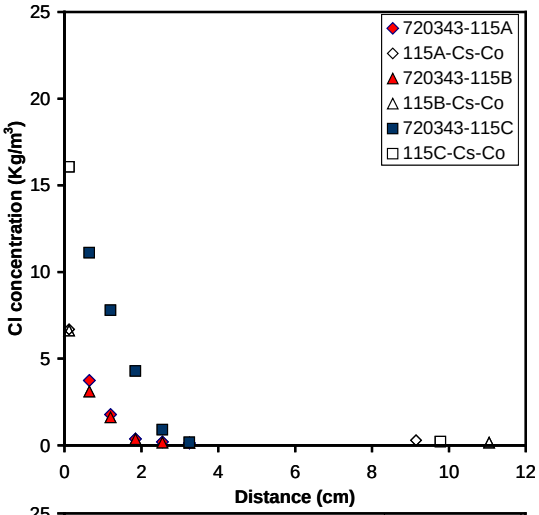
720343-115A
115A-Cs-Co
720343-115B
115B-Cs-Co
720343-115C
115C-Cs-Co
Cl concentration (Kg/m3)
Distance (cm)

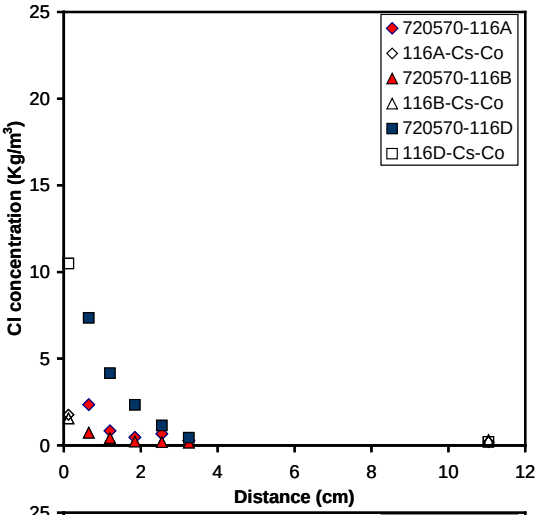
720570-116A
116A-Cs-Co
720570-116B
116B-Cs-Co
720570-116D
116D-Cs-Co
Cl concentration (Kg/m3)
Distance (cm)

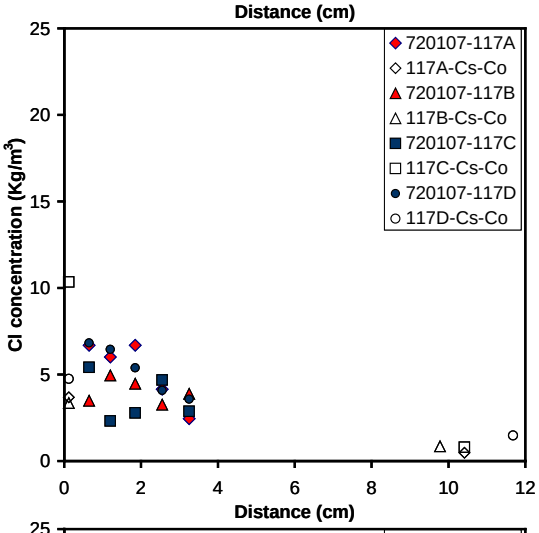
720107-117A
117A-Cs-Co
720107-117B
117B-Cs-Co
720107-117C
117C-Cs-Co
720107-117D
117D-Cs-Co
Cl concentration (Kg/m3)
Distance (cm)

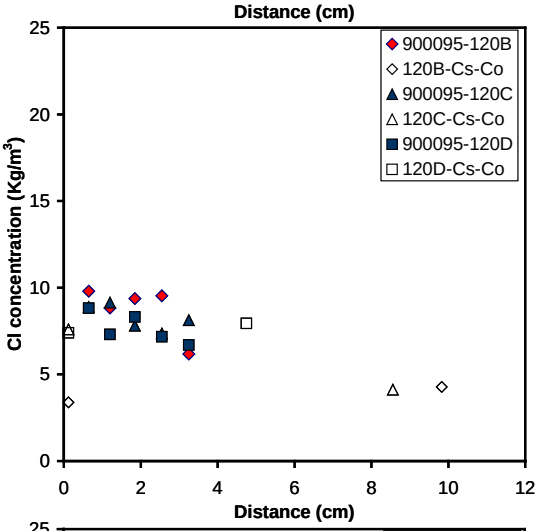
900095-120B
120B-Cs-Co
900095-120C
120C-Cs-Co
900095-120D
120D-Cs-Co
Cl concentration (Kg/m3)
Distance (cm)

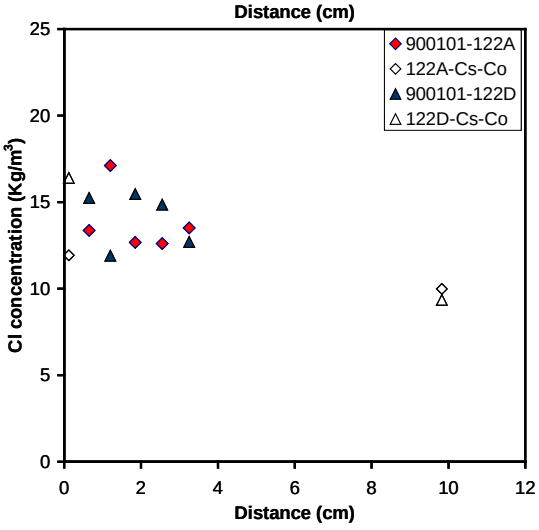
900101-122A
122A-Cs-Co
900101-122D
122D-Cs-Co
Cl concentration (Kg/m3)
Distance (cm)

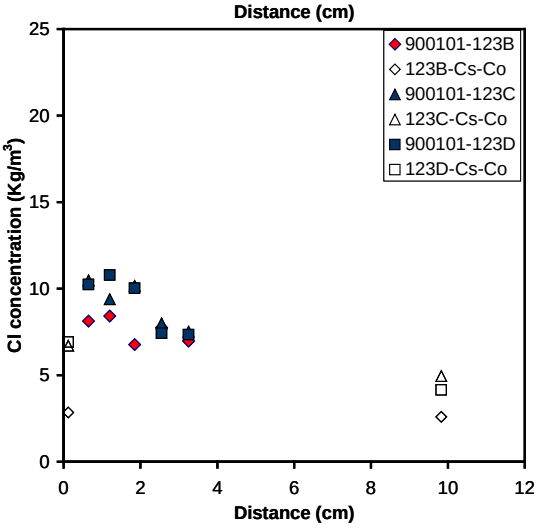
900101-123B
123B-Cs-Co
900101-123C
123C-Cs-Co
900101-123D
123D-Cs-Co
Cl concentration (Kg/m3)
Distance (cm)

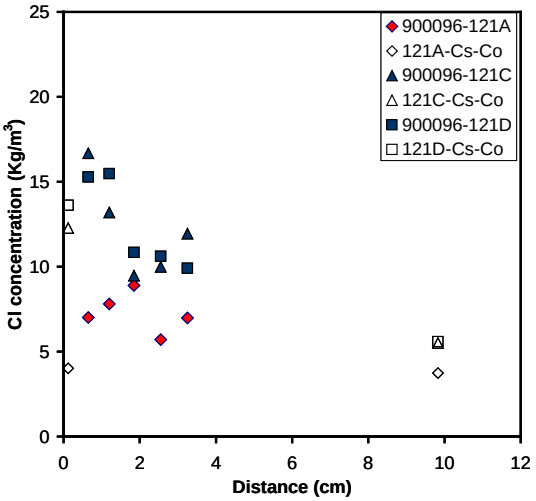
900096-121A
121A-Cs-Co
900096-121C
121C-Cs-Co
900096-121D
121D-Cs-Co
Cl concentration (Kg/m3)
Distance (cm)

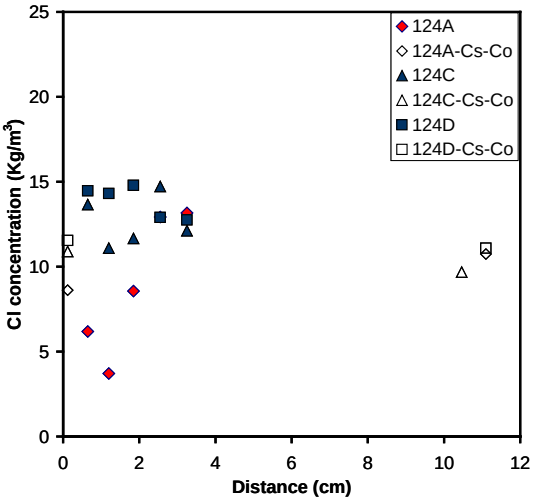
124A
124A-Cs-Co
124C
124C-Cs-Co
124D
124D-Cs-Co
Cl concentration (Kg/m3)
Distance (cm)

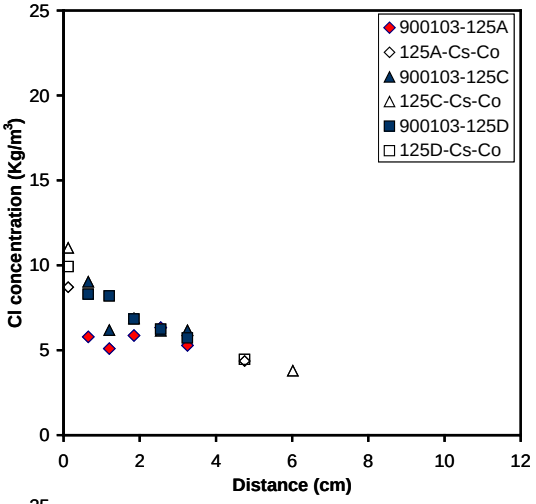
900103-125A
125A-Cs-Co
900103-125C
125C-Cs-Co
900103-125D
125D-Cs-Co
Cl concentration (Kg/m3)
Distance (cm)

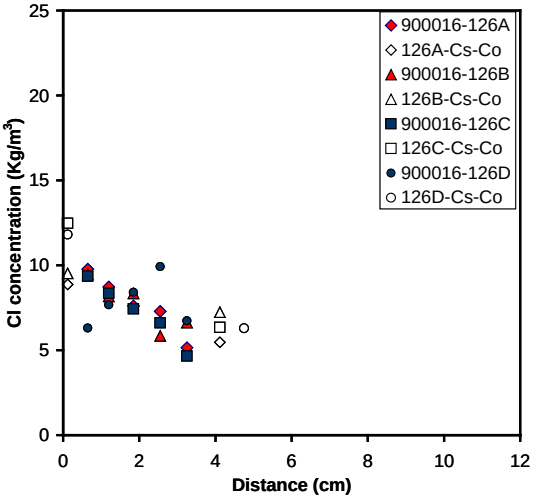
900016-126A
126A-Cs-Co
900016-126B
126B-Cs-Co
900016-126C
126C-Cs-Co
900016-126D
126D-Cs-Co
Cl concentration (Kg/m3)
Distance (cm)

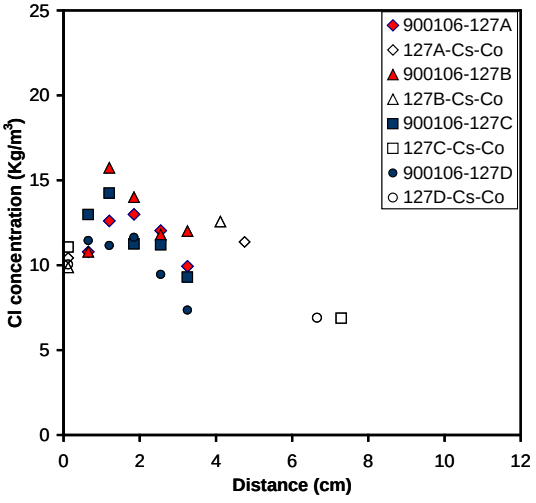
900106-127A
127A-Cs-Co
900106-127B
127B-Cs-Co
900106-127C
127C-Cs-Co
900106-127D
127D-Cs-Co
Cl concentration (Kg/m3)
Distance (cm)

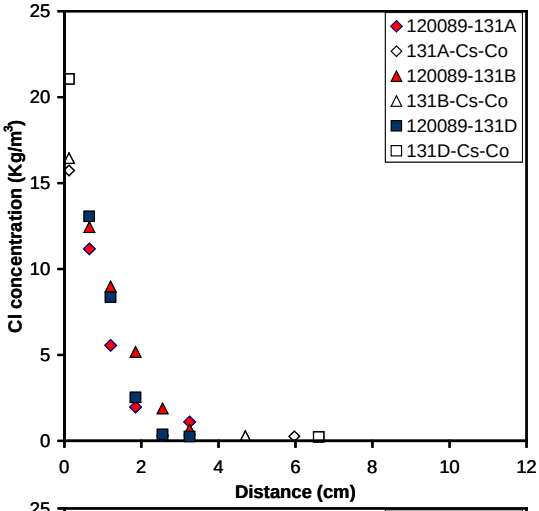
120089-131A
131A-Cs-Co
120089-131B
131B-Cs-Co
120089-131D
131D-Cs-Co
Cl concentration (Kg/m3)
Distance (cm)

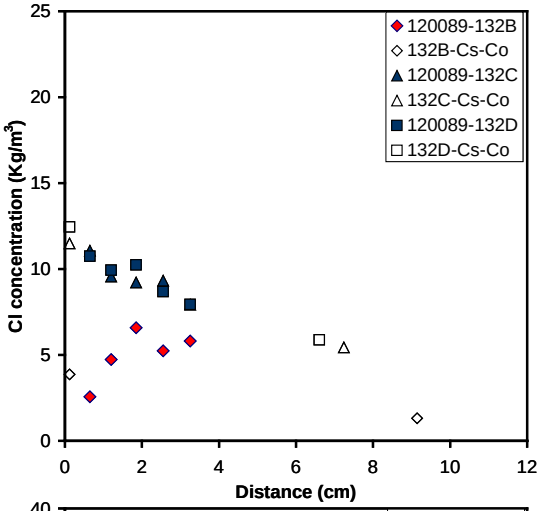
120089-132B
132B-Cs-Co
120089-132C
132C-Cs-Co
120089-132D
132D-Cs-Co
Cl concentration (Kg/m3)
Distance (cm)

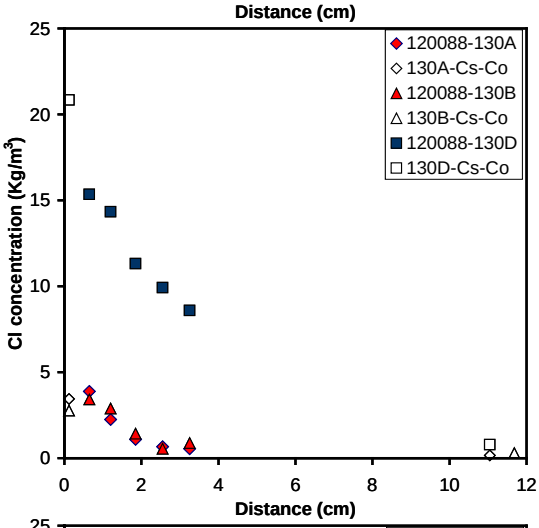
120088-130A
130A-Cs-Co
120088-130B
130B-Cs-Co
120088-130D
130D-Cs-Co
Cl concentration (Kg/m3)
Distance (cm)

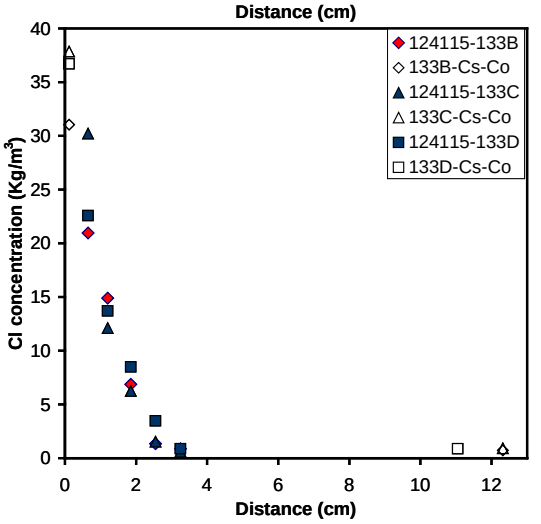
124115-133B
133B-Cs-Co
124115-133C
133C-Cs-Co
124115-133D
133D-Cs-Co
Cl concentration (Kg/m3)
Distance (cm)

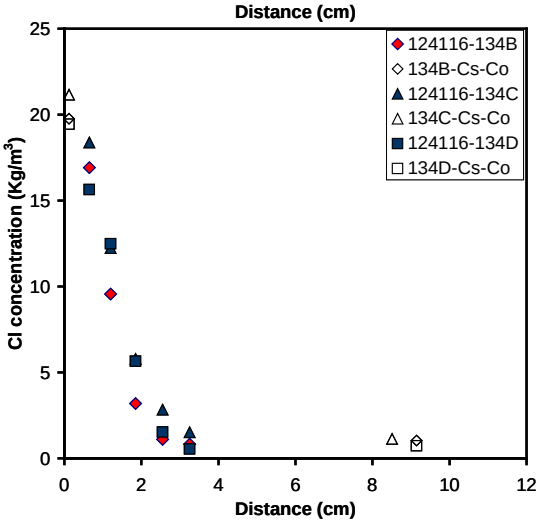
124116-134B
134B-Cs-Co
124116-134C
134C-Cs-Co
124116-134D
134D-Cs-Co
Cl concentration (Kg/m3)
Distance (cm)

Appendix 5. Resistivity profiles as a function of elevation at bridge # 136502

Note. Each page contains 6 plots, left column performed using a=3 cm, right column using a=5 cm, when available recorded concrete cover is also included.

Results from four visits to KRB #136502 are documented in this appendix.

136502
Key Royale Bridge
Bent 2 Pile 1 North Face
C Cover: 3 in

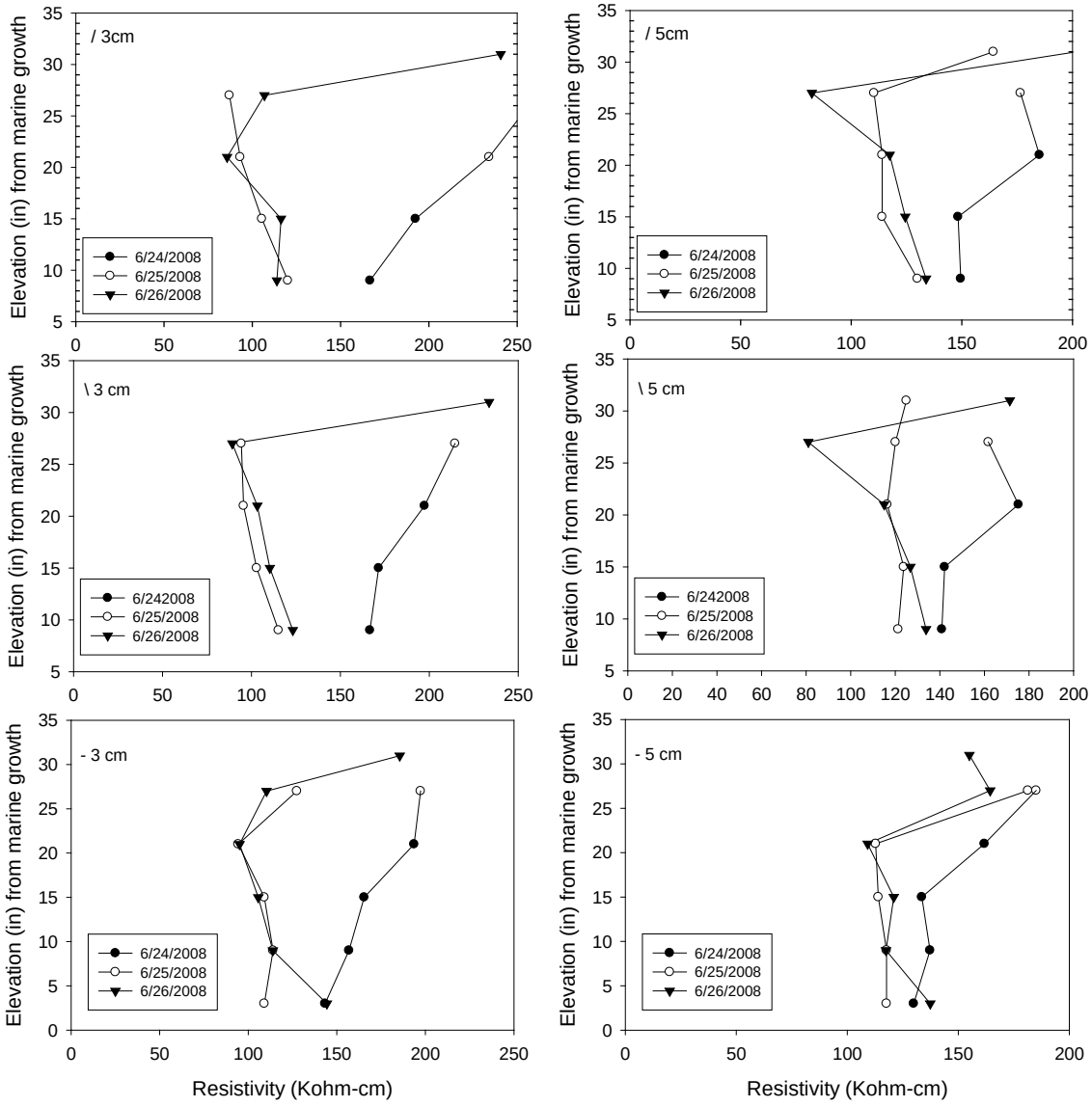

136502
Key Royale Bridge
Bent 2 Pile 2 South Face
C Cover: 3 in

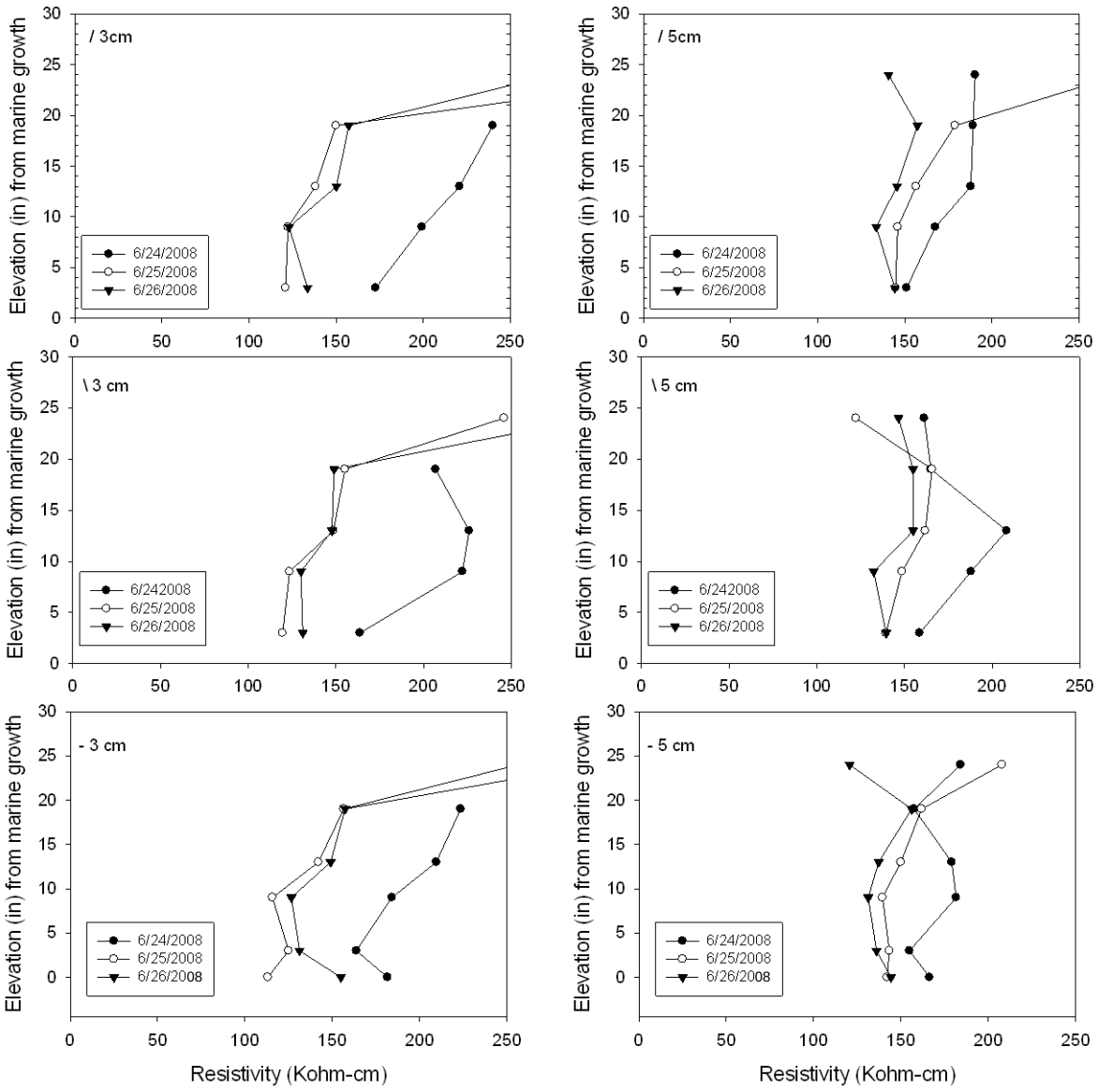

136502
Key Royale Bridge
Bent 2 Pile 3 North Face
C Cover: 3 in

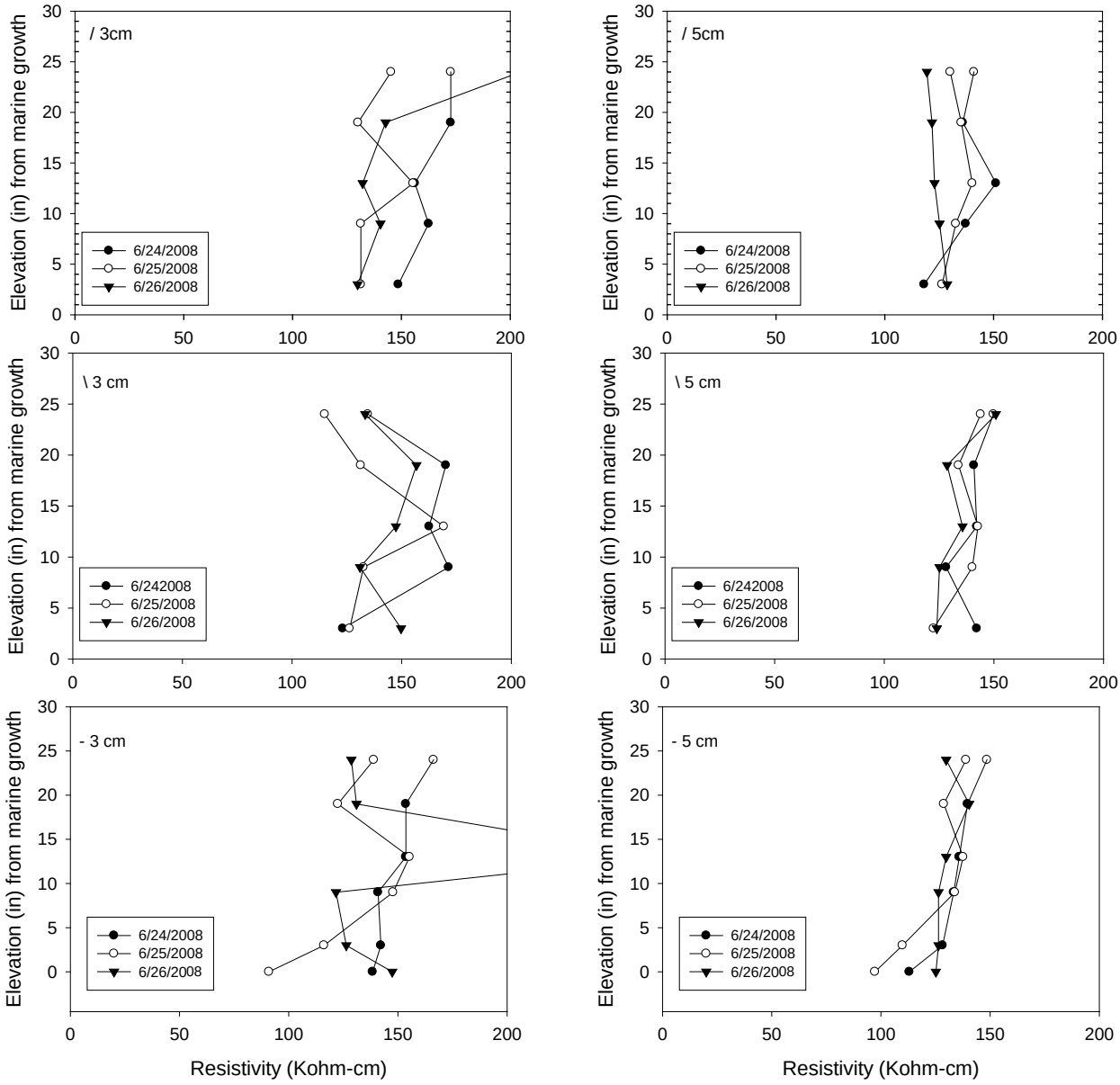

136502
Key Royale Bridge
Bent 2 Pile 4 North Face
C Cover: 3 in

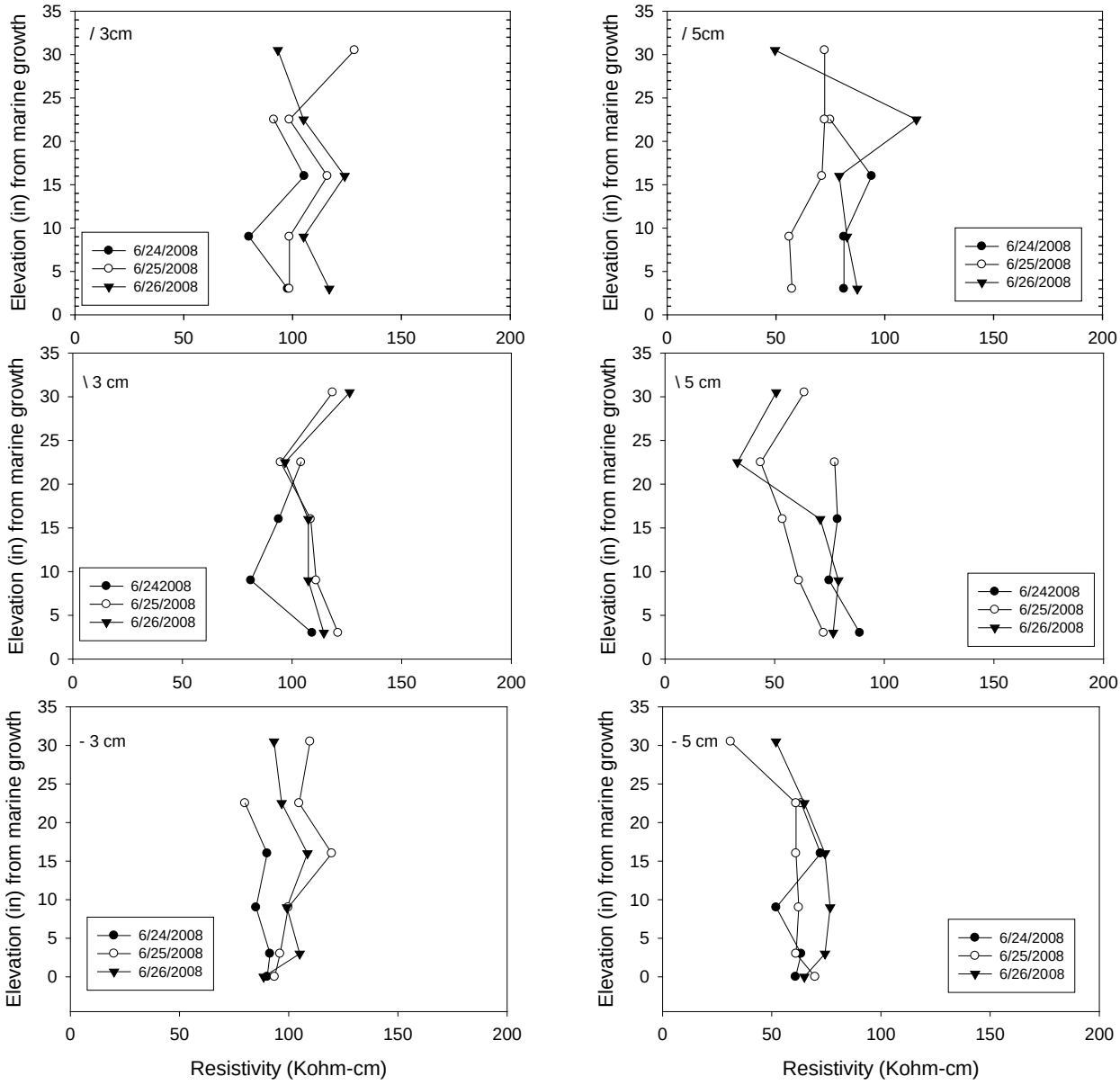

136502
Key Royale Bridge
Bent 2 Pile 5 North Face
C Cover: 3 in

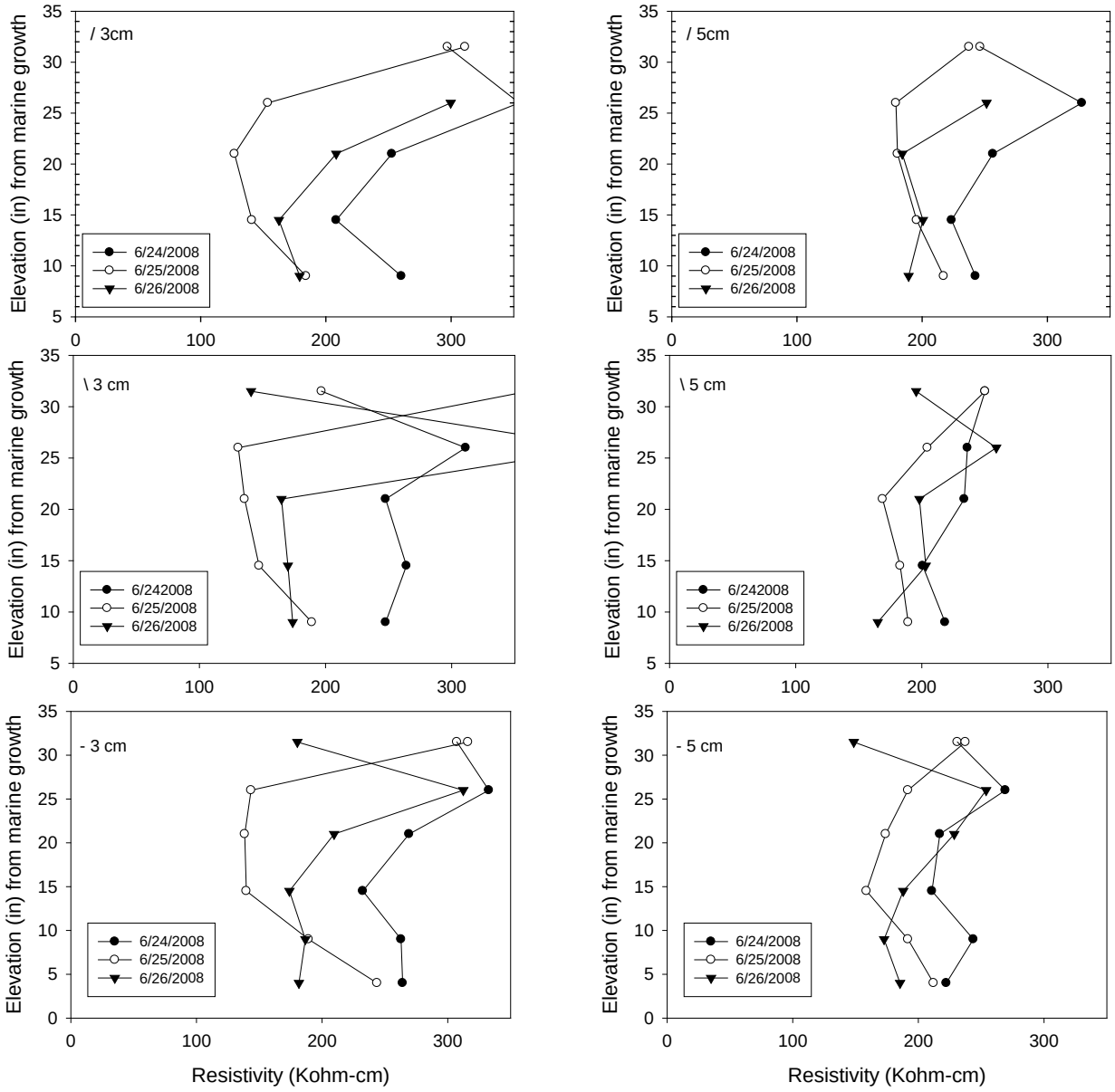

136502
Key Royale Bridge
Bent 3 Pile 1 North Face
C Cover: 3 in
Towels

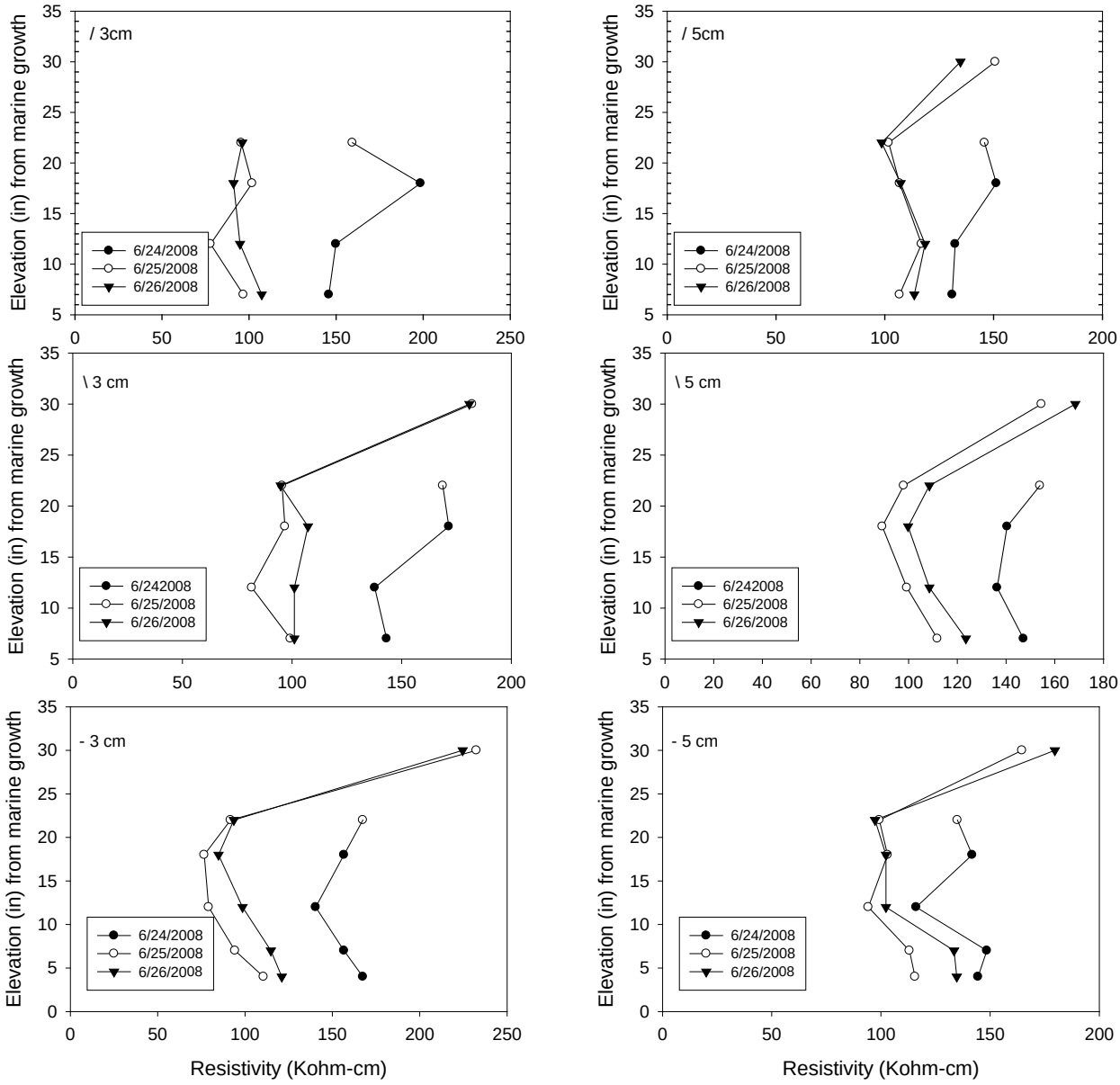

136502
Key Royale Bridge
Bent 3 Pile 2 South Face
C Cover: 3 in
Towels

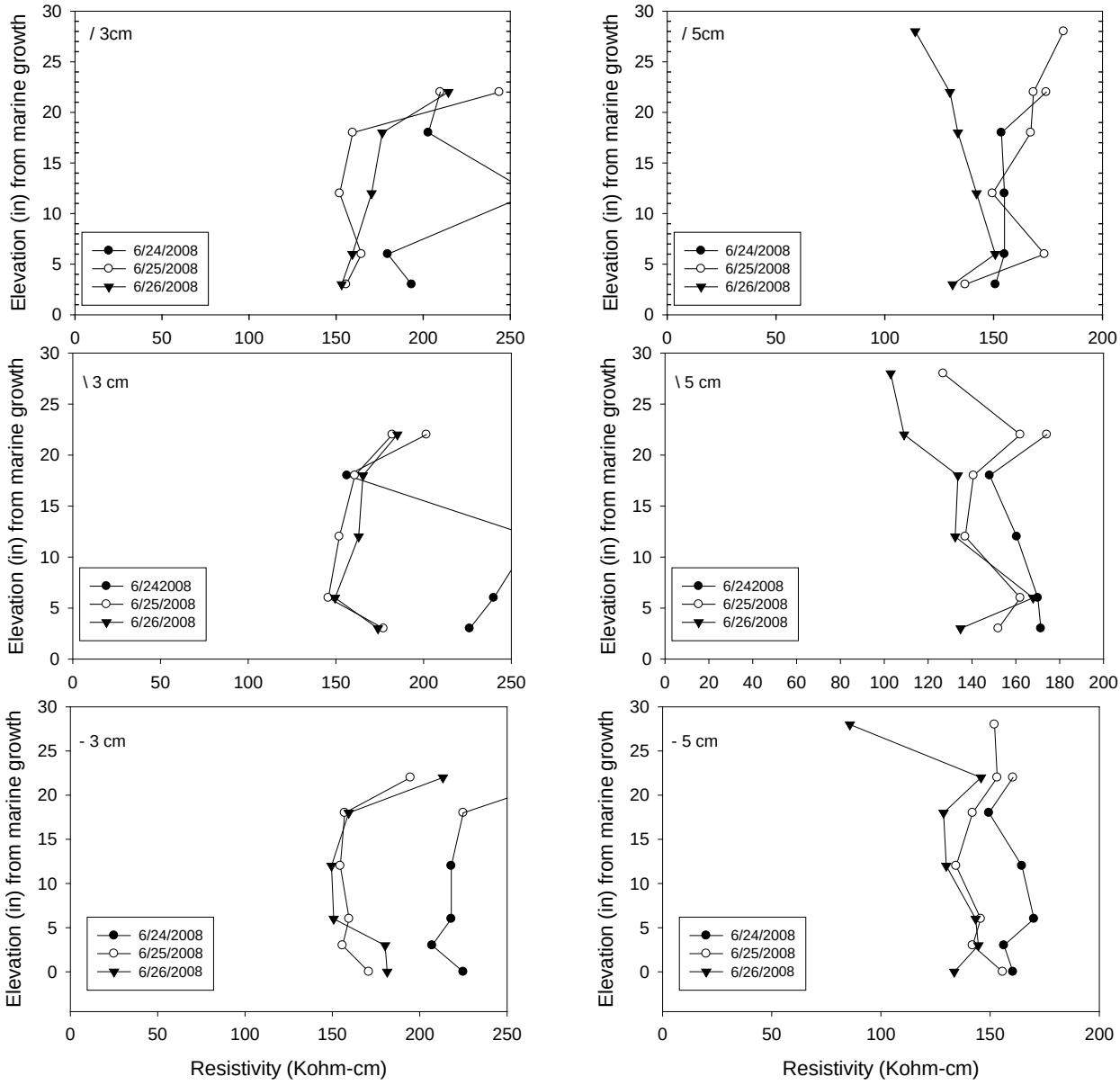

136502
Key Royale Bridge
Bent 3 Pile 3 North Face
C Cover: 3 in
Towels

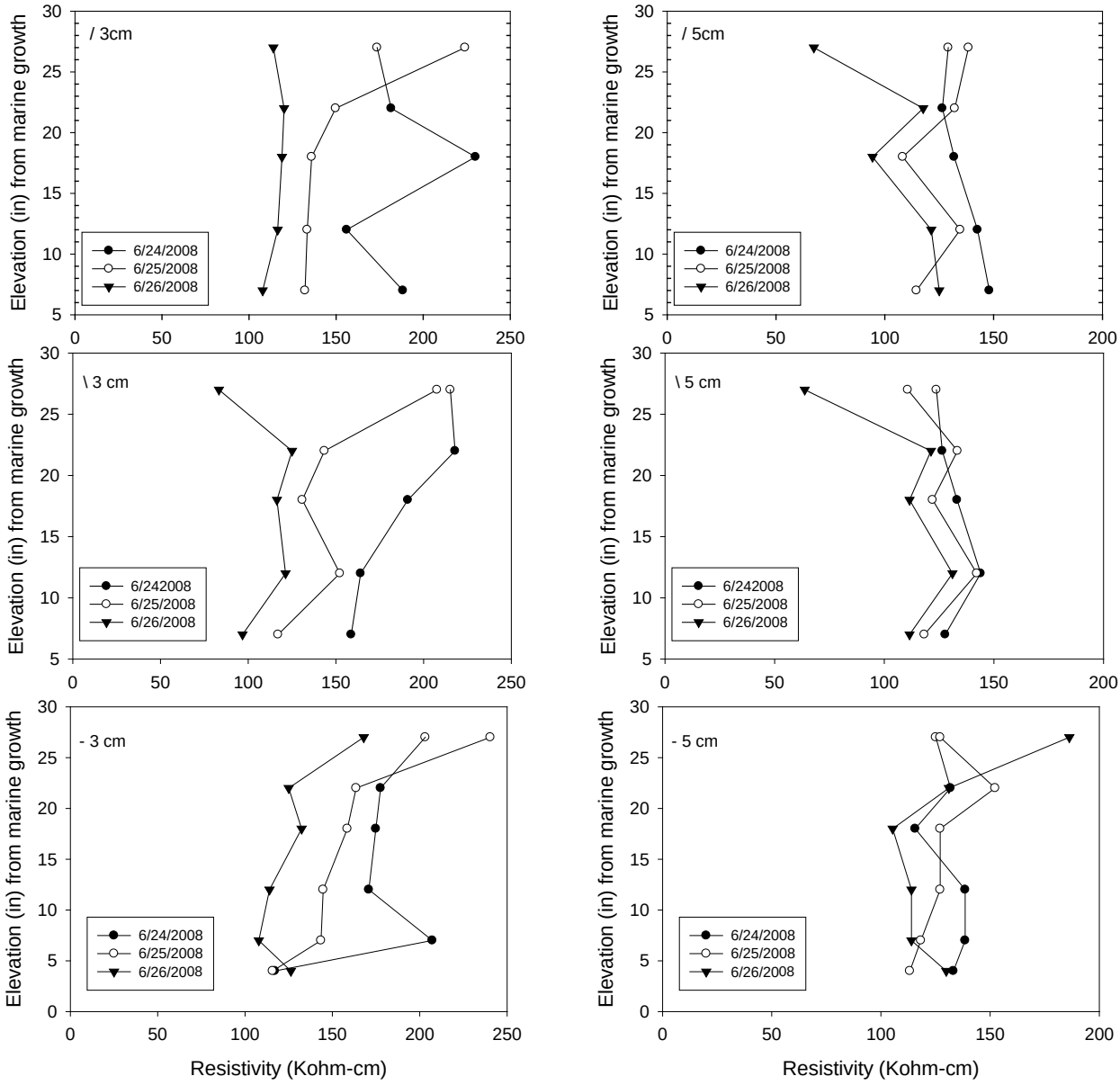

136502
Key Royale Bridge
Bent 3 Pile 4 North Face
C Cover: 3 in
Towels

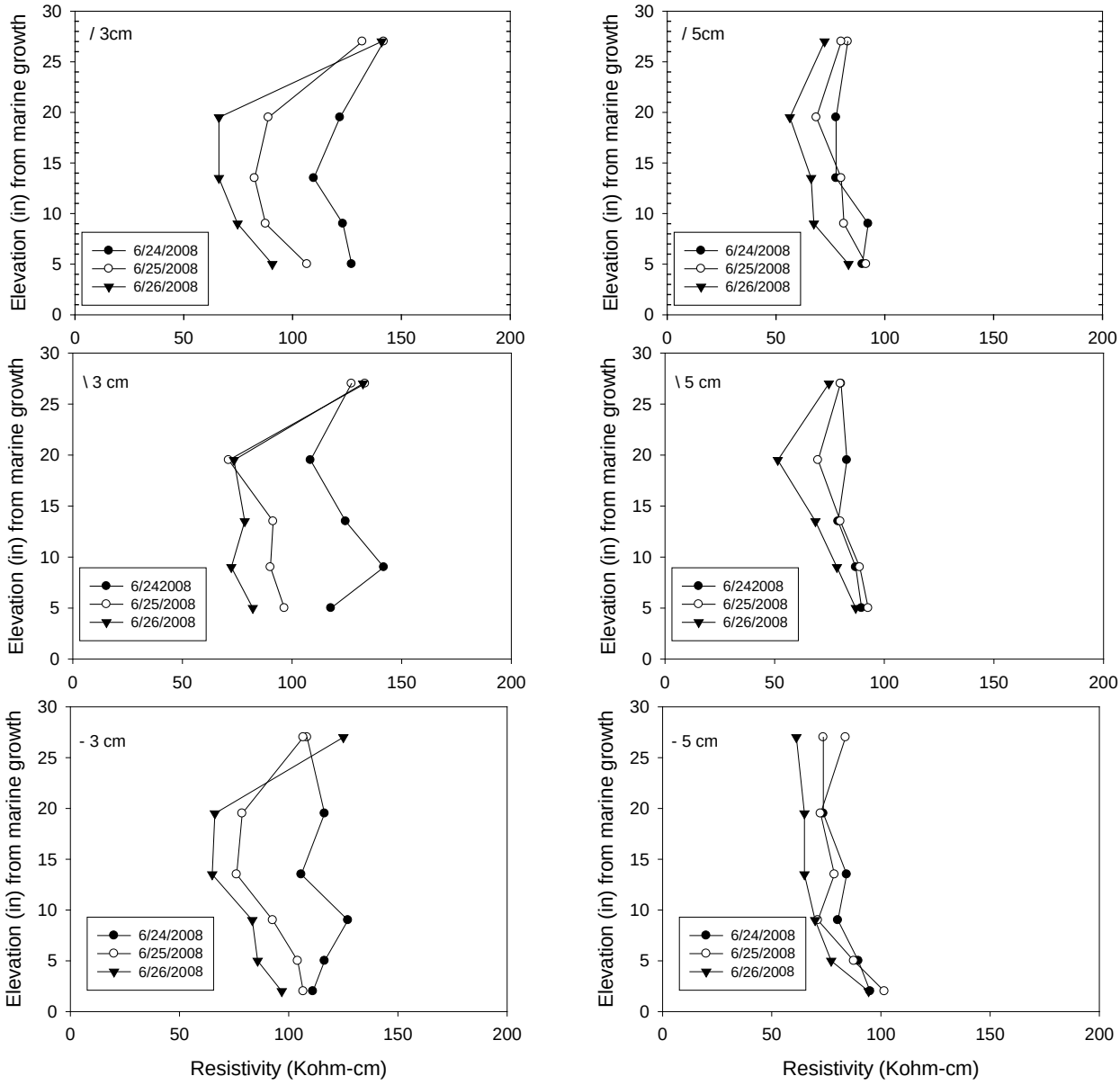

136502
Key Royale Bridge
Bent 3 Pile 5 North Face
C Cover: 3 in
Towels

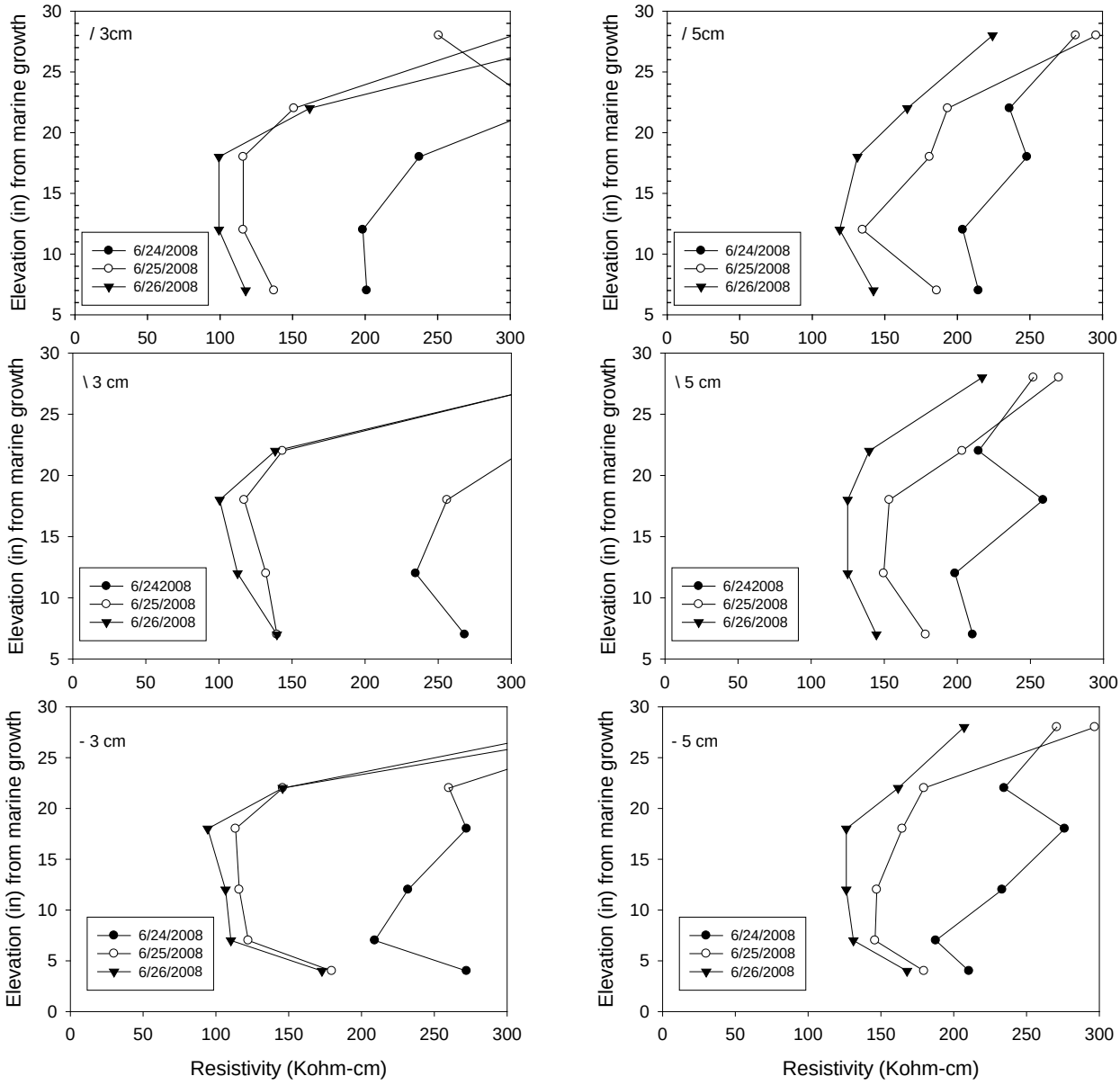

136502
Key Royale Bridge
Bent 2 Pile 1 North Face
C Cover: 3 in

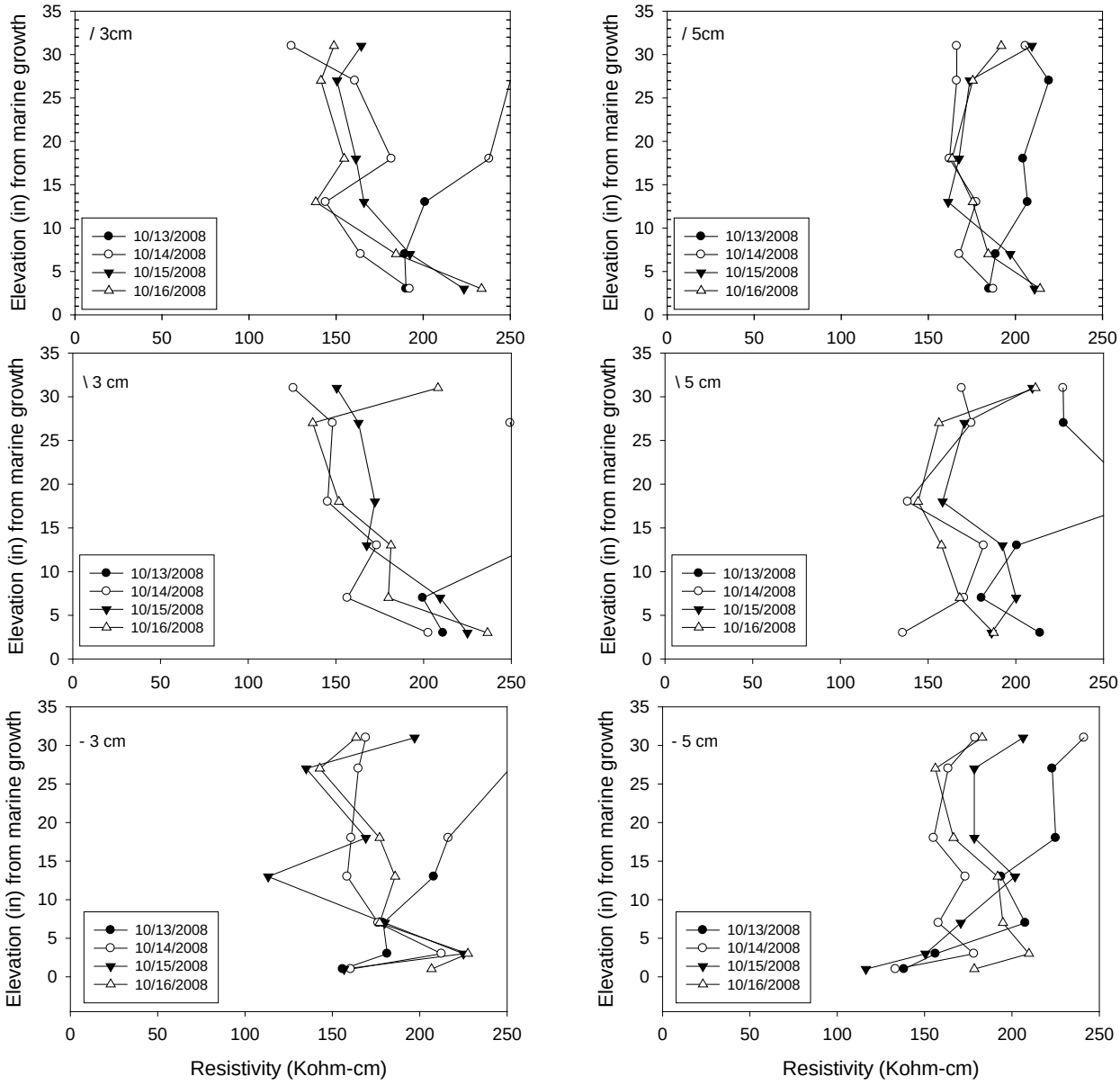

136502
Key Royale Bridge
Bent 2 Pile 2 South Face
C Cover: 3 in

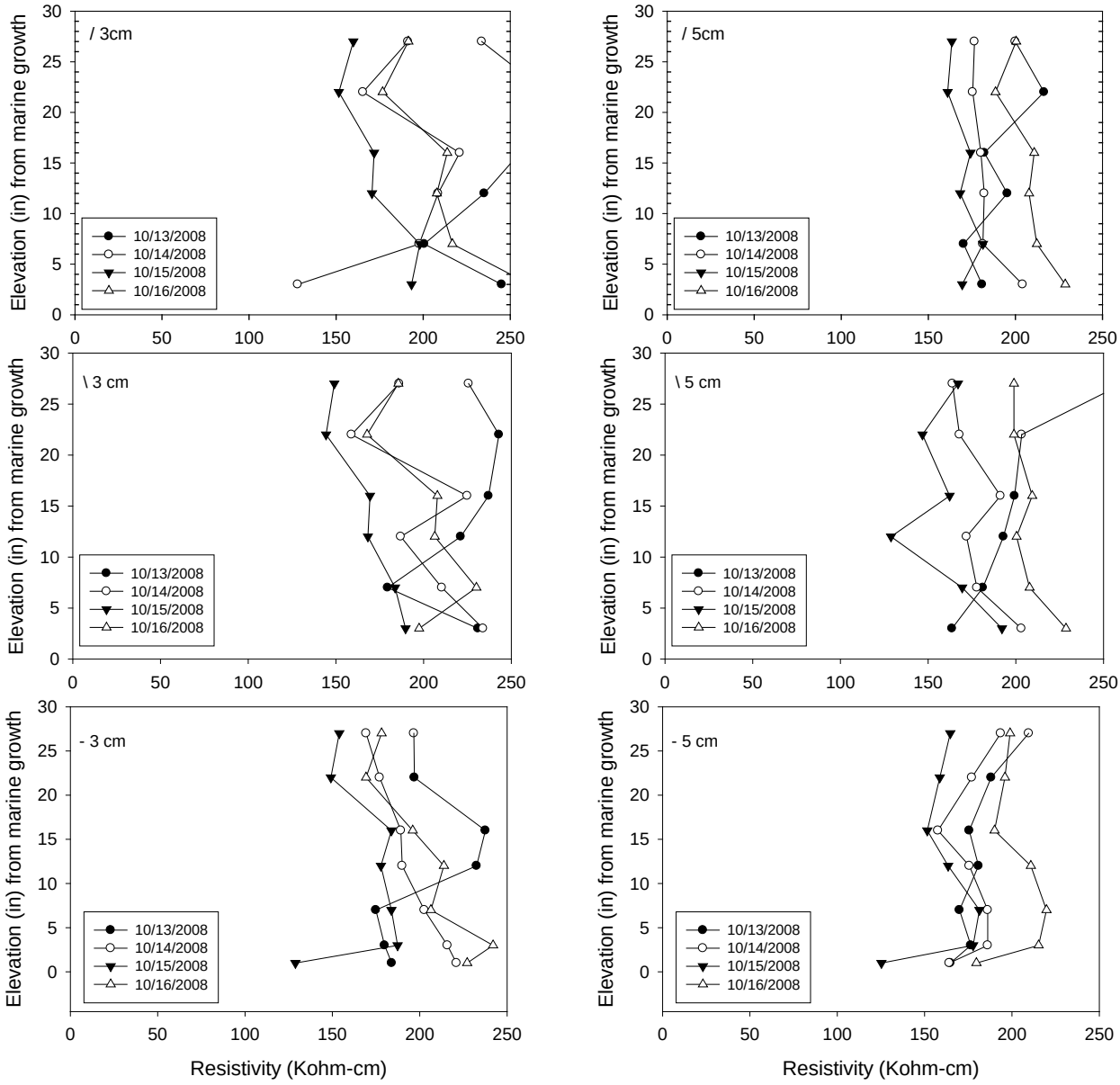

136502
Key Royale Bridge
Bent 2 Pile 3 North Face
C Cover: 3 in

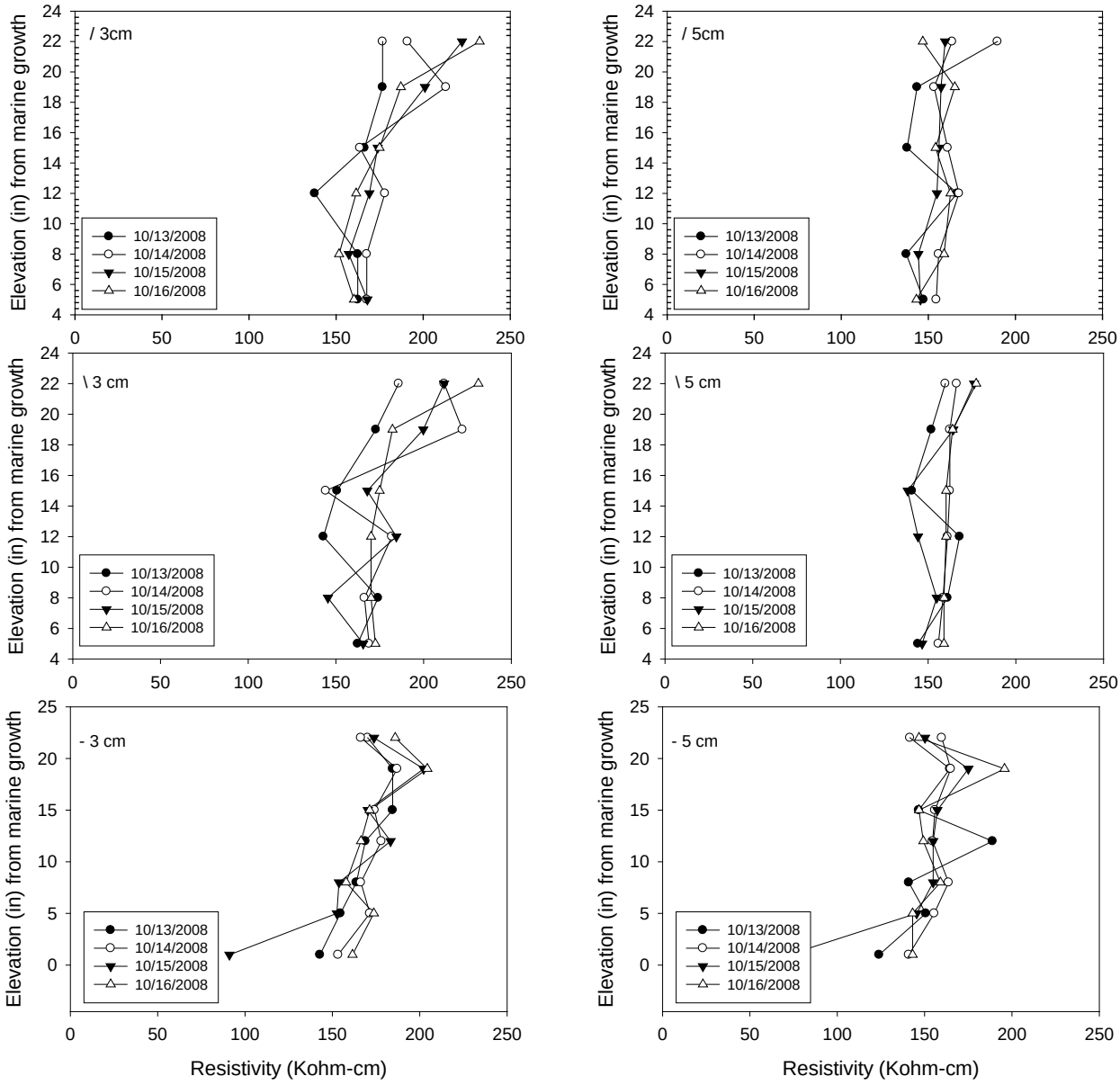

136502
Key Royale Bridge
Bent 2 Pile 4 North Face
C Cover: 3 in

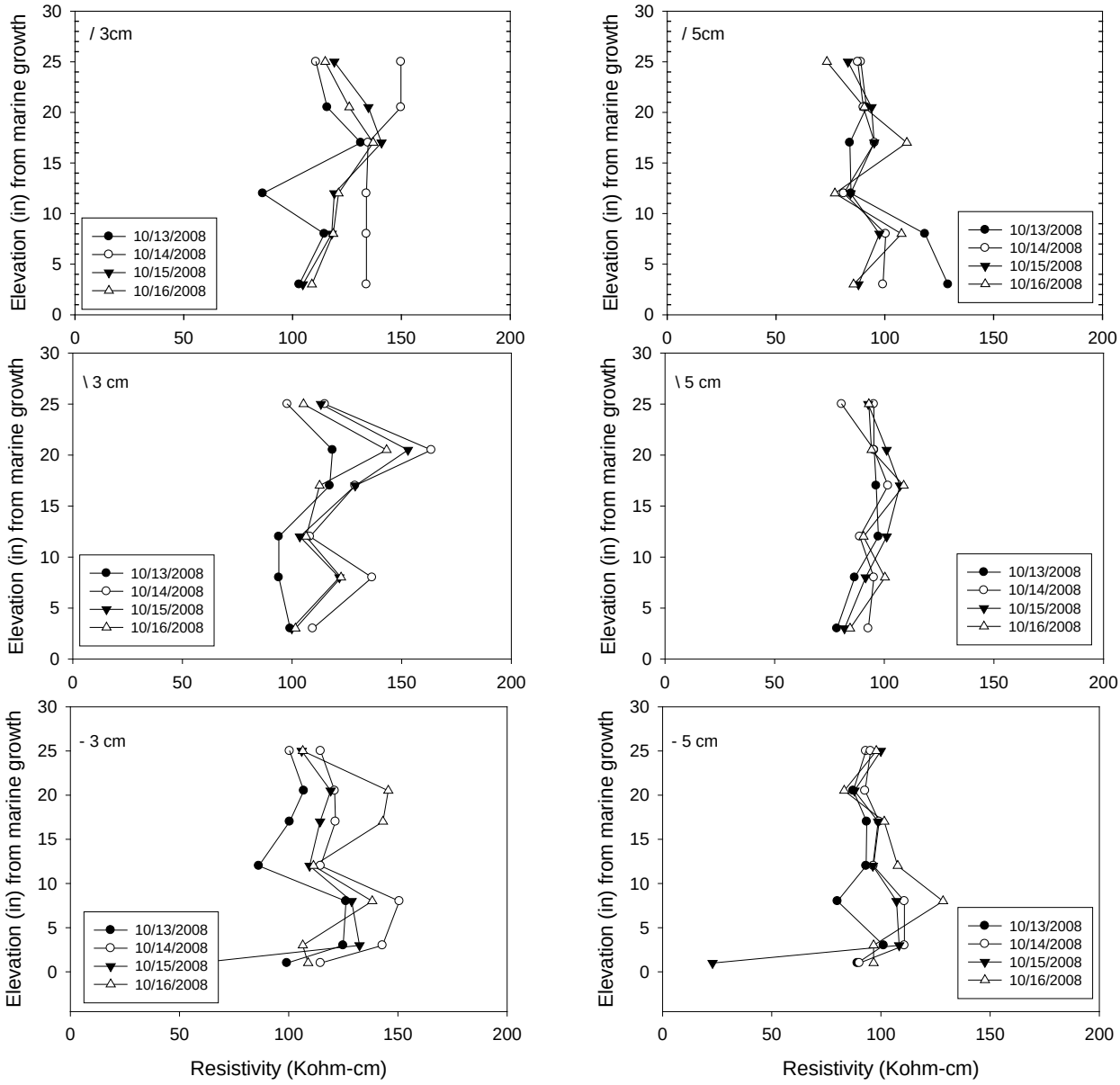

136502
Key Royale Bridge
Bent 2 Pile 5 North Face
C Cover: 3 in

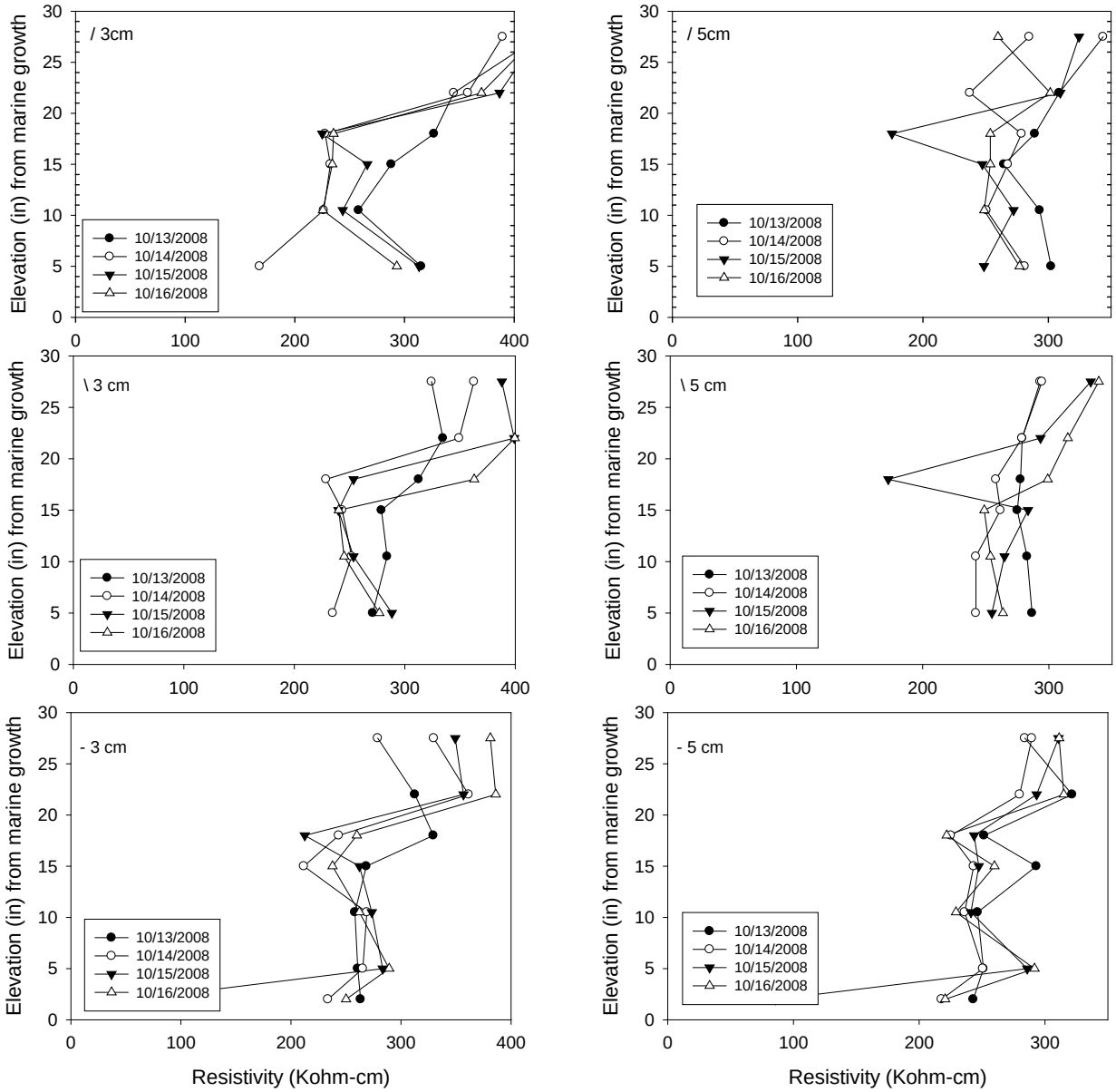

136502
Key Royale Bridge
Bent 3 Pile 1 North Face
C Cover: 3 in

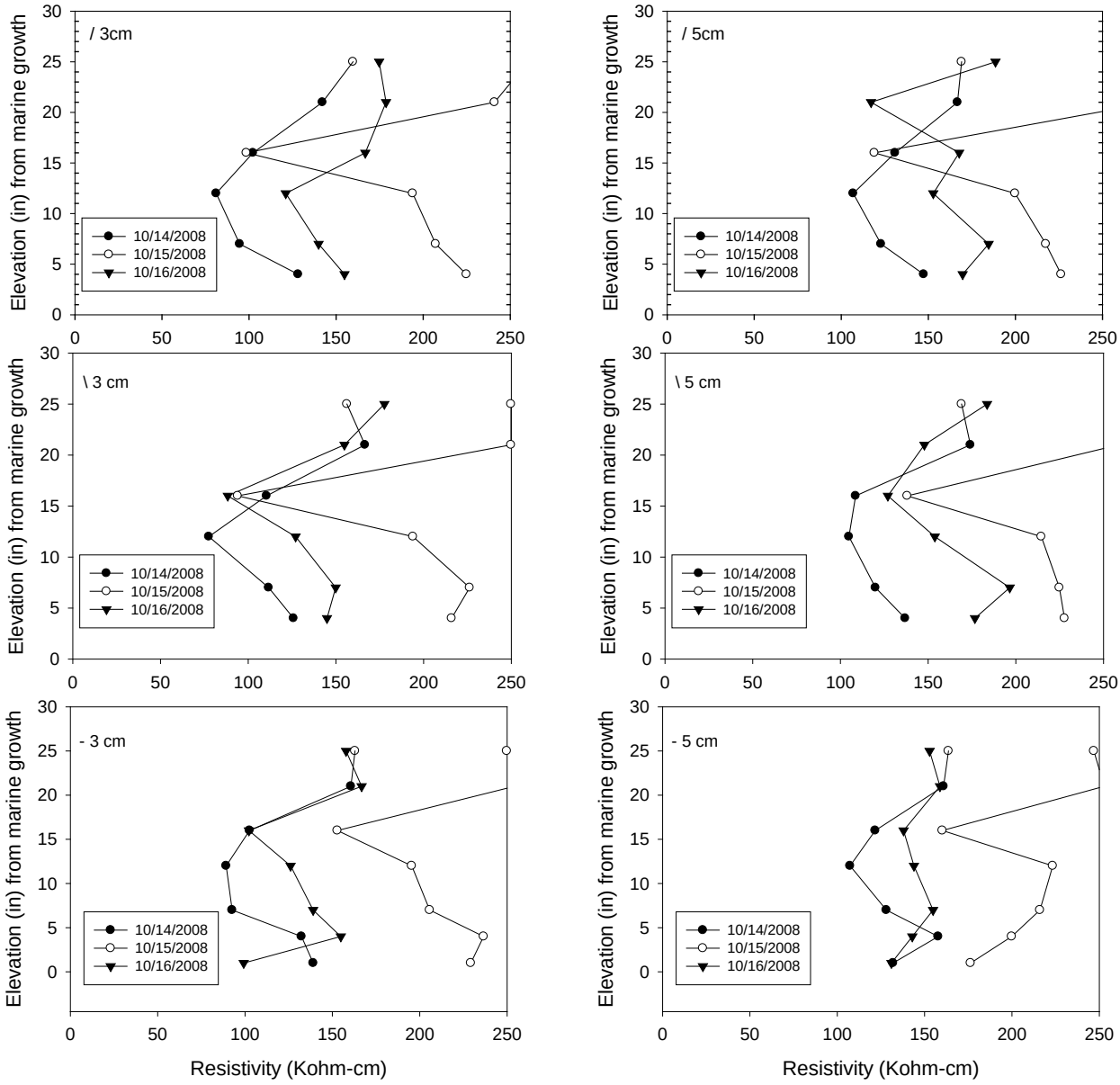

136502
Key Royale Bridge
Bent 3 Pile 2 South Face
C Cover: 3 in

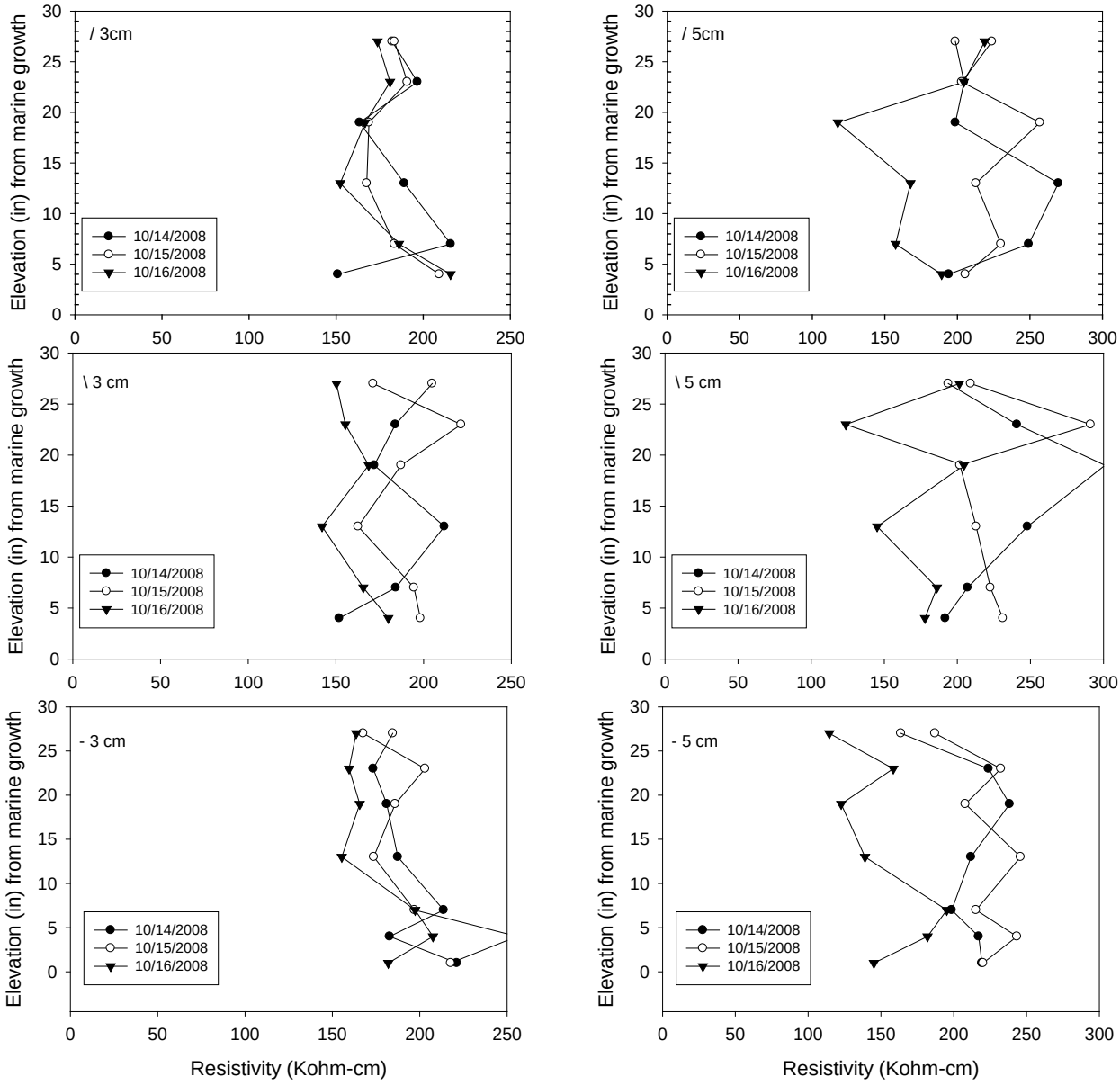

136502
Key Royale Bridge
Bent 3 Pile 3 North Face
C Cover: 3 in

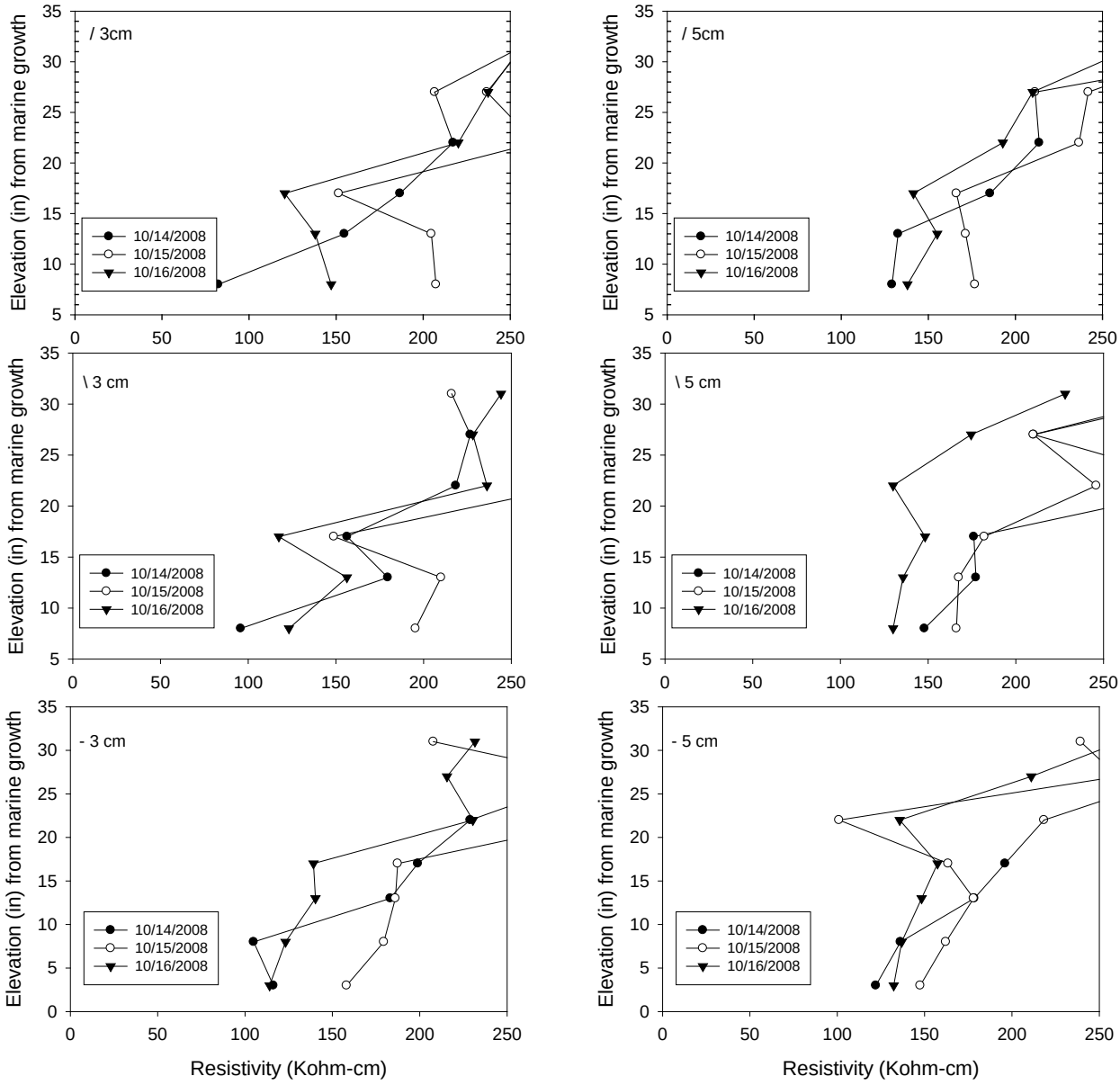

136502
Key Royale Bridge
Bent 3 Pile 4 North Face
C Cover: 3 in

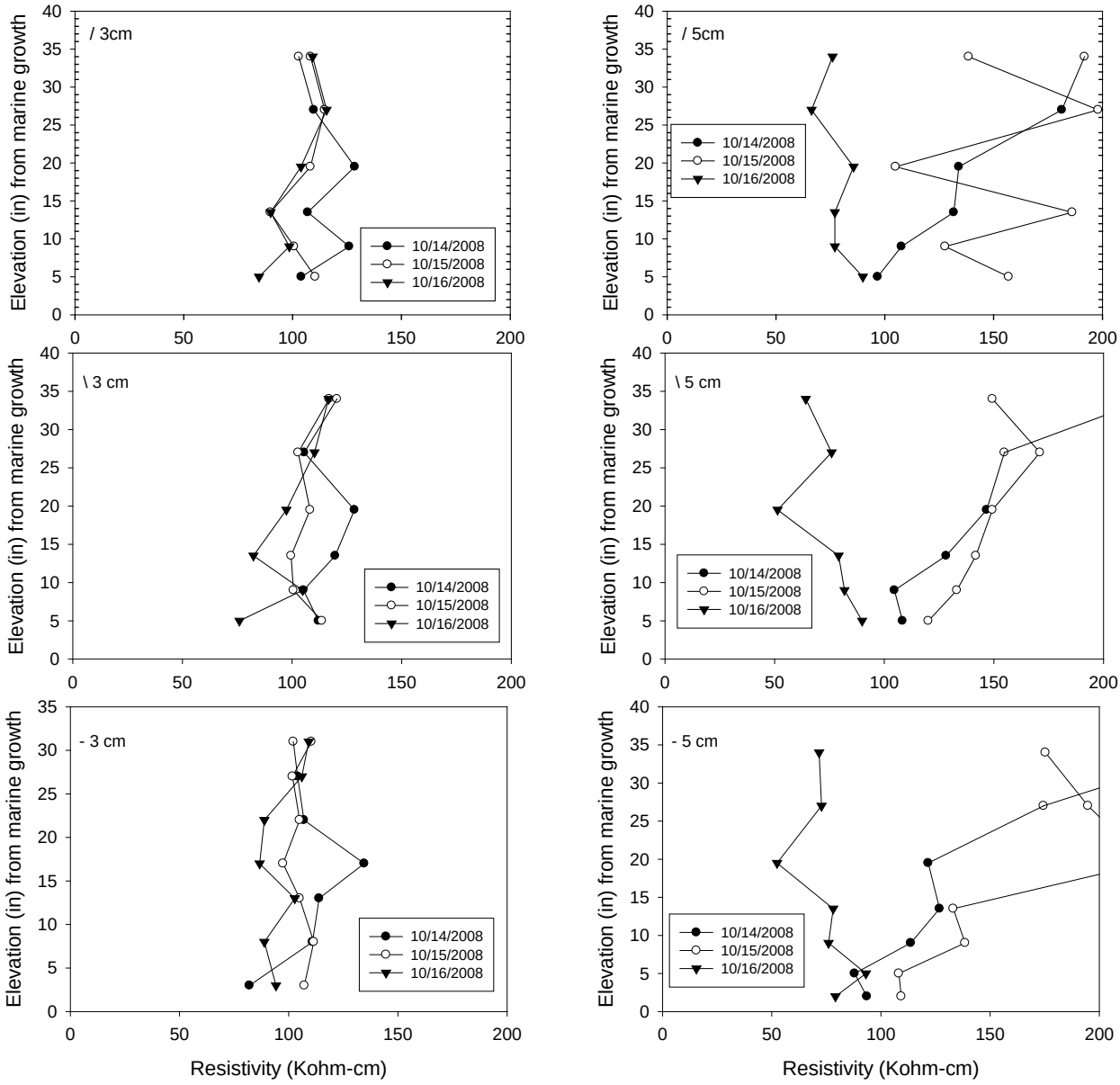

136502
Key Royale Bridge
Bent 3 Pile 5 North Face
C Cover: 3 in

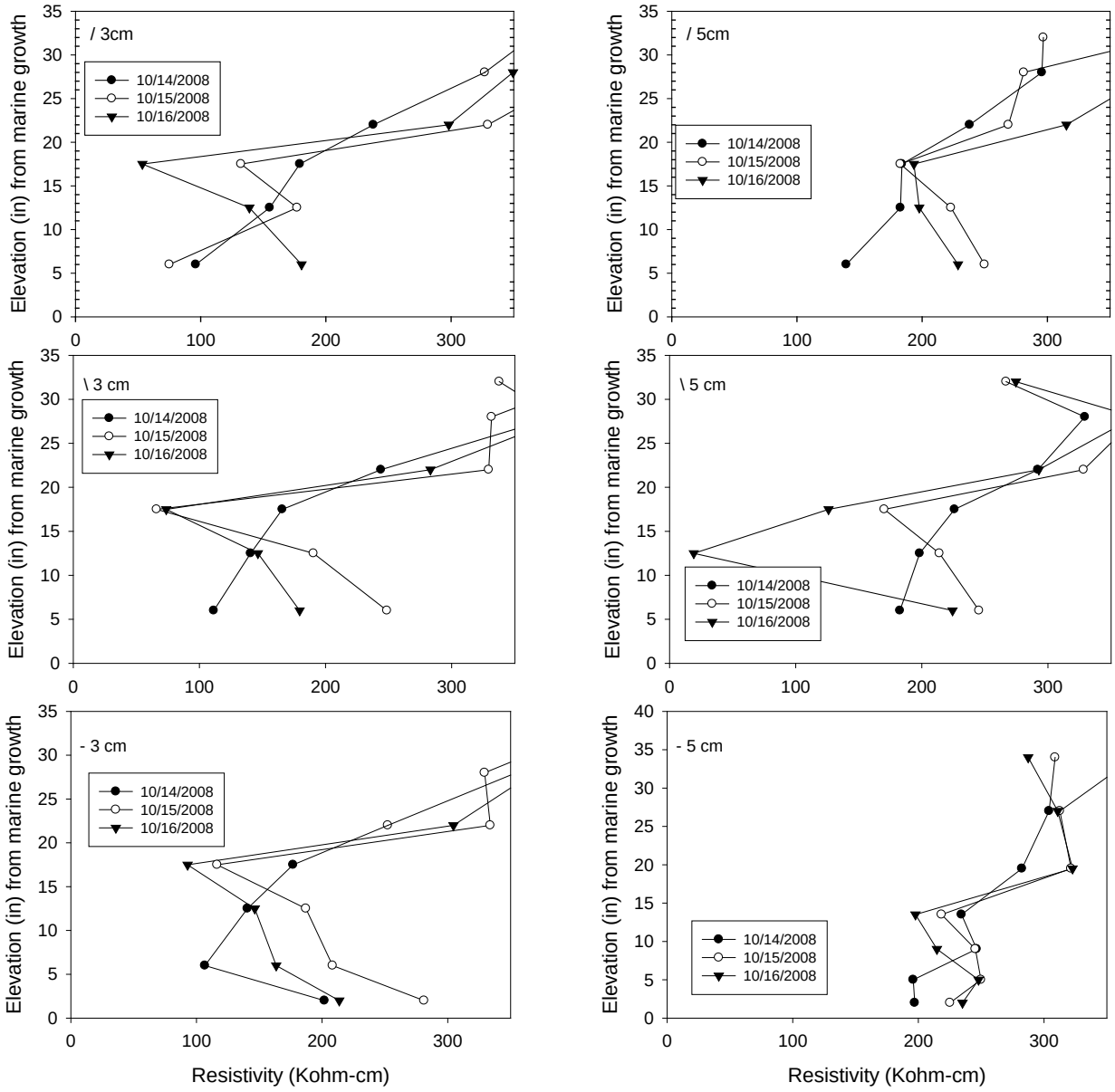

136502
Key Royale Bridge
Bent 2 Pile 1 North Face
C Cover: 3 in

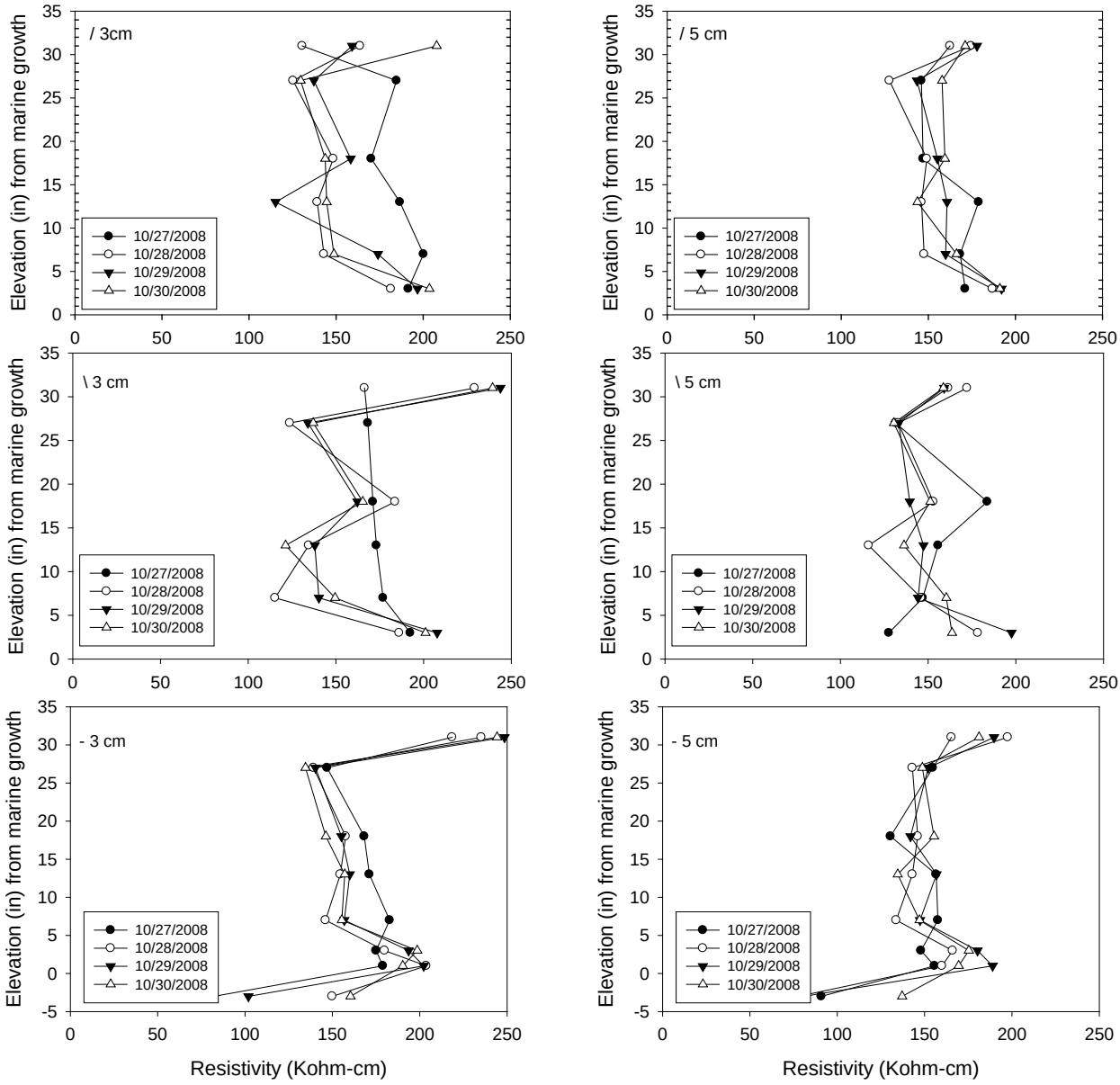

136502
Key Royale Bridge
Bent 2 Pile 2 South Face
C Cover: 3 in

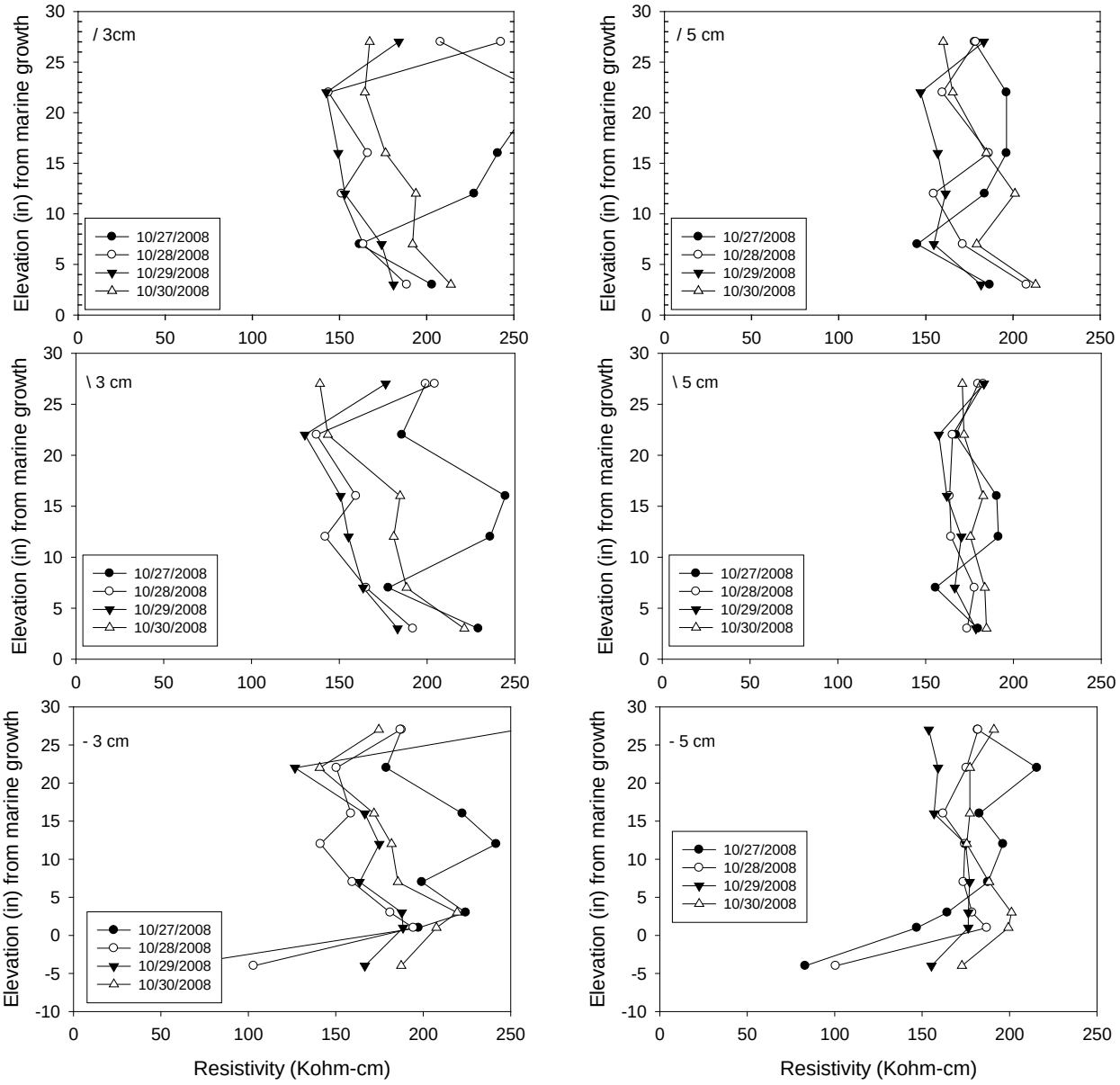

136502
Key Royale Bridge
Bent 2 Pile 3 North Face
C Cover: 3 in

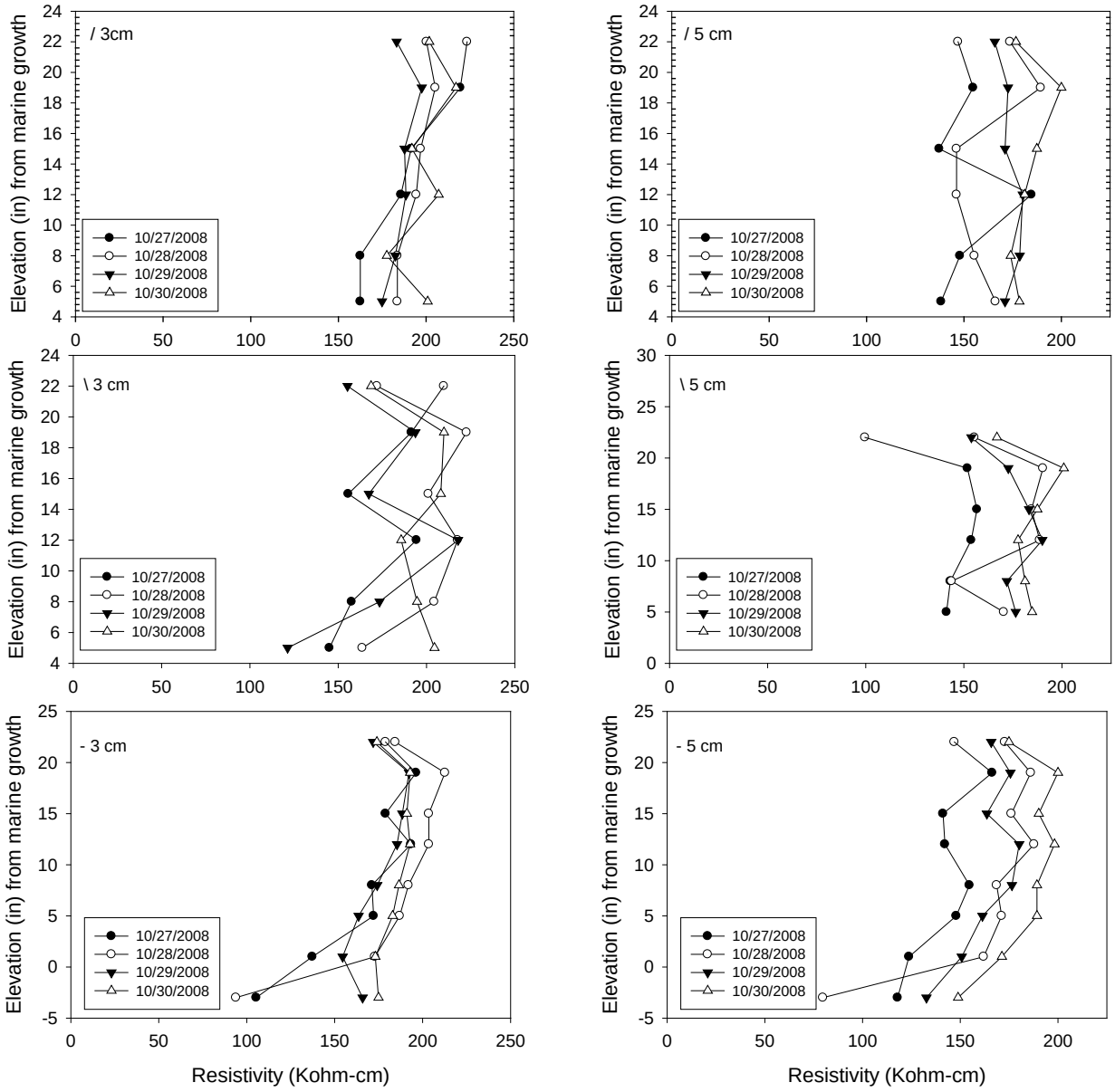

136502
Key Royale Bridge
Bent 2 Pile 4 North Face
C Cover: 3 in

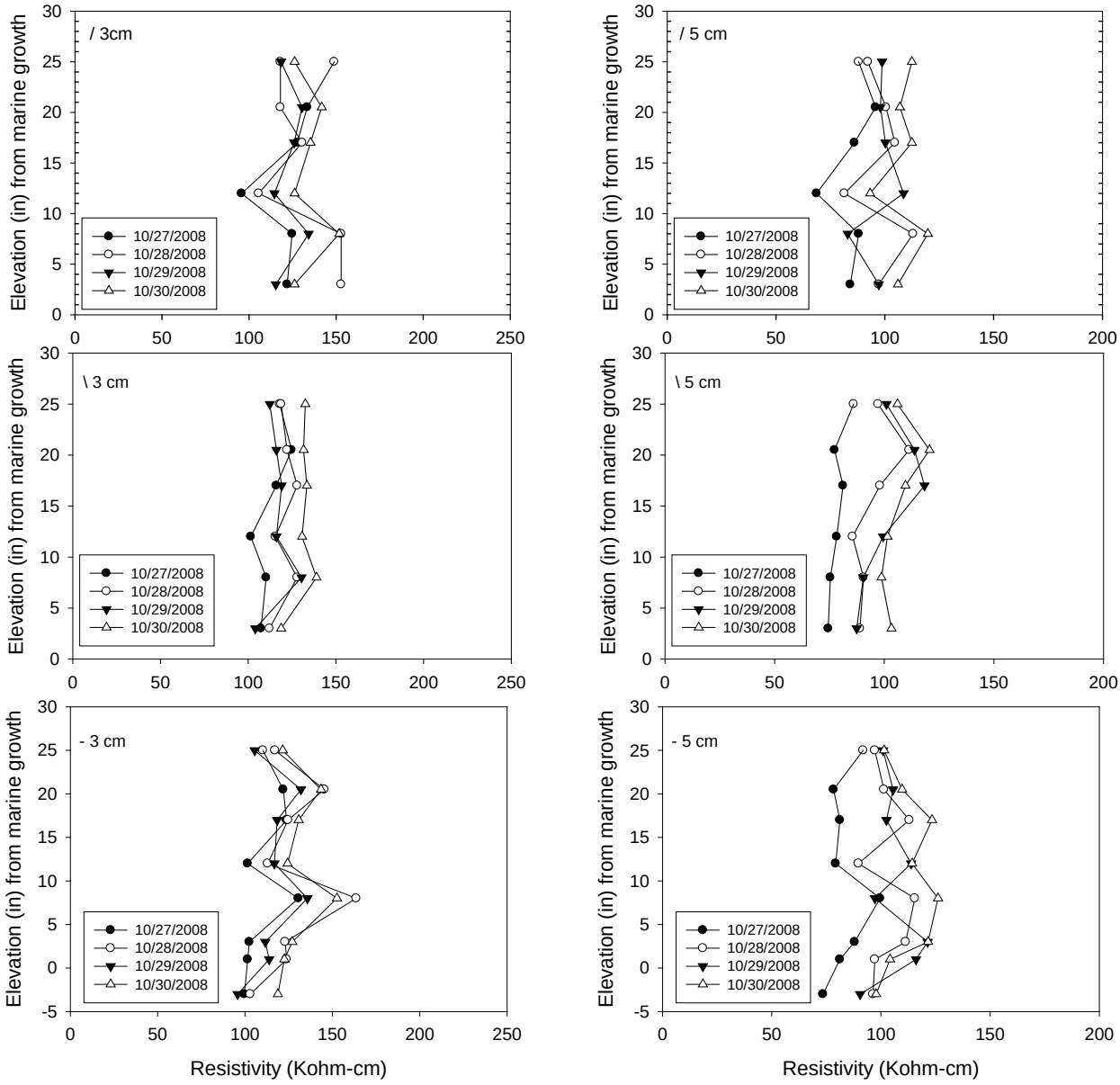

136502
Key Royale Bridge
Bent 2 Pile 5 North Face
C Cover: 3 in

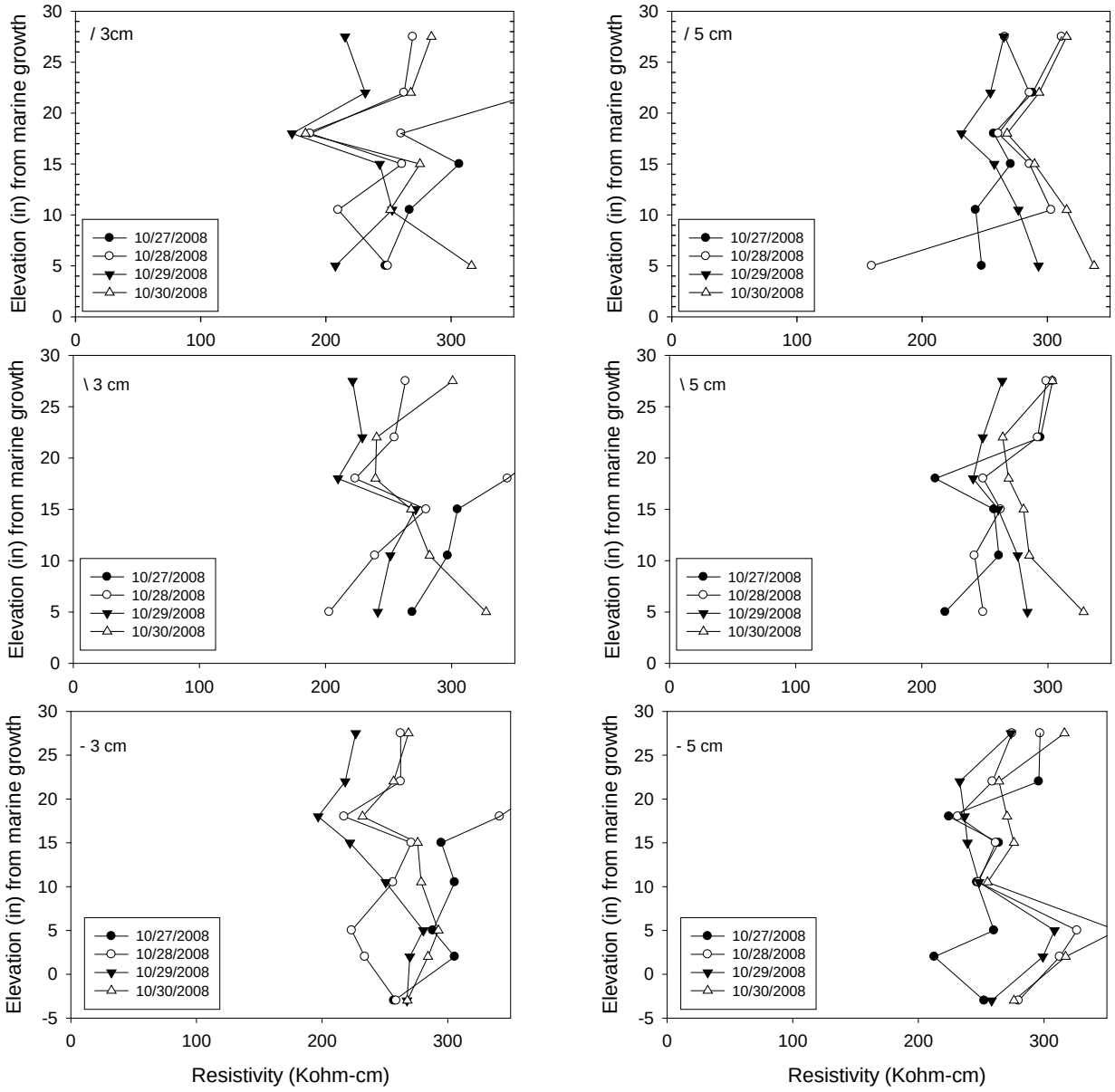

136502
Key Royale Bridge
Bent 3 Pile 1 North Face
C Cover: 3 in

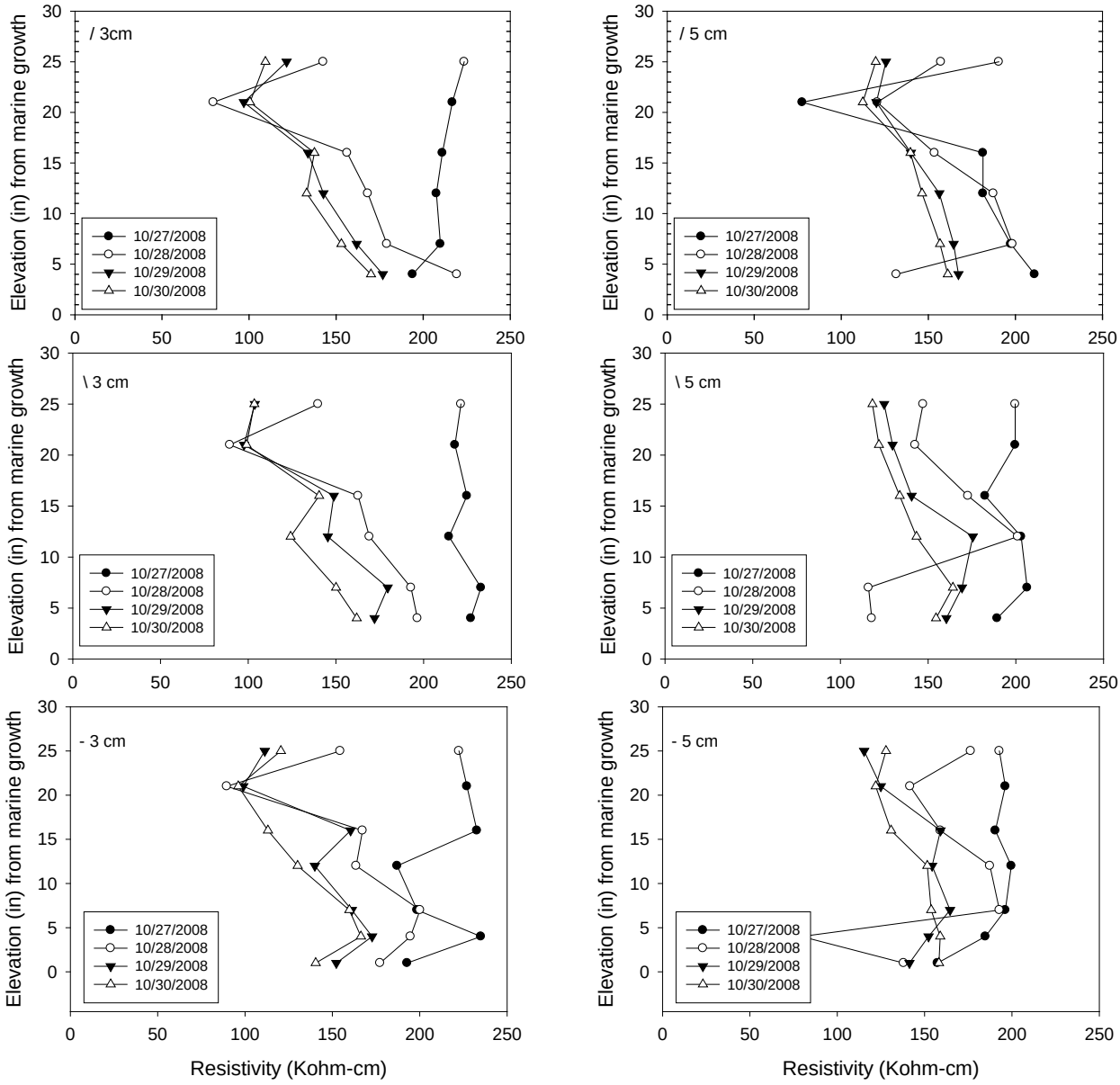

136502
Key Royale Bridge
Bent 3 Pile 2 South Face
C Cover: 3 in

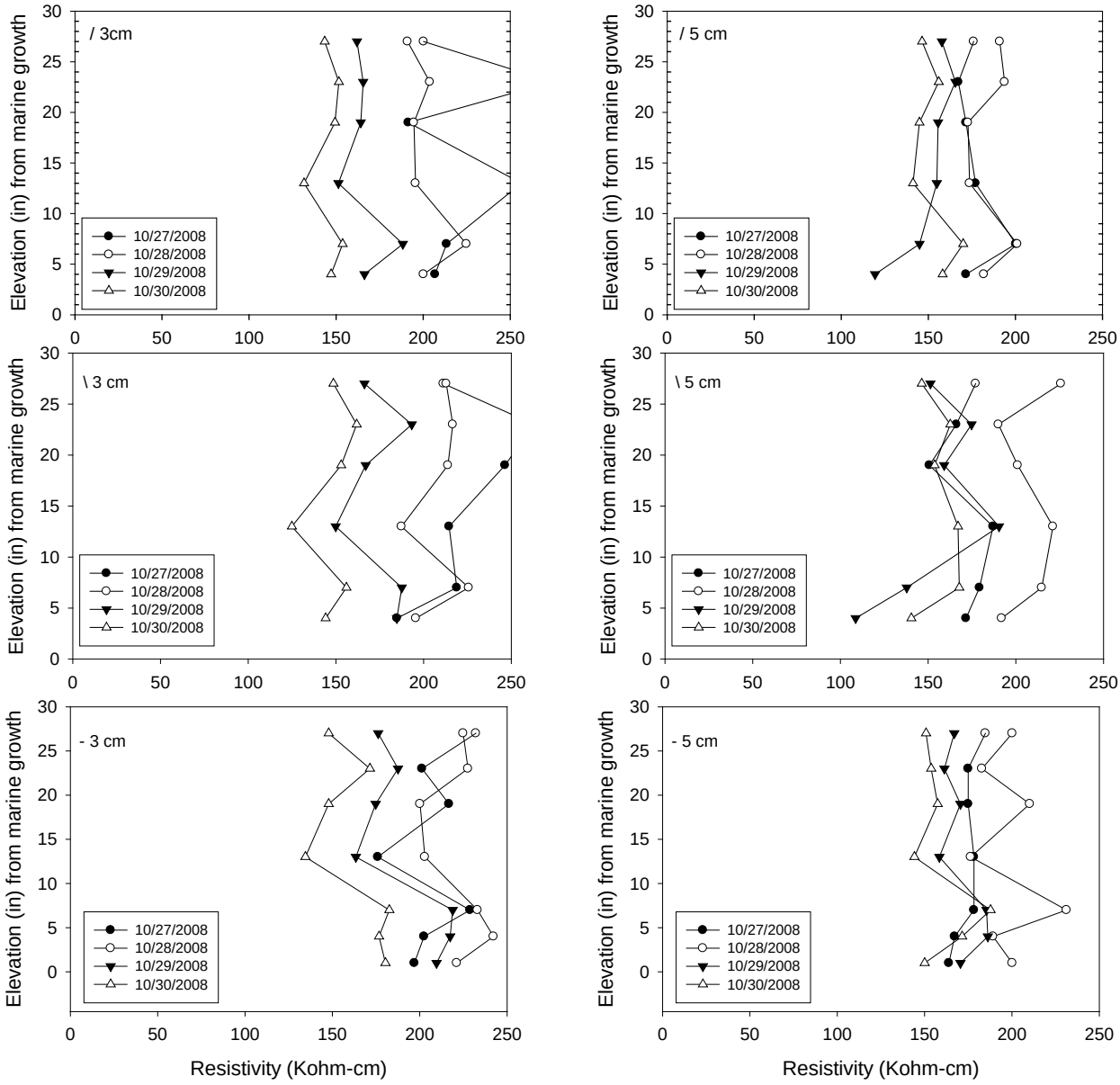

136502
Key Royale Bridge
Bent 3 Pile 3 North Face
C Cover: 3 in

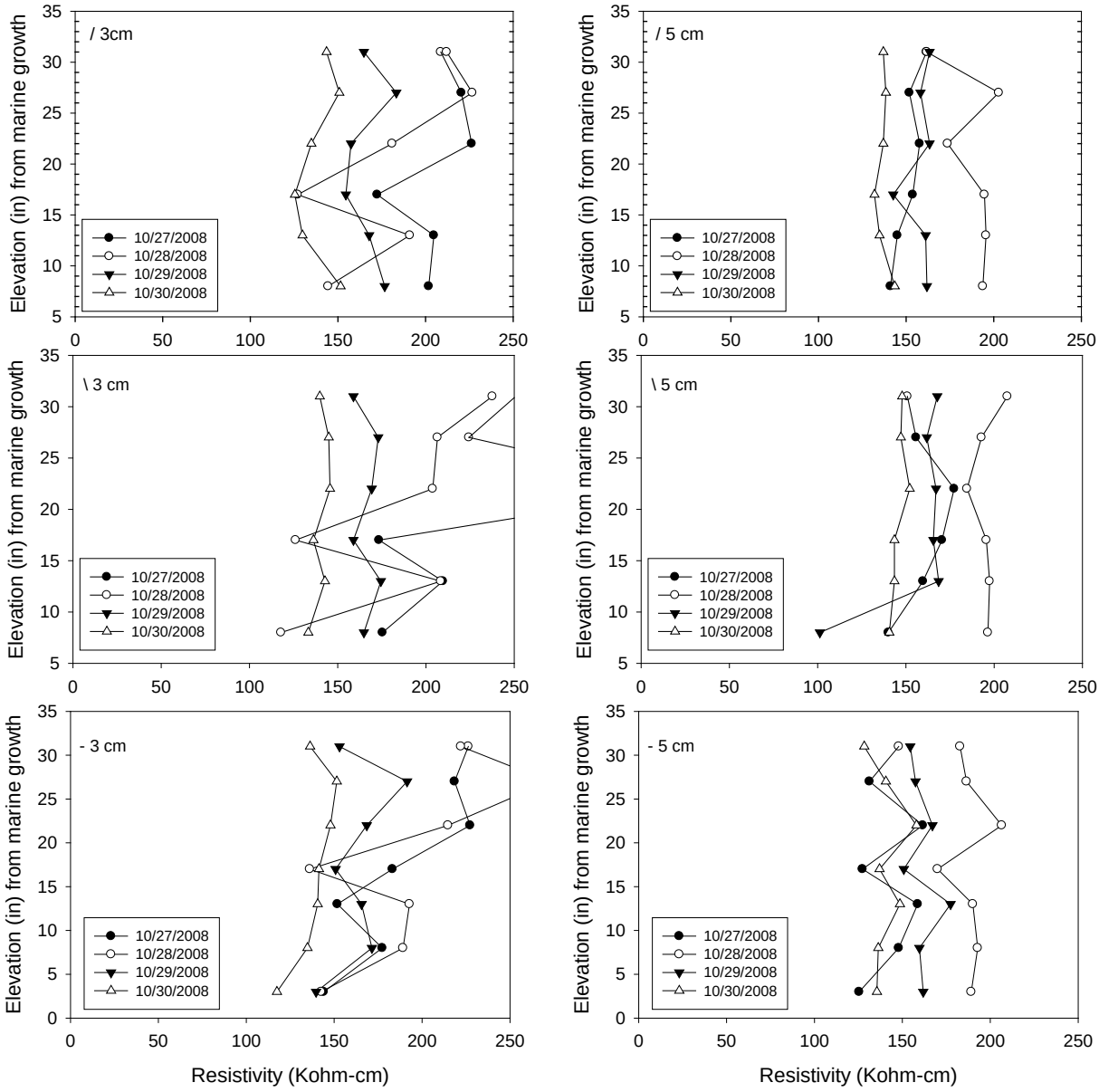

136502
Key Royale Bridge
Bent 3 Pile 4 North Face
C Cover: 3 in

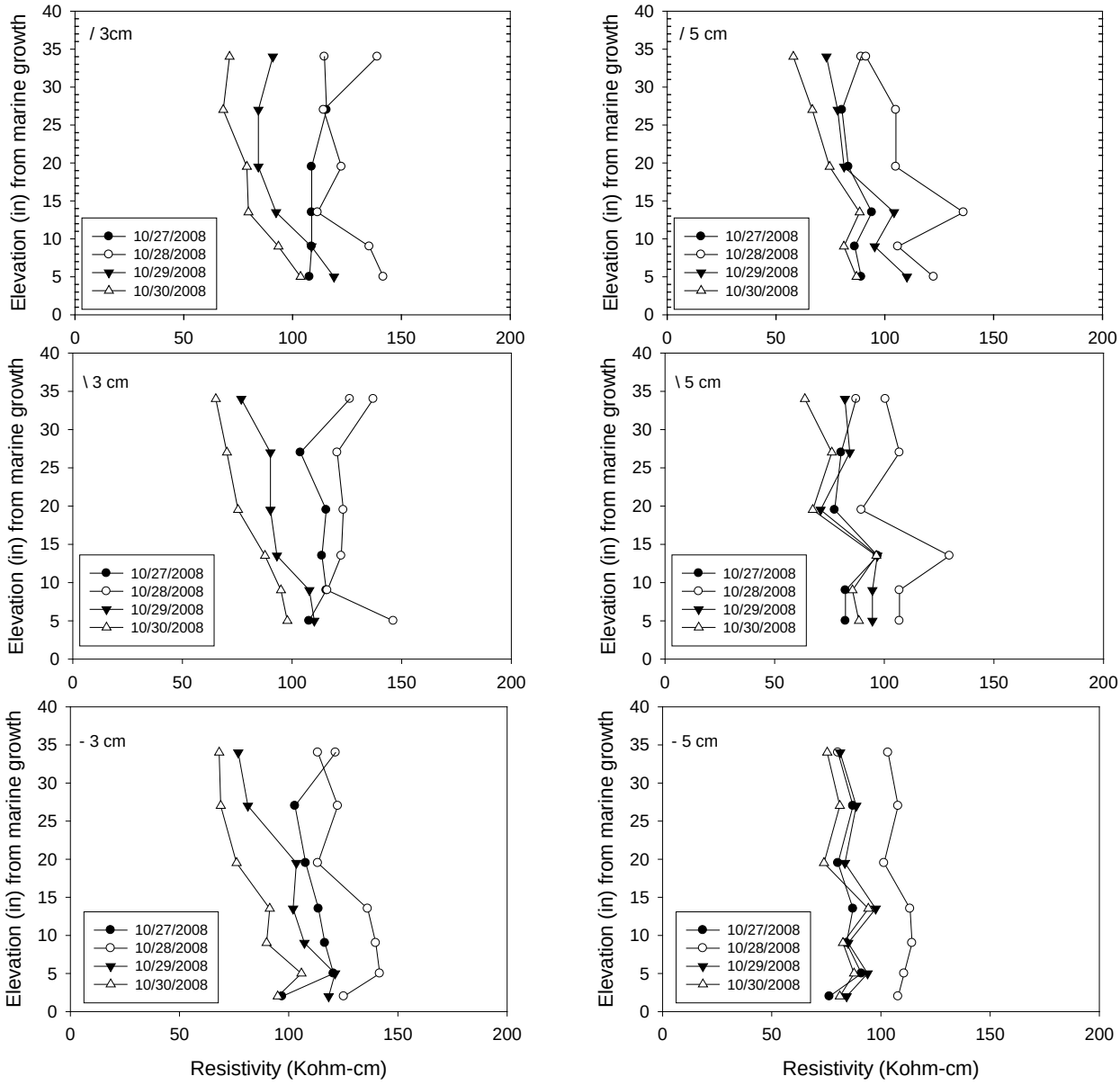

136502
Key Royale Bridge
Bent 3 Pile 5 North Face
C Cover: 3 in

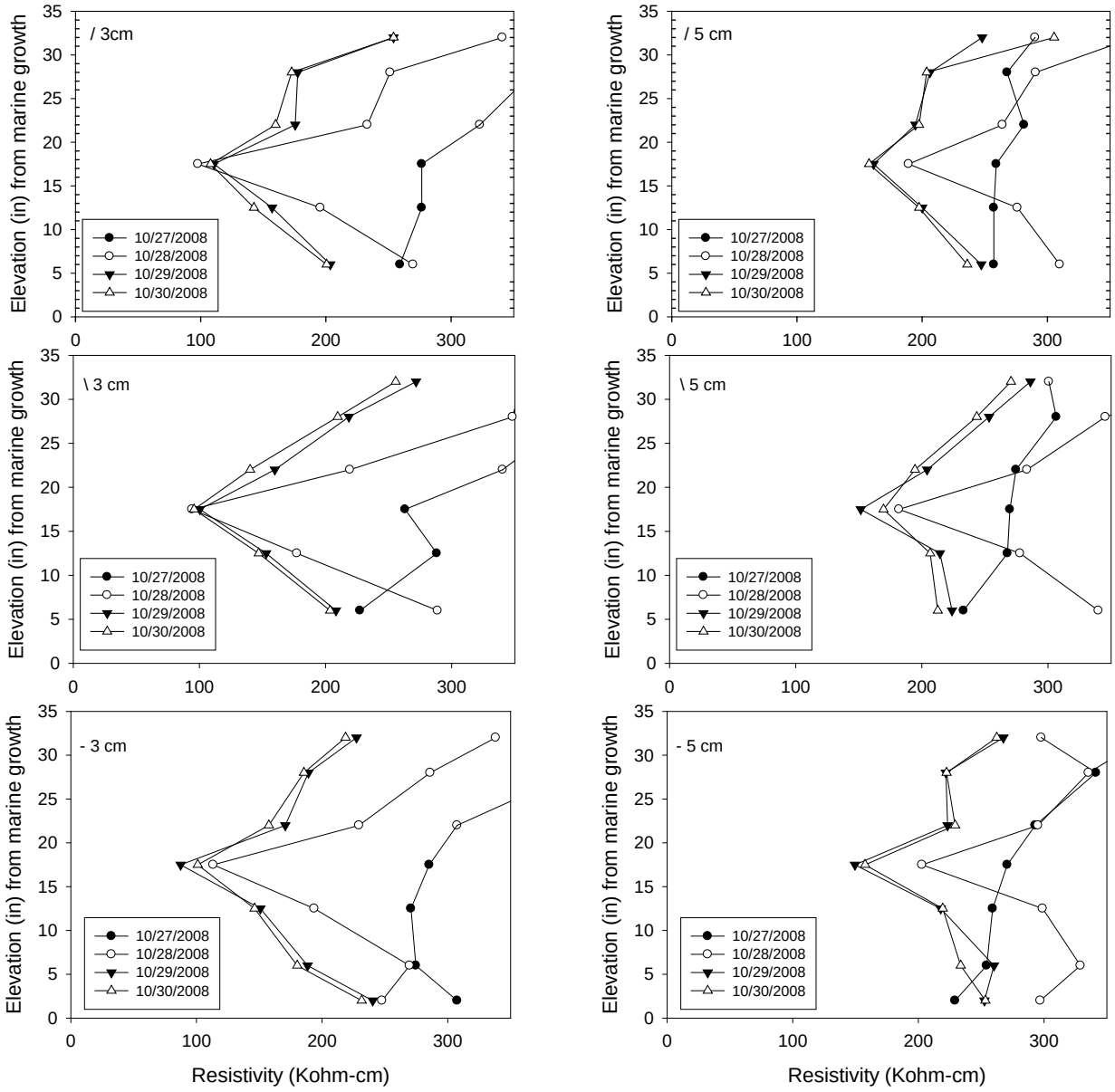

136502
Key Royale Bridge
Bent 2 Pile 1 North Face
C Cover: 3 in
UFA+FA

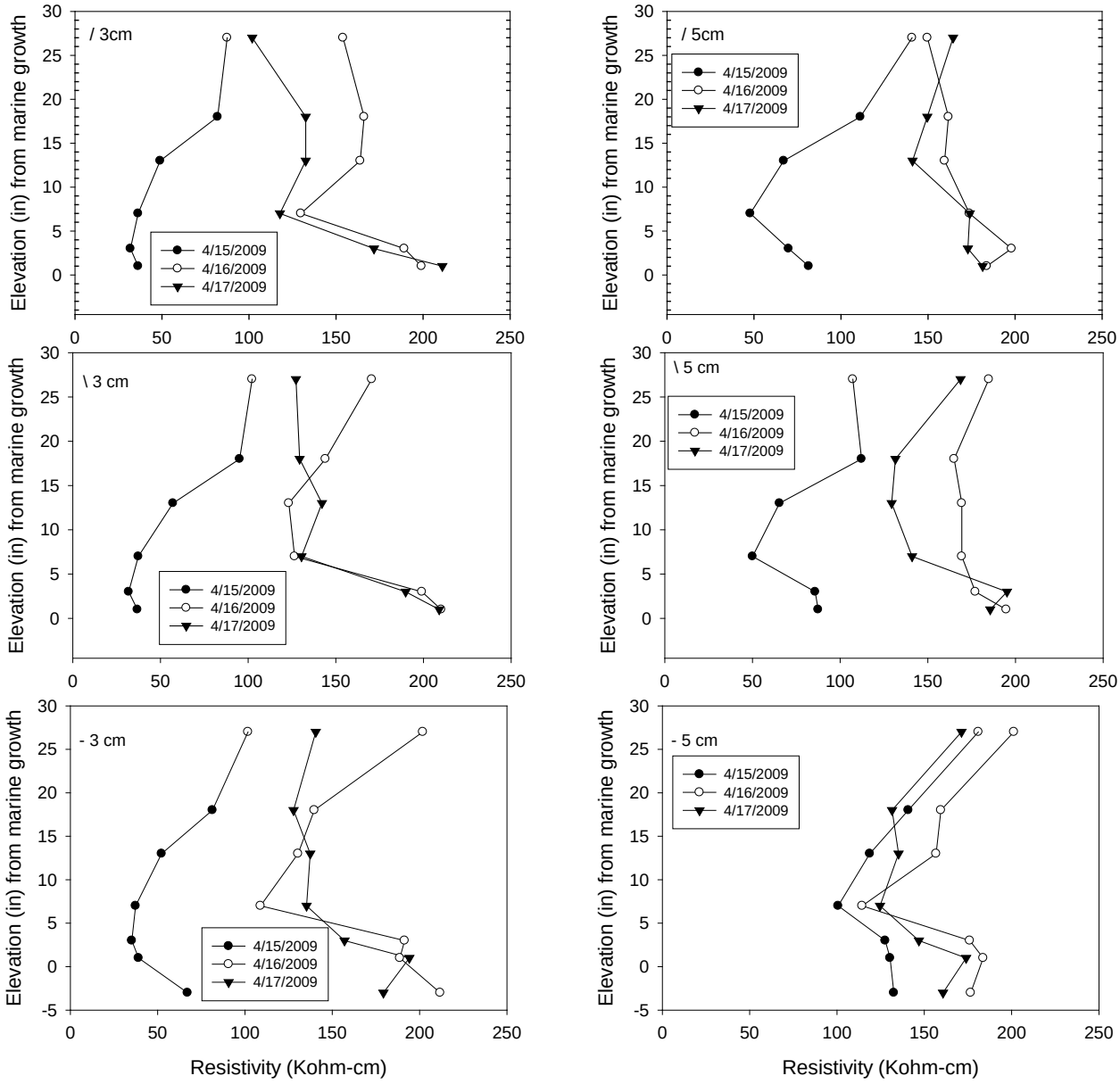

136502
Key Royale Bridge
Bent 2 Pile 2 South Face
C Cover: 3 in

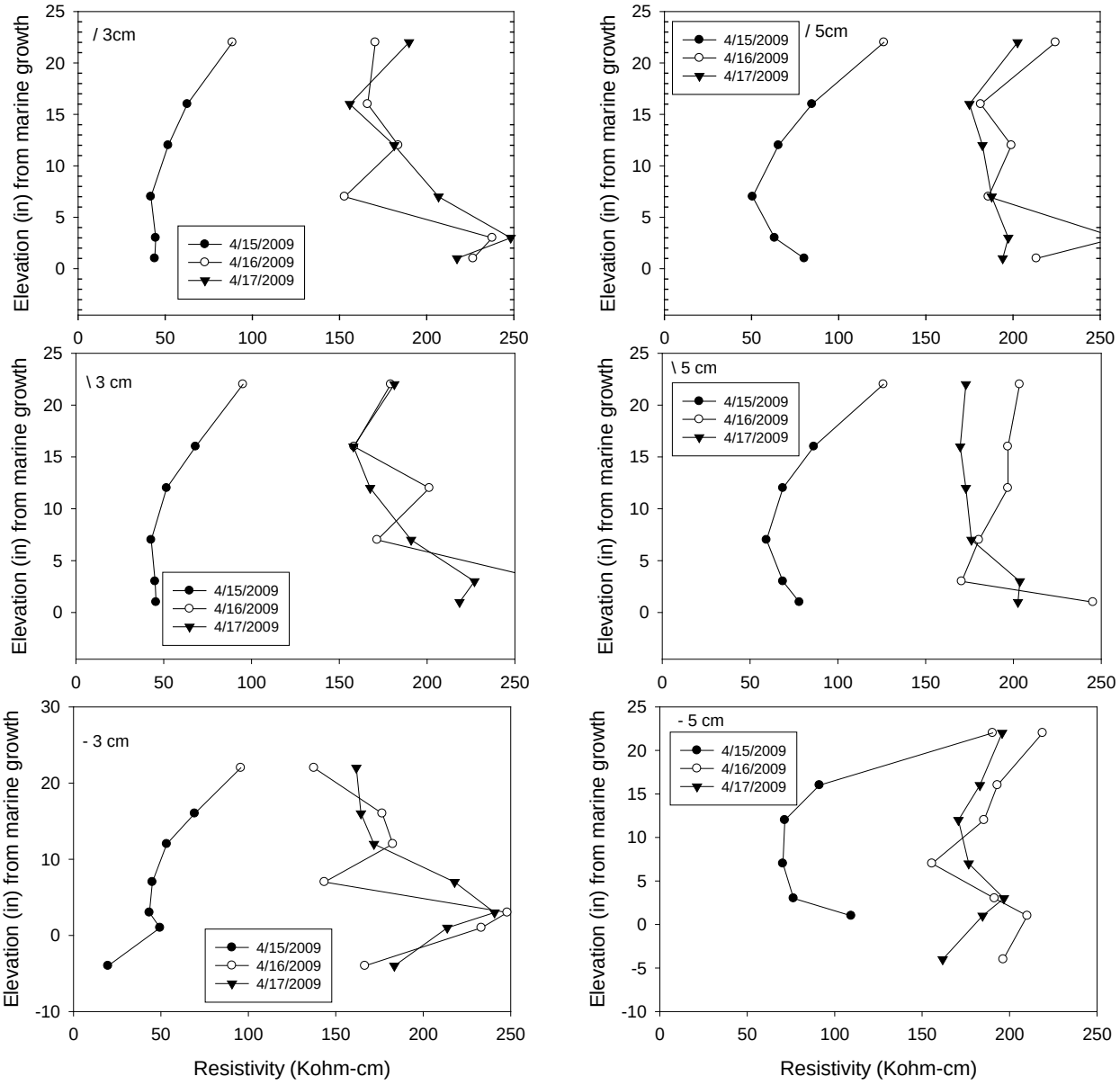

136502
Key Royale Bridge
Bent 2 Pile 3 North Face
C Cover: 3 in

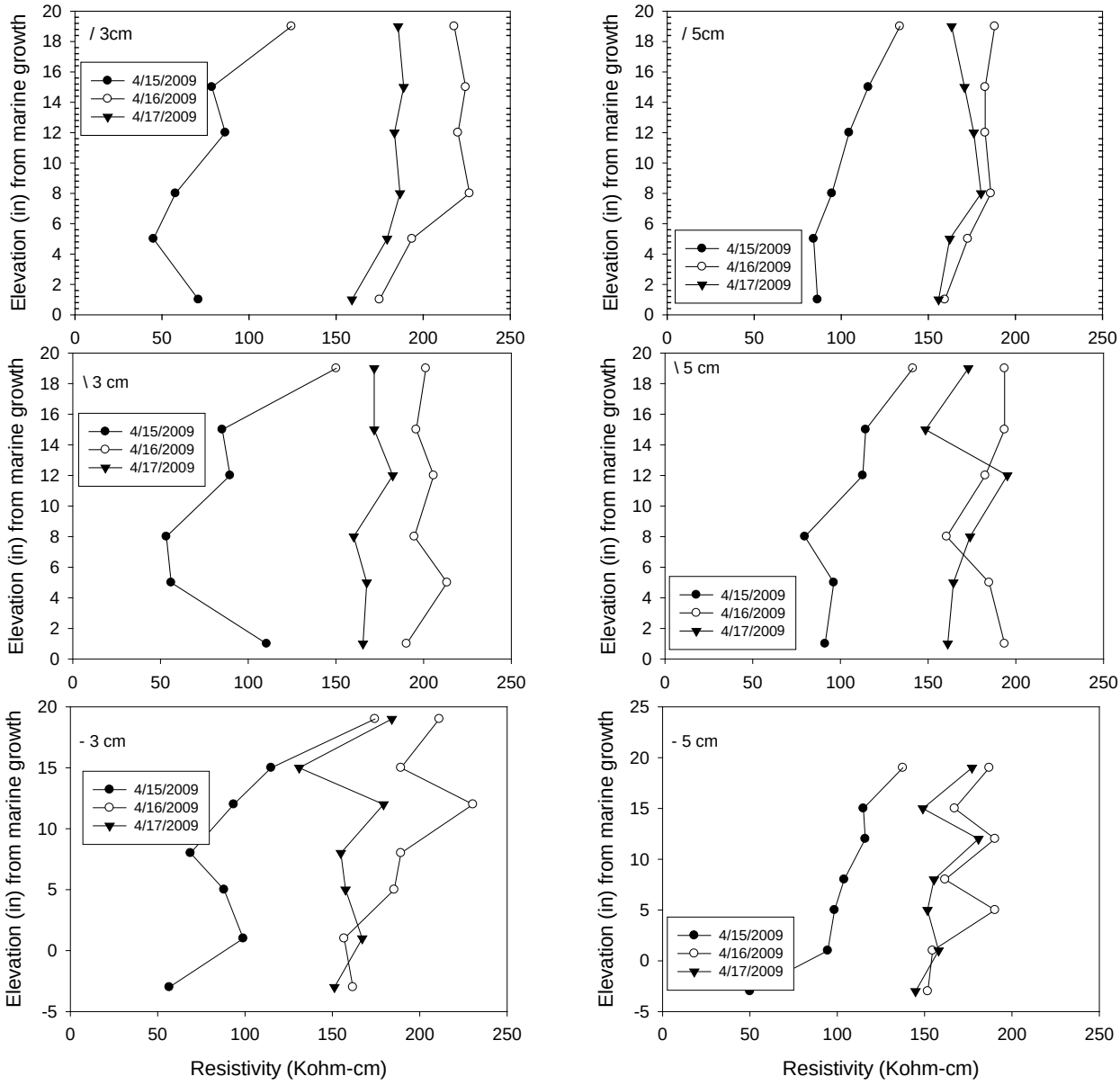

136502
Key Royale Bridge
Bent 2 Pile 4 North Face
C Cover: 3 in

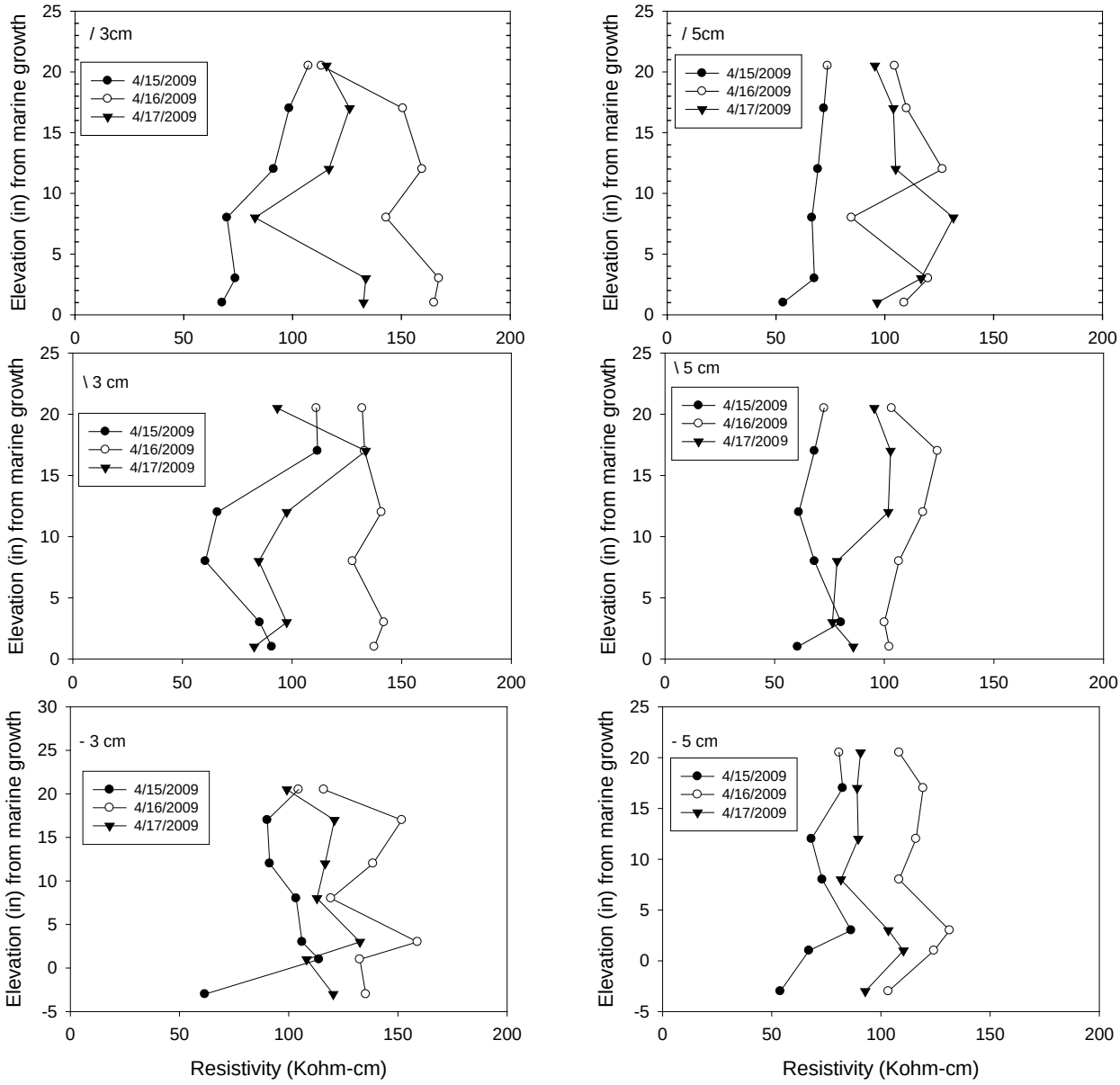

136502
Key Royale Bridge
Bent 2 Pile 5 North Face
C Cover: 3 in

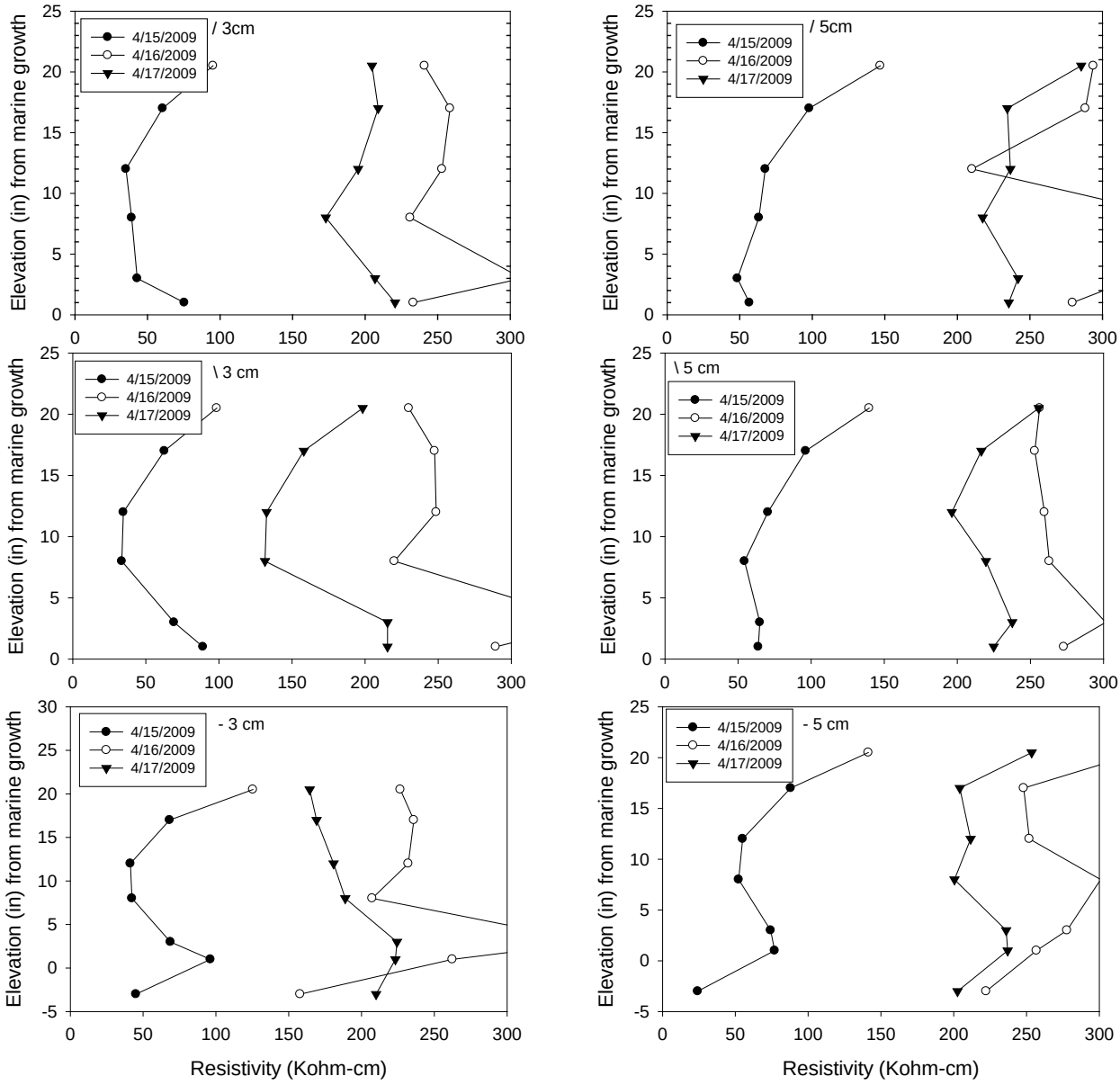

136502
Key Royale Bridge
Bent 3 Pile 1 North Face
C Cover: 3 in

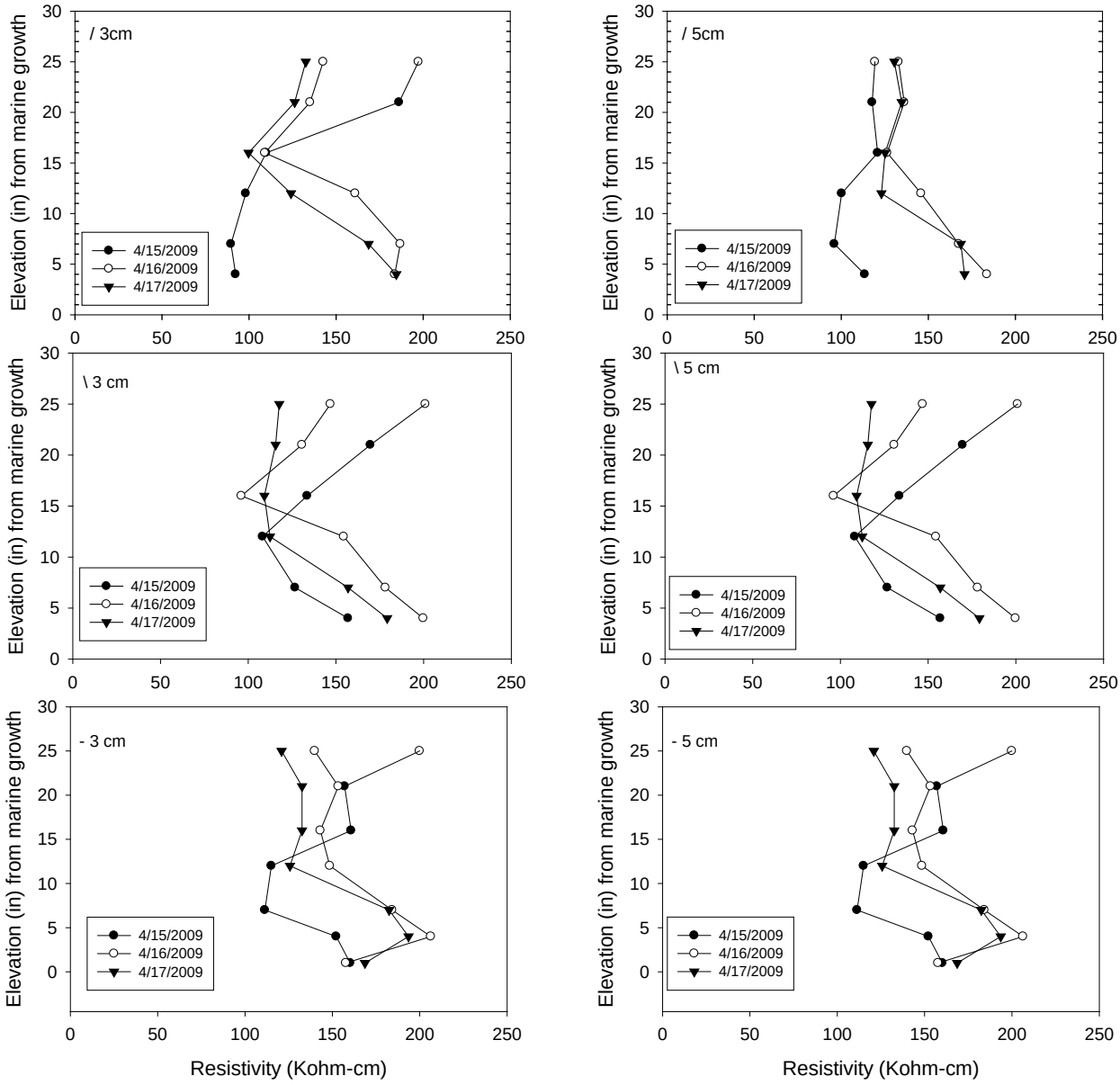

136502
Key Royale Bridge
Bent 3 Pile 2 South Face
C Cover: 3 in

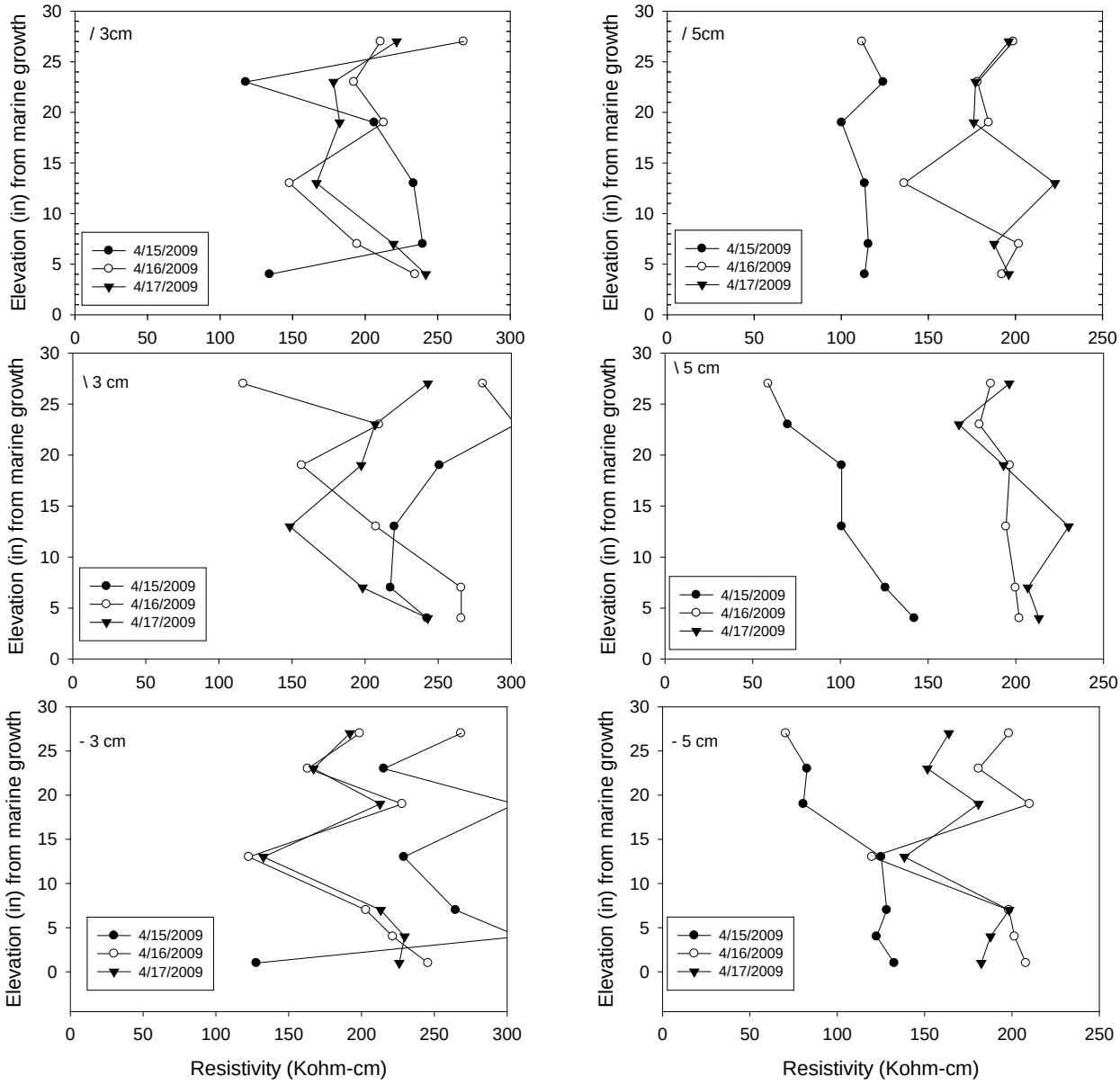

136502
Key Royale Bridge
Bent 3 Pile 3 North Face
C Cover: 3 in

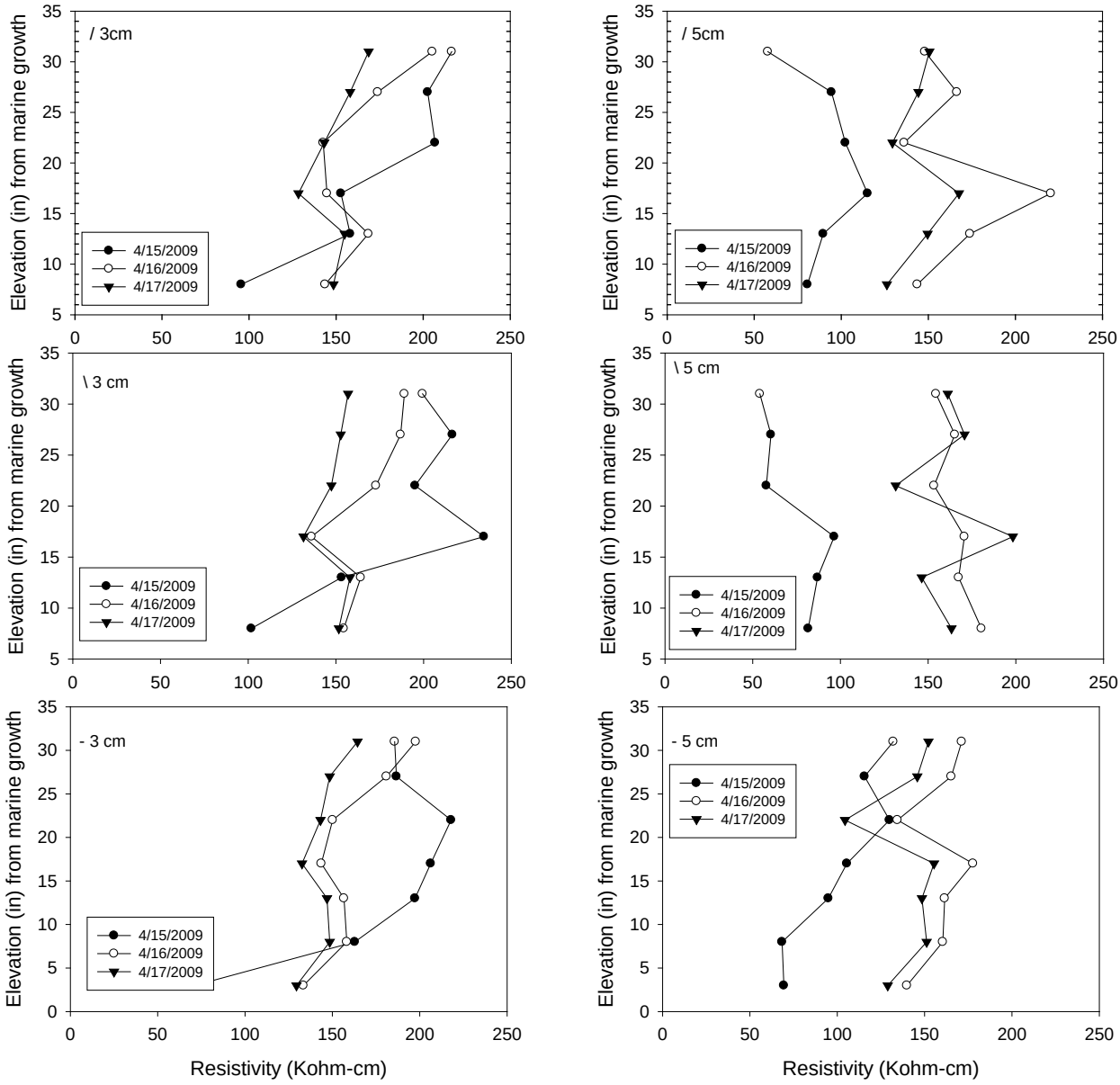

136502
Key Royale Bridge
Bent 3 Pile 4 North Face
C Cover: 3 in

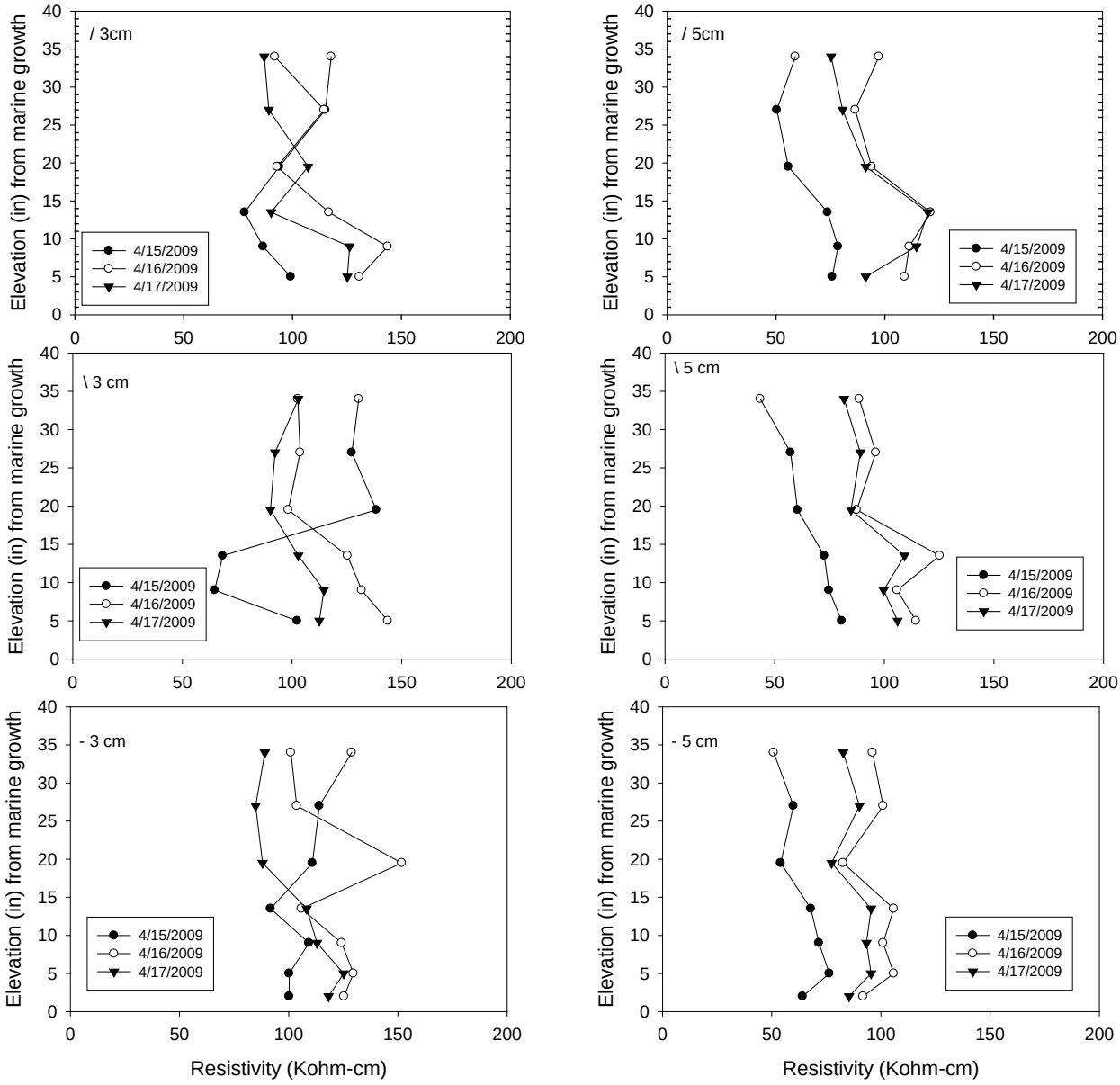

136502
Key Royale Bridge
Bent 3 Pile 5 North Face
C Cover: 3 in

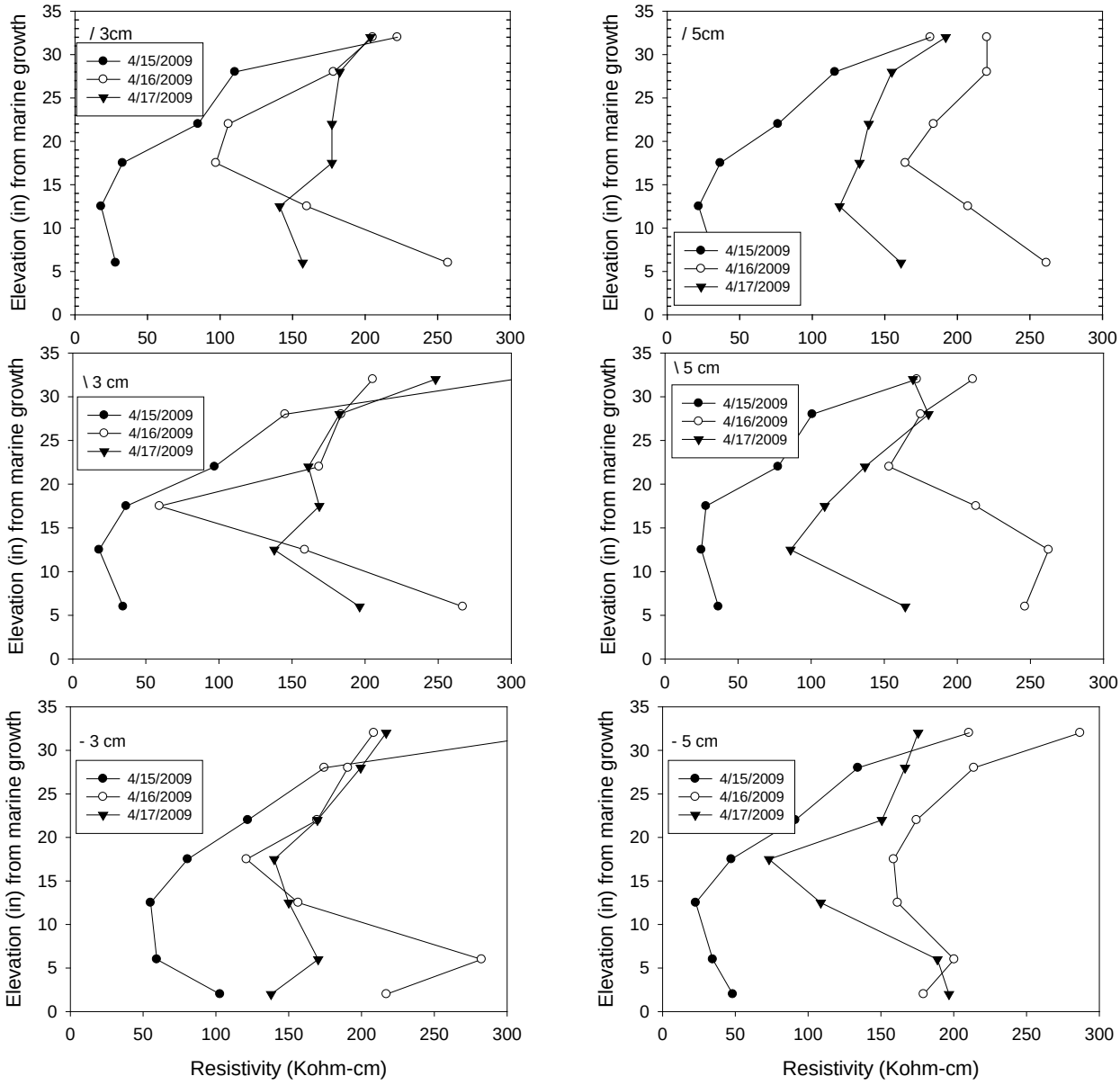

Appendix 6. Resistivity profiles as a function of elevation for all other bridges

#700006
US-1 Crane Cr. & City St
Bent 5 Pile 13 East Face
Concrete Cover ~ 3.65 in

#700006
US-1 Crane Cr. & City St
Bent 5 Pile 14 East Face
Concrete Cover ~ 3.65 in

700193
Sykes Creek
Bent 3 Pile 11 North Face
C Cover: 3 in

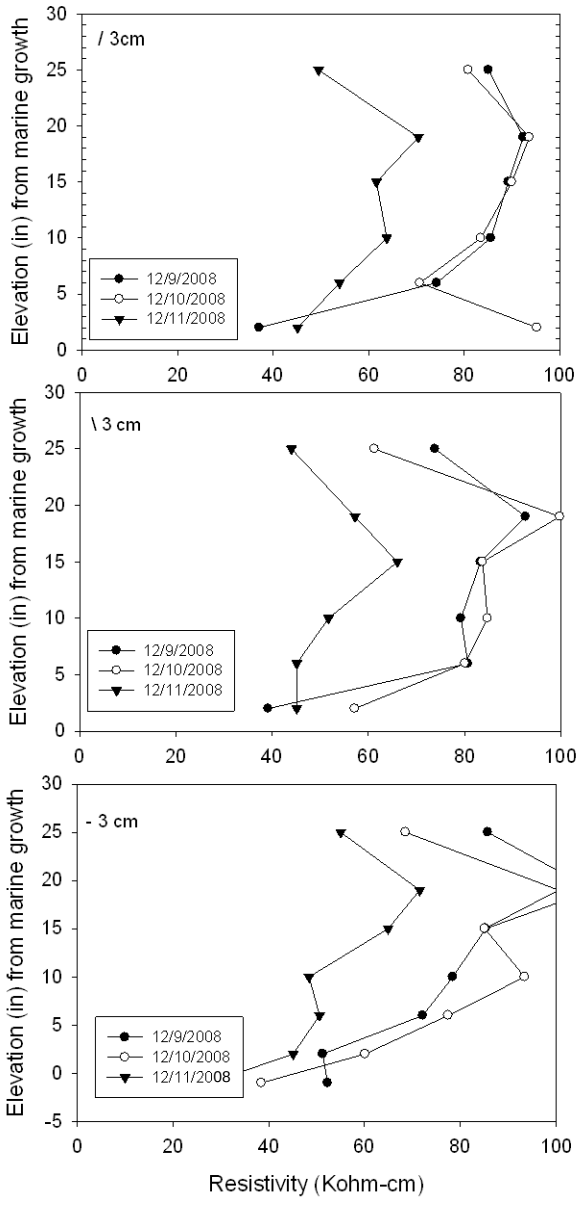

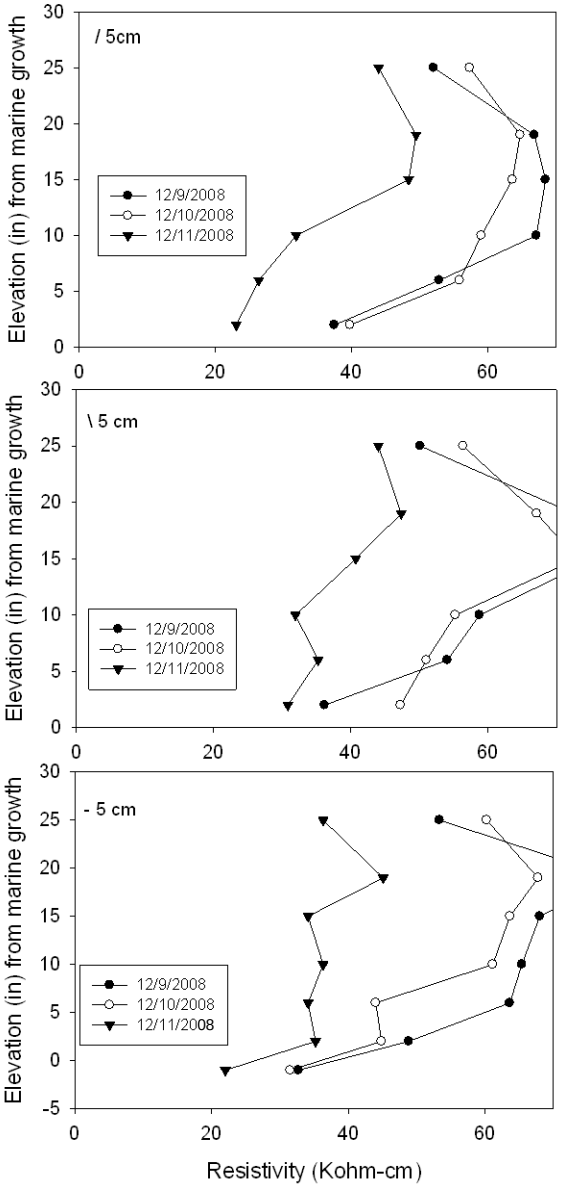

700193
Sykes Creek
Bent 4 Pile 11 North Face
C Cover: 2.9 in

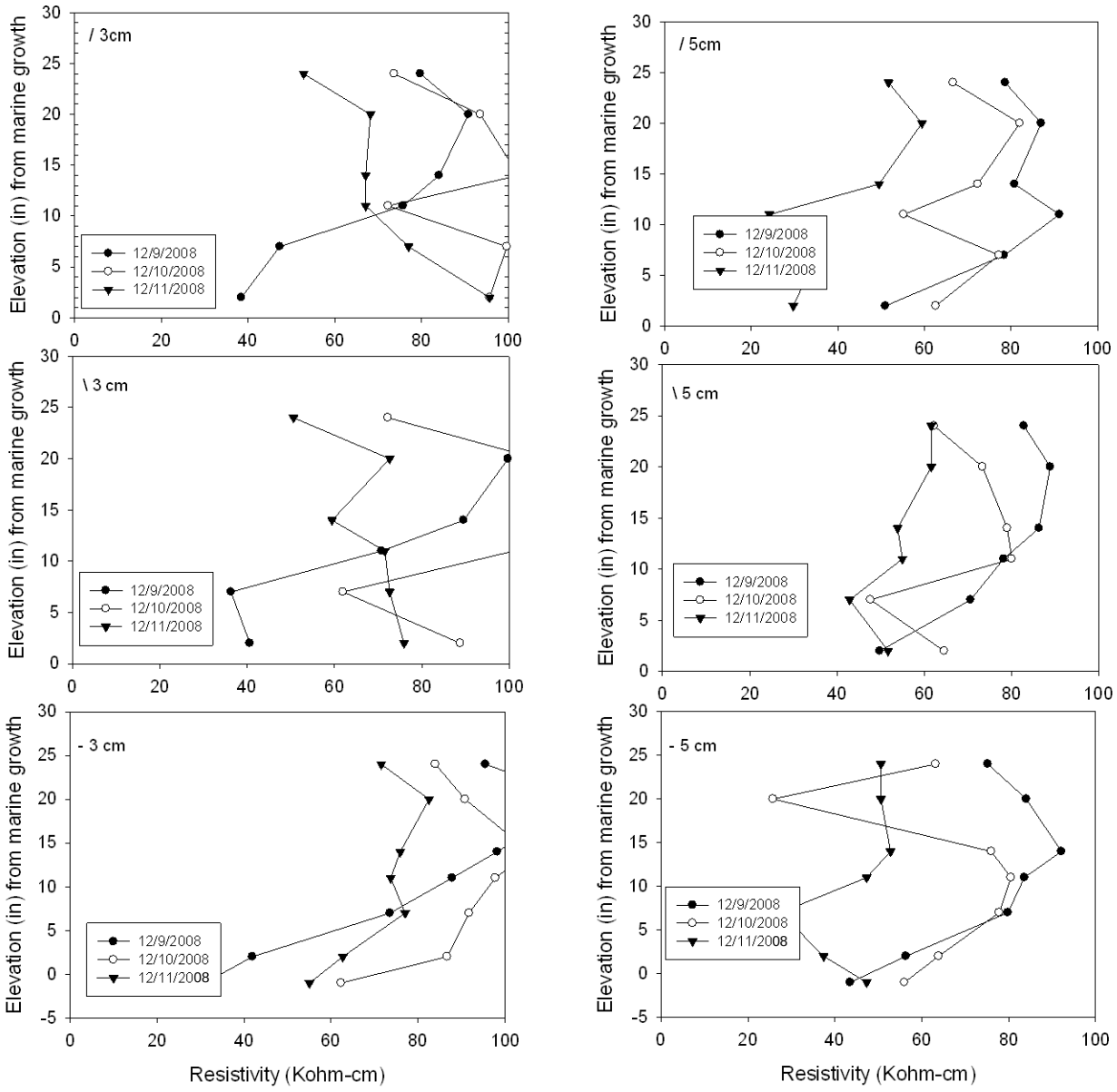

700203
Turkey Creek
Bent 3 Pile 15 West Face
C Cover: 3 in

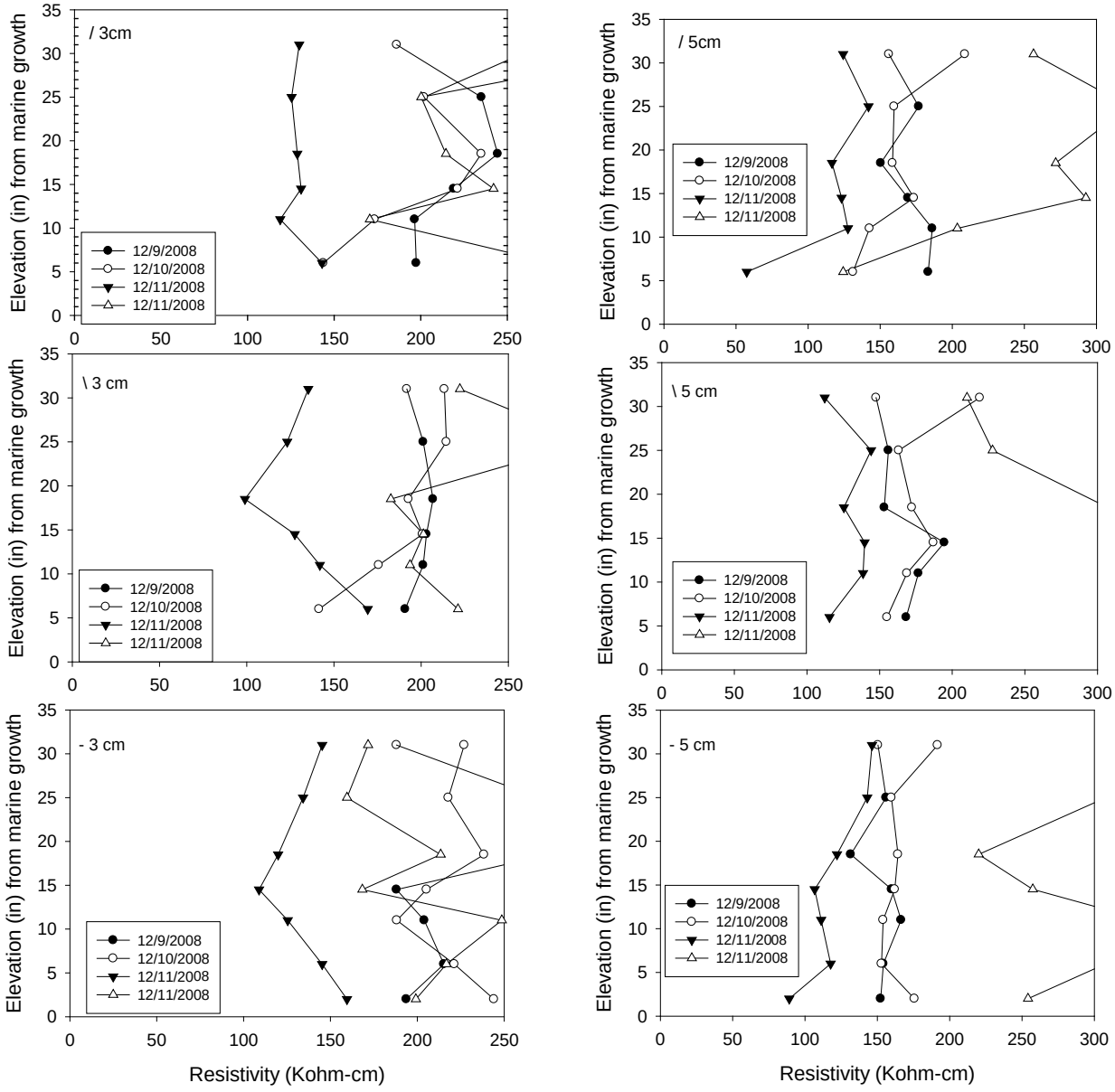

700203
Turkey Creek
Bent 5 Pile 14 East Face
C Cover: 3 in

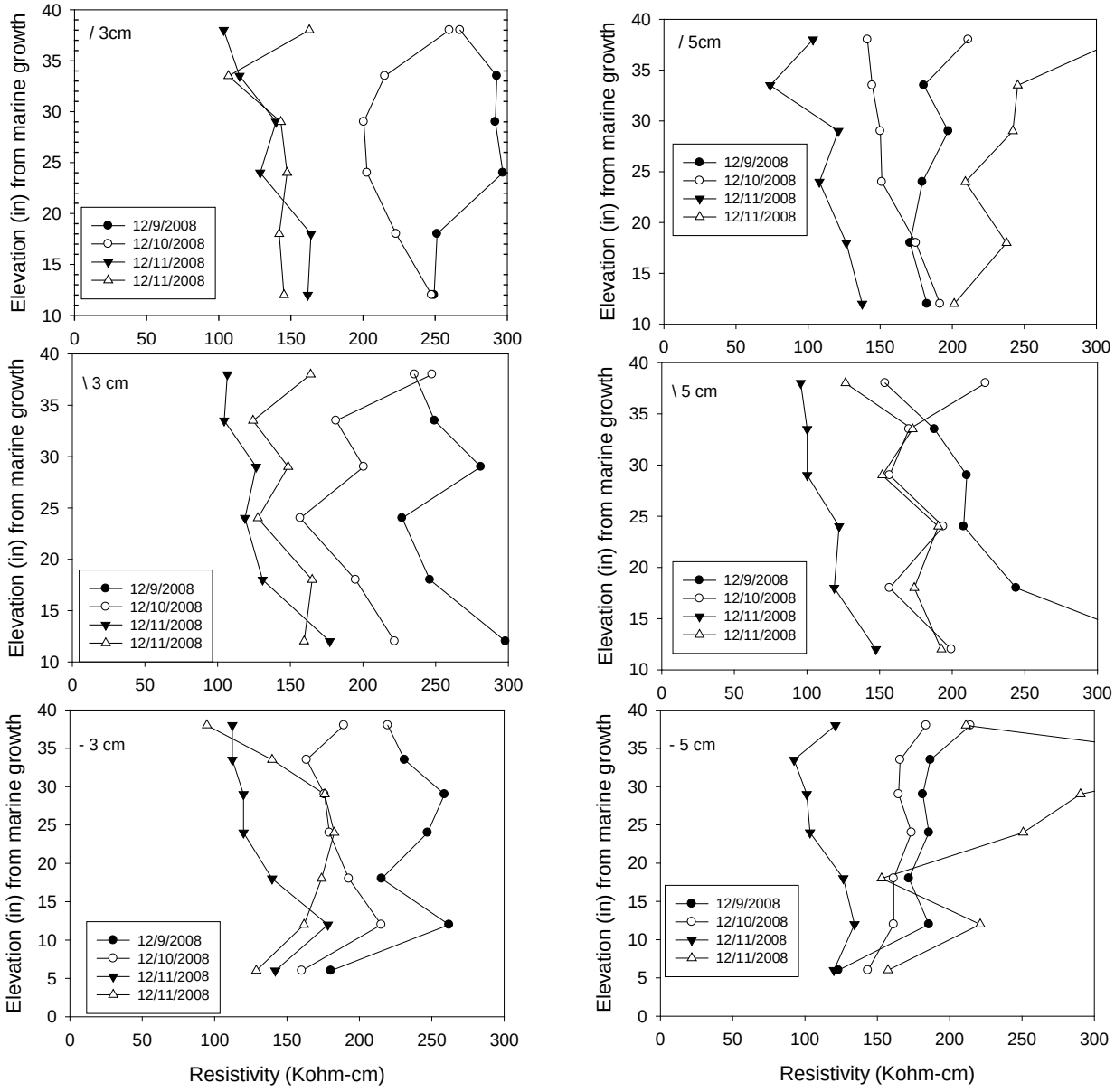

700203
Turkey Creek
Bent 5 Pile 15 West Face
C Cover: 3 in

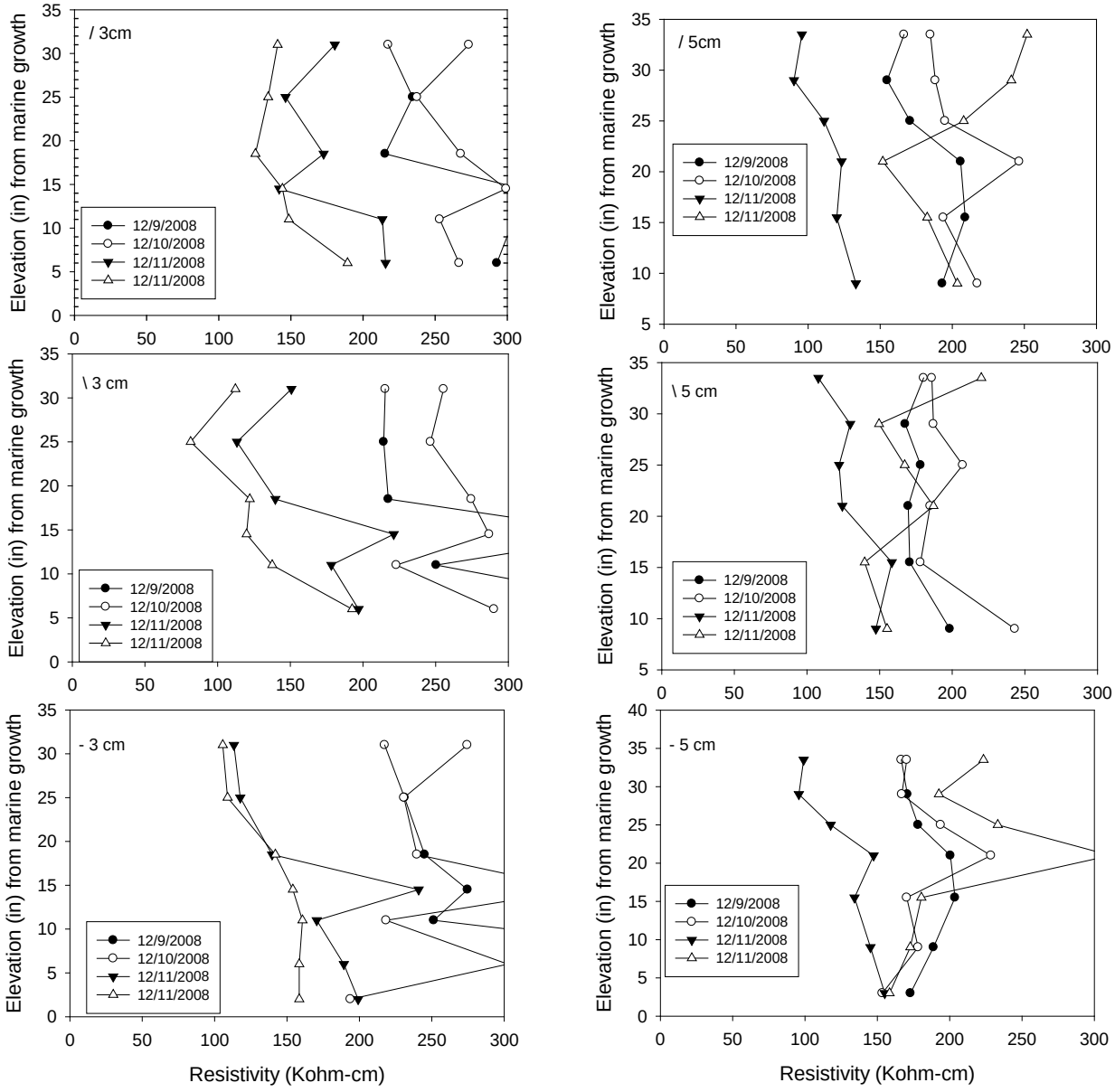

794004
Main Street - Daytona
Bent 16 Pile 3 North Face

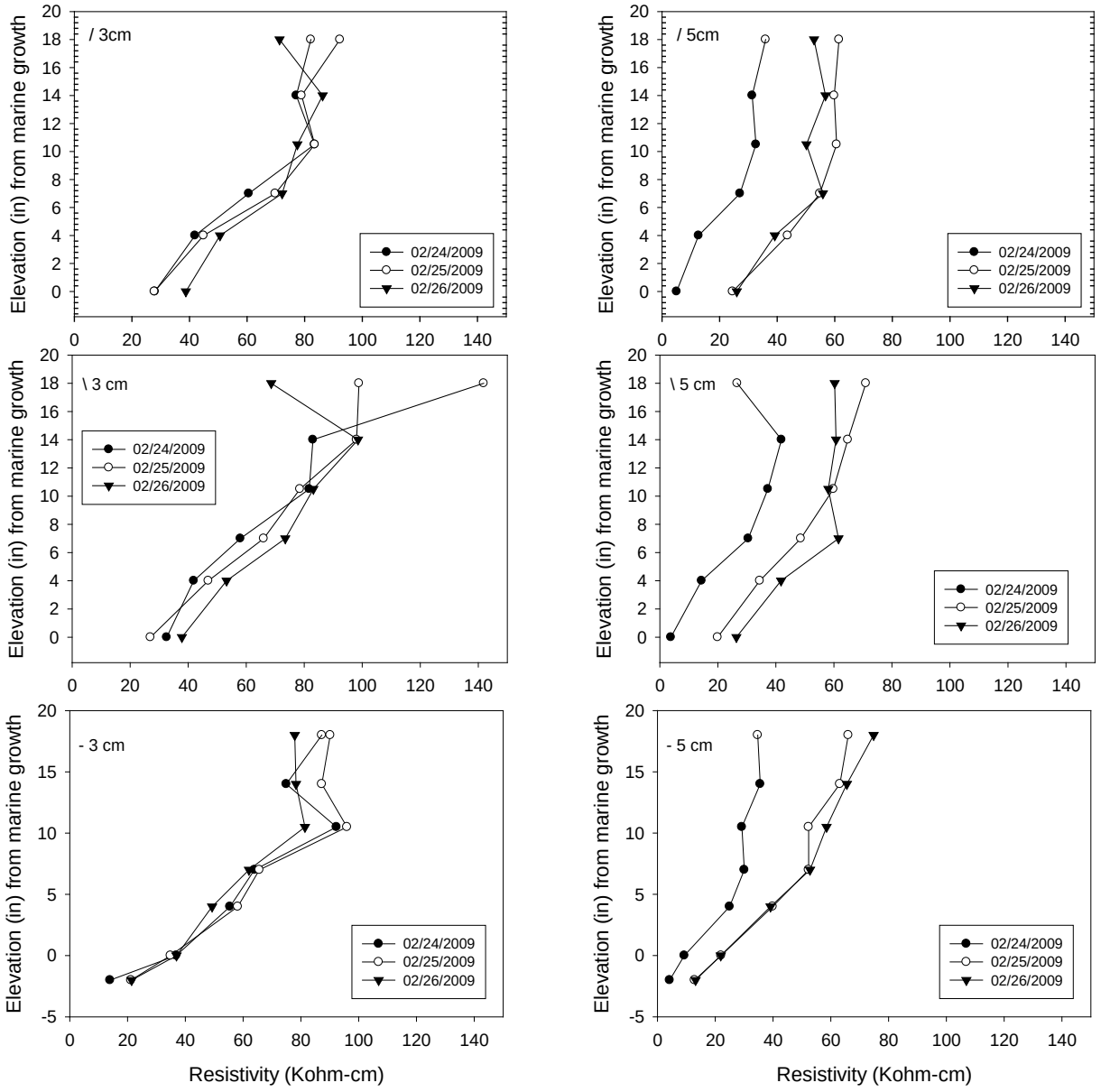

794004
Main Street - Daytona
Bent 16 Pile 4 East Face

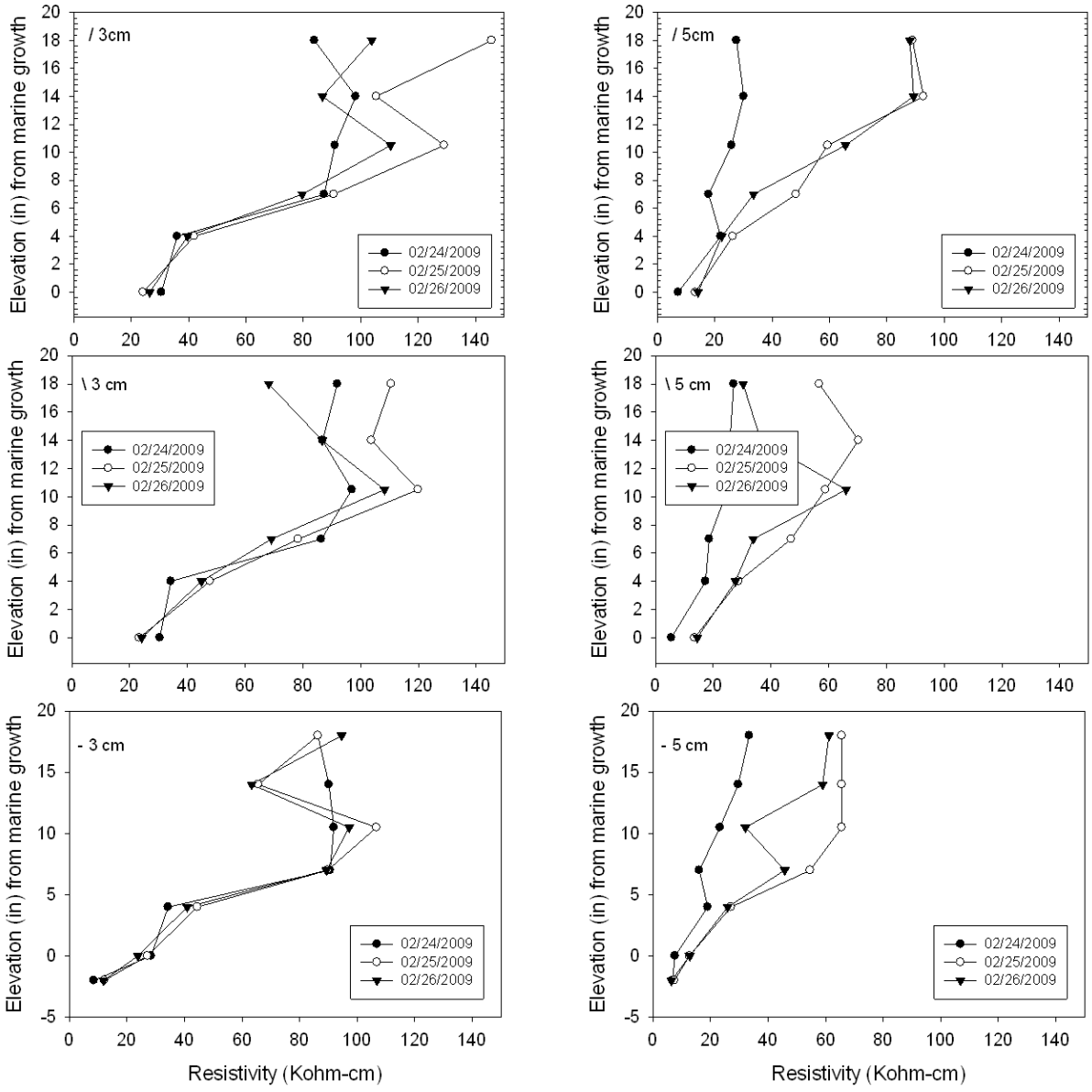

790187
International Speedway
Bent 8 Pile 2(N) West Face
C Cover: 2.75 in

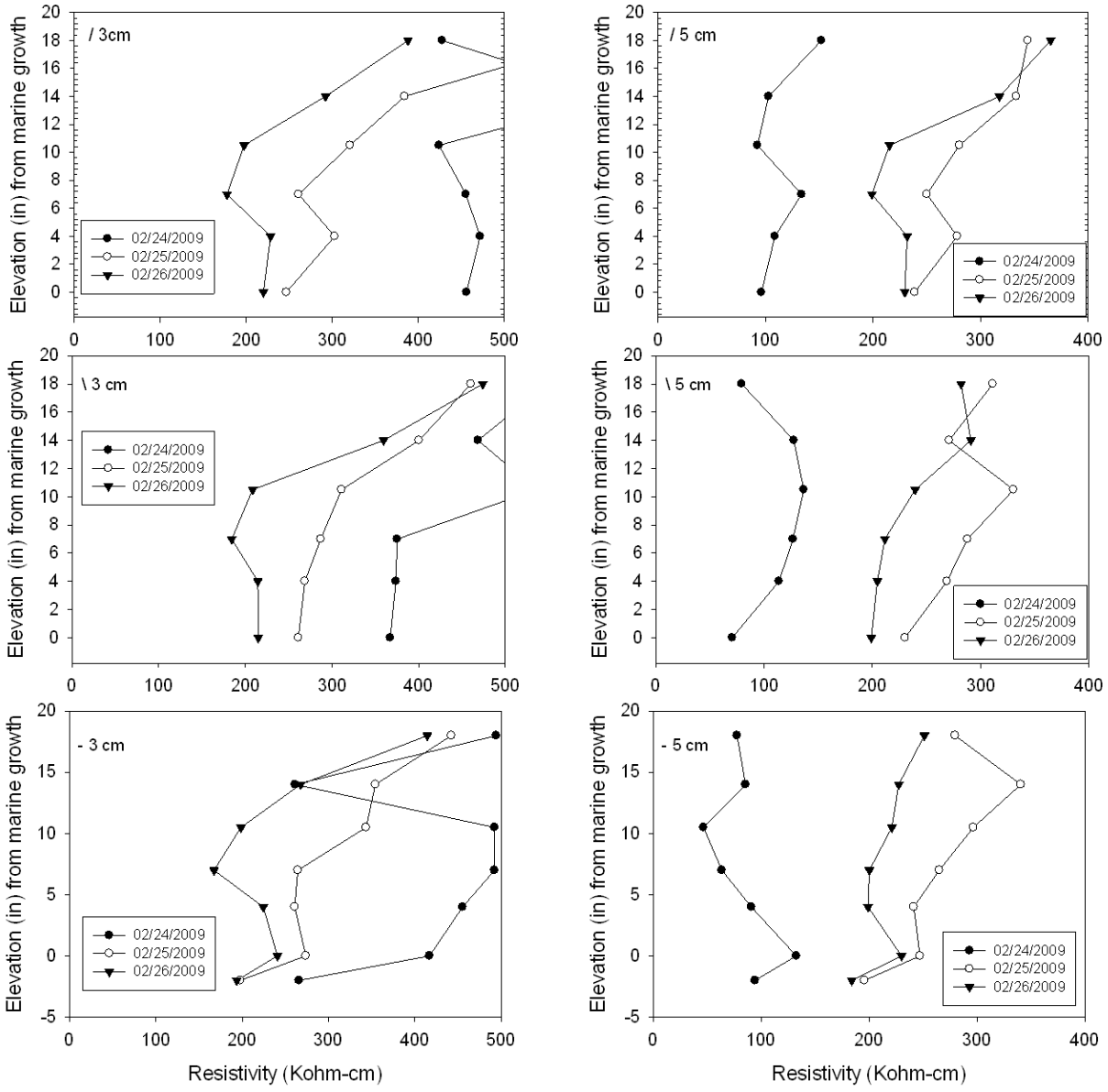

790187
International Speedway
Bent 8 Pile 1(S) North Face
C Cover: 3.85 in

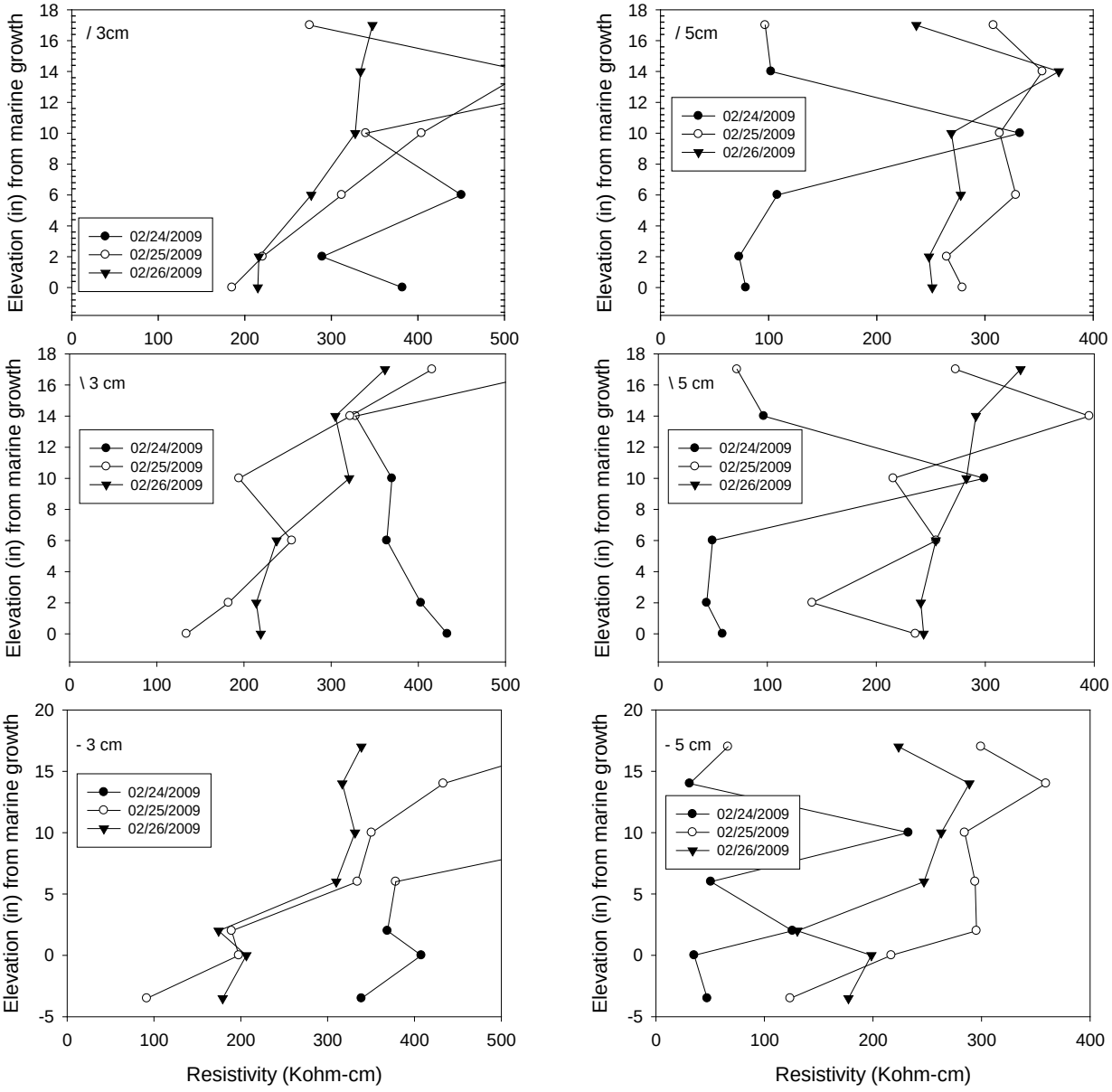

790175
Oakridge - Daytona
Bent 6 West Face

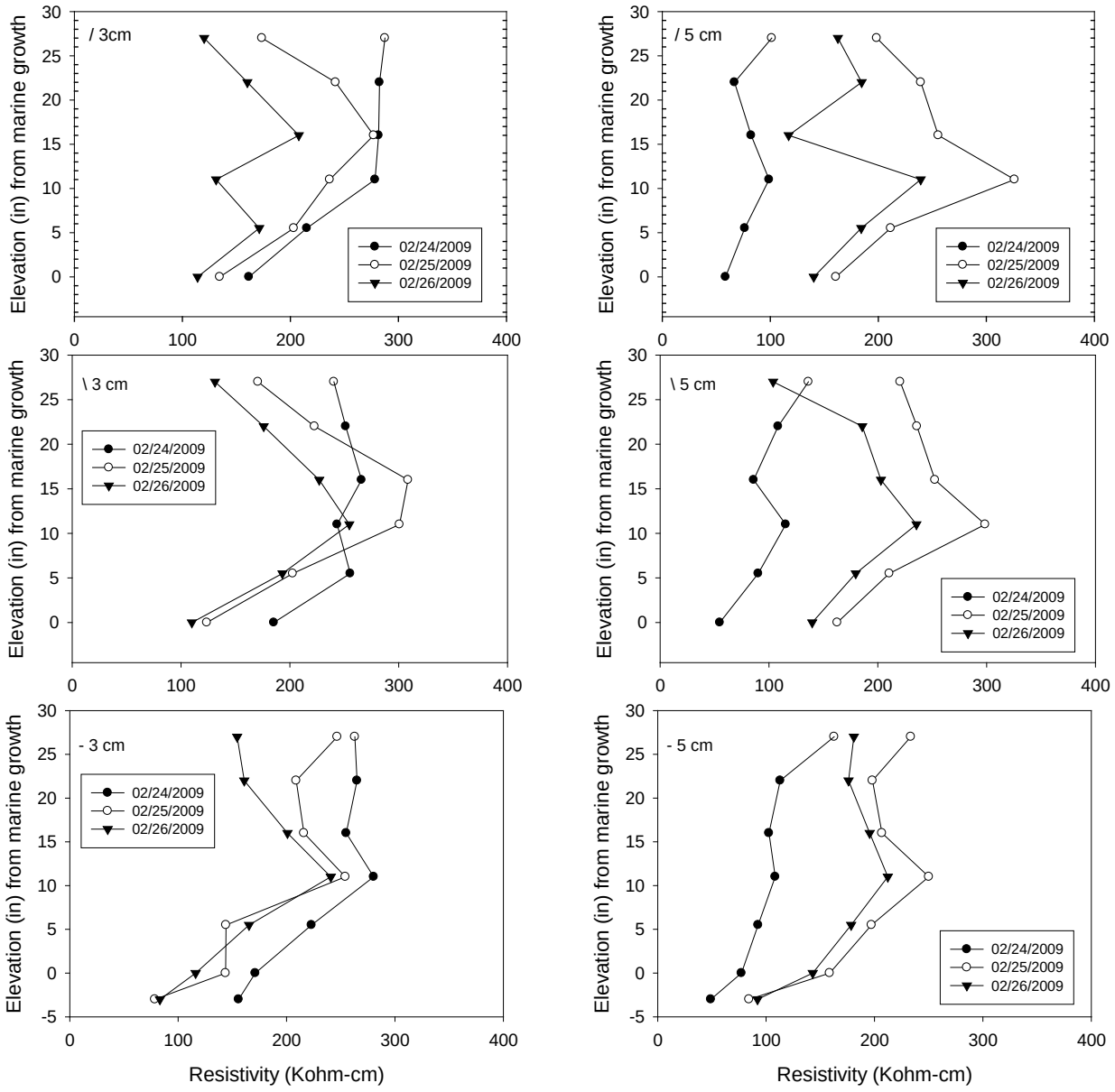

790174
Seabreeze - Daytona
Bent 6 South Face

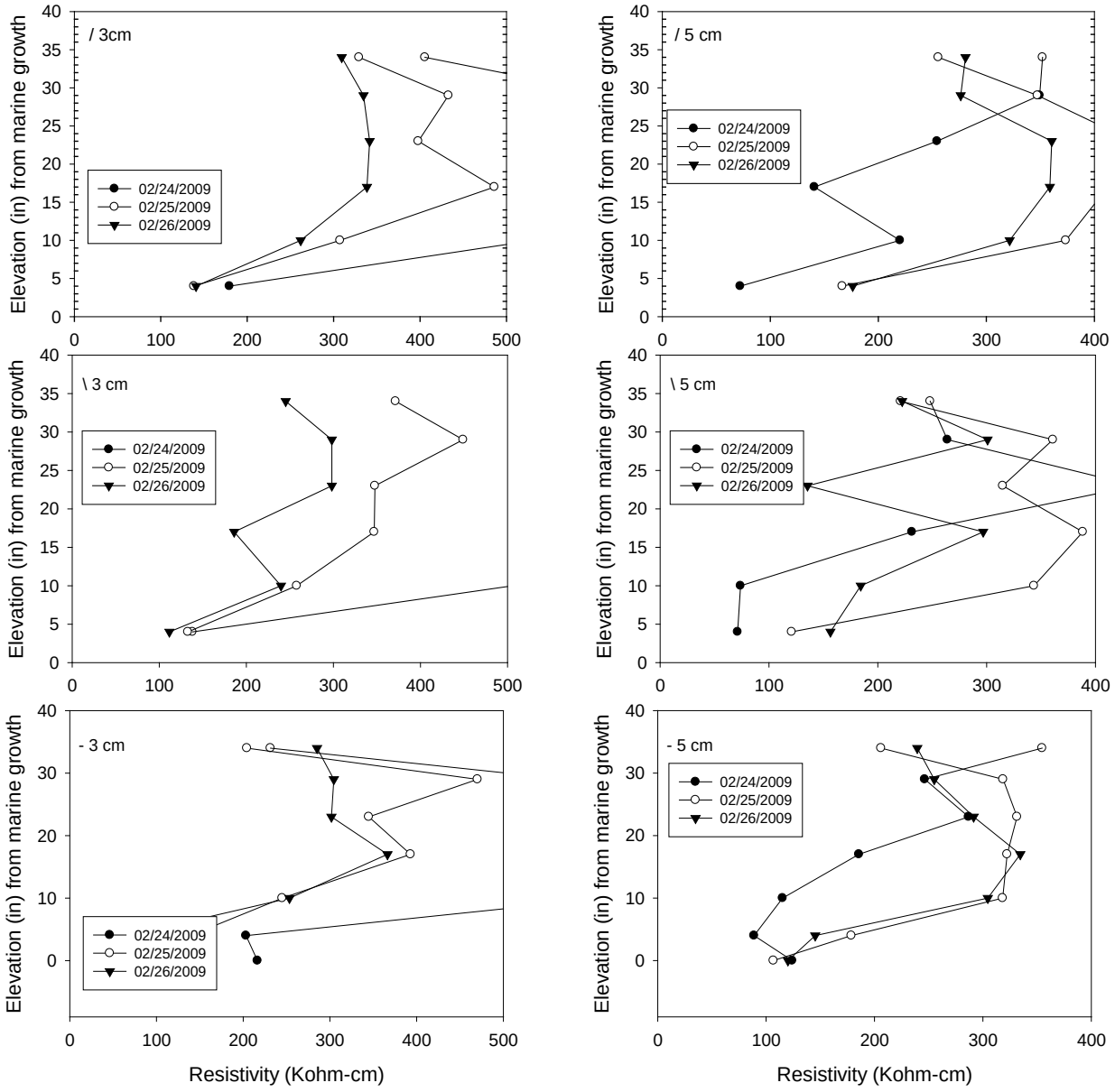

790174
Seabreeze - Daytona
Bent 7 West Face

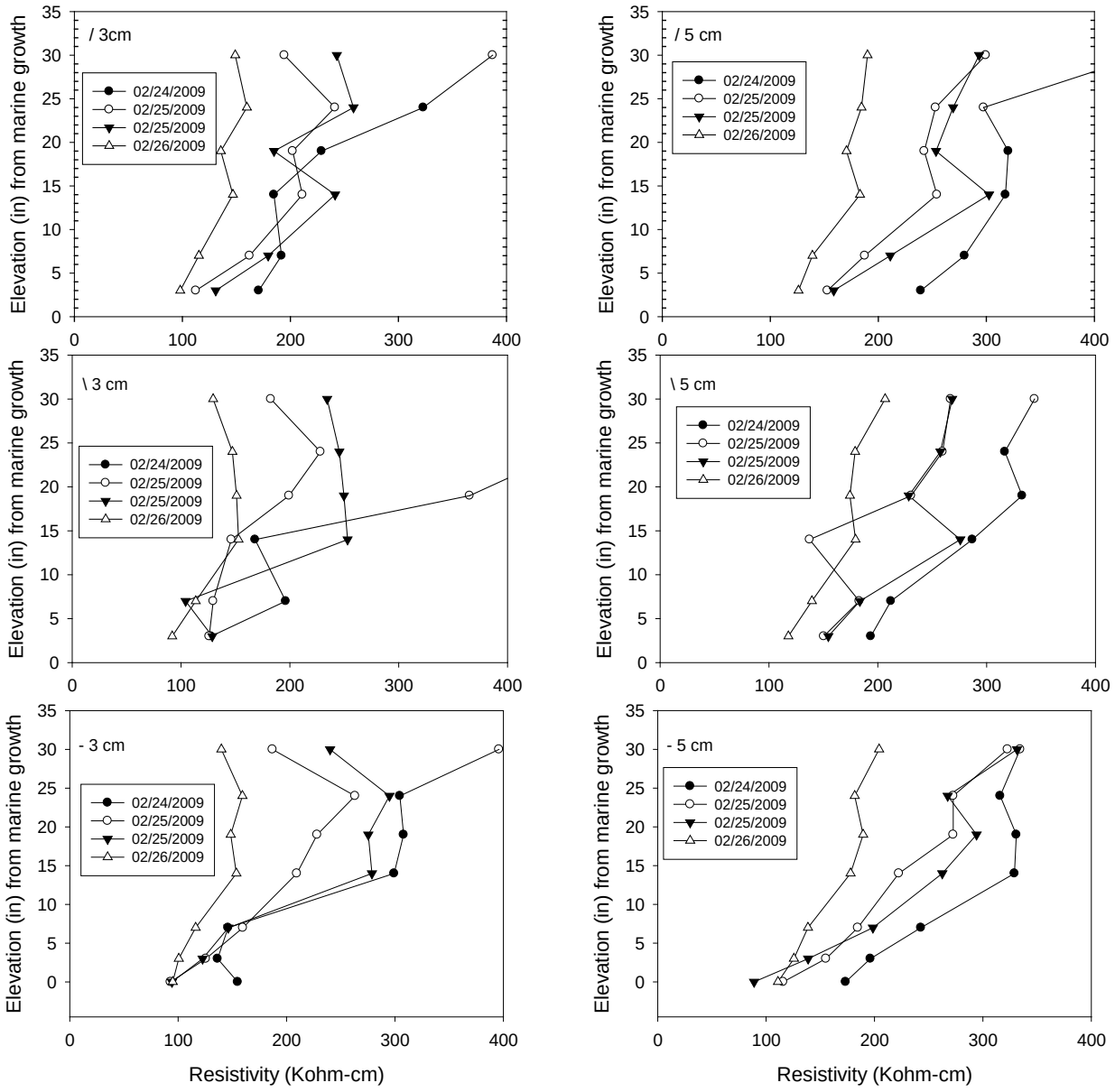

490032
Apalachicola Bay
Bent 125 Pile 3 South Face
C Cover: 3.85 in

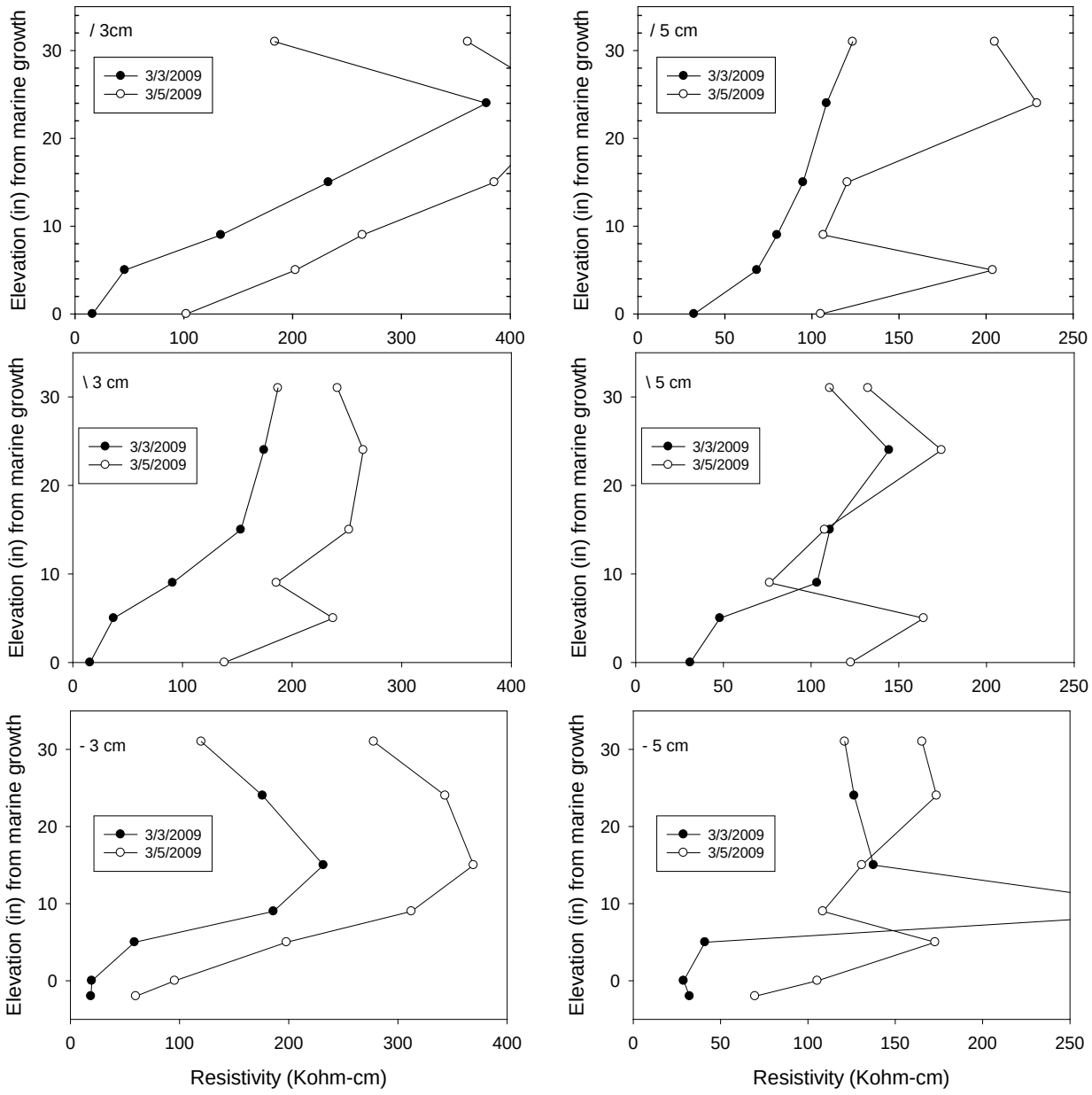

490031
Apalachicola River
Bent 15 Column above footer South Face
C Cover: 3.85 in

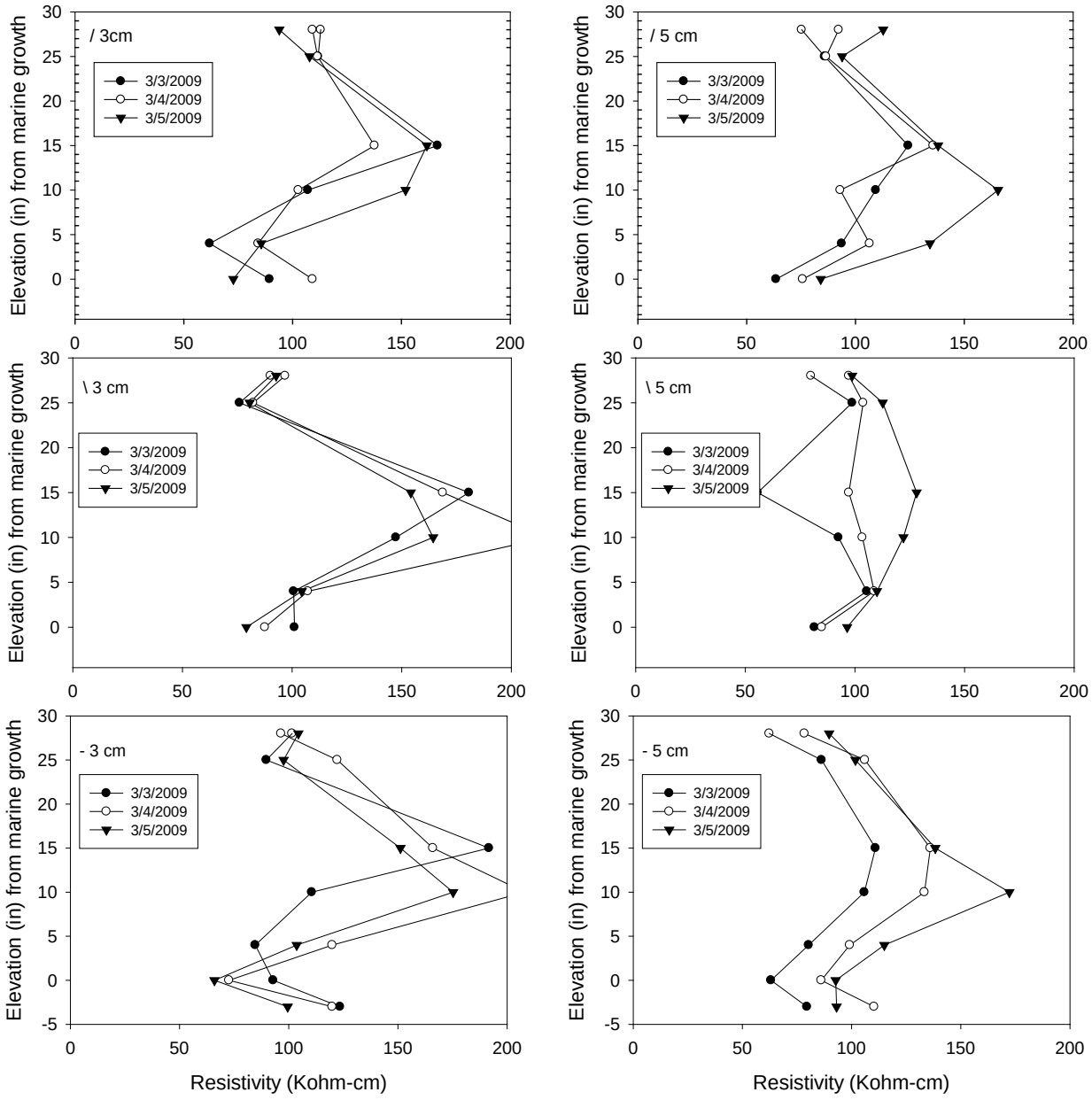

490031
Apalachicola Bay
Bent 12 Pile 3 South Face
C Cover: 2.5 in

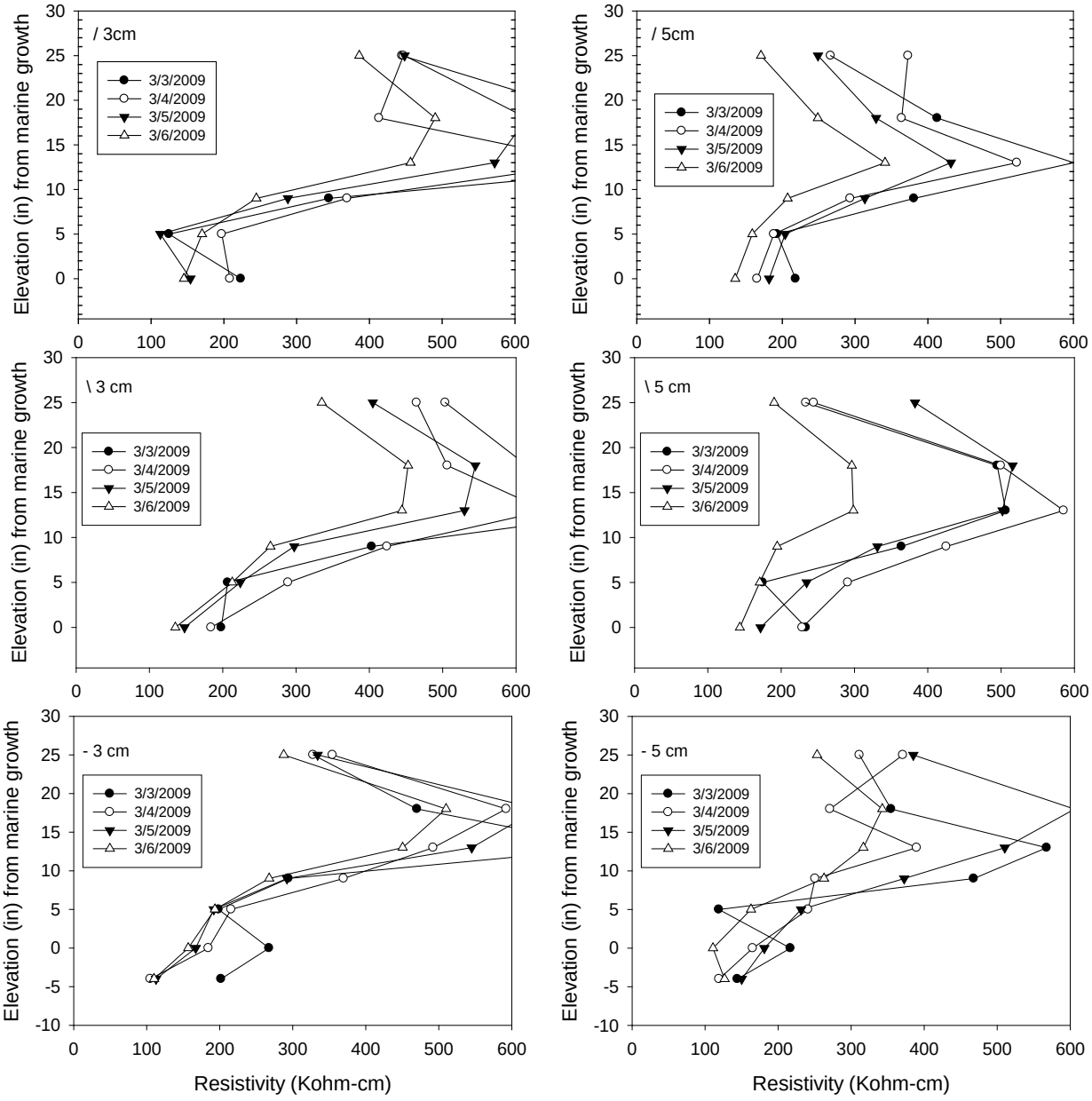

490031
Apalachicola River
Bent 15 – Pr - South Face
C Cover: 3.85 in

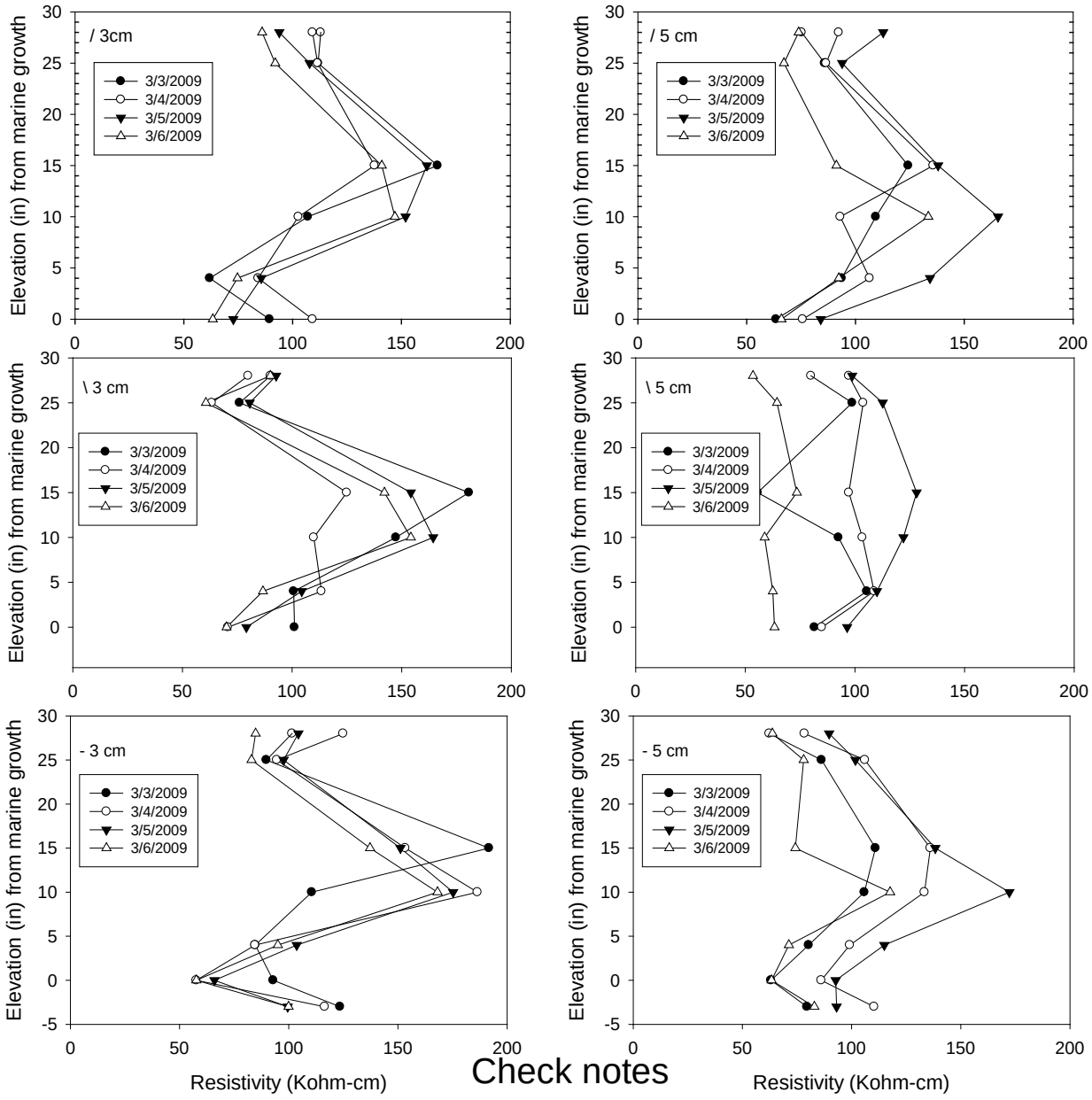

Check notes

490100
St George
Bent 19 Pile 1 West Face
C Cover: 2.7 in

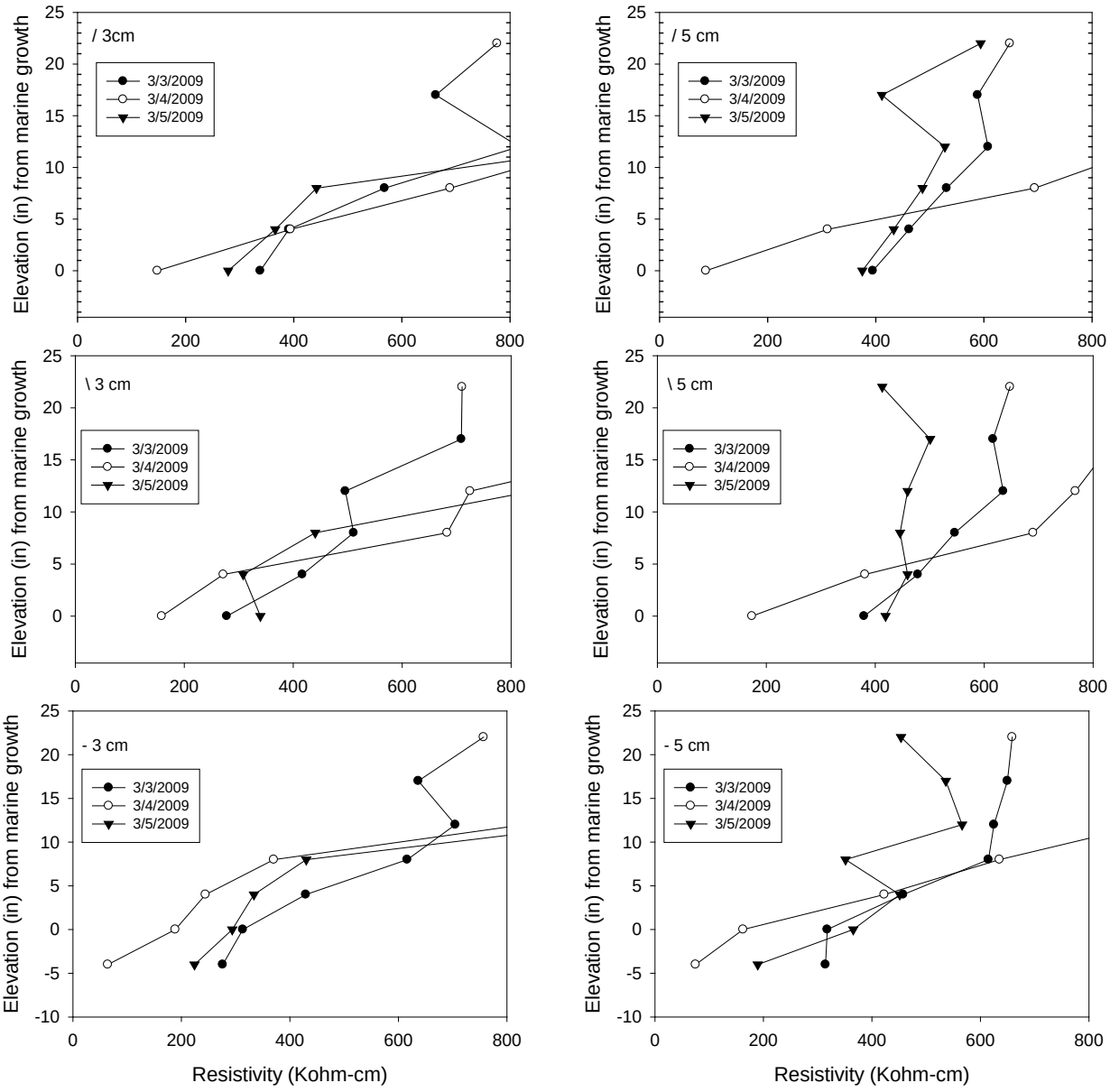

490100
St George
Bent 19 Pile 2 Southwest Face
C Cover: 2.65 in

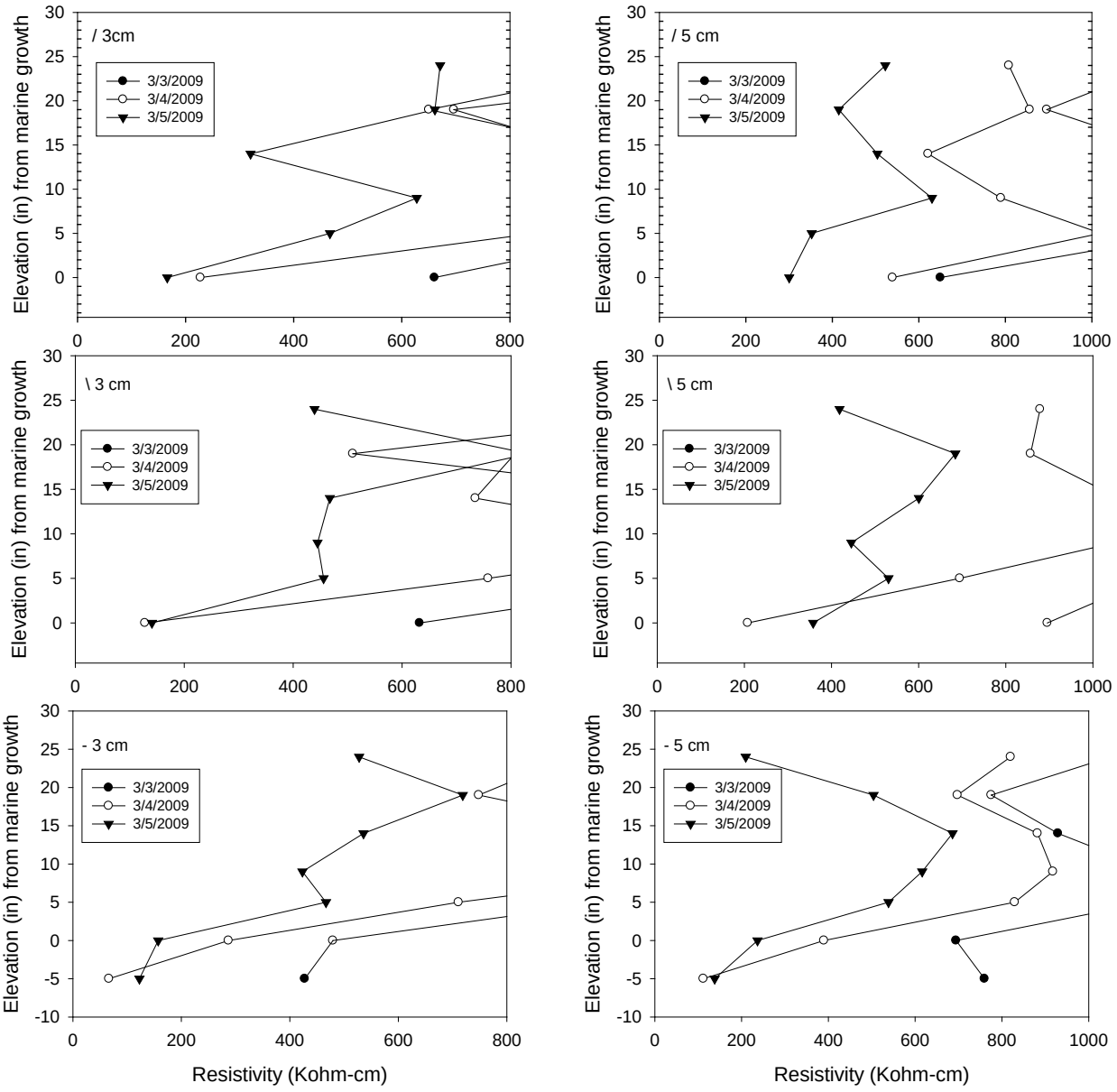

490100
St George, test p
Cutoff Pile Parallel to Bent 20 West Southwest Face
C Cover: 3.5 in

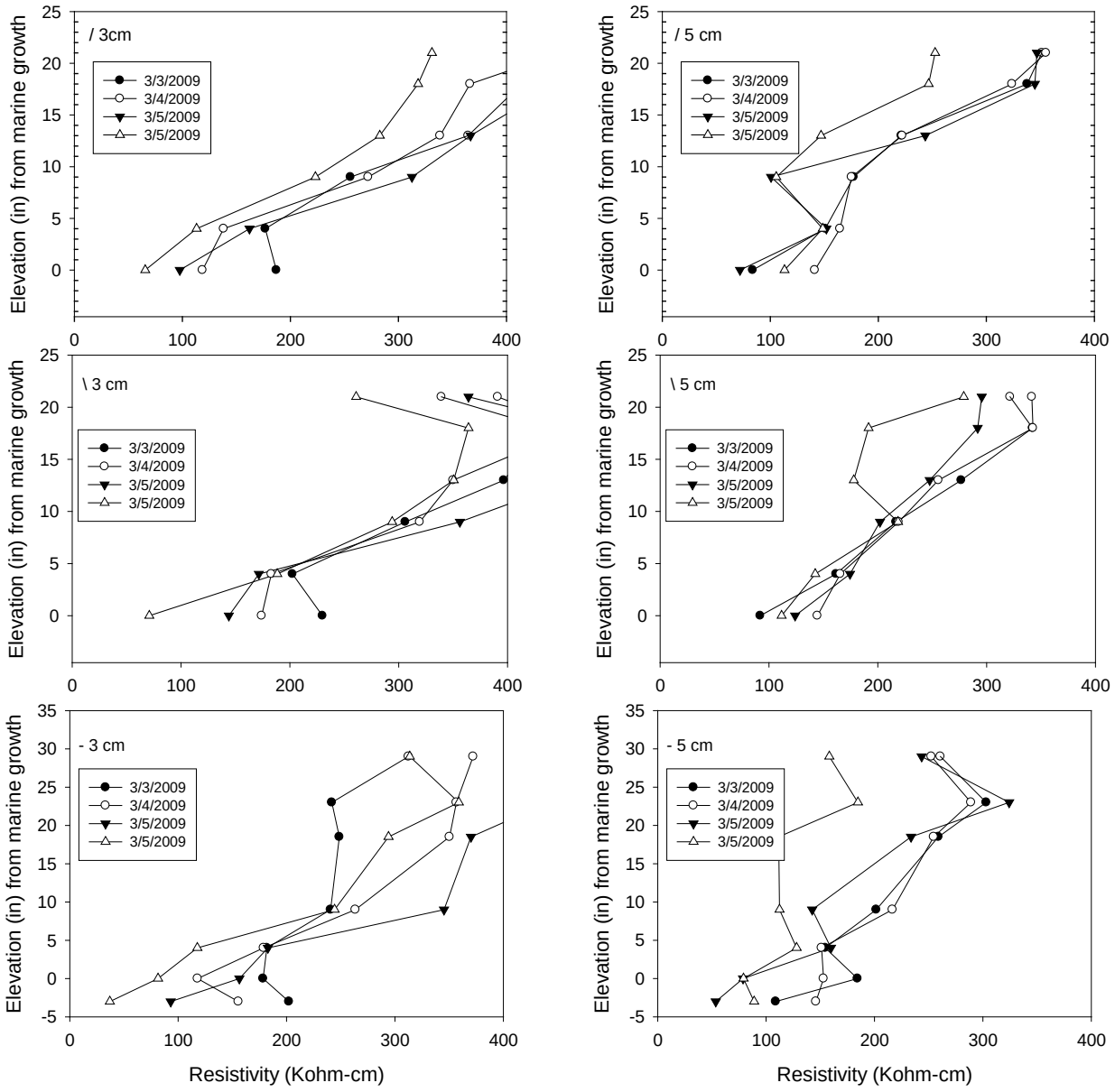

490100
St George, test p
Cutoff Pile Parallel to Bent 36 West Southwest Face
C Cover: 2.7 in

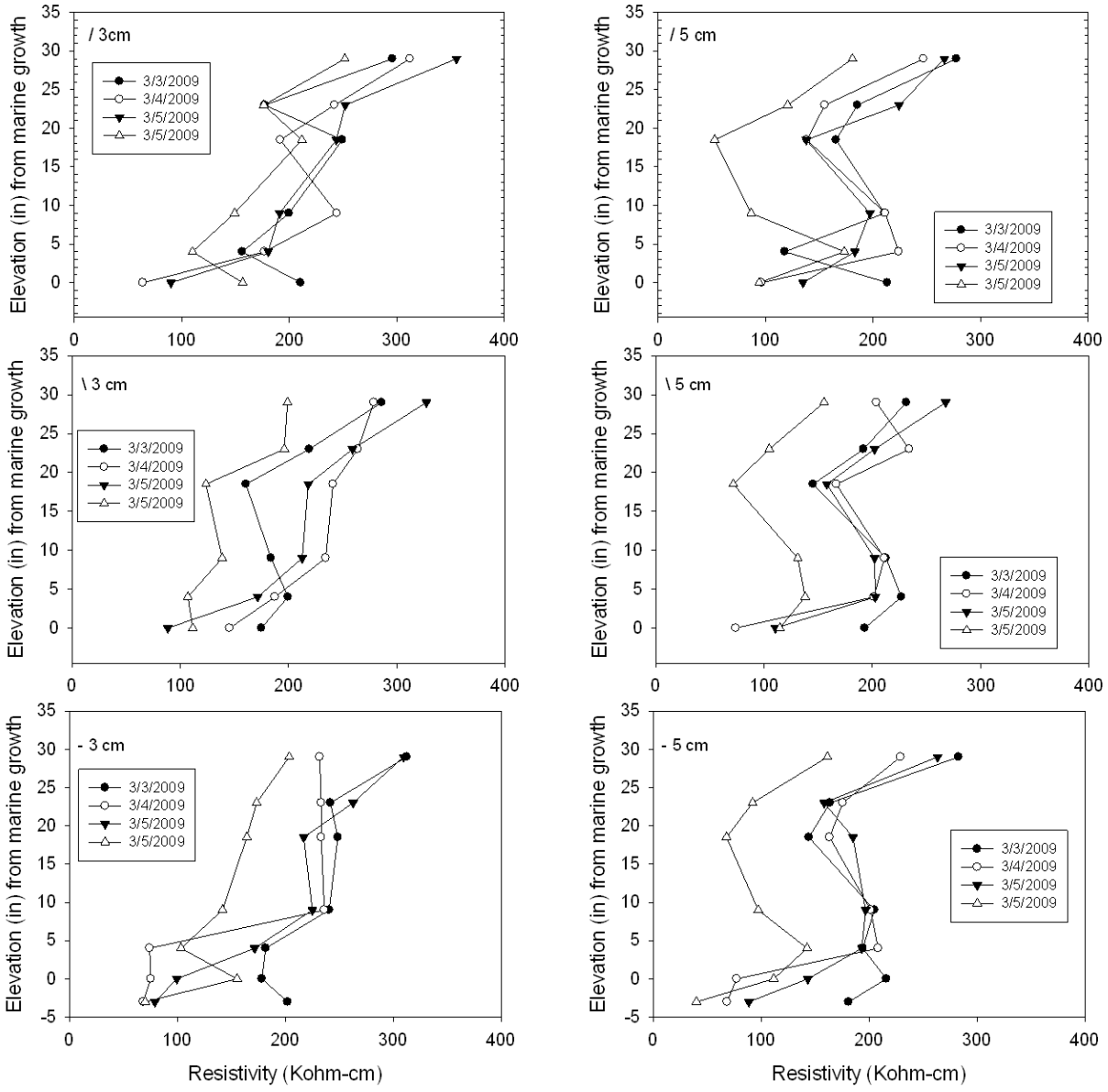

Old Saint George (fishing pier)
Bent 21 Pile 1 West Face
C Cover: 3.65 in

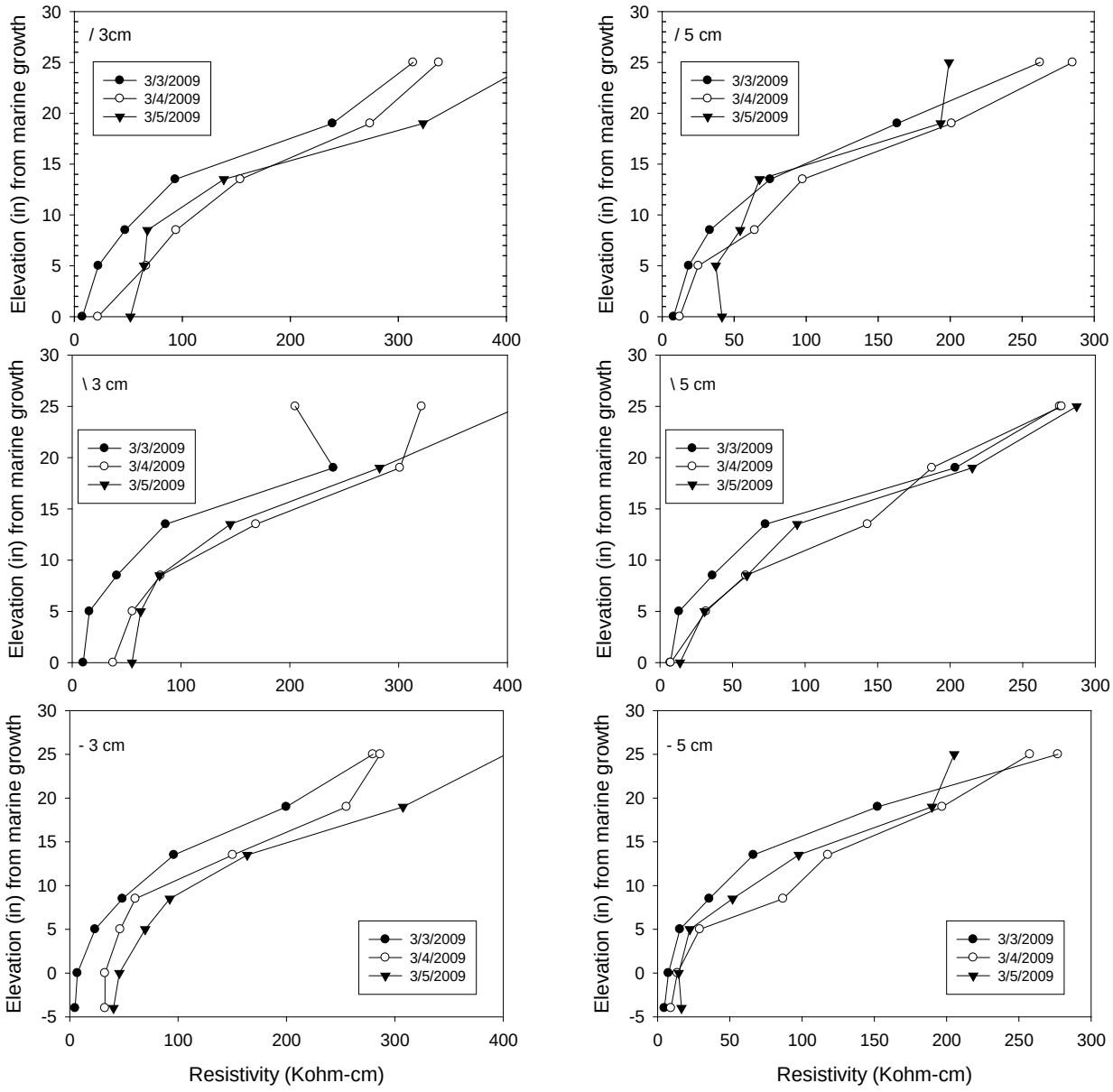

150138
Courtney Cambell
Bent 10 Pile 6 West Face
C Cover: 3.8 in

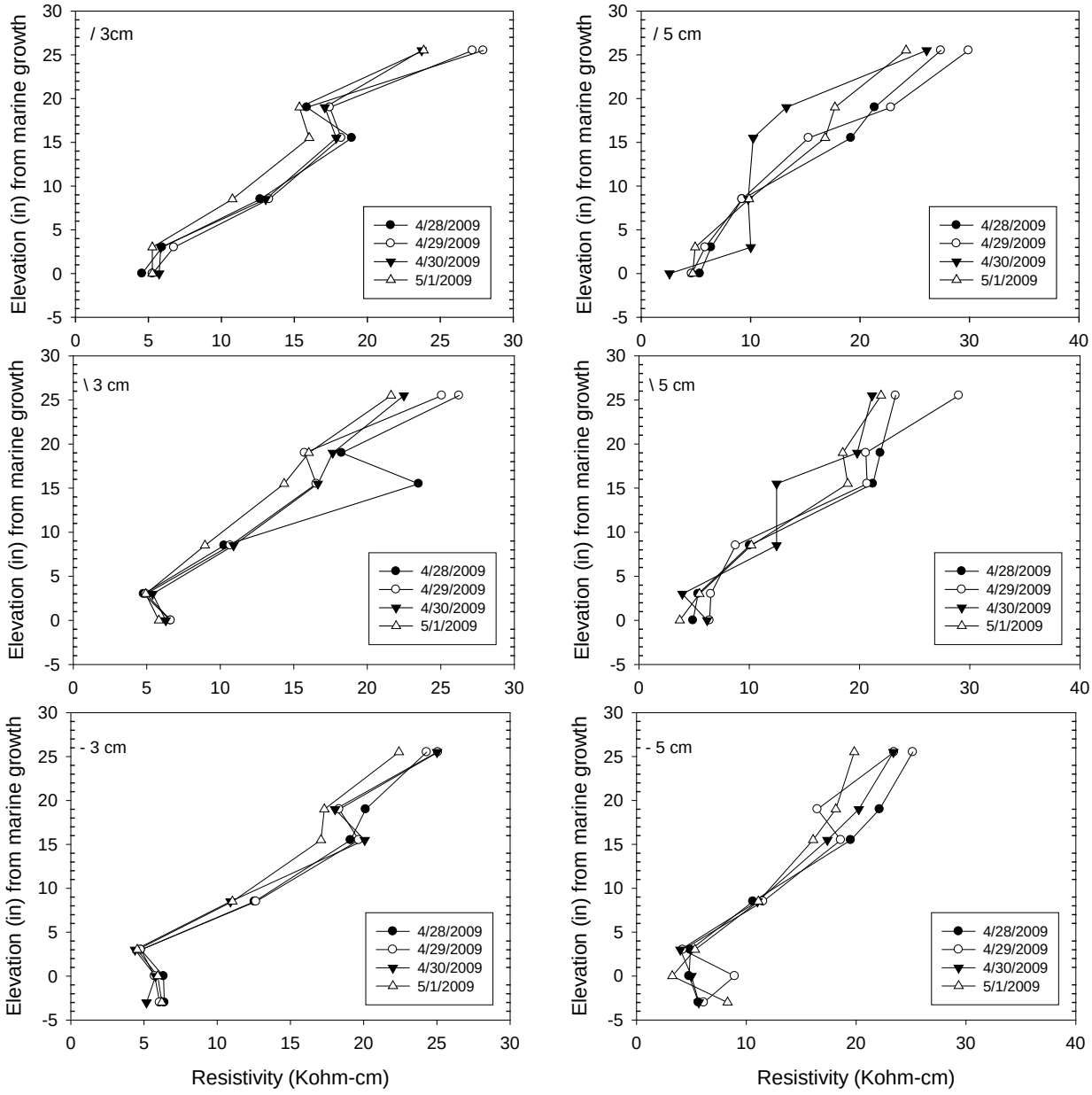

150138
Courtney Cambell
Bent 23 Footer West Face

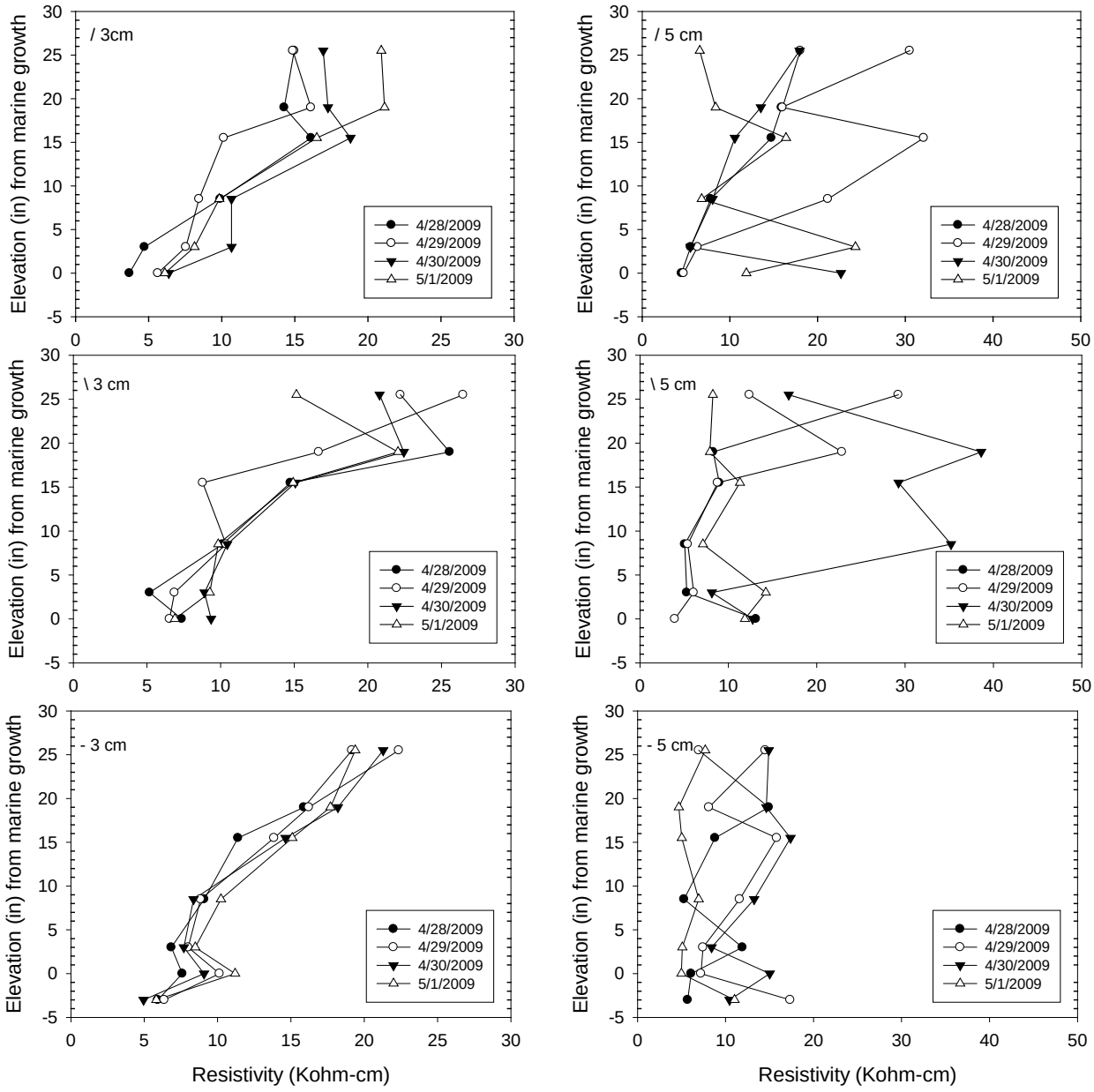

150210
New Howard Franklin
Bent 26 Pile 1 Footer East Face
C Cover: 5.5 in

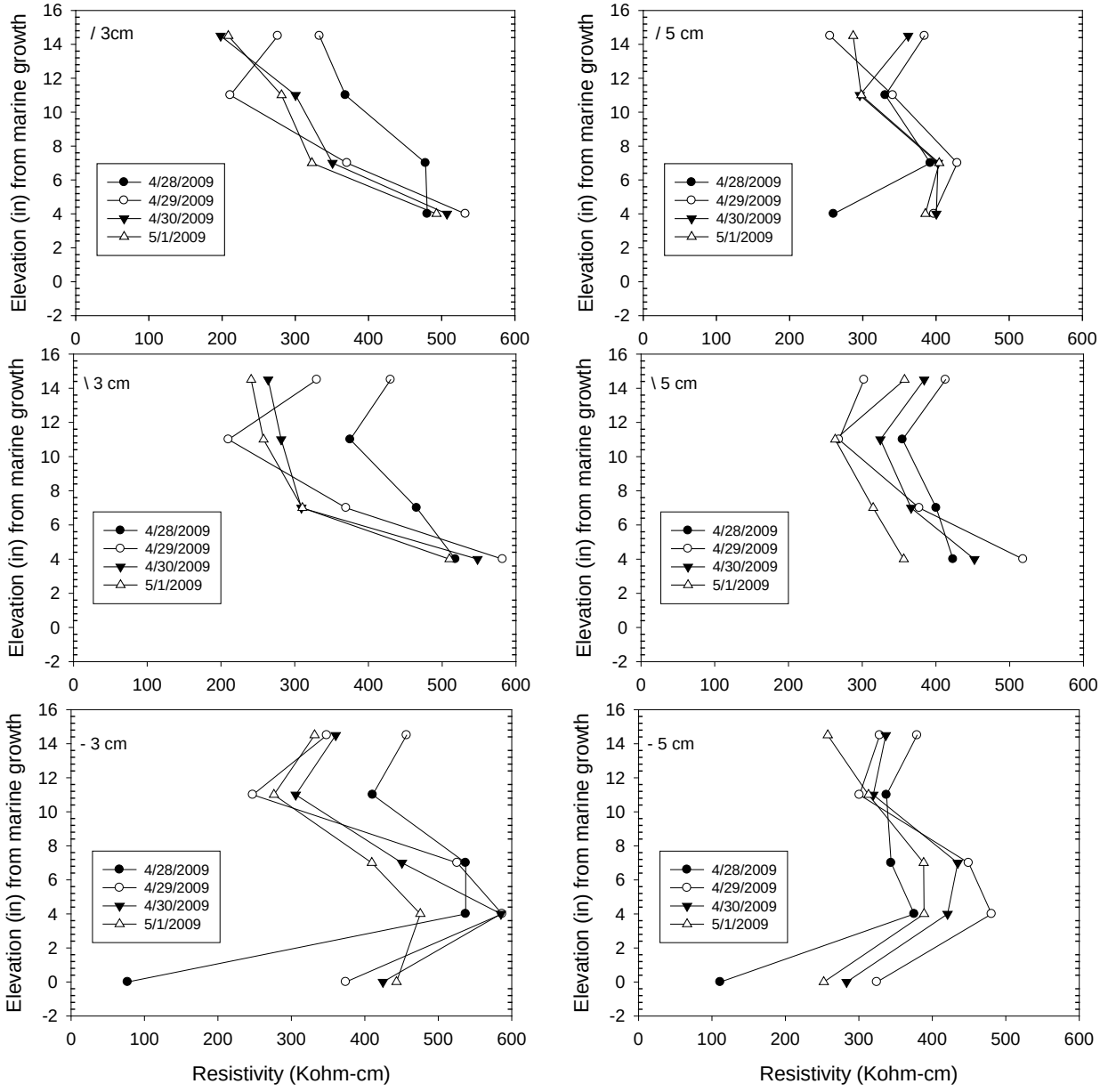

150210
New Howard Franklin
Bent 44 Single Footer East Face
Cover: 5.5 in

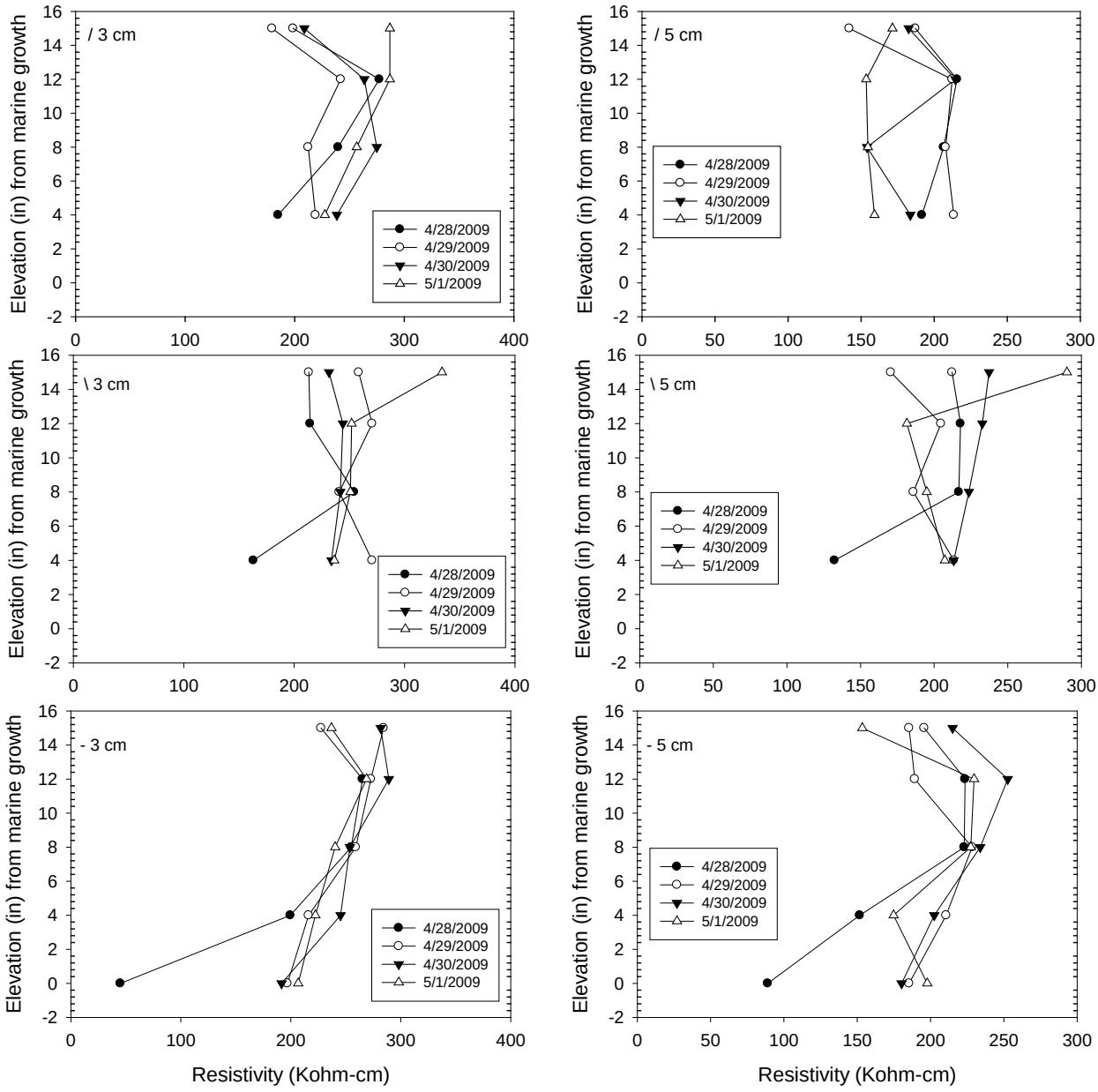

150107
Old Howard Franklin Bridge
Bent 141 Pile 8 South Face
C Cover: 3.45 in

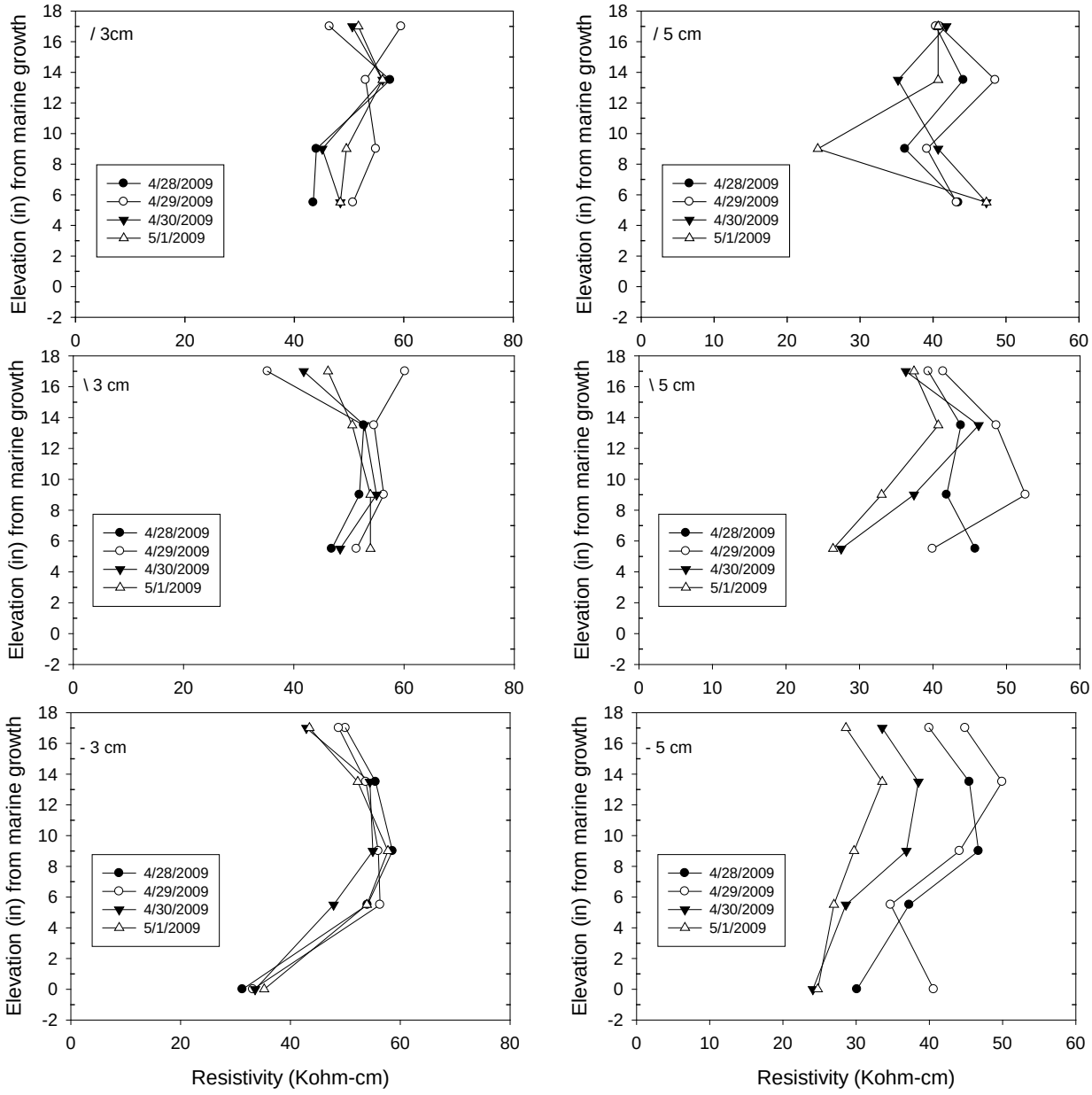

100300
Ghandy Eastbound
Bent 250 Pile 5 North Face
Cover: 3.4 in

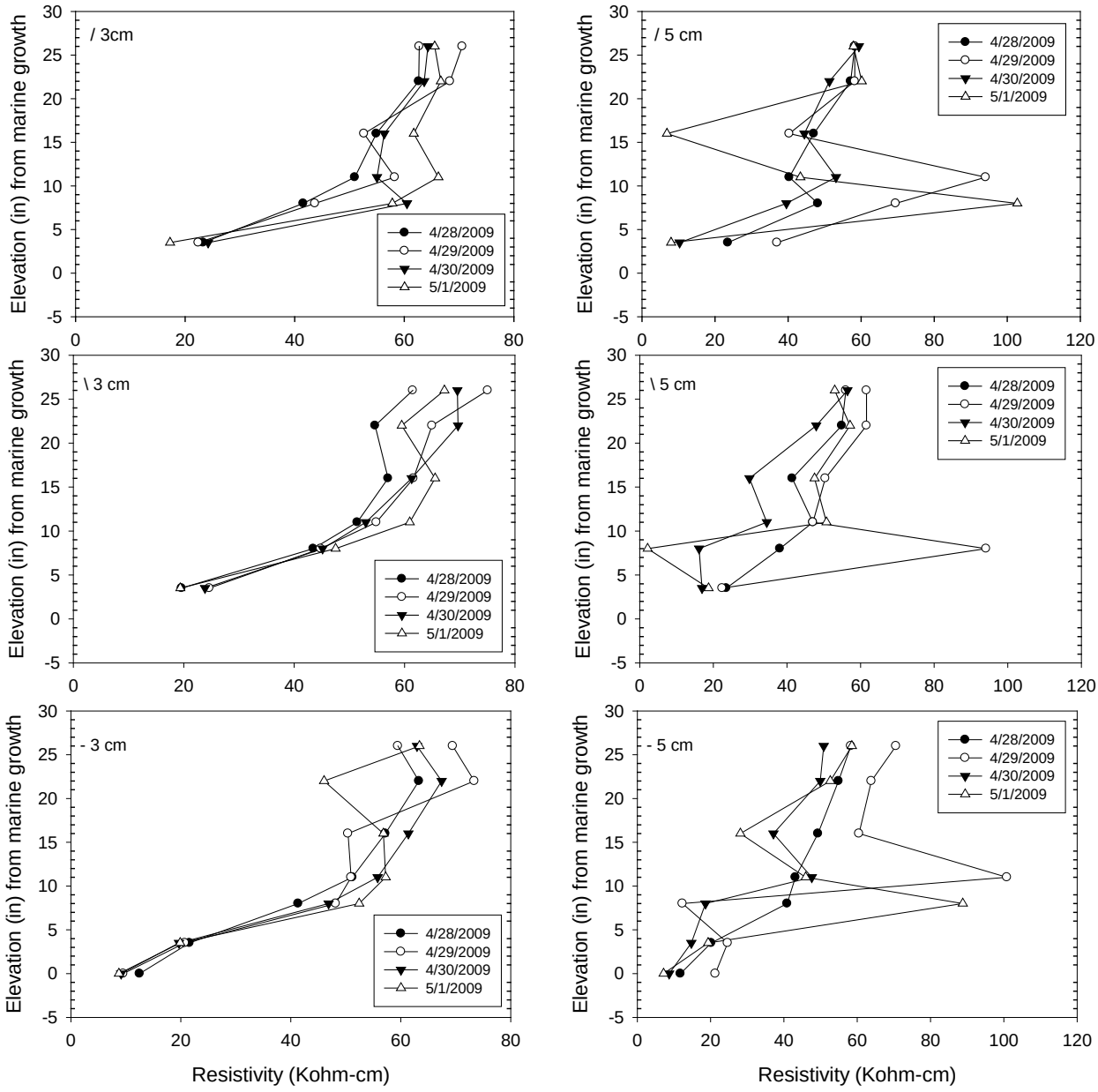

100585
Ghandy Eastbound
Bent 83 Footer West Face
C Cover: 4.7 in

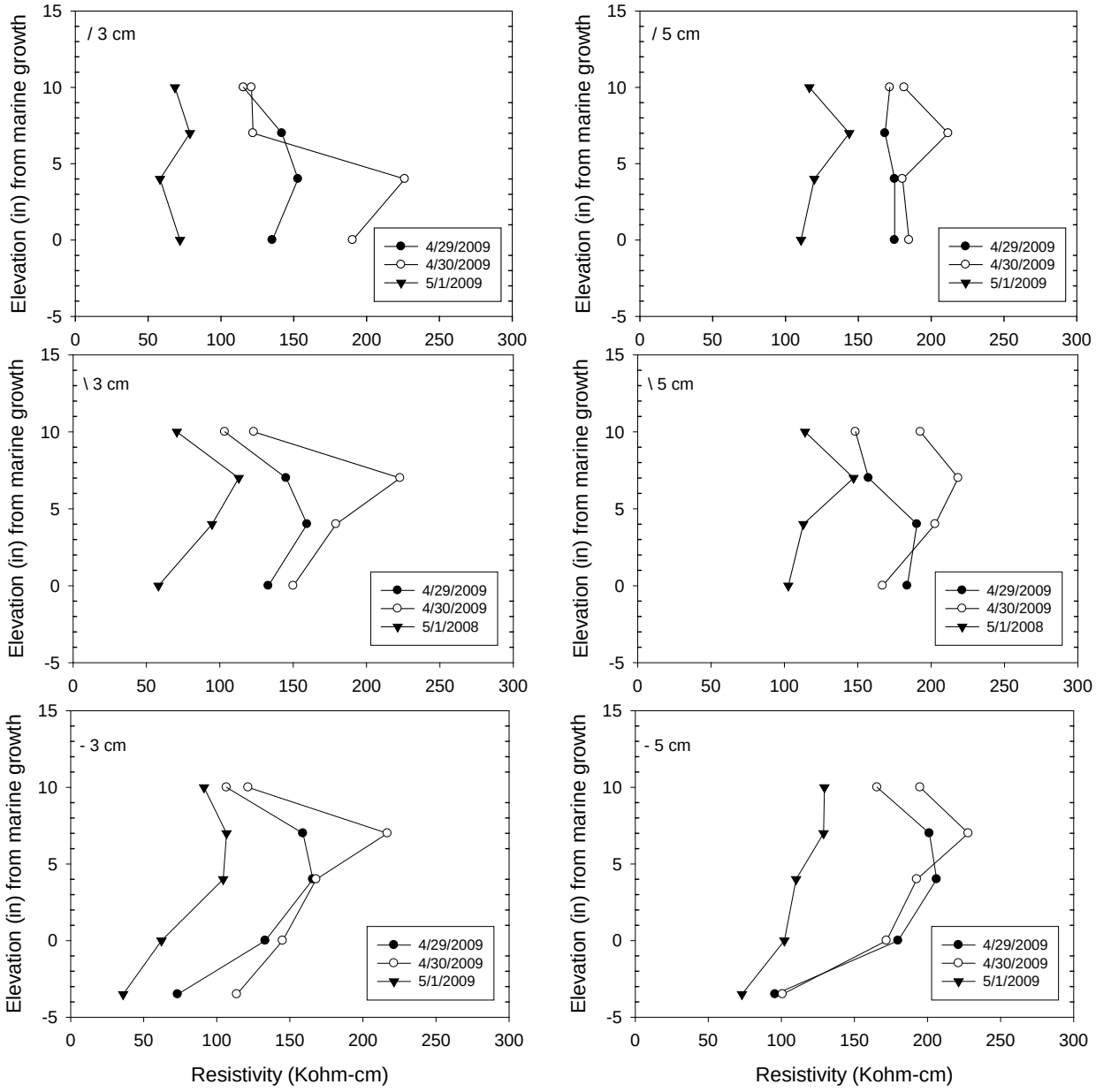

860467
Sunrise Blvd IWW Eastbound
Bent 2 Pile 4 South Face

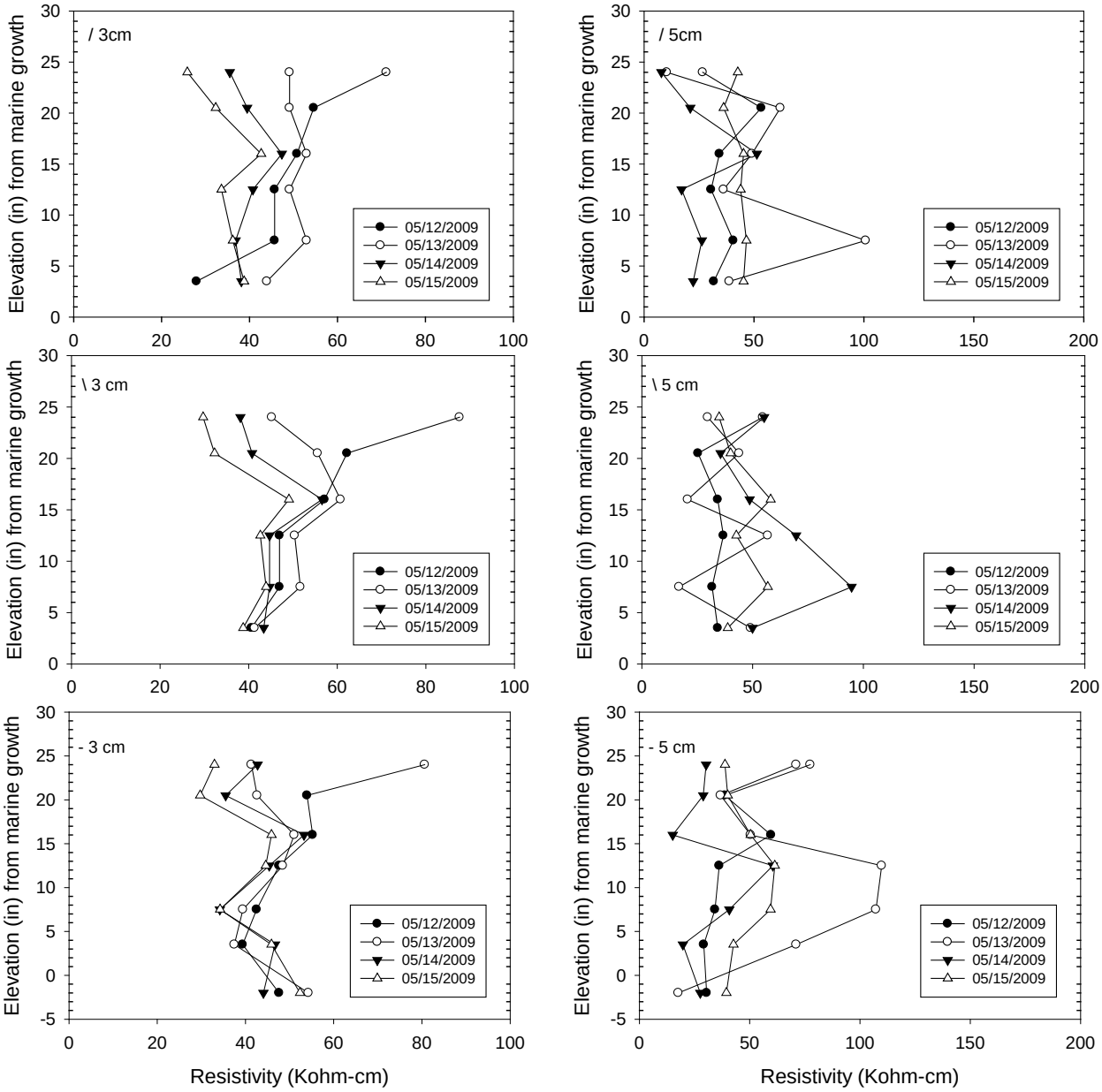

860466
Sunrise Blvd IWW Westbound
Bent 2 Pile 3 South Face

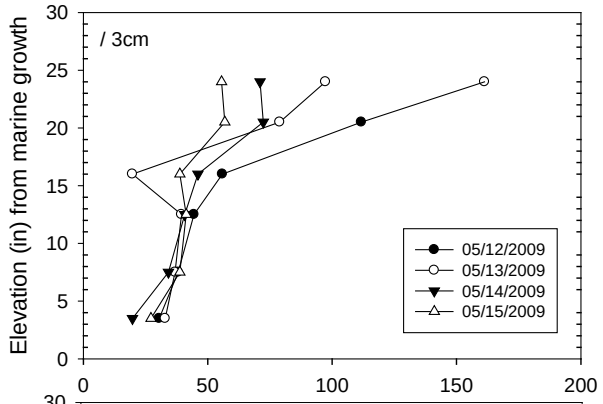

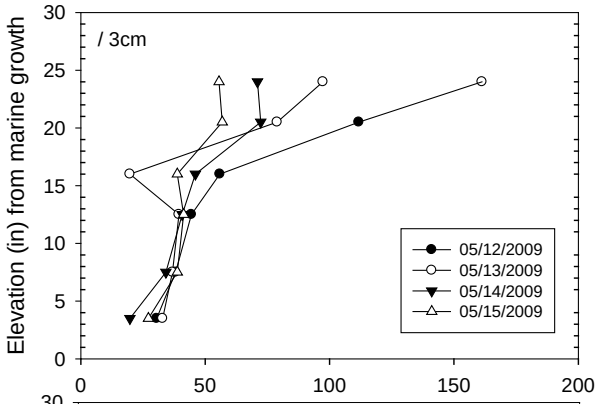

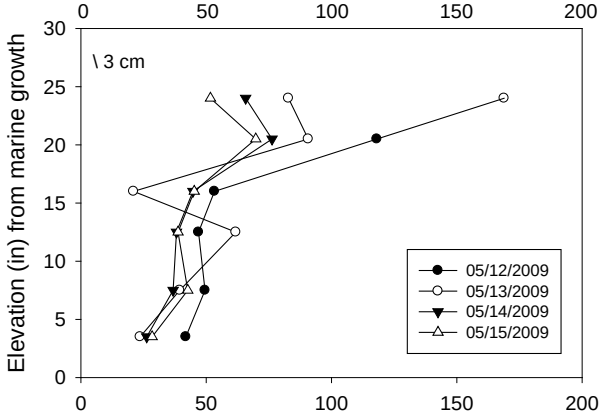

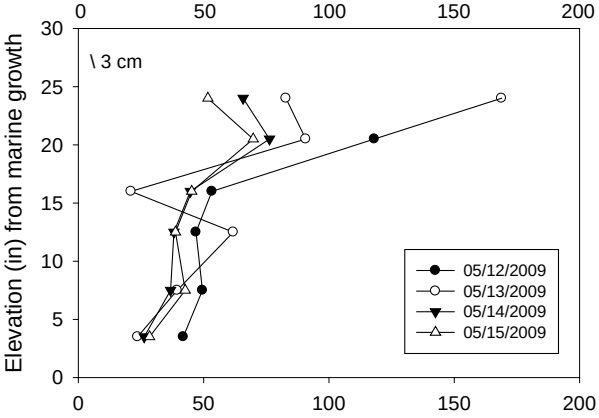

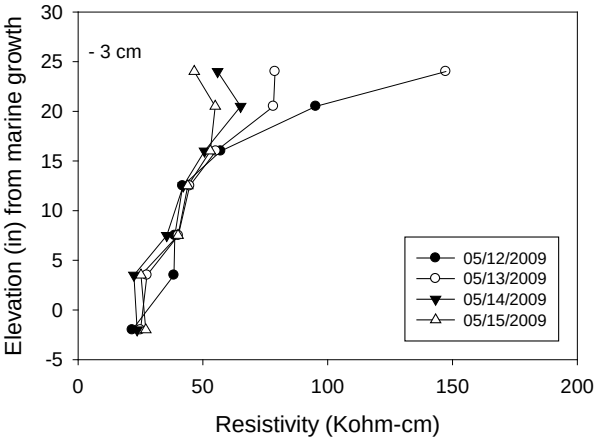

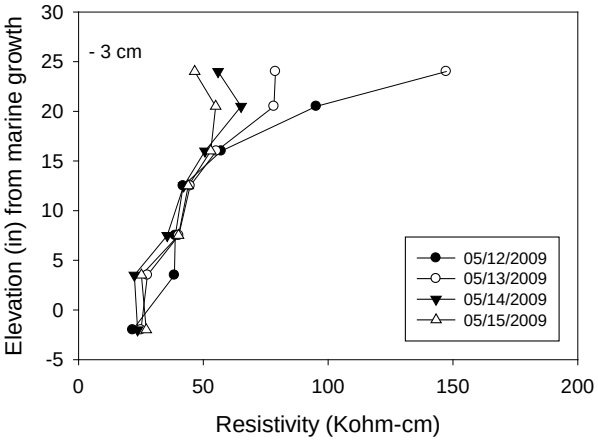

860061
Sunrise Blvd West Eastbound
Bent 2 Pile 10 East Face

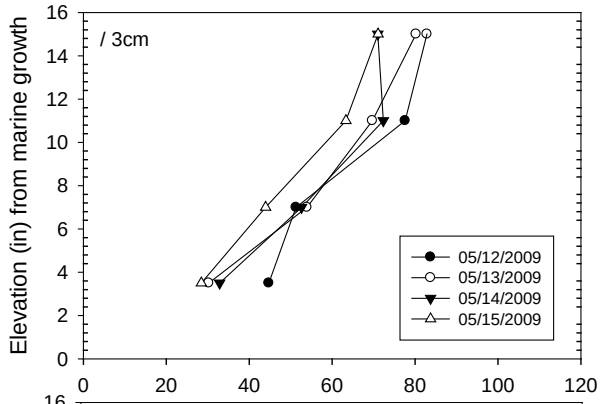

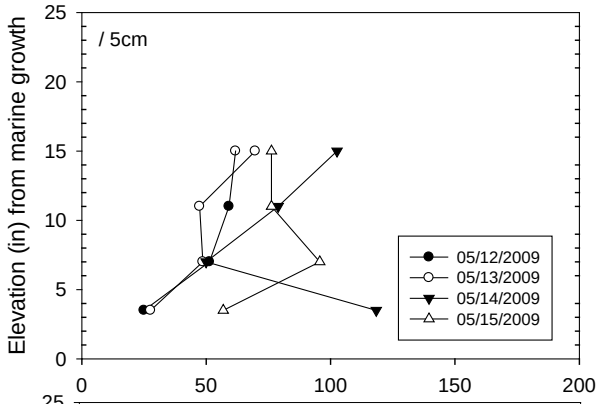

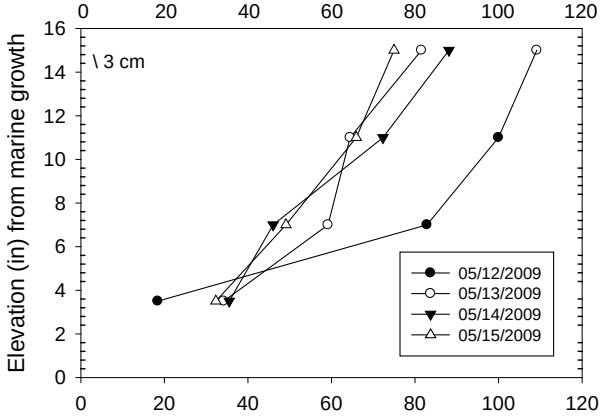

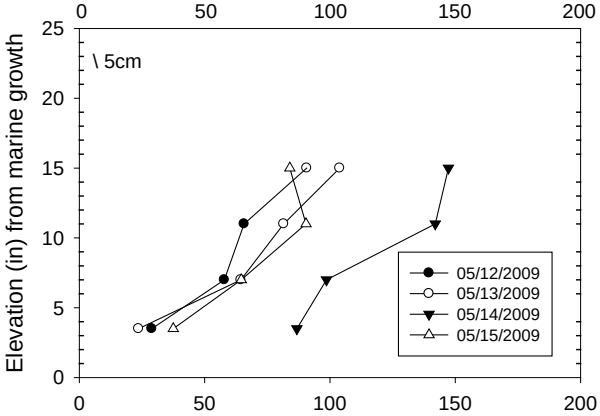

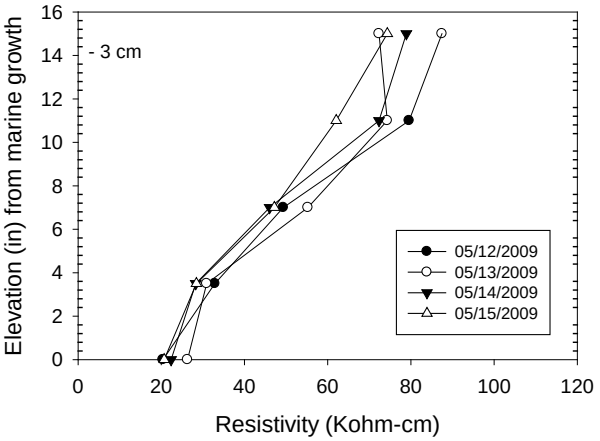

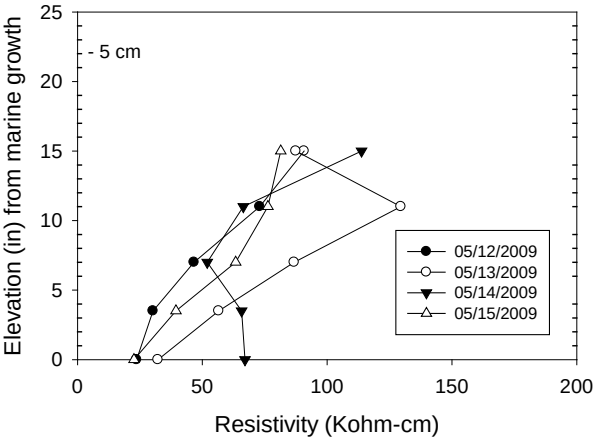

860061
Sunrise Blvd West Westbound
Bent 2 Pile 14 East Face

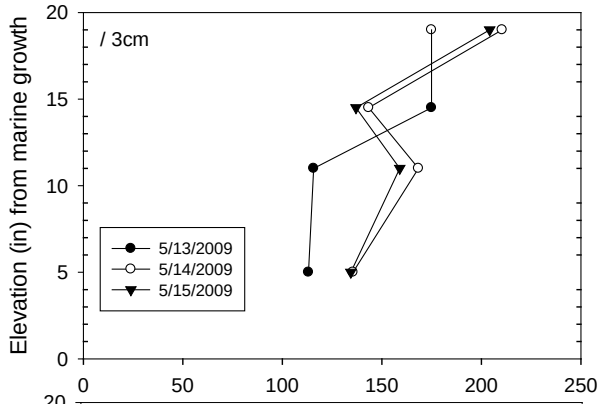

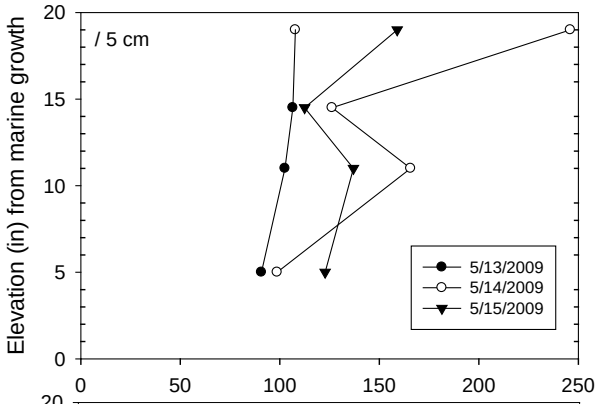

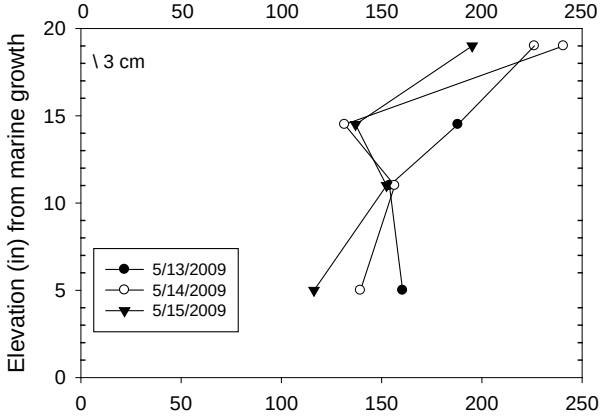

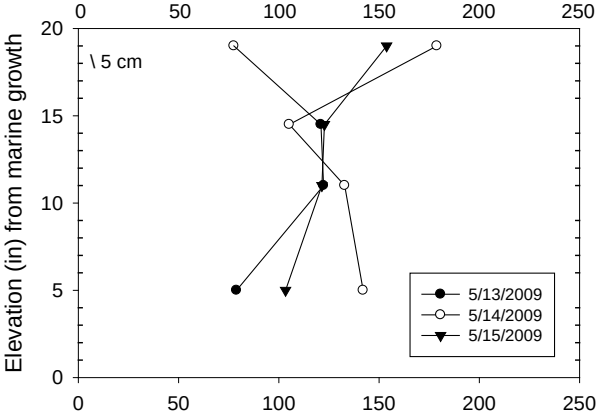

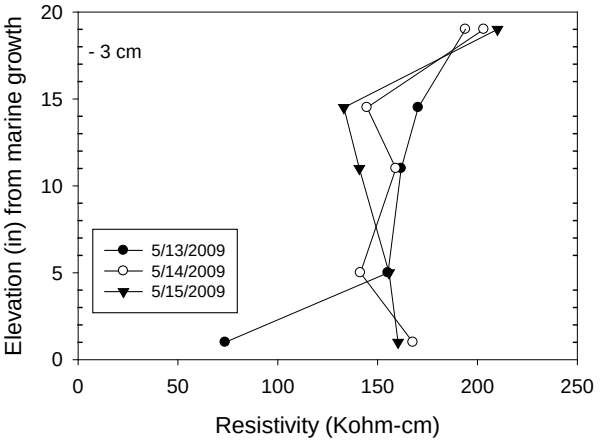

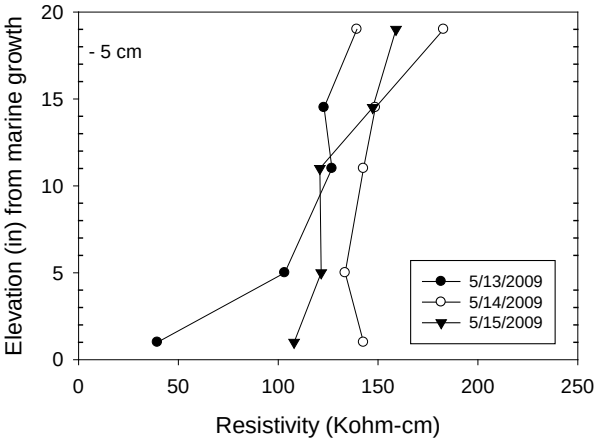

860018
Las Olas Blvd.
Bent 2 Pile 5 East Face

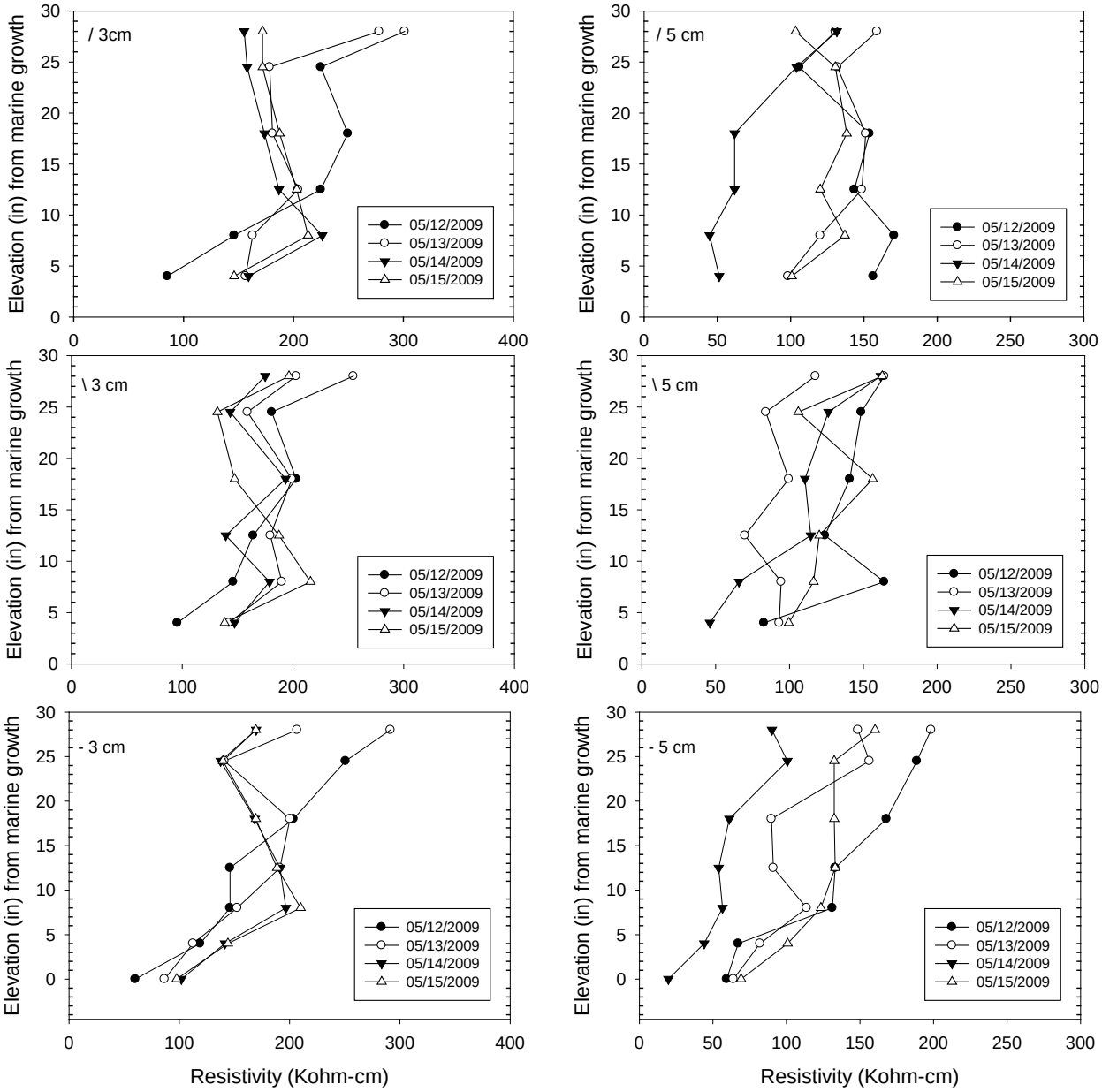

860018
Las Olas Blvd.
Bent 6 Pile 2 Footer North Face

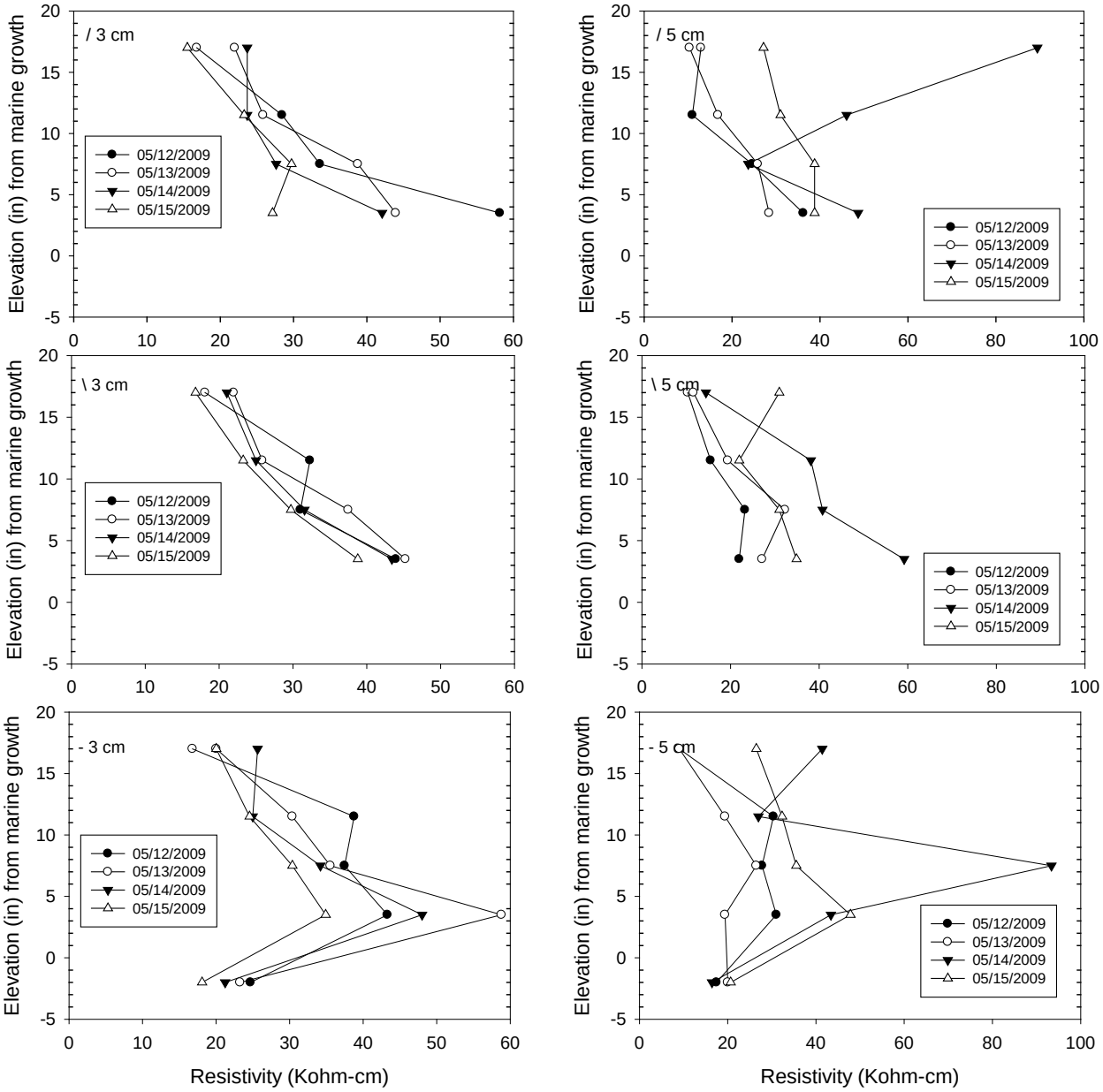

860043
Sheridan Bridge
Bent 5 Pile 1 West

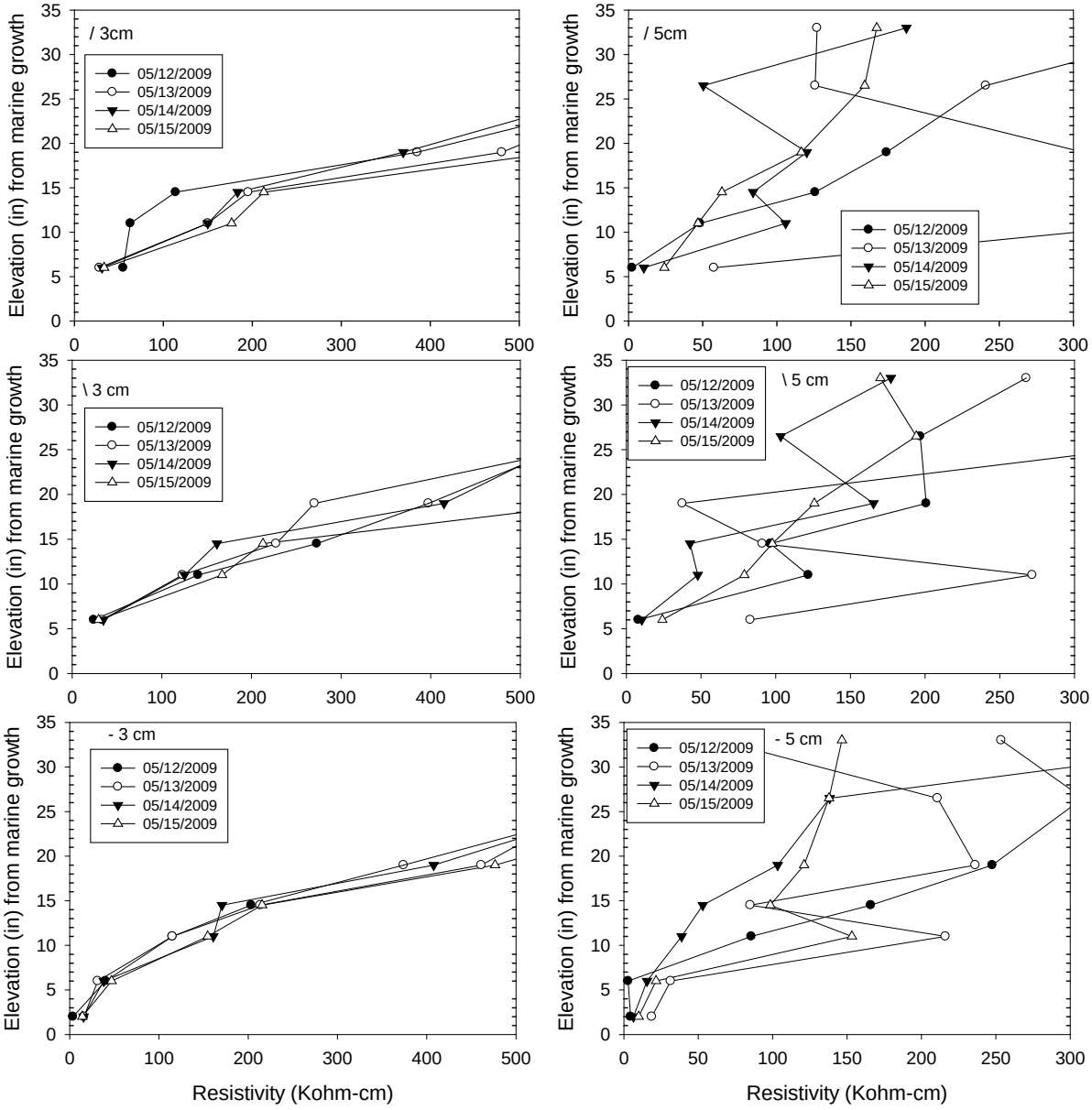

150189
Sunshine Sky Way 1 Northbound
Bent 171 Footer 1 North Face

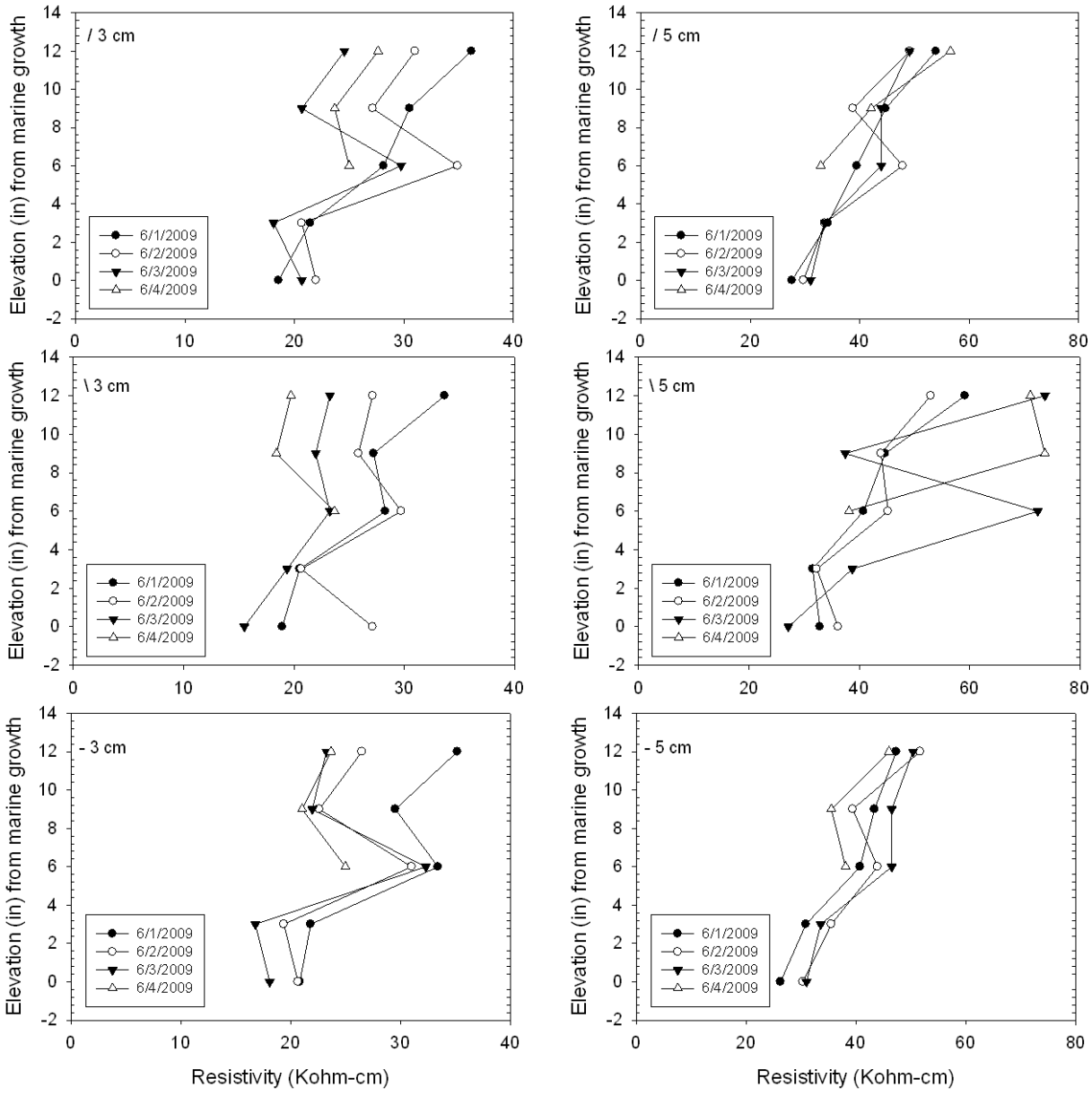

150213
Dick Misener Bridge SB, I-275 SB
Bent 11 Pile 7 West
Concrete Cover ~3.1 in

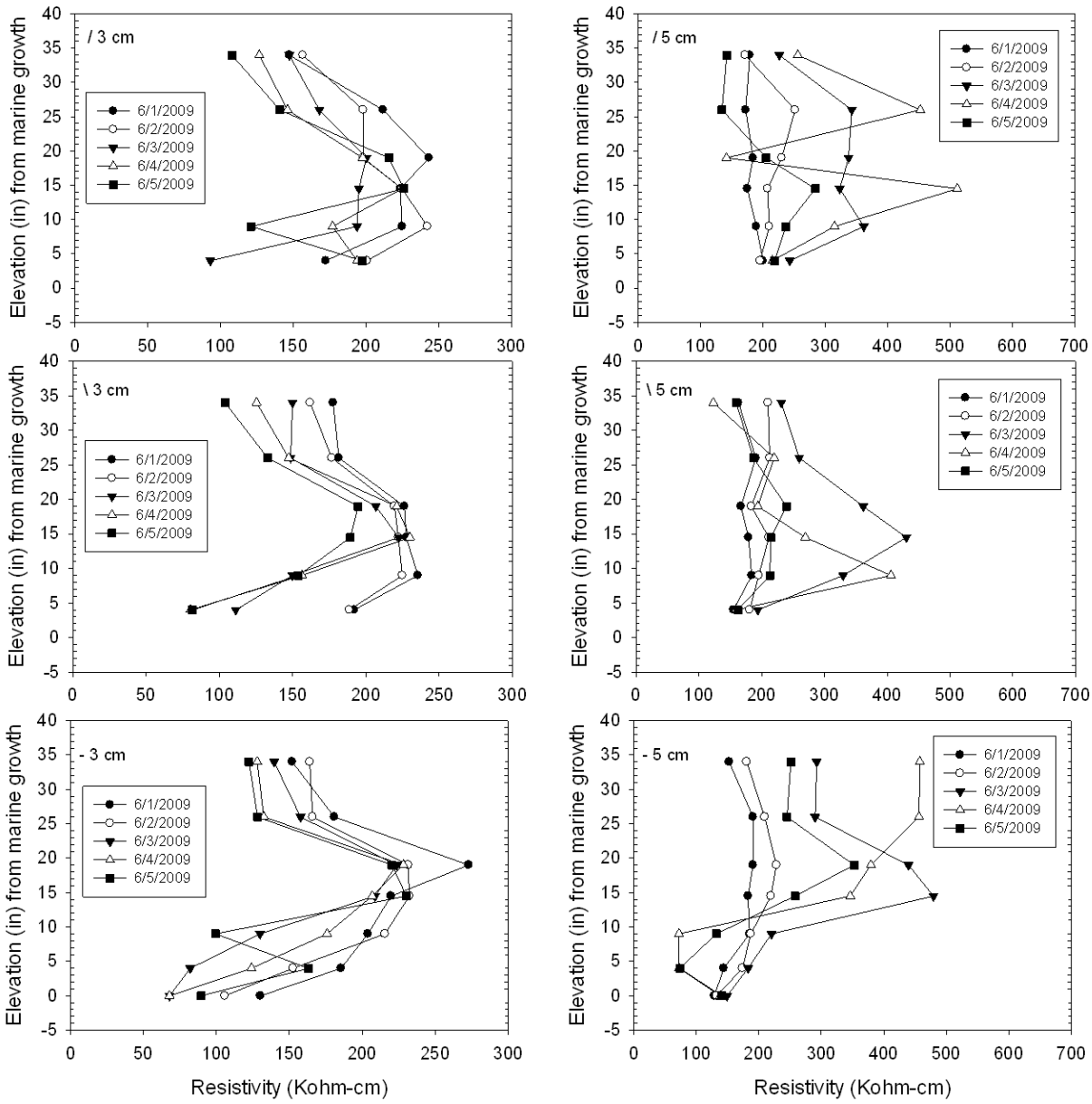

150214
Dick Misener Bridge SB, I-275 NB
Bent 22 Pile 4 North
Concrete Cover ~3.2 in

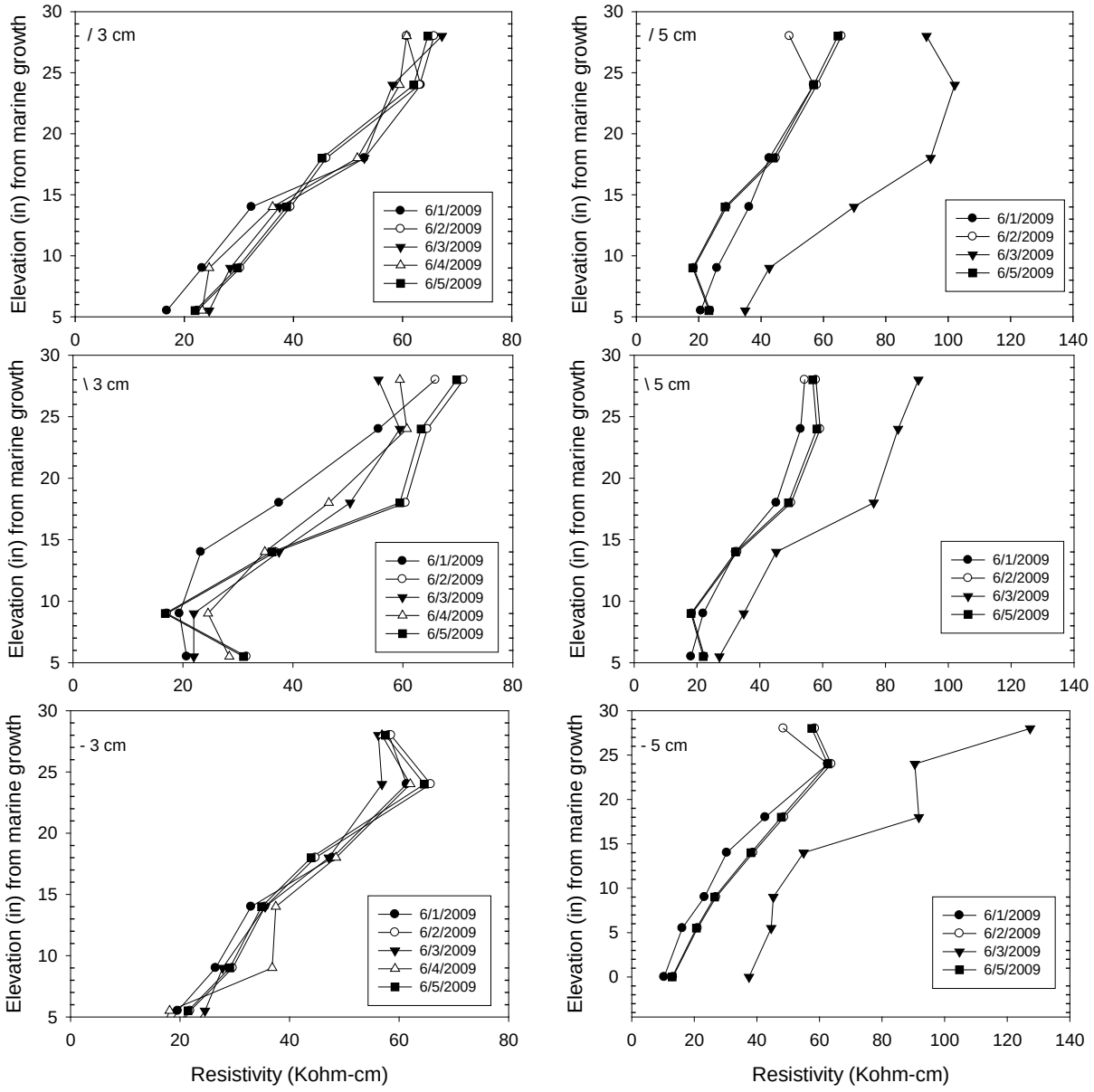

#150211
I-275 NB Over Bunce Pass
Bent 13 Footer 1 West Face

#150038
I-275 SB Over Bunce Pass
Bent 17 Footer 1 South

150243
Bunces Pass
Bent 11 Pile 2 Column East Face
C Cover: 3.85 in

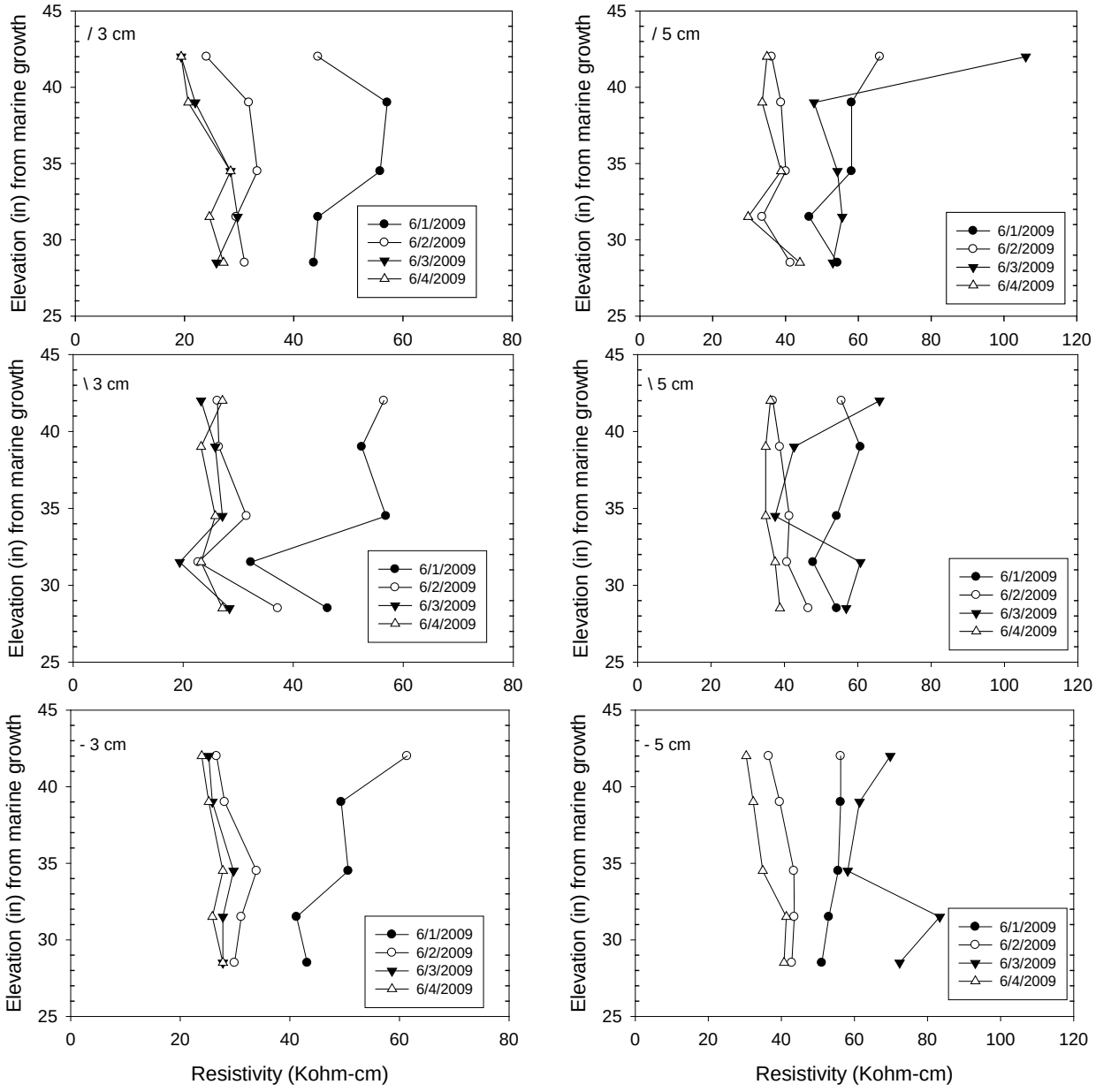

150243
Buncess Pass
Bent 11 Footer 2 East Face
Cover: 6.2 in

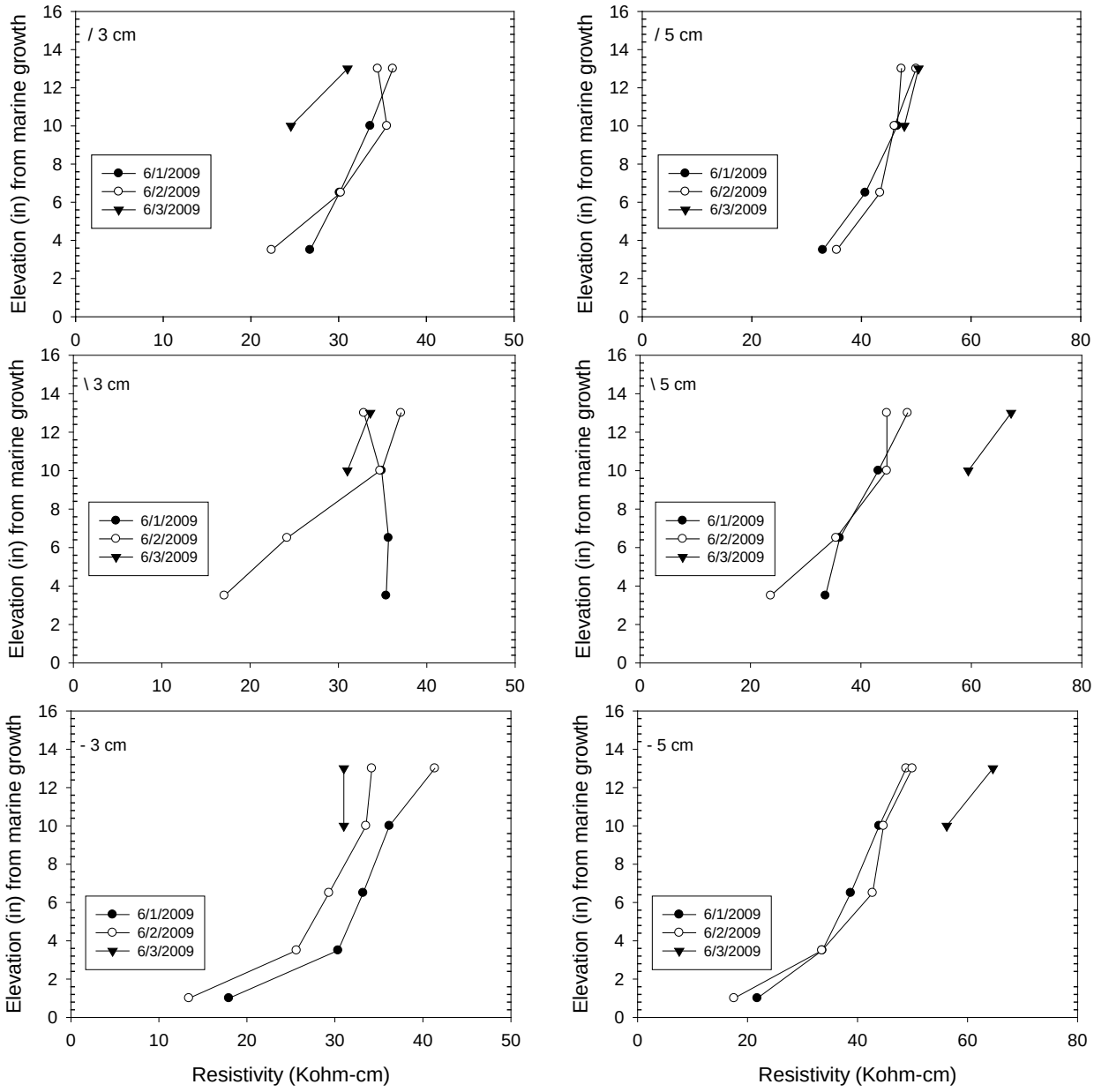

150050
Structure C
BP
C Cover: 2.85 in

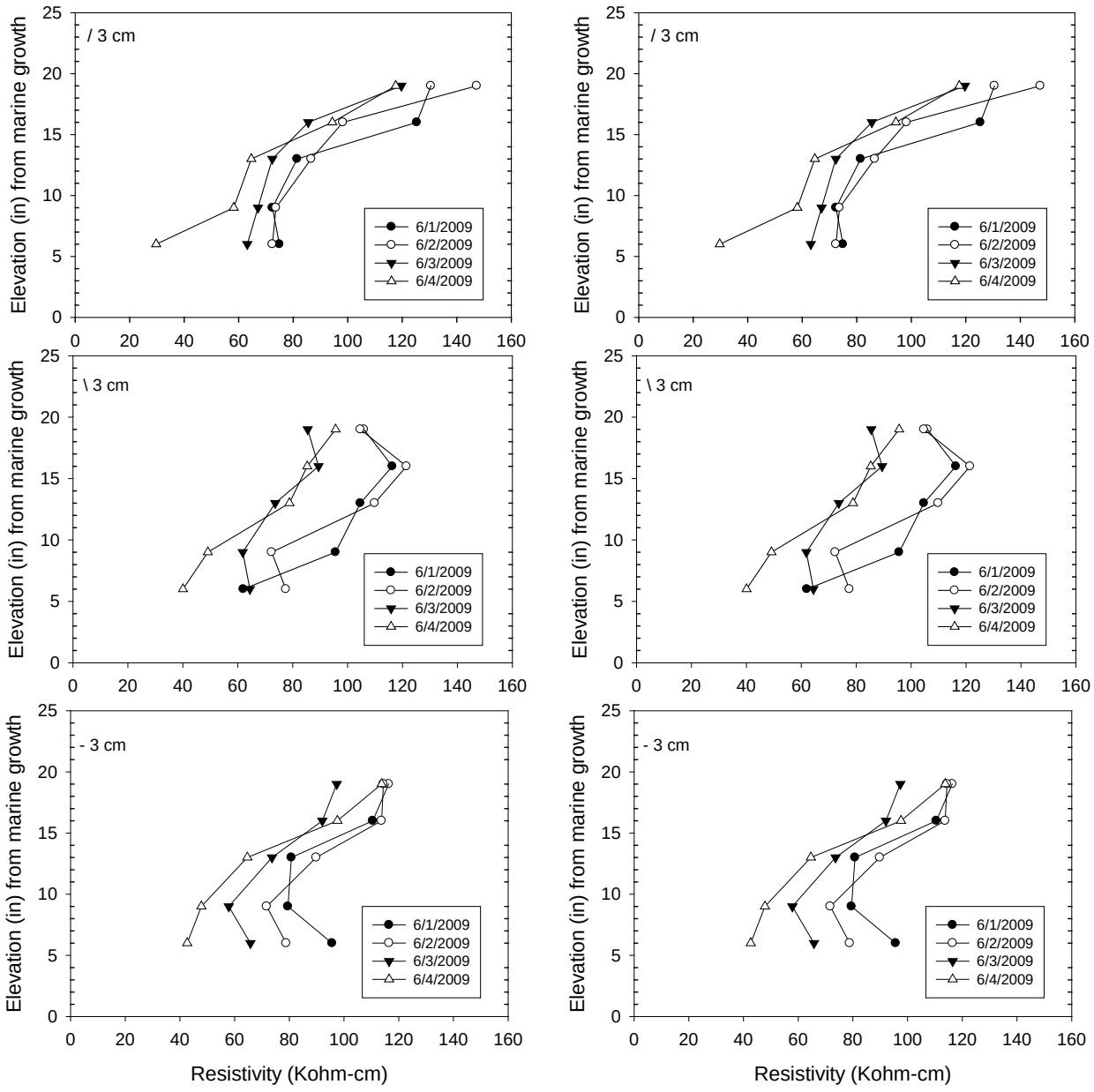

150049
Structure E
Bent 6 Pile 3 North Face

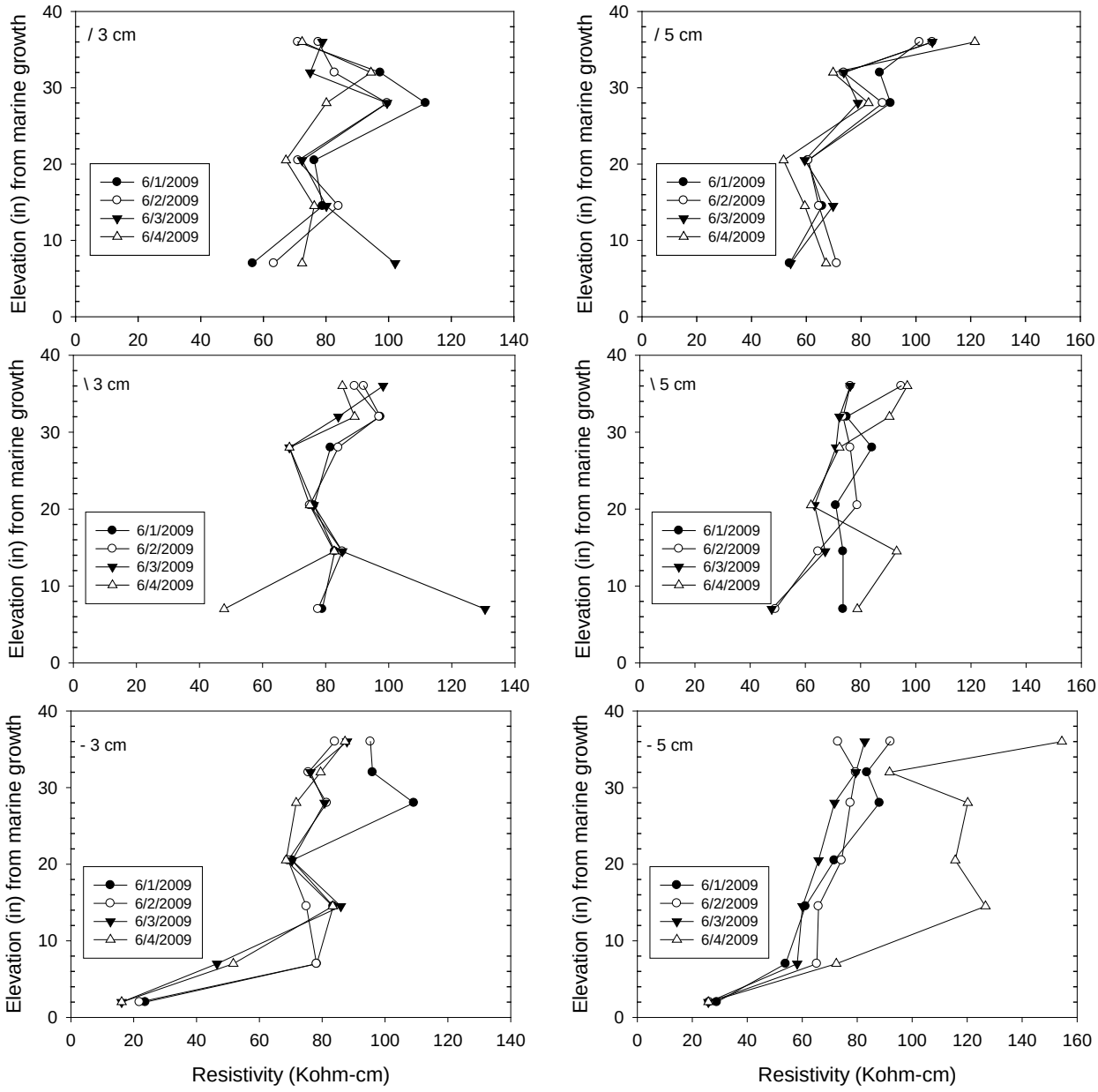

894037
Palm City SR 174 Okeechobee Waterway mile 9.5 Westbound
Bent 10 Footer North Face
C Cover: 6 in

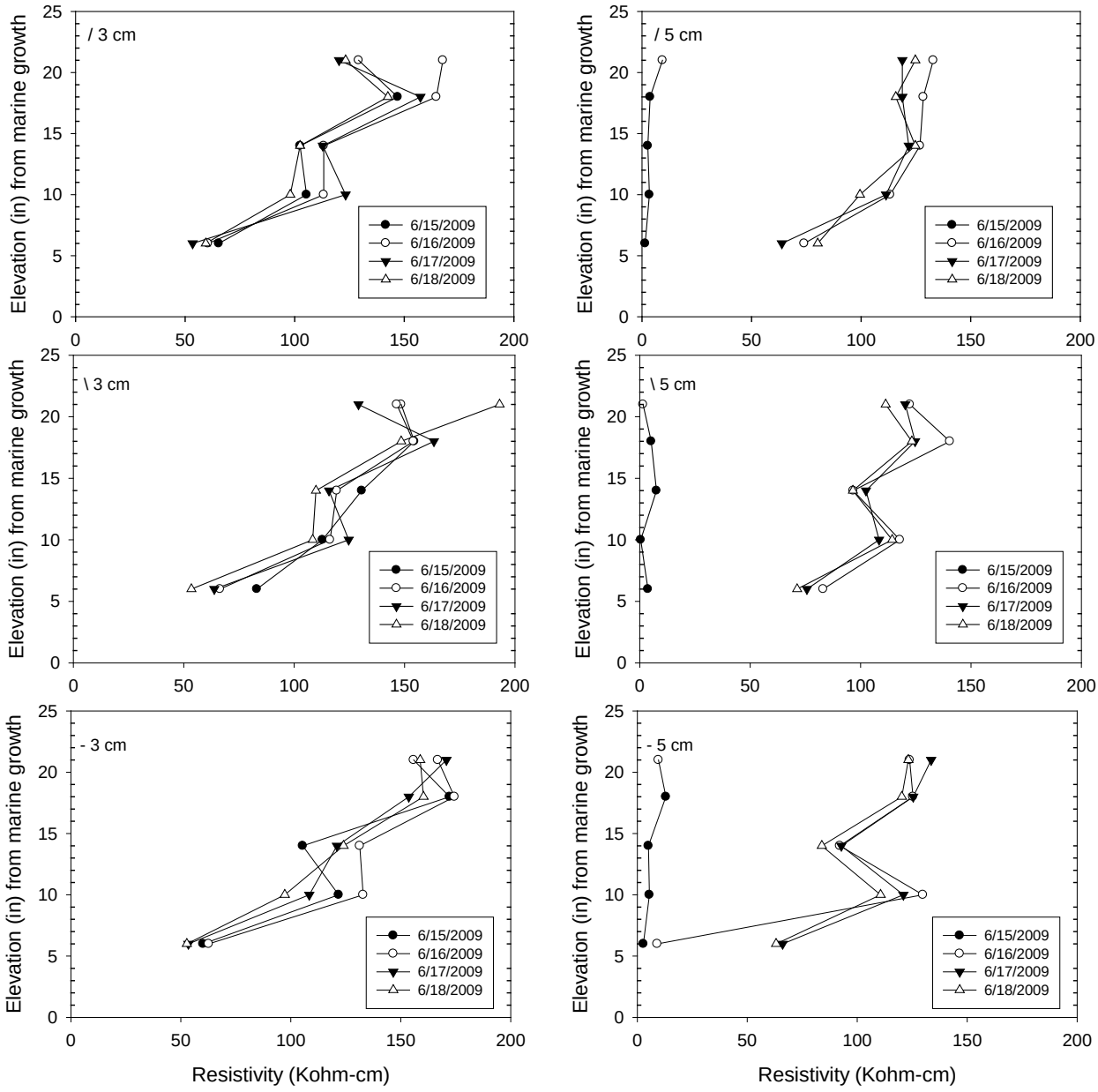

890003
Roosevelt Bridge (opens)
Bent 22
C Cover: 2.65 in

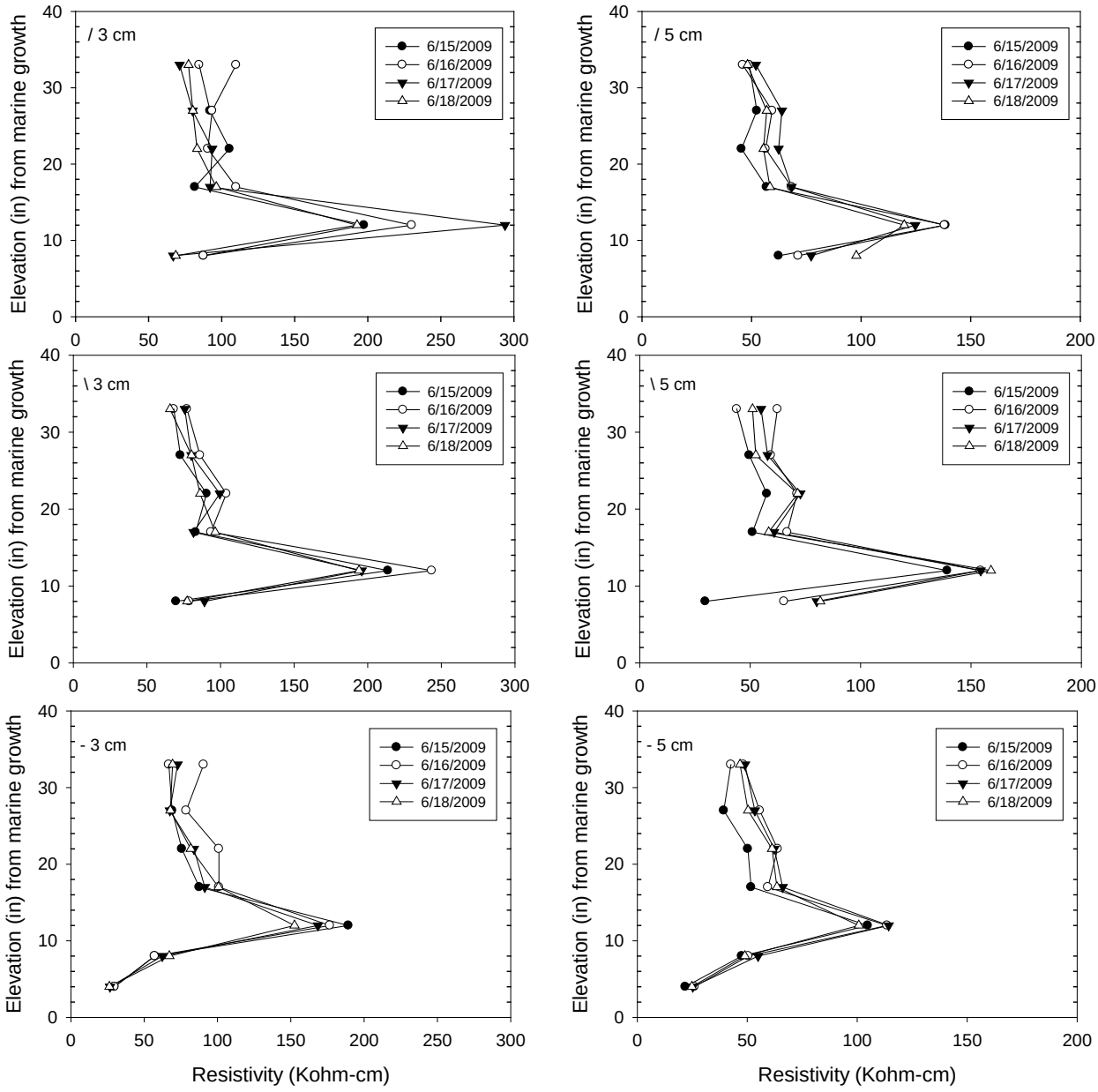

890145 W, 890146 E
SR 732 Jensen Beach Causeway
Bent 10 Footer North Face
C Cover: 4 in

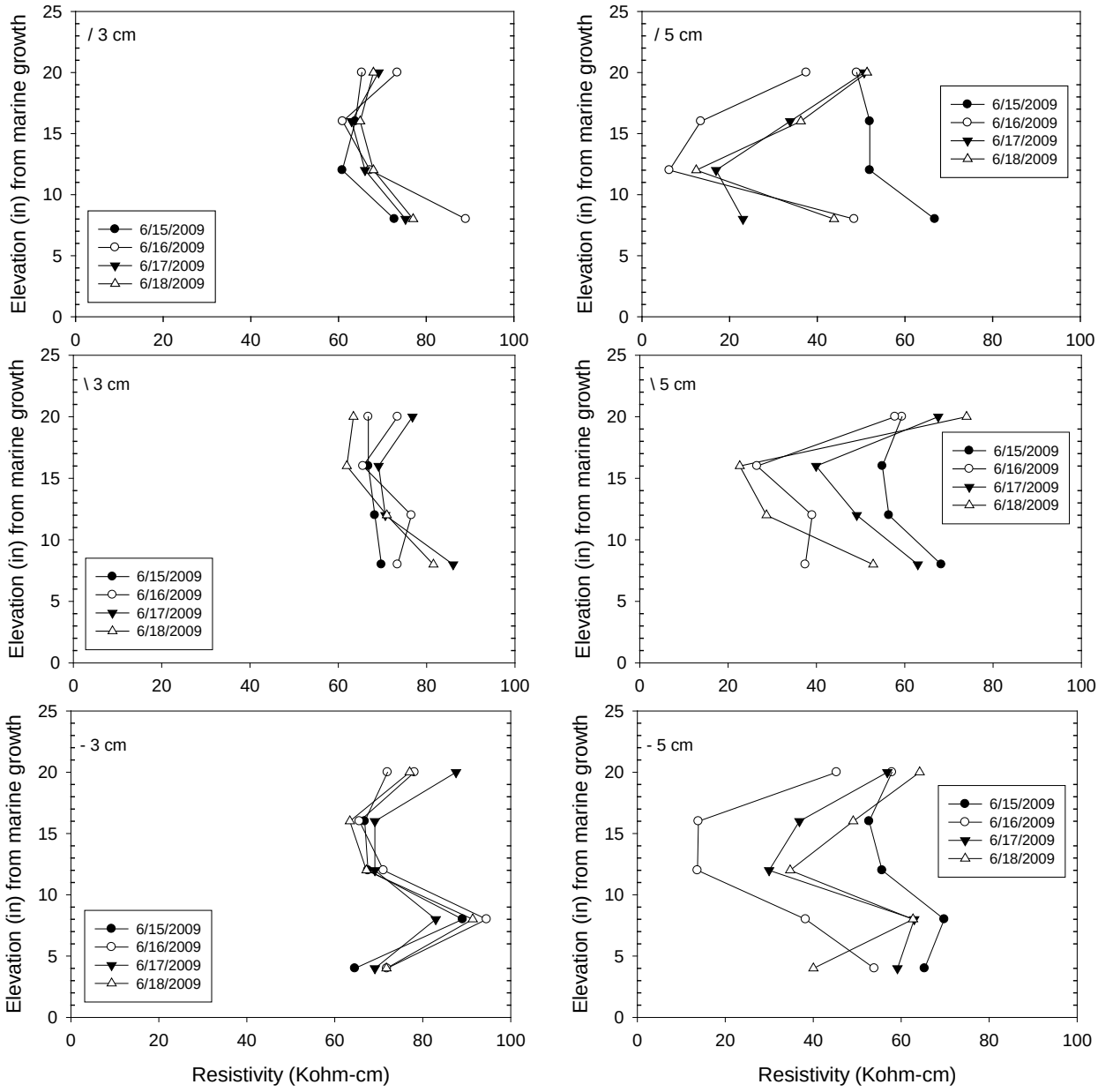

890145 W, 890146 E
SR 732 Jensen Beach Causeway relief bridge
Bent 9 Pile 2 West Face
C Cover: 3.15 in

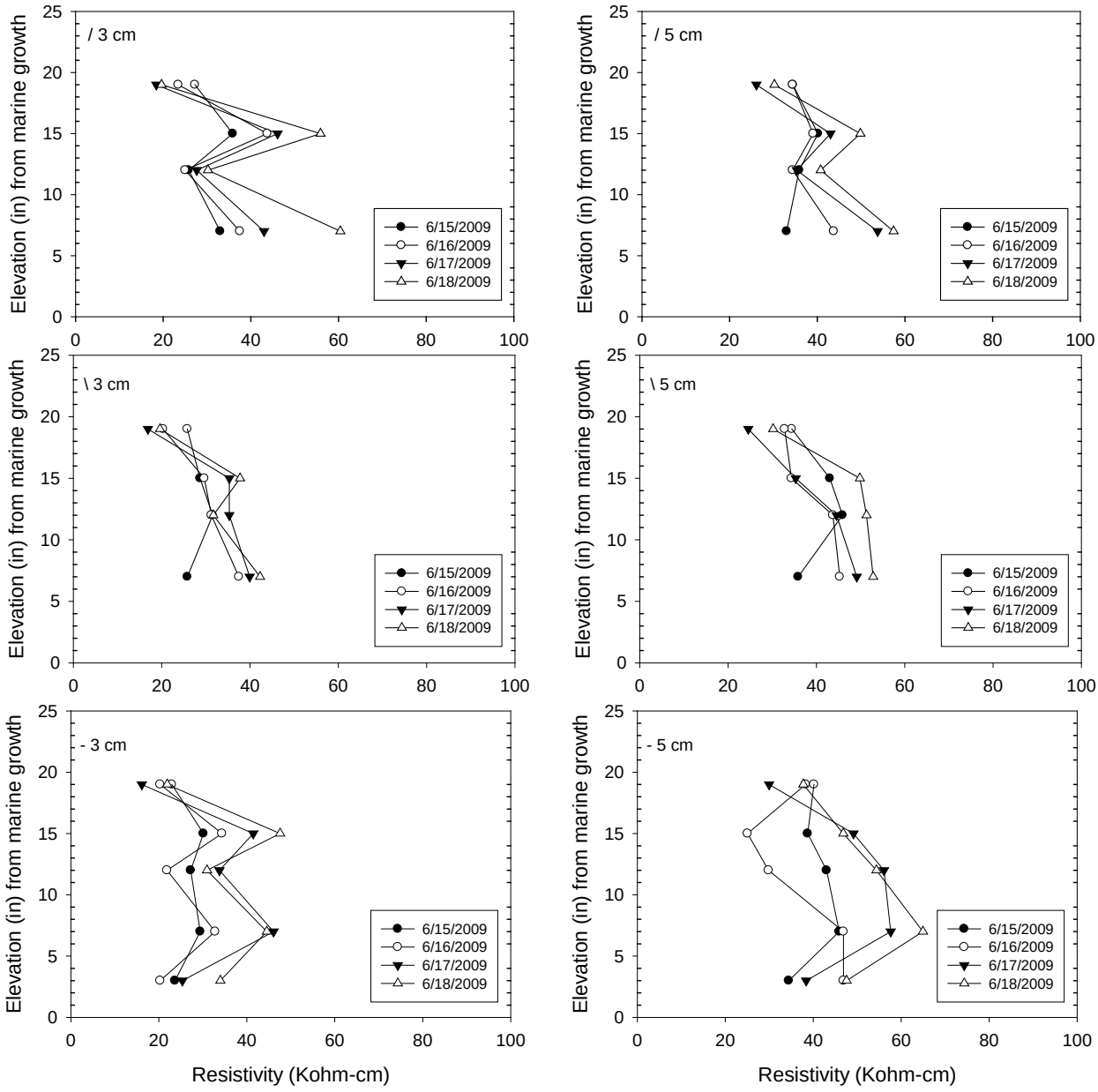

890158/60 River
SE Ocean Blvd
Bent 15 Footer East Face
C Cover: 3.8 in

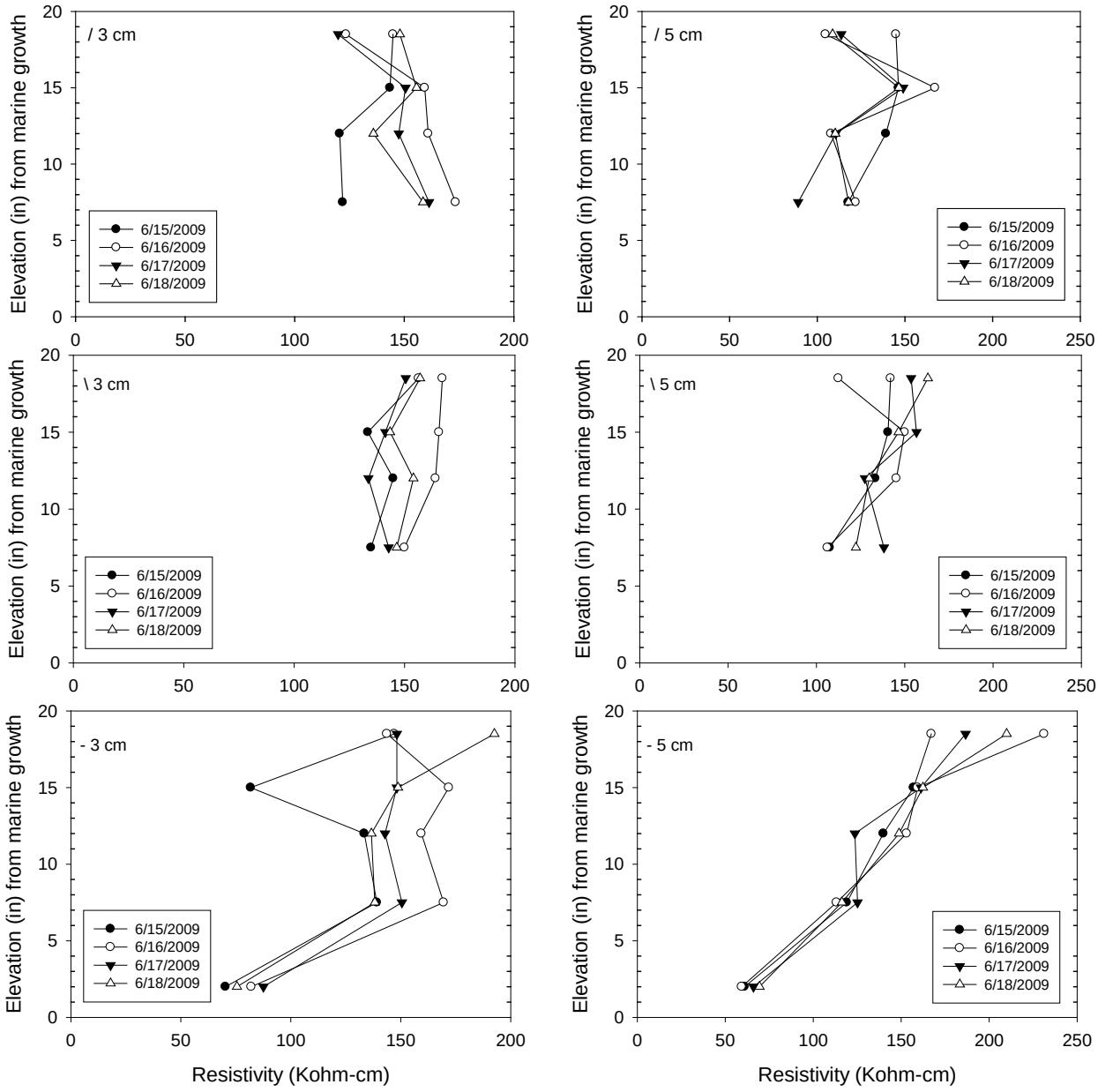

890150 Intercoastal
SE Ocean Blvd Westbound
Bent 10 Footer East Face
C Cover: 4 in

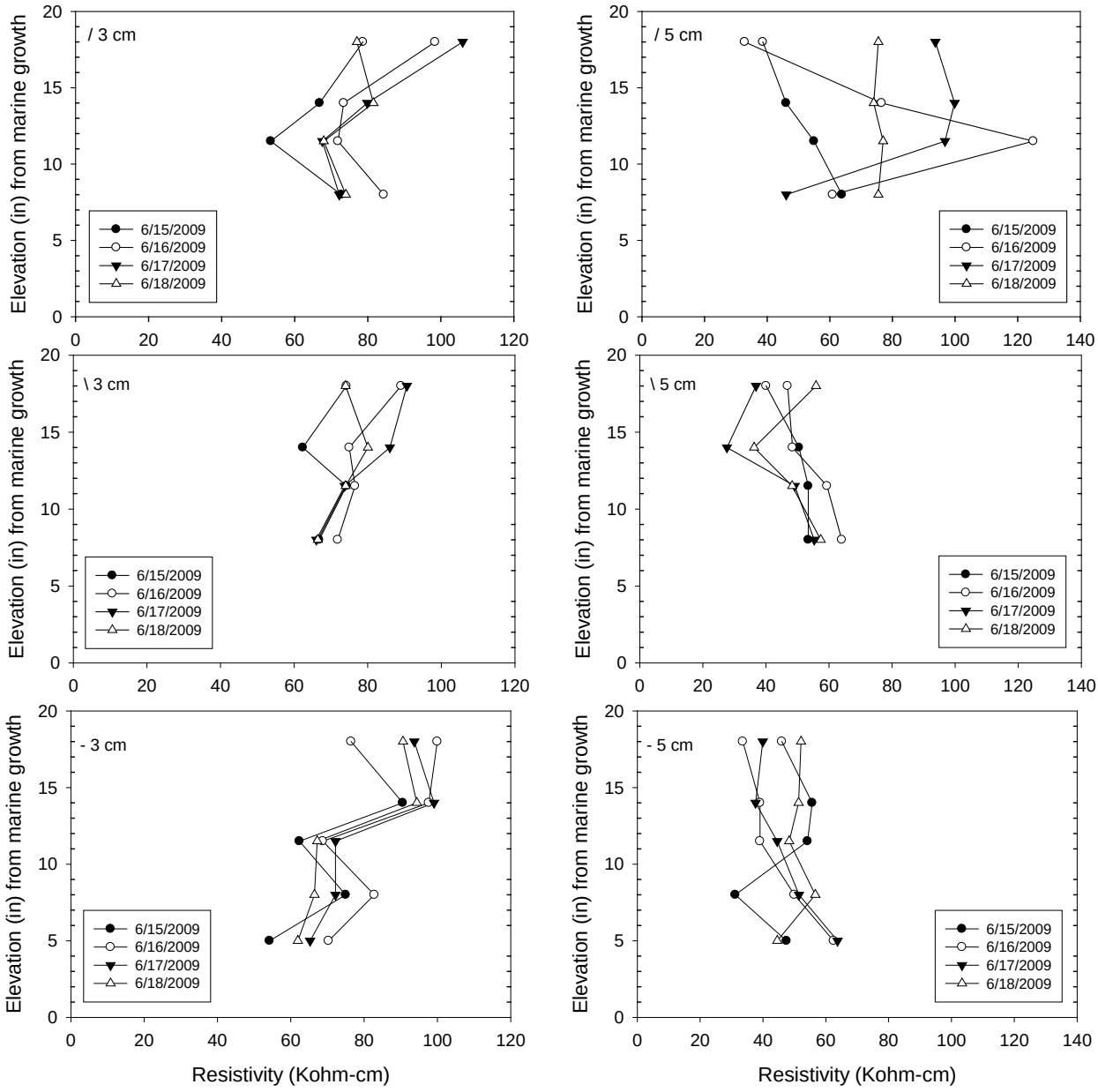

460112
Hathaway
Bent 4 Footer 1 East Face
C Cover: 3.5 in

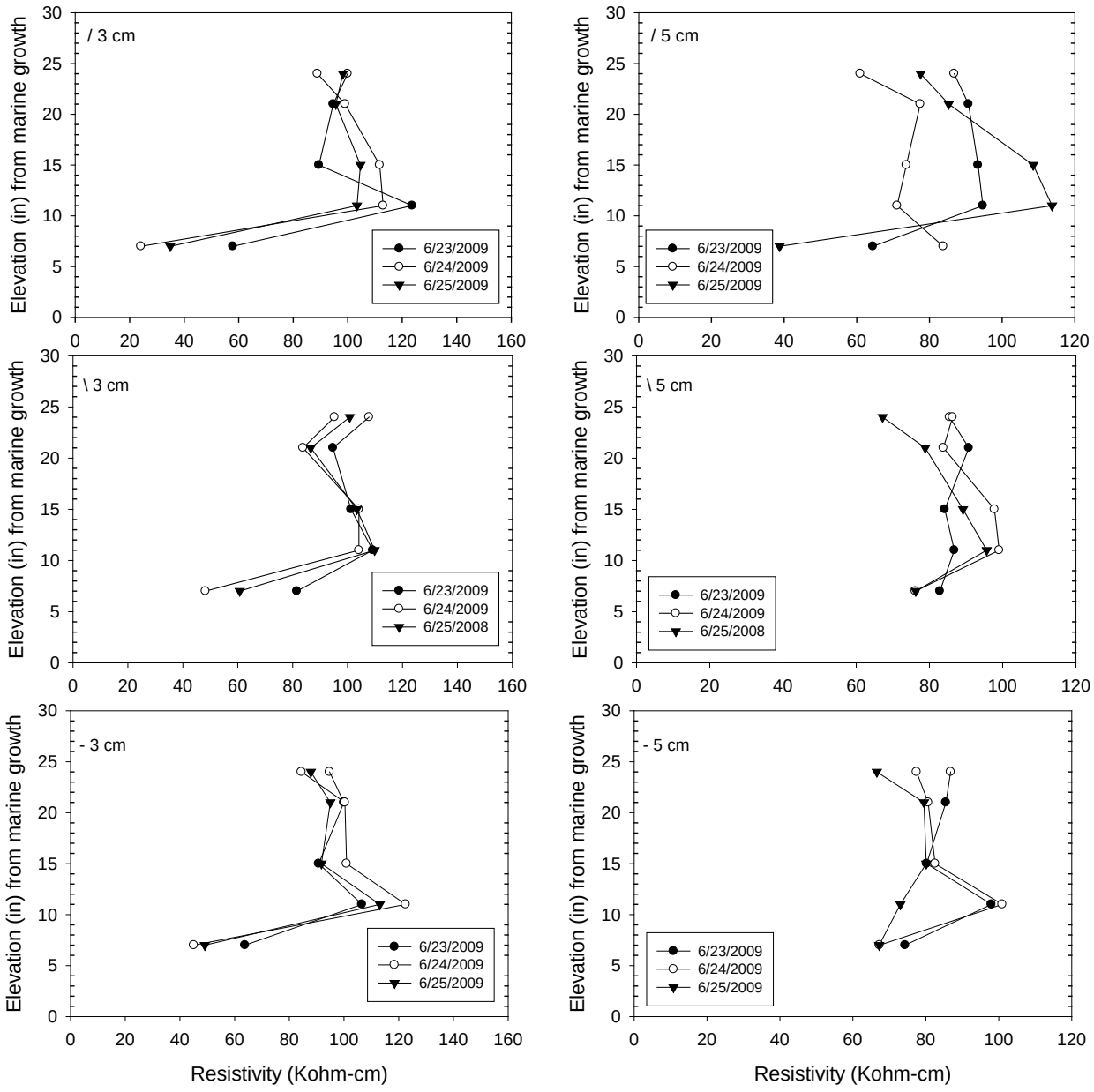

460112
Hathaway
Bent 4 Footer 2
C Cover: 3.5 in

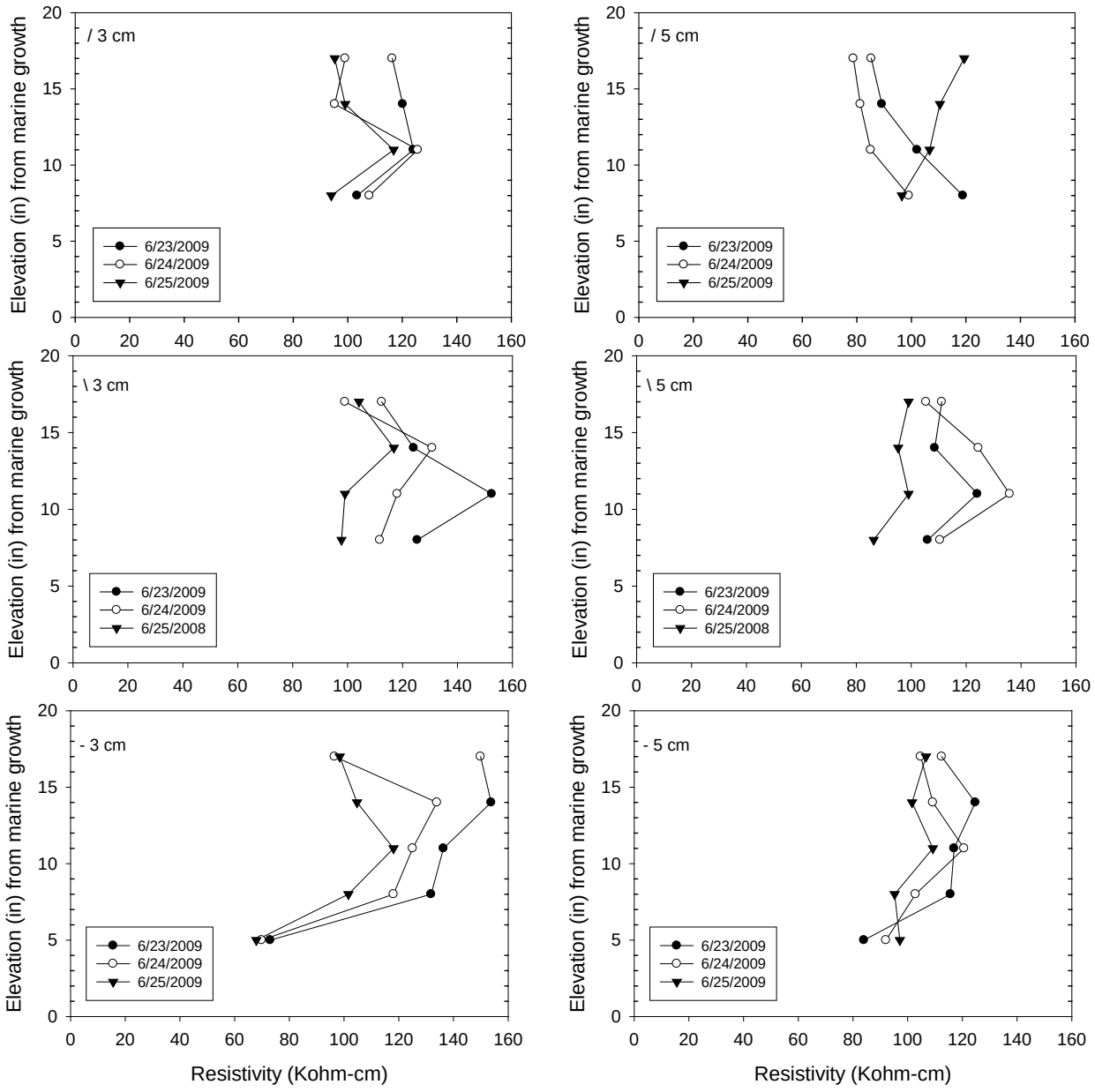

460072
Philips Inlet
Bent 16 Pile 2 East Face

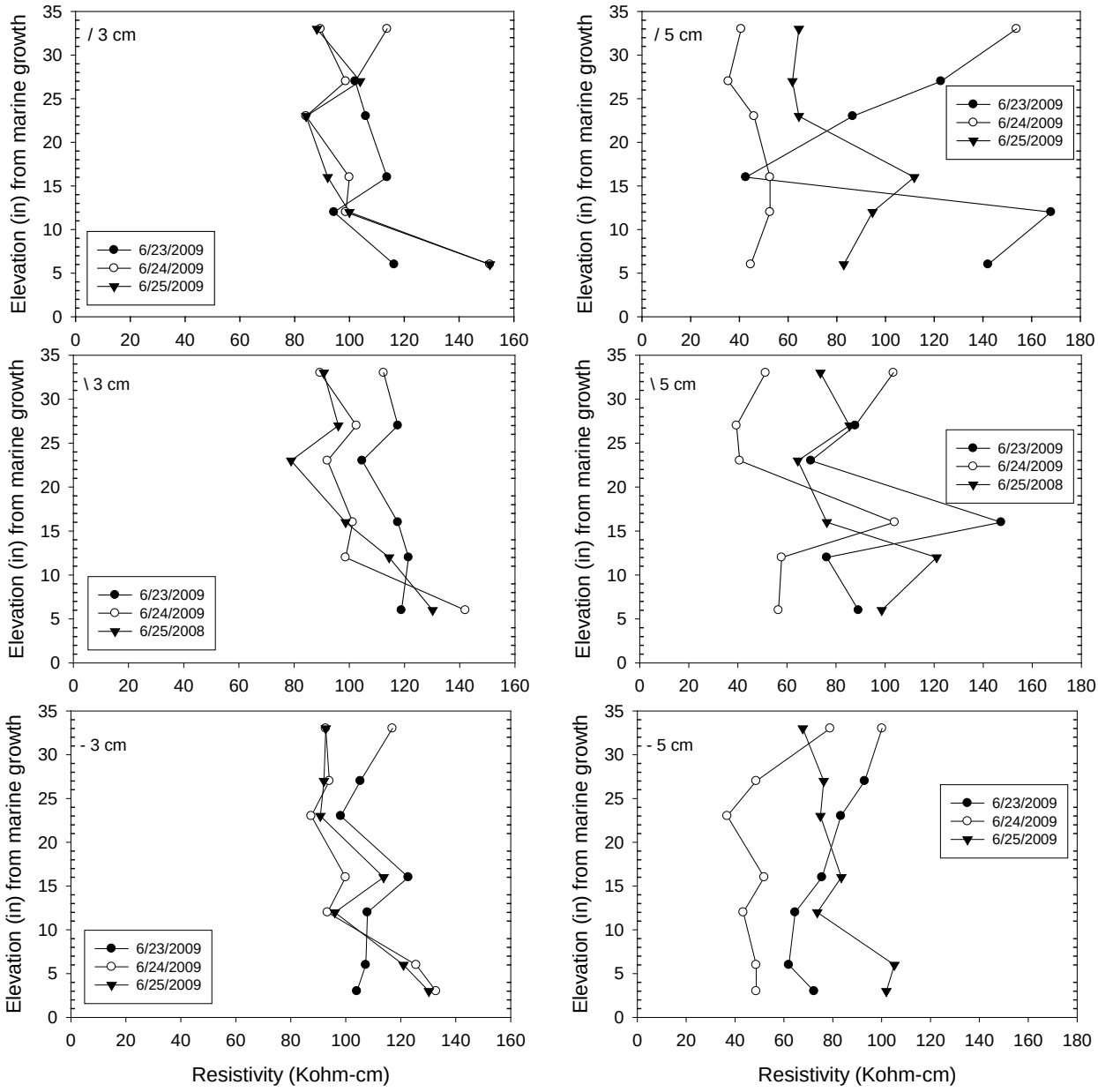

460072
Philips Inlet
Bent 18 Pile 2 East Face

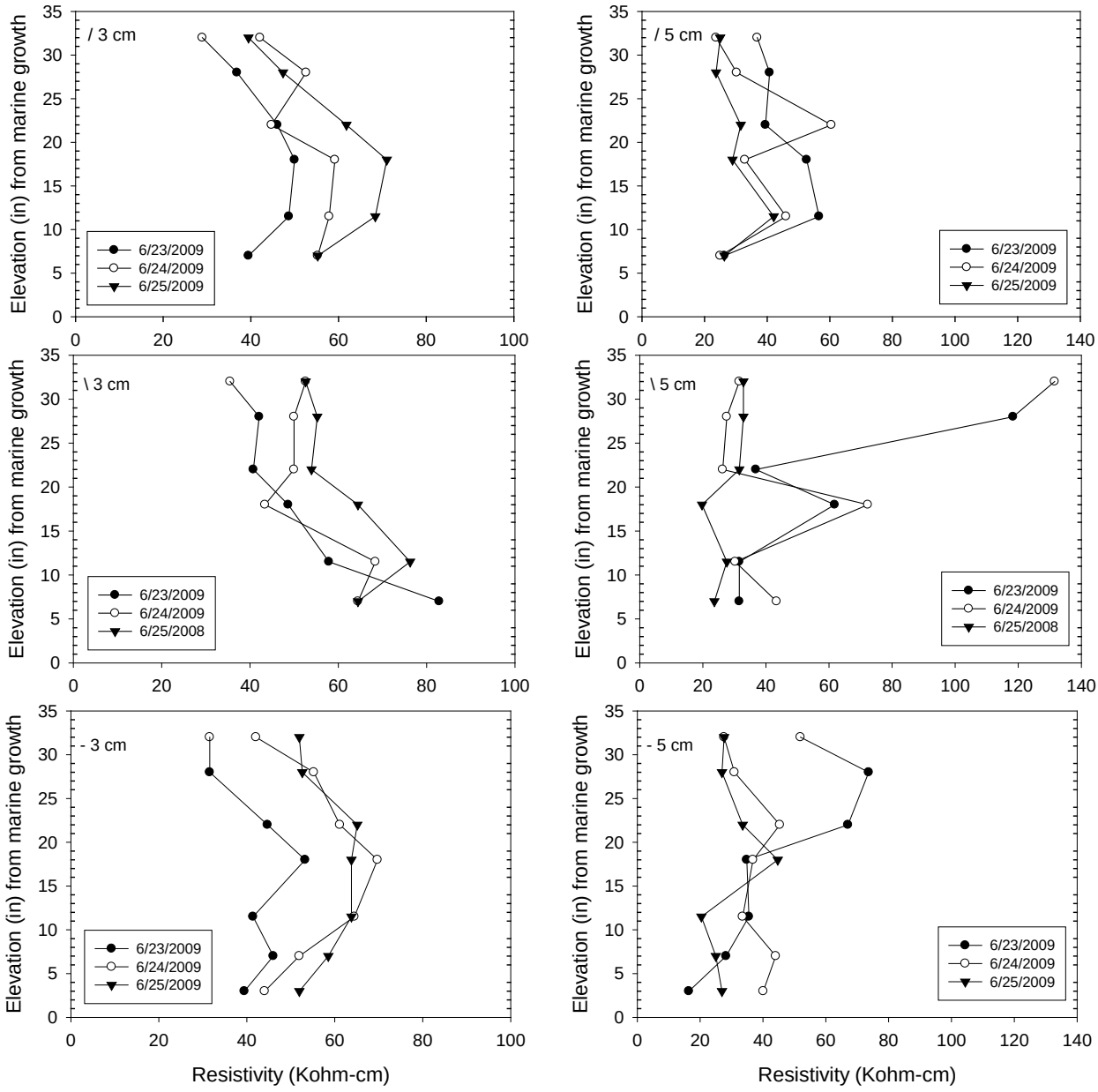

570082
William Marter
Bent 19 Footer 1 East Face

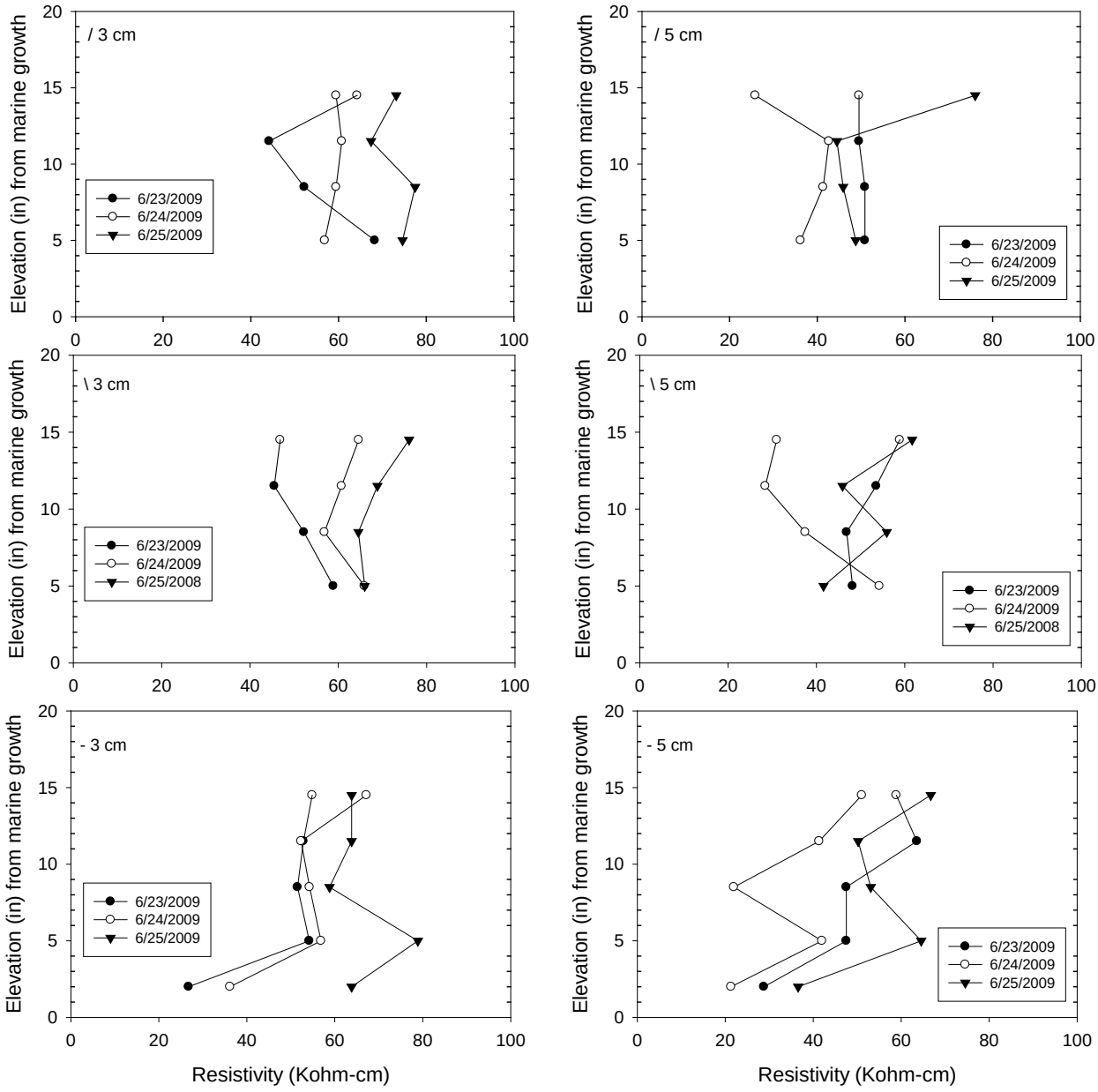

570082
William Marter Eastbound
Bent 20 Pile 3 West Face
C Cover: 3 in

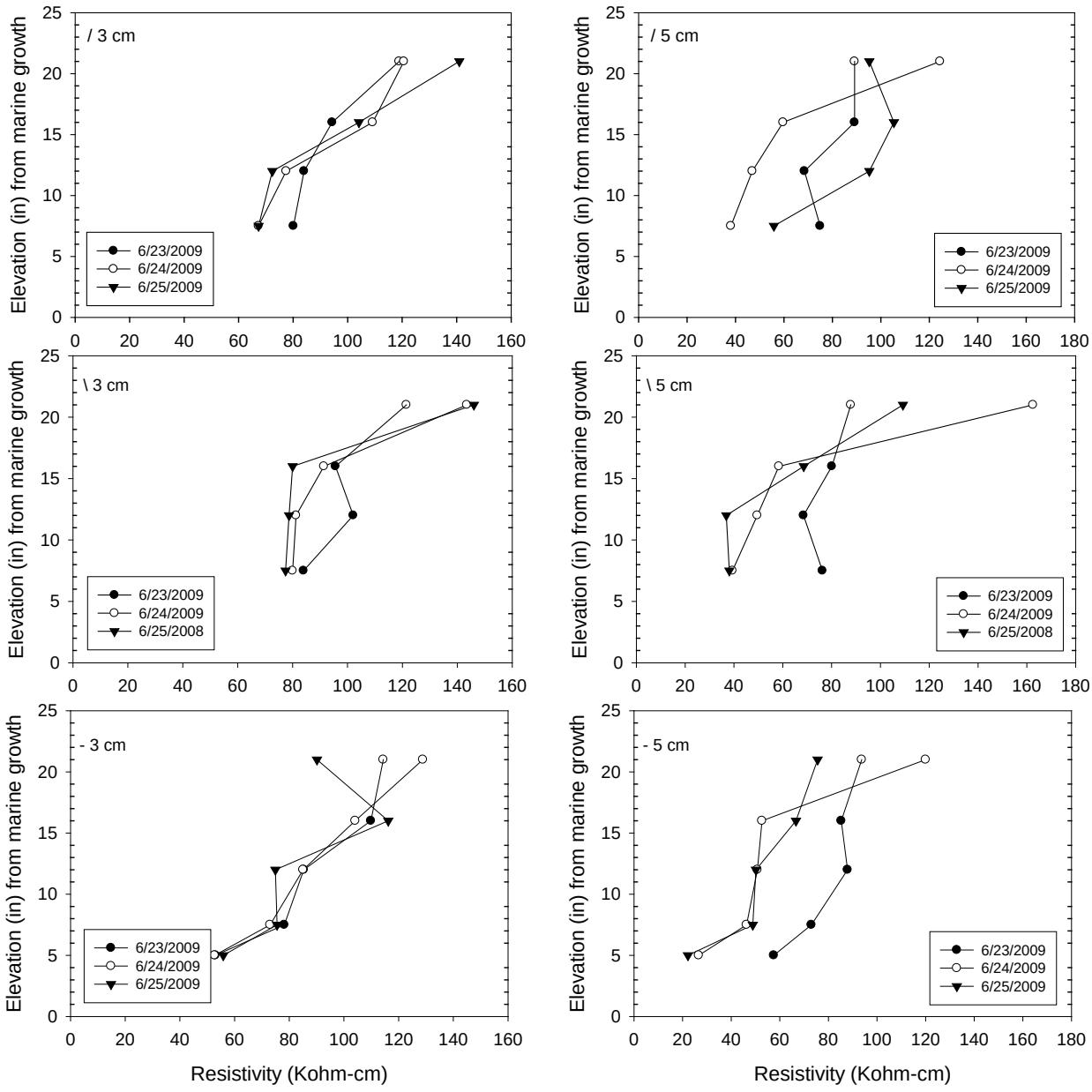

780090
Crescent Beach
Bent 34 Pile 8 South Face

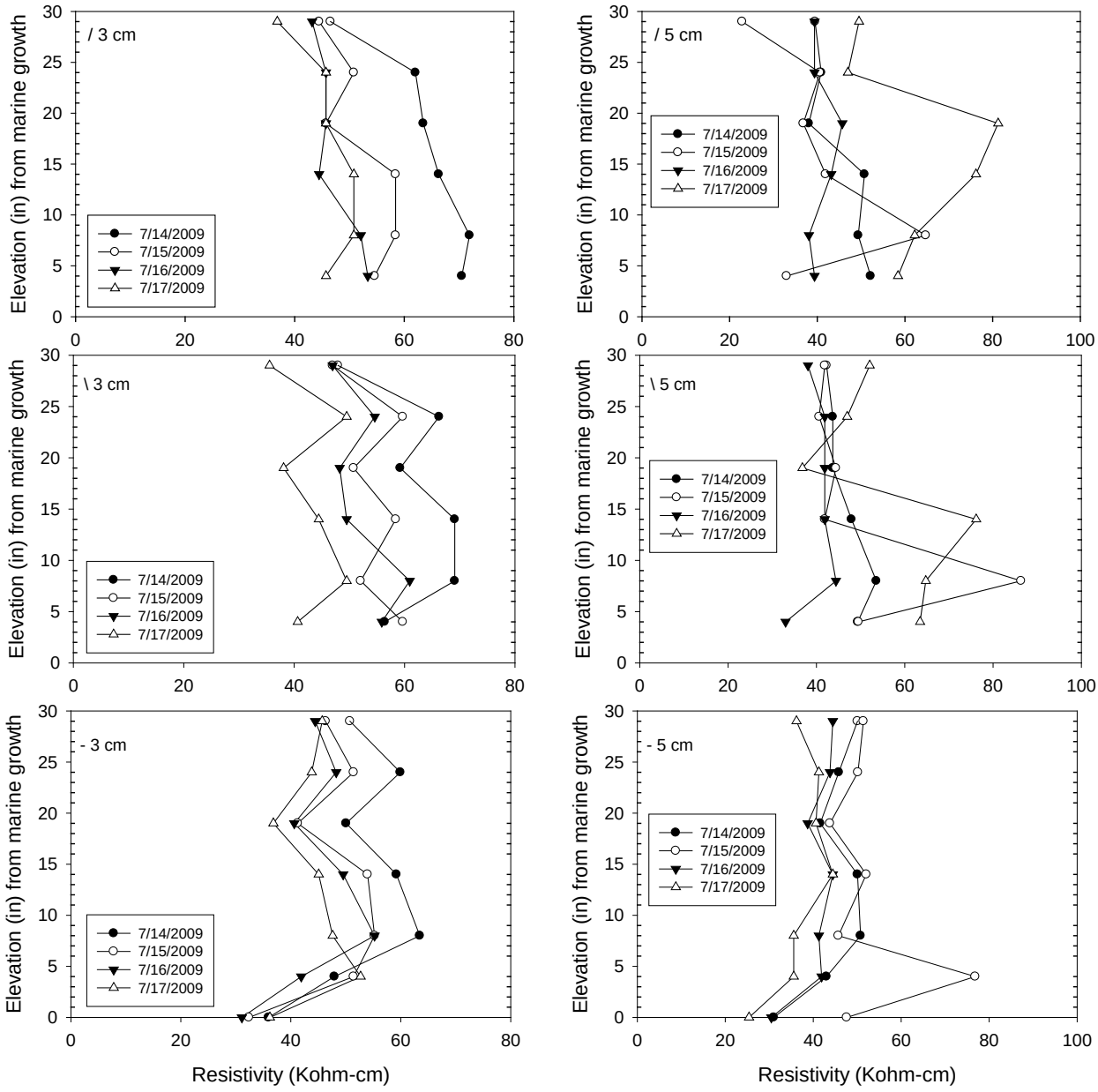

780099
Vilano
Bent 18 Pile 2 North Face

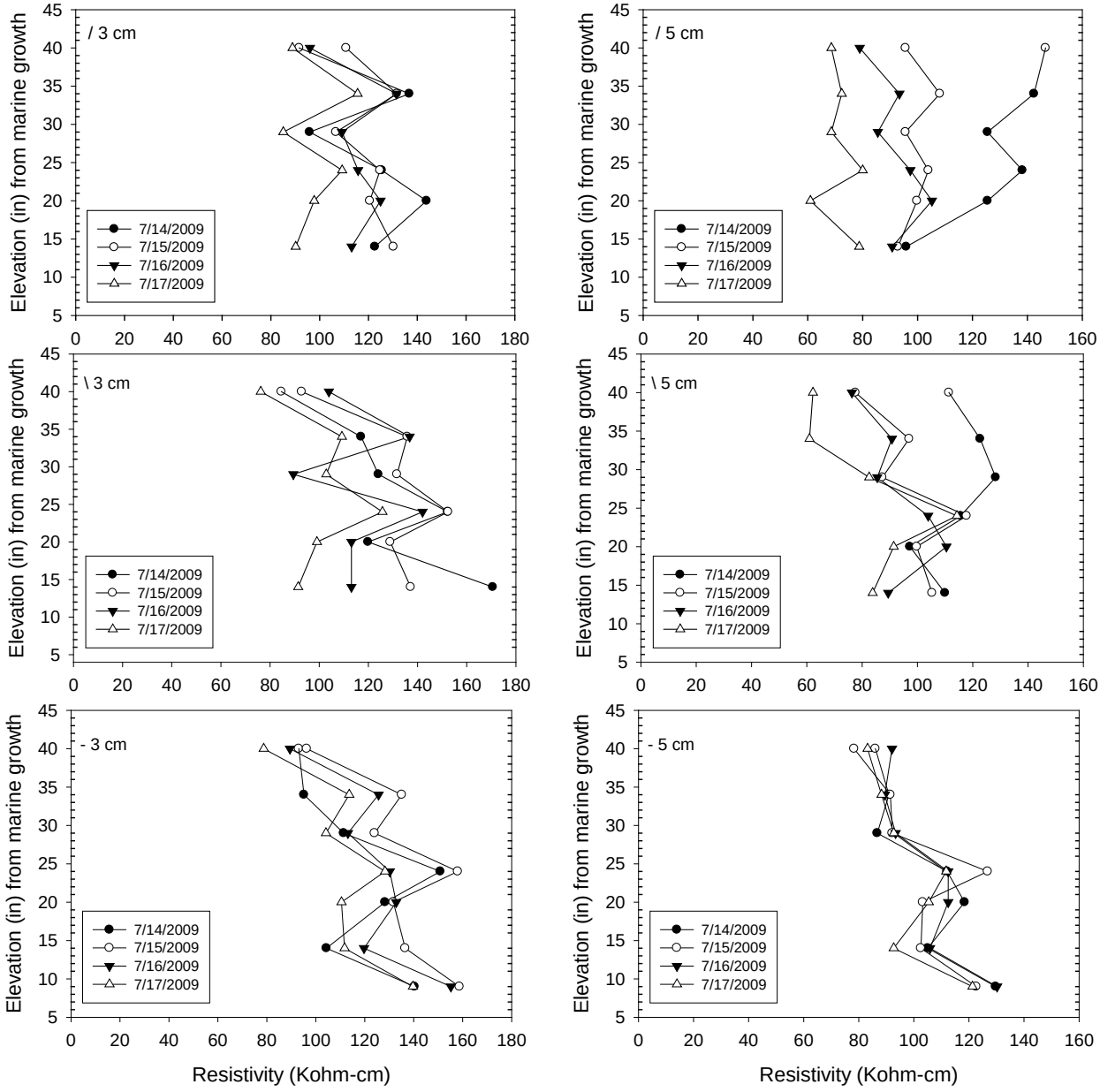

Temporary Bridge
Bent 19 Pile 4 East Face

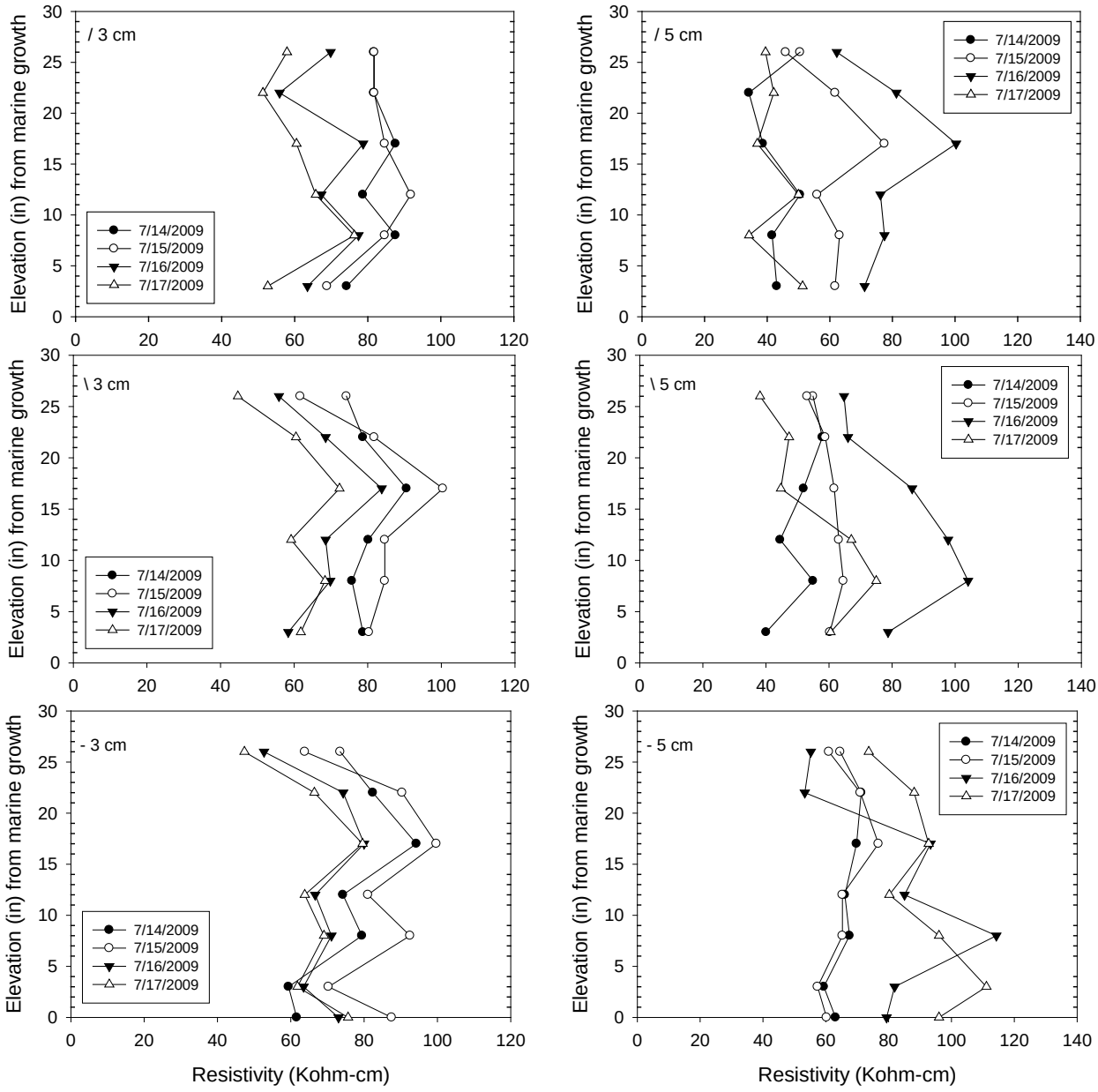

720249
Buckman Eastbound
Bent 104 Footer 1 West Face
C Cover: 3 in

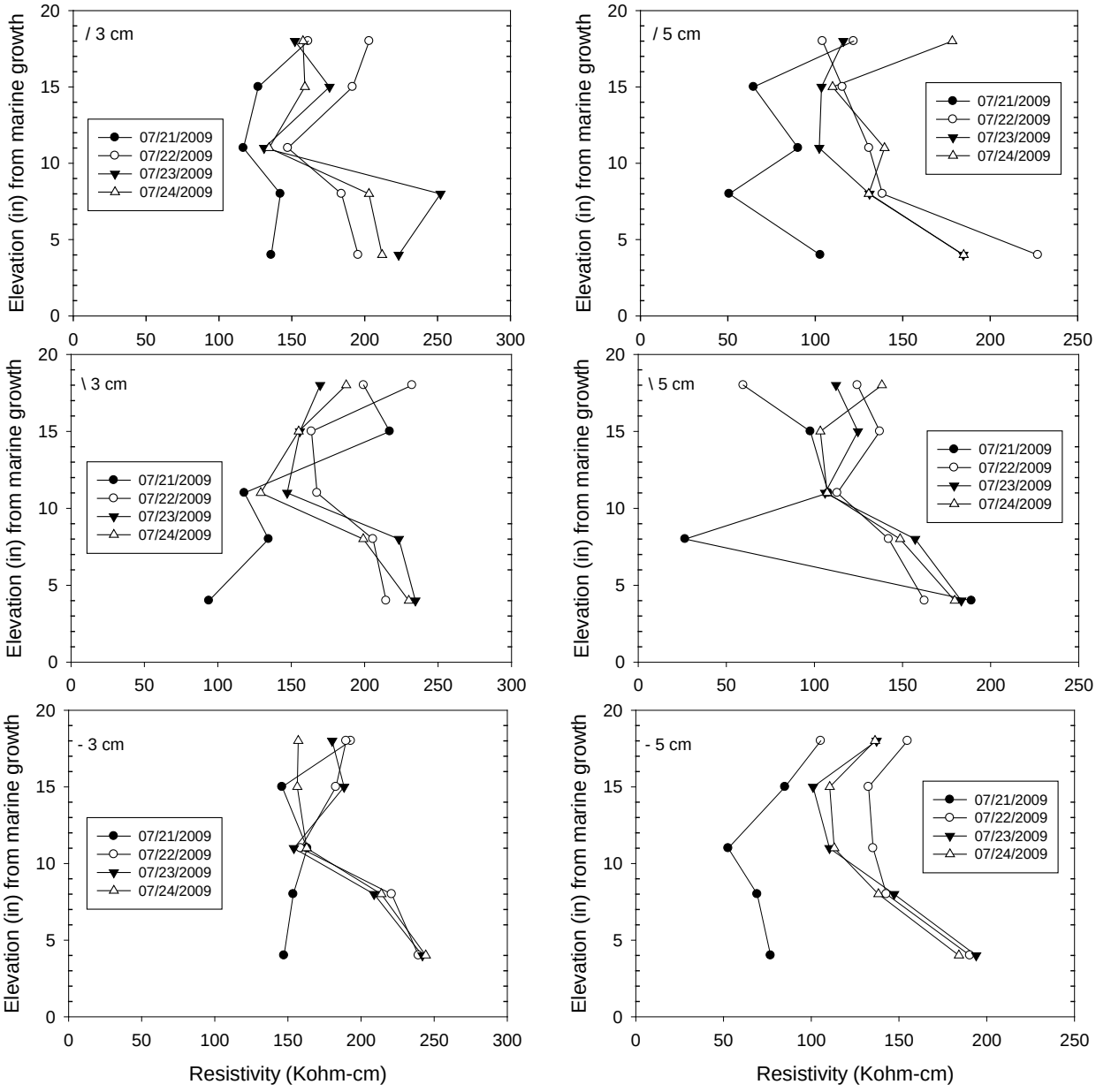

720249
Buckman Eastbound
Bent 123 Pile 3 West Face
C Cover: 2.5 in

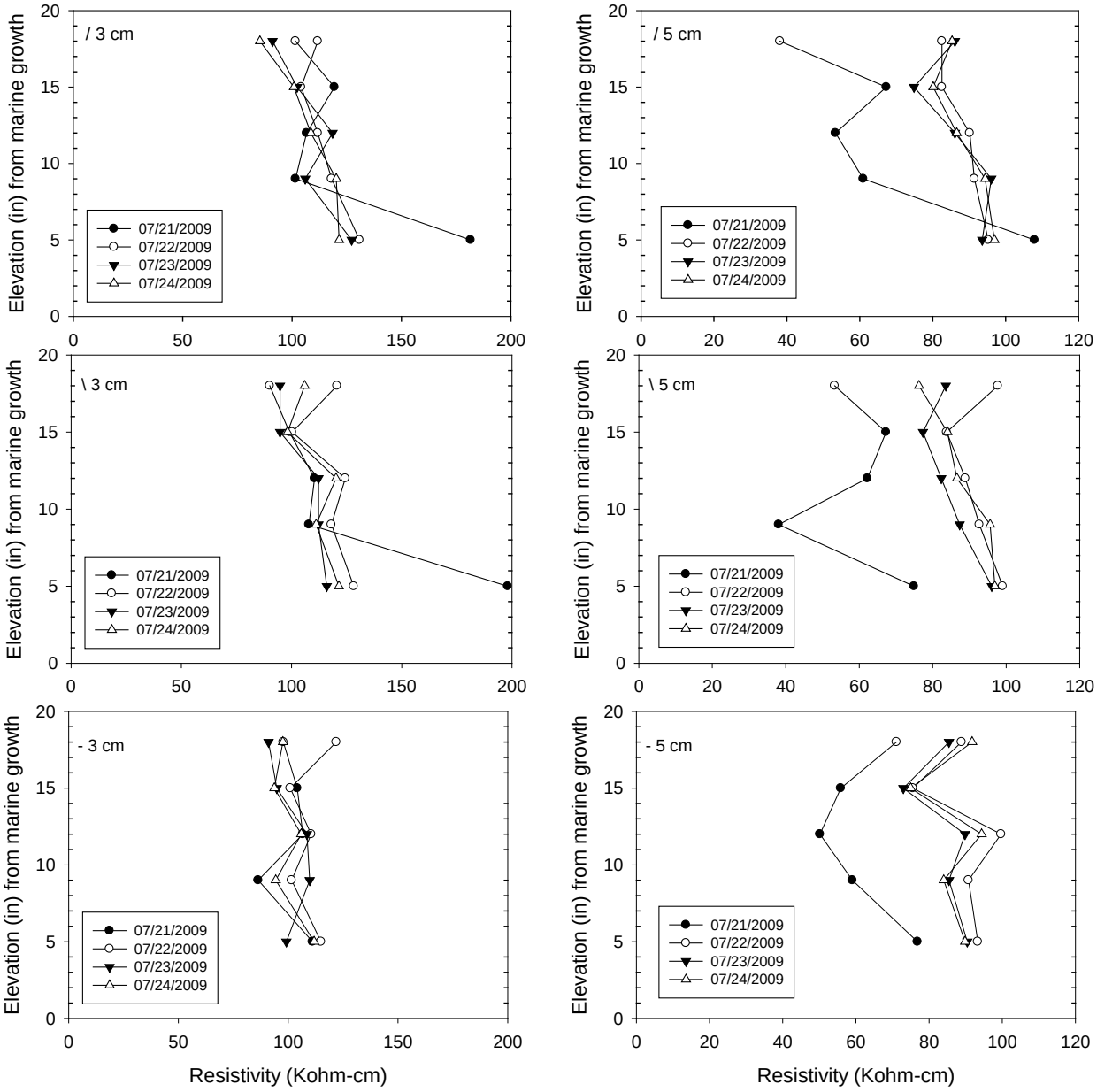

720249
Buckman Eastbound
Bent 123 Pile 7 West Face
C Cover: 2.5 in

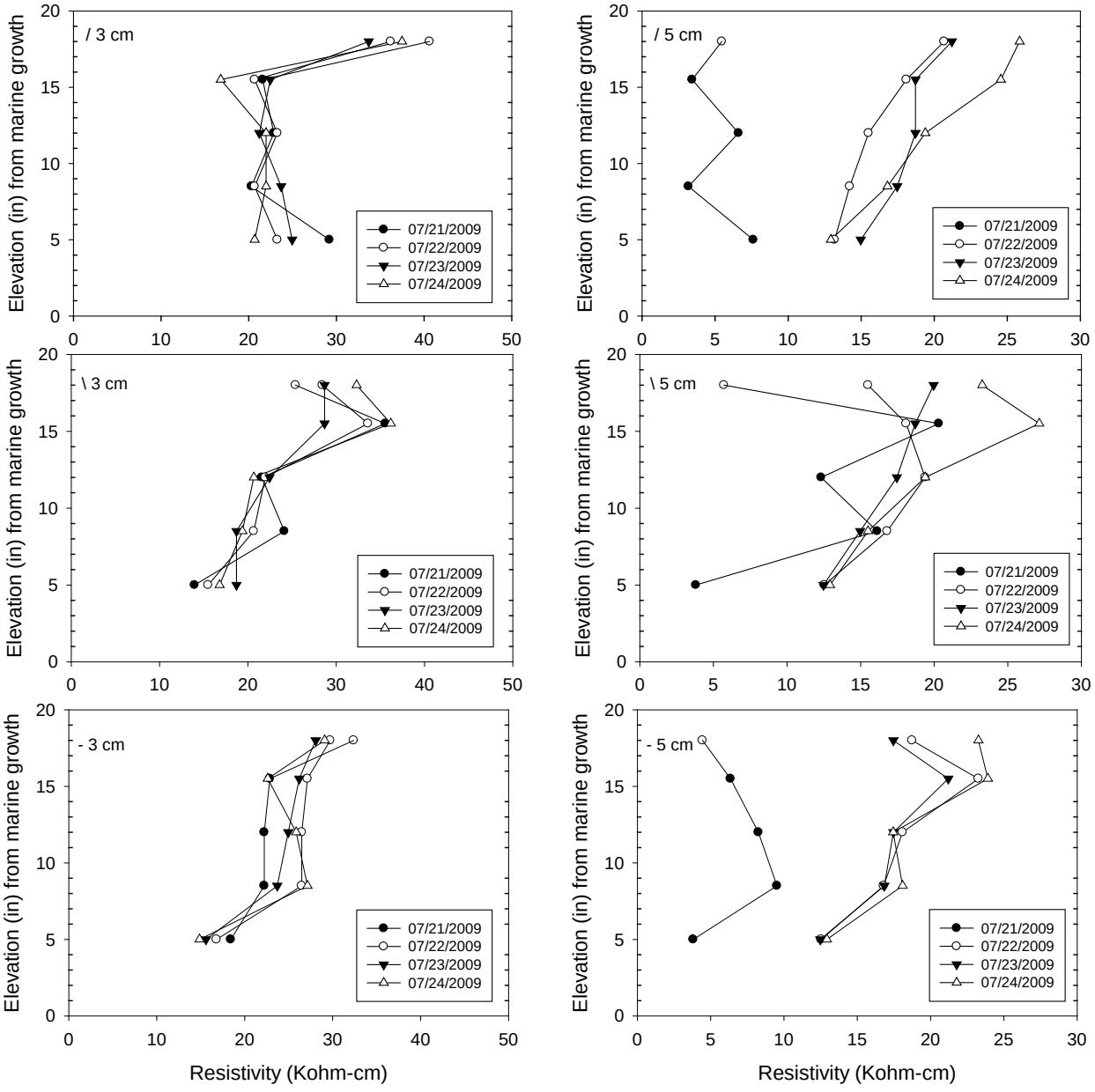

720343
Buckman Westbound
Bent 123 Pile 5 West Face
C Cover: 3.1 in

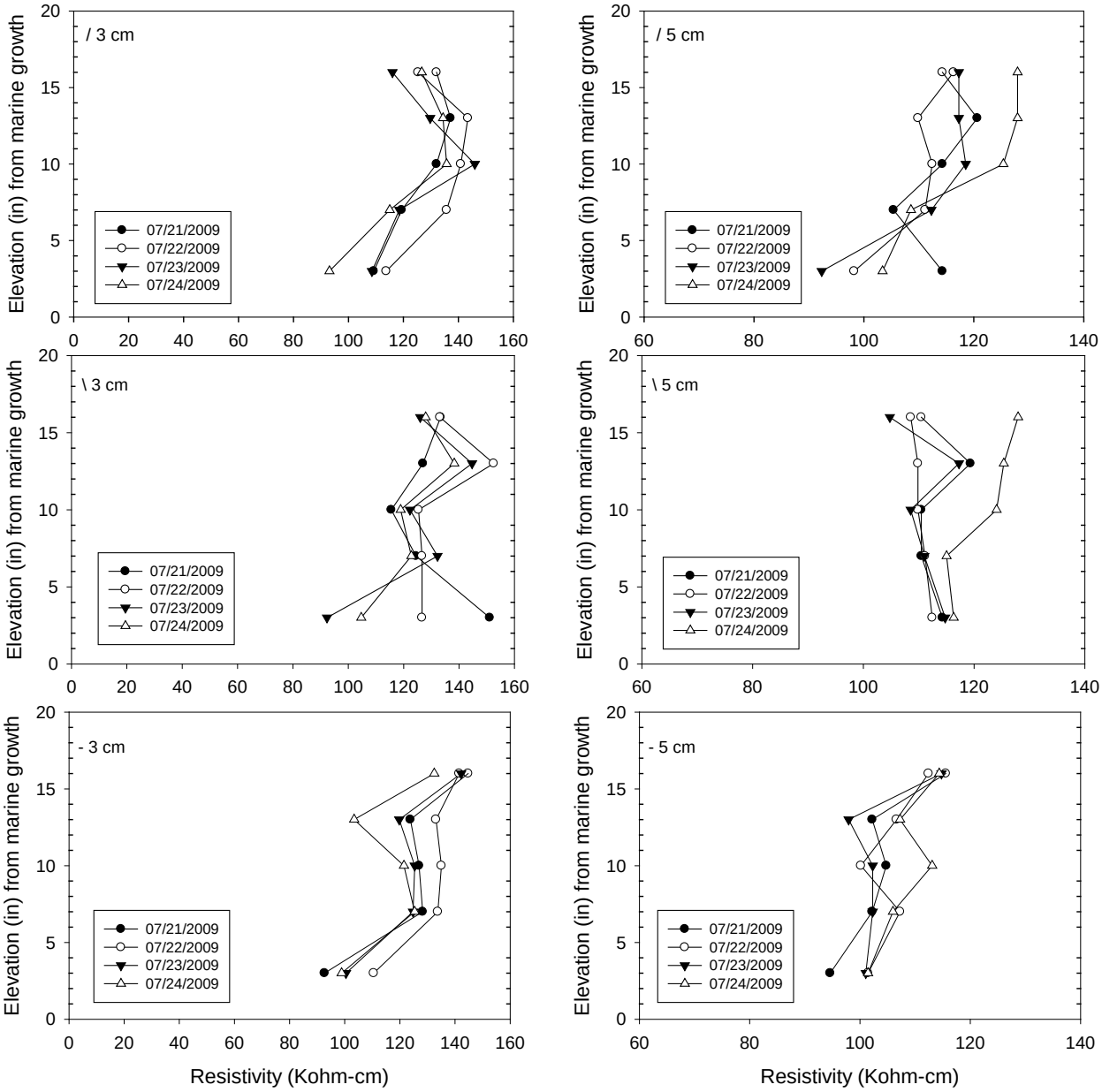

720343
Buckman Westbound
Bent 123 Pile 3 South Face
C Cover: 3.1 in

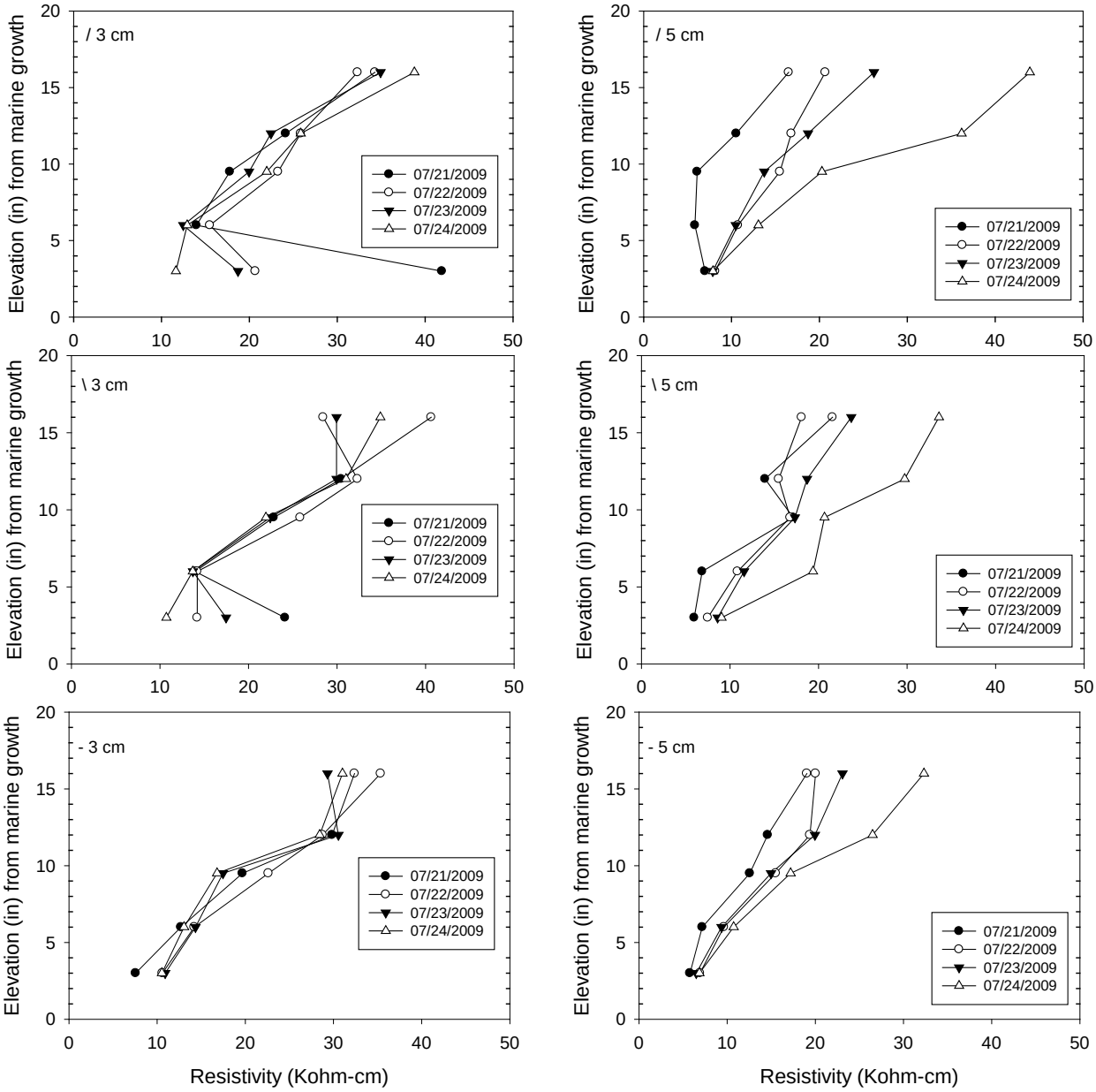

720343
Fuller Warn East to West
Bent 21 Footer 1
C Cover: 3.1

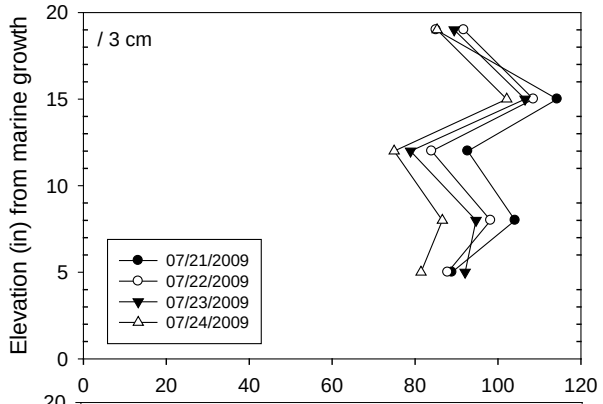

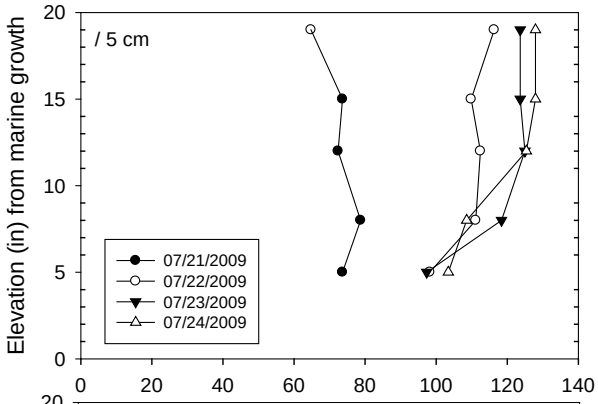

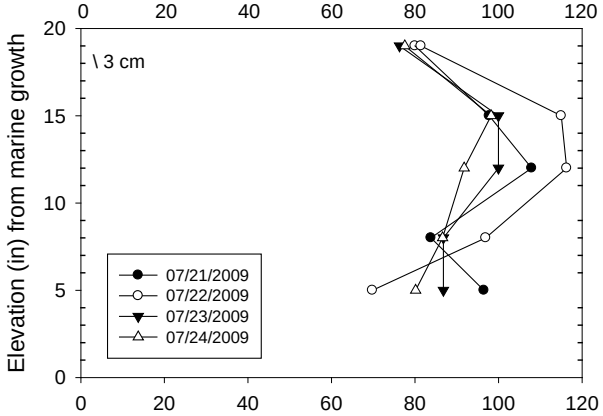

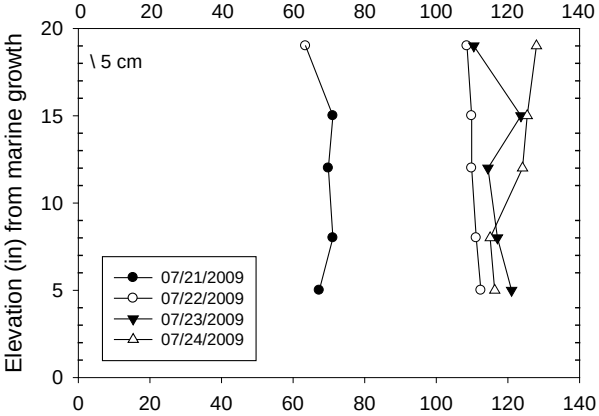

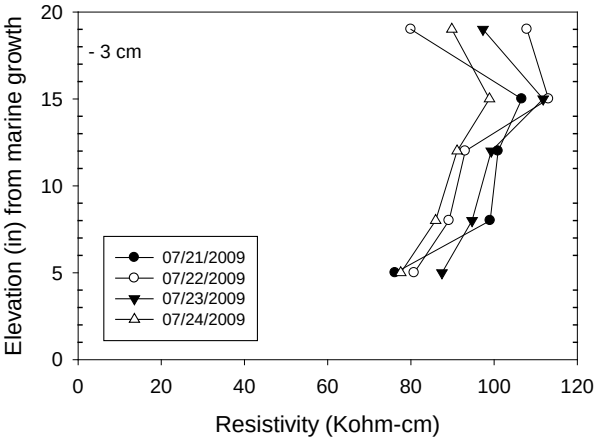

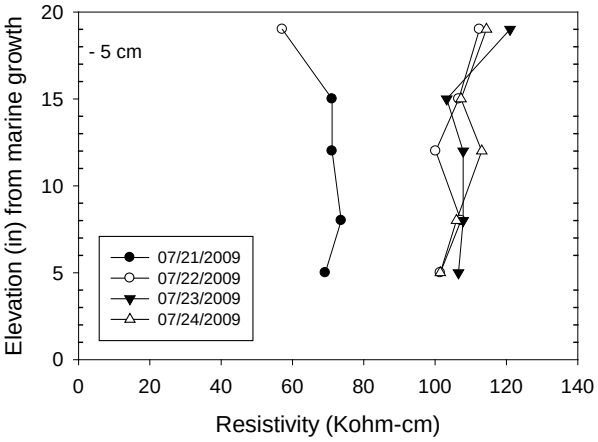

720570
Acosta Southbound
Bent 2 Footer South Face
C Cover: 3.1 in

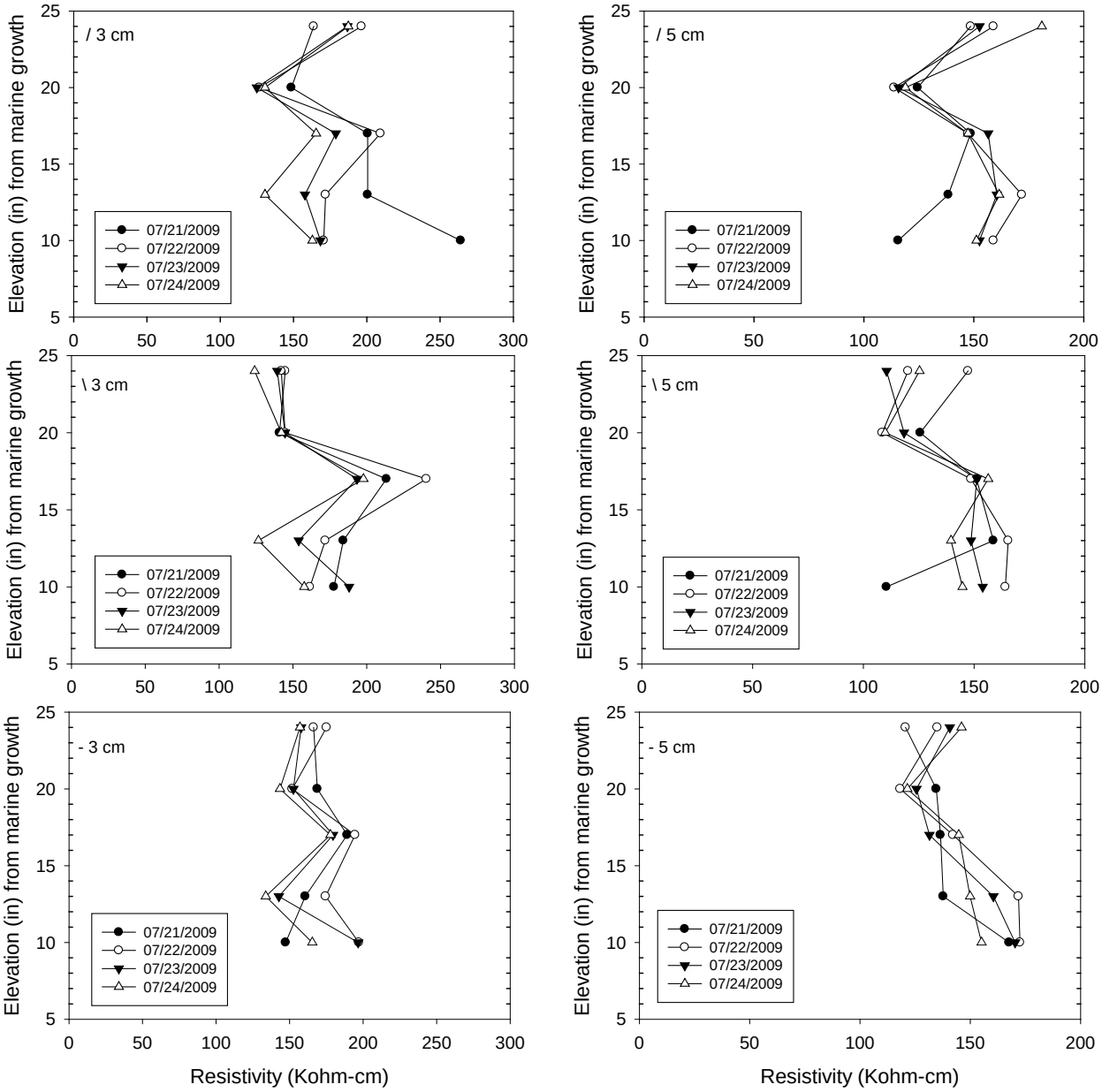

720570
Acosta
Bent 2 Footer(2)
C Cover: 3.1

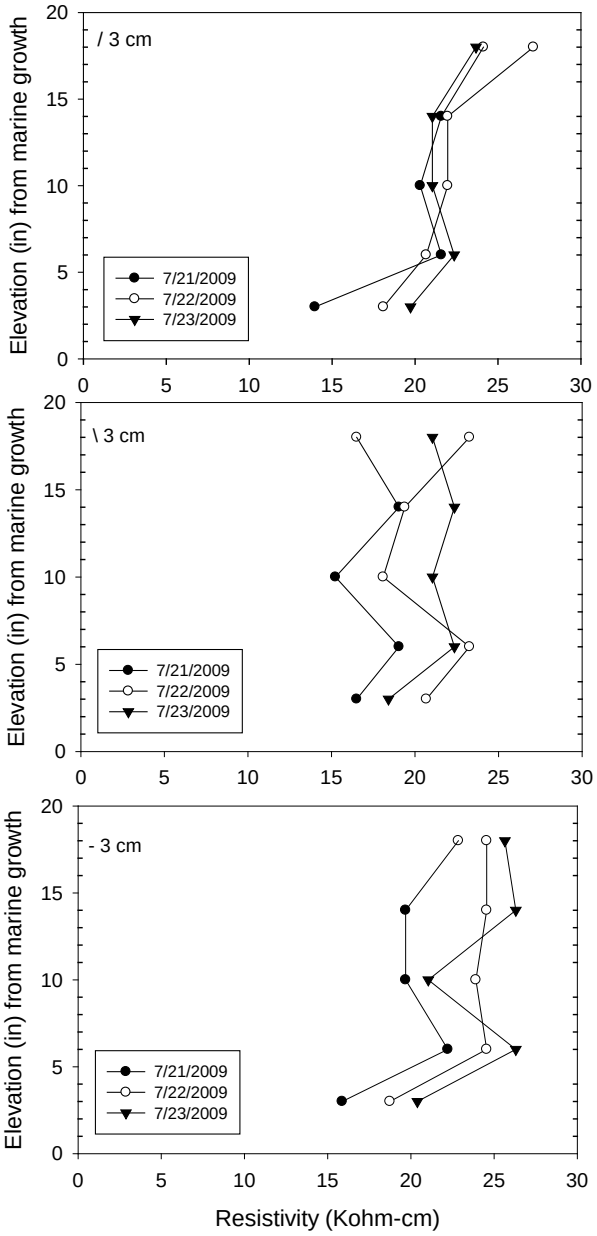

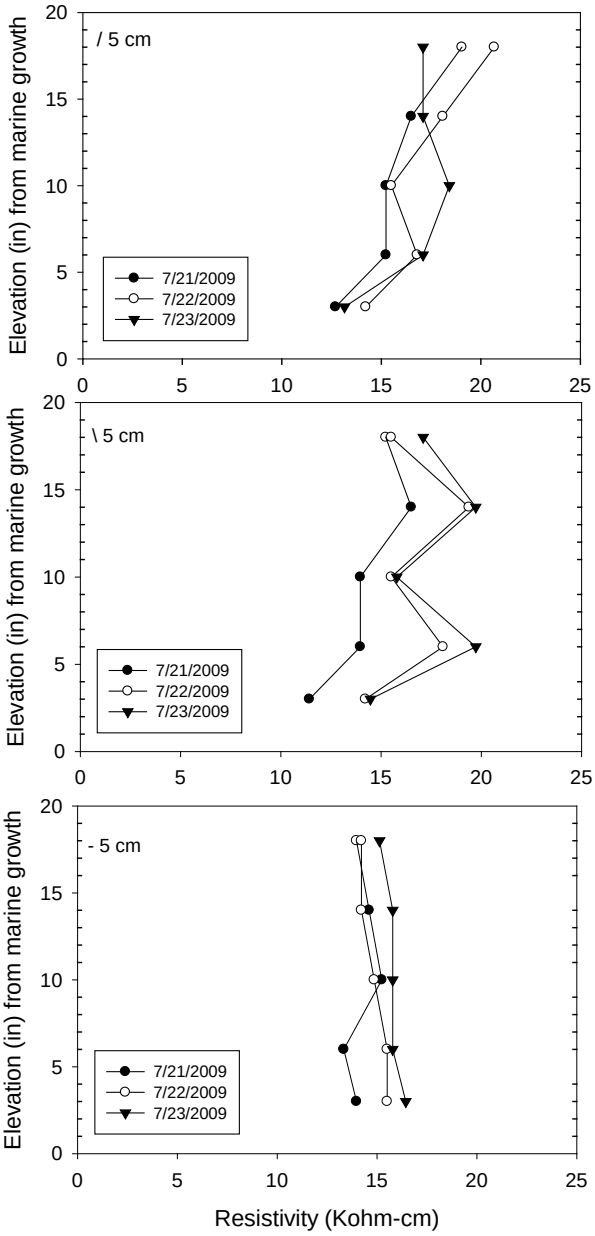

900095
Indian Way
Bent 17 Pile 1

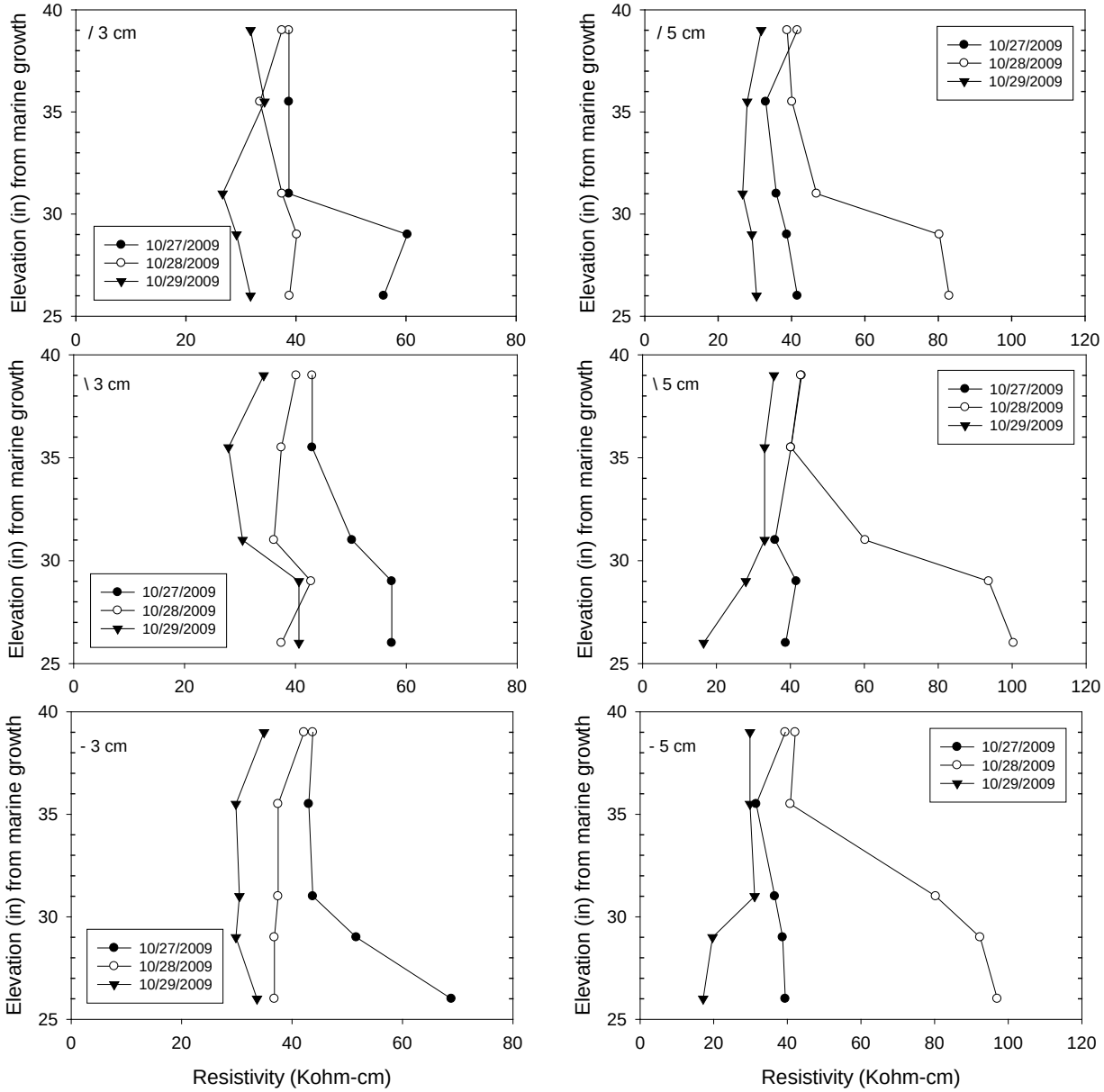

900096
LignumVitae
Bent 9 Pile 2

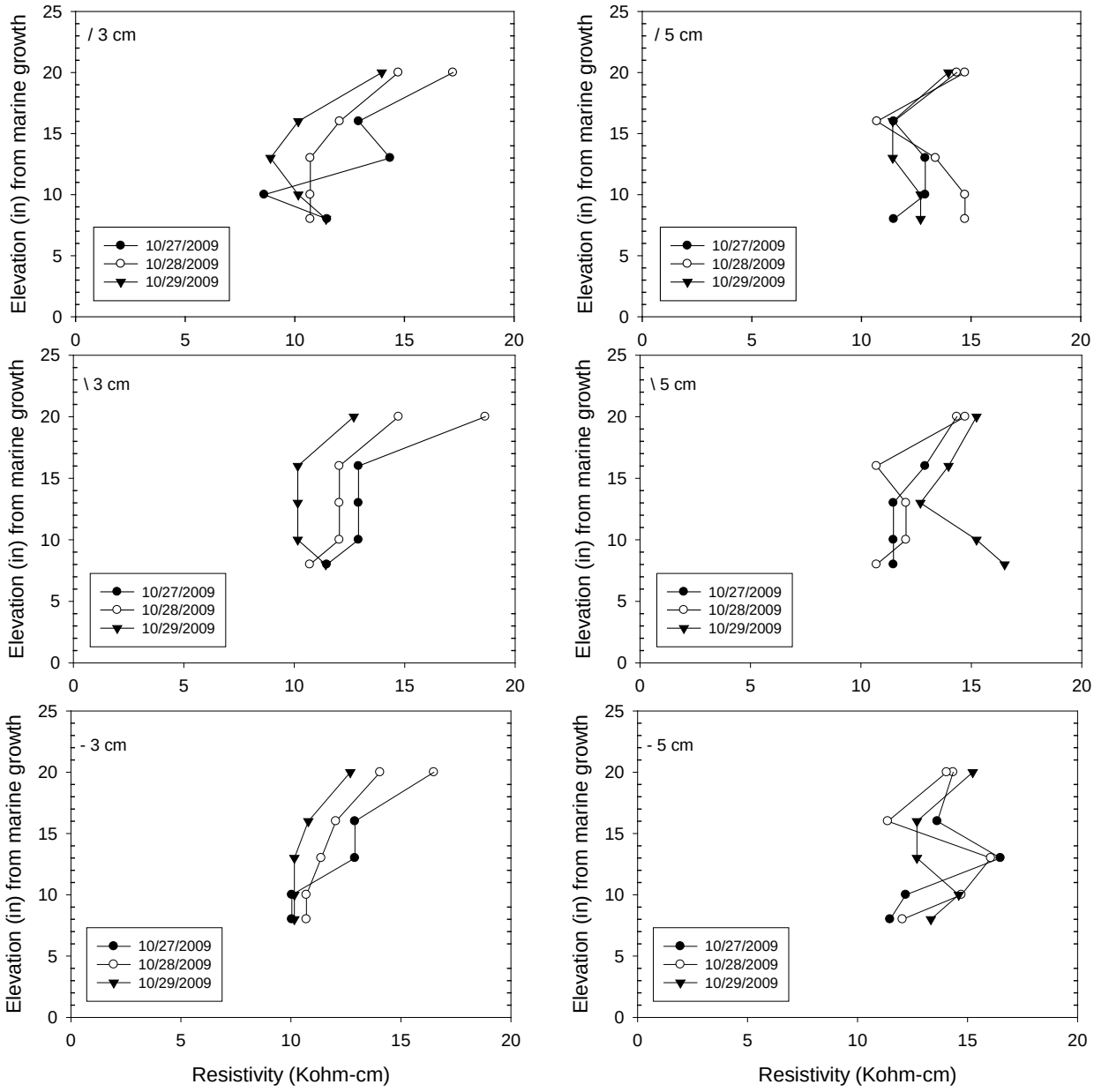

900101
7 Mile Bridge
Bent 14 Pile 2 Down

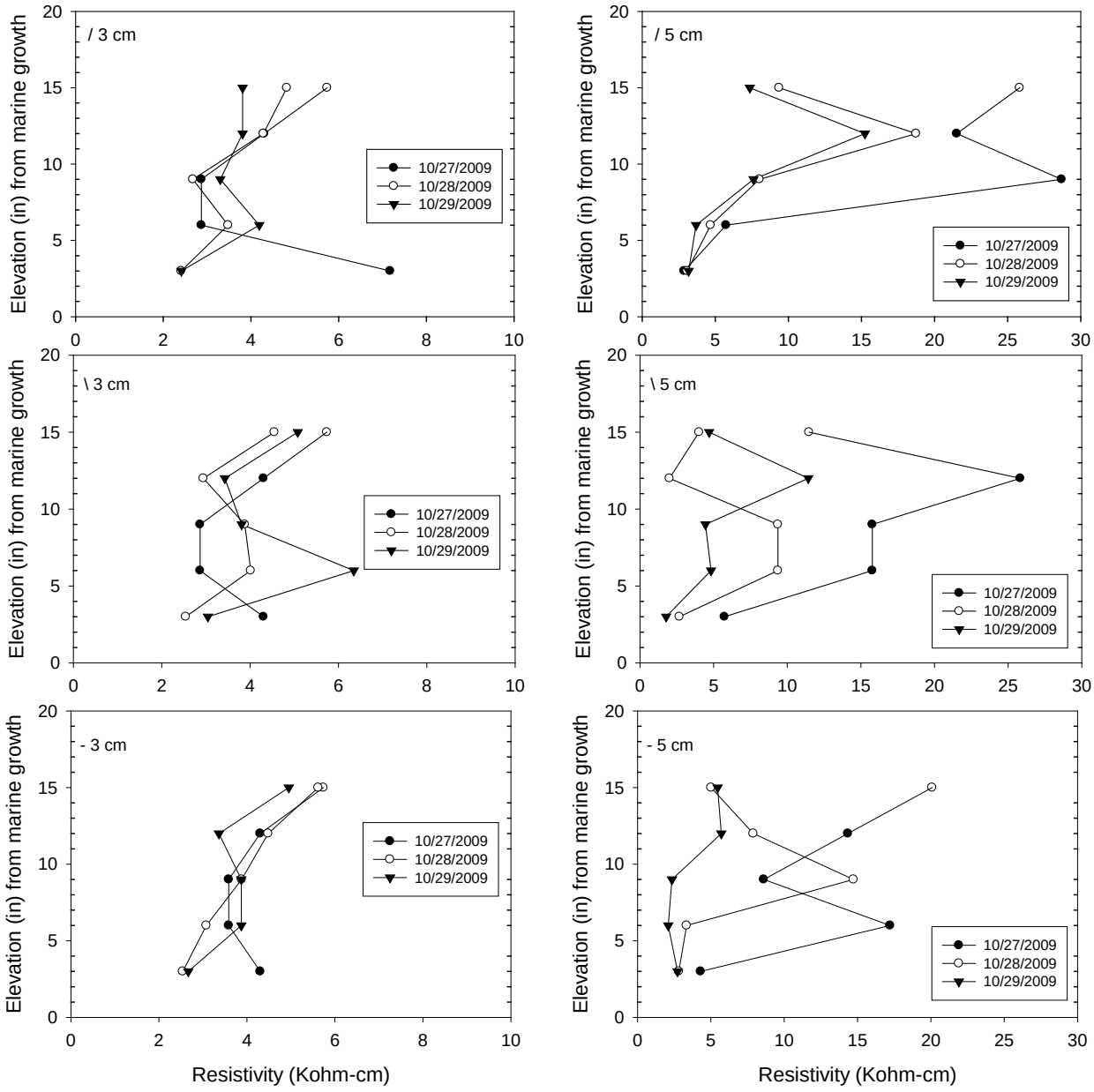

900101
7 Mile Bridge
Bent 14 Pile 2 Up

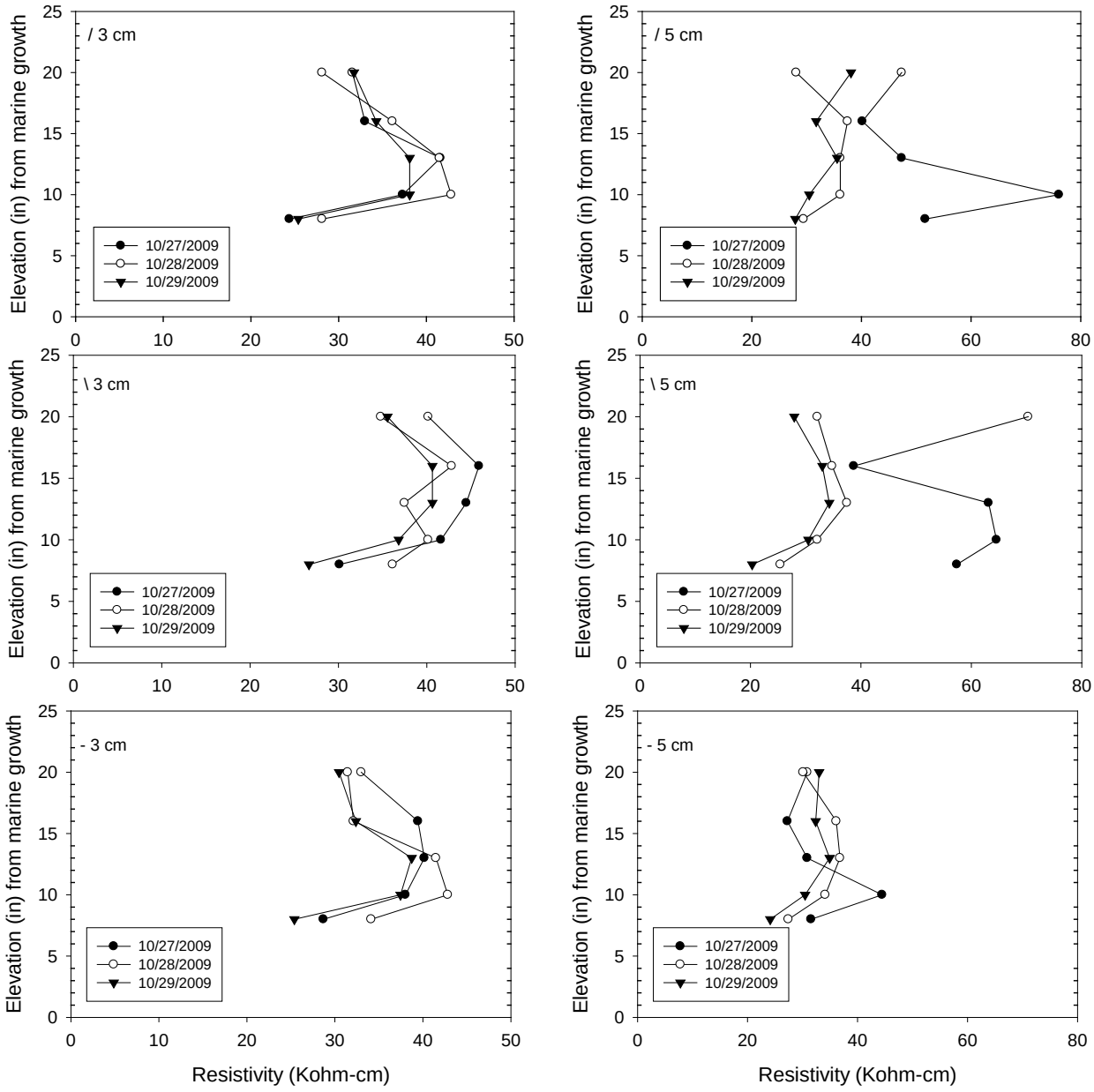

900103
Missouri Little Duck
Bent 7 Pile 2

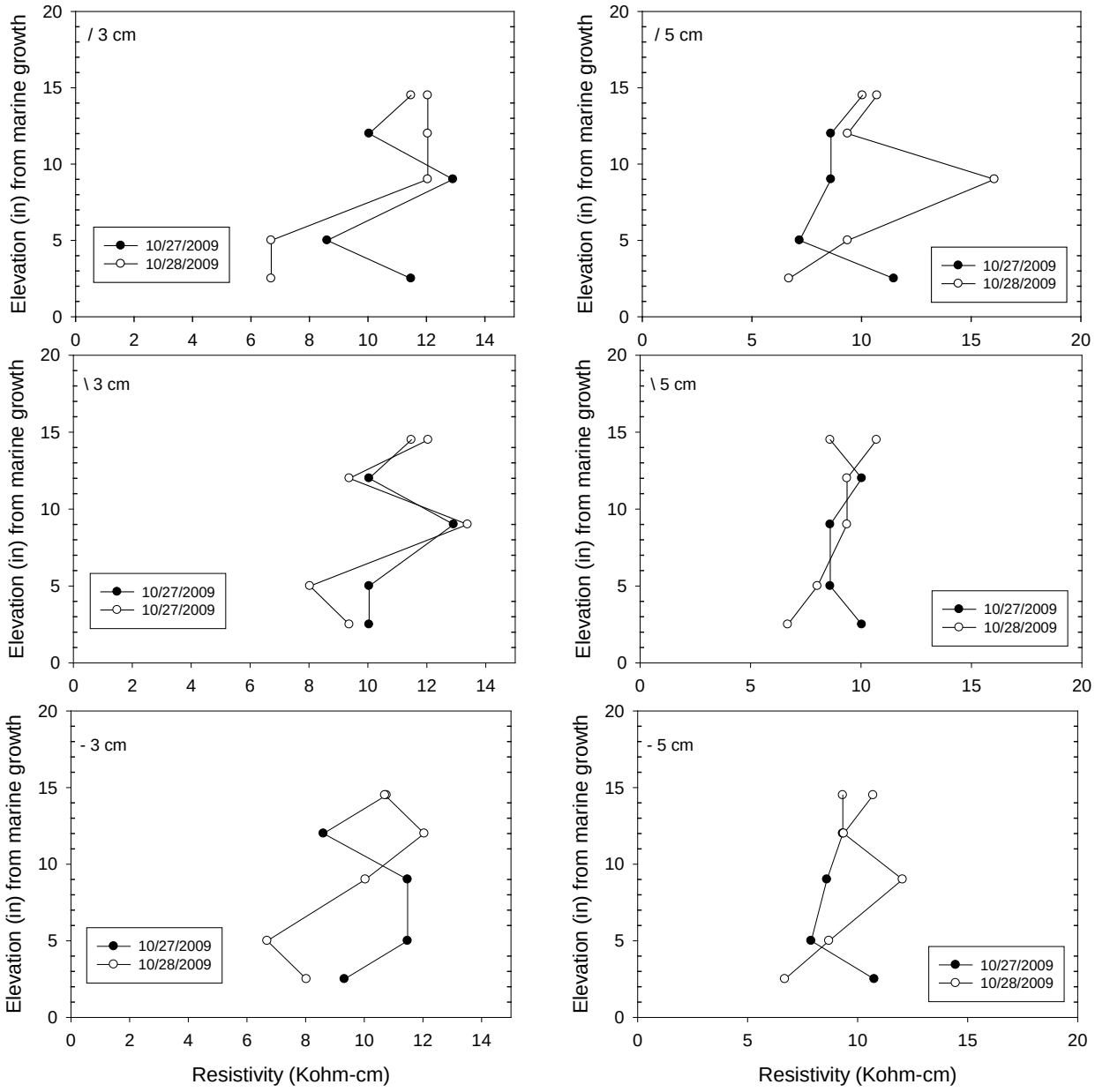

900016
Bahia Honda Southbound
Bent 69 Pile 5

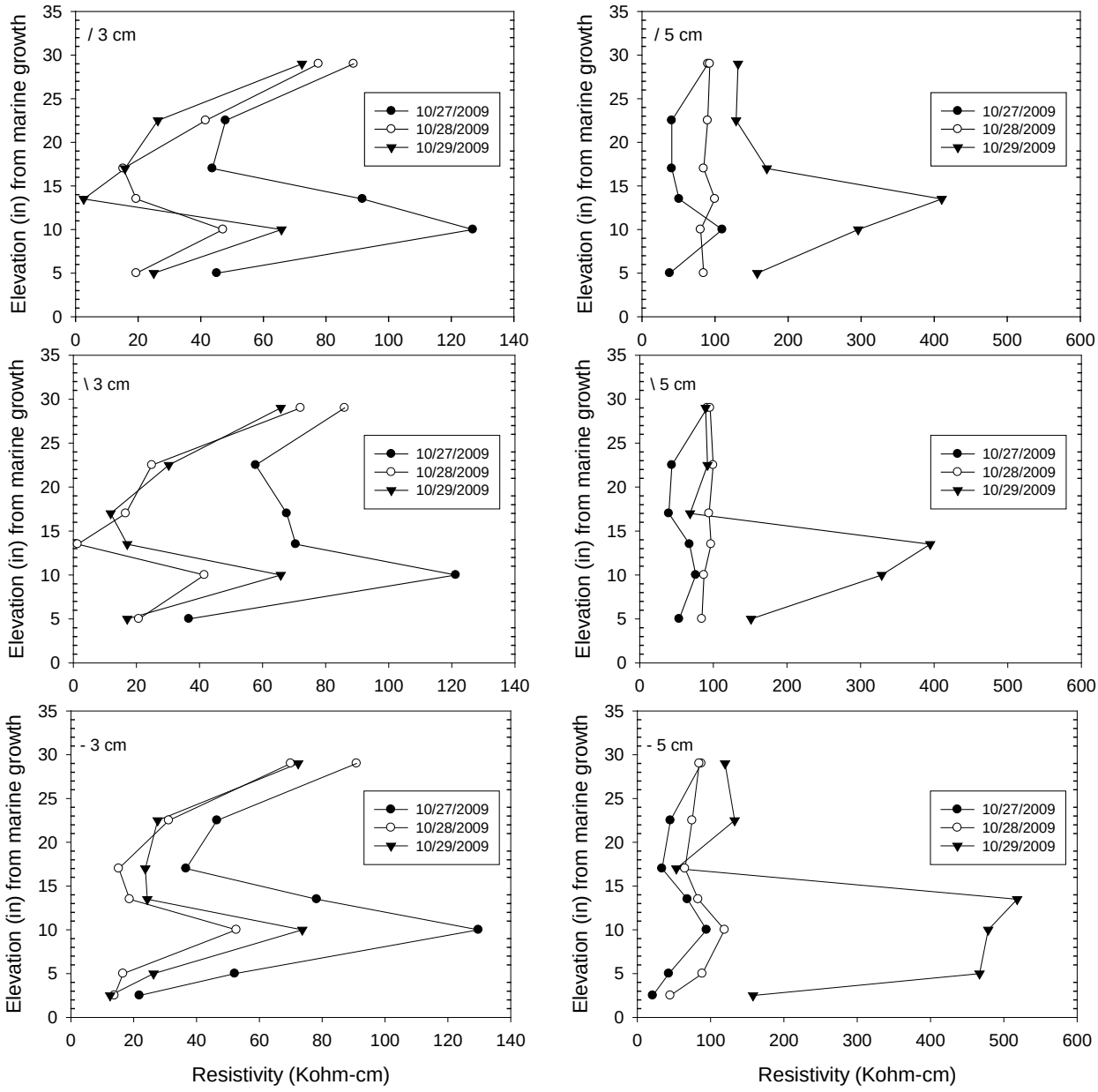

900106
Bogie Channel
Bent 35 Pile 4

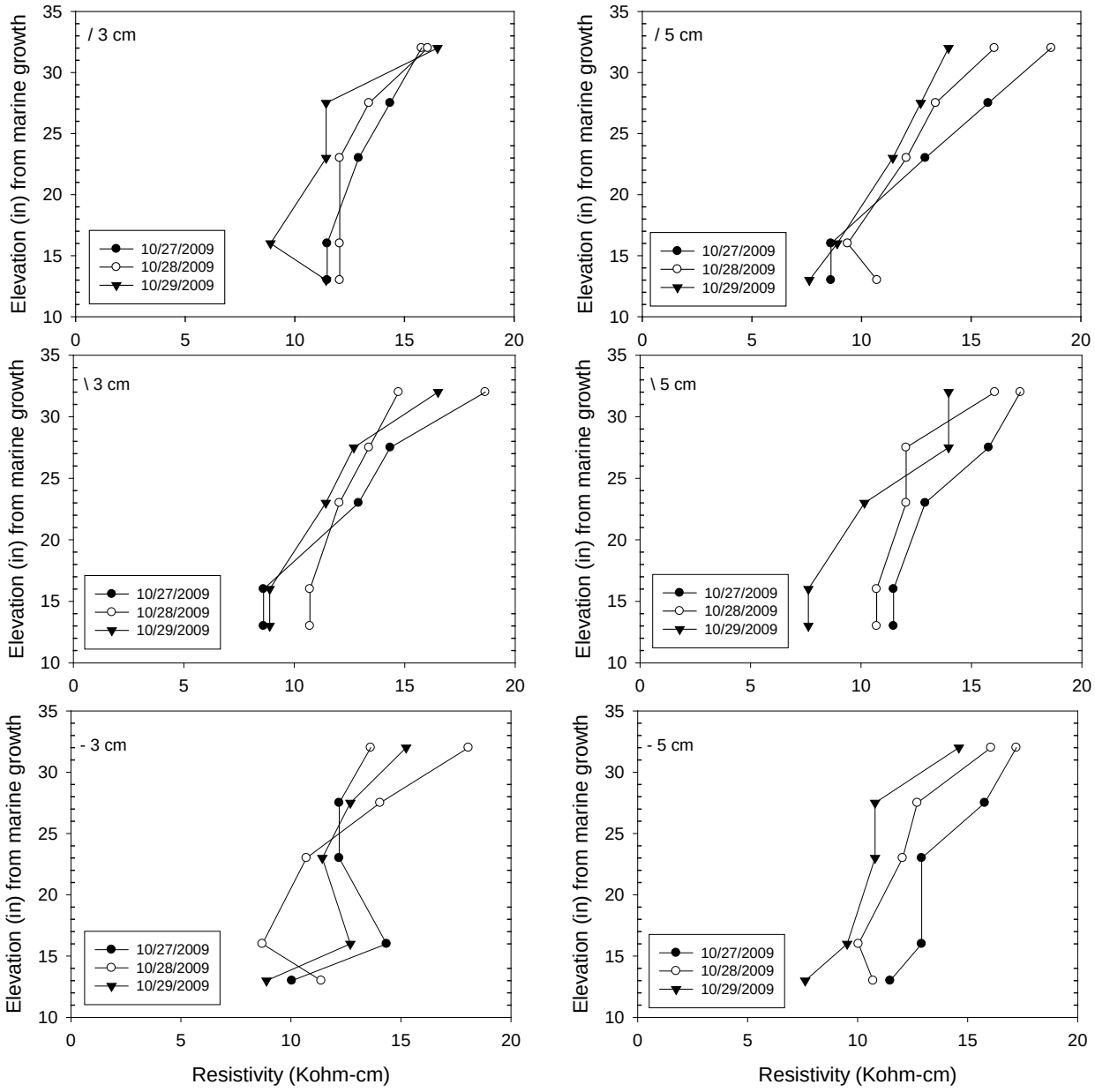

124116
Structure A Sanibel Causeway
Bent 13 Footer East Face
C Cover: 3.5 in

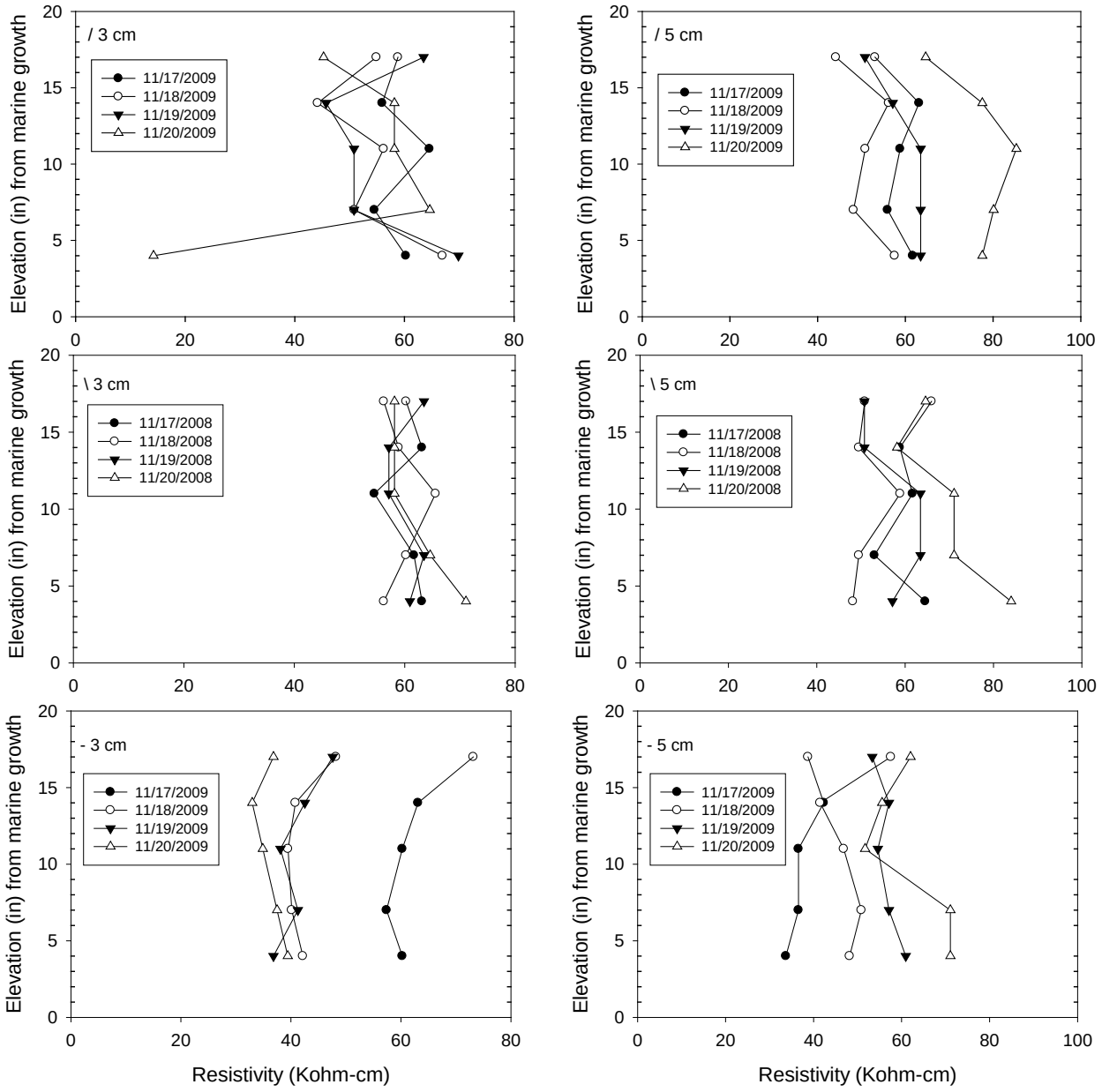

124115
Structure B Sanibel Causeway
Bent 2 Footer East Face
C Cover: 4 in

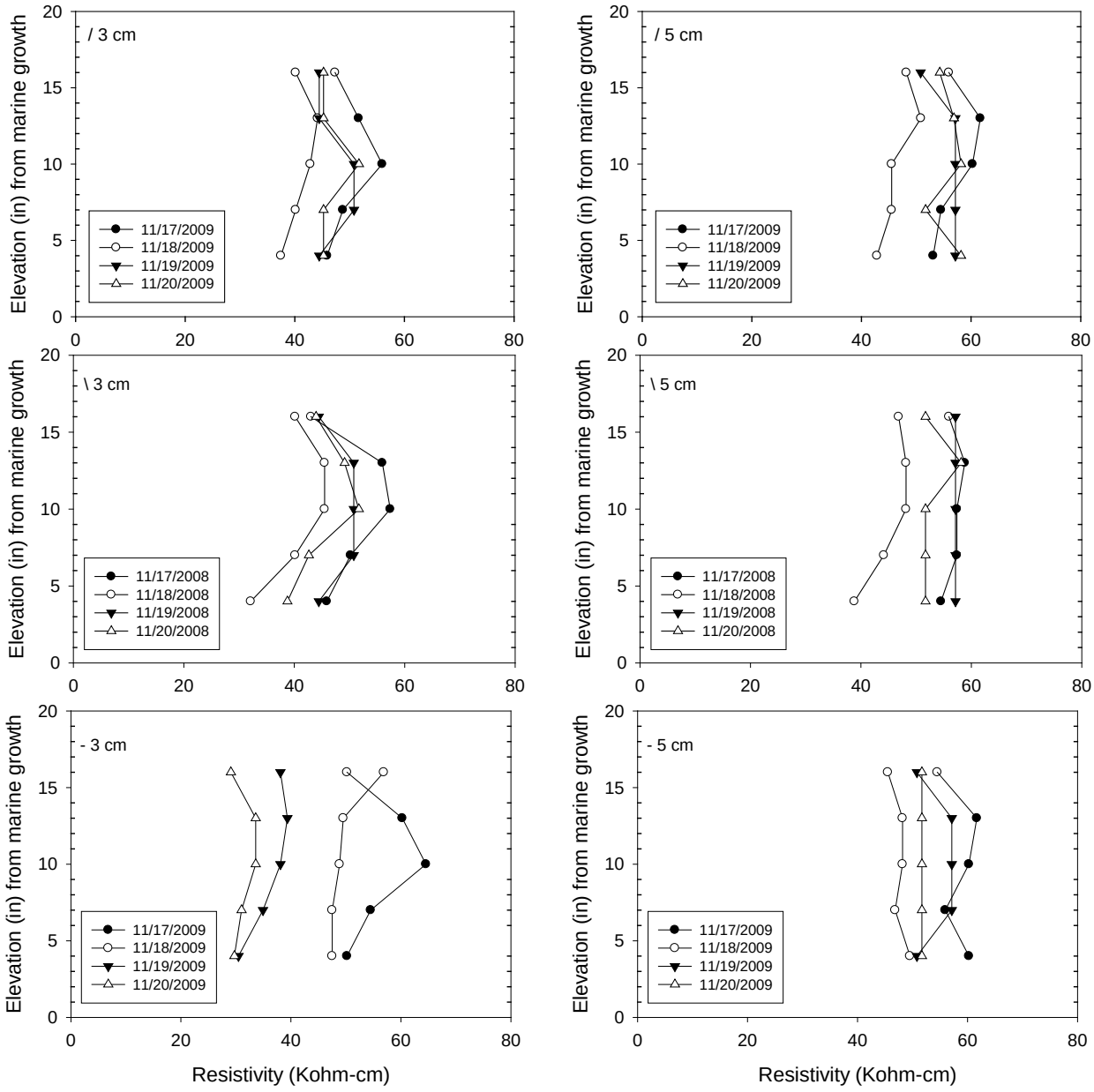

120088
Mantanzas Bay Bridge
Bent 11 Footer North Face
C Cover: 3.85 in

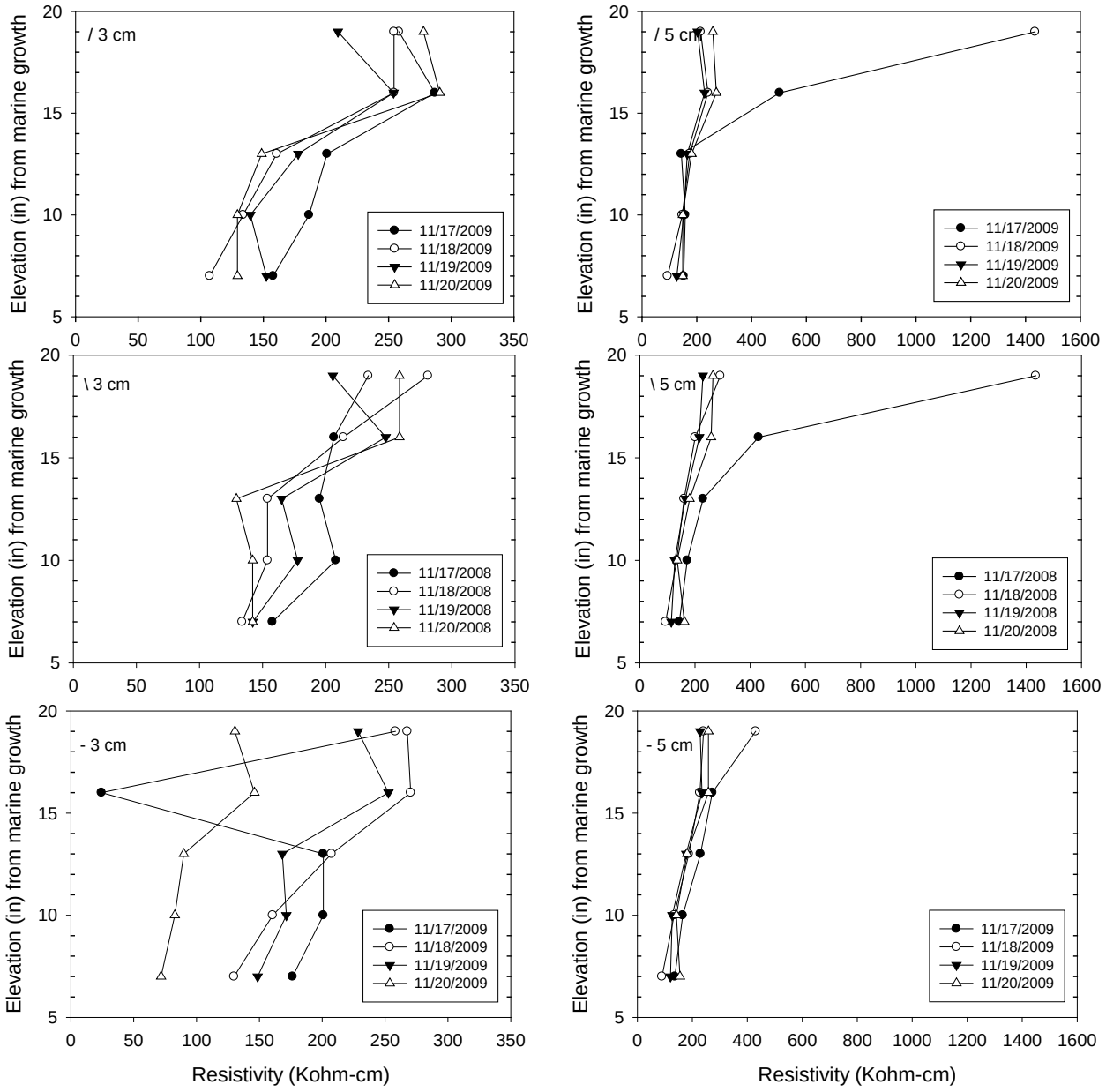

#120089
SR865- Over Hurricane Bay
Bent 8 Pile 1
Concrete Cover ~ 2.4 in

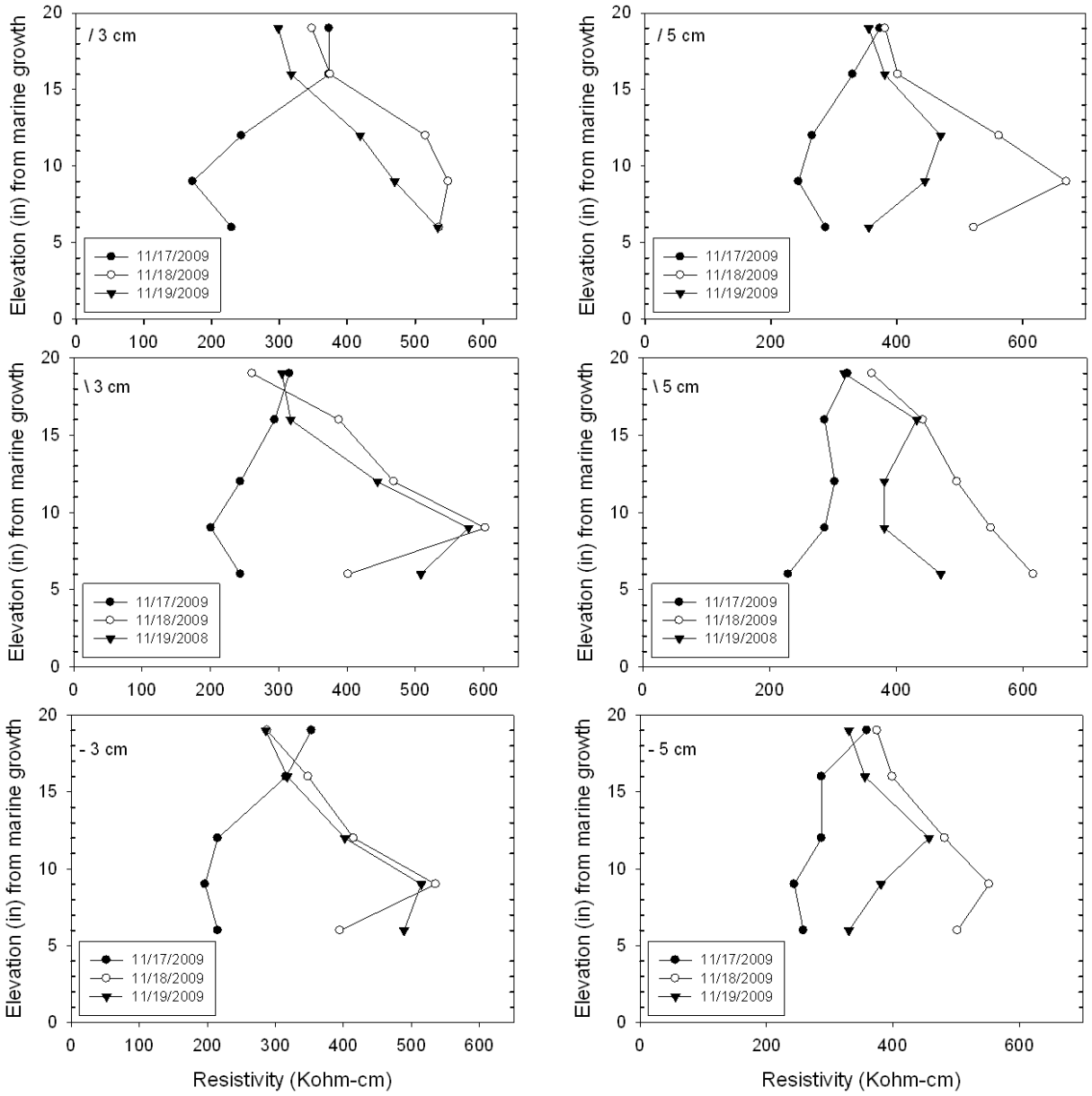

#120089
SR865- Over Hurricane Bay
Bent 8 Pile 4
Concrete Cover ~ 3.5 in